Tangellapalli Srinivas

Thermal Polygeneration

Ane Books Pvt. Ltd.

Springer

Thermal Polygeneration

Tangellapalli Srinivas

Thermal Polygeneration

Tangellapalli Srinivas
Department of Mechanical Engineering
Dr. B. R. Ambedkar National Institute
of Technology
Jalandhar, India

ISBN 978-3-031-37885-0 ISBN 978-3-031-37886-7 (eBook)
https://doi.org/10.1007/978-3-031-37886-7

Jointly published with Ane Books Pvt. Ltd.
The print edition is not for sale in South Asia (India, Pakistan, Sri Lanka, Bangladesh, Nepal and Bhutan) and Africa. Customers from South Asia and Africa can please order the print book from: ANE Books Pvt. Ltd.
ISBN of the Co-Publisher's country edition: 978-93-94883-33-8

1st edition: © Author 2023

This Springer imprint is published by the registered company Springer Nature Switzerland AG
The registered company address is: Gewerbestrasse 11, 6330 Cham, Switzerland

Foreword

A customer will expect quality and more benefits for his or her payment. Polygeneration's main focus is offering multiple benefits to meet the expectation. Certainly, the process, modelling, simulation, analysis and optimization ensures the quality of the system. I am sure that this book, thermal polygeneration meets the expectations of the readers by giving the knowledge at the basic level and advanced level to understand and develop the innovative integrations. The reader can find all the required information in the chapters and the properties data in the Annexure.

It is an honour for me to write the foreword for the book titled "Thermal Polygeneration" written by Dr T Srinivas. The scope of the book is in the area of solar thermal heat recovery for power generation, cooling production, freshwater and heat with the analysis. The needs are increasing with the high living standards. There is a need to develop new technologies that meet the needs. This type of thermal polygeneration offers the high tapping of the products from the energy source that will reduce greenhouse gas emissions. The book covers various thermal power plants, cooling systems, and thermal desalination for the polygeneration integration.

The book incorporates recent advances in research and developments in solar thermal polygeneration systems. I am confident that the book will be very useful to senior undergraduate level students, graduate-level students, researchers working in the area of thermal engineering and practising engineers in the area of polygeneration, waste heat recovery and energy management.

Dr T. M. Indra Mahlia
Distinguished Professor
University of Technology Sydney, Sydney

Foreword

The system-level developments are done very well in the research community. There is a need to integrate the individual system to meet the multiple needs of the society with the offers of low cost, flexibility, emission-free, and technically sound elements. As per the organization's behavior, it is difficult to expect eight human qualities such as decision making, organization, coordination, leadership, communication, etc., But we can expect all these qualities from a selected team. Polygeneration is such a team that meets all the expectations.

The multiple generations from renewable energy sources offer carbon dioxide-free generation to the environment. Therefore, these thermal polygeneration plants have more demand to generate more with added energy conversion. I wish this book on thermal polygeneration nurtures the new ideas of polygeneration integrations to tap the energy sources with the goal of more outputs. This book is dealing the thermodynamic analysis of very important thermal power plants with many possible options in the subsystem. The polygeneration modeling to the optimization of performance conditions results in the best practices for the effective implementation of the polygeneration. I know that Dr. T. Srinivas is also an author of 'Flexible Kalina Cycle Systems' which is focused on cooling cogeneration cycle based on Kalina cycle working principle. This book on thermal polygeneration offers more insights on the integrated energy systems based on various thermodynamic characteristics that may be very useful to the students and researchers. I wish this book, 'thermal polygeneration' contributes to understanding the polygeneration concepts, design, and development of new plants to the students, scholars, faculty, and practicing engineers for innovative developments.

Dr. R. Velraj

Professor and Vice Chancellor

Anna University, Chennai 600 025, India

Preface

Today a smart phone is playing many roles such as phone, camera for photos and videos, internet, chatting, message etc. In food technology, formers are paying interest to harvest tree having multiple fruits such as orange, apple, banana etc. What is the speciality of this type of systems? The answer is versatility. The human needs are increasing with increase in living standards. Generation of multi outputs increases the usage of the system at the domestic, commercial and industrial levels. It also increases the energy conversion capacity of the unit. The common human needs in daily life are drinking water, electricity, hot air for space heating, cold air for space cooling, hot water for regular use, process heat etc. The development of single system to meet the multiple needs minimizes the waste energy as the waste heat or similar will be recovered for multi generation. It also saves the floor space as units are combined together into a compact system.

This book is focused on description and development of polygeneration systems to generate electricity, fresh water, hot air, cold air and hot water from the single source of energy. The renewable energy sources such as solar thermal energy and photo voltaic (PV) panels have been applied to result all these outcomes. The main highlights of the focused polygeneration are no pressure parts in the desalination process, use of vapour compression refrigeration (VCR) cycle as a heat pump and also refrigerator, usage of binary fluid system for the polygeneration, compact unit to minimize the floor area and flexible operation for heating and cooling.

The thermal desalination selected is humidification-dehumidification (HDH) desalination to suit the thermal polygeneration. HDH works on a simple water cycle principle to convert the raw water into portable water or create the fresh water. The other systems such as heating and cooling are supplements the desalination processes. The selected polygeneration unit operates at the atmospheric pressure without having pressure parts. The methods are processes

are safe as it would not use any chemicals. The operation and maintenance is easy due to simple working principle.

The alternative options in this polygeneration plant are studied to highlight the best practices. Four polygeneration configurations are studied viz. binary fluid polygeneration with single stage HDH, binary fluid polygeneration with double stage HDH, heat pump polygeneration with single stage HDH and heat pump polygeneration with double stage polygeneration. The VCR is analysed with water cooled condenser. Another option of binary fluid system in place of VCR is also studied for the polygeneration development. The heat pump element with the water cooled heat exchanger to support the HDH cycle is analysed to develop the best operational conditions. The HDH plant with single stage operation and double stage operation are simulated with the objective of maximum yield and maximum energy conversion for binary fluid polygeneration and heat pump polygeneration.

The results show that the single stage HDH can be adopted in polygeneration for higher energy performance ratio (EPR) of the polygeneration compared to the double stage HDH. The double stage generates higher outputs compared to single stage HDH in polygeneration but with a penalty in the EPR. The polygeneration cycle EPR is crossing more than 100% with all the configurations. The resulted optimum refrigerant's evaporator is same for maximum cycle EPR and maximum plant EPR in a binary fluid polygeneration. But in the heat pump polygeneration, the optimum evaporator temperature for the maximum cycle EPR is greater than the maximum plant EPR. Since the phase change temperature is variable in binary fluid polygeneration, the refrigerant exit temperature from the evaporator is relatively high compared to heat pump polygeneration where the evaporator temperature is constant during the phase change.

Dr. Tangellapalli Srinivas

Acknowledgements

I greatly acknowledge the project grant of the Science and Engineering Research Board (SERB) under Impacting Research Innovation and Technology (IMPRINT-2), PAC Water Resources & River Systems, New Delhi, India (IMP/2019/000444). The title of the project is 'Experimental Investigation on Tower Type Hybrid Vapour Compression Refrigeration (VCR) and Humidification-Dehumidification (HDH) Desalination Plant' and implemented at NIT Jalandhar. The work has been extended to polygeneration to generate electricity, freshwater, heating, cooling and hot water. My hearty wishes and thanks to Dr Rajeev Kukreja, Co-Investigator of this SERB (IMPRINT-2) project in supporting every stage of the development of the technology. It is my pleasure to acknowledge the support from industrial partners, Er. Madhusudhana Rao, Oorja Energy Engineering, Hyderabad and Er. Ashraf Batti, Green Builders, Jalandhar.

My sincere gratitude goes to my research advisor, Dr. P. K. Nag, Professor, IIT Kharagpur, India for showing the road map and inspiration. I am extremely happy to express deepest thanks to my doctoral degree guide, Dr. A.V.S.S.K.S. Gupta, Professor, JNT University, Hyderabad for sculpturing me by refining the thoughts and works. It is my fortune to get dynamic and energetic guide Dr. B. V. Reddy, Professor at Ontario Tech University (OTU), Canada for my post-doctoral work.

The contributions of the doctoral scholars Dr. Shankar Ganesh, Dr. Ch.Chiranjeevi, Dr. M. Natarajan, Dr R Shankar, Mr. Akash Saxena, Mr Vajeer Baba, Mr. Adarsh Kumar Yadav and Mr. Aakash Kumar Nimesh added great weightage to this book. In additional to the doctoral scholars, UG and PG students are contributed well in shaping this book.

My special thanks to the institutes Gudlavalleru Engineering College, Gudlavalleru, India, Vellore Institute of Technology, Velore, India, Ontario Tech University, Canada and Dr B R Ambedkar National Institute of Technology, India for valuable support to nurture the innovation.

I would like to express my deep sense of gratitude and respect to parents who shaped my hard work and strong determination in the field of engineering from the beginning. My heart felt gratitude to my wife, Kavitha Devi, elder son Rahul and younger son Jignesh without their regular support and boosting, I can not do this much.

Finally, thanks to all who involved in this work directly or indirectly to shape this book in fruitful form.

Dr. Tangellapalli Srinivas

Nomenclature

AP	approach point
c	specific heat, kJ/kg K
COP	coefficient of performance
EPR	energy performance ratio
G	solar global radiation, W/m^2
h	specific enthalpy, kJ/kg
m	mass, kg
P	pressure, bar
PP	pinch point, K
Q	heat, kJ
q	specific heat, kJ/kg
s	specific entropy, kJ/kg K
T	temperature, K
TTD	terminal temperature difference, K
W	work, kJ
w	specific work output, kJ/kg
x	mass fraction of ammonia, kg/kg mixture
y	ammonia concentration in vapour phase
ɘ	effectiveness
J	energy, kJ
η	efficiency
δ	dryness fraction
Ø	relative humidity, %
ω	specific humidity, kg/kg da

Subscripts

a	ambient
bp	bubble point
c	cycle
co	compressor
cond	condenser
cw	cooling water
da	dry air
deph	dephlegmator
e	evaporator
es	electrical supply
f	fluid
fi	fluid inlet
fw	freshwater
g	generator
h	hot
hf	hot fluid
hw	hot water
HTF	heat transfer fluid
HTR	high temperature regenerator
KC	Kalina cycle
l	liquid
LTR	low temperature regenerator
m	mechanical
net	net output
p	pump
pt	plant
r	refrigerant/refrigeration
sep	separator
sh	superheater
ss	strong solution
st	steam turbine
t	turbine
th	thermal
tot	total
v	vapour
vt	vapour turbine
w	water
wa	wet air
wi	water inlet
u	universal
v	vapour
0	reference state

Contents

Foreword *v*
Foreword *vii*
Preface *ix*
Acknowledgements *xi*
Nomenclature *xiii*
1. Introduction 1
2. Power Generation 14
3. Binary Fluid Properties and Processes 56
4. Binary Fluid Power 91
5. Binary Fluid Cooling 107
6. Vapour Compression Refrigeration 123
7. Humidification-Dehumidification Desalination 146
8. Binary Fluid Polygeneration 207
9. Heat Pump Polygeneration 246
10. Polygeneration – A Comparative Study 283

Appendix - A

Binary Fluid Properties – Ammonia-Water Mixture 292

Appendix - B

Refrigerants and Psychrometric Properties 373

References *387*

1 Introduction

Abstract

Thinking big leads to success and elevates the ordinary to the extraordinary. Polgeneration is an idea to think more about technological novelty without any boundaries or limits. Polygeneration is a system that generates many outputs, at least four of which are power, which is the many outputs from a single or hybrid source of energy. The chapter gives an introduction to polygenration, its need, and classification. The significance of polygeneration has been highlighted. The research studies are reviewed with the literature survey. The chapters of the book have been discussed.

1.1 Introduction

Human and societal needs are increasing with an increase in living standards. Polygeneration, or multigenerational, produces four or more outputs from the energy supply. Cogeneration and trigeneration produce two and three outputs, respectively. For example, a smart phone can be used for talking, location sharing, chatting, texting, internet, whatsapp, internet, photos, videos, etc. The usage of smart phones has increased because of their multiple features. While purchasing a new item, a customer expects additional benefits or features compared to the existing models. Therefore, an engineer has to think about the multi-utility product to meet the needs of the customer. Zebra has the features of speed and load carrying capacity. Formers are interesting trees to harvest for their multiple fruits. This type of tree gives us different types of fruits such as apples, oranges, bananas, pineapples, etc. Instead of planting many trees, one tree will give different fruits. A broomstick can be extended to clean the ceiling in addition to the floor cleaning. A vaporising lamp gives light, and the room gets fragrant with the good smell. The top of the vaporising lamp has a cavity where the oil can be poured to heat with the lamp heat. Therefore, it offers the benefits of lighting and fragrance. Polygeneration

T. Srinivas, *Thermal Polygeneration*,
https://doi.org/10.1007/978-3-031-37886-7_1

is a unit having many features and benefits that attract the market for its easy commercialization.

Fig. 1.1 shows the energy conversion units such as (a) power generation, (b) cogeneration, (c) trigeneration, and (d) polygeneration. The power plant only produces electricity, and a lot of the energy supply is wasted in the form of heat. In a typical thermal power plant, nearly 2/3 of the energy supply (66.6%) is wasted into the atmosphere. If this unit is redesigned by utilising some parts of waste heat into useful forms, such as space heating, drying of food, etc., the energy conversion increases and is called cogeneration. In trigeneration, the cogeneration is extended with the additional benefit of cooling. As a result, in general, trigeneration produces electricity, process heat, and cooling. Finally, polygeneration is the next version of trigeneration where one more outcome (freshwater in this case) has been added in addition to electricity, process heat, and cooling. The shown polygeneration results in four outputs (or more), viz., electricity, process heat, cooling, and freshwater.

The technology has been developed well at the individual level, such as internal combustion (IC) engines, power plants, refrigeration, air-conditioning, drinking water plants, etc. But the smart integration of such units needs more refinement for the novel integration of energy systems.

The concept of integration is interdependent. For example, if we consider three systems, viz., power, water, and fields, as shown in *Fig. 1.2,* these three units are interlinked with each other. Electricity is required for the irrigation of fields, plants, and agriculture. Similarly, it also drives the water plants, which is an essential requirement. The fields provide the fuel, such as bio-fuels, for the power generation, and the plants cause the rain, which is the input to the water plants. Water is required for the irrigation of fields and is used in a power plant as a working fluid and medium to reject the heat in a water-cooled condenser.

In a polygeneration, also, if we are able to identify the interdependent features, processes, and units, it is easy to develop a potential polygeneration. For example, an air-conditioning unit has psychrometric processes such as sensible heating, humidification, cooling, dehumidification, etc., which are similar to those of humidification-dehumidification (HDH) desalination. These two can be merged together to become an integrated unit. Electricity is required to drive these two units. The thermal power plant also rejects the heat, which can be supplied to drive the units operated by heat, such as thermal desalination. This may result in a tri-generation. This trigeneration can also be extended to polygeneration. Therefore, the dependency of subsystems gives ideas for inventing new polygenerations.

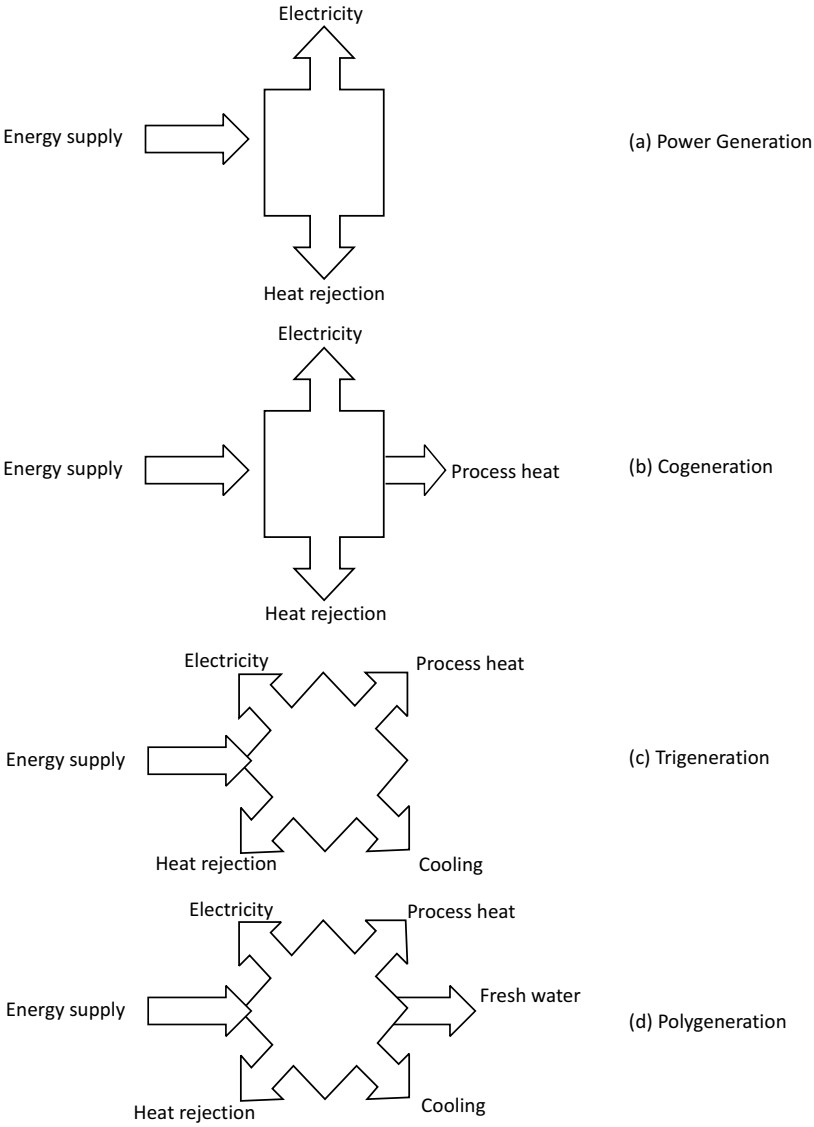

Fig. 1.1: Energy conversion units (a) power plant, (b) cogeneration, (c) trigeneation, and (d) polygeneration

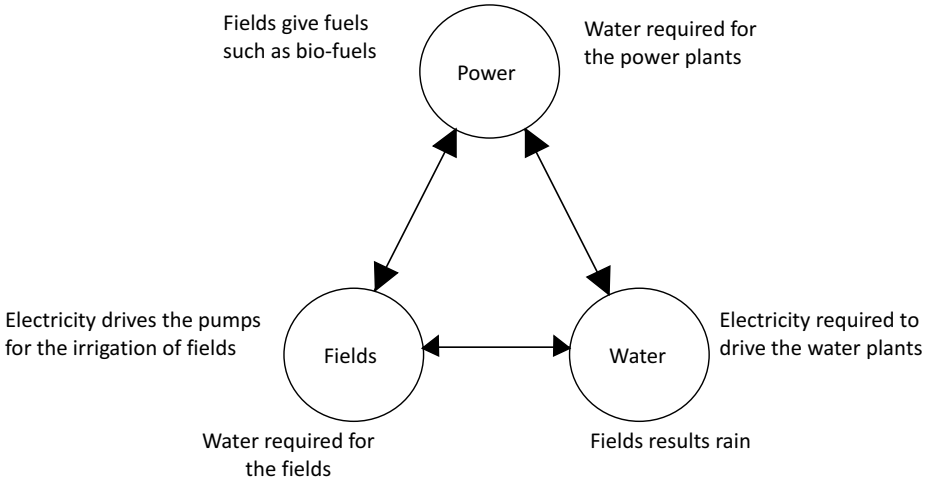

Fig. 1.2: Interdependency of systems

The following are the benefits of polygeneration.

1. Minimises the energy losses and maximises energy conversion efficiency.
2. It allows more flexibility in design and provides a custom based design.
3. Results in a compact unit compared to the total size of the individual systems.
4. It meets the multiple needs.
5. Carbon dioxide mitigation.

Polygeneration offers a higher coefficient of performance (COP) compared to the refrigerator and heat pump.

In a refrigeration, COP of refrigeration,

$$COP_r = \frac{Q_e}{W_{co}} \tag{1.1}$$

where Q_e and W_{co} are the heat absorption in an evaporator and work supplied to the compressor.

Similarly, the COP of heat pump,

$$COP_{hp} = \frac{Q_{cond}}{W_{co}} \tag{1.2}$$

In the above equation, Q_{cond} is the heat rejection in a condenser.

As per the energy balance,

$$Q_{cond} = W_{co} + Q_e \tag{1.3}$$

Therefore,

$$COP_{hp} = \frac{W_{co} + Q_e}{W_{co}} = 1 + COP_r \quad (1.4)$$

If a polygeneration is using the refrigerating effect and heat rejection for the polygeneration operations,

The COP of the polygeneration,

$$COP_{poly} = \frac{Q_e + Q_{cond}}{W_{co}} \quad (1.5)$$

$$= \frac{Q_e}{W_{co}} + \frac{Q_{cond}}{W_{co}} \quad (1.6)$$

$$= COP_r + 1 + COP_r$$

$$COP_{poly} = 2\text{COPr} + 1 \quad (1.7)$$

or

$$COP_{poly} = COP_r + COP_{hp}$$

$$= COP_{hp} - 1 + COP_{hp}$$

$$COP_{poly} = 2COP_{hp} - 1 \quad (1.8)$$

Therefore,

$$COP_{poly} = COP_r + COP_{hp} = 2COP_r + 1 = 2COP_{hp} - 1 \quad (1.9)$$

For example

If $COP_r = 3$,

Then, $COP_{hp} = 3 + 1 = 4$

and $COP_{poly} = COP_r + COP_{hp} = 3 + 4 = 7$.

It shows that the COP of polygeneration is higher than the COP of refrigerator and COP of the heat pump. In addition to the benefits, polygeneration increases the capital cost, and proper justification is required for the increased cost. Polygeneration can be developed by integrating the components and subsystems or may be a single system that generates many.

Some of the elements of polygeneration are:

1. Energy sources (gasification, fuel firing, solar thermal, solar photovoltaic (PV), PV/T, heat recovery, hybrid sources, etc.).
2. Power generation.
3. Process heat.
4. Cooling (vapour absorption refrigeration (VAR), vapour compression refrigeration (VCR), ejector, hybrid, etc.
5. Desalination
6. Hot water
7. Fuel

1.2 Studies on Polygeneration

The need for polygeneration is driven by the fast-growing world population and increasing demands. The shortage of energy sources also demands new solutions such as polygeneration. Global pollution from conventional fuels can be controlled with the development of polygeneration. Polygeneration meets the needs by converting energy into multiple outputs. The cost of electricity and fuel is increasing exponentially and we need to think about the alternatives.

Polygeneration is a single plant that supplies multiple outputs such as electricity, process heat, cooling, fuel, freshwater, etc. *(Jana et al., 2017)*. Polygeneration is an extension or modified version of cogeneration *(Murugan and Horák, 2017)*. Polygeneration generates energy, viz. electricity, process heat, cooling, as well as products such as fuel, fertilizers, food, drinking water, etc. *(Calise et al., 2018)*. Therefore, it has more flexibility in design to suit customer expectations. The consumption of water and energy is increasing with increasing demand. Polygeneration offers efficient utilisation of natural resources by minimising environmental effects *(Serra et al., 2009)*. Liu et al. (2007) used Mixed-Integer Programming (MIP) for long-term decisions on polygeneration infrastructure investment. The work has proved that the polygeneration systems are superior to the stand-alone systems. According to the *Chen et al. (2012)* findings, biomass-based pyrolysis has great adoptability for polygeneration as it results in solid, liquid, and gaseous fuels. Solar-driven polygeneration is possible with organic gas turbines, Rankine cycle (ORC), vapour absorption refrigeration (VAR), desalination, process heat etc. Solar linear focused collectors are suitable to tap the solar radiation to drive the polygeneration plants *(Kasaeian et al., 2020)*. Different renewable energy sources, such as biomass, solar, or wind, can be hybridised to drive polygeneration. Even conventional energy sources can also be combined with renewable energy sources for operation of polygeneration *(Rubio-Maya et al., 2011)*. The optimization of multi-objective units such as polygeneration is a tedious task compared to the optimization of individual units. Some of the operational conditions favour one category of system and do not favour other systems. The conditions may be supportive of each other or diverse in the total system.

The energy supplied to the polygeneration is from conventional energy systems, renewable energy systems, hybrid conventional and non-conventional energy sources, or hybrid renewable energy sources. Conventional energy sources are rich and suitable for higher polygeneration capacities, but they are harmful to the environment *(Murugan and Horák 2016)*. Renewable energy-supplied polygeneration systems are more environmentally friendly and need to be developed for improvement with sources such as solar, wind, geothermal, and bio-mass. Conventional energy sources, such as coal, oil, and natural gas, are limited and exhaustive. Currently, the majority of power generating plants

use coal and fossil fuels because of their high calorific value. As a result, mega or ultra-mega capacity power plants dominate the global power sector for producing electricity using coal, fossil fuels, etc. *(Wright 1986)*. Therefore, these energy sources can be coupled with renewables to minimise the role of conventional fuels. Similar to the flexibility in energy supply, polygeneration also has great flexibility in the selection of energy conversion technologies *(Kyriakarakos et al., 2015)*.

Zeghici et al. (2014) investigated the performance of an integrated polygeneration system coupled with a district heating unit and an aquifer thermal energy storage (ATES) unit. Fossil fuel is used as an input to this system to produce electricity, cooling and heat from energy conversion devices such as gas turbines (GT) and district heating cooling (DHC) systems. The TRANSIS simulation results show 43.5% overall performance efficiency with an 82% emissions reduction. Ortiga et al. (2007) reported the design and optimization studies of a polygeneration system. Polygeneration increases system complexity, improves energy efficiency, decreases emissions and waste, and boosts economic value (Sahoo et al., 2015).

Li and Barton (2015) mathematically investigated the optimal design of a polygeneration system to generate electricity, diesel, naphtha, and methanol from coal and bio-mass sources. This polygeneration system is equipped with coal and bio-mass conversion cycles to evaluate the overall performance of the system. The Integrated Gasification Combined Cycle (IGCC) with carbon capture and sequestration (CCS) and the Biomass Converting Plant (Biomass to liquid (BTL) via gasification) are the energy conversion devices. Mixed-integer non-linear programme (MINLP) and non-convex generalised Benders Decomposition (NGBD) programming methods were used to optimise the design, and they achieved 44.07% energy efficiency with less environmental impact. Using this combined coal-biomass-based polygeneration system, they produced 5.17 MW of electricity. Gao et al. (2004) investigated the energy analysis of a coal-based polygeneration system to generate power from a cascade system and chemicals from the methanol production process. The Aspen Plus simulation tool is used to simulate the mathematical model to evaluate the performance and energy of the coal-based polygeneration system. Simulation results were compared with previous models (IGCC coupled polygeneration system) and achieved 45.2% energy efficiency with the cascade system in the polygeneration system. Hao and Feng (2012) applied the exergo-economics analysis to a polygeneration system equipped with IGCC-CCS. The system produces power and chemical liquids from energy conversion devices, IGCC, and a methanol production plant. Guo et al. (2014) designed a new polygeneration system for producing power, methanol, and oil from coal and lignite inputs. This polygeneration system is coupled with a new circulating fluidized bed power plant for evaluating the electrical performance. The ASPEN Plus results

show an output of 1259.6 MW of power and 43.2% energy efficiency. From a techno-economic point of view, Ng and Hernandez (2016) simulated the reuse of CO_2 in a polygeneration system equipped with carbon capture and storage. In the simulation process, they evaluated the energy efficiency and economic analysis of the coal-fired polygeneration system with a CO_2 reuse scheme. Ng et al. (2013) investigate the techno-economic performance and trade-off analysis of an integrated decarbonised coal-based polygeneration system coupled with CO_2 reusing technology. Using this technology, they improved the methanol production rate and reduced CO_2 emissions. They showed a 75% conversion of CO_2 emissions into methanol. Polygeneration with coal-biomass supply and a carbon capturing system is beneficial from both an economic and environmental standpoint (Williams et al., 2009). Hu et al. (2011) compared polygeneration with and without CO_2 recovery. The results concluded that the polygeneration efficiency was improved by 42.4% of the IGCC coupled with CO_2 recovery units. Meerman et al. (2011) investigated the performance and technical feasibility of a flexible integrated gasification polygeneration (IGPG) system. A coal-supplied polygeneration system coupled with a CO_2 capturing device achieves 51% overall performance efficiency compared to bio-mass and syngas-based polygeneraiton systems. Yi et al. (2014) proposed a novel dual gas polygeneration system equipped with an IGCC and carbon capturing and reforming units. This dual-polygeneration cycle uses coal gasification gas (CGG) and coke oven gas (COG) as primary inputs to evaluate the thermal and electrical performance. The Dual gas polygeneration system improves CO_2 utilisation and overall performance efficiency by up to 53% as compared to IGSS-CCS, IGCC-CRS, and PL-CCS (polygeneration with carbon capturing system) performance. The polygeneration studies are classified as theoretical, experimental, and pilot plants, but at the commercial level, these plants are not operated. Most of the works on polygeneration reported in the open literature are theoretical studies.

According to primary input energy, polygeneration systems may be classified. Table 1.1 overviews coal-based polygeneration modelling and simulation with the performance levels. The particulars are energy supplied, outputs, energy conversion devices, methodology, efficiency, and output. As per the performance and socio-economic conditions, the IGCC is a promising technology for electricity, liquid fuels, chemicals, potable water, etc.

Table 1.1 Outputs of coal powered IGCC polygeneration

Author (Year)	Input	Outputs
Lin Hu et al., (2014)	coke oven gas	electricity, methanol, Sulphur, and fuels
Yi Qun et al., (2013)	coal	electricity, chemicals and fuels

Gutkowski Gary., (1983)	coal	electricity, liquid hydrogen, gaseous nitrogen, and heat
Li et al., (2014)	coal	electricity, methanol, and fuel
Yu and Chien, (2015)	coal	electricity and fuel
Guo et al., (2015)	coal	electricity, oil, Sulphur, and methanol
Ahmadi et al., (2012)	coal	Electricity, heating, cooling, and hot water
Zhu et al., (2016)	coal	electricity, chemicals and fuel
Farhat and Reichelstein (2016)	coal	electricity, fuels and fertilizers
Ortiga et al., (2012)	natural gas	electricity, cooling, fuel and heating
Kaniyal et al., (2013)	solar, coal	electricity and fuel
Meerman et al., (2012)	coal	electricity, fertilizers, chemicals and fuels
Lin et al., (2014)	coke oven gas	electricity, cooling and fuels
James et al., (2013)	coal	electricity and fuels
Yu et al., (2010)	coal	electricity, and fuels

Table 1.2 Input and output energies of gas based polygeneration

Author, Year	Input	Outputs
Rubio-Maya et al., (2011)	natural gas, biomass and solar energy	electricity, heating, cooling and freshwater
Ng et al., (2013)	syngas	electricity, chemicals, and fuel
Gao et al., (2008)	natural gas	electricity, and fuel
Li et al., (2011)	Syngas and coke oven gas	electricity, fuel, and chemical
Yi, Feng and Li, (2012)	coke oven gas and syngas	electricity, chemical and fuels
Khojasteh Salkuyeh and Adams, (2015a)	shale gas	electricity, chemical and fuel
Khojasteh Salkuyeh and Adams (2015b)	petroleum coke and natural gas	electricity, chemicals, olefins and fuel (Transportation)
Hao et al., (2015)	coke oven gas and coal gasified gas	electricity, DME, and ethanol

Aichmayer et al., (2014)	solar and natural gas	electricity, cooling and hot water
Wang et al., (2009)	natural gas	electricity, fuel and chemical

Table 1.3 Biomass polygeneration

Author (Year)	Input	Outputs
Maraver et al., (2012)	biomass	electricity, cooling and freshwater
Jana and De (2015)	coconut fiber	electricity, heating, cooling and freshwater
Lythcke-Jørgensen and Haglind (2015)	wheat straw	electricity, heat and bio-fuel
Gassner and Maréchal (2012)	biomass	electricity, Synthatic gas, and heat
Chen et al., (2011)	coal and biomass	electricity, chemicals and liquid fuels
Khan and Martin (2015)	biomass	electricity, cooking gas and pure water
Chen et al., (2016a)	biomass	bio-char, Bio-gas, Bio-oil
Chen et al., (2016b)	biomass	bio-gas, liquid oil, acids, ketones, phenols
Salomón et al., (2013)	palm oil residues	electricity, heat, palm oil pellets and biodiesel
Xin et al., (2013)	biomass	fuels (solid char, liquid oil and bio-gas)

Table 1.4: Renewable energy operated polygeneration

Author (Year)	Input	Outputs
Sahoo et al., (2015)	solar and biomass	electricity, heating, cooling and freshwater
Kyriakarakos et al., (2011)	solar and wind	electricity, freshwater, and hydrogen
Calise et al., (2012)	vegetable oil and solar	electricity, freshwater, cooling, and heating
Buonomano et al., (2014)	solar	electricity, cooling and heating
El-Emam and Dincer (2017)	solar and biomass	electricity, cooling, and hydrogen
Bracco et al., (2012)	solar and wind	electricity, and heat

Mata-Torres et al., (2017)	solar	electricity, and freshwater
Calise et al., (2017)	solar and geothermal	electricity, desalinated water, cooling and heating
Kribus and Mittelman, (2008)	solar	electricity, cooling and heating
Vidal and Martín, (2015)	biomass and solar	electricity, hydrogen and bio-fuel
Ray et al., (2017)	solar and biomass	electricity, methanol, and cooling
Rossi et al., (2016)	solar and wind	electrical and heat
Paleta et al., (2014)	solar and wind	electricity (Lighting, heating, conditioning)
Soutullo et al., (2016)	solar and biomass	electrical and thermal performance

Table 1.3 to Table 1.4 is focused on studies on polygeneration systems with renewable energy sources.

The study on polygeneration demonstrates the potential of integration and possible future inventions to meet societal needs. It has been observed that the vapour compression refrigeration- humidification dehumidification (VCR-HDH) and binary fluid cooling cogeneration – humidification dehumidification (BFCC-HDH) polygenerations are not reported in the open literature. This work is aimed at a review of available polygeneration systems and maximising the EPR of proposed polygeneration plants by optimising the evaporator's temperature.

1.3 Overview of the book

This book consists of 10 chapters. The following is a short description of the chapters of this thermal polygeneration book.

Chapter 1: Introduction: This chapter provides an overview of polygeneration, including definitions, the need for it, an introduction, classification, potentials, history, and literature.The elements of polygeneration have been discussed with the various technologies and contributions. The potential of the polygeneration system has been highlighted compared to the other systems. The literature is reviewed with the latest research developments in the area of polygeneration.

Chapter 2: Power Generation: Power generation is the primary outcome of polygeneration. The chapter details the thermal power plants with the working fluids of steam and organic fluids. The conventional Rankine cycle and flash cycle are elaborated with the plant layout, energy modelling, simulation and analysis.

Chapter 3: Binary Fluid System – Properties and Processes: Knowledge and solutions to binary fluid properties and processes are required to evaluate binary fluid polygeneration. This chapter details the thermodynamic properties of the binary fluid system and the process solutions.

Chapter 4: Binary Fluid Power: Polygeneration with a low temperature heat source can be associated with a low temperature operated thermal power plant. Power plant is the Binary Fluid Power Plant. Kalina invented this binary fluid cycle, hence it is known as the Kalina cycle. The chapter is focused on the development and performance study of a binary fluid power plant.

Chapter 5: Binary Fluid Cooling: Similar to binary fluid power, binary fluid cooling can be developed with the reversed cycle, which is also called a vapour absorption refrigeration (VAR) cycle. The chapter details the ammonia-water-based binary fluid cooling plant for the integration of polygeneration.

Chapter 6: Vapour Compression Refrigeration: Depending on the energy source of the polygeneration, VAR or VCR can be used to generate the cooling effect. The basics of VCR have been discussed to support VCR based polygeneration. The influence of operating conditions on VCR has been analysed.

Chapter 7: Humidification-Dehumidification Desalination: HDH desalination is a type of thermal desalination that can be used in thermal polygeneration.Since HDH has more compatibility with the air conditioning processes, it has been modelled and simulated. The performance conditions are analysed to derive the suitable operational conditions for the maximum desalination yield and energy efficiency.

Chapter 8: Binary Fluid Polygeneration: An ammonia and water mixture has been used as a working fluid in the binary fluid polygeneration. Binary fluid polygeneration integrates binary fluid cooling cogeneration (BFCC) and HDH desalination. The polygeneration configuration has been studied with the single-stage HDH and double-stage HDH units. These two polygeneration plants are analysed with the goal of optimising the cooling system's evaporator exit temperature to maximise the energy performance ratio (EPR).

Chapter 9: Heat Pump Polygeneration: Similar to binary fluid polygeneration, heat pump polygeneration has been studied with single stage HDH and double-stage HDH. The heat absorption and heat rejection characteristics of the heat pump have been used for the polygeneration processes. The performance characteristics are analysed to optimise the evaporator temperature for the maximum EPR.

Chapter 10: Polygeneration – A Comparative Study: The binary fluid polygeneration and the heat pump polygeneration are compared with the single fluid HDH and double HDH. These four polygeneration characteristics are compared to draw the relative merits and demerits of each.

1.4 Summary

The basics of polygeneration are discussed with the need, significance, and potential. The research outputs and developments are examined in order to determine the current state and future scope of polygeneration. The equations for the COP of the refrigeration, heat pump, and combined refrigeration and heat pump are formulated. The chapters of this book are surveyed.

Review questions

1. What is the difference between trigeneration and polygeneration?
2. The basic drive of the polygeneration is the interdependency of the systems. Justify with suitable examples.
3. Highlights the merits and challenges of polygeneration.
4. In a polygeneration, if the heat absorption and heat rejection of the refrigeration cycle have been used for the polygeneration, show that the COP of polygeneration is the sum of COP of the refrigeration and COP of the heat pump.

❐

2 Power Generation

Abstract

Electrical power is the primary product of polygeneration. As a result, power plants play a significant role in polygeneration integration. Power can be generated through direct energy conversion such as a fuel cell, solar photovoltaic (PV) panel, and thermos-electric effect or similar. The indirect methods of power generation include thermal power plants such as biomass gasifiers, wind turbines, solar thermal power plants, combined cycle power plants etc. This chapter is focused on various thermal power cycles for power generation suitable to a thermal polygeneration. The studied thermal power cycles are the steam Rankine cycle (SRC), steam flash cycle (SFC), organic Rankine cycle (ORC), and organic flash cycle (OFC). The power plant layout with solar concentrating collectors, evaluation model with equations and the results are presented to understand and evaluate the various solar thermal power plants.

2.1 Introduction

Thermal power plants have more adoptability to polygeneration as they have lot of waste heat. This heat can be used for process heat, such as cooling, thermal desalination, hot water, etc. or can be used for power generation. This chapter is limited to thermal power plants with a single fluid operation. The binary fluid-based thermal power plants are discussed in another chapter. Four thermal power cycles are studied with thermal modelling, simulation, analysis and optimization. The study of these thermal cycles can be extended to polygeneration for the multiple utilisation of process heat from the power plant. The organic fluid and steam are used to create single fluid power plants such as the Rankine cycle and flash cycles. The elaborated cycles are the steam

T. Srinivas, *Thermal Polygeneration*,
https://doi.org/10.1007/978-3-031-37886-7_2

Rankine cycle (SRC), steam flash cycle (SFC), organic Rankine cycle (ORC), and organic flash cycle (OFC). This chapter details the power plant layout, its workings, formulation and analysis, with the recommendations. The objective of this chapter is to develop the optimum operational conditions of thermal power plants to achieve the maximum power generation and thermal efficiency. The performance conditions studied under this chapter are power generation, cycle thermal efficiency, solar concentrating collector's thermal efficiency, and solar thermal power plant's thermal efficiency.

2.2 Steam Rankine Cycle

Fig. 2.1 depicts the solar thermal power plant's layout with water as a working fluid. The cylindrical parabolic collector (CPC) has been used to raise the temperature of heat transfer fluid (HTF), which is Therminol oil in this case. The solar collector is integrated with a thermal storage unit to supply the heat irrespective of the available solar energy. From the cold side of HTF, the fluid enters (10) into the series of collectors and the heated fluid (11) is supplied to the storage tank. The hot fluid (13) is communicated to the HRSG and the fluid (16) has been pumped to the storage tank after the heat transfer. The power cycle is a Rankine cycle with a deaerator. The heat from the HTF has been transferred to the working fluid (water) in the heat recovery steam generator (HRSG). The hot fluid (13–16) in HRSG generates the superheated steam (1) from the feedwater (7). The boiler, or HRSG, consists of three sections, viz., economizer (7-8), evaporator (8–9), and superheater (9–1). The superheated steam is expanded in the turbine (1-3) and generates electricity in the alternator. The expanded steam (3) is supplied to the water cooled condenser (3-4) and condensed to a saturated water state by rejecting the heat to the surroundings (17-18). The condensate is pumped to a deaerator pressure from the condenser pressure. A deaerator is an open feedwater heater where the steam (2) and water (5) directly mix with each other to produce saturated water (6). It removes the dissolved gases from the working fluid and increases the temperature of the feedwater heater (regeneration). This improves the performance of heat transfer and also increases the thermal efficiency of the plant. A portion of the turbine's steam (2) is trapped and supplied to a deaerator (5–6) for feedwater heating. Again, the condensate from the deaerator is pumped (6-7) from the deaerator pressure to HRSG pressure. In HRSG, the feedwater (7) is heated and the superheated steam (1) has been generated for the power generation. The cycle repeats for the continuous operation.

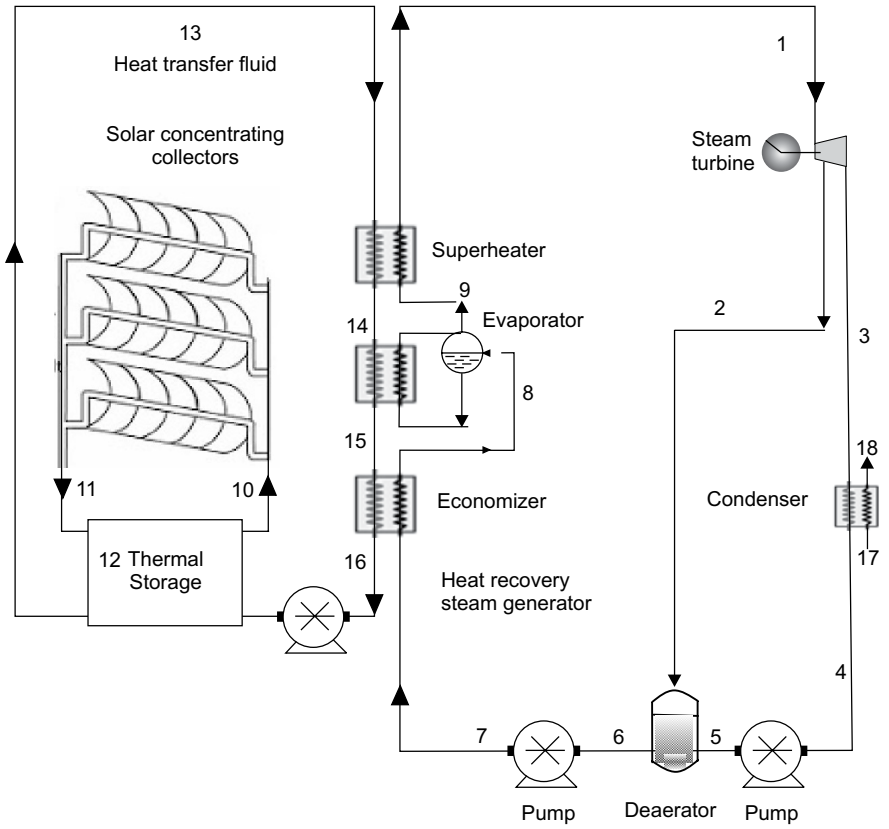

Fig. 2.1: Schematic plant layout of SRC with a deaerator

Fig. 2.2 shows the temperature-specific entropy diagram of SRC with source and sink fluids. The cycle operates on three pressures, viz., high pressure (boiler), intermediate pressure (deaerator), and low pressure (condenser). Since the sink temperature is below 100 °C, the condenser pressure is a vacuum pressure. The turbine inlet temperature is selected as per the condition of the solar thermal collector and HTF. The HTF temperature in HRSG (13-16) decreased. State 15 is determined by the pinch point (PP) constraint. The PP and AP are defined in the next modelling section. A small approach point (AP) is also considered between the economiser and the evaporator (state 8). The circulating water temperature is increased (17–18) in the water cooling condenser with the heat absorption.

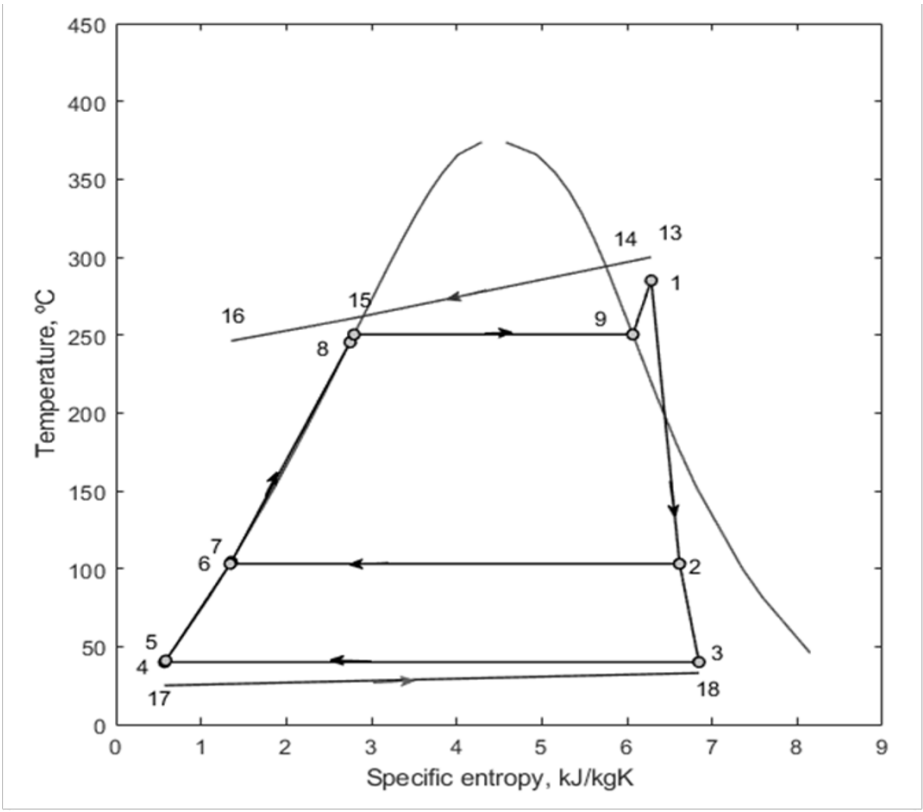

Fig. 2.2: Temperature-entropy diagram for SRC with a deaerator

The SRC has been modelled with the solar CPC and Rankine cycle. The assumptions in this model are that flows

The steam flow rate at the inlet of the turbine is 100 kg/s. The steam supply temperature at the inlet of the turbine is determined by the source temperature, i.e., the thermic oil temperature coming from the solar concentrating collector. In a heat exchanger, the terminal temperature difference (TTD) has been fixed as a constraint to ensure the heat transfer from the hot fluid to the cold fluid. In a superheater, the TTD is 15 K. TTD in the condenser is 10 K. PP is a minimum temperature difference between hot fluid and the working fluid in the evaporator. In the direction of the working fluid, the inlet of the evaporator has a minimum temperature difference. It ensures the positive heat transfer from the HTF to the working fluid. With this limit at the known quantity of working fluid, the required amount of HTF can be determined in the design, or vice versa. AP is the temperature difference within the working fluid, i.e., between the evaporator temperature and the economizer exit temperature. At zero AP, these two temperatures are the same. But to ensure a smooth transmission of phase from liquid to vapour at the interphase, AP has been maintained.

With this AP, a slightly subcooled liquid has been supplied to the evaporator to avoid the sudden transition in phase and pitting with the bubbles. At Jalandhar (31.33° N, 75.58 ° E), Punjab, India, the beam radiation and global radiation determined at the equinox time (between summer and winter) are 340 W/m^2 and 515 W/m^2, respectively.

The turbine inlet temperature from the supply temperature of HTF and TTD in superheater,

$$T_1 = T_{13} - TTD_{sh} \tag{2.1}$$

The economizer exit temperature from the AP and boiler saturation temperature,

$$T_8 = T_{HRSG,\,sat} + AP \tag{2.2}$$

The HTF flow from the energy balance in evaporator and superheater with the constraint of PP,

$$m_{13} = \frac{m_1(h_1 - h_8)}{c_{p,HTF,13}T_{13} - c_{p,HTF,15}T_{15}} \tag{2.3}$$

In the above equation, specific heat of heat transfer fluid, $c_{p,\,HTF}$ has been determined as a function of temperature.

Enthalpy of heat transfer fluid at the inlet of superheater from the energy balance in superheater,

$$h_{14} = h_{13} - \frac{m_9(h_1 - h_9)}{m_{14}} \tag{2.4}$$

T_{14} is simulated from h_{14}.

Similarly, the enthalpy of HTF at the exit of economizer from the heat balance in economizer,

$$h_{16} = h_{15} - \frac{m_8(h_8 - h_7)}{m_{16}} \tag{2.5}$$

T_{16} is iterated from h_{16}.

The size of solar concentrating collector has been simulated from the HTF flow, fluid inlet temperature (T_{10}) and fluid exit temperature (T_{11}) using analytical method.

The water flow in the condenser, from the energy balance in condenser,

$$m_{17} = \frac{m_3(h_3 - h_4)}{c_{pw}(T_{18} - T_{17})} \tag{2.6}$$

The steam turbine gross power,

$$W_{st} = m_1 (h_1 - h_2) + m_3 (h_2 - h_3) \tag{2.7}$$

The pump supply,

$$W_p = m_4 (h_5 - h_4) + m_6 (h_7 - h_6) \quad (2.8)$$

The net power generation,

$$W_{net} = W_{st} - W_p \quad (2.9)$$

Solar thermal power plant efficiency,

$$\eta_{pt} = \frac{W_{net}}{0.001 G A_{CPC}} \times 100 \quad (2.10)$$

Table 2.1 summarises the thermodynamic properties of the SRC with the solar thermal energy source. The listed properties are pressure, temperature, flow rate, specific enthalpy, and specific entropy. The required thermic oil in the linier solar concentrating collector is 2106.53 kg/s to generate 100 kg/s of the working fluid in boiler. The source temperature of the oil from the collectors is 300 °C. With the TTD, the turbine inlet temperature is 285 °C at 40 bar pressure. Because of the deaerator, there are three pressures in this thermal power plant: high pressure, deaerator pressure, and condenser pressure. They are 40 bar, 1.13 bar, and 0.07 bar, respectively, at the boiler, deaerator, and condenser. After transferring the heat to the thermal power plant, the thermic oil exit temperature from the HRSG or supply temperature of the solar thermal collector is 246.19 °C.

Table 2.1 Results of thermodynamic model applied to solar thermal power plant with SRC

State	P, bar	T,ºC	m, kg/s	h, kJ/kg	s, kJ/kg K
1	40.00	285.00	100.00	2917.55	6.29
2	1.13	103.10	11.60	2417.27	6.62
3	0.07	40.00	88.40	2132.02	6.85
4	0.07	40.00	88.40	167.45	0.57
5	1.13	41.00	88.40	171.64	0.59
6	1.13	103.10	100.00	432.14	1.34
7	40.00	104.29	100.00	437.17	1.36
8	40.00	245.33	100.00	1063.03	2.75
9	40.00	250.33	100.00	2800.34	6.07
10	1.01	253.04	2106.53	457.51	1.14
11	1.01	300.00	2106.53	573.77	1.36
12	1.01	300.00	2106.53	573.77	1.36
13	1.01	300.00	2106.53	573.77	1.36
14	1.01	297.82	2106.53	568.21	1.35
15	1.01	265.33	2106.53	487.22	1.20
16	1.01	253.04	2106.53	457.51	1.14
17	1.01	25.00	5193.41	0.00	0.00
18	1.01	33.00	5193.41	33.44	0.11

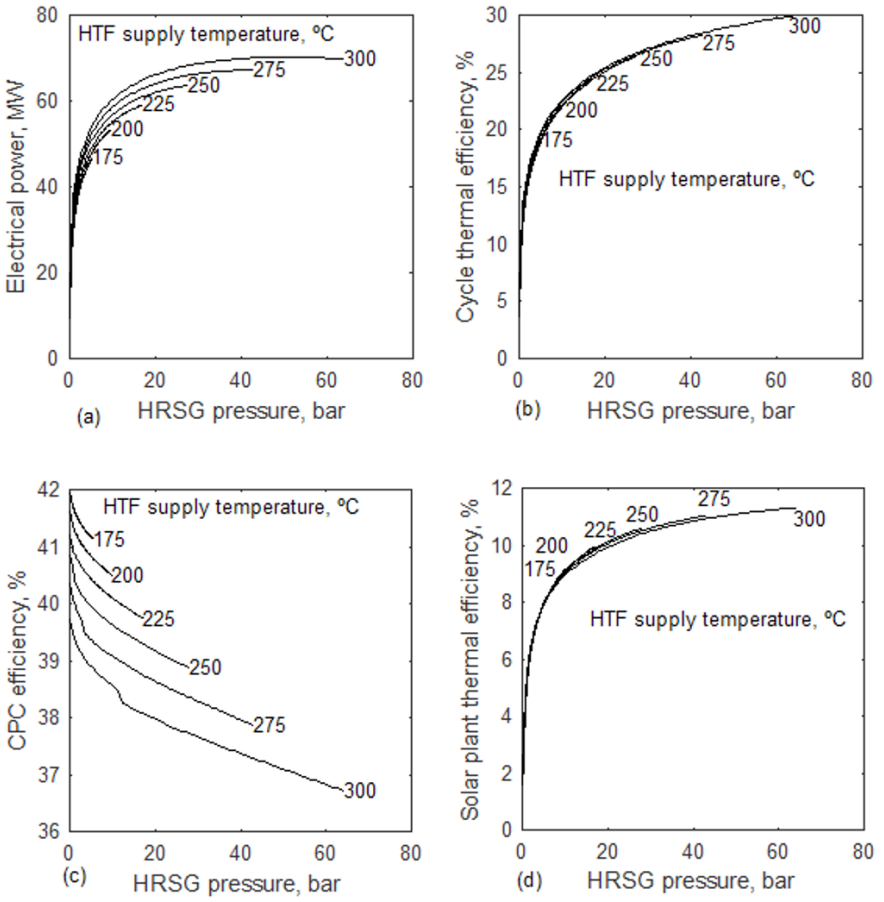

Fig. 2.3: Performance characteristics of solar thermal power plant with SRC integration

Fig. 2.3 analyses the changes in (a) power generation, (b) SRC thermal efficiency, (c) CPC collector's efficiency, and (d) solar thermal power plant efficiency with a change in HRSG pressure and HTF supply temperature. The power generation is analysed at the fixed working fluid in the SRC i.e., 100 kg/s. This power generation is increasing with an increase in HTF supply temperature and also with the boiler pressure. At the higher HTF supply temperature, and high boiler's pressure, the power generation is diminishing as it demands more energy to drive the high pressure pumps. The cycle's thermal efficiency is increasing with an increase in HTF supply temperature and the boiler pressure.

The CPC collector's efficiency decreases with an increase in HRSG pressure and HTF supply temperature. The solar thermal power plant's efficiency increases with an increase in HTF supply temperature. But at the

same boiler pressure, the power plant's efficiency decreases with an increase in HTF supply temperature as the energy supply increases with an increase in source temperature. The high temperature fluid results more heat transfer losses and low thermal efficiency. Therefore, the HTF supply temperature is restricted to 300 °C.

2.3 Steam Flash Cycle

Fig. 2.4 shows the solar thermal power plant layout with the steam flash cycle configuration. It is a double flash cycle. A flasher is a device provided to expand the fluid from the high pressure to a low pressure to produce a liquid-vapour mixture. In SFC, the pressurised water at the exit of the economizer is expanded from the boiler pressure to flasher pressure, which is maintained between the condenser pressure and the boiler pressure. It results in the liquid and vapour being separated from which the vapour is supplied to the turbine. The superheated steam (1) generated in HRSG is supplied to the turbine and expands (1-6) from the boiler pressure to the condenser pressure. The turbine, in addition to the superheated steam, also receives steam from the flashers. By rejecting heat to the circulating water (28-29), the expanded steam (6) is condensed (6-7) in a water-cooled condenser. The condensate is pumped from the condenser pressure to the flasher pressure. The saturated liquid from the second flasher (19) is mixed with the pumped water (8). The mixed fluid (9) is again pumped (9–10) from the flasher pressure to the boiler pressure. Since the second pump is handling additional water received from the flasher, the heat load in the economizer (10–11) is greater compared to a power plant without using a flasher. At the exit of the economizer, the liquid (11) is separated into two parts; one is supplied to the further evaporator and superheater, and the other is supplied to the high pressure (HP) flasher. The liquid (14) is flashed (14–15) from the boiler pressure to the low pressure (LP) flasher pressure. The flashed fluid is separated into liquid (16) and vapour (17). The separated vapour is connected to the turbine, and the separated water is flashed (16-17) from the HP flasher to the LP flasher. The mixture in the LP flasher is again separated into water (19) and vapour (20). This vapour (20) is supplied to the turbine, and the water (19) is mixed with the pumped water (8). Therefore, the turbine is receiving two streams of vapour, i.e., from the LP flasher (20) and the HP flasher (17), in addition to the superheated steam (1). This additional steam in the turbine enhances the power generation from the turbine. But the heat load in the HRSG, i.e., the economizer part, is greater compared to the conventional power plant. Therefore, it will decrease the thermal efficiency with the power augmentation.

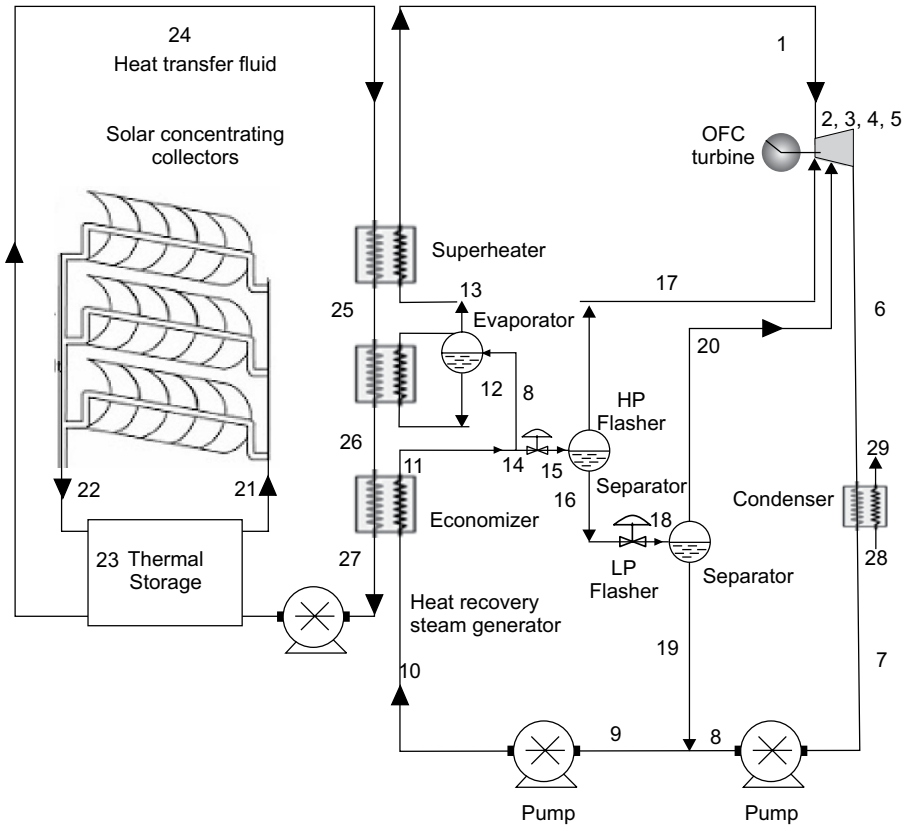

Fig. 2.4: SFC with two flashers

Fig. 2.5 shows the temperature-specific entropy of SFC with two flashers and source and sink temperature profiles. The double flash SFC operates on four pressures, viz. boiler pressure, HP flasher pressure, LP flasher pressure, and condenser pressure. The HTF fluid temperature is decreasing (24–27) by rejecting heat to the working fluid (10.1). The separated saturated vapour is mixed with the turbine stream. Since the flashed vapour is small in quantity, the mixed temperature is close to the turbine stream temperature. The circulating water temperature is increased (28–29) by absorbing the latent heat of steam.

The same assumptions listed in the SRC are used in the SFC. The HP flasher's pressure is the midpoint between the HRSG pressure and the LP flasher's pressure. Similarly, the LP flasher's pressure is the midpoint between the HP flasher's pressure and the condenser pressure (Pradeep Varma and Srinivas, 2017).

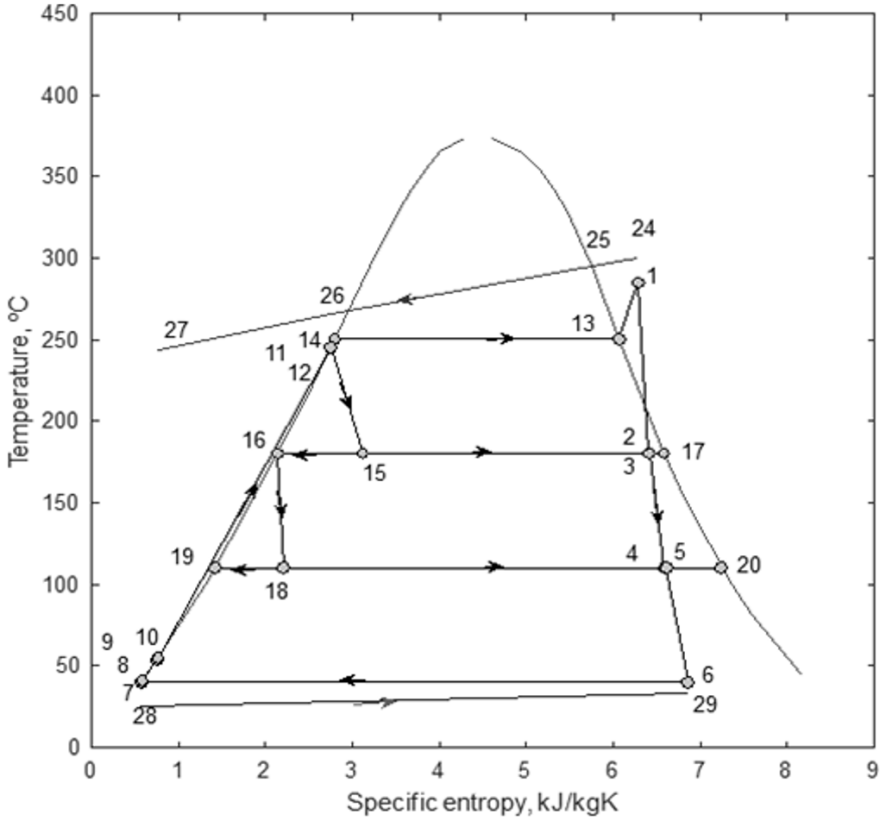

Fig. 2.5: Temperature-specific entropy diagram for SFC with two flashers

The heat transfer fluid in HRSG from the heat balance in evaporator and superheater,

$$m_{24} = \frac{m_1(h_1 - h_{12})}{c_{p,HTF,24}T_{24} - c_{p,HTF,26}T_{26}} \tag{2.11}$$

Enthalpy of HTF at the exit of superheater,

$$h_{25} = h_{24} - \frac{m_1(h_1 - h_{13})}{m_{25}} \tag{2.12}$$

Similarly, the enthalpy of HTF at the exit of economizer from the heat balance in economizer,

$$h_{25} = h_{24} - \frac{m_1(h_1 - h_{13})}{m_{25}} \tag{2.13}$$

The required water flow in the condenser from the heat balance in the condenser,

$$m_{28} = \frac{m_6(h_6 - h_7)}{c_{pw}(T_{29} - T_{28})} \quad (2.14)$$

The steam turbine gross power,

$$W_{st} = m_1 (h_1 - h_2) + m_3 (h_3 - h_4) + m_5 (h_5 - h_6) \quad (2.15)$$

The pump supply,

$$W_p = m_7 (h_8 - h_7) + m_9 (h_{10} - h_9) \quad (2.16)$$

Table 2.2 lists the thermodynamic properties of the SFC with two flashers and a solar concentrating collector. The plant is using two flashers for the power augmentation. Therefore, there are four pressures in the plant, viz., high pressure, HP flasher's pressure, LP flasher's pressure, and condenser pressure. These pressures are 40 bar, 10.08 bar, 1.44 bar, and 0.07 bar, respectively, in the boiler, HP flasher, LP flasher, and condenser. Therefore, the steam expands in three stages in the steam turbine. The required thermic oil flow in the collector to generate 100 kg/s of the working fluid in HRSG is 2106.53 kg/s. In HRSG, the energy balance has been applied together with the evaporator and superheater, considering the pinch point to find the thermic oil requirement. Therefore, the oil requirements in SRC and SFC are the same with this evaluation. But, the economizer loads in SRC and SFC are different. Hence, the supply oil temperature to the solar collector is relatively low with SFC.

Table 2.2 Results of power plant simulation with SFC and two flashers

State	P, bar	T,°C	m, kg/s	h, kJ/kg	s, kJ/kg K
1	40.00	285.00	100.00	2917.55	6.29
2	10.08	180.22	100.00	2697.83	6.41
3	10.08	180.22	104.95	2701.54	6.41
4	1.44	110.11	104.95	2441.26	6.58
5	1.44	110.11	108.80	2450.11	6.61
6	0.07	40.00	108.80	2136.03	6.86
7	0.07	40.00	108.80	167.45	0.57
8	1.44	41.00	108.80	171.64	0.59
9	1.44	53.83	133.33	225.39	0.75
10	40.00	54.88	133.33	229.66	0.77
11	40.00	245.33	133.33	1063.03	2.75
12	40.00	245.33	100.00	1063.03	2.75
13	40.00	250.33	100.00	2800.34	6.07
14	40.00	245.33	33.33	1063.03	2.75
15	10.08	180.22	33.33	1063.03	3.12
16	10.08	180.22	28.38	764.04	2.14

17	10.08	180.22	4.95	2776.46	6.58
18	1.44	110.11	28.38	764.04	2.21
19	1.44	110.11	24.53	461.77	1.42
20	1.44	110.11	3.85	2691.47	7.24
21	1.01	243.36	2106.53	434.47	1.09
22	1.01	300.00	2106.53	573.77	1.36
23	1.01	300.00	2106.53	573.77	1.36
24	1.01	300.00	2106.53	573.77	1.36
25	1.01	297.82	2106.53	568.21	1.35
26	1.01	265.33	2106.53	487.22	1.20
27	1.01	243.36	2106.53	434.47	1.09
28	1.01	25.00	6404.94	0.00	0.00
29	1.01	33.00	6404.94	33.44	0.11

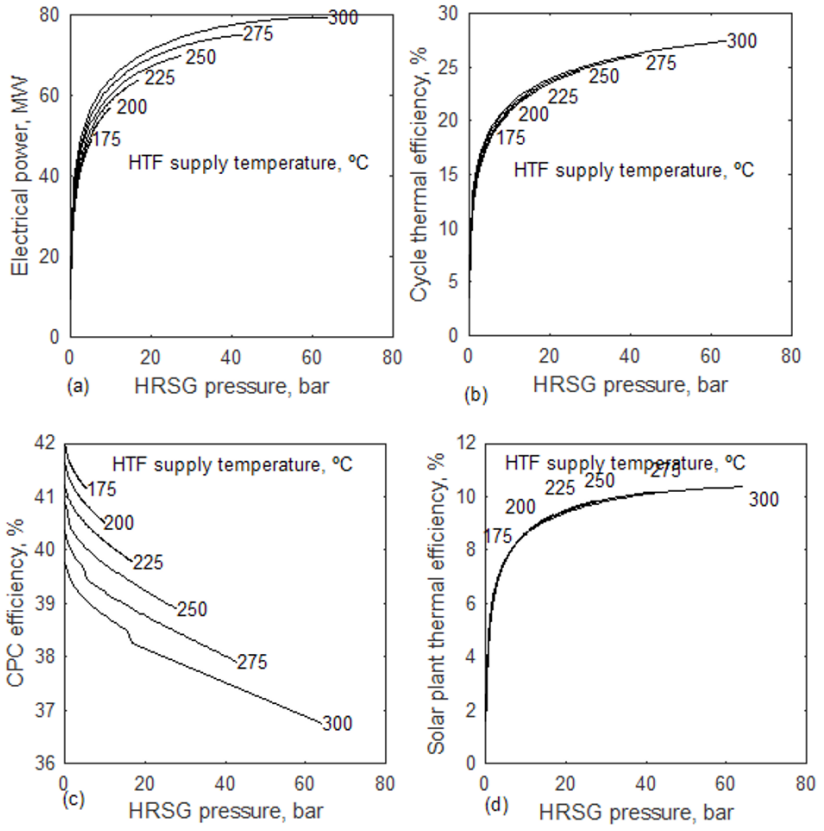

Fig. 2.6: Performance characteristics of solar thermal power plant with SFC integration

Fig. 2.6 analyses the (a) power generation, (b) SFC thermal efficiency, (c) CPC collector's efficiency, and (d) solar thermal power plant's efficiency with a change in HRSG pressure and HTF supply temperature. The power generation is analysed at the working fluid flow rate of 100 kg/s at the turbine inlet. The power generation from SFC is also increasing with an increase in HTF supply temperature and boiler pressure. As discussed in the earlier section, the power is increasing in a diminishing rate at the higher pressures. Compared to the SRC, the power generation from the SFC is high with the additional working fluid generation in the flashers. The cycle's thermal efficiency is increasing with an increase in the supply temperature and boiler pressure. It can be noticed that the cycle efficiency with SFC is decreasing compared to the SRC with the added heat load in the economizer.

The CPC collector's efficiency decreases with an increase in HTF supply temperature and boiler pressure. The power plant's efficiency increases with an increase in HTF supply temperature at a diminishing rate. At the higher supply temperature, the energy supply is increasing and the solar collector's efficiency is decreasing. The plant efficiency of SFC is decreasing compared to SRC as the economizer load increases even though power is augmented.

2.4 Organic Rankine Cycle

Fig. 2.7 shows the solar thermal power plant layout with the ORC configuration. The ORC is suitable to a low-temperature heat source compared to the steam power plant. By properly selecting the organic fluid, it is possible to design the ORC to suit the available source temperature. Organic fluid is a carbon compound-based fluid. The molecular weight of organic fluids is higher than other fluids like water. Therefore, the speed of this vapour turbine is less than the steam turbine. It reduces vibrations and the maintenance of moving parts. The density of the organic fluid is also high, which results in more electricity being generated due to the heavy working fluid. But there is a chemical decay at high temperatures. Since the ORC is designed with a lower source temperature, it is not a big problem with this fluid. With reference to Fig. 2.7, the superheated vapour (1) is generated in the heat recovery vapour generator (HRVG). The vapour is expanded in the turbine (1-2) from boiler pressure to condenser pressure. At the exit of the turbine, the temperature of the fluid is high enough to recover the heat to raise the temperature of the feed solution to the boiler. The internal heat recovery is a heat exchanger, which is called a regenerator. After the regenerator, the vapour moves to the condenser (3–4) to form the saturated liquid (4). In the water-cooled condenser (16-17), heat is rejected into the surroundings. In the steam power plant, the exit steam temperature is close to the condenser temperature. Therefore, there is no such regenerator in SRC or SFC. The regenerator in ORC saves the size of the condenser and HRVG (economizer section). In the regenerator, the exit

vapours temperature decreases (2-3) by rejecting heat to the pumped solution. The pumped solution temperature rises (5–6) in the regenerator. Superheated vapour is generated in the HRVG, which expands, and the cycle repeats.

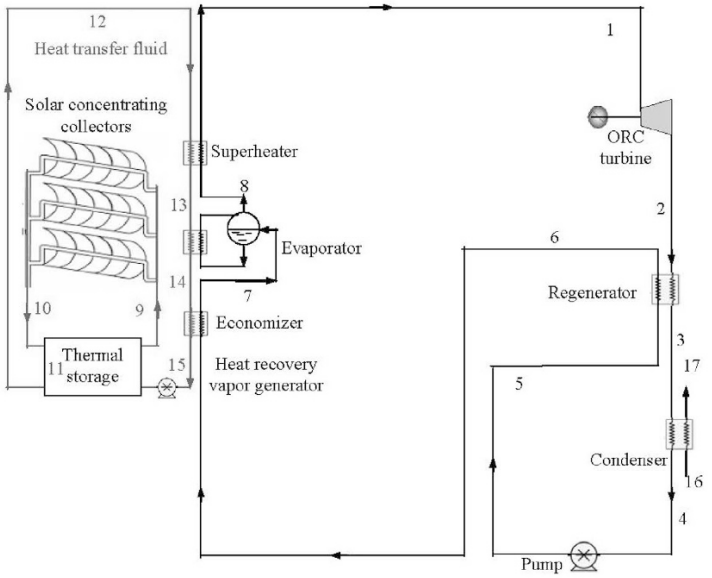

Fig. 2.7: Organic Rankine cycle with regenerator

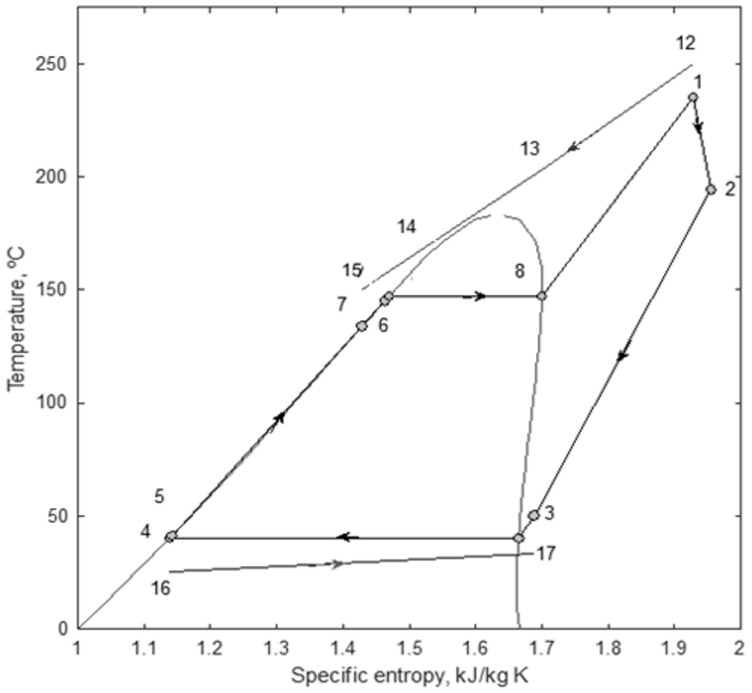

Fig. 2.8: Temperature-entropy diagram of ORC with regenerator

Fig. 2.8 shows the temperature-specific entropy diagram of ORC with the regenerator, heat source, and heat sink conditions. By rejecting heat to the organic fluid in the HRVG, the HTF temperature is reduced (12–15). The specific heat of vapour is less than the specific heat of liquid. Therefore, the temperature drop in vapour is higher than the temperature rises in fluid at the same flow rate.

The assumptions used to develop the following formulations are used to analyse the ORC.

The terminal temperature difference (TTD) in the superheater and condenser is 15 K and 10 K, respectively. The pinch point and approach point in the heat recovery vapour generator are 10 K and 2 K respectively. The average global solar radiation and average beam radiation are 515 W/m^2 and 340 W/m^2, respectively. The supply temperature of the heat transfer fluid (Therminol) to the plant is 250 °C. The temperature of the circulating water supply in the water-cooled condenser is 30 °C. Isentropic efficiencies of pump and vapour turbine are 75% and 80%, respectively (Varma and Srinivas, 2017).

The condensate temperature,

$$T_{cond} = T_{wi} + TTD_{cond} \tag{2.17}$$

The economizer exit temperature,

$$T_7 = T_8 - AP \tag{2.18}$$

From the energy balance in regenerator,

$$h_3 = h_2 - (h_6 - h_5) \tag{2.19}$$

The heat transfer fluid temperature in HRVG using pinch point,

$$T_{14} = T_8 + PP \tag{2.20}$$

The heat transfer fluid in HRVG from the energy balance in evaporator and superheater,

$$m_{12} = \frac{m_1(h_1 - h_7)}{c_{p,HTF,12}T_{12} - c_{p,HTF,14}T_{14}} \tag{2.21}$$

Enthalpy of HTF at the inlet of evaporator from the heat balance in superheater,

$$h_{13} = h_{12} - \frac{m_8(h_1 - h_8)}{m_{13}} \tag{2.22}$$

Similarly, the enthalpy of heat transfer fluid at the exit of economizer,

$$h_{15} = h_{14} - \frac{m_8(h_7 - h_6)}{m_{15}} \tag{2.23}$$

In the condenser, from the energy balance, the circulating water flow,

$$m_{16} = \frac{m_3(h_3 - h_4)}{c_{pw}(T_{17} - T_{16})} \tag{2.24}$$

The vapour turbine gross power,

$$W_{vt} = m_1 (h_1 - h_2) \quad (2.25)$$

The pump supply,

$$W_p = m_4 (h_5 - h_4) \quad (2.26)$$

Table 2.3 results the thermodynamic simulation results of the ORC with the source of solar thermal energy. ORC is working between two pressures i.e. boiler pressure and condenser pressure respectively 20 bar and 1.54 bar. The condenser pressure is positive pressure therefore there is no need of vacuum pump which is required in a steam thermal power plant. The required thermic oil in the solar concentrating collector is 97.35 kg/s to generate 100 kg/s of the working fluid. Compared to the steam power plant, this is low due to lower heat load in HRVG.

Table 2.3 Thermodynamic properties of ORC with the regenerator

State	P, bar	T,°C	m, kg/s	h, kJ/kg	s, kJ/kg K
1	20.00	235.00	100.00	565.86	1.93
2	1.54	194.16	100.00	517.15	1.95
3	1.54	50.00	100.00	412.78	1.69
4	1.54	40.00	100.00	240.59	1.14
5	20.00	41.19	100.00	241.83	1.14
6	20.00	133.91	100.00	346.20	1.43
7	20.00	145.12	100.00	360.66	1.46
8	20.00	147.12	100.00	460.15	1.70
9	1.01	149.89	97.35	228.56	0.64
10	1.01	250.00	97.35	450.24	1.13
11	1.01	250.00	97.35	450.24	1.13
12	1.01	250.00	97.35	450.24	1.13
13	1.01	202.89	97.35	341.66	0.90
14	1.01	157.12	97.35	243.43	0.68
15	1.01	149.89	97.35	228.56	0.64
16	1.01	25.00	514.92	0.00	0.00
17	1.01	33.00	514.92	33.44	0.11

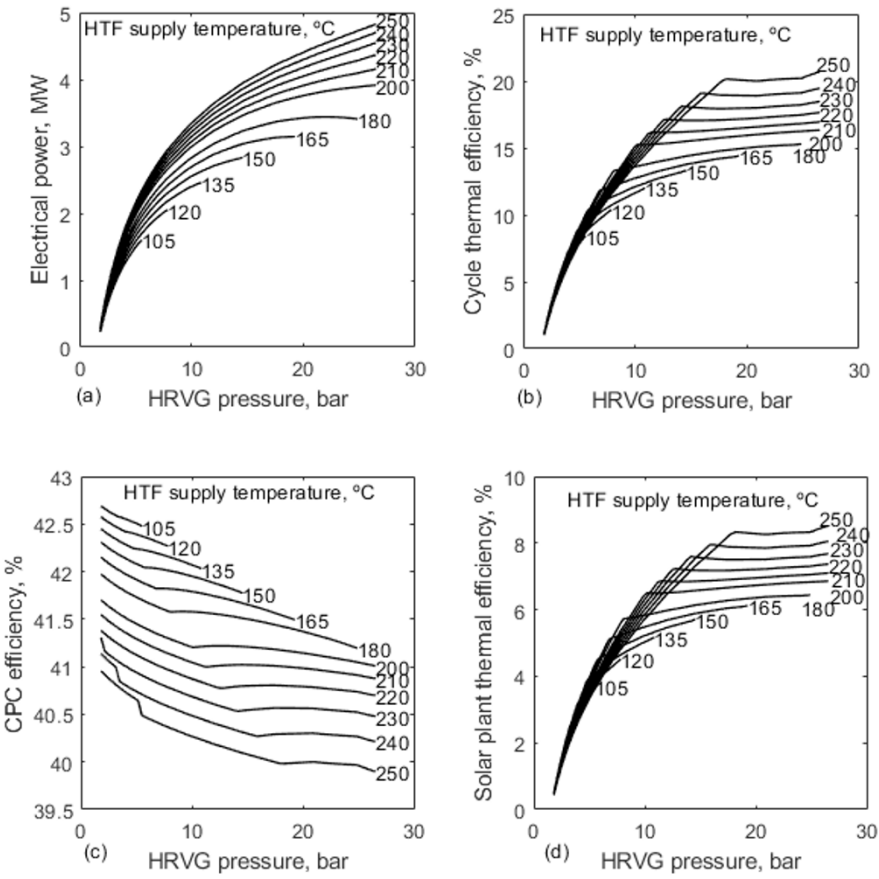

Fig. 2.9: Performance characteristics of solar thermal power plant with ORC integration

Fig. 2.9 analyses the performance of (a) power generation, (b) cycle thermal efficiency, (c) thermal efficiency of solar concentrating collector, and (d) solar thermal power plant with a change in boiler (HRVG) pressure and heat transfer fluid (HTF) supply temperature to the power plant. The critical temperature of the steam is less than the critical temperature of the organic fluid. Since ORC is designed at the lower supply temperature compared to the steam, the supply temperature is changed below and above the critical temperature of the working fluid. The power generation and cycle thermal efficiency are increasing with an increase in HTF temperature and boiler pressure. The rate of increase with pressure is in diminishing rate.

The solar thermal collector's efficiency depends on fluid inlet temperature, outlet temperature, and fluid flow rate. These three conditions have been simulated for the area of collector. These three conditions vary with the stated

changes in the plant. Therefore, the collector efficiency is affected by boiler pressure and HTF supply temperature. The working fluid flow rate is fixed at 100 kg/s. At the fluid temperatures and the energy balance in the HRVG, the HTF flow rate is evaluated. The energy balance in the economizer results from the collector fluid inlet temperature. The heat transfer losses (conduction, convection, and radiation) from the solar collector increase with an increase in collector fluid temperature, i.e., both the inlet and outlet. The collector inlet temperature increases as the boiler pressure increases. As shown in Fig. 2.9 (a), the collector efficiency decreases with an increase in fluid temperature in the collector. A solar thermal power plant's efficiency depends on both electricity generation and solar radiation energy supplied to the collector. The energy conversion efficiency from solar radiation to electricity is known as a solar thermal power plant's efficiency. Hence, power generation increases with an increase in pressure, resulting in an efficiency that also increases with the pressure. The increase in source temperature also increases the output, but with the added energy supply. Since the increase in power generation is dominating the additional energy supply, the plant's efficiency has been increasing with an increase in source temperature, but at a diminishing rate. The thermal efficiency of the plant is reaching to a maximum value with an increase in the boiler pressure. Later there is no much significant increase in the thermal efficiency. Therefore, the boiler pressure can be selected as per the resulted higher thermal efficiency.

2.5 Organic Flash Cycle

Fig. 2.10 shows the solar thermal power plant's layout with OFC and double flashers. Similar to the SFC, the OFC also works, but the only difference is the regenerator. As per the earlier discussion, the exit temperature of the vapour turbine is high enough to recover the heat and raise the temperature of the feed to the boiler. The superheated vapour (1) is expanded (1–6) in the turbine for power generation. The vapour temperature is decreased (6-7) in the regenerator by rejecting heat to the feed (9-10). By rejecting heat to the surroundings (30–31), the vapour is condensed (7-8) to a saturated liquid in a condenser. The capacity of the condenser and economizer decreases with the use of the regenerator. The condensate is pumped (8-9) from the condenser pressure to the LP flasher pressure. The preheated liquid (10) from the regenerator and the separated liquid (21) from the LP flasher mix with each other, and this is pumped (11–12) again from the LP flasher pressure to the boiler pressure. In the economizer, the main fluid coming from the condenser and the separated liquid from the LP flasher were heated (12–13) and reached the saturated liquid state (13) in the boiler. This high-pressure saturated liquid is divided into two parts, viz., and stream to the HP flasher (16) and steam to the evaporator (14). The evaporator stream is higher than the flasher stream as the flashed fluid is restricted to the exit temperature of HTF. In the HP

flasher, the liquid (16) is expanded (16-17) from the boiler pressure to the HP flasher pressure. This expanded fluid is separated into liquid (18) and vapour (19). Similarly, the liquid from the HP flasher (18) is expanded (18–20) from the HP flasher's pressure to the LP flasher's pressure. Also, the flashed mass (20) is separated into liquid (21) and vapour (22) at the LP flasher's pressure. Therefore, the turbine is receiving three streams, viz., superheated vapour (1), HP flasher's vapour (19) and LP flasher's vapour (22). It augments the power generation with this excess amount of working fluid.

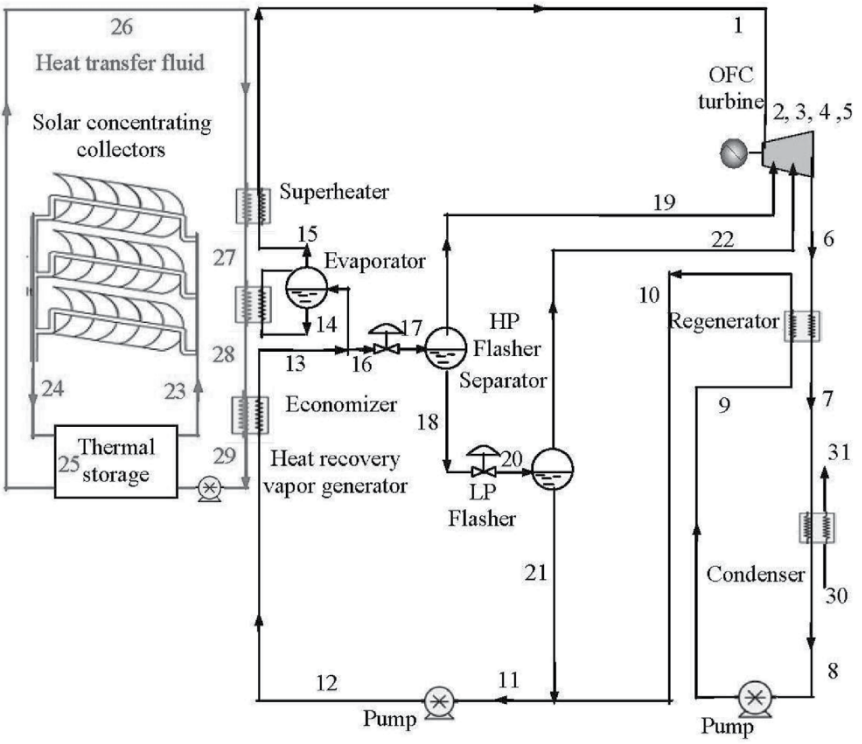

Fig. 2.10: Organic flash cycle with two flashers

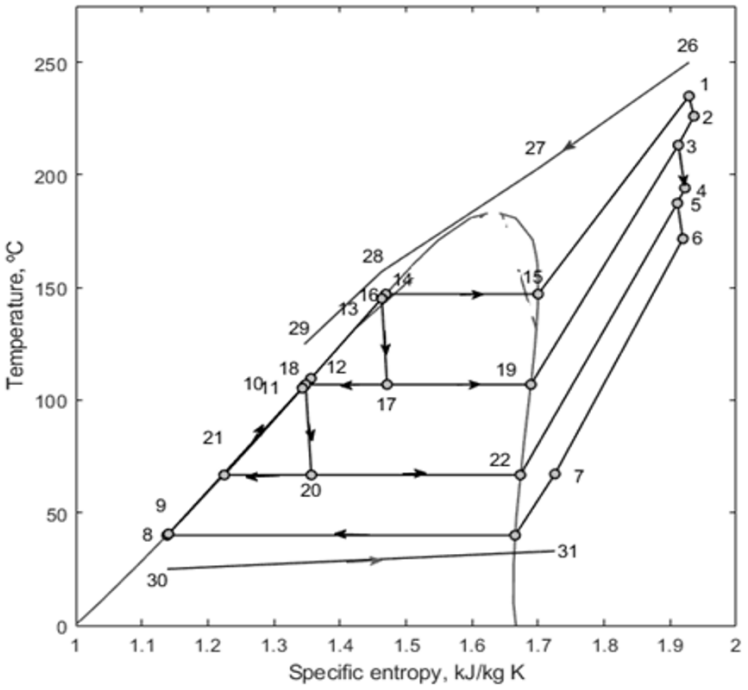

Fig. 2.11: Temperature-specific entropy diagram of OFC with two flashers

Fig. 2.11 shows the temperature-specific entropy diagram of the OFC with two flashers. It shows the four pressures, viz. HRVG pressure, HP flasher pressure, LP flasher pressure, and condenser pressure. By rejecting heat to the working fluid (12-1) the HTF temperature is reduced (26-29). The saturated vapour from the flasher is mixed with the expanded vapour in the turbine. The turbine inlet temperature is above the critical temperature of the working fluid. Since there is a temperature gap between the saturated vapour and the exit vapour temperature, the mixed vapour temperature is slightly decreased compared to the turbine exit vapour.

The economizer exit temperature from the AP and saturation temperature of boiler,

$$T_{13} = T_{15} - AP \tag{2.27}$$

From the energy balance in regenerator,

$$h_3 = h_6 - (h_{10} - h_9) \tag{2.28}$$

The HTF temperature in HRVG using pinch point,

$$T_{28} = T_{15} + PP \tag{2.29}$$

The HTF flow in HRVG from the energy balance of evaporator and superheater,

$$m_{26} = \frac{m_1(h_1 - h_{14})}{c_{p,HTF,26}T_{26} - c_{p,HTF,28}T_{28}} \tag{2.30}$$

Enthalpy of HTF at the inlet of evaporator from the heat balance in superheater,

$$h_{27} = h_{26} - \frac{m_1(h_1 - h_{15})}{m_{27}} \tag{2.31}$$

Similarly, the enthalpy of HTF at the exit of economizer, from the heat balance in economizer,

$$h_{29} = h_{28} - \frac{m_{13}(h_{13} - h_{12})}{m_{29}} \tag{2.32}$$

The circulating water required from the heat balance in the condenser,

$$m_{30} = \frac{m_7(h_7 - h_8)}{c_{pw}(T_{31} - T_{30})} \tag{2.33}$$

The vapour turbine gross power,

$$W_{vt} = m_1 (h_1 - h_2) + m_3 (h_3 - h_4) + m_5 (h_5 - h_6) \tag{2.34}$$

The pump supply,

$$W_p = m_8 (h_9 - h_8) + m_{11} (h_{12} - h_{11}) \tag{2.35}$$

Table 2.4 summarises the thermodynamic properties of the OFC with two flashers and a solar thermal collector. Similar to SFC, OFC is also working on four pressures, viz., boiler pressure, HP flasher's pressure, LP flasher's pressure, and condenser pressure, respectively, of 20 bar, 9.18 bar, 3.46 bar, and 1.54 bar. The required thermic oil in the solar concentrating collector is 97.35 kg/s for the generation of 100 kg/s of the working fluid in HRVG. This is the same as the ORC plant. The thermic oil has been determined with the same constraint of pinch point in the evaporator with the energy balance of the evaporator and superheater without adding the economizer. Therefore, the solar collector's fluid flow is the same in both ORC and OFC. With this same fluid flow of oil, the oil exit temperature from the economizer is lower in OFC compared to ORC. The economizer load in the OFC is higher than the economizer load in the ORC. Hence, the oil supply temperature to the solar thermal collector is lower with OFC compared to ORC.

Table 2.4 Thermodynamic Properties of OFC with two flashers and Solar Thermal Energy Supply

State	P, bar	T,°C	m, kg/s	h, kJ/kg	s, kJ/kg K
1	20.00	235.00	100.00	565.86	1.93
2	9.18	226.10	100.00	551.16	1.94
3	9.18	213.27	112.06	539.55	1.91
4	3.46	194.19	112.06	521.05	1.92
5	3.46	187.45	118.32	515.77	1.91
6	1.54	171.68	118.32	500.88	1.92
7	1.54	67.24	118.32	425.26	1.73
8	1.54	40.00	118.32	240.59	1.14
9	3.46	40.65	118.32	241.26	1.14
10	3.46	109.67	118.32	316.88	1.36
11	3.46	105.30	133.33	311.94	1.34
12	20.00	106.30	133.33	313.04	1.35
13	20.00	145.12	133.33	360.66	1.46
14	20.00	145.12	100.00	360.66	1.46
15	20.00	147.12	100.00	460.15	1.70
16	20.00	145.12	33.33	360.66	1.46
17	9.18	106.95	33.33	360.66	1.47
18	9.18	106.95	21.27	313.80	1.35
19	9.18	106.95	12.06	443.32	1.69
20	3.46	66.78	21.27	313.80	1.36
21	3.46	66.78	15.01	268.94	1.22
22	3.46	66.78	6.26	421.34	1.67
23	1.01	124.71	97.35	178.20	0.52
24	1.01	250.00	97.35	450.24	1.13
25	1.01	250.00	97.35	450.24	1.13
26	1.01	250.00	97.35	450.24	1.13
27	1.01	202.89	97.35	341.66	0.90
28	1.01	157.12	97.35	243.43	0.68
29	1.01	124.71	97.35	178.20	0.52
30	1.01	25.00	653.43	0.00	0.00
31	1.01	33.00	653.43	33.44	0.11

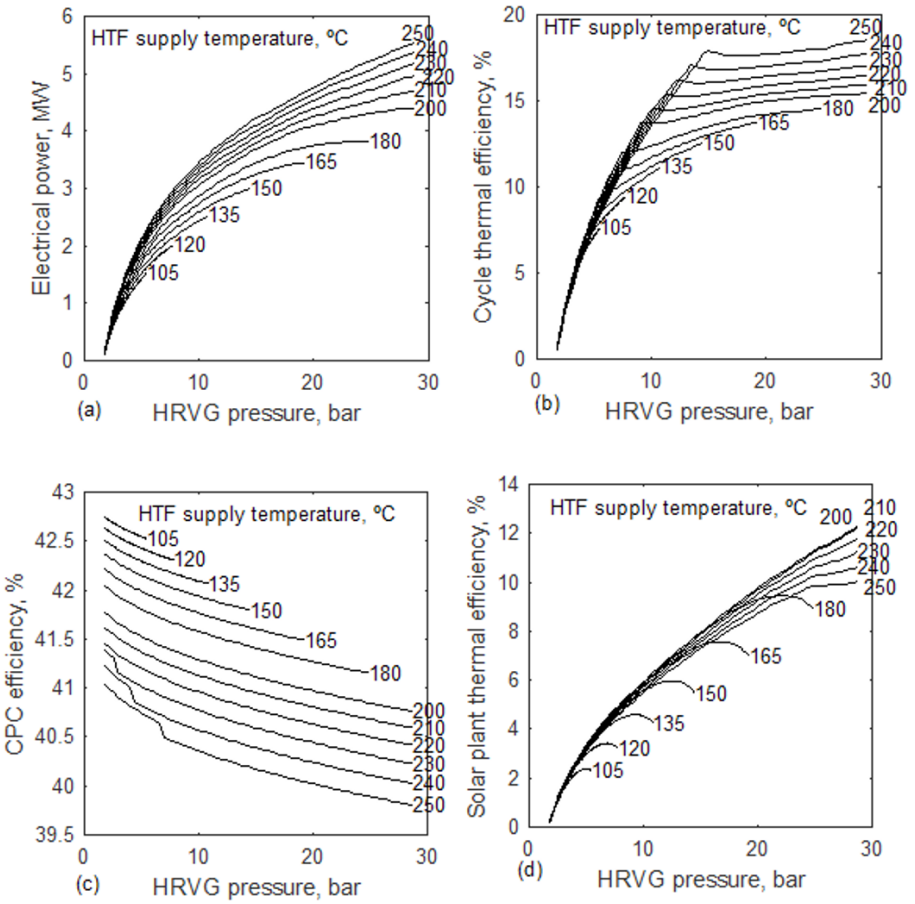

Fig. 2.12: Performance characteristics of solar thermal power plant with OFC integration

Fig. 2.12 analyses the (a) power generation, (b) cycle thermal efficiency, (c) CPC efficiency, and (d) solar thermal power plant efficiency with a change in HRVG pressure and HTF source temperature. The supply temperature is changed below and above the critical temperature of the working fluid due to a lower critical temperature of organic fluid compared to steam. In the analysis of steam power plant, the source temperature is kept below the critical temperature of steam to suit the solar thermal collector's generation temperature. The slope of the power curves and efficiency curves are higher with OFC compared to the ORC.

With reference to the earlier discussion, the CPC efficiency is decreasing with an increase in boiler pressure and source temperature. The boiler pressure increases with an increase in HTF supply temperature. The power generation increases with increase in boiler pressure but the fluid generation in the HRVG decreases with an increase in the pressure. Therefore, the power increases and drops with an increase in the HRVG pressure. The pressure is optimised with the turbine inlet temperature below the critical temperature of the working fluid for the maximum plant efficiency. Above this temperature, the plant efficiency is decreasing with an increase in the source temperature. The increasing power with increase in HRVG pressure increases the thermal efficiency with an increase in source temperature. A further increase in pressure decreases the power. Hence, the thermal efficiency decreases with an increase in source temperature. At the high pressures, the cycle efficiencies are decreasing with the OFC whereas the plant efficiencies are increasing with the OFC compared to ORC. With the more economizer load with OFC, the fluid temperature in the solar thermal collector is decreasing and resulting relatively a higher collection temperature. Hence, the solar thermal power plant efficiency is benefiting with the flashers.

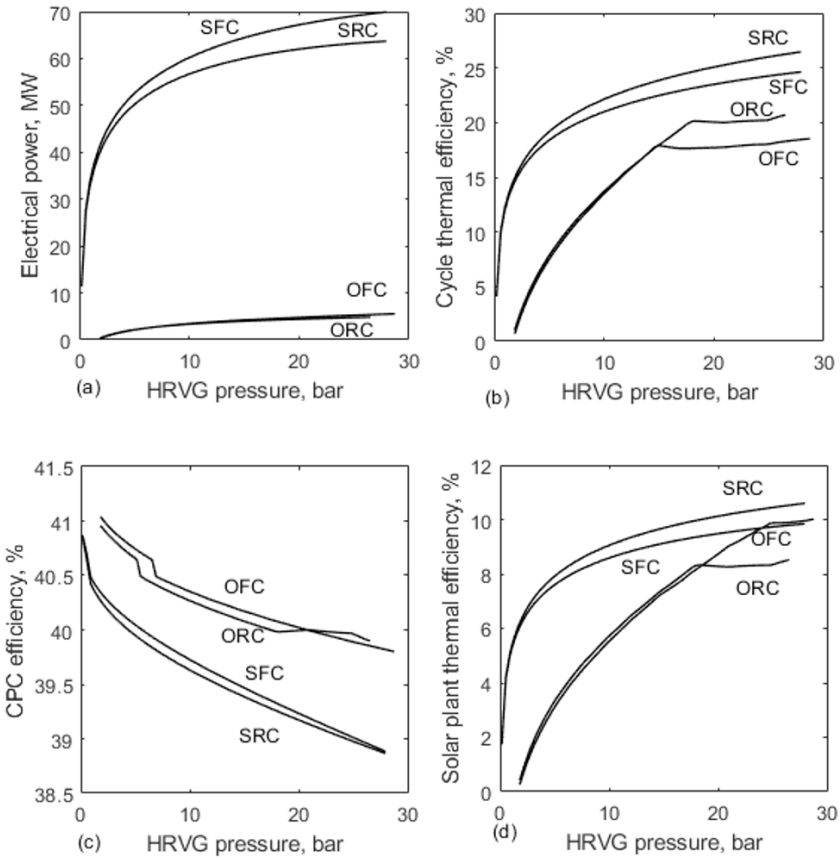

Fig. 2.13: Comparison of four thermal power cycles with solar thermal energy supply at the working fluid flow rate of 100 kg/s at the turbine inlet

Fig. 2.13 compares the performance conditions of the four solar thermal power plants under this study with the aim of polygeneration adoption. The steam results highest specific power compared to the other working fluids. The power augmentation with flash cycle is more with steam fluid compared to the organic fluid. The cycle efficiency is decreasing with flasher in both steam fluid and organic fluid. The solar collector efficiency is increasing with the flash cycle with a drop in fluid temperature in the collectors. With the solar thermal collectors, integration, flash cycle is favouring the solar thermal power plant efficiency with the organic fluid. But it is not able to boost the solar thermal power plant's efficiency with the steam fluid.

2.6 Summary

A few thermal cycles for power generation suitable for polygeneration are studied and presented with their performance characteristics coupled with the solar thermal energy supply. This chapter is limited to a single fluid system in the power plant configuration that has been used as the binary fluid is elaborated in some other chapters. The flashing of working fluid at the end of the economizer part of HRVG is being studied to identify the potential benefits and challenges. The study revealed the scope of the flasher to augment the power generation at the same condition as the turbine inlet. Compared to steam as a working fluid, organic fluid can be used with the additional benefit of regeneration at the end of the vapour turbine and positive pressure condenser. The increase in source temperature will not result in more improvement in the performance of solar thermal power plants as the solar thermal losses will increase with an increase in the system temperature. Therefore, a suitable source temperature can be selected to collect the maximum solar energy and achieve maximum power generation efficiency. If the polygeneration is designed with waste heat recovery, gasification, or fuel firing, the performance characteristics and the operational conditions will vary. Therefore, the optimization results depend on the source and the power plant configuration. The power augmentation and drop in thermal efficiency are noticeable with SFC compared to SRC. The results showed that the power generation and thermal efficiency of solar thermal power plants with OFC increased compared to ORC. The flashers are supporting the solar thermal power plant efficiency compared to the cycle efficiency at the high boiler pressure with the influence of power augmentation.

Numerical Solutions

Steam Rankine Cycle: Hot gas temperature in a coal fired furnace is 1000 °C and it is leaving to 180 °C after rejecting heat to boiler components. How much steam can be generated at 120 bar pressure with superheated temperature of 500 °C at the hot gas supply of 100000 kg/h. Construct a simple Rankine cycle without irreversibilities in turbine and pump. In water cooled condenser maintained at 0.1 bar, the circulating water inlet temperature is 28 °C. Maintain a terminal temperature difference of 8 K at the inlet of condenser (steam direction). What is the circulating water demand in the condenser at these conditions? Find the steam rate, heat rate, power generation and thermal efficiency. Take the specific heat of hot gas as 1.1 kJ/kg K.

Solution

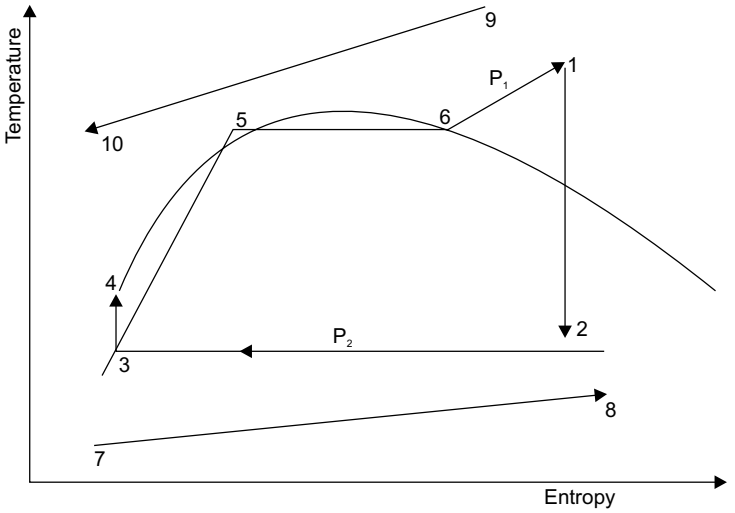

Fig. 2.14: Planning of simple Rankine cycle with temperature-entropy diagram

$T_9 = 1000$ °C, $T_{10} = 180$ °C, $m_g = 100000$ kg/h, $c_{pg} = 1.1$ kJ/kg K
$P_1 = 120$ bar, $T_1 = 500$ °C, $P_2 = 0.1$ bar
From steam tables at 120 bar and 500 °C (superheated steam),

$$h_1 = 3349.6 \text{ kJ/kg}$$
$$s_1 = 6.4906 \text{ kJ/kgK}$$

Since the entropy is constant in turbine with reversible process,

$$s_2 = s_1 = 6.4906 \text{ kJ/kgK}$$

At the condenser pressure

$$h_w = 191.8 \text{ kJ/kg}$$
$$h_v = 2584.8 \text{ kJ/kg}$$
$$s_w = 0.6493 \text{ kJ/kg}$$
$$s_v = 8.1511 \text{ kJ/kg K}$$

Since $s_2 < s_v$
The condition of steam at the exit of turbine is wet steam.

Now from the actual entropy at the exit of turbine, the dryness fraction of steam (quality) can be determined as follows

$$s_2 = s_w + x_2 (s_v - s_w)$$

$$x_2 = \frac{s_2 - s_w}{s_v - s_w} = \frac{6.4906 - 0.6493}{8.1511 - 0.6493} = 0.7787$$

Therefore, the enthalpy at the exit of steam turbine

$$h_2 = h_w + x_2 (h_v - h_w)$$
$$= 191.8 + 0.7787 \times (2584.8 - 191.8)$$
$$= 2055.1 \text{ kJ/kg}$$

From the steam tables at saturated water condition and condenser pressure,

h_3 = 191.8 kJ/kg
s_3 = 0.6493 kJ/kg K
v_3 = 0.001010 m^3/kg

From the SFEE and –vdP work in pump,

$h_4 = h_3 + v_3 (P_4 - P_3)100$
$= 191.8 + 0.00110 \times (120 - 0.1) \times 100$
$= 205.7$ kJ/kg

From the energy balance in boiler and furnace, the mass of steam generation

$$m_s = \frac{m_9 c_{pg} (T_9 - T_{10})}{h_1 - h_4} = \frac{100000 \times 1.1 \times (1000 - 180)}{3600 \times (3349.6 - 205.7)} = 7.97 \ kg/s$$

Similar to boiler, from the energy balance applied to condenser
The saturation temperature in condenser = 45.83 °C.
The circulating water exit temperature in the condenser

$= T_{sat\ condenser} - TTD = 45.83 - 8$

$= 37.83$ °C

$$m_w = m_7 = \frac{m_2 (h_2 - h_3)}{c_w (T_8 - T_7)} = \frac{7.97 \times (2055.1 - 191.8)}{4.18 \times (37.83 - 28)} = 361.4 \ kg/s$$

Steam turbine output,
$W_t = m_1 (h_1 - h_2) = 7.97\ (3349.6 - 2055.1) = 10317$ kW

Work supply to pump,

$W_p = m_3 (h_4 - h_3) = 7.97\ (205.7 - 191.8) = 110.93$ kW

Net power generation,

$W_{net} = W_t - W_p = 10317 - 110.93 = 10206$ kW
Heat supply,
$Q_{supply} = m_9 c_{pg} (T_9 - T_{10}) = m_1 (h_1 - h_4) = 7.97\ (3349.6 - 205.7) = 25056$ kW

First law efficiency

$$\eta_I = \frac{W_{net}}{Q_{sup\ ply}} \times 100 = \frac{10206}{25056} = 40.73\%$$

$$Steam\ rate = \frac{3600 \times m_{steam}}{W_{net}} = \frac{3600 \times 7.97}{10206} = 2.81 \ kg/kWh$$

$$Heat\ rate = \frac{Q_{sup\ ply}}{W_{net}} = \frac{25056}{10206} = 2.45$$

Table 2.5: Summary of results with properties

State	P, bar	T, ºC	m, kg/s	h, kJ/kg	s, kJ/kg K
1	120.00	500.00	7.97	3349.63	6.49
2	0.10	45.83	7.97	2055.11	6.49
3	0.10	45.83	7.97	191.83	0.65
4	120.00	49.12	7.97	205.75	0.65
5	120.00	324.65	7.97	1491.33	3.50
6	120.00	324.65	7.97	2689.93	5.50
7	1.01	28.00	361.31	12.54	0.04
8	1.01	37.83	361.31	53.64	0.18
9	1.01	1000.00	27.78	1072.50	1.60
10	1.01	180.00	27.78	170.50	0.46

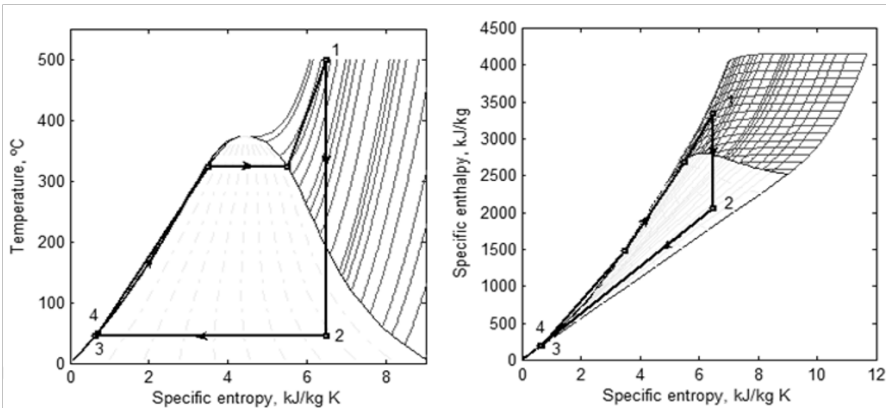

Fig. 2.15: Solution of Rankine cycle on (a) T-s diagram and (b) h-s diagram

Steam Flash Cycle: Determine the specific power and thermal efficiency of SFC with two flashers and the following operational conditions.

Solar global radiation is 516 W/m^2. The thermic oil temperature from the solar concentrating collector is 300 °C. The TTD in superheater is 15 K. The circulating water supply temperature to the condenser is 30 °C. Temperature rise of circulating water in the water cooled condenser is 8 °C. The working fluid used for the flashing is 25% of the fluid flow in the economizer. The boiler pressure is 40 bar. The temperature difference between boiler and high pressure flasher is 0.5 times of the temperature difference between boiler and condenser. Similarly, the temperature difference between low pressure

flasher and condenser is 0.5 times of the temperature difference between high pressure flasher and condenser. TTD in condenser is 10 K. Approach point in the boiler is 5 K. Isentropic efficiencies of pump and turbine are 75% and 80% respectively. Find the cycle output and efficiency.

Solution: Refer Fig. 2.5 for notations of the states.

From the properties of steam

The saturation pressure of 40 °C, the boiler pressure is 0.0738 bar.

The HRSG saturation temperature at 40 bar, $T_{13} = 250.33$ °C.

The high pressure flash temperature is the mid temperature of condenser and boiler's evaporator.

$$T_{15} = T_{16} = T_{cond} + \frac{T_e - T_{cond}}{2}$$

$$= 40 + \frac{250.33 - 40}{2} = 180.22\ ^\circ C$$

The saturation pressure of high pressure flasher at 180.22 °C is 10.07 bar.

Similarly, the low pressure flash temperature is the mid temperature of condenser and high pressure flasher.

$$T_{18} = T_{19} = T_{cond} + \frac{T_{HPF} - T_{cond}}{2}$$

$$= 40 + \frac{180.22 - 40}{2} = 110.11\ ^\circ C$$

The saturation pressure of high pressure flasher at 110.11 °C is 1.43 bar.

$$T_{11} = T_{sat,\ boiler} - AP$$

$$= 250.33 - 5 = 245.33\ ^\circ C$$

At condenser pressure, the properties of fluid are as follows

Liquid properties

$v_7 = 0.001\ m^3/kg$
$h_7 = 167.40\ kJ/kg$
$s_7 = 0.5721\ kJ/kg\ K$

Vapor properties

$h_6 = 2136.00\ kJ/kg$
$s_6 = 1.6651\ kJ/kg\ K$

At LPF, the properties of fluid are as follows

Liquid properties

$v_1 = 0.0011\ m^3/kg$
$h_{19} = 461.80\ kJ/kg$
$s_{19} = 1.4197\ kJ/kg\ K$

Vapor properties

$$h_{20} = 2691.50 \text{ kJ/kg}$$
$$s_{20} = 7.2375 \text{ kJ/kg K}$$

At HPF, the properties of fluid are as follows

Liquid properties

$$v_{16} = 0.0011 \text{ m}^3\text{/kg}$$
$$h_{16} = 764.04 \text{ kJ/kg}$$
$$s_{16} = 2.14 \text{ kJ/kg K}$$

Vapor properties

$$h_{17} = 2776.46 \text{ kJ/kg}$$
$$s_{17} = 6.58 \text{ kJ/kg K}$$

At the boiler, the properties of fluid are as follows:

Vapor properties

$$h_{13} = 2800.34 \text{ kJ/kg}$$
$$s_{13} = 6.07 \text{ kJ/kg K}$$

At T_{11}, the liquid properties,

$$h_{11} = h_{12} = h_{14} = 1063.03 \text{ kJ/kg}$$
$$s_{11} = s_{12} = s_{14} = 2.75 \text{ kJ/kg K}$$

The enthalpy before and after the flashing is same,

$$h_{14} = h_{15} = 1063.03 \text{ kJ/kg}$$

The dryness fraction of vapour at the exit of HP flasher

$$\frac{1063.03 - 764.04}{2776.46 - 764.04} = 0.1486$$

The entropy at this state,

$$s_{15} = s_{16} + \delta_{15}(s_{17} - s_{16})$$
$$= 2.14 + 0.1486\ (6.58 - 2.14)$$
$$= 3.12 \text{ kJ/kg K}$$

The dryness fraction of vapour at the exit of LP flasher

$$\delta_{18} = \frac{h_{18} - h_{19}}{h_{20} - h_{19}}$$
$$= \frac{764.04 - 461.74}{2691.47 - 461.74} = 0.1356$$

The entropy at this state,

$$s_{18} = s_{19} + \delta_{18}(s_{20} - s_{19})$$
$$= 1.42 + 0.1356\ (7.24 - 1.42)$$
$$= 2.21 \text{ kJ/kg K}$$

The liquid mass used for HP flashing,

$$m_{14} = m_{15} = m_1 \times \frac{FMR}{1 - FMR}$$
$$= 100 \times \frac{0.25}{1 - 0.25} = 33.4\ kg/s$$
$$m_{16} = (1 - \delta_{15})\, m_{15}$$
$$= (1 - 0.1486) \times 33.4 = 28.38 \text{ kg/s}$$

$$m_{17} = \delta_{15}\, m_{15} = 0.1486 \times 33.4 = 4.95 \text{ kg/s}$$
$$m_3 = m_2 + m_{17} = 100 + 4.95 = 104.95 \text{ kg/s}$$

At the turbine inlet condition i.e. superheated vapor state, 285 °C and 40 bar

$$h_1 = 2917.55 \text{ kJ/kg}$$
$$s_1 = 6.29 \text{ kJ/kg K}$$

The expansion consists of three parts. In the first state, the steam expands from HRSG pressure to HP flasher. In the second stage, the steam expands from HP flasher to LP flasher condenser pressure. Finally, the steam expands from the LP flasher to condenser.

At the end of the first stage expansion,

$$h_2 = 2697.80 \text{ kJ/kg}$$
$$s_2 = 6.4067 \text{ kJ/kg K}$$

The mixing of two fluids at the supply second stage,

$$m_2 h_2 + m_{17} h_{17} = m_3 h_3$$

After solving,

$$h_3 = 2701.50 \text{ kJ/kg}$$
$$s_3 = 6.4149 \text{ kJ/kg K}$$

At the end of the second stage expansion,

$$h_4 = 2441.30 \text{ kJ/kg}$$
$$s_4 = 6.5847 \text{ kJ/kg}$$

The mixing of two fluids at the supply final stage,

$$m_4 h_4 + m_{20} h_{20} = m_5 h_5$$

After solving,

$$h_5 = 2450.10 \text{ kJ/kg}$$
$$s_5 = 6.6078 \text{ kJ/kg K}$$

At the end of the final stage expansion,

$$h_6 = 2136.00 \text{ kJ/kg}$$
$$s_6 = 6.8585 \text{ kJ/kg K}$$

The specific power output,

$$\begin{aligned} w_{net} &= w_t - w_p \\ &= m_1(h_1 - h_2) + m_3 (h_3 - h_4) \\ &\quad + m_5 (h_5 - h_6) - m_7 (h_8 - h_7) \\ &\quad - m_9 (h_{10} - h_9) \\ &= 100 \times (1917.55 - 2697.83) + 104.05 \\ &\quad \times (2701.54 - 2441.26) + 108.80 \\ &\quad \times (2450.11 - 2136.03) - 108.80 \times \\ &\quad (171.64 - 164.45) - 133.4 \times \\ &\quad (229.66 - 225.39) \\ &= 79110.36 \text{ kW} \end{aligned}$$

Thermal efficiency of OFC cycle,

$$n_{th} = \frac{w_{net}}{q_{supply}} \times 100$$

$$q_{supply} = m_{10} (h_{11} - h_{10}) + m_{12} (h_1 - h_{12})$$

$$= 133.4\ (1063.03 - 229.66) + 100\ (2917.55 - 1063.03)$$
$$= 296570.00\ \text{kW}$$
$$= \frac{79110.36}{296570.00} \times 100$$
$$= 26.67\%$$

Organic Rankine Cycle: Determine the specific power and thermal efficiency of ORC with regenerator with the following data. Fluid: R123, Turbine inlet temperature: 165 °C, HRVG pressure: 11 bar, Condenser temperature: 40 °C. The vapor is cooled to 56 °C in the regenerator. The isentropic efficiencies of pump and turbine are respectively 75% and 80%.

Solution: Refer Fig. 2.8 for notations of the states. (the approach point is neglected)

From the properties of R123,

The saturation pressure at 40 °C is 1.54 bar.

At this condenser pressure the properties of fluid are as follows

Liquid properties

$$v_f = 0.0007\ m^3/kg = v_4$$
$$h_f = 240.59\ kJ/kg = h_4$$
$$s_f = 1.1383\ kJ/kg\ K = s_4$$

Vapor properties

$$h_v = 405.54\ kJ/kg$$
$$s_v = 1.6651\ kJ/kg\ K$$

Similarly, the saturation properties at boiler pressure of 11 bar

Liquid properties

$$h_f = 323.89\ kJ/k = h_7$$
$$s_f = 1.3739\ kJ/kg\ K = s_7$$

Vapor properties

$$h_v = 447.54\ kJ/kg = h_8$$
$$s_v = 1.6922\ kJ/kg\ K = s_8$$

At the turbine inlet condition i.e. superheated vapor state,

$$h_1 = 494.17\ kJ/kg$$
$$s_1 = 1.8051\ kJ/kg\ K$$

The properties of fluid at the exit of turbine can be determined from the isentropic efficiency of the turbine as follows

The turbine exit condition is determined from the isentropic efficiency of turbine by equating the specific entropies before and after the expansion. The specific entropy at the inlet of turbine is 1.8051 kJ/kg K. The saturated vapor entropy at the condenser pressure i.e. 1.54 bar is 1.6651 kJ/kg K. It is less that the turbine inlet entropy. Therefore, the state after the expansion is the superheated vapor condition.

After the isentropic expansion from the iteration of entropy by varying

the superheated temperature which is unknown or specific heat of vapor at this condition, the exit temperature of turbine can be determined.

$$s_2' = s_g + c_p \ln\left(\frac{T_2'}{T_{sat}}\right)$$

$$T_2' = T_{sat} \exp\left(\frac{s_2' - s_g}{c_p}\right)$$

$$T_2' = (40 + 273.15)\exp\left(\frac{1.8051 - 1.6651}{0.724}\right) - 273.15$$

$$= 106.80\ ^\circ C$$

$$h_2' = h_g + c_p\left(T_2' - T_{sat}\right)$$

$$= 405.54 + 0.724(106.80 - 40)$$

$$= 453.90\ kJ/kg$$

The isentropic efficiency of turbine is

$$\eta_t = \frac{h_1 - h_2}{h_1 - h_2'}$$

$$h_2 = h_1 - \eta_t (h_1 - h_2')$$

$$= 494.17 - 0.8 \times (494.17 - 453.90)$$

$$= 461.96\ kJ/kg$$

$$h_2 - h_g = c_p(T_2 - T_{sat})$$

$$T_2 = T_{sat} + \frac{h_2 - h_g}{c_p}$$

$$= 40 + \frac{461.96 - 405.54}{0.724}$$

$$= 117.92\ ^\circ C$$

The pump exit condition is determined from the isentropic efficiency as follows

After the isentropic pumping,

$$h_2 = h_4 + v_4 (P_5 - P_4) \times 100$$

$$= 240.59 + 0.0007 \times (11 - 1.54) \times 100$$

$$= 241.25\ kJ/kg$$

The isentropic efficiency of pump is

$$\eta_p = \frac{h_5' - h_4}{h_5 - h_4}$$

From the above equation,

$$h_5 = h_4 + \frac{h_5' - h_4}{\eta_p}$$

$$= 240.59 + \frac{241.25 - 240.59}{0.75}$$

$$= 241.47 \text{ kJ/kg}$$

The properties at the exit of pump are 1.1416 kJ/kg entropy and 41 °C.

$$T_3 = 56 \text{ °C}$$

$$h_3 = h_g + c_p (T_3 - T_{sat})$$
$$= 405.54 + 0.724 \times (56 - 40)$$
$$= 417.12 \text{ kJ/kg}$$

From energy balance in regenerator,

$$h_6 = h_5 + (h_2 - h_3)$$
$$= 241.47 + 461.96 - 417.12$$
$$= 286.31 \text{ kJ/kg}$$

From the enthalpy, h_6, T_6 is obtained as 82 °C.

The specific power output,

$$w_{net} = w_t - w_p$$
$$= h_1 - h_2 - (h_5 - h_4)$$
$$= 494.17 - 461.96 - (241.47 - 240.59)$$
$$= 31.33 \text{ kJ/kg}$$

Thermal efficiency of ORC cycle,

$$\eta_{th} = \frac{w_{net}}{q_{\sup ply}} \times 100$$

$$= \frac{w_{net}}{h_1 - h_6} \times 100$$

$$= \frac{31.33}{494.17 - 286.33} \times 100$$

$$= 15\%$$

Organic Flash Cycle: Determine the specific power and thermal efficiency of OFC-R123 with single flasher and the following operational conditions. Turbine inlet temperature state: 235 °C, 15 bar. Condenser temperature: 40 °C. The hot fluid exit temperature in the regenerator is 43.1 °C. Take the flash temperature as a mid-temperature of condenser temperature and boiler saturation temperature. The mass ratio of fluid for flashing is 0.25. The isentropic efficiencies of pump and turbine are 75% and 80% respectively. Take approach point as 2 K.

Solution. Refer Fig. 2.16 for notations of the states.

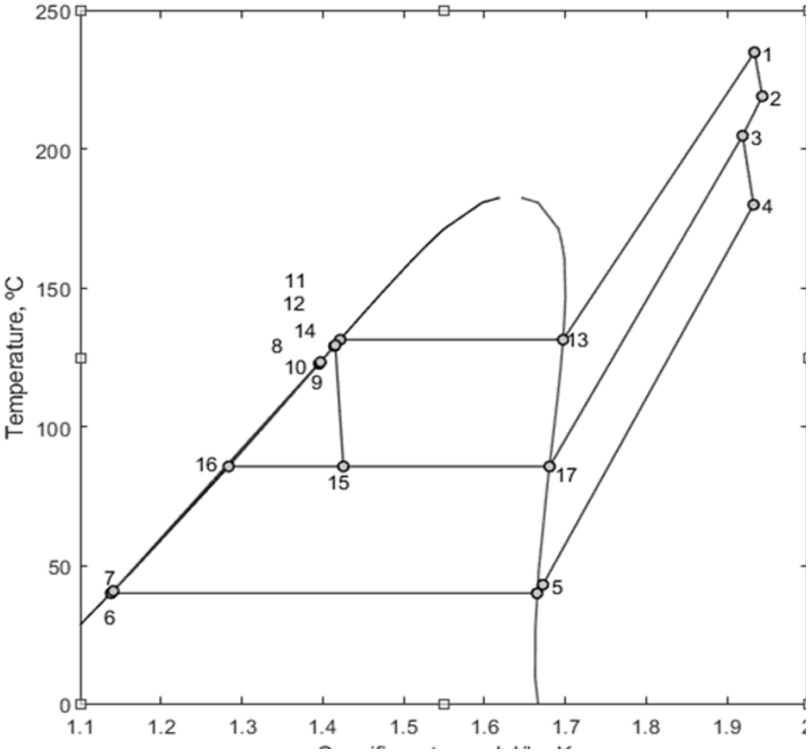

Fig. 2.16: Temperature-specific entropy diagram of OFC with single flasher given in the problem

From the properties of R123

The saturation pressure at 40 °C is 1.54 bar.

The HRVG saturation temperature at 15 bar, T_{13} = 131.41 °C.

The flash temperature is the mid temperature of condenser and evaporator.

$$T_{15} = T_{16} = T_{cond} + \frac{T_e - T_{cond}}{2}$$

$$= 40 + \frac{131.41 - 40}{2} = 85.70\,°C$$

The saturation pressure of flasher fluid at 85.70 °C is 5.63 bar.

At condenser pressure, the properties of fluid are as follows

Liquid properties

v_6 = 0.0007019 m^3/kg

h_6 = 240.59 kJ/kg

s_6 = 1.1383 kJ/kg K

Vapor properties

h_v = 405.54 kJ/kg

s_v = 1.6651 kJ/kg K

Vapor properties at 15 bar,

$$h_{13} = 454.61 \text{ kJ/kg}$$
$$s_{13} = 1.6972 \text{ kJ/kg K}$$

The evaporator inlet temperature or economizer exit temperature,

$$T_{11} = T_{12} = T_{14} = T_{13} - AP$$
$$= 131.41 - 2 = 129.41 \text{ °C}$$

At T_{11}, the liquid properties,

$$h_{11} = h_{12} = h_{14} = 340.60 \text{ kJ/kg}$$
$$s_{11} = s_{12} = s_{14} = 1.4155 \text{ kJ/kg K}$$

The enthalpy before and after the flashing is same,

$$h_{14} = h_{15} = 340.60 \text{ kJ/kg}$$

The dryness fraction of vapour at the exit of flasher

$$\delta_{15} = \frac{h_{15} - h_{16}}{h_{17} - h_{16}}$$
$$= \frac{340.60 - 289.66}{432.07 - 289.66} = 0.36$$

The entropy at this state,

$$s_{15} = s_{16} + \delta_{15} (s_{17} - s_{16})$$
$$= 1.2836 + 0.36 (1.6805 - 1.2836)$$
$$= 1.4256 \text{ kJ/kg K}$$

The liquid mass used for flashing,

$$m_{14} = m_{15} = m_1 \times \frac{FMR}{1 - FMR}$$
$$= 1 \times \frac{0.25}{1 - 0.25} = 0.334 \, kg/s$$
$$m_{10} = m_{11} = m_1 + m_{14}$$
$$= 1 + 0.334 = 1.334 \text{ kg/s}$$
$$m_{16} = (1 - \delta_{15}) m_{15}$$
$$= (1 - 0.36) \times 0.334 = 0.2141 \text{ kg/s}$$
$$m_{17} = \delta_{15} m_{15} = 0.36 \times 0.334 = 0.1192 \text{ kg/s}$$
$$m_3 = m_2 + m_{17} = 1 + 0.1192 = 1.1192 \text{ kg/s}$$

At the turbine inlet condition i.e. superheated vapor state, 235 °C and 15 bar

$$h_1 = 562.14 \text{ kJ/kg}$$
$$s_1 = 1.9339 \text{ kJ/kg K}$$

The expansion consists of two parts. In the first state, the vapour expands from HRVG pressure to flasher pressure. In the second stage, the vapour expands from flasher pressure to condenser pressure.

The specific entropy at the inlet of turbine is 1.9339 kJ/kg K. The saturated vapor entropy at the flash pressure i.e. 5.63 bar is 1.6805 kJ/kg K. It is less that the turbine inlet entropy. Therefore, the state after the expansion falls in the superheated vapor region.

After the isentropic expansion,

From the iteration of entropy by varying the superheated temperature the exit temperature can be evaluated. Alternatively, from specific heat of vapor, the exit temperature of turbine can be determined as follows,

$$s_2^{'} = s_g + c_p \ln\left(\frac{T_2^{'}}{T_{sat}}\right)$$

$$T_2^{'} = T_{sat} \exp\left(\frac{s_2^{'} - s_g}{c_p}\right)$$

$$= (85.71 + 273.15)\exp\left(\frac{1.939 - 1.6805}{0.8321}\right) - 273.15$$

$$= 213.44°C$$

$$h'_2 = h_g + c_p (T'_2 - T_{sat})$$
$$= 432.07 + 0.8321\ (213.44\text{-}85.70)$$
$$= 538.36\ kJ/kg$$

The isentropic efficiency of turbine is

$$\eta_t = \frac{h_1 - h_2}{h_1 - h_2^{'}}$$

$$h_2 = h_1 - \eta_t (h_1 - h'_2)$$
$$= 562.14 - 0.8 \times (562.14 - 538.36)$$
$$= 543.12\ kJ/kg$$

also, $h_2 - h_g = c_p(T_2 - T_{sat})$

$$T_2 = T_{sat} + \frac{h_2 - h_g}{c_p}$$

$$= 85.70 + \frac{543.12 - 432.0754}{0.8321}$$

$$= 219.16°C$$

At the exit of the turbine, two vapours i.e. flash vapour and turbine vapour are mixed.

The energy balance applied to the mixing of two streams,

$$m_2 h_2 + m_{17} h_{17} = m_3 h_3$$

$$h_3 = \frac{m_2 h_2 - m_{17} h_{17}}{m_3}$$

$$= \frac{1 \times 543.12 - 0.1192 \times 432.07}{1.1192}$$

$$= 531.29\ kJ/kg$$

also, $h_3 - h_g = c_p(T_3 - T_{sat})$

$$T_3 = T_{sat} + \frac{h_3 - h_g}{c_p}$$

$$= 85.70 + \frac{531.29 - 432.07}{0.8321}$$

$$= 204.94\ °C$$

The entropy after the mixing,

$$s_3 = s_g + c_p h\left(\frac{T_3}{T_{sat}}\right)$$

$$= 1.6805 + 0.8321 \times \ln\left(\frac{204.94 + 273.15}{85.70 + 273.15}\right)$$

$$= 1.9192\ \text{kJ/kg K}$$

Now the vapour expands in the second stage after mixing with the flash vapour.

The specific entropy at the inlet of turbine is 1.9192 kJ/kg K. The saturated vapor entropy at the condenser pressure i.e. 1.54 bar is 1.6651 kJ/kg K. It is less that the turbine inlet entropy. Therefore, the state after the expansion falls in the superheated vapor region.

After the isentropic expansion (3-4),

$$s_4' = s_g + c_p \ln\left(\frac{T_4'}{T_{sat}}\right)$$

$$T_4' = T_{sat} \exp\left(\frac{s_4' - s_g}{c_p}\right)$$

$$= (40 + 273.15) \times \exp\left(\frac{1.9192 - 1.6651}{0.7240}\right) - 273.15$$

$$= 171.65\ °C$$

$$h'_4 = h_g + c_p (T'_4 - T_{sat})$$

$$= 405.54 + 0.7240 \times (171.65\text{-}40.0)$$

$$= 500.85\ \text{kJ/kg}$$

The isentropic efficiency of turbine is

$$\eta_t = \frac{h_3 - h_4}{h_3 - h_4'}$$

$$h_4 = h_3 - \eta_t (h_3 - h'_4)$$

$$= 531.29 - 0.8 \times (531.29 - 500.85)$$

$$= 506.94\ \text{kJ/kg}$$

also, $h_4 - h_g = c_p(T_4 - T_{sat})$

$$T_4 = T_{sat} + \frac{h_4 - h_g}{c_p}$$

$$= 40.0 + \frac{506.94 - 405.54}{0.7240}$$

$$= 180.06°C$$

Since the exit condition of pump 1 is required to solve the regenerator, after evaluating the pump 1 exit state, the regenerator can be solved.

The pump exit condition is determined from the isentropic efficiency as follows

After the isentropic pumping,

$$h'_7 = h_6 + v_6 (P_7 - P_6) \times 100$$
$$= 240.59 + 0.0007 \times (5.63 - 1.54) \times 100$$
$$= 240.87 \text{ kJ/kg}$$

The isentropic efficiency of pump is

$$\eta_p = \frac{h'_7 - h_6}{h_7 - h_6}$$

From the above equation,

$$h_7 = h_6 + \frac{h'_7 - h_6}{\eta_p}$$

$$= 240.59 + \frac{240.87 - 240.59}{0.75}$$

$$= 240.97 \text{ kJ/kg}$$

Temperature at this enthalpy, $T_7 = 40.84$ °C

Since the exit state of pump is evaluated, the regenerator can be solved with the result.

The hot side exit temperature of hot fluid in the regenerator is kept above the condenser temperature.

$$T_5 = 43.1 \text{ °C}$$

Enthalpy at this temperature,

$$h_5 = h_g + c_p (T_5 - T_{sat})$$
$$= 405.54 + 0.7240 \times (43.1 - 40.0)$$
$$= 407.78 \text{ kJ/kg}$$

The energy balance in regenerator,

$$h_4 - h_5 = h_8 - h_7$$

The exit temperature of cold side fluid from regenerator,

$$h_8 = h_7 + (h_4 - h_5)$$
$$= 240.97 + (506.94 - 407.78)$$
$$= 340.13 \text{ kJ/kg}$$

Temperature of liquid at this enthalpy,

$$T_8 = 129.07 \text{ °C}$$

The mixing of two liquids at the exit of separator,

$$m_8 h_8 + m_{16} h_{16} = m_9 h_9$$

$$h_9 = \frac{m_8 h_8 + m_9 h_9}{m_9}$$

$$= \frac{1.119 \times 340.13 + 1.3334 \times 332.52}{1.334}$$

$$= 332.52 \text{ kJ/kg}$$

The temperature of liquid at this enthalpy,

$$T_9 = 122.71 \text{ °C}$$

After the isentropic pumping,

$$h'_{10} = h_9 + v_9 (P_{10} - P_9) \times 100$$

$$= 332.52 + 0.00086 \times (15 - 12.69) \times 100$$

(considered the saturation pressure at the heated temperature)

$$= 332.66 \text{ kJ/kg}$$

The isentropic efficiency of pump is

$$\eta_p = \frac{h'_{10} - h_9}{h_{10} - h_9}$$

From the above equation,

$$h_{10} = h_9 + \frac{h'_{10} - h_9}{\eta_p}$$

$$= 332.52 + \frac{332.66 - 332.52}{0.75}$$

$$= 332.72 \text{ kJ/kg}$$

Temperature at this enthalpy, $T_{10} = 123.33$ °C

The specific power output,

$$w_{net} = w_t - w_p$$

$$= m_1(h_1 - h_2) + m_3 (h_3 - h_4) - m_6 (h_7 - h_6) - m_9 (h_{10} - h_9)$$

$$= 1 \times (562.14 - 543.12) + 1.1192 \times (531.29 - 506.94) - 1.1192 \times (240.97 - 240.59) - 1.334 \times (332.72 - 332.52)$$

$$= 45.58 \text{ kJ/kg}$$

Thermal efficiency of OFC cycle,

$$\eta_{th} = \frac{w_{net}}{q_{sup\ ply}} \times 100$$

$$q_{supply} = m_{10} (h_{11} - h_{10}) + m_{12} (h_1 - h_{12})$$

$$= 1.334\,(340.60–332.72)+1(562.14 – 340.60)$$
$$= 232.05 \text{ kJ/kg}$$
$$= 19.64\%$$

Review Questions

1. Differentiate between conventional steam Rankine cycle with steam flash cycle?
2. Compare the relative merits and demerits of ORC and OFC.
3. Why superheat is not mandatory in some ORC plants?
4. The recommendations of the flash cycle depend on the nature of energy source. Justify with suitable examples.
5. Compare the elements of power generation with single fluid and binary fluid.
6. Draw the temperature profile of heat recovery with single fluid, binary fluid and flash cycle in a solar thermal power plant.
7. If the working fluid at the turbine inlet is same in Rankine cycle and flash cycle, the required thermic oil in solar thermal collector is also same in these two cycles in spite of different economizer load. Justify.
8. The oil supply temperature to solar collector in OFC is lower than the supply temperature with ORC. Analyse the reason.

❐

3

Binary Fluid Properties and Processes

Abstract

The knowledge of the thermodynamic properties and processes of binary fluid systems is essential to solve problems involving binary fluid subsystems such as power plants and cooling plants in a polygeneration. In this chapter the mathematical formulation to solve the properties and thermodynamic modelling for the evaluation of processes are detailed. The solutions can be applied to design and analyse the vapour absorption refrigeration (VAR) Kalina cycle (KC), cooling cogeneration, polygeneration and similar systems. The solutions to the processes have been depicted on a property chart drawn to scale to understand the process clearly.

3.1 Introduction

The binary fluid system is a mixture of two fluids prepared to have the required properties to meet the operation of the system. The binary fluid system enjoys the qualities of both fluids. The following are the advantages and disadvantages of the binary fluid system:

Advantages

1. A binary fluid system can be operated with a low-temperature heat source.
2. The phase change occurs at the variable temperature. Therefore, there is a good match in temperature between heat transfer fluid and working fluid, which results in low entropy generation compared to a single fluid system.
3. The binary fluid system has great flexibility to adopt in cooling cogeneration systems, i.e., combined power and cooling systems.

T. Srinivas, *Thermal Polygeneration*,
https://doi.org/10.1007/978-3-031-37886-7_3

4. It is more suitable for renewable energy sources such as solar thermal, biomass, geothermal etc.

Disadvantages

1. The system is complex in nature because of additional components such as absorbers, mixers, separators, etc.
2. The closed temperature difference between heat transfer fluid and working fluid increases the size of the heat exchanger, hence its cost.
3. Special materials are required for the equipment. For example, in an ammonia-water mixture, ammonia is corrosive to copper and its alloys. Therefore, the equipment should be free from this material.

To evaluate the subsystem with binary fluid, one needs to understand and develop the properties and processes. At the moment, the power and cooling units are also combined into a single system known as a "cooling cogeneration." Therefore, this can be extended to solve cooling cogeneration in addition to the power plant and refrigeration and air conditioning units having the binary fluid system.

3.2 Thermodynamic Properties of Binary Fluid

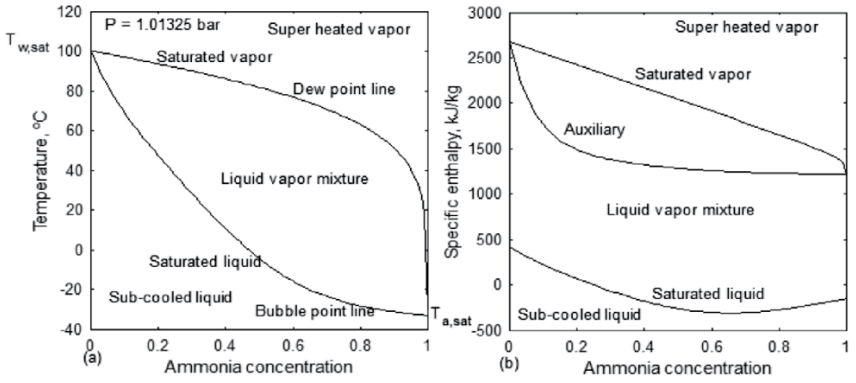

Fig. 3.1: Regions of binary fluid system

Fig. 3.1 details the regions of fluid on (a) the temperature-concentration diagram and (b) the specific enthalpy-concentration diagram. There are five regions that define the state of the fluid. They are

1. Subcooled liquid or compressed liquid,
2. Saturated liquid,
3. Liquid-vapour mixture,
4. Saturated vapour state, and
5. Superheated vapour.

The temperature-concentration diagram has two curves, viz., the saturated liquid curve and the saturated vapour curve. But the specific enthalpy-concentration diagram has three curves, viz., saturated liquid curve, auxilliary curve, and saturated vapour curve. An auxiliary curve is used to apply the lever rule to evaluate the liquid-vapour mixture state. The temperature-concentration diagram shows a loop at a constant pressure. Three properties are required to define the state of the fluid, and they are pressure, temperature, and concentration. After determining these three properties, at the stated pressure and concentration, the starting temperature of the phase change and the final temperature of the phase change of the fluid can be evaluated. The starting temperature of the phase change is called the "bubble point temperature" (BPT). Similarly, the end temperature of the phase change is known as the dew point temperature (DPT). The stated temperature should be compared with the BPT and DPT. If the fluid temperature is below the bubble point temperature, then the state of the fluid is subcooled or compressed liquid. If the temperature is equal to the bubble point temperature, the saturated liquid is called a saturated liquid. If the temperature lies between BPT and DPT, it is known as a liquid-vapour mixture. The temperature of the fluid is equal to the DPT, which indicates a saturated vapour state. Finally, a temperature greater than the DPT denotes the superheated vapour state. A single fluid exsists at a concentration of zero and one unit, respectively, for water and ammonia. For example, Fig. 3.1a shows the saturation temperature of water at 100 °C at atmospheric pressure. Similarly, the saturated temperature of ammonia at the same pressure is -33.41 °C, i.e., a fixed temperature during the phase change. Therefore, the loop is sloped in the right direction. For the binary fluid, the phase change starts with the BPT and ends with the DPT. Between these two temperatures, liquid-vapour exists.

Fig. 3.1b shows an extra curve, auxiliary in addition to the saturated liquid and saturated vapour curves on the specific enthalpy-concentration chart. This auxiliary curve is useful to solve the properties of a liquid-vapour mixture using the lever rule. The formulation and use of auxiliary curves to solve the state and processes have been detailed in the further sections. At zero concentration, the difference in specific enthalpies of saturated vapour and saturated liquid is equal to the specific latent heat of water. Similarly, the difference between the specific enthalpy of saturated vapour and the specific enthalpy of saturated vapour is the specific enthalpy of ammonia at unit concentration.

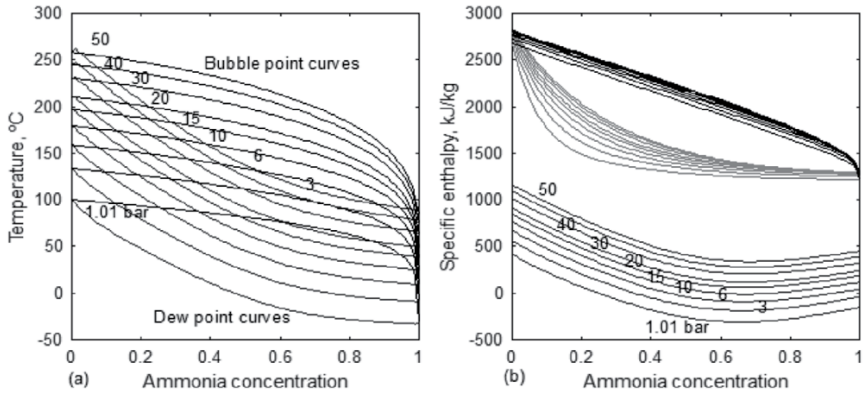

Fig. 3.2: The saturation temperatures at the beginning (BPT) and end (DPT) of phase change at various pressures

Fig. 3.1 is focused on the binary fluid properties at a fixed pressure (1.01325 bar). The properties will change with a change in pressure. Therefore, the properties have been extended with the change in pressure and are depicted in Fig. 3.2. The saturation temperatures of BPT and DPT are shown from 1.01325 bar to 50 bar pressure. It shows that the BPT and DPT increase with an increase in pressure (Fig. 3.2a). Similarly, Fix. 3.2b shows the changes in the specific enthalpies with a change in pressure. The specific enthalpy of a saturated liquid decreases because, the concentration increases after the minimum enthalpy. Therefore, the specific latent heat increases with the concentration and decreases after the peak. The specific enthalpy of saturated liquid and saturated vapour is increasing with an increase in pressure.

The thermodynamic properties required to solve a thermal system are pressure, temperature, concentration, specific internal energy, specific enthalpy, specific entropy, and specific energy. The single-phase properties can be evaluated directly without any use of dryness fraction. The dryness fraction is required to evaluate the properties of a liquid-vapour mixture. The dryness fraction of a mixture is defined as the ratio of the mass of dry vapour to the total mass of the mixture. Similarly, the wetness fraction is defined as the mass ratio of liquid to the total mass of the mixture.

Dryness fraction of liquid-vapour mixture,

$$\delta = \frac{m_v}{m} = \frac{m_v}{m_1 + m_v} \tag{3.1}$$

Similarly, the wetness fraction of liquid-vapour mixture,

$$1 - \delta = \frac{m_l}{m} = \frac{m_l}{m_l + m_v} \tag{3.2}$$

The specific enthalpy of liquid-vapour mixture,

$$h = h_l + \delta\,(h_v - h_l) \tag{3.3}$$

$$\delta = \frac{h - h_l}{h_v - h_l} \tag{3.4}$$

Similarly, the ammonia balance (mass balance) in the liquid-vapour mixture,

Total ammonia in the mixture = ammonia in liquid + ammonia in vapour

$$m\,x = m_l\,x_l + m_v\,x_v \tag{3.5}$$

where,

$$m = m_l + m_v \tag{3.6}$$

Therefore,

$$\begin{aligned} mx &= (1-\delta)\,m\,x_l + \delta\,m\,x_v \\ x &= (1-\delta)\,x_l + \delta\,x_v \\ &= x_l - \delta\,x_l + \delta\,x_v \end{aligned} \tag{3.7}$$

Therefore

$$x = x_l + \delta\,(x_v - x_l) \tag{3.8}$$

and so

$$\delta = \frac{x - x_l}{x_v - x_l}$$

Combining, these two equations,

$$\delta = \frac{x - x_l}{x_v - x_l} = \frac{h - h_l}{h_v - h_l} \tag{3.10}$$

This also can be used to find the entropy and energy of liquid-vapour mixture.

$$\delta = \frac{s - s_l}{s_v - s_l} \tag{3.11}$$

3.3 Thermodynamic Processes of Binary Fluid

The solutions of binary fluid subsystems in polygeneration, such as the binary fluid power plant and the binary fluid cooling plant, need the properties of the binary fluid detailed in the earlier section. The properties can be evaluated from the correlations available in the literature. The knowledge of these properties and process solutions is required for these subsystems' evaluation for the polygeneration. Therefore, the binary fluid processes are detailed with the formulation for analytical and the graphical solutions.

The binary fluid power generation and binary fluid cooling systems have the following thermodynamic processes.

1. Boiling
2. Separation of liquid-vapour mixture

3. Dephlegmator
4. Expansion in a turbine
5. Mixing of fluids without heat transfer (adiabatic mixing)
6. Mixing of fluids with heat transfer (diabatic mixing)
7. Condensation
8. Pumping
9. Throttling

3.3.1 Boiling

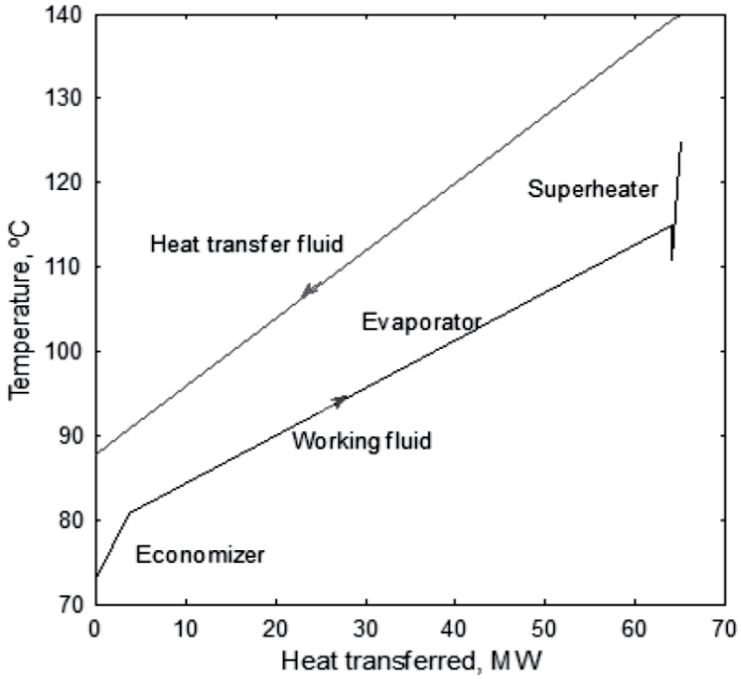

Fig. 3.3: Binary fluid system - boiling

The boiler in a binary fluid system consists of an economizer and an evaporator or an economizer, an evaporator, and a superheater. As a result, the concentration in the turbine is close to 100% ammonia fluid is an isentropic fluid, and hence the superheating is not a mandatory component of the binary fluid system. In a steam power plant, the fluid, i.e., water, is a wet fluid and superheating and reheating of steam are required to protect the turbine from the wet expansion and erosion. Fig. 3.3 shows a typical boiler working from the heat recovery of the hot fluid. This boiler is also called a heat recovery vapour generator (HRVG). It shows the temperature profile of two fluids, viz.,

heat transfer fluid (HTF) and working fluid (binary fluid). In the case of a solar thermal plant, the HTF is thermal oil, pressurised water, or glycol mixed water. In waste heat recovery, generally hot gas plays the role of HTF. A constraint in the evaporator, which is called the pinch point (PP), controls and maintains the positive temperature difference between hot fluid and cold fluid. The PP is defined as the minimum temperature difference between hot fluid and cold fluid at the inlet of the evaporator in the direction of the working fluid. In a fuel firing plant such as a coal-fired thermal power plant, PP is not used as the hot fluid temperature is too high compared to the working fluid temperature. Between the evaporator and the superheater, the fluid temperature is dropped with the heat rejection in dephlegmator.

A minor degree of superheat has been considered in this boiler to supply dry and vapour in the turbine. The temperature of the working fluid changes in all these three sections, i.e., the economizer, the evaporator, and the superheater. In the evaporator, the boiling starts with BPT. The evaporator may be complete or partial, depending on the plant configuration. In a binary fluid cooling plant, i.e., VAR, the evaporation is not complete, i.e., the exit temperature of the vapour is below the DBT. In a binary fluid power plant designed for low temperature heat recovery, the fluid temperature in the evaporator is below the DBT. After separating the vapour from the mixture, it is heated further in the superheater as shown. The binary fluid in HRVG results a close temperature match between hot fluid and cold fluid.

3.3.2 Separation of liquid-vapour mixture

At the end of the boiler of a binary fluid system, the mixture consists of liquid and vapour. These two fluids have to be separated for the plant processing. The separated vapour, which is a saturated vapour, can be used for the processing of cooling or power. Similarly, the separated liquid is a saturated liquid, which is also called a weak solution due to its lower concentration. The weak solution is used to dilute the vapour before it enters the absorber for easy condensation at a reasonable sink temperature.

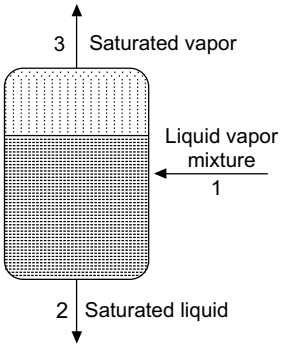

Fig. 3.4: Division of a mixture into liquid and vapour

Fig. 3.4 is the separation process that divides the mixing into saturated liquid and saturated vapour. The process is dipected on enthalpy-concentration chart (Fig. 3.5). Separator is a physical drum where the liquid collected at the bottom with gravity and the vapour at the top. The process consists of three concentrations, viz., mixture concentration, liquid concentration and vapour concentration. The mixture concentration lies between liquid concentration and vapour concentration. The separation process can be solved using lever rule in the graphical solution. Alternatively, it also can be evaluated with analytical approach.

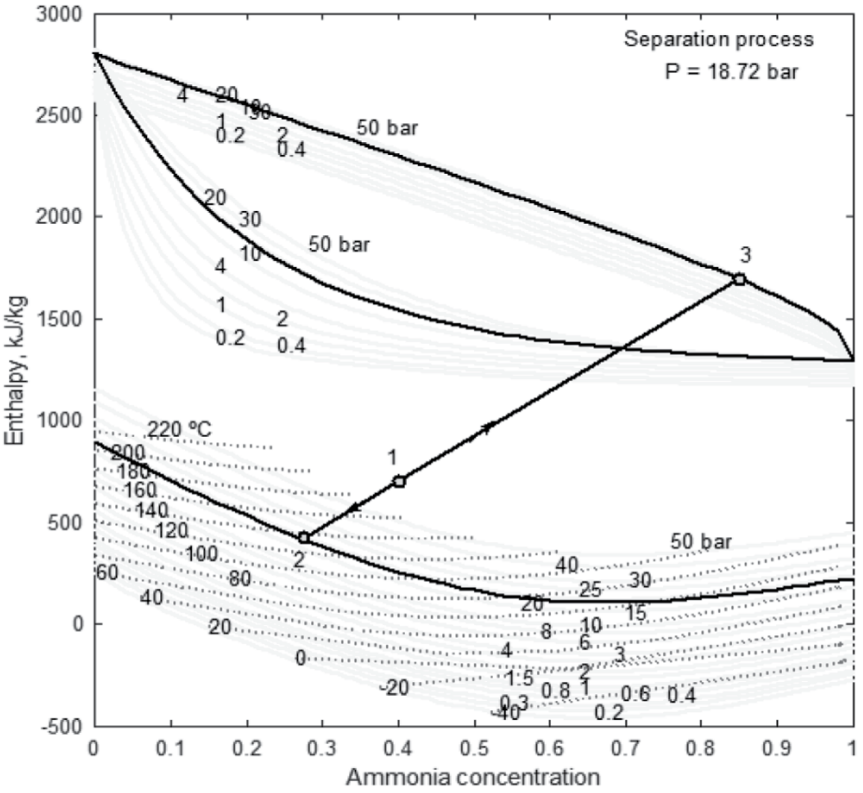

Fig. 3.5: Specific-enthalpy and concentration diagram for representation of separation process from liquid-vapour mixture into saturated liquid and saturated vapour

As per the definition of dryness fraction,

$$m_1 = m_2 + \delta\,(m_3 - m_2) \tag{3.12}$$

The Eq. 3.10 defines the dryness fraction on enthalpy scale and concentration scale.

With reference to Eq.3.8,

$$x_1 = x_2 + \delta\,(x_3 - x_2) \tag{3.13}$$

Combining these two equations,

$$x_1 = x_2 + \frac{m_3}{m_1}(x_3 - x_2) \tag{3.14}$$

$$= \frac{m_3}{m_1} = \frac{x_1 - x_2}{x_3 - x_2} \tag{3.15}$$

$x_1 - x_2$ is the distance between mixture and liquid and $x_3 - x_2$ is distance between vapour and liquid. Therefore, the length of process line between mixture and liquid is proportional to the vapour mass. And the length of process line between vapour and liquid is proportional to the mixture mass. It shows that the length towards the liquid is proportional to vapour mass the total length of the process is proportional to the total mass. This is the lever rule. The length towards the vapour from the mixture is proportional to the liquid mass.

Since the dryness fraction can also be defined as a function of enthalpies, the length between mixture enthalpy and liquid enthalpy is proportional to the vapour. From the similar triangles, the lever rule can be applied as a function of concentration or enthalpy. If the diagram is drawn with entropy, the lever rule can also be applied as a function of specific enthalpy.

Therefore

$$\frac{m_3}{m_1} = \frac{h_1 - h_2}{h_3 - h_2} \tag{3.16}$$

Similarly,

$$\frac{m_2}{m_1} = \frac{x_3 - x_1}{x_3 - x_2} = \frac{h_3 - h_1}{h_3 - h_2} \tag{3.17}$$

3.3.3 Dephlegmator

Fig. 3.6 shows the fluid flow and workings of the dephlegmator in a binary fluid system. The fluid at the exit of the evaporator section of the boiler is in a liquid-vapour mixture state. The liquid and vapour have to be separated, respectively, to dilute the vapour in the absorber and power/cooling process. The separated liquid is called a “weak solution” due to its lower concentration. The separated vapour is supplied to the dephlegmator. In the dephlegmator, the heat exchanger coil provides a cold body to reject the heat from the dephlegmator. In a dephlegmator, the two processes are heat rejection and separation of the mixture into liquid and vapour. Finally, the separated vapour from the dephlegmator has a greater concentration compared to the vapour from a separator.

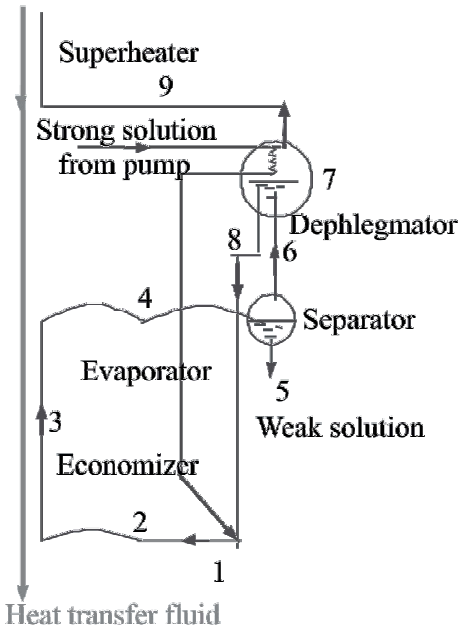

Fig. 3.6: Binary fluid system with boiler, separator and dephlegmator

The high concentration fluid offers more cooling and coefficient of performance (COP) to a cooling plant. It also allows operating the boiler at a lower pressure compared to a boiler without connecting a dephlegmator. In a typical two-plant setup, viz., with a dephlgamator and without a dephlegmator, If the concentration of the fluid in the cooling components (condenser, throttling, and evaporator) or power components (turbine, etc.) is the same, the boiler concentration differs in these two cases. The concentration of the boiler is the same as with a plant without a dephlegmator. However, the boiler concentration is less than the dephlegmator exit concentration in a plant having a dephlegmator. Therefore, the boiler pressure, which is a function of temperature and concentration, is low compared to without the dephlegmator. The dephlegmator not only favours the cooling performance, it also allows the boiler to operate at a low pressure without compromising on concentration. A dephlegmator is used in a binary fluid system to enhance the concentration of fluid. The distillation of fluid by cooling condenses the water from the vapour. To condense the water from the vapour mixture, heat has to be rejected from the dephlegmator. In the current case, instead of rejecting the heat to the surroundings, some strong solution has been used to absorb the heat from the dephlegmator. While cooling the vapour in the dephlegmator, first the water vapour starts to condense due to its higher boiling point compared to the ammonia.

From Fig. 3.6, it can be understood that the processes consist of two separation processes, viz., in the separator and the dephlegmator. Therefore, two dryness fractions can be evaluated for the separator and the dephlegmator.

The dryness fraction in separator,

$$\delta_{sep} = \frac{x_4 - x_5}{x_6 - x_5} \tag{3.18}$$

Similarly, the dryness fraction in dephlegmator,

$$\delta_{deph} = \frac{x_7 - x_8}{x_9 - x_8} \tag{3.19}$$

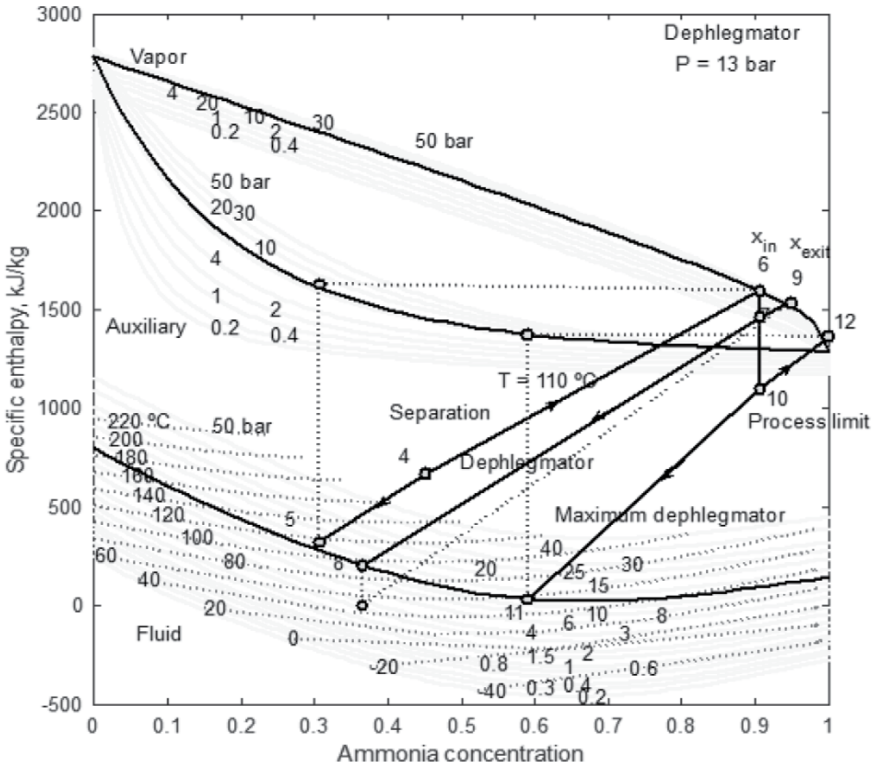

Fig. 3.7: Representation of dephlegmator process after the vapor separation

Fig. 3.7 shows the dephlegmator process in a specific enthalpy-concentration diagram. It also shows the maximum extent of distillation of the vapour to reach a 100% concentration. The effectiveness of a dephlegmator is determined by the ratio of actual concentration raised to maximum concentration raised. The maximum rise in concentration is a hypothetical limit shown as a process limit.

$$\varepsilon_{deph} = \frac{x_9 - x_6}{1 - x_6} \tag{3.20}$$

3.3.4 Expansion in a turbine

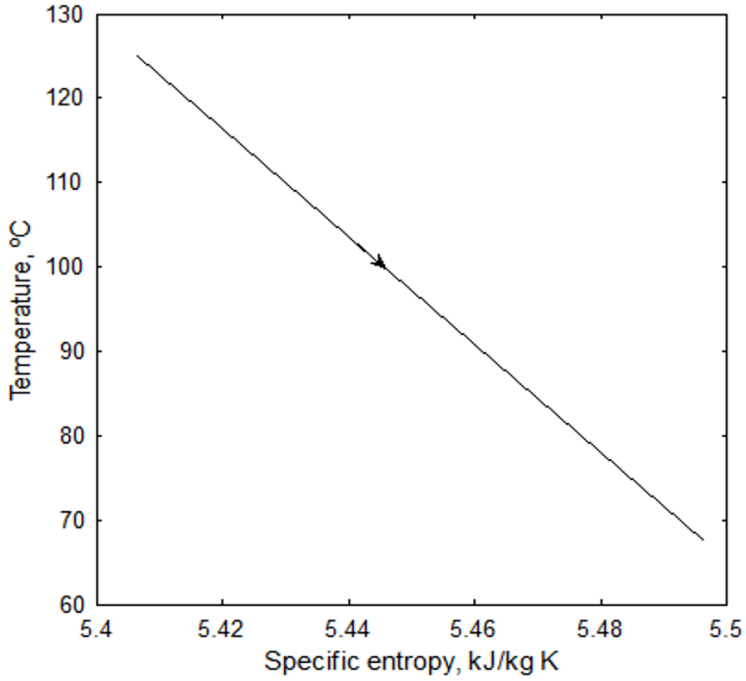

Fig. 3.8: Expansion of vapour in a turbine on temperature-specific entropy diagram

Fig. 3.8 shows the expansion of vapour in a turbine in a binary fluid system. As per the isentropic efficiency value, the entropy of the vapour increases in the expansion process with a drop in temperature. The mixture is a combination of wet fluid (water) and isentropic fluid (ammonia). But the concentration of vapour in the turbine is nearly more than 90%, which follows the properties of isentropic fluid. Therefore, in a binary fluid power plant, a superheater is not a mandatory component. In some cases, a small degree of superheat can be used. In the steam power plant, since the fluid is wet, superheating and steam reheating protect the steam turbine from wet expansion.

3.3.5 Mixing of fluids without heat transfer (adiabatic mixing)

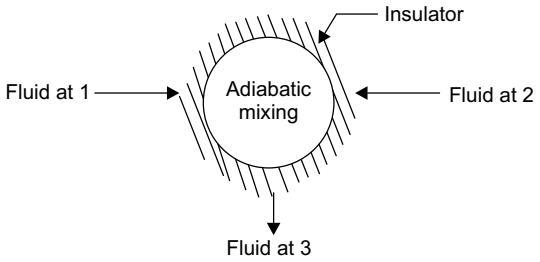

Fig. 3.9: Adding two fluids without heat transfer (adiabatic mixing)

Fig. 3.9 shows the mixing of two streams into a new stream without adding or rejecting the heat transfer. It is called adiabatic mixing of fluids. This mixing has been depicted on specific enthalpy and concentration diagrams. It is the reverse process of separation. In a binary fluid system, the mixing of two streams at the inlet of the absorber plays an important role in condensing the vapour. In this case, the mixing of vapour into water is called absorption. Hence, the cycle is called the absorption cycle. Condensing ammonia-rich vapour by rejecting heat to the surroundings is difficult as it demands a very low temperature. To avoid this difficulty, the vapour is mixed with the weak solution to decrease the concentration. This allows the easy and complete condensation of vapour into the saturated liquid state.

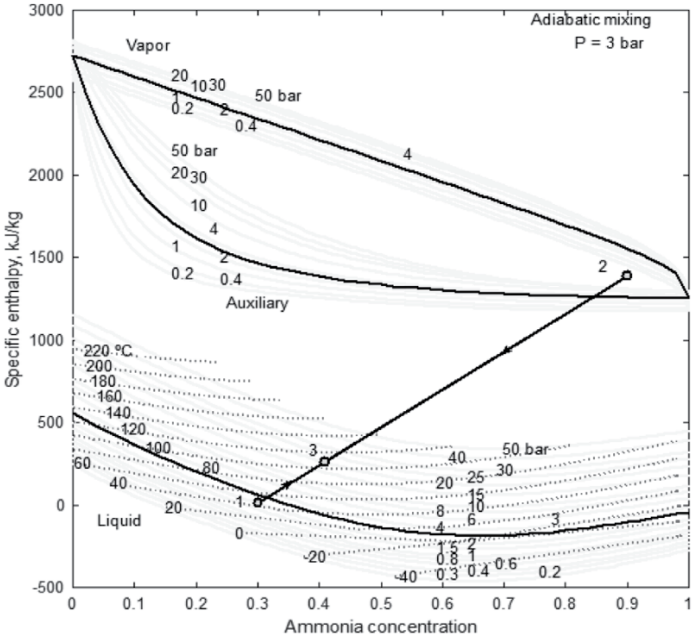

Fig. 3.10: Binary fluid system –adiabatic mixing

Fig. 3.10 shows the mixing process of two fluids on specific enthalpy-ammonia concentration diagram.

The simplification of the mass and energy balance equations, of mixing process results the final concentration and specific enthalpy of the mixer.

The mass balance equations are,

$$m_1 + m_2 = m_3 \tag{3.21}$$

and

$$m_1 x_1 + m_2 x_2 = m_3 x_3 \tag{3.22}$$

Similarly, the energy balance equation,

$$m_1 h_1 + m_2 h_2 = m_3 h_3 \tag{3.23}$$

Alternatively, the final concentration and specific enthalpy of the mixture can be evaluated from the lever rule without simplifications of the above three equations.

With reference to the Fig. 3.10, applying the lever rule,

$$\frac{m_2}{m_3} = \frac{x_3 - x_1}{x_2 - x_1} = \frac{h_3 - h_1}{h_2 - h_1} \tag{3.24}$$

$$x_3 = x_1 + \frac{m_2}{m_3}\left(x_2 - x_1\right) \tag{3.25}$$

Similarly,

$$h_3 = h_1 + \frac{m_2}{m_3}\left(h_2 - h_1\right) \tag{3.26}$$

3.3.6 Mixing of fluids with heat transfer (diabatic mixing)

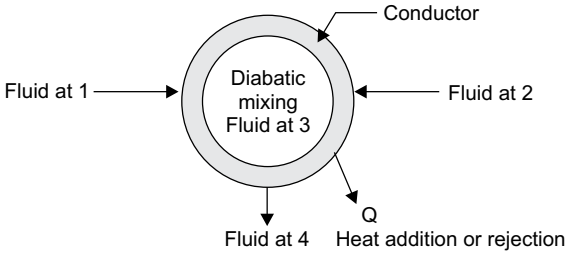

Fig. 3.11: Diabatic mixing of two fluids

Figure 3.11 depicts the heat transfer mixing of two steams into another stream.In an absorption system, the vapour absorbs into the weak solution and is followed by a heat rejection for the condensation of the liquid-vapour mixture. This is an example of diabatic mixing. In diabatic mixing, two fluids mix with each other and undergo either heat addition or heat rejection. Generally, these two processes happen simultaneously. For simplicity, these two processes are shown separately as adiabatically mixed and followed by a

heat transfer process.

Fig. 3.12 details the diabatic mixing on specific enthalpy and ammonia concentration diagrams. The line 1-3-2 shows the adiabatic process. The line 3-4 is the heat transfer process. The diabatic process is 1-2-4. In this process, heat has been rejected to condense the vapour.

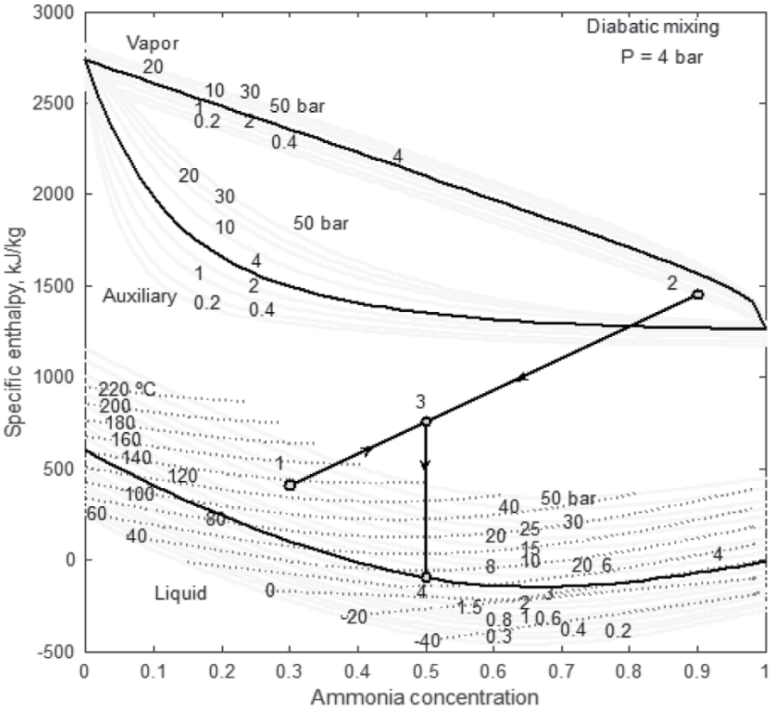

Fig. 3.12: Diabatic mixing in absorber to result a saturated liquid solution

The final concentration and specific enthalpy of the adiabatic process can be determined from the earlier formulation.

After the heat transfer, the concentration is the same as the mixture concentration. But the specific enthalpy changes as per the quantity of the heat transfer.

$$m_4 h_4 = m_3 h_3 + Q \text{ (+ for heat addition)} \tag{3.27}$$

$$m_4 h_4 = m_3\left(h_1 + \frac{m_2}{m_3}(h_2 - h_1)\right) + Q \tag{3.28}$$

$$h_4 = h_1 + \frac{m_2}{m_3}(h_2 - h_1) + \frac{Q}{m_3} \tag{3.29}$$

In case of heat rejection from the system,

$$h_4 = h_1 + \frac{m_2}{m_3}(h_2 - h_1) - \frac{Q}{m_3} \tag{3.30}$$

The general form is,

$$h_4 = h_1 + \frac{m_2}{m_3}(h_2 - h_1) \pm \frac{Q}{m_3} \tag{3.31}$$

In Eq. 3.31, the sign convention of heat transfer shows the direction of heat transfer. The positive sign indicates the heat addition as shown in Fig. 3.13 and the negative sigh is the heat rejection (Fig. 3.12). An absorber is a good example of a mixing and heat rejection process. At the inlet of the dephlegmator, two fluids, viz., from the pump and from the dephlegmator, mix with each other and are followed by a heat addition in the boiler (Fig. 3.6).

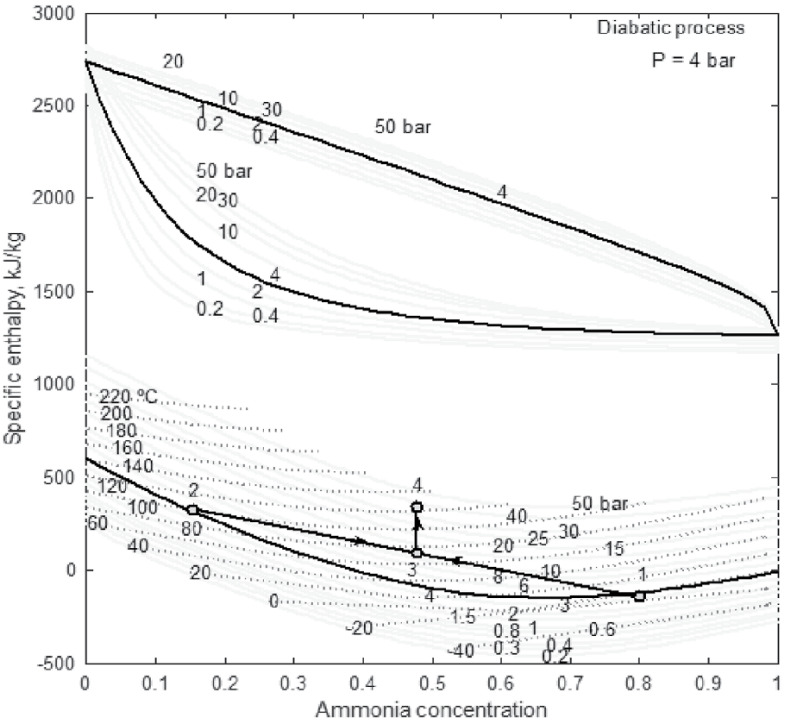

Fig. 3.13: Diabatic process with heat addition

3.3.7 Condensation

Fig. 3.14 shows the condensation of vapour (binary fluid) with the water-cooled condenser. As discussed in the earlier sections, during the phase change operation, the temperature of the binary fluid is variable, not a constant temperature. It results in a lower temperature difference between hot fluid (working fluid) and cold fluid (heat transfer fluid in this case). But a low temperature difference in a heat exchanger results a large surface area being heated at the same time. In a binary fluid cooling system, the vapour from the boiler is condensed at a high pressure and higher concentration. Since the pressure is high, the vapour can be condensed without diluting with the water at the surrounding (sink) temperature. But in the absorber, which is at low pressure, condensing the high concentration of vapour at the surrounding temperature is difficult as it demands a very low temperature for the condensation. Therefore, at the absorber, the condensation precedes a dilution of vapour with the water (weak mixture).

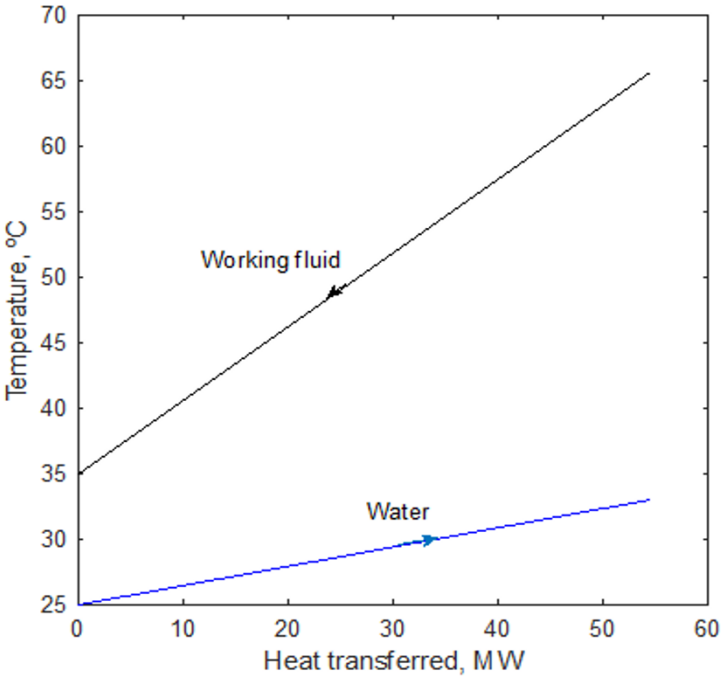

Fig. 3.14: Binary fluid system - condensation

3.3.8 Pumping

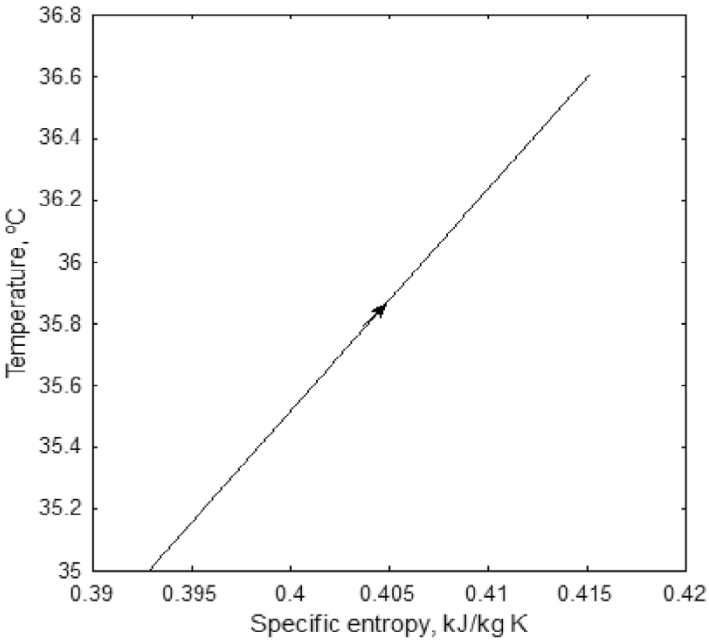

Fig. 3.15: Pumping of liquid solution from condenser pressure to boiler pressure

After condensing the vapour in the absorber, the solution has to be pumped to the boiler pressure. The pumping energy is a function of pressure, temperature, and concentration at the inlet and, similarly, pressure, temperature, and concentration at the outlet of the pump. Pressure and concentration play a major role compared to the temperature, which experiences a marginal increase in temperature through the pumping. Fig. 3.15 shows the temperature-specific entropy diagram of a pumping process in a binary fluid system. The temperature rises by less than 1 °C, depending on the specified process conditions. As a result of the dissipative effects, the entropy is increased as shown.

3.3.9 Throttling

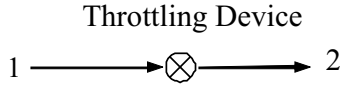

Fig. 3.16: Expansion of binary fluid through a restricted passage

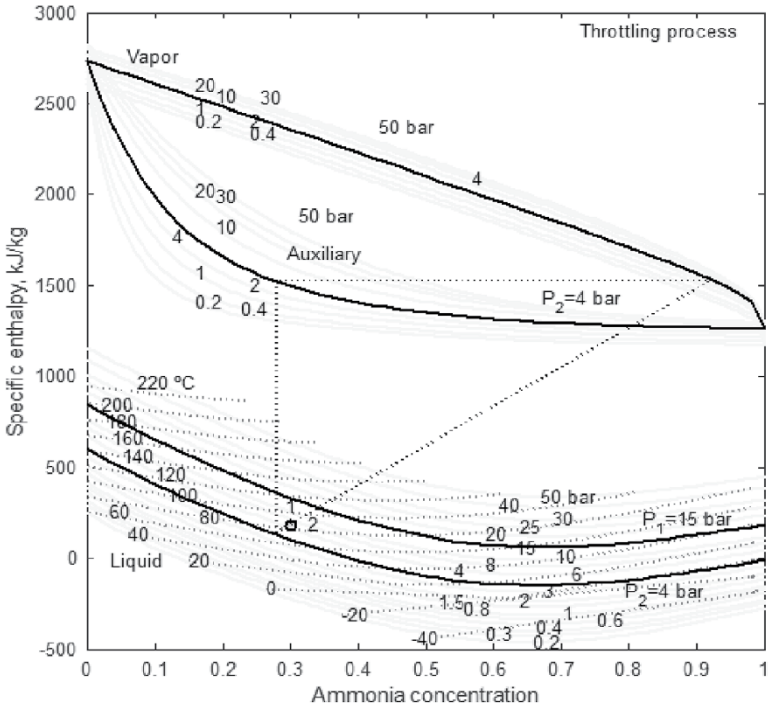

Fig. 3.17: Effect of concentration on throttling exit temperature

Fig. 3.16 shows the throttling of fluid through a restricted passage from high pressure to low pressure. The process has been shown in Fig. 3.17 as points 1-2. On a specific enthalpy and concentration diagram, the initial state and final state are the same due to no change in enthalpy and concentration during the process. In a binary fluid system, two throttling devices are used in a binary fluid cooling system. One is in the weak mixture path and the other one is in the vapour line. The concentration of a weak mixture is lower than the vapour concentration. Therefore, there is only expansion of the fluid from high pressure to low pressure without much change in the temperature. But the vapour concentration is high and the condensate of this concentration results in a very low temperature after the throttling. The temperature of the fluid decreases in the throttling process with the higher concentrations. This low temperature can be used for refrigeration and air conditioning applications. Then the question will come, how to show the inlet temperature and outlet temperature on the enthalpy-concentration chart. Fig. 3.17 shows the expansion of a weak mixture from high pressure to low pressure. State 1 with reference to high pressure is subcooled liquid, as it lies below the bubble point temperature curve of the high pressure. With reference to the low pressure, state 2 is a liquid-vapour mixture as it lies between the bubble point temperature curve

and the dew point temperature curve of the low pressure. The exit temperature of the throttling in this graphical solution can be obtained through the iteration method. Initially, a temperature has been assumed, a vertical line drawn till the auxiliary curve, a horizontal line till the dew point curve of the low pressure, and a meeting point between this point and the initial point. If the line is passing through the state of expansion, then the isothermal line shows the exit temperature, which has to be repeated for consistency.

Summary

Understanding and evaluating binary fluid systems requires a thorough understanding of binary fluid properties and processes. This chapter discussed the basics of the binary fluid system with the regions and particulars of the thermodynamic processes. It is simple to solve complex, binary fluid systems such as power plants, cooling plants, and cooling cogeneration plants with assistance.

Numerical Solutions

1. Solve the separation process at the exit of the evaporator of a binary fluid power plant with the following data. The boiler pressure, temperature and concentration at the inlet of separator 20 bar, 120 °C and 0.50 respectively.

Solution:

Boiler pressure, P = 20 bar
Separator temperature, T_{sep} = 120 °C
Strong solution concentration, x_{ss} = 0.5

At 20 bar and 120 °C, by referring the saturated liquid curve, we can identify the meeting point to find the liquid concentration. The same can be find from the property tables by refereeing bubble point temperatures and concentrations at the zero dryness fraction which is given for the reference.

Table 3.1: Saturated liquid properties of ammonia-water mixture at 20 bar

Property	Ammonia concentration (mass fraction), x										
	0	0.1	0.2	0.3	0.4	0.5	0.6	0.7	0.8	0.9	1
T, °C	213.15	182.30	155.92	131.82	110.10	91.66	77.16	66.61	59.25	53.84	49.15
v, m^3/kg	0.00	0.00	0.00	0.00	0.00	0.00	0.00	0.00	0.00	0.00	0.00
h, kJ/kg	911.87	719.80	547.89	395.47	269.88	179.55	129.46	118.95	141.40	185.36	237.05
s, kJ/kg K	2.46	2.24	1.96	1.66	1.38	1.14	0.97	0.87	0.83	0.83	0.80
x_l, kg/kg	0.00	0.10	0.20	0.30	0.40	0.50	0.60	0.70	0.80	0.90	1.00
x_v, kg/kg	0.00	0.00	0.00	0.00	0.00	0.00	0.00	0.00	0.00	0.00	0.00

The table indicates that the liquid concentration lies between 0.3 and 0.4 as the temperature is 120 °C. Between these two stages, the liquid concertation can be iterated.

The resulted concentration for the liquid,

$$x_l = 0.35$$

From the h-x diagram a vertical line from saturated liquid state up to the auxiliary curve and followed by a horizontal line till the saturation vapour curve results the vapour concentration as 0.92.

$$x_v = 0.92$$

Dryness fraction,

$$\delta = \frac{m_v}{m_l + m_v} = \frac{x - x_l}{x_v - x_l} = \frac{0.5 - 0.35}{0.92 - 0.35} = 0.26$$

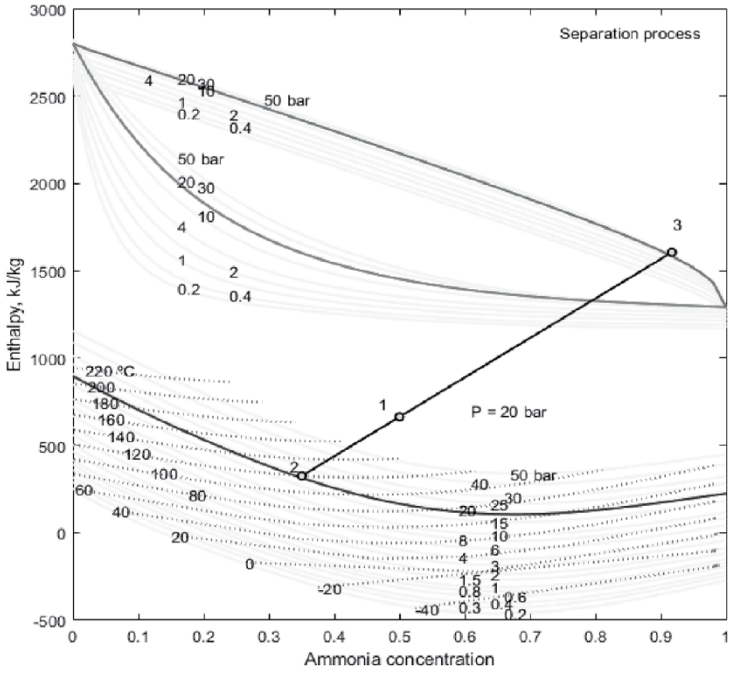

Fig. 3.18: Solution of separation process

If the mixture mass, m = 1 kg/s
Mass of liquid, $m_l = (1-\delta)\ m = 1 - 0.26 = 0.74$ kg/s
Mass of vapour separated, $m_v = \delta\ m = 0.26$ kg/s

Table 3.2 Saturated vapour properties of ammonia-water mixture at 20 bar

Property	Ammonia concentration (mass fraction), x										
	0	**0.1**	**0.2**	**0.3**	**0.4**	**0.5**	**0.6**	**0.7**	**0.8**	**0.9**	**1**
T, °C	210.36	206.10	201.05	195.16	188.35	180.48	171.29	160.27	146.25	125.54	47.51
v, m^3/kg	0.10	0.10	0.10	0.10	0.10	0.10	0.10	0.10	0.09	0.09	0.06
h, kJ/kg	279.42	267.08	255.84	242.54	230.95	217.68	205.06	191.79	171.80	165.22	125.60
s, kJ/kg K	6.34	6.36	6.30	6.20	6.07	5.92	5.74	5.53	5.28	4.95	4.12
x_l, kg/kg	0.00	0.00	0.00	0.00	0.00	0.00	0.00	0.00	0.00	0.00	0.00
x_v, kg/kg	0.00	0.10	0.20	0.30	0.40	0.50	0.60	0.70	0.80	0.90	1.00

From the chart or tables, at the pressure and liquid concentration, the enthalpy of liquid,

$$h_l = 329.05 \text{ kJ/kg}$$

From the chart or tables, at the pressure and liquid concentration, the enthalpy of vapour,

$$h_v = 1584.2 \text{ kJ/kg}$$

The enthalpy of the mixture,

$$\begin{aligned} h &= (1 - d)\ h_l + d\ h_v \\ &= (1 - 0.26)\ 329.05 + 0.26 \times 1584.2 \text{ kJ/kg} \\ &= 660.23 \text{ kJ/kg} \end{aligned}$$

2. A subcooled liquid of 0.82 kg/s of aqua–ammonia ($x_1 = 0.3$) at 47 °C and 3 bar mixes adiabatically with another liquid–vapor mixture with flow rate of 0.18 kg/s, 0.90 concentration and 60 °C at the same pressure. Establish the state points on *h–x* diagram and result, the mixture concentration, mixture enthalpy and isotherm through the mixture state using analytical or graphical method.

Solution

Given data

$$\begin{aligned} \text{Pressure} &= P_1 = P_2 = P = 3 \text{ bar} \\ m_1 &= 0.82 \text{ kg/s} \\ x_1 &= 0.3 \\ T_1 &= 47\ ^\circ\text{C} \\ m_2 &= 0.18 \text{ kg/s} \\ x_2 &= 0.90 \\ T_2 &= 60\ ^\circ\text{C} \end{aligned}$$

Analytical method

Table 3.3: Saturated liquid properties at 3 bar

Property	Ammonia concentration (mass fraction), x										
	0	**0.1**	**0.2**	**0.3**	**0.4**	**0.5**	**0.6**	**0.7**	**0.8**	**0.9**	**1**
T, °C	13.178	10.514	79.297	58.415	39.465	23.382	10.984	2.3846	-3.0981	-6.6712	-9.5568
v, m^3/kg	0.0011	0.001	0.001	0.001	0.0011	0.0012	0.0013	0.0014	0.0015	0.0015	0.0015
h, kJ/kg	56.256	36.027	20.845	62.559	-52.869	-15.334	-17.133	-18.812	-15.062	-10.788	-43.682
s, kJ/kg K	1.6718	1.3845	1.0776	0.7614	0.4562	0.1933	0.0005	-0.1087	-0.1431	-0.134	-0.1507

Table 3.4: Saturated vapour properties at 3 bar

Property	Ammonia concentration (mass fraction), x										
	0	0.1	0.2	0.3	0.4	0.5	0.6	0.7	0.8	0.9	1
T, °C	133.685	130.093	126.254	121.675	116.759	111.237	105.302	97.754	88.463	74.623	-8.468
v, m^3/kg	0.6046	0.6037	0.6022	0.5999	0.5968	0.5926	0.5871	0.5796	0.569	0.5504	0.4075
h, kJ/kg	275.27	257.21	249.51	232.12	214.88	207.36	199.36	189.83	167.22	155.11	123.72
s, kJ/kg K	6.9953	7.0076	6.9411	6.8399	6.7124	6.5617	6.388	6.187	5.959	5.641	4.775

Table 3.5: Liquid-vapour mixture properties at 3 bar, θ = 0.8

Property	Ammonia concentration (mass fraction), x								
	0.1	**0.2**	**0.3**	**0.4**	**0.5**	**0.6**	**0.7**	**0.8**	**0.9**
T, °C	124.5107	116.6792	108.9773	101.2736	93.679	86.2209	78.649	70.1772	58.3714
v, m^3/kg	0.2598	0.289	0.3126	0.336	0.3632	0.3946	0.4288	0.4628	0.4896
h, kJ/kg	135.3746	132.542	128.9566	125.6	124.3368	125.9512	128.1642	133.5248	133.4426
s, kJ/kg K	3.9108	4.0642	4.1481	4.2241	4.3364	4.4999	4.7069	4.9333	5.1331
x_l, kg/kg	0.0255	0.0503	0.0773	0.1069	0.1383	0.1709	0.2053	0.2451	0.3
x_v, kg/kg	0.247	0.4105	0.5464	0.6604	0.7528	0.8246	0.8735	0.9191	0.9585
h_l, kJ/kg	524.3762	467.9168	415.0521	361.806	308.74	256.4496	203.7158	145.7839	62.3553
h_v, kJ/kg	241.8312	220.5833	202.2564	188.4531	176.637	166.7657	161.8211	154.4797	146.4363

Table 3.6: Liquid-vapour mixture properties at 3 bar, θ = 0.9

Property	Ammonia concentration (mass fraction), x								
	0.1	**0.2**	**0.3**	**0.4**	**0.5**	**0.6**	**0.7**	**0.8**	**0.9**
T, °C	127.26	121.3523	115.2974	108.9997	102.4664	95.6255	88.1822	79.3368	66.5018
v, m^3/kg	0.4101	0.4235	0.435	0.4466	0.4608	0.4779	0.4965	0.5137	0.5225
h, kJ/kg	190.8145	182.2991	174.3163	166.5278	160.4373	156.5834	153.5988	150.7359	147.4247
s, kJ/kg K	5.2774	5.3204	5.3206	5.3059	5.308	5.3369	5.3859	5.4347	5.4364
x_l, kg/kg	0.0175	0.0352	0.0549	0.0772	0.1022	0.1301	0.1622	0.2021	0.2627
x_v, kg/kg	0.1823	0.3164	0.4366	0.546	0.6441	0.731	0.8075	0.8689	0.934
h_l, kJ/kg	548.1982	500.7047	458.4064	415.2056	370.0908	322.3799	270.1891	208.4766	121.1614
h_v, kJ/kg	249.2542	232.4759	216.3725	202.7212	190.5476	179.4144	168.2365	161.3758	151.0959

$$m_3 = m_1 + m_2 = 0.82 + 0.18 = 1.0 \text{ kg/s}$$

From the saturated liquid properties, at 3 bar, 0.3 concentration, and 47 °C, the liquid condition is subcooled, since the bubble-point temperature at this condition is 58.41 °C. 0.3 concentration vertical line and 47, °C will meet a point (State 1).

From the saturated tables with a pressure (2.1 bar) below the saturated pressure (3 bar)

$$h_1 = 13.10 \text{ kJ/kg}$$

At 3 bar, 60 °C liquid–vapor mixture and the concentration of 0.90,

$$\theta = \frac{T - T_{bp}}{T_{dp} - T_{bp}} = \frac{60 - (-6.6712)}{74.6323 - (-6.6712)} = 0.82$$

From the liquid-vapour mixture properties and iteration of properties between θ = 0.8 and 0.9,

$$h_2 = 1392.2 \text{ kJ/kg}$$

After the mixing of fluid 1 and fluid 2,

$$x_3 = x_1 + \frac{m_2}{m_3}(x_2 - x_1) = 0.3 + \frac{0.18}{1}(0.9 - 0.3) = 0.41$$

$$h_3 = h_1 + \frac{m_2}{m_3}(h_2 - h_1) = 13.10 + \frac{0.18}{1}(1392.2 - 13.10)$$

By referring the unsaturated properties at 3 bar and 0.41 concentration, the temperature of the mixture can be iterated with reference to the specific enthalpy.

The temperature after mixing is 55.3 °C

Graphical solution

The mixture obtained in the two-phase region is a blend of compressed liquid and liquid–vapor mixture. As per the lever rule, the distance between 1 and 3 is the ratio of mass at 2 to mass at 3 and between 2 and 3 is the ratio of mass at 1 to mass at 3. The solution is shown in enthalpy–concentration chart in Fig.3.19.

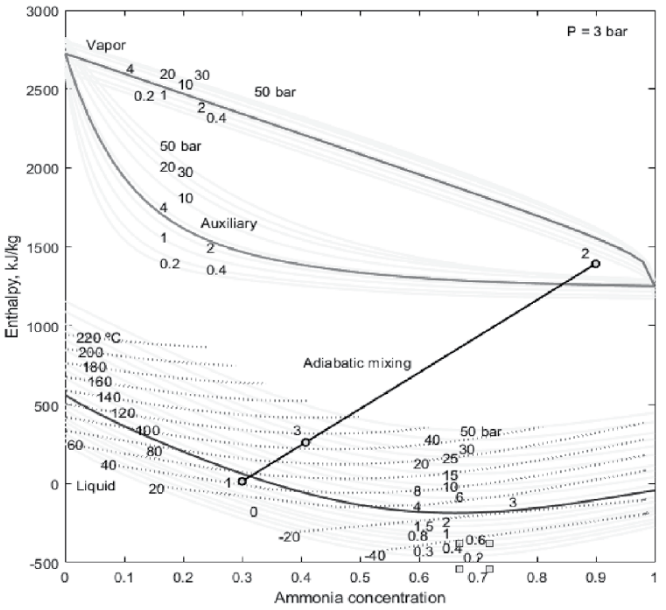

Fig. 3.19: Adiabatic mixing on enthalpy–concentration chart.

State 1 is established on the concentration enthalpy chart as the intersection of concentration and temperature 47°C. With reference to the saturation liquid curve, State 1 can be defined. If the state is below the curve, it is subcooled or compressed liquid on the curve shows the saturation state and above the state reveals the liquid–vapor mixture. Since State 1 lies below the saturation curve, it is subcooled state. State 2 can be obtained by drawing isotherm at 60 °C from saturated liquid at 3 bar, extension vertically up till auxiliary, followed by horizontal line till vapor curve and finally joint this saturation vapor point to the initial saturation liquid state. This inclined line is called isotherm. The isotherm will intersect the 0.90 concentration vertical line and it is termed as State 2. State 3 is located on the line joining 1–2 at the distance $m_2/m_3 = 0.18/1$, that is, 18% of the total length measured to the line 1 – 3.

From the graph, we can read the properties as follows

$x_3 = 0.41$, $h_3 = 261.33$ kJ/kg and $T_3 = 55.3$ °C.

3. A fluid of 20 kg/s of aqua–ammonia ($x_1 = 0.30$) at 85 °C and 4.0 bar mixes diabatically with liquid–vapor mixture supplied from a turbine with flow rate of 10 kg/s, 0.9 concentration and 70 °C at the same pressure. Heat is rejected from the system to the surroundings to condense the vapor into saturated liquid. Solve the diabatic mixing process in an absorber of Kalina cycle power plant.

Solution

Given data,

Pressure = $P_1 = P_2 = P_3 = P_4 = 4$ bar

$m_1 = 20$ kg/s

$x_1 = 0.3$

$T_1 = 85$ °C

$m_2 = 10$ kg/s

$x_2 = 0.9$

$T_2 = 70$ °C

Using tables:

At 4 bar, 0.3 concentration, the bubble-point temperature and dew point temperature are 67.67 °C and 131.14 °C respectively. Since the temperature of the fluid at state 1 (85 °C) lies between bubble point temperature and dew point temperature, this state is liquid-vapour mixture.

$$\theta_1 = \frac{T_1 - T_{bp}}{T_{dp} - T_{bp}} = \frac{85 - 67.67}{131.14 - 67.67} = 0.27$$

Iteration from the unsaturated fluid properties, between θ = 0.2 and 0.3,

$$h_1 = 407.89 \text{ kJ/kg}$$

At 4 bar, 0.9 concentration, the bubble-point temperature and dew point temperature are 0.88 °C and 81.41 °C respectively. Since the temperature of the fluid at state 1 (70 °C) lies between bubble point temperature and dew point temperature, this state is liquid-vapour mixture.

Table 3.7 Liquid-vapour mixture at 4 bar, θ = 0.2 and θ = 0.3

θ	Property	Ammonia concentration (mass fraction), x								
		0.1	0.2	0.3	0.4	0.5	0.6	0.7	0.8	0.9
0.2	T, °C	118.1154	98.3558	80.3663	63.8675	49.5864	38.1266	29.4918	22.96	16.9881
	v, m^3/kg	0.0239	0.0328	0.0426	0.0556	0.0745	0.1022	0.1411	0.1918	0.252
	h, kJ/kg	528.543	416.198	325.663	271.379	268.416	332.071	469.436	677.401	943.973
	s, kJ/kg K	1.8092	1.6614	1.5227	1.4435	1.4837	1.7015	2.1381	2.7966	3.6437
	x_l, kg/kg	0.0813	0.1609	0.2418	0.3163	0.3904	0.4566	0.5136	0.5633	0.6171
	x_v, kJ/kg	0.5405	0.7836	0.9027	0.9597	0.9827	0.9921	0.996	0.9978	0.9989
	h_l, kJ/kg	451.9022	314.8868	191.5818	79.8451	-5.9095	-67.4764	-107.4007	-131.823	-147.0848
	h_v, kg/kg	2050.483	1732.889	1580.108	1475.462	1412.617	1371.592	1344.887	1326.186	1309.734
0.3	T, °C	120.8396	103.0321	86.7131	71.631	58.4102	47.5574	39.0318	32.0959	25.0414
	v, m^3/kg	0.0379	0.0507	0.064	0.0809	0.1039	0.1351	0.1753	0.2235	0.2765
	h, kJ/kg	601.0573	510.4553	438.9752	402.3463	415.7579	488.7943	622.6948	808.932	1033.3331
	s, kJ/kg K	1.9933	1.9136	1.8401	1.828	1.9326	2.1958	2.6345	3.2319	3.9486
	x_l, kg/kg	0.0713	0.141	0.2126	0.2832	0.3438	0.4016	0.4511	0.4955	0.5466
	x_v, kg/kg	0.4974	0.7368	0.8669	0.9383	0.9705	0.9848	0.9915	0.995	0.9973
	h_l, kJ/kg	470.609	347.4358	234.5202	134.0461	46.1149	-17.3628	-62.9201	-96.1171	-124.7416
	h_v, kJ/kg	2105.6858	1795.575	1634.3376	1519.2741	1449.0406	1404.3645	1374.5545	1352.6749	1331.9885

Table 3.8: Liquid-vapour mixture at 4 bar, θ = 0.8 and θ = 0.9

θ	Pro-perty	Ammonia concentration (mass fraction), x								
		0.1	0.2	0.3	0.4	0.5	0.6	0.7	0.8	0.9
0.8	T, °C	134.4603	126.4136	118.4468	110.4484	102.5293	94.7111	86.7321	77.7758	65.3078
	v, m^3/kg	0.2052	0.2271	0.2443	0.2616	0.2816	0.3049	0.3303	0.3553	0.3744
	h, kJ/kg	1415.7706	1388.2173	1343.9579	1306.1449	1289.404	1297.2496	1325.2399	1363.7221	1396.2167
	s, kJ/kg K	4.0083	4.1501	4.2183	4.2787	4.3738	4.5176	4.7021	4.9032	5.0731
	x_l, kg/kg	0.0264	0.052	0.08	0.1107	0.1431	0.1768	0.2125	0.254	0.3092
	x_v, kJ/kg	0.2403	0.4011	0.5354	0.649	0.7421	0.8157	0.8668	0.9148	0.9563
	h_l, kJ/kg	567.2965	508.9585	454.1797	398.9865	343.9348	289.5787	234.6511	174.3093	88.9202
	h_v, kg/kg	2433.1038	2228.4847	2057.0381	1910.5568	1788.4777	1689.0896	1634.5155	1560.5675	1482.9896
0.9	T, °C	137.1845	131.0899	124.7935	118.2118	111.3531	104.1419	96.2722	86.9118	73.3611
	v, m^3/kg	0.3202	0.3311	0.3389	0.3467	0.3565	0.3686	0.382	0.3941	0.3995
	h, kJ/kg	1957.124	1883.7217	1798.8833	1717.6539	1651.3122	1602.4532	1567.6037	1538.6676	1498.9194
	s, kJ/kg K	5.3269	5.3752	5.3614	5.3308	5.3165	5.3282	5.3595	5.3894	5.3688
	x_l, kg/kg	0.0184	0.0368	0.0575	0.0809	0.1071	0.1364	0.17	0.2117	0.2749
	x_v, kg/kg	0.1788	0.3112	0.4303	0.539	0.6372	0.7247	0.8024	0.8657	0.9323
	h_l, kJ/kg	591.0581	541.8927	497.7745	452.5653	405.2529	355.1627	300.4078	235.878	145.2729
	h_v, kJ/kg	2511.4453	2342.9706	2191.358	2052.3861	1925.9283	1811.5513	1707.3196	1636.1967	1530.2392

$$\theta_2 = \frac{T_2 - T_{bp}}{T_{dp} - T_{bp}} = \frac{70 - 0.88}{81.41 - 0.88} = 0.86$$

Iteration from the unsaturated fluid properties, between θ = 0.8 and 0.9,

$$h_2 = 1453.3 \text{ kJ/kg}$$

After properties at state 3, (without considering heat transfer)

$$x_3 = x_1 + \frac{m_2}{m_3}(x_2 - x_1) = 0.3 + \frac{10}{30}(0.9 - 0.3) = 0.5$$

$$h_3 = h_1 + \frac{m_2}{m_3}(h_2 - h_1) = 407.89 + \frac{10}{30}(1453.3 - 407.89)$$

$$= 756.35 \text{ kJ/kg}$$

The state after the diabatic mixing is a saturated liquid condition. Therefore, the bubble point temperature at pressure and concentration at state 4 gives the saturation temperature.

From tables, the bubble point temperature,

$$T_4 = 31.94 \text{ °C}$$

Since it is the saturated liquid, from the saturated liquid properties

$$h_4 = -96.78 \text{ kJ/kg}$$

$$\frac{Q}{m_3} = h_1 + \frac{m_2}{m_3}(h_2 - h_1) - h_4$$

$$\frac{Q}{30} = 407.89 + \frac{10}{30}(1453.3 - 407.89) - (-96.78)$$

$$= 236.16 \text{ kJ/kg}$$

$$Q = 25594 \text{ kW}$$

Using chart:

State 1 is established on the concentration enthalpy chart from the temperature, pressure and concentration by drawing a vertical line and reaching via auxiliary line. Similarly, state 2 also can be located. Using the scale, and division of line proportional to the mass ratios, state 3 on line 1 - 2 can be located. Draw a vertical line to meet the saturated liquid state after the mixing.

$$T_4 = 32 \text{ °C}$$

Q can be calculated from the properties collected from the h-x graph.

$$Q = 25600 \text{ kW}$$

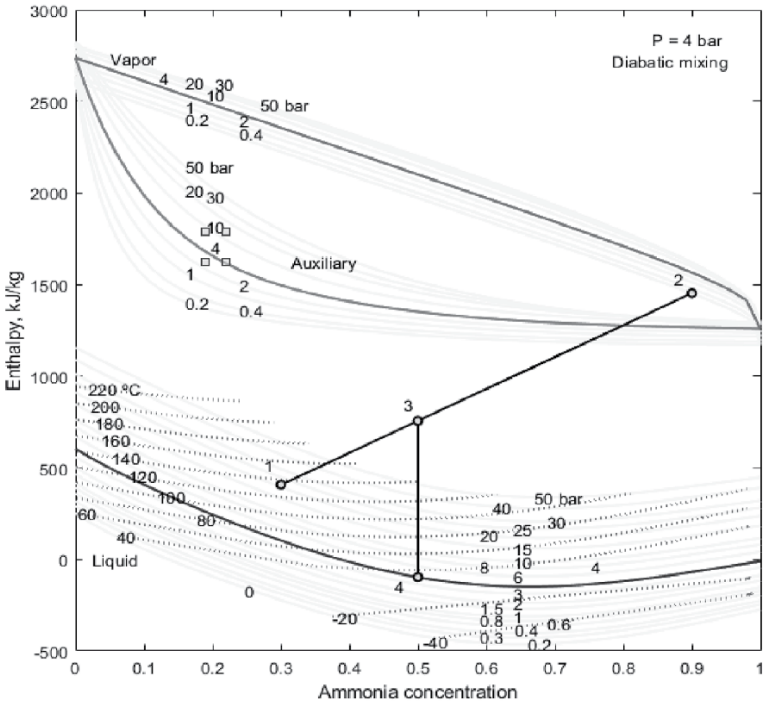

Fig. 3.20: Diabatic mixing on enthalpy–concentration chart

4. In a typical Kalina power plant, the weak solution is throttled from 15 bar to 4 bar with the ammonia mass concentration of 0.3. The temperature before throttling is 85 °C. Find the exit temperature of the fluid.

Solution

At 15 bar and 0.3 concentration

$$T_{bp} = 118.60\ °C$$

Since the temperature of the fluid is less than this bubble point temperature, the state 1 is a sub cooled liquid state as shown in Fig. 3.21.

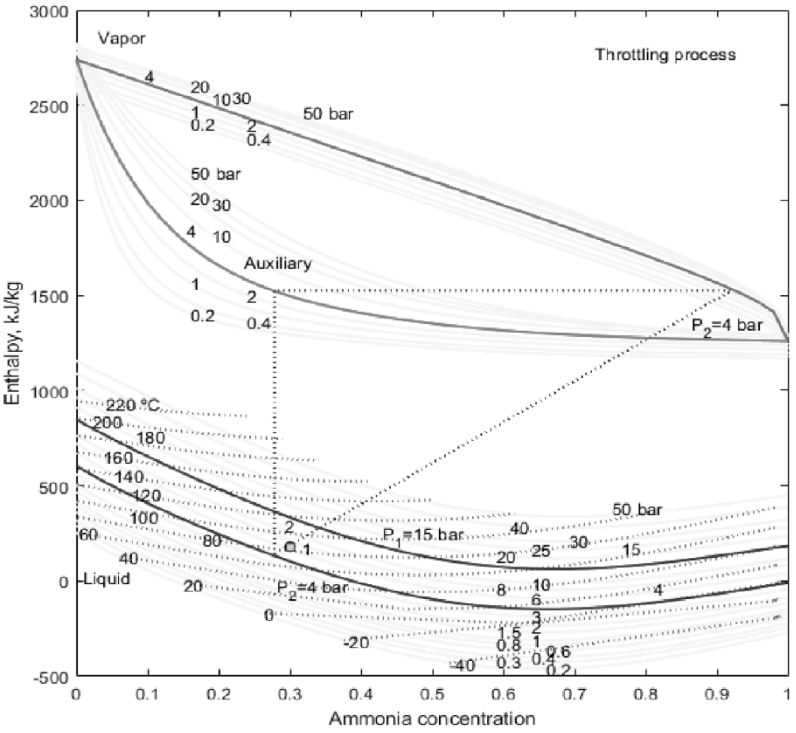

Fig. 3.21: Throttling of weak solution at 0.3 concentration

At 7 bar and 0.3 concentration

$$T_{bp} = 87.43\ °C$$ and specific enthalpy is 190.34 kJ/kg

After the iteration at $T_1 = 85\ °C$ at 0.3 concentration,

$$h_1 = 180.01\ kJ/kg$$

$$h_2 = h_1 = 180.01\ kJ/kg$$

With reference to the state 2, at 4 bar and 0.3 concentration,

$$T_{bp} = 67.67\ °C$$

The specific enthalpy at the bubble point temperature and low pressure is 102.97 kJ/kg. Since this enthalpy is less than h_2, the state should be above the bubble point temperature. Referring to unsaturated fluid properties,

At $\theta = 0.1$,

The temperature is 74.02°C.

Specific enthalpy is 214.86 kJ/kg

Therefore, interpolating the θ between 0 and 0.1,

The resulted temperature after throttling,

$$T_2 = 72.60\ °C$$

5. A fluid is expanding from 15 bar and 31 °C to 4 bar at the concentration of 0.75. Find the exit temperature of the fluid after throttling.

Solution

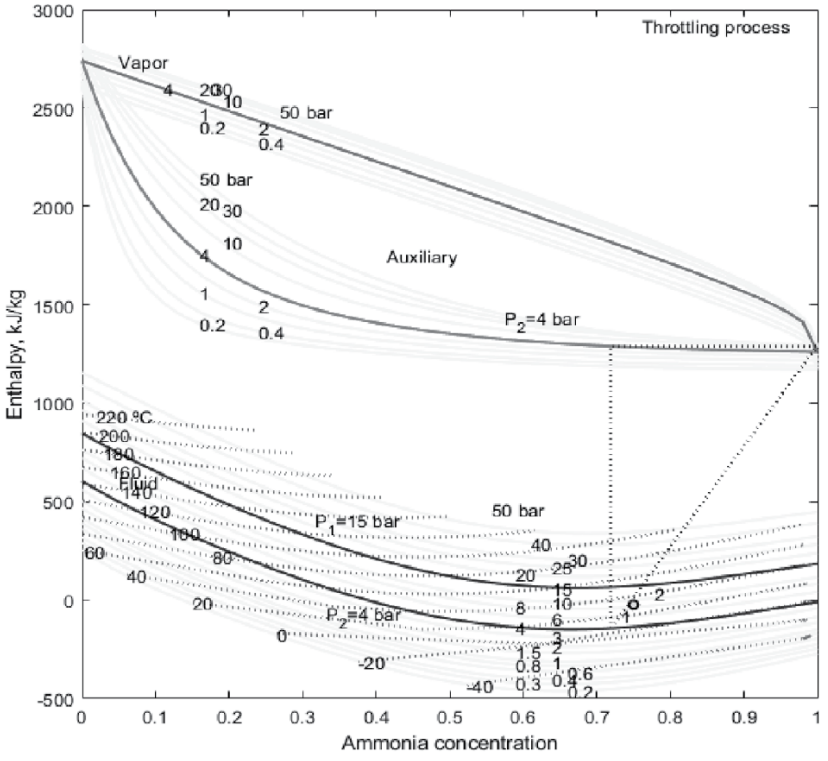

Fig. 3.22: Throttling of liquid at 0.75 concentration

Fig. 3.22 is plotted for the throttling solution, with the solution concentration 0.75. It results an exit temperature of 8.63 °C.

After the final iteration, the solution shows that an isotherm of 8.63 °C is passing through the state points 1 and 2.

At the exit of the state, i.e., state 2, the vapour concentration and liquid concentration of the liquid-vapour mixture are 0.99 and 0.72 respectively.

The dryness fraction of fluid after throttling,

$$\delta = \frac{m_v}{m} = \frac{x - x_1}{x_v - x_1} = \frac{0.75 - 0.72}{0.99 - 0.72} = 0.11$$

$$m_v = 0.11 \text{ kg/s}$$

The liquid mass is then,

$$m_l = m - m_v = 1 - 0.11 = 0.89 \text{ kg/s}$$

The vapour and liquid mass are 0.089 kg/s and 0.11 kg/s with the total mass of 1 kg/s mixture.

6. In the above problem if the concentration is changed to 0.95 in place of 0.75 keeping other conditions are same, find the exit temperature of the fluid after throttling.

Solution

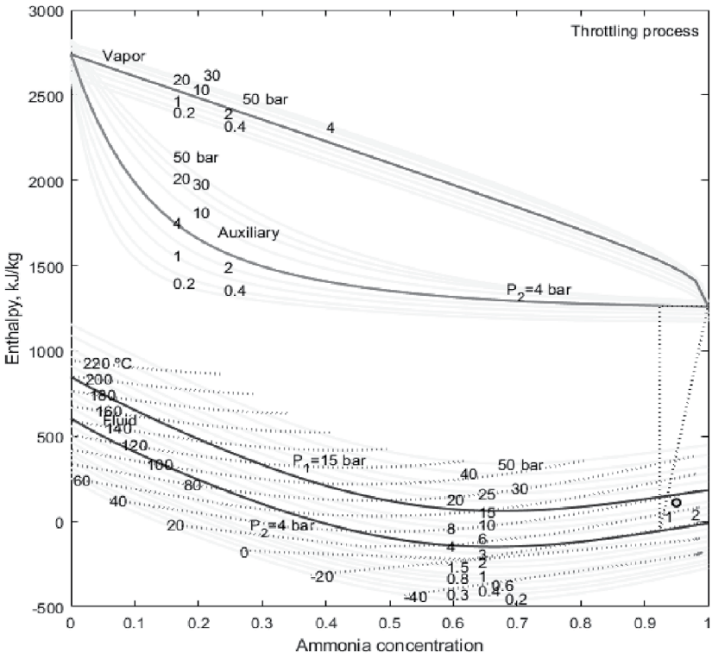

Fig. 3.23: Throttling on enthalpy–concentration chart with 0.95 concentration

Fig. 3.23 is plotted for the throttling solution, with the solution concentration 0.95.

The states before throttling and after throttling are subcooled liquid and liquid-vapour mixture respectively.

The throttling results an exit temperature of -0.49 °C. This is lower than the earlier solution. Therefore, it can be understood that the exit temperature of the throttling decreases with an increase in the concentration. Therefore, dephlegmator is used in the cooling system to result low temperature for heat absorption.

After the final iteration, the solution shows that an isotherm of -0.49 °C is passing through the state points 1 and 2.

At the exit of the state, i.e., state 2, the vapour concentration and liquid concentration of the liquid-vapour mixture are 1.0 and 0.92 respectively.

The dryness fraction of fluid after throttling,

$$\delta = \frac{m_v}{m} = \frac{x - x_1}{x_v - x_1} = \frac{0.95 - 0.92}{1.0 - 0.92} = 0.34$$

$$m_v = 0.34 \text{ kg/s}$$

The liquid mass is then,

$$m_l = m - m_v = 1 - 0.34 = 0.66 \text{ kg/s}$$

The vapour and liquid mass are 0.34 kg/s and 0.66 kg/s with the total mass of 1 kg/s mixture.

It can be noticed that, not only decreasing the low temperature in the throttling with the increase in the concentration, the vapour quantity also is increasing.

7. The boiler pressure in a typical vapour absorption system is 15 bar. The effectiveness of dephlegmator is 0.5. Consider the strong solution concentration as 0.5. The fluid at the inlet of the separator is 1 kg/s. The separator temperature is 110 °C. Solve the dephlegmator conditions.

Solution. (Fig. 3.24)

Refer Fig. 3.6 for the schematic arrangement of dephlemgator with the boiler.

The strong solution concentration, $x_{ss} = 0.5$

At 15 bar and 110 °C,

The separation process can be solved with the pressure and separator temperature.

The liquid concentration, $x_5 = 0.34$

The vapour concentration, $x_6 = 0.92$

From the effectiveness of dephlegmator and separator vapour concentration, the concentration at the exit of the dephlegmator can be determined.

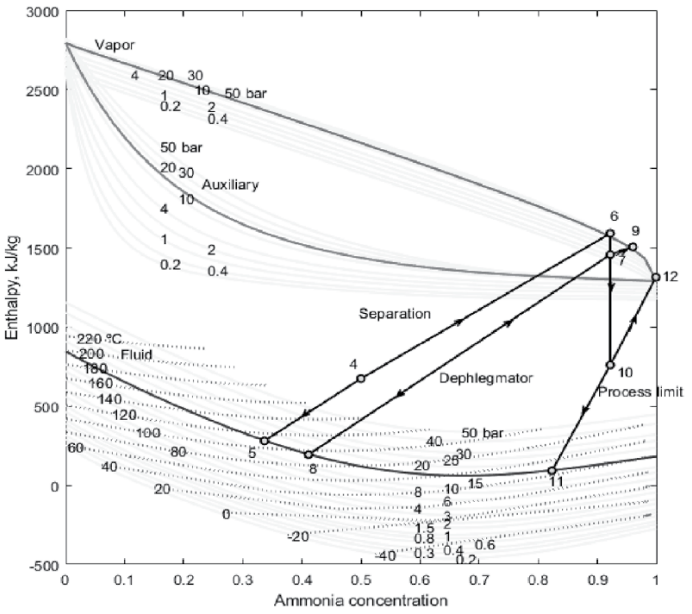

Fig. 3.24: Dephlegmator process and its process limit on enthalpy–concentration chart

The effectiveness of dephlegmator,

$$\text{Э}_{deph} = \frac{x_9 - x_6}{1 - x_6}$$

The concentration at the exit of dephlegmator,

$$\begin{aligned} x_9 &= x_6 + \delta_{deph}\,(1\text{-}x_6) \\ &= 0.92 + 0.5\,(1 - 0.92) \\ &= 0.96 \end{aligned}$$

The dryness fraction in the separator,

$$\delta_{sep} = \frac{m_v}{m} = \frac{x_4 - x_5}{x_6 - x_5} = \frac{0.5 - 0.34}{0.92 - 0.34} = 0.28$$

Mass of vapor separated from m_4,

$$m_6 = \delta_{sep} m_4 = 0.28 \times 1 = 0.28 \text{ kg/s}$$

Mass of liquid separated from m_4,

$$m_5 = (1 - \delta_{sep}) m_4 = (1 - 0.28) \times 1 = 0.72 \text{ kg/s}$$

The enthalpies can be obtained as

$$\begin{aligned} h_4 &= 674.8 \text{ kJ/kg} \\ h_5 &= 281.6 \text{ kJ/kg} \\ h_6 &= 1591.8 \text{ kJ/kg} \end{aligned}$$

From the pressure and concentration at state, 9

The dew point temperature, $T_9 = 94.62$ °C

At 15 bar and 94.62 °C,

The separation process can be solved with the pressure and separator temperature.

The liquid concentration, $x_8 = 0.34$

The vapour concentration, $x_9 = 0.96$

The enthalpies can be obtained as

$$h_7 = 1457.5 \text{ kJ/kg}$$
$$h_8 = 194.9 \text{ kJ/kg}$$
$$h_9 = 1506.9 \text{ kJ/kg}$$

The dryness fraction in the dephlegmator,

$$\delta_{deph,\max} = \frac{m_v}{m} = \frac{x_7 - x_8}{x_9 - x_8} = \frac{0.92 - 0.34}{0.96 - 0.34} = 0.93$$

Mass of vapor separated from m_7,

$$m_9 = \delta_{\text{deph}} m_7 = 0.93 \times 0.28 = 0.26 \text{ kg/s}$$

Mass of liquid separated from m_7,

$$m_8 = (1 - \delta_{\text{deph}}) m_7 = (1 - 0.93) \times 0.28$$
$$= 0.019 \text{ kg/s}$$

At the ideal case, the exit concentration of dephlegmator is 100%.

From the pressure and concentration (100%) at state, 12

The dew point temperature, $T_{12} = 46.13$ °C

At 15 bar and 46.13 °C,

The separation process can be solved with the pressure and separator temperature.

The liquid concentration, $x_{11} = 0.83$

The vapour concentration, $x_{12} = 1.00$

The dryness fraction in the dephlegmator with maximum process limit,

$$\delta_{deph,\max} = \frac{m_v}{m} = \frac{x_{10} - x_{11}}{x_{12} - x_{11}} = \frac{0.92 - 0.83}{1.00 - 0.83} = 0.56$$

Mass of vapor separated from m_{10},

$$m_{12} = \delta_{\text{deph, max}} m_{10} = 0.56 \times 0.28 = 0.16 \text{ kg/s}$$

Mass of liquid separated from m_7,

$$m_{11} = (1 - \delta_{\text{deph, max}}) m_{10} = (1 - 0.56) \times 0.28$$
$$= 0.12 \text{ kg/s}$$

The enthalpies can be obtained as

$$h_{10} = 760.2 \text{ kJ/kg}$$
$$h_{11} = 92.4 \text{ kJ/kg}$$
$$h_{12} = 1315.0 \text{ kJ/kg}$$

Review Questions

1. Prove the following to find the heat rejection from a diabatic mixing process.

$$\frac{Q}{m_3} = h_1 + \frac{m_2}{m}(h_2 - h_1) - h_4$$

   where state 1, 2 and 3 represents the adiabatic mixing and 3-4 for heat rejection.
2. Distillation of fluid at the exit of evaporator of boiler has merits and demerits. Analyze these two.
3. How to apply the lever rule in a binary fluid system?
4. Formulate the separation of two fluids in a binary fluid system with mass balance and energy balance.

❒

4 Binary Fluid Power

Abstract

The power plant designed with the binary fluid can be operated at a lower source temperature compared to the thermal power plant with water/steam as the fluid. A Kalina cycle (KC) uses an ammonia-water mixture as a working fluid. KC is also a modified Rankine cycle with added processes and components. In a polygeneration KC has a special role in the recovery of waste heat at the low temperature for the power generation in the KC analysis. The identified independent process conditions are strong solution concentration, the separator's vapour concentration, and source temperature. This chapter details the thermal model with analysis to determine the optimum process conditions.

4.1 Introduction

The Kalina cycle (KC) works with a binary fluid system suitable for the power generation. Power generation through binary fluid offers more benefits compared to the single fluid system. They are variable temperature of working fluid during phase change to get close temperature difference between hot fluid and working fluid, positive pressure in condenser (absorber) more internal heat recovery from weak solution to strong solution which minimises the economizer heat load, suitability to low heat source, flexibility to switch into cooling cogeneration, adoptability to polygeneration, and suitability to various heat sources such as geothermal, solar thermal, biomass, waste heat recovery etc. Compared to steam power plant, organic Rankine cycle (ORC) plant also has the benefit of internal heat recovery with the regenerator. But

T. Srinivas, *Thermal Polygeneration*,
https://doi.org/10.1007/978-3-031-37886-7_4

the amount of internal heat recovery in KC is much higher than the ORC plant. The subsequent chapters deal the ORC and organic flash cycle (OFC) for the power generation models. The OFC has more heat load in the economizer. The KC has least heat load in the economizer compared to the other thermal power plants. KC has the limitation in the selection of material for the equipment of the plant. Since ammonia is corrosive with copper and its alloys, these materials should be avoided in the plant components. Still, more research is needed to overcome the current challenges in the implementation, operation and maintenance of the plant for the power generation.

4.2 Kalina Cycle

Fig. 4.1 shows the plant layout of KC with a solar thermal collector as an energy source. The working fluid is ammonia-water mixture. Therefore, it holds the benefits of ORC and steam Rankine cycle. The plant configuration shown in Fig. 4.1 is suitable to low temperature heat recovery which is more common in use. The configuration changes with change in the level of source temperature. The components of KC are solar thermal concentrating collector, thermal storage, heat recovery vapour generator (HRVG) or boiler, separator, dephlegmator, vapour turbine, mixer, low temperature regenerator (LTR), absorber, solution pump, and high temperature regenerator (HTR). The HRVG consists of three sections viz. economizer, evaporator and superheater. The heat transfer fluid (HTF) in solar collecting system is VP therminol (solar fluid). The fluid generated in the evaporator is liquid-vapour mixture (14). Therefore, at the exit of evaporator, the liquid (15) and vapour (16) have been separated. The separated vapour has been distilled (16-21) in the dephlegmator to increase the vapour concentration. Dephlemgator is an optional component in the KC plant. It facilitates to operate the boiler at the low pressure at the same turbine concentration. In the binary fluid cooling system, it plays a major role as it increases the cooling effect and also coefficient of performance (COP) of vapour absorption refrigeration (VAR) unit. The distilled vapour (21) is a saturated vapour condition. Therefore, it has been superheated (21-1) before supplying to vapour turbine. Since the concentration in turbine is more compared to other components, the superheating is also an optional component. Water is a wet fluid, hence superheating and steam reheating is mandatory to save the steam turbine from the erosion. Since ammonia is an isentropic fluid, a small amount of degree of superheat is enough for the operation of binary fluid (ammonia and water) expansion. The superheated vapour is expanded in the turbine (1-2) and generates the electricity. This expanded vapour (2) to be condensed into saturated liquid state. But it is difficulty to condense this vapour as it needs very low temperature as the concentration of vapour is high. Therefore, it is diluted with the weak solution (19) for the easy condensation in the absorber. Absorber may be air cooled or water cooled heat exchanger. In this case, absorber is a water cooled condenser (4-5). The

vapour is absorbed into the liquid by rejecting the heat to the environment. The dilution of the vapour decreases the concentration (2-3) and increases the condensation temperature as the water's saturation temperature is higher than the ammonia's saturation temperature at the same pressure. The temperature at the exit of steam turbine is closed to the condensation temperature, hence therefore no internal heat recovery or regenerator at the exit of steam turbine. But the vapour temperature at the exit of vapour turbine is higher than the condensation temperature. Therefore, there is a scope for internal heat recovery before suppling to the absorber. After diluting the vapour with the weak solution, it is capable of transferring the heat to the pumped solution. It also saves the boiler load apart from the absorber capacity. The temperature of mixture is decreased in the LTR (3-4) by rejecting the heat to the strong solution (7-10). At the exit of absorber, the state of fluid is saturated liquid (5) and it is also called as strong solution as its concentration is higher than the weak solution's concentration. The strong solution is pumped (5-6) from the absorber pressure to boiler pressure. This strong solution has been parted in to two streams viz. steam to boiler (7) and stream to dephlegmator's cooling (8). The use of strong solution as a cooling medium in the dephlegmator instead of rejecting the heat to surroundings increases the efficiency of the system. The main stream of strong solution passes into LTR (7-10), gains heat and flows in the HTR (10-11) for the internal heat recovery. At the exit of HTR, the fluid (11) is mixed with the heated strong solution (9) and liquid return (20) from the dephlegmator. This mixed fluid (12) is supplied to the HRVG. In the first part of HRVG, i.e. economizer, the fluid temperature is increased (12-13) up to the bubble point temperature (BPT). Later, the fluid temperature is increased in the evaporator (13-14). In the evaporator the fluid temperature increases as it is a binary fluid. The fluid is not heated up to the dew point temperature (DPT). Below the DPT and above the BPT, the fluid exists in liquid vapour mixture (14). The liquid (15) and vapour (16) have been divided in the separator unit. The vapour is supplied to the dephlegmator, where, the fluid is cooled (16-17) with the parted strong solution. The water (20) from the fluid in dephlegmator is condensed first with the cooling as its condensation temperature is higher than the ammonia concentration. The concentration of vapour is increased by removing the water which is also called as distillation of the fluid. Another part from the separator is saturated liquid (15) which is known as weak solution due to its lower concentration. The weak solution is also capable of internal heat recovery. The heat rejection from the weak solution to the feed solution at the higher temperature is formed as HTR. The HTR saves the size of absorber and condenser. The weak solution throttles in the valve from the boiler pressure to absorber pressure (18-19). The weak solution, turbine exit vapour mixed at the low pressure. The cycle repeats for the continuous generation of electricity. The source consists of series of solar thermal collector. The HTF flows between collectors, and working fluid.

The collector also consists of storage for the uniform generation of electricity irrespective status of sun beam.

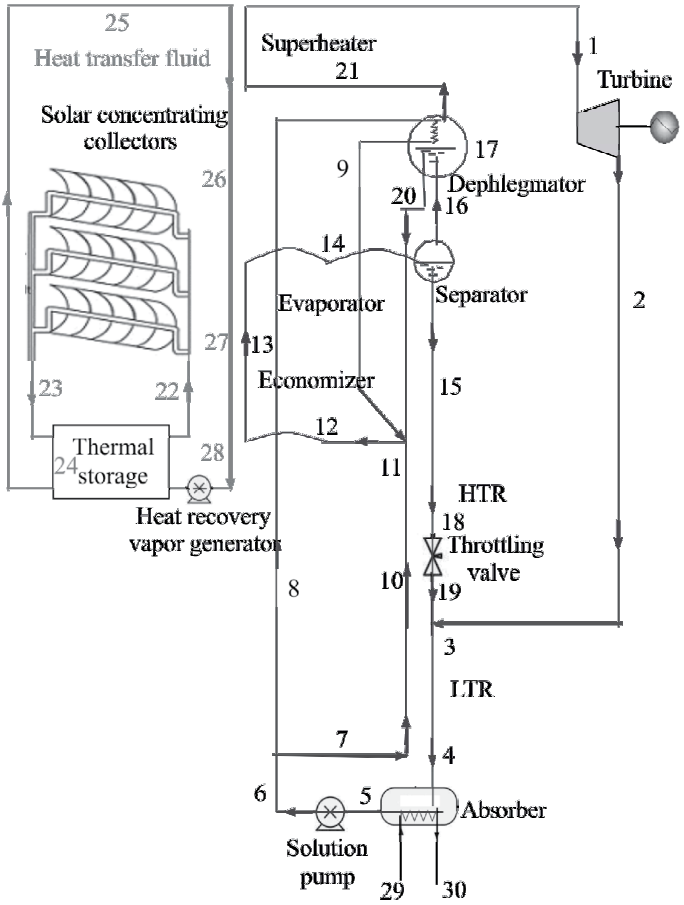

Fig. 4.1: Binary fluid system for power generation

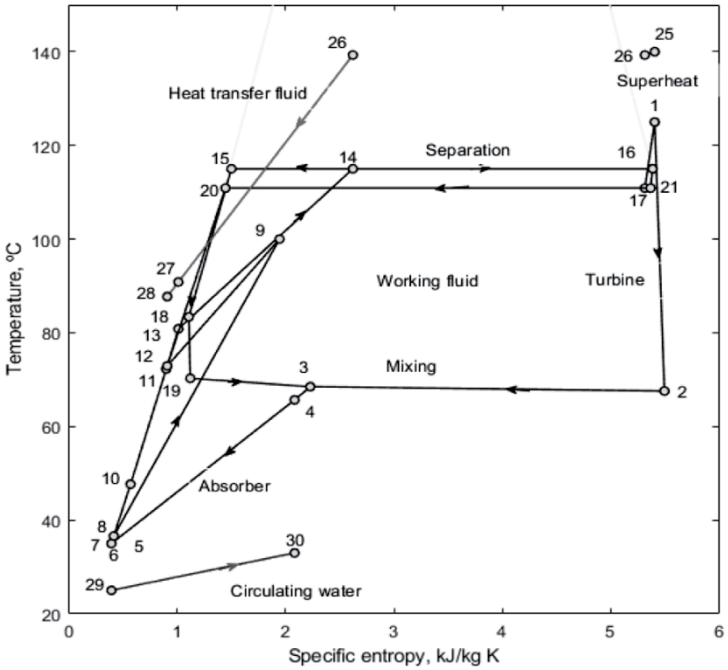

Fig. 4.2: Binary fluid power plant on temperature-specific entropy diagram

Fig. 4.2 shows the KC on the temperature-specific entropy (T-s) diagram. Binary fluid processes are different compared to single fluid processes. In particular, the phase change occurs with the variable temperature. The T-s diagram also adds the heat source and heat sink fluids, viz., HTF and circulating water, respectively, at HRVG and absorber. The separation of fluid at the exit of the boiler is shown as a horizontal line (15-14-16). Similarly, the distillation in the dephlegmator is a horizontal line (20-17-21). The mixing process has been shown as a line (19-3-2). The condensation process in the absorber is a variable temperature line (3–4-5). Similarly, the heat addition in the evaporator is also a variable temperature line (13–14).

4.3 Thermal Model of Binary Fluid Power Plant

Thermodynamic properties of binary fluid have been developed to solve the processes involved in the KC power plant. The following are the assumptions used in the thermal modelling of the solar thermal power plant.

The solar concentrator used for power generation is a cylindrical parabolic collector (CPC). The average solar radiation at the local conditions (Jalandhar, India) has been simulated, and it is 515 W/m^2 of the global component. The circulating water supply temperature to the absorber is 30°C. The degree of superheat under consideration is 10 °C. The terminal temperature difference

(TTD) in the superheater between HTF and the turbine inlet temperature is 15 °C. The TTD in the condenser is the temperature difference between the binary fluid and the circulating water exit temperature, and it is 5 °C. The boiler maximum pressure is determined by the separator temperature and strong solution concentration. Similarly, the boiler minimum pressure is determined by the absorber exit pressure and strong solution concentration. The maximum and minimum boiler pressures are used in the analysis of plants with a change in boiler pressure between these two limits. A dephlegmator is used to increase the concentration of vapour after the boiler. The maximum limit of concentration is 100%. The effectiveness of a dephlegmator is defined as the actual concentration rose to the maximum concentration change through the distillation process in the dephlegmator. In the current analysis, the effectiveness of dephlegmator is kept at 15% as a minor amount is sufficient in the KC plant. The strong solution flow rate in the absorber is 100 kg/s (Ganesh and Srinivas, 2012).

The simplification of mass balance equations in the separator results in the dryness fraction in the separator.

The dryness fraction in separator,

$$\delta_{\text{sep}} = \frac{m_v}{m_{mixture}}$$

$$= \frac{x_{14} - x_{15}}{x_{16} - x_{15}} \tag{4.1}$$

Similarly, the dryness fraction in dephlegmator,

$$\delta_{deph} = \frac{x_{16} - x_{20}}{x_{21} - x_{20}} \tag{4.2}$$

After the simplification of equations, the working fluid in the turbine,

$$m_1 = \frac{\delta_{sep}\delta_{deph}m_3}{1 + \delta_{sep}\delta_{deph} - d_{sep}} \tag{4.3}$$

The working fluid in the boiler,

$$m_{12} = \frac{m_1}{\delta_{sep}\delta_{deph}} \tag{4.4}$$

The weak solution,

$$m_{12} = \frac{1 - \delta_{sep}m_1}{\delta_{sep}\delta_{deph}} \tag{4.5}$$

From the energy balance in dephlegmator,

$$m_8 = \frac{m_{16}(h_{16} - h_{17})}{(h_9 - h_8)} \tag{4.6}$$

From the energy balance in HTR,

$$h_{18} = h_{15} - \frac{m_{10}(h_{11} - h_{10})}{m_{15}} \tag{4.7}$$

From the mixing/absorption of the fluids at the inlet of absorber,

$$x_3 = \frac{m_2 x_2 + m_{19} x_{19}}{m_3} \tag{4.8}$$

and

$$h_3 = \frac{m_2 h_2 + m_{19} h_{19}}{m_3} \tag{4.9}$$

From the mixing of fluids at the inlet of boiler,

$$h_{12} = \frac{m_9 h_9 + m_{11} h_{11} + m_{20} h_{20}}{m_{12}} \tag{4.10}$$

From the energy balance in LTR,

$$h_4 = h_3 - \frac{m_7(h_{10} - h_7)}{m_4} \tag{4.11}$$

The circulating water requirement in the absorber for the condensation of vapour,

$$m_{29} = \frac{m_4(h_4 - h_5)}{c_{pw}(T_{30} - T_{29})} \tag{4.12}$$

The HTF in the boiler from the solar concentrating collector is evaluated from the energy balance in evaporator and superheater,

$$m_{25} = \frac{m_{13}(h_{14} - h_{13}) + m_1(h_1 - h_{21})}{c_{p\ HTF,25} T_{25} - c_{p\ HTF,27} T_{27}} \tag{4.13}$$

From the energy balance in superheater,

$$h_{26} = h_{25} - \frac{m_1(h_1 - h_{21})}{m_{25}} \tag{4.14}$$

From the energy balance in economizer,

$$h_{28} = h_{27} - \frac{m_{12}(h_{13} - h_{12})}{m_{28}} \quad (4.15)$$

The size of the CPC has been determined from the standard heat transfer correlations and equations of the solar concentrating collector (Duffie and Beckman, 2013).

The power generation in vapour turbine,

$$W_t = m_1 (h_1 - h_2) \quad (4.16)$$

The energy supply to pump,

$$W_p = m_5 (h_6 - h_5) \quad (4.17)$$

Thermal efficiency of solar thermal power plant,

$$\eta_{pt} = \frac{W_t - W_{solution\ p} - W_{cw\ p} - W_{HTF\ p}}{0.001 G A_{CPC}} \quad (4.18)$$

In the above equation, G is the global solar radiation and A_{CPC} is the solar collector's area.

4.4 Results and Discussions

The identified key independent KC conditions are HTF source temperature, strong solution concentration, and HRVG pressure. Fig. 4.3 shows the effect of these three conditions on the power generation of the plant. Fig. 4.3a-f shows the effect of strong solution concentration from a concentration of 0.3 to 0.55. The temperature of the HTF supply has been raised from 135 °C to 160 °C. The HRVG pressure is changed from the minimum pressure related to the sink to the maximum pressure related to the source. The pressure range changes with the changes in the operational conditions. The power generation capacity is decreasing with an increase in strong solution concentration. A low concentration fluid generates more power due to the presence of more steam. The expansion in the turbine increases with an increase in the source temperature. Therefore, the power generation increases with an increase in the HTF supply temperature. The lower concentration has no effect on the peak in power generation. From the concentration of 0.4 onwards, power peaks result from the change in HRVG pressure. HRVG demands low pressure at all the strong solution concentrations. The pinch point constraint in the HRVG limits the optimum boiler pressure to a low pressure. In conventional thermal power plants, such as fuel-fired units, there is no such pinch point limit. Therefore, these conventional thermal power plants demand high-pressure boilers. The low pressure boiler with heat recovery facilitates the low maintenance and low cost equipment.

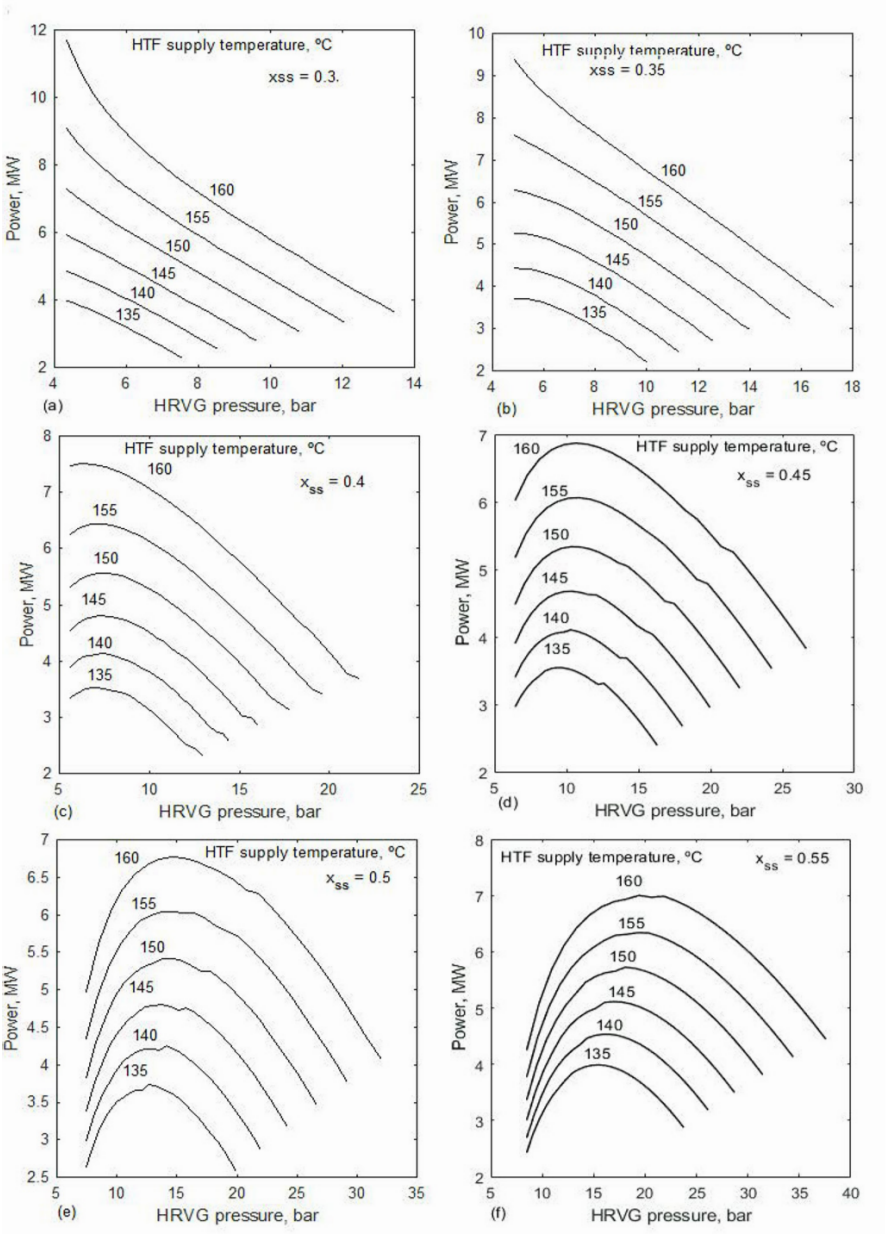

Fig. 4.3: Power generation from binary fluid solar thermal power plant as a function of HTF supply temperature, strong solution concentration and boiler pressure

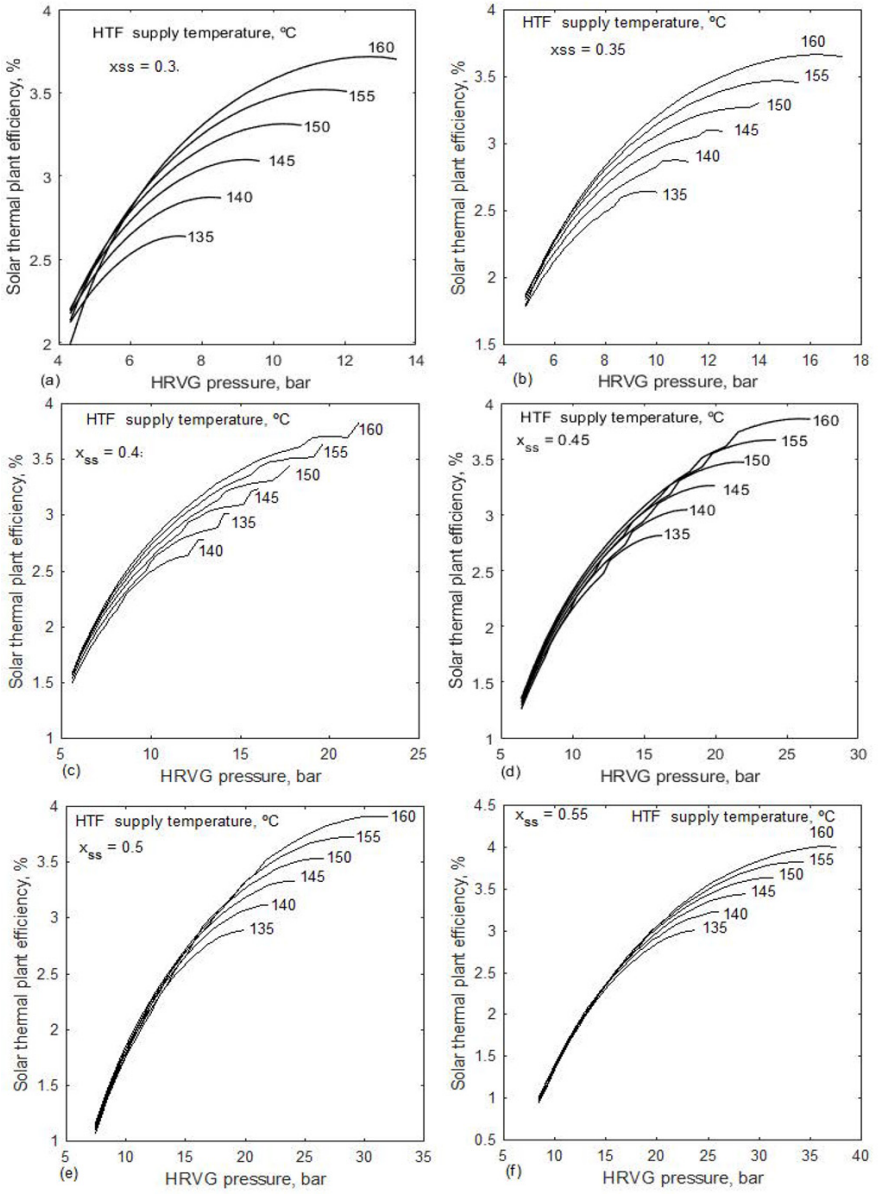

Fig. 4.4: Thermal efficiency of binary fluid solar thermal power plant as a function of HTF supply temperature, strong solution concentration and boiler pressure

Fig. 4.4 analyses the effect of HTF supply temperature, boiler pressure, and strong solution concentration on the thermal efficiency of a solar thermal

power plant. Fig. 4.4a-f studies the effect of strong solution concentration from 0.3 to 0.55. With an increase in strong solution concentration, the performance curves are tightening around each other. It shows the influence of the HTF source temperature. The efficiency of the plant is increasing with an increase in the boiler's pressure but declining due to the drop in output. Even though the power is decreasing with an increase in the strong solution concentration, the thermal efficiency of the solar power plant is increasing with an increase in the concentration. Based on the objective, a strong solution concentration can be selected. If the focus is on maximum power generation, a lower strong solution concentration is recommended. A higher concentration is required for the higher thermal efficiency.

Table 4.1 lists the thermodynamic simulation results evaluated at the optimum boiler pressure of 17.47 bar. To generate 100 kg/s of strong solution, the required thermic fluid in the solar thermal concentrating collector is 680.51 kg/s. The high pressure and low pressure in this Kalina cycle are 17.47 and 5.49, respectively, at HRVG and absorber. Five concentrations are observed in the power cycle, viz., 0.34, 0.36, 0.55, 0.92, and 0.93, because of the dephlegmator with internal heat recovery. The weak solution concentration and strong solution concentration are 0.34 and 0.55, respectively. As per the selected role of dephlegmator (15%), the concentration is increased from 0.92 to 0.93. The power plant's thermodynamic fluid supply temperature is 140 °C. With this supply temperature, the turbine inlet temperature is 125 °C. After the heat recovery in the HRVG, the thermic fluid supply temperature to the solar collector is 84.68 °C.

Table 4.1 Thermodynamic properties of the binary fluid power plant with solar thermal concentrating collector at the optimum boiler pressure.

State	P, bar	T,°C	x	m, kg/s	h, kJ/kg	s, kJ/kg K
1	17.47	125.00	0.93	34.93	1590.54	4.96
2	5.49	67.33	0.93	34.93	1425.79	5.04
3	5.49	70.40	0.55	100.00	602.71	2.46
4	5.49	67.37	0.55	100.00	555.97	2.33
5	5.49	35.00	0.55	100.00	-79.00	0.36
6	17.47	36.71	0.55	100.00	-70.27	0.39
7	17.47	36.71	0.55	98.78	-70.27	0.39
8	17.47	36.71	0.55	1.22	-70.27	0.39
9	17.47	100.00	0.55	1.22	556.58	2.17
10	17.47	47.10	0.55	98.78	-22.95	0.54
11	17.47	67.24	0.55	98.78	70.12	0.82
12	17.47	68.91	0.55	100.75	77.73	0.84
13	17.47	78.27	0.55	100.75	122.03	0.97
14	17.47	115.00	0.55	100.75	795.46	2.79

15	17.47	115.00	0.34	65.07	303.14	1.45
16	17.47	115.00	0.92	35.68	1597.98	4.97
17	17.47	111.44	0.92	35.68	1576.57	4.92
18	17.47	84.23	0.34	65.07	161.36	1.07
19	5.49	73.21	0.34	65.07	163.80	1.08
20	17.47	111.44	0.36	0.75	282.57	1.40
21	17.47	111.44	0.93	34.93	1553.79	4.87
22	1.01	84.68	- -	680.51	102.59	0.31
23	1.01	140.00	- -	680.51	208.53	0.59
24	1.01	140.00	- -	680.51	208.53	0.59
25	1.01	140.00	- -	680.51	208.53	0.59
26	1.01	139.06	- -	680.51	206.64	0.59
27	1.01	88.27	- -	680.51	109.14	0.33
28	1.01	84.68	- -	680.51	102.59	0.31
29	1.01	25.00	- -	1898.83	0.00	0.00
30	1.01	33.00	- -	1898.83	33.44	0.11

4.5 Summary

The boiler pressure can be optimised to generate the maximum power from the thermal power plant with waste heat recovery. Keeping this in mind, the analysis has been focused on optimising the boiler pressure with a change in strong solution concentration and thermic fluid supply temperature. The results show that the optimum boiler pressure increases with an increase in strong solution concentration for the maximum power production. No significant change in optimum boiler pressure has been observed with the change in heat transfer fluid supply temperature for maximum power generation. The maximum thermal efficiency demands a high-pressure boiler, a strong solution concentration, and a high heat transfer fluid supply temperature. The strong solution is playing differently on power and thermal efficiency. Low and high-strength solution concentrations are recommended for maximum power and maximum thermal efficiency, respectively.

Numerical Solutions

1. The layout of a basic Kalina cycle consists of turbine, absorber, pump, boiler (economizer and evaporator), separator and throttling. The separator temperature is 150 °C. The boiler pressure is 15 bar. The strong solution concentration is 0.4. In the absorber, the fluid is condensed to 35 °C. For unit mass flow of strong solution, find the capacity of heat exchangers, power generation and thermal efficiency of a simple KC. Assume an isentropic process in pump and turbine.

Solution

With reference to Fig. 4.5 the given data of KC is

$P_7 = 15$ bar
$T_7 = 150$ °C
$T_4 = 35$ °C
$x_{ss} = x_4 = 0.4$

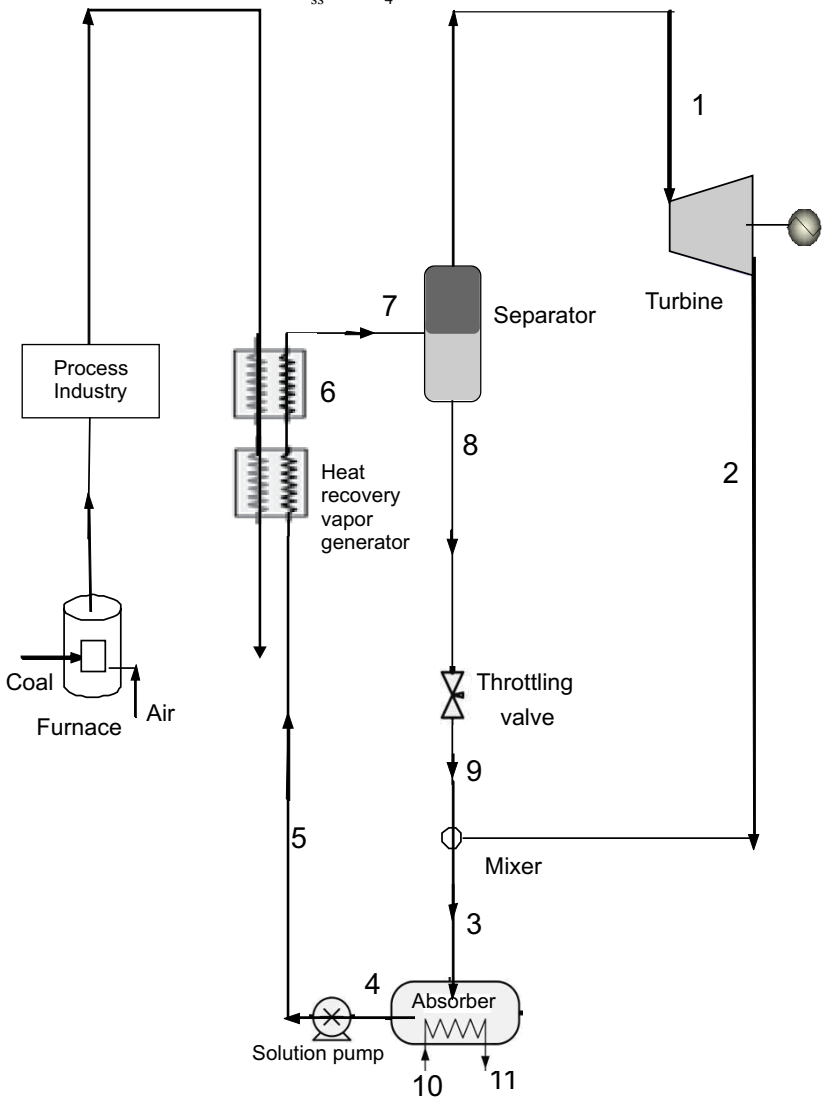

Fig. 4.5: Basic Kalina cycle

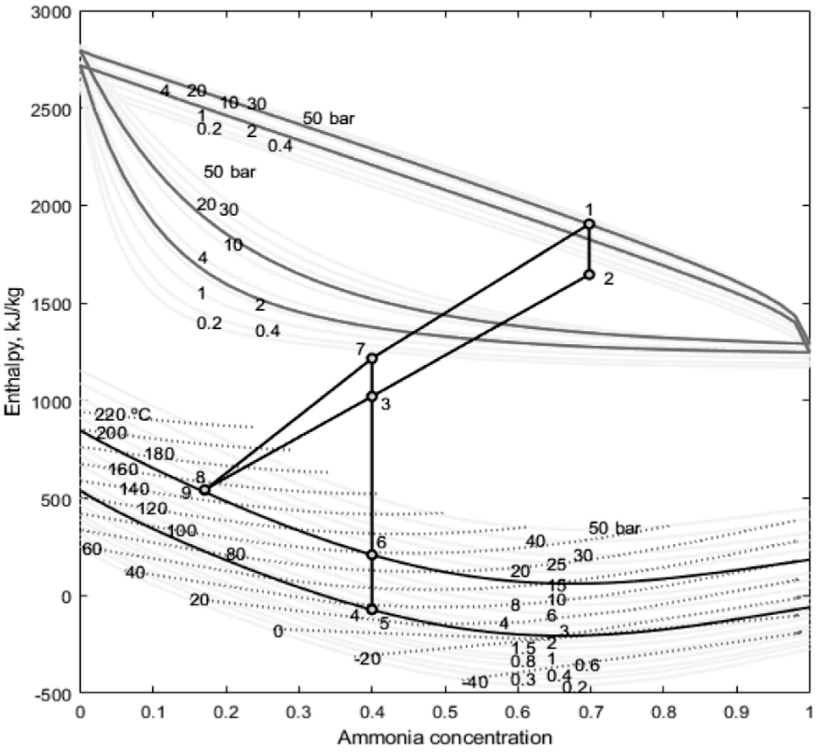

Fig. 4.6: Basic KC enthalpy-concentration chart

The separator can be solved from the given pressure and temperature, The pressure and temperature results liquid concentration and vapour concentration.

From the saturated liquid tables at 15 bar and 150 °C,

$$x_l = x_8 = 0.17$$

Similarly, from the saturated vapour tables at 15 bar and 150 °C,

$$x_v = x_1 = x_2 = 0.698$$

The low pressure in absorber can be determined from the sink temperature (saturated liquid temperature) and strong solution concentration.

From the saturated liquid properties, at 0.4 concentration and 35 °C,

$$P_4 = 2.58 \text{ bar}$$

For isentropic process in pump,

$$s_4 = s_5 = 0.40 \text{ kJ/kg K}$$

The state after pumping can be referred from the saturated liquid properties,

At 0.4 concentration and 0.4 kJ/kg K of specific entropy,

$$T_5 = 35.25 \text{ °C}$$

The dryness fraction of separator,

$$\delta_{sep} = \frac{x_m - x_l}{x_v - x_l} = \frac{x_7 - x_8}{x_1 - x_8} = \frac{0.4 - 0.17}{0.698\text{-}0.17} = 0.435$$

Let the strong solution, $m_4 = 1$ kg/s

The mass flow in turbine, $m_1 = \delta_{sep}\, m_7 = 0.435 \times 1 = 0.435$ kg/s

The weak solution flow rate, $m_8 = (1 - \delta_{sep})\, m_7 = (1 - 0.435) \times 1 = 0.565$ kg/s

The temperature between economizer and evaporator is the bubble point temperature. Therefore, from the saturated liquid properties at 0.4 of strong solution concentration and 15 bar pressure,

$$T_{bp} = T_6 = 97.34\ °C$$

Similar to the pump, in turbine, for isentropic expansion, with reference to the specific entropy, the exit state can be determined.

The specific entropy, at the inlet of turbine,

$$s_1 = s_2 = 5.63\ \text{kJ/kg K}$$

After the expansion, we can refer liquid-vapour mixture properties to find the temperature at the exit of turbine.

Between $\theta = 0.9$ and 1, we can calculate the temperature,

$$T_2 = 86.74\ °C$$

The state after mixing can be determined from the mass balance and energy balance equations

$$m_2 h_2 + m_9 h_9 = m_3 h_3$$

$$h_3 = \frac{m_2 h_2 + m_9 h_9}{m_3}$$

$$= \frac{0.435 \times 1599.7 + 0.564 \times 540.7}{1}$$

$$= 1001.5\ \text{kJ/kg}$$

At 2.58 bar, 0.4 concentration and 1001.5 kJ/kg enthalpy from the liquid-vapour properties,

Between $\theta = 0.7$ and 0.8, we can calculate the temperature,

$$T_3 = 90.20\ °C$$

Heat load of absorber,

$$Q_a = m_1 (h_3 - h_4) = 1 \times (1001.8 - (-72.6))$$

$$= 467.45\ \text{kW}$$

Heat load of economizer,

$$Q_{eco} = m_5 (h_6 - h_5) = 1 \times (209.2 - (-70.4))$$

$$= 279.64\ \text{kW}$$

Heat load of evaporator,

$$Q_{evap} = m_6 (h_7 - h_6) = 1 \times (1216.1 - 209.2)$$

$$= 1006.9\ \text{kW}$$

Heat load of HRVG,

$$Q_{HRVG} = Q_{eco} + Q_{evap} = 279.64 + 1006.9 = 1286.5 \text{ kW}$$

Work from turbine,

$$W_t = m_1 (h_1 - h_2) = 0.4351 \times (1905.1 - 1599.7)$$

$$= 125 \text{ kW}$$

Work to pump,

$$W_p = m_4 (h_5 - h_4) = 1 \times (-70.4 - (-72.6))$$

$$= 2.2 \text{ kW}$$

Net output,

$$W_{net} = W_t - W_p = 125 - 2.2 = 122.8 \text{ kW}$$

Thermal efficiency of cycle,

$$\eta_{th} = \frac{W_{net}}{Q_{HRVG}} \times 100 = \frac{122.8}{1286.5} \times 100 = 9.5\%$$

Table 4.2 Summarizes the mass balance and energy balance equations of the solution.

Table 4.2 Thermodynamic properties of basic KC

State	P, bar	T,°C	x	m, kg/s	h, kJ/kg	s, kJ/kg K
1	15.00	150.00	0.70	0.44	1905.08	5.64
2	2.58	86.74	0.70	0.44	1599.72	5.63
3	2.58	90.20	0.40	1.00	1001.77	3.58
4	2.58	35.00	0.40	1.00	-72.57	0.39
5	15.00	35.24	0.40	1.00	-70.42	0.40
6	15.00	97.34	0.40	1.00	209.22	1.22
7	15.00	150.00	0.40	1.00	1216.12	3.73
8	15.00	150.00	0.17	0.56	540.71	1.91
9	2.58	96.54	0.17	0.56	543.11	1.98
10	1.01	30.00	0.00	4.92	20.90	0.07
11	1.01	82.20	0.00	4.92	239.09	0.73

Review Questions

1. The separation with heat addition and the mixing (absorption) with heat rejection drive the binary fluid power plant. Elaborate.
2. What is the need for diluting vapour before sending it to the absorber?
3. What are the challenges of a binary fluid power plant compared to a single fluid system?
4. Analyze the optimum boiler pressure to achieve the maximum performance under the operating conditions.
5. What is the role of strong solution concentration in power generation and thermal efficiency of binary fluid power plants?

❐

5
Binary Fluid Cooling

Abstract

Following power generation, the cooling effect is critical in polygeneration. The current chapter is focused on the binary fluid system for the cooling generation, which is also called vapour absorption refrigeration (VAR). The method of thermodynamic evaluation has been detailed with the formulation. The study has been extended to include an energy analysis and is followed by parametric optimization. The identified key operational conditions are heat transfer fluid (HTF) supply temperature, strong solution concentration, exit temperature of the evaporator, and effectiveness of the dephlegmator. An optimum strong solution concentration has been generated to result in a maximum coefficient of performance (COP) for the solar thermal cooling plant as a function of HTF supply temperature, evaporator's exit temperature, and effectiveness of the dephlegmator. The recommended strong solution concentration for the maximum COP of the plant is around 0.5. For more cooling, high HTF supply temperature, high evaporator temperature, and high effectiveness of the dephlegmator are recommended. Similarly, for high COP of the plant, low HTF supply temperature, high evaporator temperature, and high effectiveness of the dephlegmator are suggested.

T. Srinivas, *Thermal Polygeneration*,
https://doi.org/10.1007/978-3-031-37886-7_5

5.1 Introduction

In many cases, the cooling demand is equal to or greater than the power demand. Therefore, polygeneration gives preference to cooling production to meet the current increasing demand. Cooling can be generated using a low-grade energy supply, a high-grade energy supply, or a combination of the two. Vapour absorption refrigeration (VAR) can be operated with low grade energy such as heat. To drive the mechanical compressor, the vapour compression refrigeration (VCR) requires high grade energy, i.e., electricity. A hybrid refrigeration system needs both low-grade and high-grade energy. A suitable cooling system can be selected to meet the polygeneration conditions. VAR has the benefit of operating with low grade energy even though its coefficient of performance (COP) is low compared to others. The benefits applied to the binary fluid system discussed in the Kalina cycle (KC) can also be claimed for the VAR system.

5.2 Vapour Absorption Refrigeration System

The components used in the binary fluid solar thermal cooling plant are the solar collectors, condenser, subcooler, throttling device, evaporator, absorber, solution pump, low temperature regenerator (LTR), high temperature regenerator (HTR), boiler, separator, and dephlegmator (Fig. 5.1). The boiler generates working fluid (11) from the heat recovery of solar thermic fluid. The working fluid consists of liquid and vapour mixture. The vapour has to be separated and circulated in the cooling plant's main components, viz., condenser, throttling, and evaporator. The subcooler is an additional component for the internal heat recovery. In the separator, the separated liquid (12) is a weak solution used to increase the concentration of vapour at the inlet of the absorber. The concentration of the vapour is increased (13-19) in the dephlegmator. The increased concentration in the cooling plant increases the performance of the cooling system. To increase the concentration in the dephlegmator, some portion of strong solution (5-6) has been used without rejecting the heat. The distilled vapour (19) is passed through the condenser to condense the vapour into saturated liquid at high pressure. A highly concentrated vapour can be condensed at high pressure without any difficulty and dilution. But this is not possible at the low pressure of the absorber. Therefore, the mixing of the weak solution and vapour dilutes the vapour for easy condensation at the absorber. After the condenser (19–20), the fluid passes into the subcooler (20–21) to lose the heat to low temperature vapour from the evaporator. After the subcooler, the subcooled liquid is throttled (21-22), resulting in a low temperature liquid-vapour mixture (22). This mixture is capable of producing the cooling effect in the evaporator (22-23) by absorbing the heat from the surroundings. The vapour is diluted with the weak solution (17) at the inlet of the absorber. The vapour is condensed to the saturated liquid state (2) in the absorber. The heat

from the weak solution is recovered in HTR and LTR. The weak solution is throttled from the high pressure to the low pressure (12–15) to mix in the low pressure stream. The saturated liquid from the absorber is pumped to the boiler for recirculation.

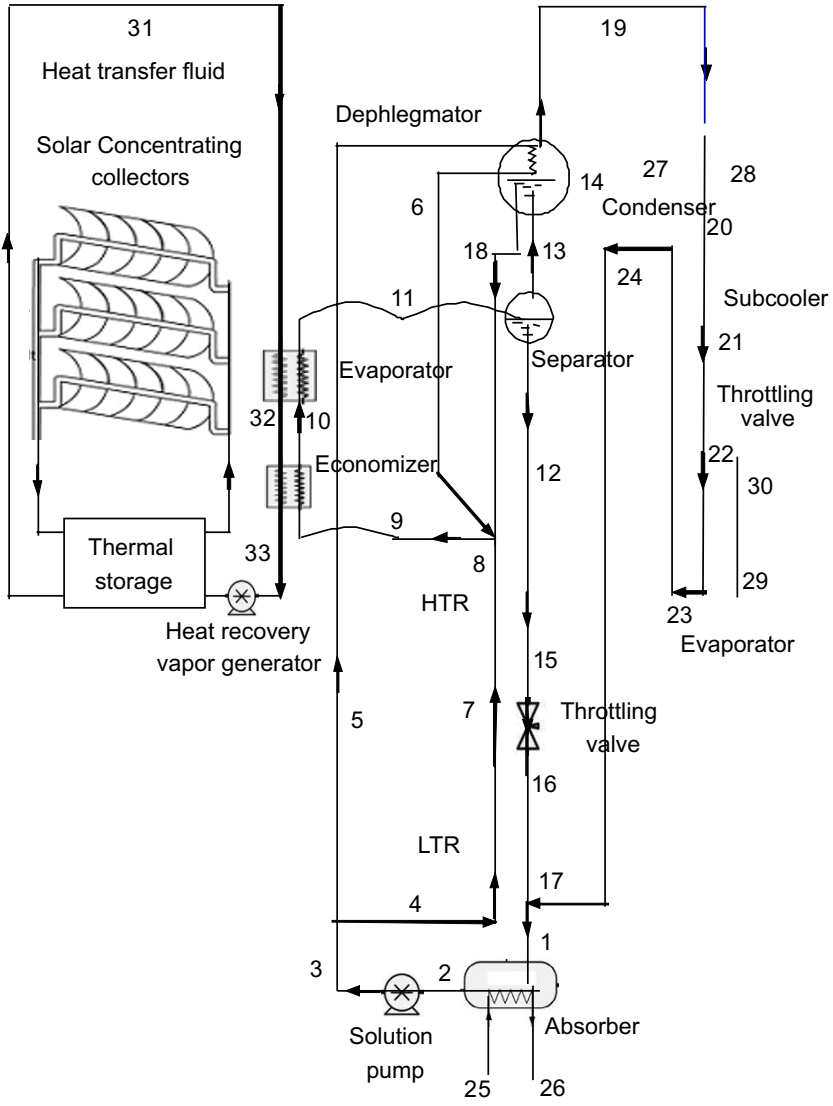

Fig. 5.1: Binary fluid solar thermal cooling plant

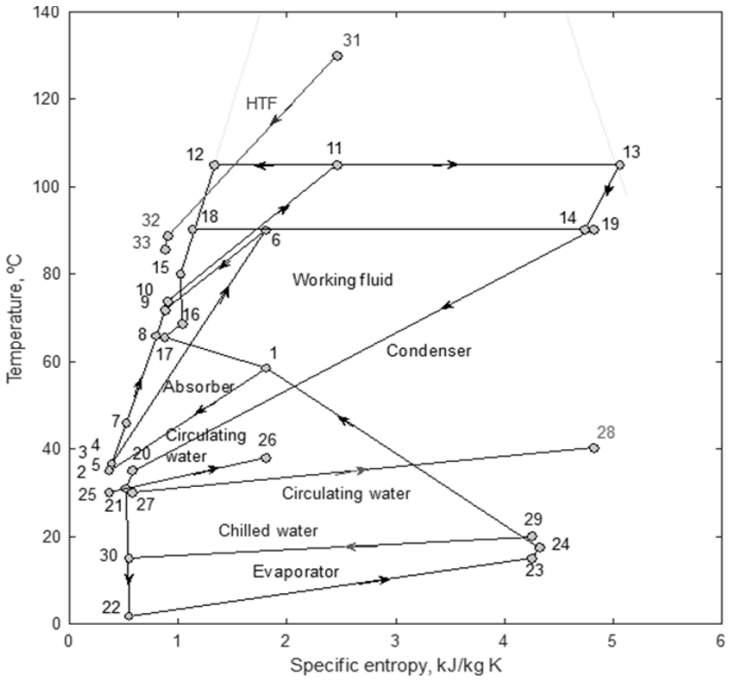

Fig. 5.2: Binary fluid cooling system on temperature-specific entropy diagram

Fig. 5.2 summarises the binary fluid cooling cycle on a temperature-specific entropy plot. The heat addition (9–10–11) is shown with the variable temperature line. The length of heat addition shows that the evaporator load is much higher than the economizer load. The use of LTR and HTR saves the economizer load (4-7-8) as shown. The heat rejection in the condenser (19–20) and absorber (1–2) are also shown as variable temperature lines. The length of the heat rejection line in the condenser is longer than the length of the heat rejection line in the absorber. But the fluid flow in the absorber is higher than the fluid in the condenser. Therefore, the heat load in the absorber is greater than the condenser load. The two horizontal lines (12-11-13) and (18-14-19) are the separation of fluids in the separator and dephlegmator respectively. In addition to the working fluid states, the other fluids, viz., HTF (31-32-33), circulating water (27-28), and chilled water (29-30) states have also been depicted as external fluids.

5.3 Thermodynamic Model

The average global radiation has been simulated using the standard solar radiation models at the considered location (Jalandhar, India) during the equinox period. The average global radiation is 515 W/m^2. The identified independent variables in the simulation of VAR are HTF supply temperature, strong solution concentration, evaporator temperature, and the effectiveness

of the dephlegmator. The terminal temperature difference (TTD) in the heat sink is 5 °C, which is the temperature difference between the working fluid's exit temperature and the circulating water supply temperature. This TTD is maintained in the condenser and absorber. Therefore, the exit temperature of the condenser and absorber is determined by the water supply temperature and TTD. VAR works on two pressures, viz., and high pressure (HP) and low pressure (LP). The exit conditions of absorber (2) result in the LP. The LP is determined. LP is the function of saturated liquid temperature (T_2) and strong solution concentration (x_2) at the exit of the absorber.

Similarly, the HP is the function of saturated liquid temperature (T_{20}) and concentration (x_{20}) at the exit of the condenser. But the concentration at the exit of the condenser is not known. But these concentrations, i.e., concentration at the exit of the condenser and weak solution concentration, are functions of strong solution concentration, evaporator temperature, separator temperature, and water supply temperature. Therefore, the vapour concentration at the exit of the separator (x_{13}) has been iterated. The saturated vapour condition at the exit of separator (13) supports this iteration.

A dephlegmator is used to distil the fluid before supplying the refrigeration components, viz., condenser, throttling, and evaporator. The maximum limit for the distillation is pure ammonia, i.e., 100% concentration. The degree of dephlegmation is determined by its effectiveness. The actual concentration rise in the dephlegmator is $x_{19}–x_{13}$, against the maximum increase of $1–x_{13}$.

Effectiveness of dephlegmator,

$$э_{deph} = \frac{x_{19} - x_{13}}{1 - x_{13}} \tag{5.1}$$

According to the degree of dephlegmator, the exit concentration from the dephlegmator is determined. In the current simulation, the assumed degree of dephlegmator is 0.5. The pressure and temperature of the separator also result in the weak solution concentration at its liquid exit. The liquid concentration from the dephlegmator (18) is determined by the temperature and pressure (14).

The simplification of mass balance equations with the dryness fraction (mass of vapour to total mass) in the separator and dephlegmator in the VAR loops solves all the fluid flow in the VAR unit.

The dryness fraction of fluid in separator,

$$\delta_{sep} = \frac{x_{11} - x_{12}}{x_{13} - x_{12}} \tag{5.2}$$

The fluid generated for refrigeration unit which is flowing in condenser, throttling and evaporator,

$$m_{19} = \frac{\delta_{sep}\delta_{deph}m_1}{\delta_{sep}\delta_{deph} + 1 - \delta_{sep}} \tag{5.3}$$

The dryness fraction of fluid in dephlegmator,

$$\delta_{deph} = \frac{x_{13} - x_{18}}{x_{19} - x_{18}} \tag{5.4}$$

The fluid in the boiler,

$$m_{11} = \frac{m_{19}}{\delta_{sep}\delta_{deph}} \tag{5.5}$$

The weak solution,

$$m_{12} = \frac{\left(1 - \delta_{sep}\right)m_{19}}{\delta_{sep}\delta_{deph}} \tag{5.6}$$

The energy balance in subcooler results the temperature, T_{24}

$$h_{24} = h_{23} + (h_{20} - h_{21}) \tag{5.7}$$

Similarly, the exit temperature from HTR, T_{15} is determined from its energy balance,

$$h_{15} = \frac{h_{12} - m_7(h_8 - h_7)}{m_{12}} \tag{5.8}$$

The exit temperature from LTR, T_{17} is determined from its energy balance,

$$h_{17} = \frac{h_{16} - m_7(h_7 - h_4)}{m_{17}} \tag{5.9}$$

The coefficient of performance (COP) of VAR cycle,

$$COP_c = \frac{m_{22}(h_{23} - h_{22})}{m_9(h_{11} - h_9) + y_e W_{es}} \tag{5.10}$$

The coefficient of performance (COP) of solar thermal cooling plant,

$$\mathrm{COP}_{\mathrm{pt}} = \frac{m_{22}(h_{23} - h_{22})}{0.001GA_{CPC} + y_e W_{es}}$$

W_{es} is the electrical supply to drive the plant components such as circulating pumps. In the plant, two pumps have been used one for solution and another for the circulating water.

Table 5.1 Material balance and energy balance results of solar thermal cooling plant

State	P, bar	T, °C	x	ψ	m, kg/s	h, kJ/kg	s, kJ/kg K	ε, kJ/kg
1	4.41	58.50	0.50	0.24	1.00	379.03	1.81	-160.73
2	4.41	35.00	0.50	0.00	1.00	-82.98	0.37	-192.08
3	13.00	36.63	0.50	0.00	1.00	-74.93	0.39	-190.77
4	13.00	36.63	0.50	0.00	0.93	-74.93	0.39	-190.77
5	13.00	36.63	0.50	0.00	0.07	-74.93	0.39	-190.77
6	13.00	90.00	0.50	0.18	0.07	415.22	1.81	-123.34

7	13.00	45.91	0.50	0.00	0.93	-33.11	0.52	-188.61
8	13.00	65.93	0.50	0.00	0.93	58.17	0.80	-180.05
9	13.00	71.79	0.50	0.00	1.02	85.23	0.88	-176.66
10	13.00	73.76	0.50	0.00	1.02	94.37	0.90	-175.40
11	13.00	105.00	0.50	0.30	1.02	659.54	2.46	-74.13
12	13.00	105.00	0.33	0.00	0.73	259.84	1.33	-137.62
13	13.00	105.00	0.93	1.00	0.29	1582.81	5.06	73.35
14	13.00	90.21	0.93	0.97	0.29	1456.50	4.74	43.20
15	13.00	80.05	0.33	0.00	0.73	146.62	1.02	-158.51
16	4.41	68.61	0.33	0.03	0.73	149.06	1.04	-159.97
17	4.41	65.53	0.33	0.01	0.73	93.85	0.87	-166.83
18	13.00	90.21	0.40	0.00	0.02	175.41	1.13	-161.43
19	13.00	90.21	0.96	1.00	0.27	1483.75	4.82	45.34
20	13.00	35.00	0.96	0.00	0.27	138.56	0.58	-34.53
21	13.00	31.00	0.96	0.00	0.27	119.13	0.52	-35.03
22	4.41	1.72	0.96	0.11	0.27	119.38	0.55	-44.18
23	4.41	15.00	0.96	0.89	0.27	1144.69	4.25	-123.32
24	4.41	17.39	0.96	0.90	0.27	1165.61	4.32	-123.80
25	1.01	30.00	- -	0.00	13.84	20.87	0.07	0.17
26	1.01	38.00	- -	0.00	13.84	54.26	0.18	1.15
27	1.01	30.00	- -	0.00	8.44	20.87	0.07	0.17
28	1.01	40.21	- -	0.00	8.44	63.48	0.21	1.57
29	1.01	20.00	- -	0.00	13.14	-20.87	-0.07	0.18
30	1.01	15.00	- -	0.00	13.14	-41.74	-0.14	0.72
31	1.01	130.00	- -	0.00	7.33	188.60	0.54	27.02
32	1.01	88.76	- -	0.00	7.33	110.03	0.33	10.32
33	1.01	85.55	- -	0.00	7.33	104.16	0.32	9.33

5.4 Performance Characteristics

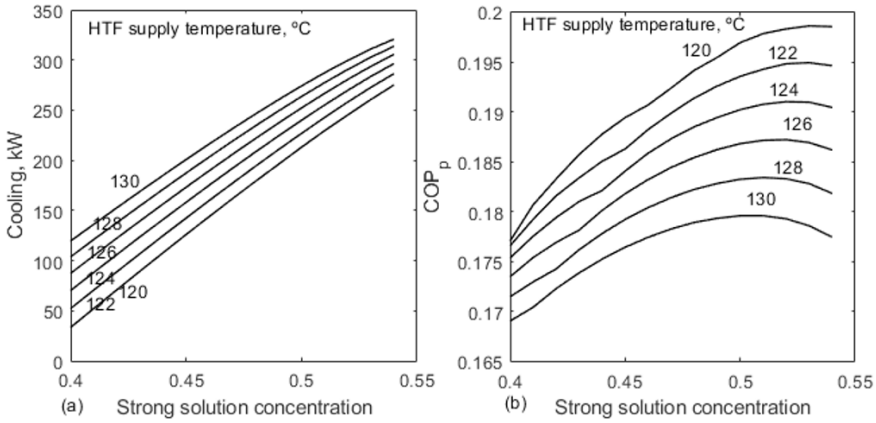

Fig. 5.3: Effect of HTF supply temperature and strong solution concentration on cooling generation and COP of solar thermal cooling plant

Fig. 5.3 shows the effect of the HTF supply temperature with strong solution concentration. The increase in supply temperature increases the boiler pressure and allows more expansion in the throttling. More expansion decreases the low temperature at the inlet of evaporator and results more heat absorption. It increases the cooling effect generated in the evaporator. But the increase in supply temperature increases the energy supply to the plant. Therefore, the COP of the cooling unit is decreasing with an increase in HTF supply temperature. The increase in strong solution concentration also increases the cooling effect as it increases the ammonia concentration. The boiling point of ammonia is very low compared to water at the same temperature. Compared to the water, ammonia role in the cooling production and generating low temperature is significant. The cooling effect is increasing with an increase in strong solution concentration. COP is function of cooling output and energy supply. The energy supply to the plant includes the collected solar radiation, solution pump work and circulating water pump supply work. The water circulating pump capacity is increasing with an increase in HTF supply temperature and strong solution concentration. The energy supply is increasing with increase in HTF temperature and strong solution concentration. The increase in cooling effect and energy supply with an increase in HTF temperature and strong solution concentration results COP peaks in the analysis. The COP of the plant is maximum at the optimum strong solution concentration and is function of HTF supply temperature. The optimum strong solution concentration is increasing with an increase in HTF supply temperature to result maximum COP.

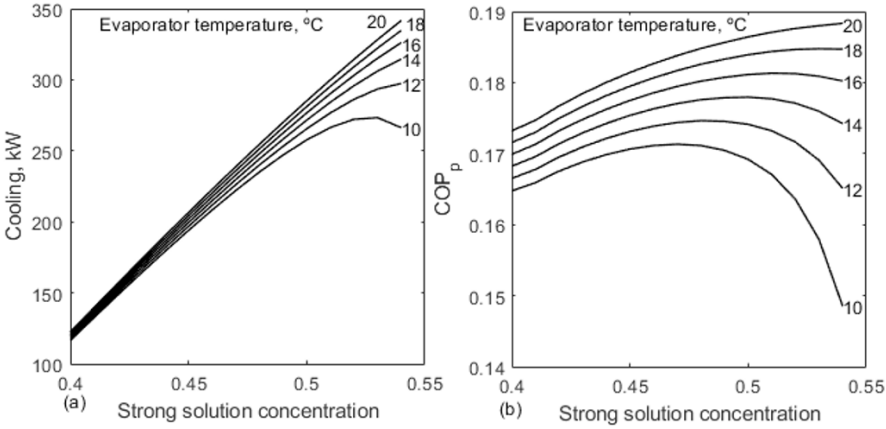

Fig. 5.4: Effect of evaporator temperature and strong solution concentration on cooling generation and COP of solar thermal cooling plant

Fig. 5.4 shows the effect of evaporator temperature and strong solution concentration on the cooling effect and COP of a solar thermal cooling plant. The evaporator temperature is the saturation temperature of the fluid in the evaporator. In a single fluid system, the evaporator temperature is the saturation temperature of the refrigerant. But in the binary fluid system, the temperature of the fluid during the phase change is not constant. The evaporator temperature exit temperature results in the cold body or fluid temperature for the refrigerating effect. Therefore, the evaporator exit temperature is considered as an evaporator temperature for the parametric analysis to find the optimum evaporator temperature. The evaporator temperature depends on the load conditions. Under light cooling load, the evaporator temperature decreases, and it increases with an increase in cooling load. The cooling load has been shown with the chilled water generation. The water has been circulated in the evaporator to produce chilled water for the cooling generation. Unlike the source temperature, the increase in evaporator temperature supports both the cooling and the COP of the plant. The evaporator temperature influences cooling but not the energy supply in the boiler. But the circulating water pump capacity increases with an increase in evaporator temperature as it increases the cooling generation. Therefore, the COP of the plant is increasing with an increase in evaporator temperature with the diminishing rate. At the lower strong solution concentration, the effect of evaporator temperature is low compared to the higher strong solution concentration. It is because the circulating water capacity is increasing with an increase in strong solution concentration. Similar to the HTF supply temperature, the optimum strong solution concentration is also increasing with an increase in evaporator temperature.

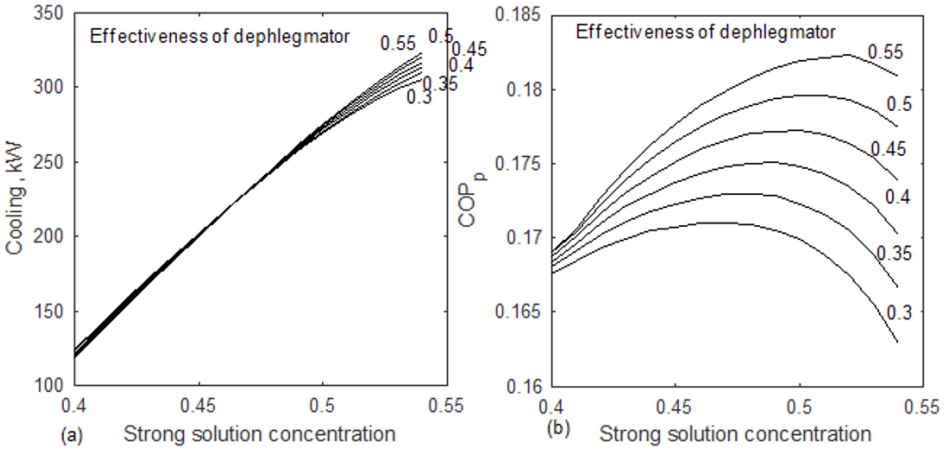

Fig. 5.5: Effect of degree of dephlegmator and strong solution concentration on cooling generation and COP of solar thermal cooling plant

Fig. 5.5 depicts the effect of effectiveness of dephlegmator and strong solution concentration on cooling and COP of the solar thermal cooling plant. Dephlegmator is a heat exchanger that transfers the heat between vapour and strong solution to increase the concentration of vapour by condensing water vapour. The effectiveness of dephlegmator has been changed from 0.3 to 0.55. The zero dephlegmator represents the operation of cooling plant without using dephlegmator (not shown here). The maximum extent of distillation of vapour is to 100% i.e. pure ammonia. At this condition, the effectiveness of dephlegmator becomes maximum i.e. 100%. Therefore, the effectiveness of dephlegmator has been defined as the ratio of actual rise in concentration in the dephlegmator to the maximum concentration rise (hypothetical). The increase in effectiveness of dephlegmator is favouring the cooling and COP of the plant. The increase in dephlegmator's effectiveness increases the concentration of vapour in the throttling and evaporator. This high concentrated fluid in the throttling decreases its exit temperature hence, more scope for the cooling. On other side, the increase in dephlegmator, drops the fluid flow in the throttling and evaporator as water is condensed from the vapour and returns back to boiler. The dephlegmator is giving positive results with the higher strong solution concentrations i.e. around after 0.47 concentration. Therefore a higher strong solution concentration and higher dephlegmator's effectiveness gives more cooling. The energy supply to the boiler is decreasing with an increase in effectiveness of dephlegmator as it decreases the boiler pressure. The solution pump capacity and circulating pump capacity are increasing with an increase in effectiveness of dephlegmator. An optimum strong solution concentration is resulted for the maximum COP of the plant. The optimum concentration is increasing with an increase in effectiveness of dephlegmator.

Table 5.2 summarises the specifications of the solar thermal cooling plant. Based on the unit flow (1 kg/s) in the absorber, the HTF flow in the solar collector has been determined. The resultant HTF is 7.33 kg/s. It has been circulated between the collector and the heat recovery vapour generator (HRVG). The simulation of the collector at the given HTF supply temperature (82.5 °C) and exit temperature (130 °C) and fluid flow (7.33 kg/s) resulted in a 42.27% thermal efficiency at the average global radiation. At these conditions, the simulated CPC area is 2805 m^2. The energy supply to the solar thermal cooling plant includes thermal energy to the solar collector (619 kW), electrical energy supply to the solution pump (8 kW) and water circulation pump (15.5 kW). The resultant cooling effect is 274.21 kW. The COP of the cycle and plant are 0.47 and 0.18, respectively, at the stated operating conditions. The comparison shows that the heat load in the HTR is higher than the LTR. They also save the heat load in the economizer of the boiler. Therefore, the major load on the boiler is its evaporation only. Due to higher fluid flow in the absorber, its heat load is greater than the condenser's load.

Table 5.2 Specifications of solar thermal power plant at 130 °C of HTF supply temperature, 0.5 strong solution concentration, 15 °C of evaporator exit temperature and 0.5 effectiveness of dephlegmator

S. No.	Description	Result
1.	HTF at unit flow in absorber, kg/s	7.33
2.	CPC efficiency at noon time at the stated period and location, %	42.27
3.	Area of CPC, m^2	2805.00
4.	CPC fluid supply temperature, °C	85.50
5.	CPC fluid exit temperature, °C	130.00
6.	Work supply to solution pump, kW	8.00
7.	Work supply to circulating water pump, kW	15.50
8.	Subcooler, kW	5.19
9.	LTR, kW	38.73
10.	HTR, kW	84.54
11.	Heat supplied to boiler, kW	619.00
12.	Boiler's economizer load, kW	9.31
13.	Boiler's evaporator load, kW	608.69
14.	Condenser load, kW	359.76
15.	Absorber load, kW	462.01
16.	Cooling effect, kW	274.21
17.	COP of the VAR cycle	0.47
18.	COP of the solar thermal cooling plant	0.18

5.5 Summary

The solar thermal cooling plant has been developed and studied with thermal modelling and analysis with the goal of identifying the best operating conditions for the efficient operation of the plant. The identified key independent conditions are: HTF supply temperature, strong solution concentration, evaporator temperature, and effectiveness of the dephlegmator. The study shows that strong solution concentration has a role in the resulting maximum COP for the considered solar thermal cooling plant. The plant's supply temperature has a contrast effect on cooling and COP. The rise in HTF supply temperature benefits cooling but not COP. Optimum strong solution concentration has been achieved as a function of HTF supply temperature, evaporator temperature, and effectiveness of the dephlegmator. This optimum strong solution concentration is increased with an increase in HTF supply temperature, evaporator temperature, and effectiveness of the dephlegmator. The dephlegmator with a lower strong solution concentration is not resulting in positive results for the cooling generation. The resultant optimum strong solution concentration is around 0.5 at the stated operational conditions.

Numerical solutions

1. In an ammonia-absorption system with an analyzer but without a dephlegmator, the following data are given: Condenser pressure = 20.3 bar. Evaporator pressure = 2.1 bar. Generator temperature = 156 °C. Absorber temperature = 40 °C. Specific volume of liquid solution at inlet of pump is 1.251×10^{-3} m^3/kg. Determine per unit mass of the vapor distilled, (i) specific solution circulation rates (ii) temperature at inlet to evaporator if the liquid from the condenser is cooled by 13 °C in the liquid-vapor heat exchanger. (iii) the refrigerating effect if the maximum refrigeration temperature is 5 °C (iv) the heat transfer in the liquid-liquid heat exchanger (v) the heat added in the generator (vi) the pump work (vii) the coefficient of performance (viii) the heat rejected in the absorber and condenser and (ix) energy balance of the system. Take saturated liquid temperature at low pressure and weak solution concentration at inlet and outlet of throttle valve at inlet of absorber.

Solution Refer Fig.5.6 and Fig. 5.7

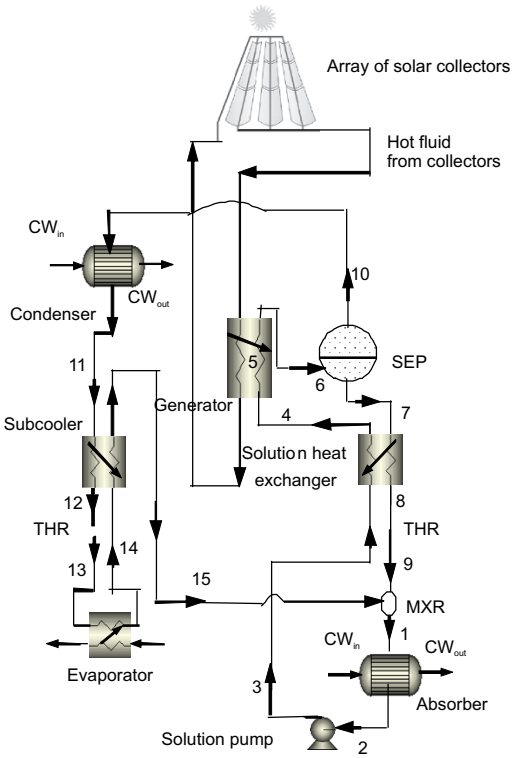

Fig. 5.6: Vapor absorption refrigeration system with subcooler and solution heat exchanger and without dephlegmator

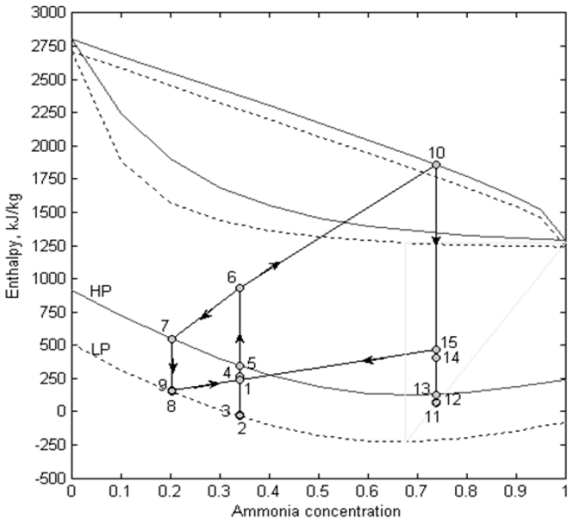

Fig. 5.7: Enthalpy-concentration diagram for vapor absorption refrigeration system

Table 5.3: VAR properties

State	P, bar	T, ºC	x	m, kg/s	h, kJ/kg	DF
1	2.1	55.16	0.34	3.9	240.42	0.12
2	2.1	40	0.34	3.9	-33.22	0
3	20.3	41.38	0.34	3.9	-25.65	0
4	20.3	107.03	0.34	3.9	268.07	0
5	20.3	123.46	0.34	3.9	344.64	0
6	20.3	156	0.34	3.9	931.03	0.29
7	20.3	156	0.2	2.9	547.12	0
8	20.3	67.47	0.2	2.9	151.99	0
9	2.1	68.11	0.2	2.9	161.91	0
10	20.3	156	0.74	1	1859.75	1
11	20.3	64.08	0.74	1	127.28	0
12	20.3	51.08	0.74	1	64.27	0
13	2.1	-5.11	0.74	1	64.27	0.2
14	2.1	5	0.74	1	404.82	0.41
15	2.1	8.12	0.74	1	467.82	0.45

At 20.3 bar and 156 °C

Weak solution concentration, $x_7 = 0.2$

At 2.1 bar and 40 °C saturated liquid condition, rich solution concentration, $x_2 = 0.34$

Also the concentration of vapor leaving the analyzer in equilibrium with the entering rich solution is

$$x_{10} = 0.74$$

It is convenient to put the thermodynamic properties and flow rates at various section in a tabular form in table.

(a) Specific strong solution circulation rate

$$\lambda_{ss} = \frac{m_6}{m_{10}} = \frac{x_{10} - x_7}{x_6 - x_7} = \frac{0.74 - 0.2}{0.34 - 0.2} = 3.85 \text{ kg/kg vapor}$$

Specific weak solution circulation rate

$\lambda_{ws} = \lambda_{ss} - 1 = 3.85 - 1 = 2.85$ kg/kg vapor

Temperature after condensation

$T_{11} = 64$ °C saturated liquid at 0.74 composition and 20.3 bar.

Temperature after subcooling,

$T_{12} = 64 - 13 = 51$ °C

For throttling expansion process at inlet of evaporator,

$h_{12} = h_{13} = 64.27$ kJ/kg

There are two variables, temperature T_{13} and vapor concentration at point 10. A trail and error solution can be obtained by assuming T_{13}. But in such a solution with the h-x diagram, point 13 fluctuates greatly. A simpler and quite accurate method is to assume the vapor state at x = 1 and then join of this point to 12 which gives the temperature after expansion and the temperature at inlet to evaporator as

$$T_{13} = -5°C$$

Pump work

Specific volume of solution at 40 °C, at the inlet to the pump,

$$V_2 = x_2 v_{NH3} + (1-x_2) v_{H2O}$$
$$= 0.34 (1.726 \times 10^{-3}) + 0.66 (1.008 \times 10^{-3})$$
$$= 1.251 \times 10^{-3} \text{ m}^3/\text{kg}$$

Pump work, $w_p = 1.251 \times 10^{-3} (20.3 - 2.1) \times 10^2 = 2.277$ kJ/kg vapor

From chart $h_2 = -33.22$ kJ/kg

$h_3 = h_2 + w_p = -33.22 + 2.277 = -35.49$ kJ/kg

(c) Temperature after the evaporator, $T_{14} = 5$ °C

Draw the isothermal tie line for 5 °C and 2.1 bar.

The intersection with $x_{14} = 0.74$ locates point 14.

Refrigerating effect, $Q_e = m_{13} (h_{14} - h_{13}) = 404.8 - 73.7 = 331$ kJ/kg

(d) Heat transfer in the liquid-liquid heat exchanger (solution heat exchanger)

$$Q_{shex} = m_7 (h_7 - h_8) = m_3 (h_4 - h_3)$$

(Take $h_8 = h_9$)

$$2.9 (547.12 - 151.99) = 3.9 (h_4 - 25.62)$$
$$h_1 = 240.42 \text{ kJ/kg}$$

(d) heat added in generator, $Q_g = m_4 (h_6 - h_4)$

$$= 3.9 (931 - 268) = 2583.2 \text{ kJ/kg}$$

Coefficient of performance,

$$\text{COP} = \frac{Q_e}{Q_g + W_p} = \frac{331}{2583.2 + 29.49} = 0.13$$

From heat exchanger, $h_{15} = h_{14} + (h_{11} - h_{12})$

$$= 404.8 + (127.8 - 64.27) = 467.82 \text{ kJkg}$$

Heat rejected in absorber,

$$Q_a = m_1 (h_1 - h_2)$$
$$3.9 (240.42—33.22) = 1066 \text{ kJ/kg}$$

Heat rejected in condenser

$$Q_c = m_{10} (h_{10} - h_{11}) = 1 (1859.2 - 127.28)$$
$$= 1732.4 \text{ kJ/kg}$$

(i) Energy balance

Heat rejected

$$Q_k = Q_a + Q_c = 1066.2 + 1732.4$$
$$= 2798.6 \text{ kJ/kg}$$

Heat received

$$Q_r = Q_g + Q_e + W_p$$
$$= 2583.2 + 331.08 + 29.49$$
$$= 2943.75 \text{ kJ/kg}$$

Review Questions

1. What are the common features and components between binary fluid power and binary fluid cooling?
2. What is the working principle of the binary fluid cooling system?
3. What are the merits and demerits of binary fluid cooling compared to vapour compression refrigeration?
4. In binary fluid cooling, the thermal compressor demands low grade energy. Elaborate.

❒

6 Vapour Compression Refrigeration

Abstract

Vapour compression refrigeration system (VCR) operates on reversed organic Rankine cycle with the replacement of pump with the throttling. It is driven by a mechanical compressor and has high coefficient of performance (COP) compared to a vapour absorption refrigeration (VAR) system. VCR has been modelled and analysed with the evaporator pressure, condenser pressure, subcooling at the exit of condenser and superheating at the inlet of the compressor. The performance levels are studied with the auxiliary components.

6.1 Introduction

In refrigeration, heat flows from a low temperature body to high temperature body with the supply of energy (low grade or high grade). It has many applications such as refrigeration, air conditioning (AC), cold storage, centralised air conditioning, automobile air conditioning, aeroplane air conditioning, food preservation, heating, ventilation, and air conditioning (HVAC), and so on. Air conditioning refers to creating a comfortable environment by controlling temperature, moisture, velocity of air, and health conditions. Research on refrigerants, compressors, and methods of cooling are the main phases of the history of refrigeration.

Naturally, heat will flow from a high temperature to a low temperature without any work. The Clasius second law of thermodynamics says that it is impossible to construct a heat pump or refrigerator to draw heat from a low-temperature body to a high-temperature body without the use of an external agency. So some input is required to transfer the heat from a low temperature

T. Srinivas, *Thermal Polygeneration*,
https://doi.org/10.1007/978-3-031-37886-7_6

to a high temperature. The input may be high grade energy or low grade energy. The high grade energy, i.e., work, is supplied to a VCR system and the low grade heat is supplied to a VAR system. Table 6.1 shows the difference between VCR and VAR.

Table 6.1 VCR versus VAR

S. No.	VCR	VAR
1.	High grade energy is used to drive the VCR.	Low grade energy is used to drive the VAR.
2.	Mechanical vapour compressor is used to increase the pressure and create the vapour.	Thermal compressor (boiler with solution pump) is used to increase the pressure and create the vapour.
3.	High COP.	Low COP.
4.	Less number of components.	More number of components
5.	The size of the total system is small.	The size of the total system is large.
6.	Low cost.	High cost.
7,	Low maintenance.	High maintenance.

6.2 Carnot Refrigeration Cycle

Based on the nature of the fluid, refrigeration can be grouped into two, they are vapour refrigeration and gas refrigeration. It is with sensible heat transfer without phase change in gas refrigeration. Vapour refrigeration works with latent heat transfer and phase change. Air refrigeration working on the Bellcolemann cycle is an example of gas refrigeration. Due to the benefits, the majority of the refrigeration systems are in the vapour refrigeration category. Gas refrigeration is used in special cases, such as aeroplanes where light weight has primary importance.

Fig. 6.1 shows the Carnot vapour compression refrigeration cycle where the vapour is compressed in the compressor and shown in the vapour dome. There is no phase change during the processes of air or gas refrigeration. But in vapour compression refrigeration, the condensation and evaporation occur with phase change. The advantage of VCR compared to gas refrigeration is the increased heat transfer in the condenser and evaporator due to latent heat handling.

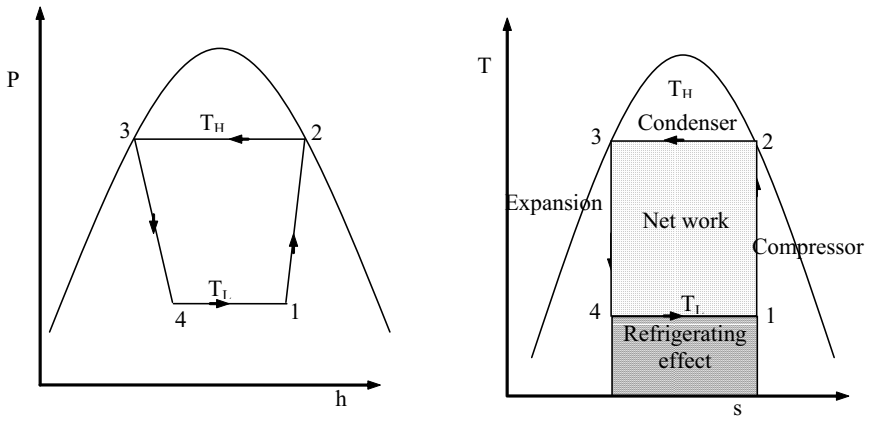

Fig. 6.1: Carnot vapour compression refrigerator
(a) P-V diagram and (b) T-s diagram

Heat rejected in the condenser,

$$Q_1 = T_H \Delta S \tag{6.1}$$

Heat absorption in evaporator,

$$Q_2 = T_L \Delta S \tag{6.2}$$

From the first law of thermodynamics,

$$\sum_c Q_{net} = \sum_c W_{net} \tag{6.3}$$

$$Q_1 - Q_2 = W_{net} \tag{6.4}$$

Coefficient of performance (COP)

$$COP = \frac{Q_2}{W_{net}} = \frac{Q_2}{Q_1 - Q_2} = \frac{T_L}{T_H - T_L} \tag{6.5}$$

The above equation shows that the COP is the function of higher temperature (condenser) of heat rejection and heat absorption (evaporator) at a low temperature. The COP increases with an increase in low temperatures and decreases with an increase in high temperatures. Therefore, to minimise the work supply, i.e., area in the PV diagram, the evaporator temperature should be high and the condenser temperature be low. Practically, Carnot VCR is not possible due to some difficulties in the process implementation and irreversibilities associated. The heat transfer in the condenser and evaporator happens with the external fluid association. For example, in a water-cooled condenser, the circulating water temperature in the condenser should be low enough to reject the complete latent heat from the water. Similarly, the air temperature should be low enough to reject the heat from the air-cooled condenser. If the evaporator is designed to generate chilled water, the chilled

water temperature is greater than the evaporator's working fluid temperature.

6.3 Vapor Compression Refrigeration System

In a vapour compression refrigeration cycle, the working fluid undergoes phase change and the refrigeration effect is due to the vaporisation of refrigerant liquid. If the refrigerant is a pure substance, then its temperature remains constant during the phase change processes. However, if a zeotropic mixture is used as a refrigerant, then there will be a temperature glide during vaporisation and condensation (in VAR). Since the refrigeration effect is produced during phase change, a large amount of heat (latent heat) can be transferred per kilogramme of refrigerant at a near constant temperature. Hence, the required mass flow rates for a given refrigeration capacity will be much smaller compared to a gas cycle. Vapor cycles can be subdivided into vapour compression systems, vapour absorption systems, and vapour jet systems. Among these, vapour compression refrigeration systems are predominant.

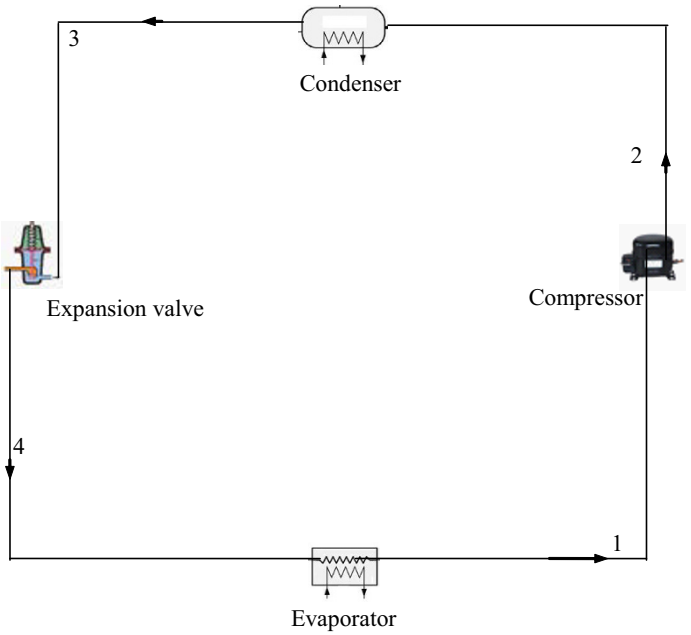

Fig. 6.2: Schematic of components arrangements in a simple vapor compression refrigeration cycle

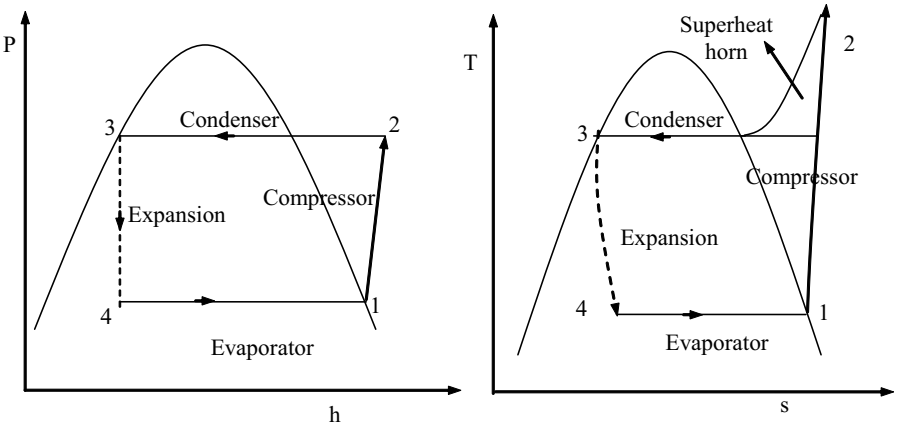

Fig. 6.3: Vapor compression refrigeration (a) P-h diagram and (b) T-s diagram

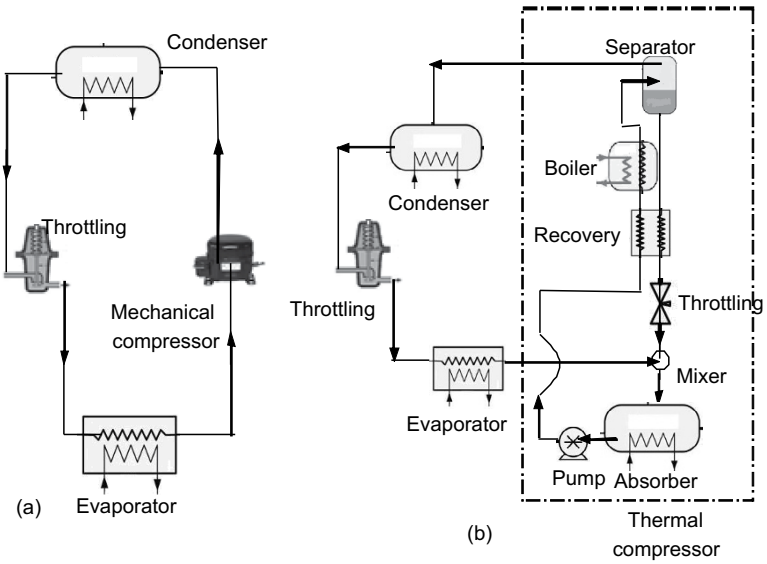

Fig. 6.4: **(a)** Mechanical compressor and
(b) thermal compressor in refrigeration

Fig. 6.4 shows the difference between VCR and VAR refrigeration systems. In the VCR, a mechanical compressor is driven by electricity (high grade energy), where as in the VAR, a thermal compressor is applied and operated by heat (low grade energy). A thermal compressor consists of a pump, boiler, separator, heat recovery, throttling, mixture, and absorber. The work input for the pump is very low compared to a vapour compressor. Heat-operated pumps are also available, such as bubble pumps, and steam jets.

As the name implies, these systems belong to the general class of vapour cycles wherein the working fluid (refrigerant) undergoes phase change at least once during one process. In a vapour compression refrigeration system, refrigeration is obtained as the refrigerant evaporates at low temperatures. The input to the system is in the form of mechanical energy required to run the compressor. Hence, these systems are also called "mechanical refrigeration systems." Vapor compression refrigeration systems are available to suit almost all applications, with refrigeration capacities ranging from a few watts to a few megawatts. A wide variety of refrigerants can be used in these systems to suit different applications, and capacities. The actual vapour compression cycle is based on the Evans-Perkins cycle, which is also called the reverse Rankine cycle. Before the actual cycle is discussed and analyzed, it is essential to find the upper limit of performance of vapour compression cycles. This limit is set by a completely reversible cycle.

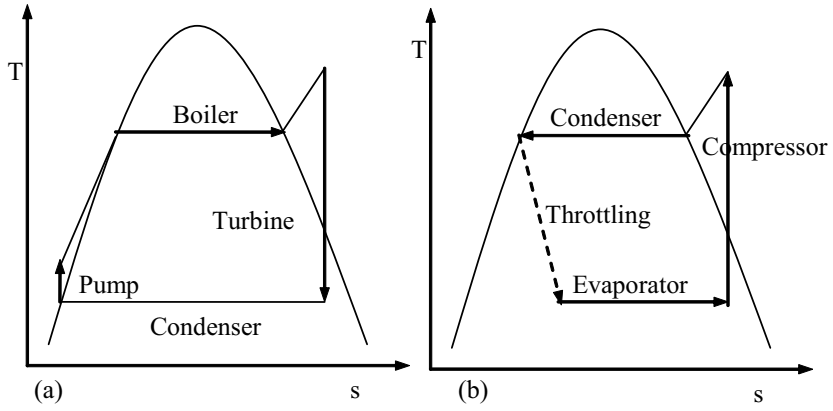

Fig. 6.5: Difference between (a) Rankine cycle and (b) VCR (reversed Rankine cycle)

Fig. 6.5 outlines the difference between Rankine cycle and VCR cycle. The components in Rankine cycle are pump, boiler, turbine and condenser. In VCR the pump is replaced by an irreversible throttling process, boiler by condenser, turbine by compressor and condenser by evaporator.

The vapor-compression refrigeration cycle has four components: the evaporator, compressor, condenser, and expansion (or throttle) valve. The most widely used refrigeration cycle is the vapor-compression refrigeration cycle. In an ideal vapor-compression refrigeration cycle, the refrigerant enters the compressor as a slightly superheated vapour at a low pressure. It then leaves the compressor and enters the condenser as a vapour at some elevated pressure, where the refrigerant is condensed as heat is transferred to the cooling water or to the surroundings. The refrigerant then leaves the condenser as a high-

pressure liquid. As the pressure of the liquid is decreased as it flows through the expansion valve, some of the liquid flashes into cold vapor. The remaining liquid, now at a low pressure and temperature, is vaporised in the evaporator as heat is transferred from the refrigerated space. This vapour then reenters the compressor.

The refrigerant enters the compressor in vapor-compression refrigeration cycles specifically have two additional advantages. First, they exploit the large thermal energy required to change a liquid to a vapour so we can remove lots of heat out of our air-conditioned space. Second, the isothermal nature of the vaporisation allows extraction of heat without raising the temperature of the working fluid to the temperature of whatever is being cooled. This is a benefit because the closer the working fluid temperature approaches that of the surroundings, the lower the rate of heat transfer. The isothermal process allows the fastest rate of heat transfer. The cycle operates at two pressures and the state points are determined by the cooling requirements and the properties of the working fluid. Most coolants are designed so that they have relatively high vapour pressures at typical application temperatures to avoid the need to maintain a significant vacuum in the refrigeration cycle.

The ideal vapor-compression cycle consists of four processes. They are

1-2 isentropic compression,

2-3 constant pressure heat rejection in the condenser,

3-4 throttling in an expansion valve and

4-1 constant pressure heat addition in the evaporator

The ordinary household refrigerator is a good example of the application of this cycle.

The energy conversions in a refrigerator can be solved using stead flow energy equation (SFEE) as outlined in the following section.

For the isentropic compression of vapor in the compressor,

$$W_{co} = m(h_2 - h_1) \tag{6.6}$$

The heat rejection in the condenser is equal to the sum of desuperheater load and evaporator load assuming zero subcooling.

$$Q_{cond} = m(h_2 - h_3) \tag{6.7}$$

The expansion process is a throttling or isenthalpic process, i.e. $h_4 = h_3$

Similar to condenser, evaporator also handles latent heat transfer. The heat absorption in the evaporator is latent heat only as at the end of evaporator, the state is considered as saturated vapor.

$$Q_e = m(h_1 - h_4) = m(h_1 - h_3) \tag{6.8}$$

The coefficient of performance is the performance index of the refrigeration

system and defined as the resulted refrigerating effect at evaporator from the work supplied to compressor.

$$\text{COP} = \frac{Q_e}{W_{co}} = \frac{q_e}{w_{co}} = \frac{h_1 - h_4}{h_2 - h_1} = \frac{h_1 - h_3}{h_2 - h_1} \tag{6.9}$$

Most of the cases, the refrigerating effect or capacity is expressed in terms of tons of refrigeration. One ton of refrigeration is the generation of one ton of ice (2000 lb) from and at 0 °C for the period of 24 hours.

The ton of refrigeration (TR) is

$$\text{TR} = \frac{907 \times 334}{24 \times 3600} = 3.506 \approx 3.5kW \tag{6.10}$$

Conversion of refrigerating effect from kW to tons is as follows,

$$Q_{ref,TR} = \frac{Q_{e,kW}}{3.5} = \frac{m(h_1 - h_3)}{3.5} \tag{6.11}$$

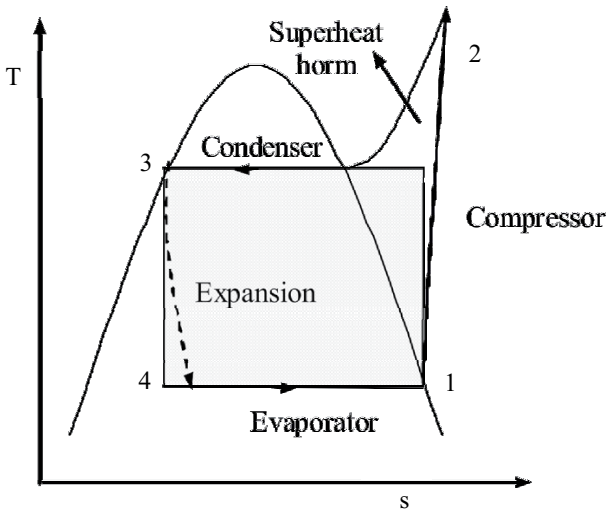

Fig. 6.6: Comparison of Carnot vapor refrigeration and vapor refrigeration

The Carnot vapour refrigeration cycle, which is imaginary, is the bench mark to compare the potential of the actual vapour compressor refrigeration cycle. The compression in Carnot and vapour compression are isentropic and adiabatic, respectively. The superheat horn deviates from the ideal cycle. The horn adds the extra area, which increases the compressor work. To decrease the compressor work, i.e., the area of the cycle, the condenser temperature should be decreased and the evaporator temperature should be at a high level. Or the evaporator and condenser temperatures should be close to each other. The expansions in Carnot and vapour compression, respectively, are isentropic

and throttling. The isentropic expansion results in relatively more wet fluid at the inlet of the evaporator and thus a greater cooling effect. For most of the refrigerants, except ammonia, the area of the superheated horn is low. As a result, the main difference between actual and Carnot vapour compression is irreversible throttling. If the throttling is replaced by an expansion process in a turbine or expander, the irreversibility decreases. But unfortunately, the operation of turbines in wet regions is difficult. Therefore, to achieve closeness to Carnot, vapour compression should be operating with as little temperature difference between the evaporator and condenser as possible.

In the evaluation, Ewing's method can be used for the suction state of the compressor for maximum COP. The COP of the simple vapour compression system may be achieved close to its ideal value by using an appropriate refrigerant and selecting operating pressure limits as close to each other as possible. The Ewing's method is based on the fact that as the point of compression proceeds away from state 4, the COP increases. If the compression started right at state 4, the COP would be zero.

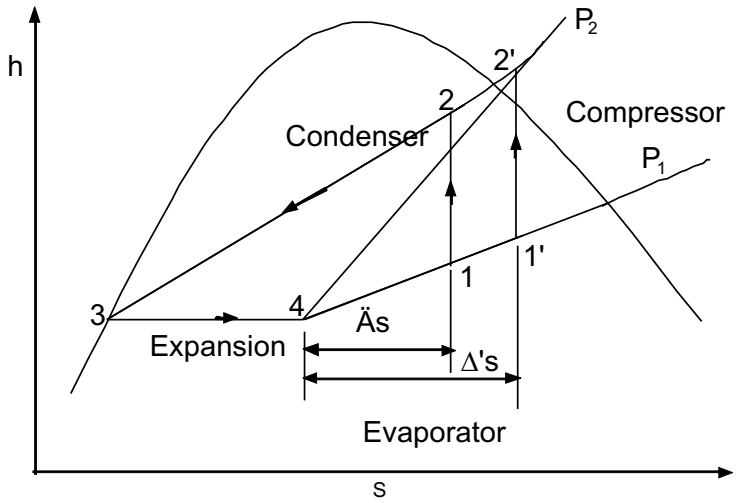

Fig. 6.7: Ewing's diagram

$$\text{COP} = \frac{h_1 - h_2}{h_2 - h_1} = \frac{T_1 \Delta s}{h_2 - h_4 - T_1 \Delta s} \tag{6.12}$$

Dividing numerator and denominator by Δs,

$$\text{COP} = \frac{T_1}{\left(h_2 - h_4 - T_1 \Delta s\right)/\Delta s} = \frac{T_1}{\left(\frac{h_2 - h_4}{\Delta s} - T_1\right)} \tag{6.13}$$

The slope $\frac{h_2 - h_4}{\Delta s}$ will be minimum corresponding to tangent to the condensing pressure line i.e.

$$\text{COP}_{\max} = \frac{T_1}{\left[\left(\frac{h_2 - h_4}{\Delta s}\right)_{\min} - T_1\right]} \tag{6.18}$$

The quantity $\left(\frac{h_2 - h_4}{\Delta s}\right)_{\min}$ is determined by drawing a line from state 4, tangent to constant pressure line p_2. In the present case this minimum value from Fig. 6.7 is

$$\left(\frac{h_2 - h_4}{\Delta s}\right)_{\min} = \left(\frac{h_2' - h_4}{s_1' - s_4}\right) \tag{6.19}$$

The line 2' – 4 is tangent to constant pressure line p_2.

In practice, Ewing's method has become obsolete these days. The wet compression in a high-speed compressor has a shortage of time for the evaporation of tiny liquid droplets. Hence, the performance would be far from the one explained above, in addition to the association of serious mechanical difficulties. The Ewing's method, on the other hand, would fail as soon as state point 1 entered the superheat region.

6.4 Internal Heat Recovery in Vapor Compression Refrigeration

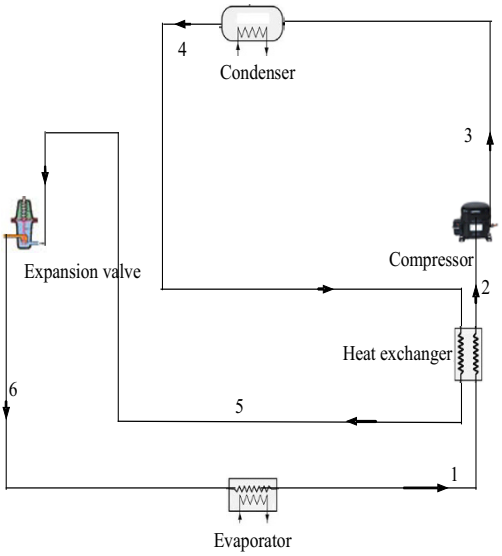

Fig. 6.8: Refrigeration system with a heat exchanger to subcool the liquid from the condenser

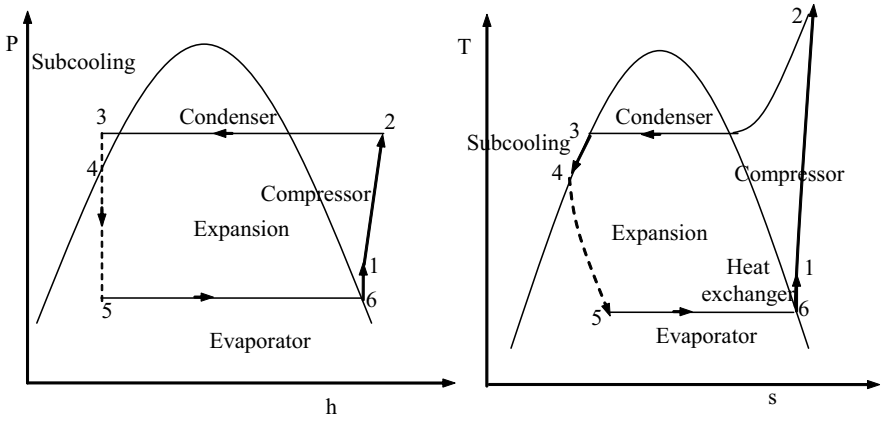

Fig. 6.9: Vapor compression refrigeration with heat exchanger on (a) P-h diagram and (b) T-s diagram

Some refrigeration systems use a liquid-to-suction heat exchanger, which subcools the liquid from the condenser with suction vapour coming from the evaporator. The arrangements are shown in Fig. 6.8, and the corresponding pressure-enthalpy and temperature-entropy diagrams are shown in Fig. 6.9. Saturated liquid at point 3 coming from the condenser is cooled to point 4 by means of vapour at point 6 being heated to point 1.

From a heat balance,

$$h_3 - h_4 = h_1 - h_6 \tag{6.20}$$

Because of the increased refrigerating effect, the system using the heat exchanger may seem to have obvious advantages compared with the standard vapour compression cycle. Both the capacity and the coefficient of performance may seem to be improved. This is not necessarily true, however. Even though the refrigerating effect is increased, the compression is pushed farther out into the superheat region, where the work of compression in kJ/kg is greater than it is close to the saturated vapour line. From the standpoint of capacity, point 1 has a higher specific volume than point 6, so that a compressor which is able to pump a certain volume delivers less mass flow if the intake is at point 1. The potential improvements in performance are thus counterbalanced and the heat exchanger probably has negligible thermodynamic advantages.

The heat exchanger is definitely justified, however, in situations where the vapour entering the compressor must be superheated to ensure that no liquid enters the compressor. Another practical reason for using the heat exchanger is to subcool the liquid from the condenser to prevent bubbles of vapour from impeding the flow of refrigerant through the expansion valve.

6.5 Actual Vapor Compression Cycle

The actual vapour compression cycle suffers from inefficiencies compared with the standard cycle. There are also other changes from the standard cycle that may be intentional or unavoidable. Some comparisons can be drawn by superimposing the actual cycle on the pressure enthalpy diagram of the standard cycle as in Fig. 6.10.

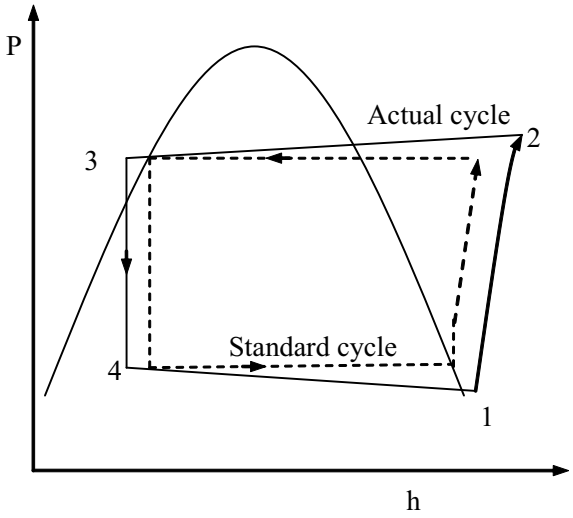

Fig. 6.10: Comparison of Carnot vapor refrigeration and vapor refrigeration

The essential differences between the actual and the standard cycle appear in the pressure drops in the condenser and evaporator, in the subcooling of the liquid leaving the condenser, and in the superheating of the vapour leaving the evaporator. The standard cycle assumes no drop in pressure in the condenser and evaporator. Because of friction, the pressure of the refrigerant drops in the actual cycle. The result of these drops in pressure is that the compression process between 1 and 2 requires more work that in the standard cycle. Subcooling of the liquid in the condenser is a normal occurrence and serves the desirable function of ensuring that 100% liquid will enter the expansion device. Superheating of the vapour usually offers in the evaporator and is recommended as a precaution against droplets of liquid being carried over into the compressor. The final difference in the actual cycle is that the compression is no longer isentropic and there are inefficiencies due to friction and other losses.

6.6 Analysis of Vapor Compression Refrigeration System

6.6.1 Effect of pressure on COP

It is difficult to operate a refrigeration system at the design conditions due to variations in ambient conditions and performance variations of the components, viz., compressor, condenser, throttling valve, and evaporator. For example, the exit state of the condenser is designed to achieve a saturated liquid state. It could be a sub-cooling condition or a liquid-vapour mixture with a change in heat load or pressure in the real world.

This section analyses the changes in the pressure on the COP of the refrigeration system. The changes in the pressure also indicate the changes in the temperature. For example, the analysis of the evaporator pressure is the same as the analysis of the evaporator temperature. The following are the pressure conditions to analyse their effect on the COP.

(i) Drop in evaporator temperature by ΔP_1, while the condenser pressure, P_2 is fixed (Fig. 6.11).

(ii) Increase in condenser pressure, P_2 by ΔP_2, while the evaporator pressure, P_1 is constant (Fig. 6.12) and

(iii) Decrease in evaporator pressure, P_1 by ΔP_1 and increase in condenser pressure, P_2 by ΔP_2 (Fig. 6.13).

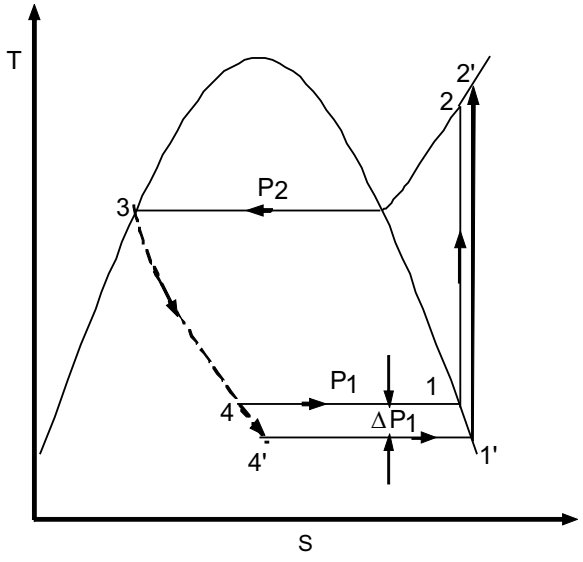

Fig. 6.11: Effect of evaporator pressure or temperature

As shown in Fig. 6.11, the decrease in evaporator pressure, P_1 causes the states 4 and 1 to shift to 4' and 1' respectively. It shows that there is not

much change in the refrigeration effect with the change in evaporator pressure or temperature. But the area under the T-s diagram and also the P-v diagram increases, which is equal to the compressor power. Therefore, the COP of the refrigeration decreases with a decrease in evaporator pressure.

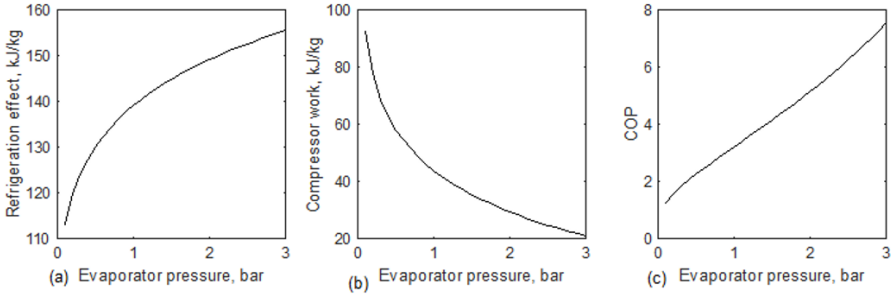

Fig. 6.12: Effect of evaporator pressure on (a) refrigeration effect, (b) compressor supply and (c) COP of the refrigeration system

Fig. 6.12 analyses the effect of evaporator pressure or its temperature on the performance of the refrigeration system. The analysis demands a higher evaporator temperature for the favorable conditions, i.e., a higher COP.

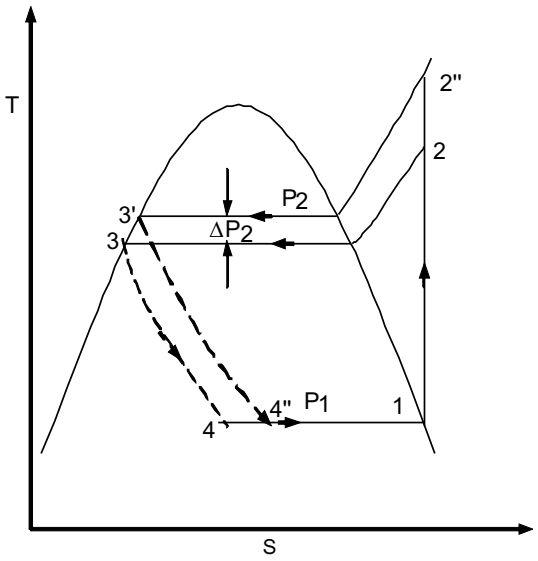

Fig. 6.13: Effect of condenser pressure or temperature

Fig. 6.13 shows the effect of condenser pressure on the COP of the refrigeration. The dryness fraction of the fluid increases at the end of the throttling, which suppresses the refrigeration effect. The area of the diagram also increases, which increases the compressor supply. Since these two factors

do not favour the COP, the COP of the refrigeration decreases with an increase in condenser pressure or temperature.

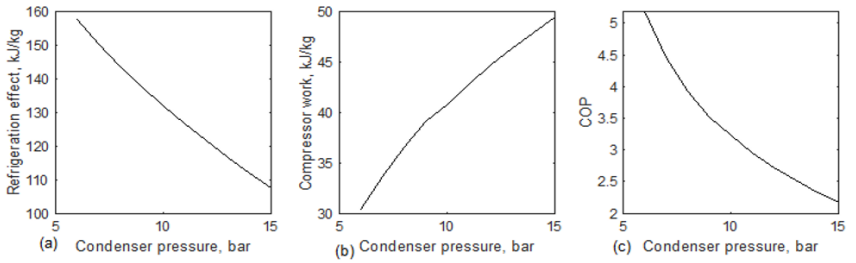

Fig. 6.14: Effect of condenser pressure on (a) refrigerating effect, (b) compressor supply and (c) COP of the refrigeration system

Fig. 6.14 shows the effect of condenser pressure on the performance of the VCR. The analysis recommends a lower condenser pressure to result in a higher COP of refrigeration.

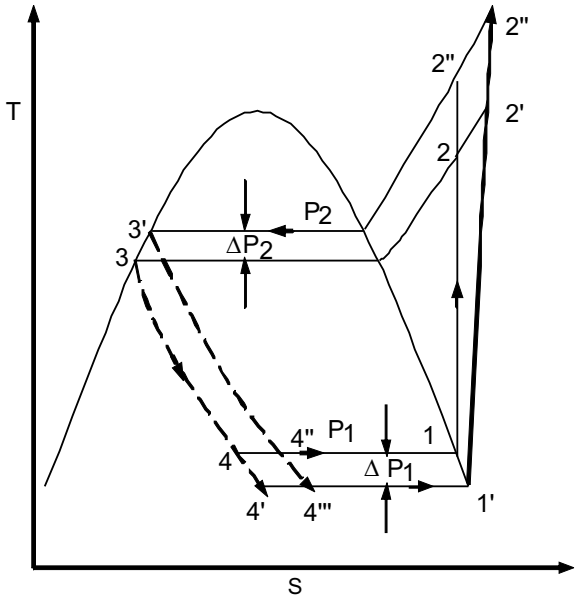

Fig. 6.15: Combined effect of evaporator pressure and condenser pressure

Fig. 6.15 shows the combined effect of the drop in evaporator pressure and the increase in condenser pressure on the refrigeration effect and the COP of the refrigerator. The decrease in evaporator pressure mainly decreases COP without much change in the refrigerating effect. The increase in the condenser

pressure effects both, i.e., the decrease in refrigerating effect and the increase in the compressor capacity. The combined effect of these two drastically increases the compressor input and drops the refrigeration output. Therefore, the COP is much lower than in the earlier two cases.

The above effects can be easily predicted approximately using thermodynamic analysis. To do this, let us define a term, "thermodynamic mean temperature," given by

$$T_m = \frac{h_2 - h_4}{s_2 - s_4} \tag{6.20}$$

The Carnot COP of the normal cycle is given by

$$COP = \frac{T_1}{T_m - T_1} \tag{6.21}$$

The three cases corresponding to decrease in pressure can be reduced to equivalent temperature changes, i.e. the change ΔP_1 is equivalent to ΔT_1, and the change ΔP_2 equivalent to ΔT_2. Then for three cases COP's are given by

$$COP_i = \frac{T_1 - \Delta T_1}{T_m + \Delta T_1 + \Delta T_2 - T_1} \tag{6.22}$$

$$COP_{ii} = \frac{T_1}{T_m + \Delta T_2 - T_1} \tag{6.23}$$

$$COP_{iii} = \frac{T_1 - \Delta T_1}{T_m + \Delta T_1 + \Delta T_2 - T_1} \tag{6.24}$$

If is assumed that $\Delta T_1 = \Delta T_2$, the above COP's of difference cases are seen to be $COP_i > COP_{ii} > COP_i > COP_{iii}$ (6.25)

This clearly demonstrates which of the above effects are more severe, undesirable, and would be taken into design consideration of the refrigeration system. The above analysis, based on the thermodynamic ideas, gives a quick tool to demonstrate which effects are going to be more pronounced.

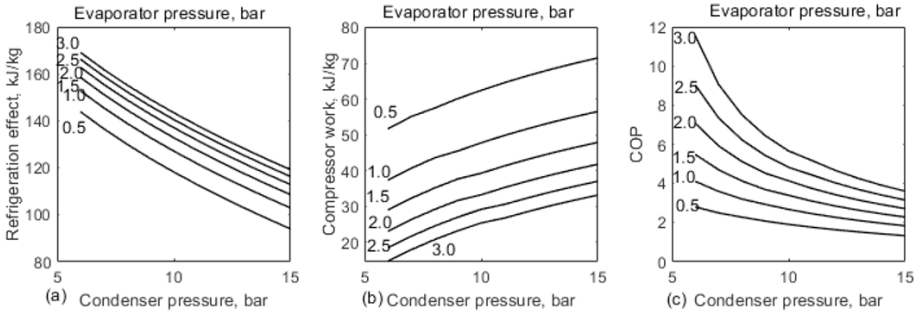

Fig. 6.16: Effect of evaporator pressure and condenser pressure on (a) refrigeration effect, (b) compressor supply work and (c) COP of the refrigeration system

Fig. 6.16 consolidates the influence of evaporator pressure and condenser pressure on (a) refrigeration effect, (b) compressor work and (c) COP of the refrigeration. The combined effect shows that the highest refrigeration effect can be resulted at the higher evaporator pressure and lower condenser pressure. At the same conditions (the higher evaporator and lower condenser pressure) a lowest compressor work is required. Therefore, at this state, COP becomes maximum.

As explained above, the variation in conditions other than design values results in different capacities of the refrigeration system. It is therefore usually practiced to define a capacity factor as the ratio of the actual capacity of a system to the normal one at design conditions. Fig. 6.17 shows the variation in capacity factor for R12 for the given condensing saturation temperature of 40 °C with changes in evaporator temperature.

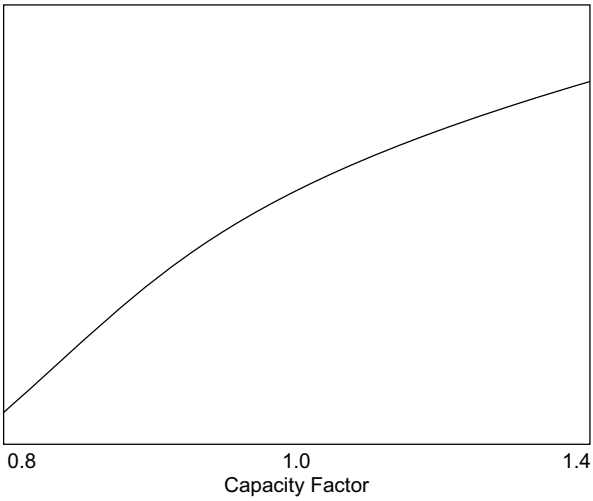

Fig. 6.17: Capacity factor with evaporator temperature changes at fixed condensing temperature

6.6.2 Effect of subcooling of condensate on COP

Fig. 6.18 shows the effect of subcooling at the end of the condenser on the performance of the refrigeration (process 4-4′). For favourable results, it is desirable to maintain a small amount of subcooling of around 5 to 10 K. The experiments demonstrated a drop in the current requirement to operate the compressor from 11 A to 9 A. It shows that the power consumption is decreasing with the subcooling at the inlet of throttling.

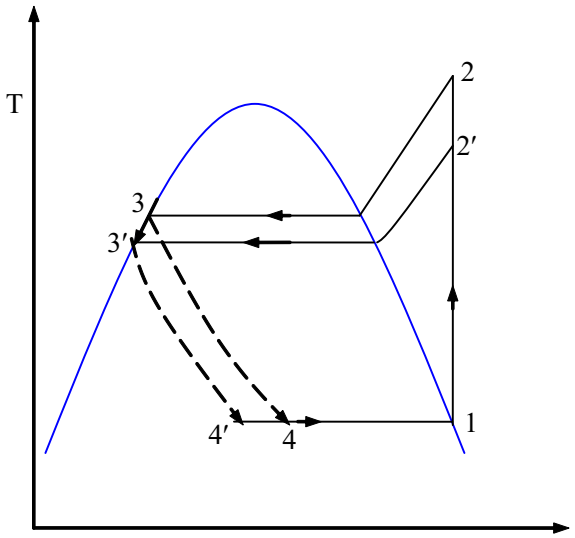

Fig. 6.18: Effect of condensate subcooling on COP

The subcooling increases the refrigeration effect considerably. Therefore, the COP of the system also increases with the subcooling. One can evaluate Δh for subcooling of condensate from the sutured enthalpy of the condensate corresponding to subcooled condensate temperature. Because the condensate is an incompressible fluid, its enthalpy depends upon temperature only as can be easily shown using the state postulate. It is seen that refrigeration effect is increased by an area under the process 4′ - 4 which is also equal to the enthalpy difference $h_4 – h_{4'}$. The large subcooling off-sets the performance of the refrigeration system. If the refrigeration cycle is represented by 1 - 2′ - 3′ - 4′, the refrigeration effect is equal to that of subcooled cycle. But work input was reduced considerably by an area 2′ - 2 – 3 - 4′. Thus subcooling of condensate improves the capacity. But too much subcooling in condenser is totally undesirable.

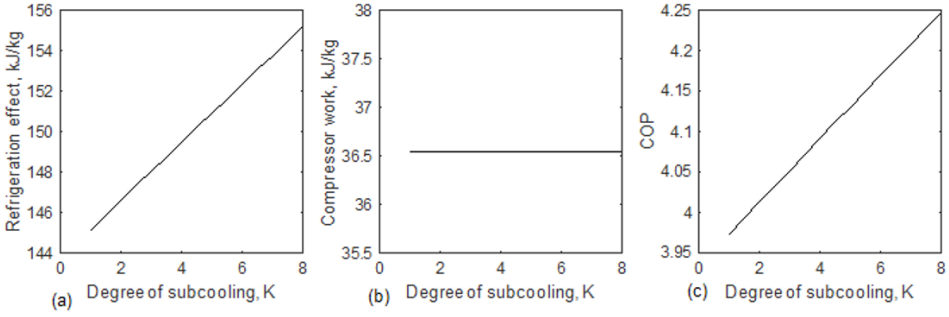

Fig. 6.19: Effect of subcooling on (a) refrigeration effect, (b) compressor supply and (c) COP of the refrigeration system

Fig. 6.19 analyses the effect of the degree of subcooling at the exit of the condenser on (a) refrigeration effect, (b) compressor supply work, and (c) COP of the refrigeration. The degree of subcooling at the end of the condenser or beginning of the throttling is desirable as it increases the refrigeration effect. Since the subcooling is not related to the vapour compressor, the supply to the compressor is constant. The increase in refrigeration effect with an increase in the degree of subcooling increases the COP of the refrigeration system.

6.6.3 Effect of superheating of vapor before compression

Fig. 6.20 shows the effect of superheating at the inlet of compression. A small degree of superheating is required at the inlet of the vapour compressor to avoid wet compression. For good results, approximately 5 to 20 K of superheat is recommended for good results in the performance. The dry compression avoids the liquid particles in the compressor and saves its life. The wet compression also causes hammer blows and many mechanical hurdles.

The superheating of vapour at the end of the evaporator or supply of the compressor happens as follows:

(i) More cooling load in the evaporator causes superheating of the vapour.

(ii) Providing the internal heat recovery between the exit of the condenser and the exit of the evaporator. This heat transfer between hot fluid (condensate) and cold fluid (vapour from the evaporator) results in a superheat before the compressor and

(iii) The transfer of heat from the surroundings to the evaporator.

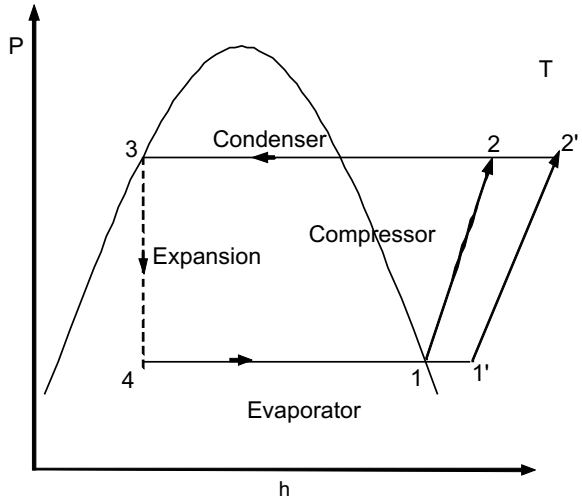

Fig. 6.20: Vapor superheating before suction

The effect of superheating is as follows:

(i) The refrigeration effect increases with the superheat.

(ii) The specific volume of the vapour at the inlet of the vapour compressor increases with the superheating. It decreases the mass of the refrigerant, resulting in a drop in the volumetric efficiency of the compressor.

(iii) The isobars in the superheating region are diverging in nature. Therefore, the superheating of the vapour at the inlet of the compressor demands more power to operate the compressor.

(iv) The COP of the refrigeration system may increase or decrease depending on the type of working fluid in the refrigeration system used.

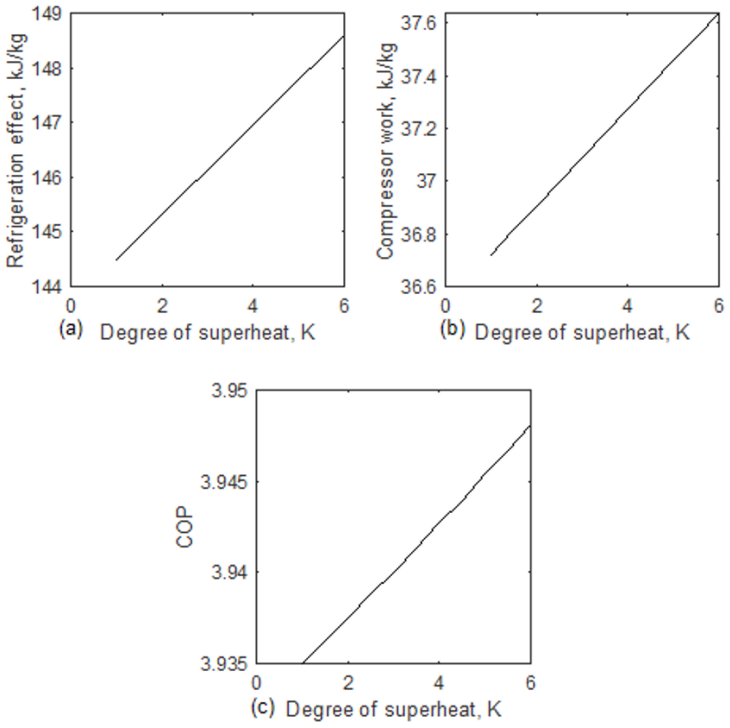

Fig. 6.21: Effect of degree of superheat on (a) refrigeration effect, (b) compressor supply work and (c) COP of refrigeration

Fig. 6.21 shows the effect of the degree of superheat on (a) refrigeration effect, (b) compressor supply work, and (c) COP of the refrigeration. The analysis shows that an increase in the degree of superheat increases the refrigeration effect, compressor work, and COP of the refrigeration system. In

the COP, the influence of the increase in refrigeration is dominating compared to the increase in compressor work. Therefore, the COP is increasing with an increase in the degree of superheat.

6.7 Summary

Vapour compression refrigeration systems have a significant role in polygeneration as they can be used for the cooling generation for multiple applications. This chapter surveyed the VCR and compared its merits and demerits with the VAR. The Carnot refrigeration is discussed to understand the bench mark cooling system for the goal setting. The influence of the decrease in evaporator pressure, the increase in the condenser pressure, the combined effect of evaporator and condenser, the degree of subcooling, and the degree of superheating on the performance of the VCR has been analyzed. For higher COP of refrigeration, higher evaporator pressure and low condenser pressure have been recommended. Subcooling at the exit of the condenser and superheating at the exit of the evaporator or supply of the compressor also favours the COP of the refrigeration.

Numerical Solutions

1. A standard vapor compression cycle developing 50 kW of refrigeration using refrigerant 134a operates with a condensing temperature of 35 °C and an evaporating temperature of -10 °C. Calculate (a) the refrigerating effect in kJ/kg, (b) the circulation rate of refrigerant in kg/s, (c) the power required by the compressor in kW, (d) the coefficient of performance, (e) the volume flow rate measured at the compressor suction, (f) the power per kW of refrigeration and (g) the compressor discharge temperature.

Solution (Fig. 6.22)

At -10 °C, $h_1 = 401.6$ kJ/kg, $v_1 = 0.0651$ m^3/kg

$h_3 = h_4 = 243.1$ kJ/kg

The enthalpy at the exit of compressor can be determined in three ways i.e. (i) using superheated vapor tables, (ii) using c_p of vapor and (iii) using p-h chart.

The superheated vapor tables are available for few refrigerants and not available for phased out refrigerants.

The c_p of vapor at 35 °C is 0.9485 kJ/kg K

$h_2 = h_g + c_p (T_2 - T_{sat})$

To find T_2 isentropic process can be used i.e. $s_2 = s_1 = 1.7658$ kJ/kg K

$$s_2 = s_g + c_p \ln\left(\frac{T_2}{T_{sat}}\right)$$

$$T_2 = T_{sat} \exp\left(\frac{s_2 - s_g}{c_p}\right)$$

$$T_2 = (35 + 273.15)\exp\left(\frac{1.7658 - 1.7049}{0.9485}\right) - 273.15 = 55.43\ ^\circ C$$

$h_2 = h_g + c_p (T_2 - T_{sat}) = 415.34 + 0.9485(55.43 - 35) = 434.72$ kJ/kg

The actual value is

$h_2 = 435.2$ kJ/kg at the superheated condition

(a) refrigerating effect

$q_e = h_1 - h_4 = 401.6 - 243.1 = 158.1$ kJ/kg

(b) the refrigerant circulation rate,

$$m = \frac{RE}{h_1 - h_4} = \frac{50}{158.1} = 0.315\ kg/s$$

(c) The power required to compressor,

$W = m (h_2 - h_1) = 0.315 (435.2 - 401.6) = 10.6$ kW

(d) coefficient of performance

$$COP = \frac{RE}{W} = \frac{50}{10.6} = 4.72$$

(e) The volume rate of flow at the compressor inlet

$V = mv_1 = 0.315 \times 0.0654 = 0.0206\ m^3/s = 20.6$ lit/s

(f) the compressor power per kW of refrigeration

$$w = \frac{W}{RE} = \frac{10.6}{50} = 0.212$$

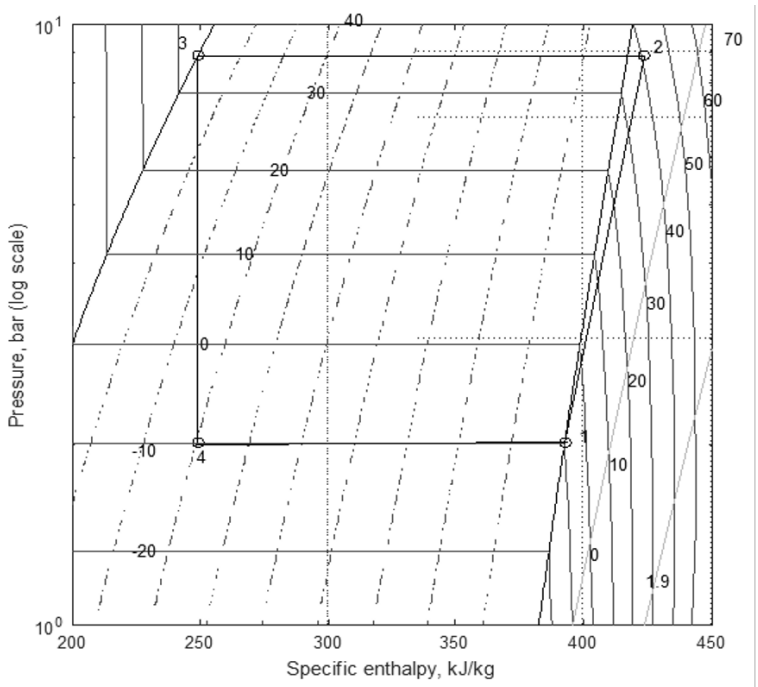

Fig. 6.22: Solution of vapor compression refrigeration

Review questions

1. State and analyse the effect of superheat horn.
2. Is subcooling and superheating at the suction of compressor is desirable?
3. What is the role of changes in evaporator pressure and condenser pressure?
4. The COP of the VCR may increase or decrease with the superheating at the inlet of the vapour compressor. Analyze these conditions.
5. Obtain the performance equations of the Carnot vapour compression refrigeration.
6. Compare gas refrigeration and vapour refrigeration.
7. What is the possibility of internal heat recovery in a VCR system?
8. Draw Ewing's diagram and discuss it.
9. Differentiate between VCR and VAR.

❐

7

Humidification-Dehumidification Desalination

Abstract

Desalination is the process that removes salts and other minerals from raw water. In the current thermal desalination, humidification-dehumidification (HDH) desalination has been studied to equip with modeling, simulation, and analysis with the motto of achieving higher desalination yields. The main processes of basic HDH desalination are preheating, humidification, and dehumidification. These three processes are formulated to evaluate the total unit. The performance conditions of the basic HDH unit are analysed by changing the hot water supply temperature, atmospheric air temperature, atmospheric air relative humidity (RH), and circulating water supply temperature. The outputs, viz., freshwater production, energy performance ratio (EPR) of the cycle and EPR of the plant, are analyzed.

The common features of HDH desalination and air conditioning processes create a hybrid humidification, dehumidification, and vapour compression refrigeration (HDH-VCR) cycle for the combined production of freshwater and air conditioning (A/C). This section is focused on the thermodynamic evaluation of the HDH-VCR cycle's process conditions and performance characteristics. Three types of single-stage HDH plants with options for dehumidifiers such as water cooled dehumidifiers (case 1), chilled water dehumidifiers (case 2), and VCR's dehumidifier (case 3) are compared to find the benefits of the hybrid HDH-VCR plant compared to other options. When compared to the other two cases (cases 1 and 2), the results support the

T. Srinivas, *Thermal Polygeneration*,
https://doi.org/10.1007/978-3-031-37886-7_7

HDH-VCR cycle (case 3). The HDH-VCR resulted in 35.40 ml/m^3 of specific freshwater, 135.83 kJ/m^3 of specific cooling and a 1.15 cycle EPR.

7.1 Introduction

There are four categories of desalination technologies. They are thermal, membrane, chemical, and adsorption. Thermal desalination has good adoptability in a polygeneration plant. It can be operated with the internal heat recovery of the polygeneration. Humidification-Dehumidification (HDH) desalination has more suitability in polygeneration as HDH can be extended to the cooling generation. The process conditions in HDH and air conditioning are similar, and hence these two units can be clubbed together into a single unit to form a subsystem in a polygeneration. HDH works on the principle of the water cycle. Therefore, the water cycle can be created to create artificial rain. In this HDH water cycle, water evaporates, which is similar to the process in a cooling tower. This process is followed by a cooling process to allow the condensation of humid air. To create a low temperature surface for the condensation of air, normal water, chilled water, or a refrigerated coil can be used for the dehumidification of air.

The benefits of HDH desalination are as follows.

1. Simple processes
2. Low cost as the material is not sophisticated
3. No pressure parts
4. The air processes are at the atmospheric conditions
5. No chemicals in the HDH processes
6. Simple to operate and control
7. More flexibility in processes control for combined water and cooling production
8. Easy to adopt into polygeneration

To understand and evaluate the HDH, psychrometry and its processes are required. Therefore, the psychrometry has also been reviewed. This chapter is focused on psychrometry, psychrometric processes, basic HDH desalination, and various options in dehumidification to get the combined freshwater production and cooling.

7.2 Psychrometry

Psychrometric is the study of the properties of a nonreactive mixture of dry air and moisture, which is the wet air. This section also elaborates on the psychrometry processes in addition to the psychrometry properties. The formulation developed for the psychrometric properties and processes can be

applied in the design and development of air conditioning systems. At least two properties are required to find the psychrometric properties of wet air. In the reported literature, psychrometric properties are available in the form of a psychrometric chart. This work presents the properties in tabular form in addition to the chart. The psychrometric property tables are available in Annexure B.

Atmospheric air consists of mainly oxygen and nitrogen, with 23% and 77% by weight, respectively. Atmospheric air also consists of moisture in the superheated form of 1% to 3% by weight. The study of the properties of dry air and water vapour mixtures is called psychrometry. In addition to oxygen, nitrogen, and water vapor, air also consists of traces of carbon dioxide, organs, hydrogen, etc. In psychrometry, these traces are not considered. Generally, psychrometric properties refer to atmospheric pressure. Using formulation, other than atmospheric pressure, psychrometric properties can also be developed with an analytical approach. The properties in a graphical form called a "psychrometric chart" are developed at atmospheric pressure. The moisture content in the atmospheric air adds unique properties to the air and differentiates the wet air from the dry air. Human comfort mainly depends on the moisture content of air, in addition to its temperature, velocity, purity, etc. For example, in summer, the human body feels more sweating due to the high humidity in the air than in winter. In the early morning, the air looks like a mist, and it is called fog as the water vapour condenses at a low temperature. The properties of wet air evaluated by psychrometry are more useful in the design of air coolers, air conditioning systems, and similar. The concentration of water in the air decreases with an increase in height. Approximately 10 km above sea level, the air is nearly dry.

The properties of moist air must be considered when designing air-conditioning systems. Evaluating the real properties of atmospheric air, including water vapor, is difficult due to the involvement of many gases. Since the pressure of air is atmospheric, the equations of perfect gas are nearly applicable to the moisture of air without much error. However, at high pressures above 3 bar, the psychrometric properties determined at atmospheric pressure result in more error. Since the air conditioning systems are designed at atmospheric pressure, there is no issue with these properties and they can be used with reasonable accuracy. Dalton's law of partial pressures can be applied to the atmospheric air. Therefore, the total pressure, or atmospheric pressure, is equal to the sum of partial pressures of oxygen, nitrogen, water vapor, etc. at the same volume and temperature. The partial pressures of oxygen and nitrogen are combined into the partial pressure of dry air. The specific properties of wet air, i.e., specific humidity, specific enthalpy, etc., are evaluated per unit mass of dry air. The unit mass of dry air is considered as a reference, and it provides an easy means of evaluation and design of specific calculations without much difficulty. Dry air is assumed to be a perfect or ideal gas.

7.2.1 Dry bulb temperature

A dry bulb temperature (DBT) is the temperature of wet air measured by a thermometer when the bulb is in a dry condition. It is the room, or ambient, temperature of the air. The temperature of the dry air and water vapour is at the DBT without undergoing any psychrometric process.

7.2.2 Wet bulb temperature

A wet bulb temperature (WBT) is the temperature of wet air measured by a thermometer; its bulb is covered by a wet wick and exposed to moving air by the rotation. Generally, the air conditioning is in an unsaturated position. The dry air absorbs the moisture till it reaches saturation, after which it cannot accommodate the water vapor. It is called "saturated air." The WBT of atmospheric air is measured by a sling psychrometer. The sling psychrometer consists of two thermometers, one with a dry bulb and another with a wet wick. It has a provision for rotation to expose the wet bulb to moving air. The wet wick provides the evaporation of water vapour into the air, and the air reaches its saturation condition. Therefore, the temperature of wet air at its saturation condition is called WBT.

7.2.3 Saturated vapor pressure

The water vapour pressure is the partial pressure as per Dalton's law of additive pressures. At atmospheric pressure, the water vapour in the air is superheated at atmospheric pressure. The saturation pressure corresponding to the temperature of air, i.e., water vapor, is called the saturated vapour pressure (Fig. 7.1). At this temperature, i.e., DBT, the saturation pressure can be determined either from the steam tables or from the Claperon equation given by the American Society of Heating, Refrigerating, and Air-Conditioning Engineers (ASHRAE). This equation can be used to find the saturation pressure from 0 to 100 °C.

$$\ln P_s = \frac{c_1}{T} + c_2 + c_3 T + c_4 T^2 + c_5 T^3 + c_6 \ln T \tag{7.1}$$

where P_s = saturated vapor pressure of water, k Pa

T = temperature, K

The regression coefficients c_1 to c_6 are as follows

$c_1 = -5.80022006 \times 10^3$

$c_2 = -5.516256$

$c_3 = -4.8640239 \times 10^{-2}$

$c_4 = 4.1764768 \times 10^{-5}$

$c_5 = -1.4452093 \times 10^{-8}$

$c_6 = 6.5459673$

7.2.4 Relative humidity

The air continuously absorbs the moisture till its saturation. The ratio of number of moles of water vapour in unsaturated condition to the number of moles of water vapour in the saturated condition at the same pressure and temperature is called as relative humidity (RH) of air. At the saturated condition, RH is 100%.

It is also equal to the ratio of partial pressure of water vapor in air to the saturation pressure of water vapor corresponding to the same temperature (Fig. 7.1).

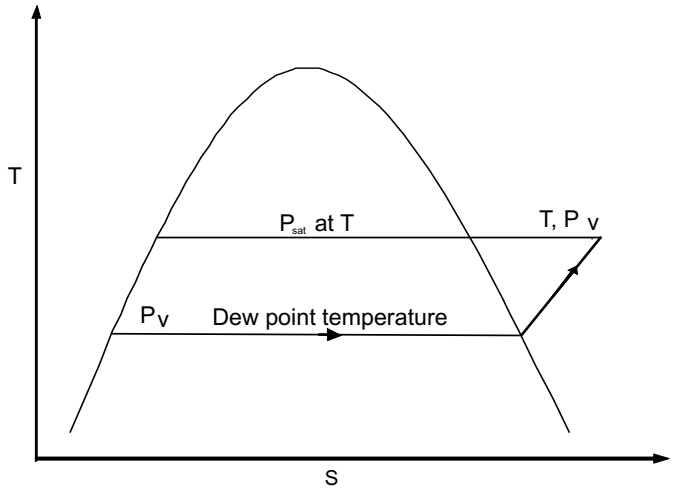

Fig. 7.1 Representation of partial pressure of water vapor and saturation pressure at the same temperature to understand the meaning of relative humidity

Using perfect gas equation, we can show that

$$\phi = \frac{partial\ \ pressure\ of\ \ water\ vapor}{saturation\ \ pressure\ of\ \ pure\ water\ vapor\ \ at\ \ sametemperature}$$

$$= \frac{P_v}{P_{sat}} = \frac{\left(\frac{n_v \bar{R}}{V}\right)}{\left(\frac{n_{sat} \bar{R}}{V}\right)} = \frac{n_v}{n_{sat}}$$

$$= \frac{number\ \ of\ \ moles\ vapor}{number\ \ of\ \ moles\ vapor\ \ at\ \ sat.\ condition}$$

Relative humidity is normally expressed as a percentage. When RH is 100%, the air is saturated.

7.2.5 Humidity ratio

The humidity ratio (or specific humidity), ω is the mass of water associated per unit mass of dry air. Assuming both water vapor and dry air to be perfect gases, the humidity ratio is given by

$$\omega = \frac{mass\ of\ water\ vapor}{mass\ of\ dry\ air} = \frac{m_v}{m_{da}} \tag{7.3}$$

$$= \frac{\left(\frac{P_v V}{R_v T}\right)}{\left(\frac{P_a V}{R_a T}\right)} = \frac{P_v R_a}{P_a R_v} = \frac{P_v R_a}{(P - P_v) R_v}$$

Therefore

$$= \frac{0.287 \times P_v}{0.4615 \times (P - P_v)}$$

$$\omega = 0.622\left(\frac{P_v}{P - P_v}\right) \tag{7.4}$$

P_v is the saturation vapor pressure determined at the temperature of the air from the equation or steam tables. P is the atmospheric pressure. The specific humidity is the function of partial pressure of water vapor and atmospheric pressure.

7.2.6 Partial pressure of water vapor

The partial pressure of water vapor in atmospheric is the pressure exerted by moist air apart from the dry air. The saturation temperature of water vapor at its partial pressure is the dew point temperature (Fig. 7.1).

If the relative humidity and saturation pressure of water vapor is known, the partial pressure of water vapor can be determined from its product as follows:

$$P_v = \phi\, P_{sat}$$

Alternatively, the partial pressure of water vapor can also be evaluated from the know specific humidity relation given below

$$\omega = 0.622\frac{P_v}{P - P_v}$$

$$P_v = \frac{P\omega}{0.622 + \omega} \tag{7.5}$$

7.2.7 Dew point temperature

When unsaturated air is cooled, the moisture from the wet air starts condensation at a temperature that is called the dew-point temperature (DPT) of air. The dew point temperature is the condensation temperature for water vapour at the partial pressure of water vapour (Figs. 7.1 and 7.2). The saturation temperature, or dew point temperature, can be found from the steam tables at the partial pressure of water vapor, P_v.

Alternatively, an approximate equation for dew-point temperature is given by

$$DPT = \frac{4030(DBT + 235)}{4030 - (DBT + 235)\mathrm{h}\ \phi} - 235 \tag{7.6}$$

where Φ is the relative humidity (in fractions). DBT and DPT are measured in degrees Celsius. Of course, since, by its definition, the dew point temperature is the saturation temperature corresponding to the vapour pressure of water vapor, it can be obtained from steam tables or by using the equation for P_{sat}.

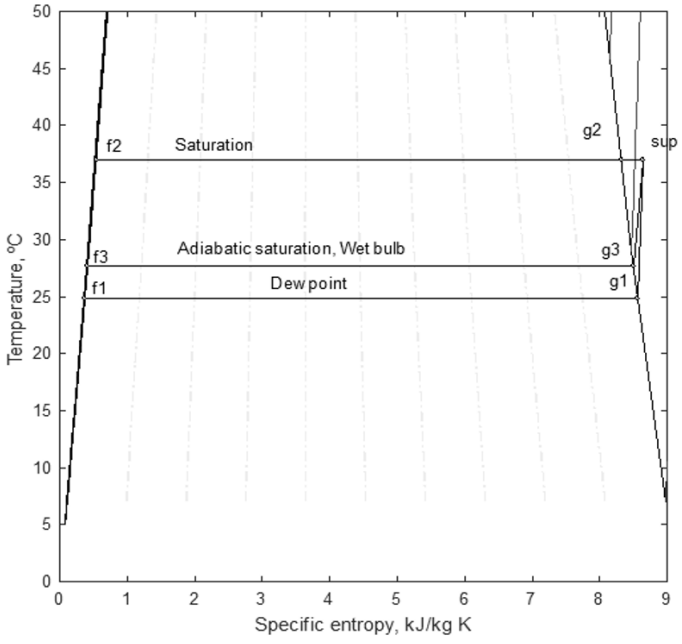

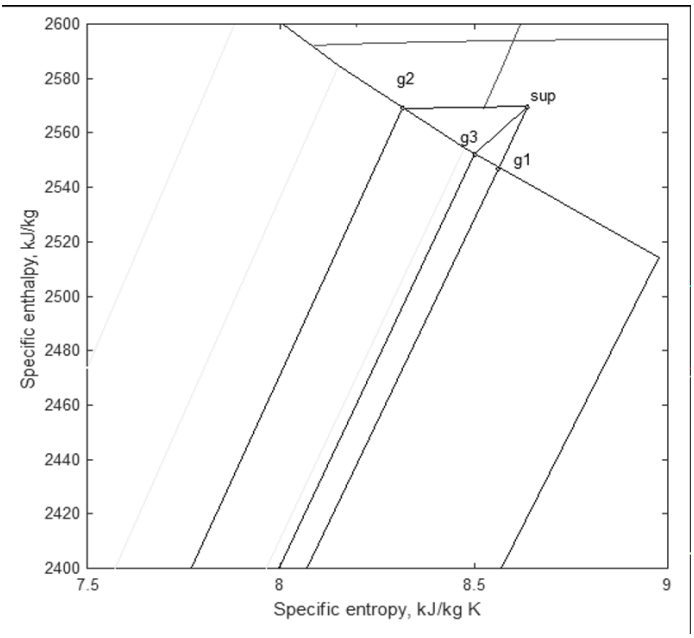

Fig. 7.2: Representation of dew point, wet bulb and saturation state on T-s and h-s diagram

7.2.8 Degree of saturation

The degree of saturation is the ratio of the humidity ratio, ω to the humidity ratio of a saturated mixture ω_s at the same temperature and pressure, i.e.

$$\mu = \left.\frac{\omega}{\omega_s}\right|_{T,\ P} \tag{7.7}$$

7.2.9 Specific volume

The specific volume is defined as the number of cubic meters of moist air per kilogram of dry air. From perfect gas equation since the volumes occupied by the individual substances are the same, the specific volume is also equal to the number of cubic meters of dry air per kilogram of dry air, i.e.,

$$v = \frac{R_a T}{P_a} = \frac{R_a T}{P - P_v}\ m^3/kg\ da \tag{7.8}$$

7.2.10 Specific enthalpy

The specific enthalpy is the total heat of wet air per unit mass of dry air. It is the sum of the enthalpy of dry air and the enthalpy of moisture. Generally,

the moisture in the wet air is in the form of superheated steam. A specific enthalpy is expressed with a reference value.

For moist air, the enthalpy of dry air is given a zero value at 0 °C, and for water vapor the enthalpy of saturated water is taken as zero at 0 °C.

The enthalpy of moist air is given by

$h = h_a + \omega h_g = c_p t + \omega (h_{g\,@\,0°C} + c_{pv} t)$ (7.9)

where c_p = specific heat of dry air at constant pressure, kJ/kg K

t = dry bulb temperature of air-vapor mixture, °C

ω = humidity ratio, kg of water vapor/kg of dry air

h_a = enthalpy of dry air at DBT, kJ/kg

h_g = enthalpy of saturated vapor at 0 °C, kJ/kg

The enthalpy of water vapor, h_g at 0 °C is 2500 kJ/kg.

$h = 1.005t + \omega (2500 + 1.88t)$ (7.10)

Though the water vapour in moist air is likely to be superheated, no appreciable error results if we assume it to be saturated. This is because of the fact that the constant temperature lines in the superheated region on a Mollier chart (*h* vs *s*) are almost horizontal. The unit of h is kJ/kg of dry air. Substituting the approximate values of c_p and h_g, we obtain the humid specific heat from the equation for the enthalpy of moist air.

The humid specific heat of moist air can be written as

$$c_{pm} = c_p + \omega c_{pw} \quad (7.11)$$

where c_{pm} = humid specific heat, kJ/kg K

c_p = specific heat of dry air, kJ/kg K

c_{pw} = specific heat of water vapor, kJ/kg

ω = humidity ratio, kg of water vapor/kg of dry air

Since the second term in the above equation (ωc_{pw}) is very small compared to the first term, for all practical purposes, the humid specific heat of moist air, c_{pm} can be taken as 1.0216 kJ/kg K dry air.

Alternatively, the enthalpy can also be determined from the following manner.

The enthalpy of air,

$$\begin{aligned} h &= c_p t + \omega h_v \\ &= c_p t + \omega (h_g + c_{pv} (t - t_{sat})) \end{aligned} \quad (7.12)$$

7.2.11 Specific entropy

Similar to enthalpy, the entropy of wet air is sum of the entropy of dry air and the entropy of the water vapor. Entropy values are always based on some

reference value.

For moist air, the entropy of dry air is given a zero value at 0 °C, and for water vapor the entropy of saturated water is taken as zero at 0 °C.

The entropy of moist air is given by

$$s = c_p \ln\left(\frac{t+273.15}{273.15}\right) - R_a \ln\left(\frac{P_a}{P_0}\right) + \omega s_g \quad (7.13)$$

where s_g = specific entropy of steam at partial pressure of water vapor (P_v) and dry bulb temperature, t, °C taken from the steam tables.

7.2.12 Specific exergy

The exergy of wet air can be determined from its enthalpy and entropy. The properties at the reference state (dead state) are P_0, T_0, and RH_0, which are 1.01325 bar, 25 °C, and 100%, respectively.

The exergy of moist air,

$$\varepsilon = h - h_0 - T_0 (s - s_0) \quad (7.14)$$

h_0 and s_0 are the specific enthalpy and specific entropy determined at P_0, T_0 and RH_0.

7.2.13 Psychrometric chart

A psychrometric chart graphically represents the thermodynamic properties of moist air. Standard psychrometric charts are bounded by the dry-bulb temperature line (abscissa) and the vapour pressure or humidity ratio (ordinate). The left hand side of the psychrometric chart is bounded by the saturation line. Fig. 7.3 shows the schematic of a psychrometric chart. Psychrometric charts are readily available for the standard barometric pressure of 101.325 kPa at sea level and for normal temperatures (0–50 °C). ASHRAE has also developed psychrometric charts for other temperatures and barometric pressures (for low temperatures of -40 to 10 °C, high temperatures of 10 to 120 °C, and very high temperatures of 100 to 120 °C).

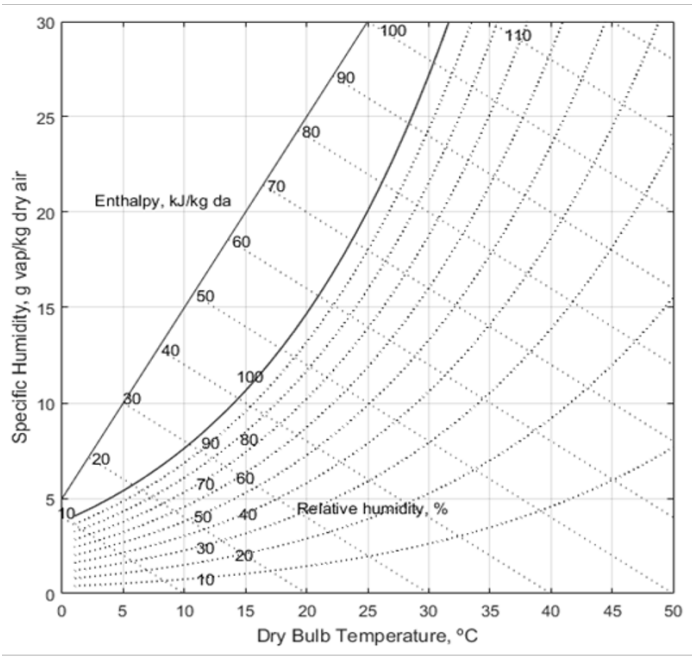

Fig. 7.3: Schematic of a psychrometric chart for a given barometric pressure

If air is evaporated with water adiabatically, the air gets saturated, and it results in an adiabatically high saturation temperature, which is called the "wet bulb temperature of the air." In an adiabatically saturator, air moves from the inlet to the outlet with the circulating fan. Air will flow over the water surface. After the contact between the air and water, the water gets evaporated and starts the saturation of the air. The mass and energy transfer between water and air. At the equilibrium condition and steady state, the saturated air temperature is equal to the water temperature. The walls of the adiabatic device are insulated. Since the water is evaporating into the air, the water level in the device decreases. To maintain a fixed water level in the device, makeup water should be supplied. This adiabatically saturated temperature is the wet bulb temperature, which is below the dry bulb temperature and above the dew point temperature of the incoming air.

To evaluate the psychrometric properties, three properties are required. For example, at the air pressure, dry bulb temperature, and wet bulb temperature, the properties can be determined with the psychrometric formulation and empirical relations. Some of the empirical correlations are as follows:

Modified Aphohn equation,

$$P_v = P'_v - \frac{1.8P(DBT - WBT')}{2700} \tag{7.18}$$

Modified Ferrel equation,

$$P_v = P'_v - 0.00066(DBT - WBT)\left(1 + \frac{1.8DBT}{1571}\right) \tag{7.19}$$

Carrier equation,

$$P_v = P'_v - \frac{1.8(P - P'_v)(DBT - WBT)}{2800 - 1.3(1.8DBT + 32)} \tag{7.20}$$

P_v is the saturation vapor pressure at wet-bulb temperature

After evaluating the vapour pressure, other properties such as specific volume, relative humidity, specific enthalpy, specific entropy, etc. can be determined from the psychrometric equations. Therefore, apart from the air pressure, two properties are required for the property solutions. In some cases, in place of dry bulb temperature and wet bulb temperature, given dry bulb temperature and given relative humidity, the psychrometric properties to be evaluated. At atmospheric pressure, the psychrometric properties can be determined from any two given properties. In most general cases, the dry bulb temperature and relative humidity are supplied. The solution is direct for these given properties. Sometimes, iterations or correlations are used to generate the psychrometric properties from the given data. There are many combinations of data supply possibilities. The following flow charts detail the evaluation of psychrometric properties from the given data.

The flow chart given in Fig. 7.4 outlines the solution of psychrometric properties from the supplied DBT and RH.

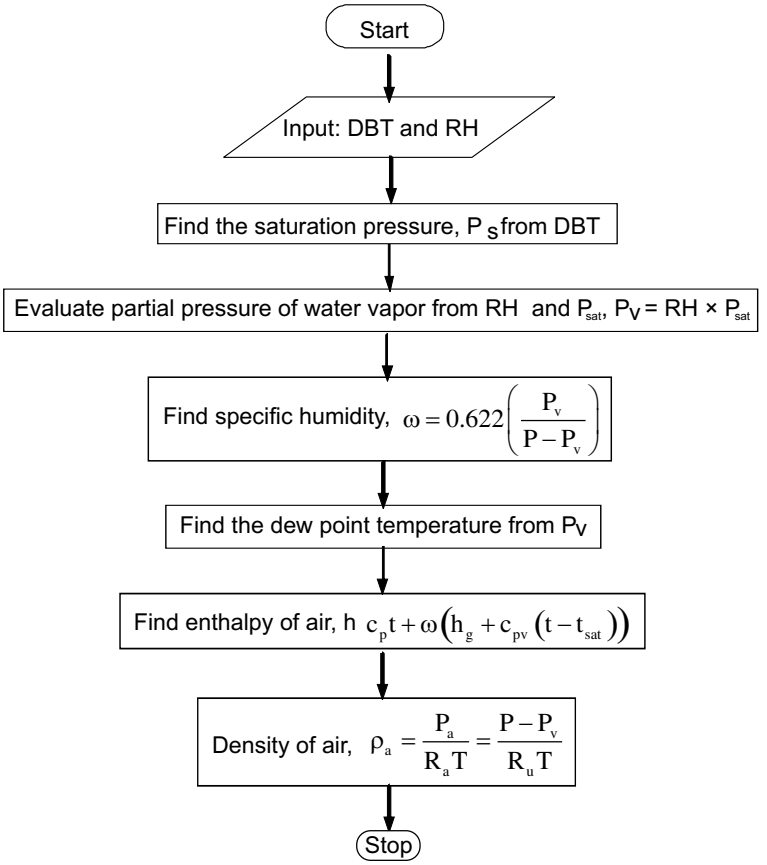

Fig. 7.4: Flow chart for thermodynamic properties of wet air from DBT and RH

The flow chart given in Fig. 7.5 outlines the solution of psychrometric properties from the supplied DBT and WBT.

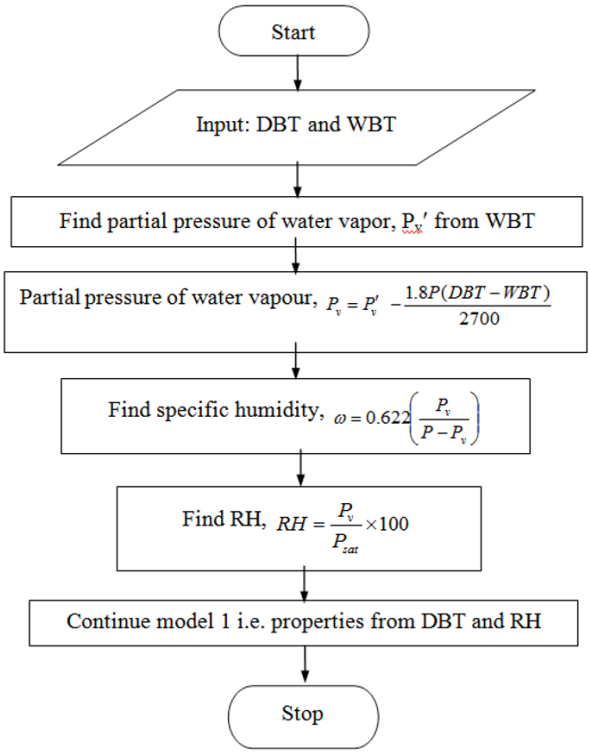

Fig. 7.5: Flow chart for psychrometric properties of wet air from DBT and WBT

The flow chart given in Fig. 7.6 outlines the solution of psychrometric properties from the supplied DBT and DPT.

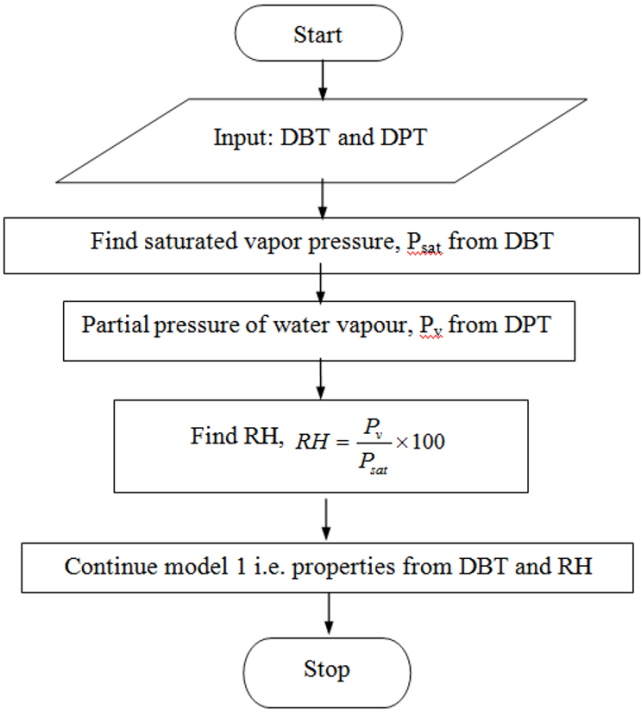

Fig. 7.6: Flow chart for thermodynamic properties of wet air from DBT and DPT

The flow chart given in Fig. 7.7 outlines the solution of psychrometric properties from the supplied DBT and ω.

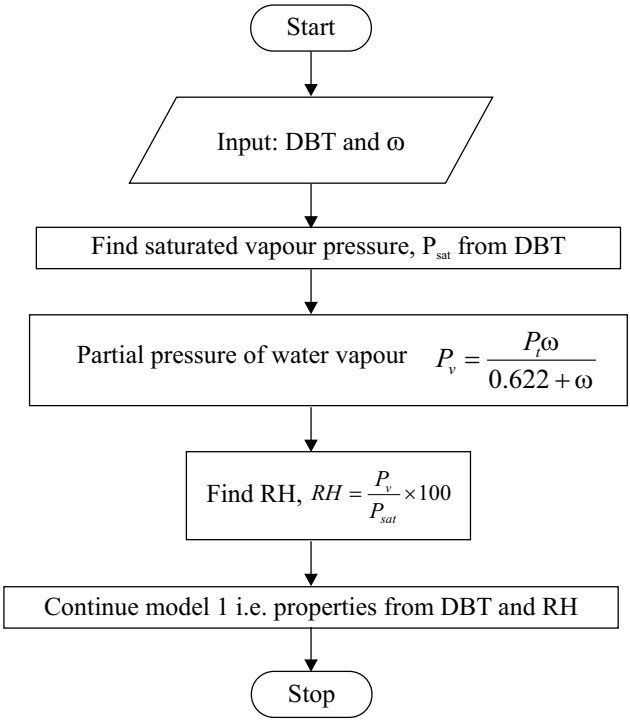

Fig. 7.7: Flow chart for thermodynamic properties of wet air from DBT and specific humidity

7.3 Psychrometric Processes

In the design and analysis of air-conditioning plants, the fundamental requirement is to identify the various processes being performed on air. Once identified, the processes can be analysed by applying the laws of conservation of mass and energy. All these processes can be plotted easily on a psychrometric chart. This is very useful for quick visualisation and also for identifying the changes taking place in important properties such as temperature, humidity ratio, enthalpy, etc. The important processes that air undergoes in a typical air-conditioning plant are discussed below.

Following are the psychrometric processes

1. Sensible cooling
2. Sensible heating
3. Adiabatic humidification
4. Adiabatic mixing
5. Heating and humidification
6. Heating and dehumidification
7. Cooling and humidification
8. Cooling and dehumidification

The psychrometric processes can be shown on a psychrometric chart to read the properties and evaluation. The horizontal lines on psychrometric charts represent sensible heat transfer. The vertical lines on psychrometric charts indicate humidification (upward) or dehumidification (downward) processes. Practically, humidification or dehumidification at a constant temperature is difficult. Therefore, a psychrometric process of vertical nature is rare. The inclined lines on the psychrometric chart represent four types of processes, viz., heating-humidification, heating-dehumidification, cooling-humidification, and cooling-dehumidification. So, except for vertical lines, there is more flexibility to show the processes on the chart.

7.3.1 Sensible cooling

During this process, the moisture content of air remains constant, but its temperature decreases as it flows over a cooling coil. To maintain constant moisture content, the cooling coil's surface should be dry and its surface temperature should be higher than the dew point temperature of air. If the cooling coil is 100% effective, then the exit temperature of air will be equal to the coil temperature. However, in practice, the exit air temperature will be higher than the cooling coil temperature. Fig. 7.8 shows the sensible cooling process (1-2) on a psychrometric chart.

Let m_c is the cold fluid flow rate used for the sensible cooling of air. Let $c_{pc,}$ T_{ci} and T_{co} are the specific heat of cold fluid, cold fluid inlet temperture and cold fluid outlet temperature respectively.

The heat transfer rate during this process is given by

$$Q_c = m_c c_{..}(T_{..} - T_{..}) = m_{.}(h_{.} - h_{.}) \quad (7.21)$$

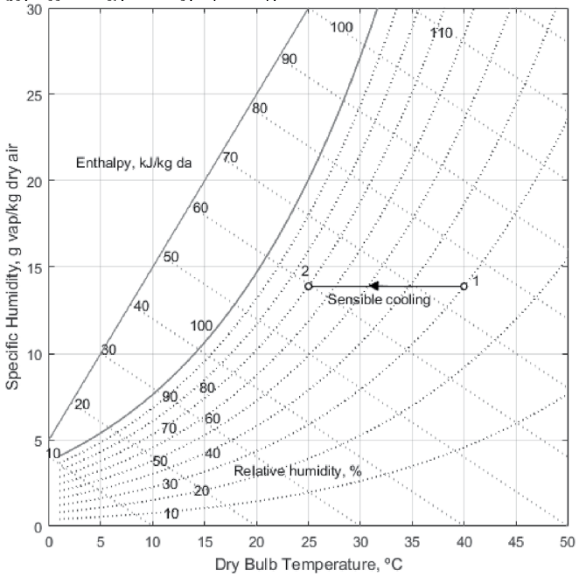

Fig. 7.8: Sensible cooling process on psychrometric chart

7.3.2 Sensible heating

During this process, the moisture content of air remains constant and its temperature increases as it flows over a heating coil (Fig. 7.9). The heat transfer rate during this process is given by

$$Q_h = m_a(h_2 - h_1) = m_a c_{pm}(T_2 - T_1) \tag{7.26}$$

where c_{pm} is the humid specific heat (≈1.0216 kJ/kg dry air) and *m* is the mass flow rate of dry air (kg/s). Figure shows the sensible heating process on a psychrometric chart.

Let m_h is the mass of the hot fluid used for the sensible heating. The temperature of the hot fluid is decreased from T_{hi} to T_{ho} with the specific heat of c_{ph}.

The heat balance in the sensible heating is

$$m_h c_{ph}(T_{hi} - T_{ho}) = m_a(h_2 - h_1) \tag{7.27}$$

The exergy balance of the sensible cooling process,

$$\varepsilon_{hi} + \varepsilon_1 = \varepsilon_{ho} + \varepsilon_2 + I_{SH} \tag{7.28}$$

After the simplification of the exergy balance, the irreversibility of sensible heating,

$$I_{SH} = T_0(m_h(s_{ho} - s_{hi}) + m_a(s_2 - s_1)) \tag{7.29}$$

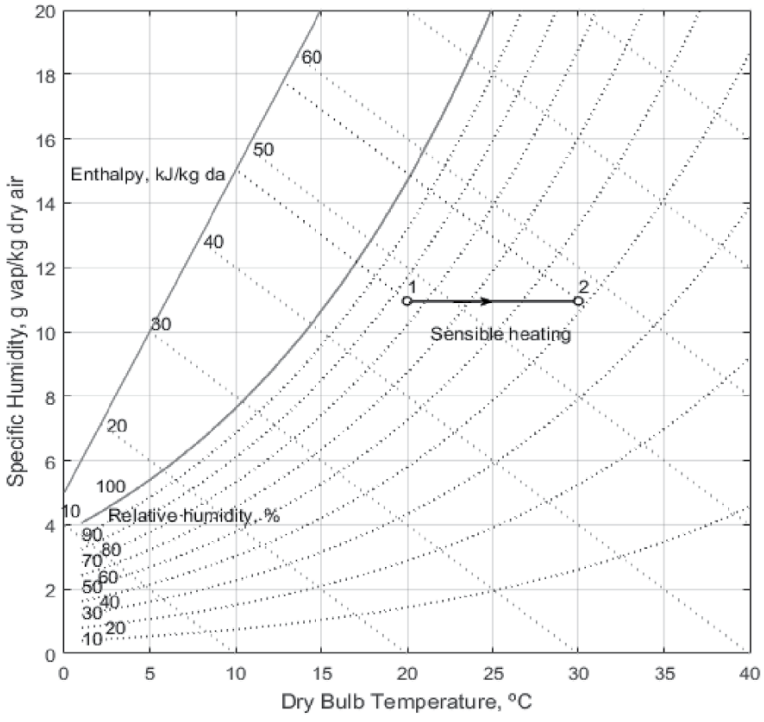

Fig. 7.9: Sensible heating process on psychrometric chart

7.3.3 Cooling and dehumidification

As a result, the temperature and humidity ratios of the air both decrease, as shown in Figs. 7.10 and 7.11. This is the process air undergoes in a typical air conditioning system. Although the actual process path will vary depending upon the type of cold surface, the surface temperature, and flow conditions, for simplicity, the process line is assumed to be a straight line. The heat and mass transfer rates can be expressed in terms of the initial and final conditions by applying the conservation of mass and conservation of energy equations as given below:

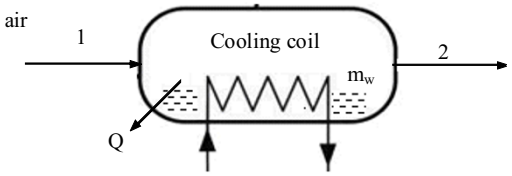

Fig. 7.10: Cooling and dehumidification process

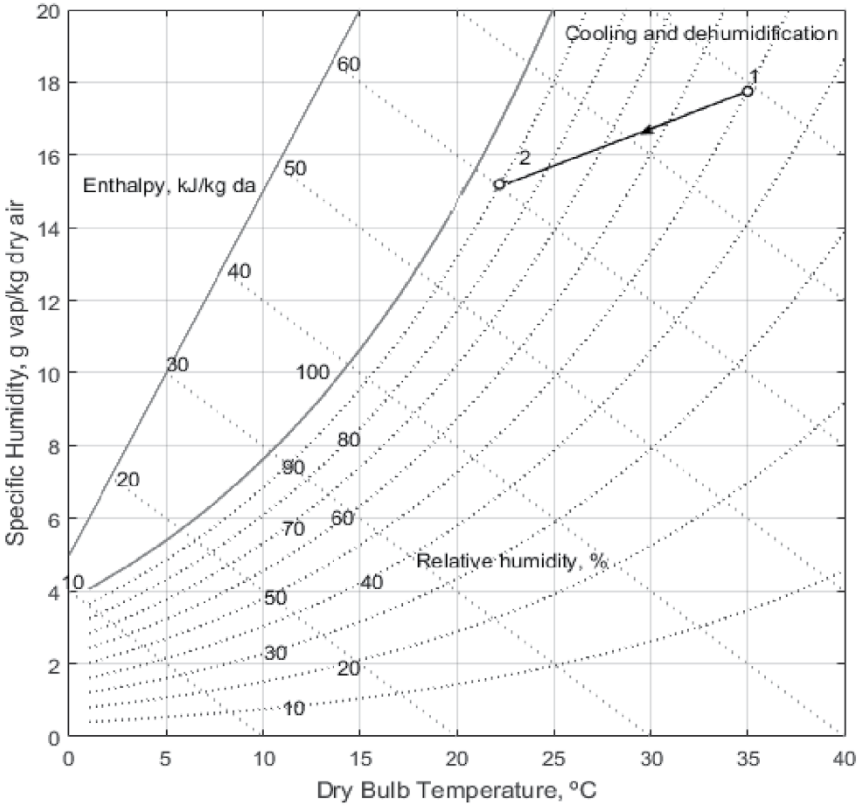

Fig. 7.11: Cooling and dehumidification process on psychrometric chart

By applying mass balance for the water

$$m_a \omega_1 = m_a \omega_2 + m_w \tag{7.30}$$

Let m_c is the cold fluid flow rate used for the cooling and dehumidification of the air. Let $c_{pc,}$ T_{ci} and T_{co} are the specific heat of fluid, cold fluid inlet temperture and cold fluid outlet temperature respectively.

By applying exergy balance

$$m_a h_1 = Q_c + m_w h_w + m_a h_2 \tag{7.31}$$

from the above two equations i.e. mass balance and exergy balances, the load on the cooling coil, Q is given by

$$Q_c = m_c c_{pc}(T_{co} - T_{ci}) = m_a (h_1 - h_2) - m_a (\omega_1 - \omega_2) h_w \tag{7.32}$$

The 2nd term on the RHS of the above equation is normally small compared to the other terms, so it can be neglected. Hence,

$$Q_c = m_a (h_1 - h_2) \tag{7.33}$$

It can be observed that the cooling and de-humidification process involves both latent and sensible heat transfer processes, hence, the total, latent and sensible heat transfer rates (Q, Q_l and Q_s) can be written as

$$Q = Q_l + Q_s \tag{7.34}$$

where

$$Q_l = m_a (h_1 - h_w) = m_a (\omega_1 - \omega_2) h_{fg} \tag{7.35}$$

$$Q_s = m_a (h_w - h_2) = m_a c_{pm} (T_1 - T_2) \tag{7.36}$$

By separating the total heat transfer rate from the cooling coil into sensible and latent heat transfer rates, a useful parameter called Sensible Heat Factor (SHF) is defined. SHF is defined as the ratio of sensible to total heat transfer rate, i.e.,

$$\text{SHF} = \frac{Q_s}{Q} = \frac{Q_s}{Q_s + Q_l} \tag{7.37}$$

From the above equation, one can deduce that a SHF of 1.0 corresponds to no latent heat transfer and a SHF of 0 corresponds to no sensible heat transfer. A SHF of 0.75 to 0.80 is quite common in air conditioning systems in normal dry climates. A lower value of SHF, say 0.6, implies a high latent heat load such as that which occurs in a humid climate. From Fig.7.12, it can be seen that the slope of the process line 1-2 is given by

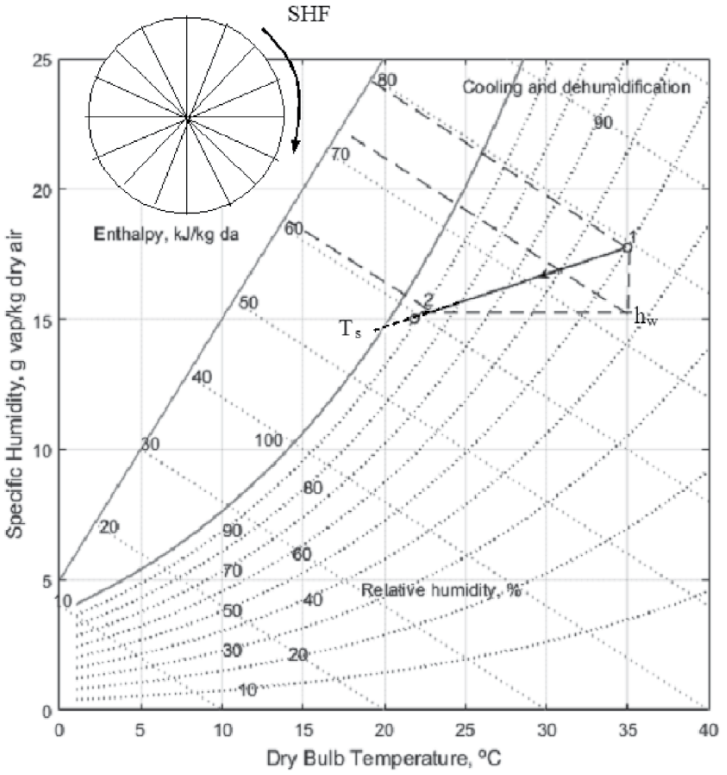

Fig. 7.12: Psychrometric chart with protractor for SHF lines

From the definition of SHF,

$$\frac{Q_l}{Q_s} = \frac{1-SHF}{SHF} = \frac{m_a \Delta\omega h_{fg}}{m_a c_{pm} \Delta T} = \frac{2501\Delta\omega}{1.0216\Delta T} = 2451\frac{\Delta\omega}{\Delta T} \tag{7.38}$$

From the above equations, we can write the slope as

$$\tan\theta = \frac{\Delta\omega}{\Delta T} = \frac{1}{2451}\left(\frac{1-SHF}{SHF}\right) \tag{7.39}$$

$$\frac{1}{SHF} - 1 = 2451 \times \frac{\Delta\omega}{\Delta T} \qquad SHF = \frac{1}{1 + 2451 \times \left(\frac{\Delta\omega}{\Delta T}\right)}$$

$$SHF = \frac{\Delta T}{\Delta T + 2451\Delta\omega} \tag{7.40}$$

Thus, we can see that the slope of the cooling and dehumidification line is purely a function of the sensible heat factor, SHF. Hence, we can draw the cooling and dehumidification lines on the psychrometric chart if the initial state and the SHF are known. In some standard psychrometric charts, a protractor with different values of SHF is provided. The process line is drawn through the initial state point and in parallel to the given SHF line from the protractor, as shown in Fig. 7.12.

In Fig. 7.12, the temperature T_s is the effective surface temperature of the cooling coil, and is known as the apparatus dew-point (ADP) temperature. In an ideal situation, when all the air comes into perfect contact with the cooling coil surface, the air temperature will be the same as the ADP of the coil. However, in actual cases, the exit temperature of air will always be greater than the apparatus dew-point temperature due to boundary layer development as air flows over the cooling coil surface and also due to temperature variation along the fins, etc. Hence, we can define a by-pass factor (BF) as

$$BF = \frac{T_2 - T_S}{T_1 - T_S} = \frac{h_2 - h_S}{h_1 - h_S} = \frac{\omega_2 - \omega_S}{\omega_1 - \omega_S} \tag{7.41}$$

It is clear that the higher the by-pass factor, the greater the difference in temperature between the air outlet and the cooling coil. When BF is 1.0, all the air bypasses the coil, and there will not be any cooling or dehumidification. In practice, the by-pass factor can be increased by increasing the number of rows in a cooling coil, by decreasing the air velocity, or by reducing the fin pitch. Alternatively, a contact factor (CF) can be defined, which is given by

$$CF = 1 - BF \tag{7.42}$$

The exergy balance applied to the cooling and dehumidification process,

$$\varepsilon_{ci} + \varepsilon_1 = \varepsilon_{co} + \varepsilon_2 + \varepsilon_w + I_{CDH} \tag{7.43}$$

Substituting the enthalpy and entropy for energy,

$$m_c (h - T_0 s)_{ci} + m_a (h - T_0 s)_1 = m_c (h - T_0 s)_{co} + m_a (h - T_0 s)_2 + m_a (\omega_1 - \omega_2) (h - T_0 s)_w + I_{SC} \tag{7.44}$$

After the simplification of the exergy balance, the irreversibility of cooling and dehumidification,

$$I_{CDH} = T_0 (m_c (s_{co} - s_{ci}) + m_a (s_2 - s_1) + m_a (\omega_1 - \omega_2) s_w) \tag{7.45}$$

7.3.4 Heating and humidification

During winter, it is essential to add heat and humidity to the room air for comfort. As shown in Figs. 7.13 and 7.14, this is done by hot water spray for air heating and humidification. The water temperature decreases and the air temperature increases in this process.

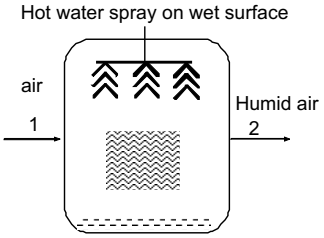

Fig. 7.13: Heating and humidification process

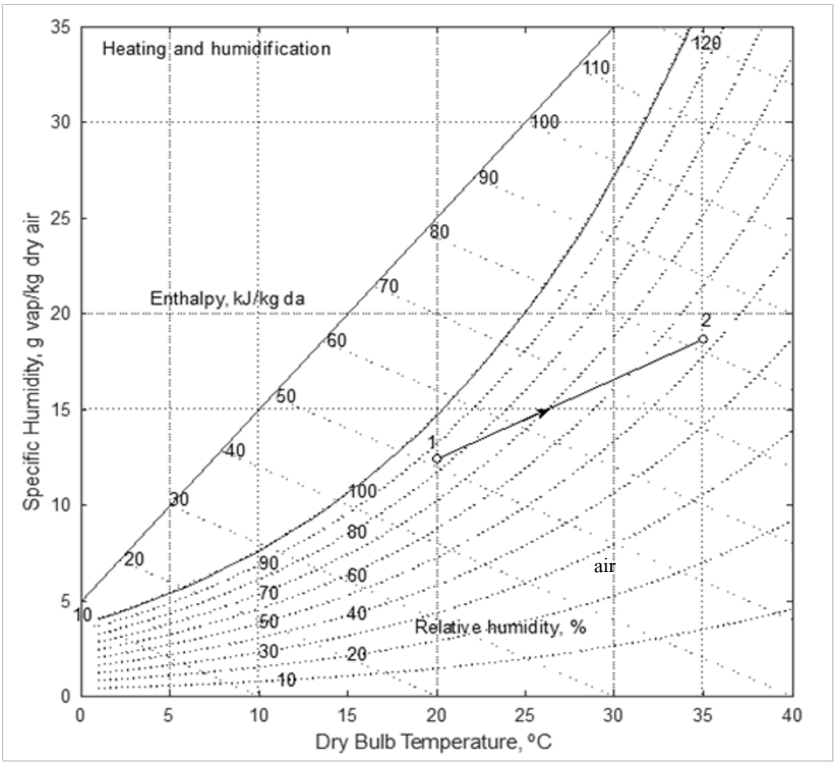

Fig. 7.14: Heating and humidification on a psychrometric chart

Let m_{hi} and m_{ho} are the mass flow rate at the inlet and outlet of the humidifier. The mass balance of water vapor for the control volume yields the rate at which water has been added to air, i.e., m_w

$$m_w = m_a(\omega_o - \omega_i) \quad (7.46)$$

where m_a is the mass flow rate of dry air.

From energy balance,

$$Q_h = m_{hi}h_{hi} - m_{ho}h_{ho} = m_a(h_2 - h_1) \quad (7.47)$$

where

$$m_{ho} = m_{hi} - m_a(\omega_o - \omega_i) \quad (7.48)$$

where Q_h is the heat supplied through the hot water. Since this process also involves simultaneous heat and mass transfer, we can define a sensible heat factor for the process in a way similar to that of a cooling and dehumidification process.

The exergy balance applied to the heating and humidification process,

$$\varepsilon_{hi} + \varepsilon_1 = \varepsilon_{ho} + \varepsilon_2 + I_{HH} \quad (7.49)$$

Substituting the enthalpy and entropy in energy,

$$m_{hi}(h - T_0s)_{hi} + m_a(h - T_0s)_1 = m_{ho}(h - T_0s)_{ho} + m_a(h - T_0s)_2 + I_{HH} \quad (7.50)$$

After the simplification of the exergy balance, the irreversibility of heating and humdidification,

$$I_{HH} = T_0[(m_{ho}s_{ho} - m_{hi}s_{hi}) + m_a(s_2 - s_1)] \quad (7.51)$$

7.3.5 Cooling and humidification

As the name implies, during this process, the air temperature drops and its humidity increases. This process is shown in Figs. 7.15 and 7.16. As shown in the figure, this can be achieved by spraying cool water into the air stream. The temperature of water should be lower than the dry-bulb temperature of air but higher than its dew-point temperature to avoid condensation ($T_{DPT} < T_w < T_1$).

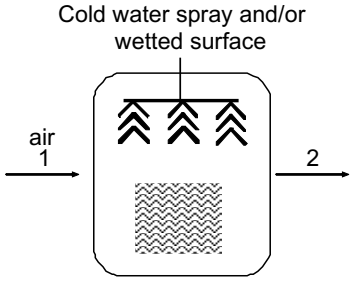

Fig. 7.15: Cooling and humidification process

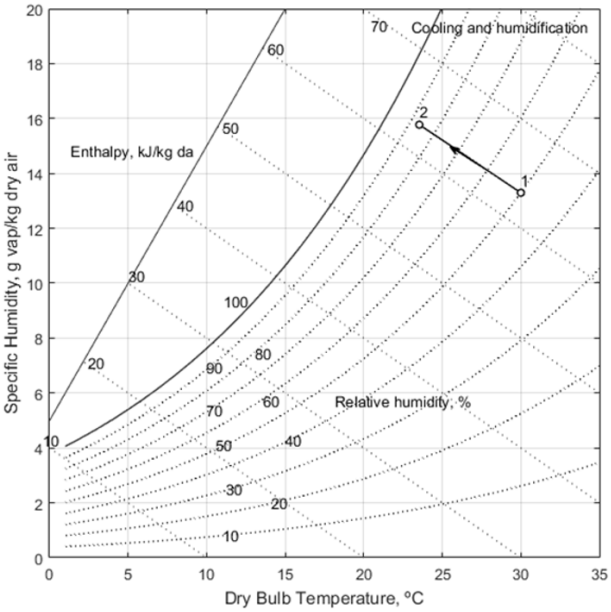

Fig. 7.16: Cooling and humidification process on psychrometric chart

It can be seen that during this process there is sensible heat transfer from air to water and latent heat transfer from water to air. Hence, the total heat transfer depends upon the water temperature. If the temperature of the water sprayed is equal to the wet bulb temperature of air, then the net transfer rate will be zero as the sensible heat transfer from air to water will be equal to the latent heat transfer from water to air. If the water temperature is greater than WBT, then there will be a net heat transfer from water to air. If the water temperature is lower than WBT, then the net heat transfer will be from air to water. In a special case when the spray water is entirely recirculated and is neither heated nor cooled, the system is perfectly insulated and the make-up water is supplied at WBT. Then, at steady-state, the air undergoes an adiabatic saturation process, during which its WBT remains constant. This is the process of adiabatic saturation. The process of cooling and humidification is encountered in a wide variety of devices such as evaporative coolers, cooling towers, etc.

The formulation created for heating and humidification can also be used for cooling and humidification.

7.3.6 Heating and dehumidification

This process can be achieved by using a hygroscopic material, which absorbs or adsorbs the water vapor from the moisture. If this process is thermally isolated, then the enthalpy of air remains constant, as a result the temperature of air increases as its moisture content decreases as shown in Fig. 7.17. This hygroscopic material can be a solid or a liquid. In general, the absorption of water by the hygroscopic material is an exothermic reaction, as a result heat is released during this process, which is transferred to air and the enthalpy of air increases.

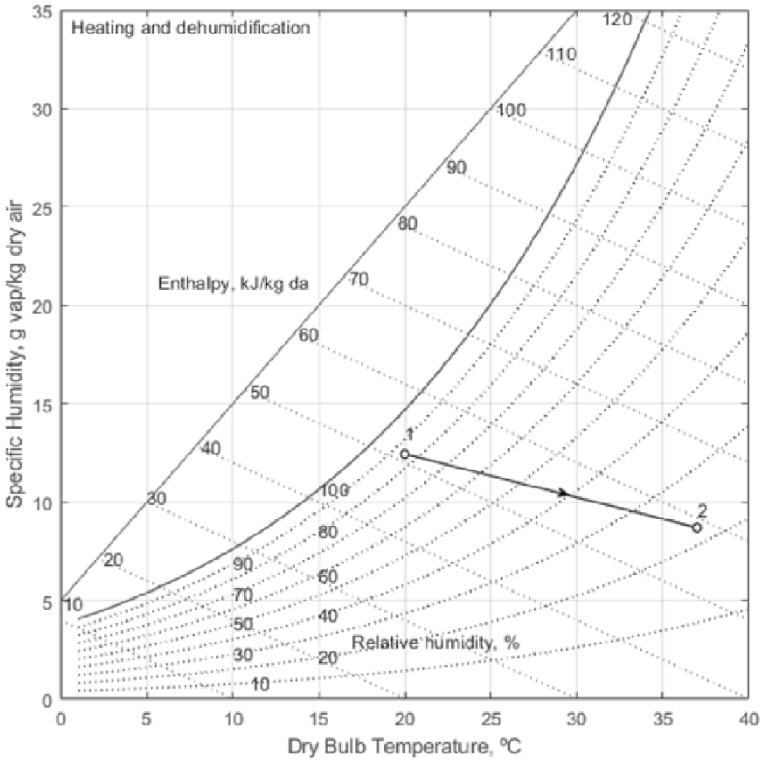

Fig. 7.17: Heating and dehumidification on a psychrometric chart

7.3.7 Mixing without condensation

Mixing of air streams at different states is commonly encountered in many processes, including air conditioning (Fig. 7.18). Depending upon the state of the individual streams, the mixing process can take place with or without condensation of moisture.

The figure shows the adiabatic mixing of two moist air streams during which no condensation of moisture takes place. As shown in the figure, when two air streams at state points 1 and 2 mix, the resulting mixture condition 3 can be obtained from mass and energy balance.

From the mass balance of dry air and water vapor,

$$m_{a1}\,\omega_1 + m_{a2}\,\omega_2 = m_{a3}\,\omega_3 = (m_{a1} + m_{a2})\,\omega_3 \tag{7.52}$$

From energy balance

$$m_{a1}\,h_1 + m_{a2}\,h_2 = m_{a3}\,h_3 = (m_{a1} + m_{a2})\,h_3 \tag{7.53}$$

From the above equations, it can be observed that the final enthalpy and humidity ratio of a mixture are weighted averages of the inlet enthalpies and humidity ratios. A generally valid approximation is that the final temperature of the mixture is the weighted average of the inlet temperatures. With this approximation, the point on the psychrometric chart representing the mixture lies on a straight line connecting the two inlet states. Hence, the ratio of distances on the line, i.e., (1-3)/(2-3) is equal to the ratio of flow rates $m_{a,2}$ / $m_{a,1}$. The resulting error (due to the assumption that the humid specific heat is constant) is usually less than 1 percent.

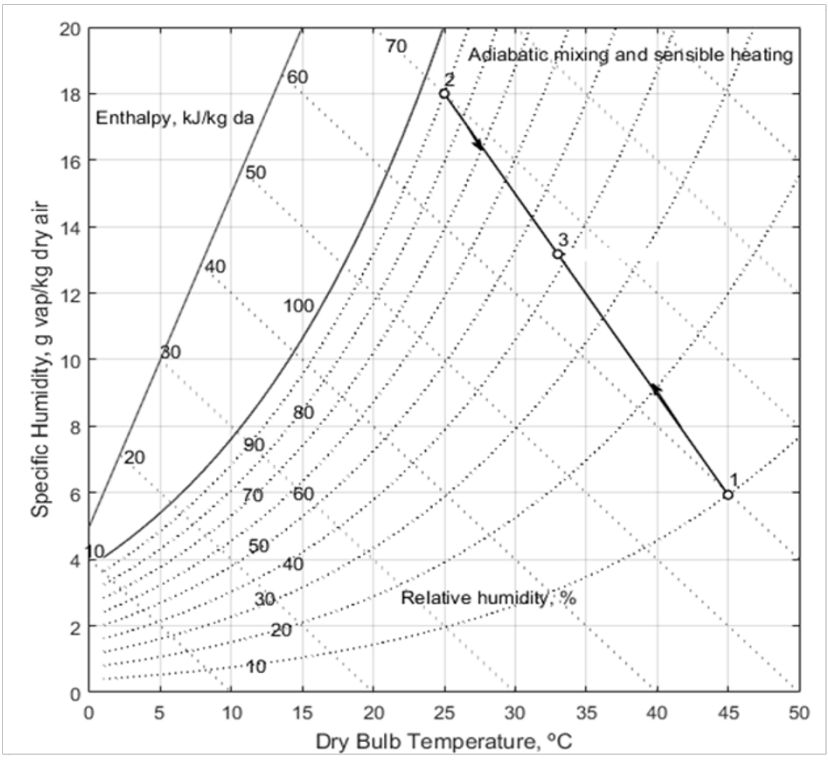

Fig. 7.18: Mixing of two air streams without condensation

The exergy balance of mixing process,

$$\varepsilon_1 + \varepsilon_2 = \varepsilon_3 + I_{mixing} \tag{7.54}$$

Substituting the enthalpy and entropy for energy,

$$m_{a1}(h - T_0 s)_1 + m_{a2}(h - T_0 s)_2 = m_{a3}(h - T_0 s)_3 + I_{mixing} \tag{7.55}$$

After the simplification of the exergy balance, the irreversibility of mixing process,

$$I_{mixing} = T_0 (m_{a3} s_3 - m_{a1} s_1 - m_{a2} s_2) \tag{7.56}$$

7.3.8 Mixing with condensation

When very cold and dry air mixes with warm air at high relative humidity, the resulting mixture condition may lie in the two-phase region. As a result, there will be condensation of water vapour and some amount of water will leave the system as liquid water. Due to this, the humidity ratio of the resulting mixture (point 3) will be less than that of point 4 (Fig. 7.19). Corresponding to this will be an increase in the temperature of the air due to the release of latent heat from condensation. This process rarely occurs in an air conditioning system, but this is the phenomenon that results in the formation of fog or frost (if the mixture temperature is below 0 °C). This happens in winter when the cold air near the earth mixes with the humid and warm air that develops in the evening or after rain.

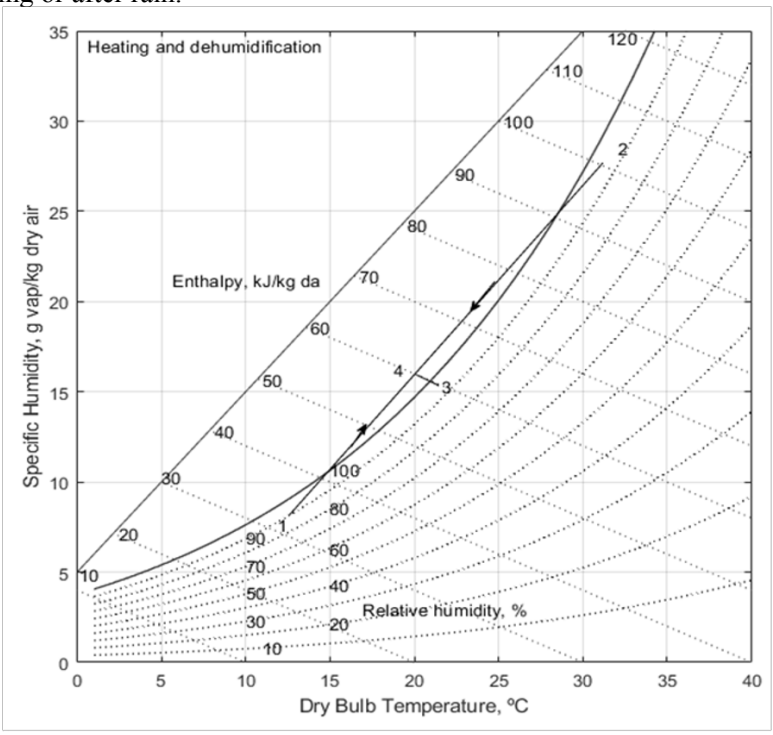

Fig. 7.19: Mixing with condensation on psychrometric chart

7.3.9 Constraints of humidification/dehumidification and heating/cooling

In a humidifier, air flows against the water flow on packing similar to a cooling tower. During this process, both heat and mass transfer occur with the direct contact of air and water. The heat flows in the direction of the temperature drop. Similarly, the mass transfer occurs in the direction of a decrease in the vapour pressure. The temperature of the exit air depends on the temperature of the water spray and air inlet conditions. In the case of sensible heat transfer, in place of water spray, either a heating coil or a cooling coil is placed, respectively for sensible heating and sensible cooling. In heating and dehumidification, water spray can be replaced with the hygroscopic material. Fig. 7.20 summarises all the psychrometric processes as per the process constraints.

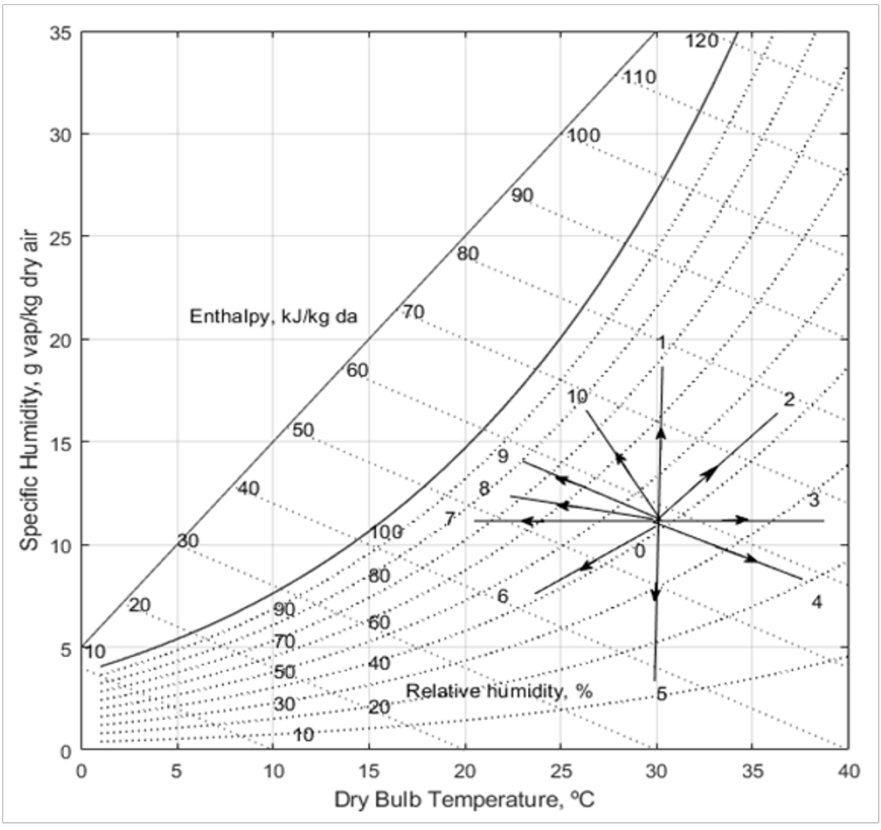

Fig. 7.20: Psychrometric processes on psychrometric chart

Following details, the psychrometric processes with reference to the chart shown in Fig. 7.20.

0-1: Humidification

In the process of only humidification, mass transfer occurs with latent heat transfer. The temperature of the air is maintained constant, similar to the isothermal process. Humidification happens in hot conditions by evaporating water into the air.

0-2: Heating and humidification ($t_w > t_{DBT}$)

If the temperature of the water spray is higher than the dry bulb temperature of the supply air, the resultant process is heating and humidification. In heating and humidification, sensible heat and latent heat transfer. In the cooling tower of a typical thermal power plant, the psychrometric process is the heating and humidification of air. The result is cooled water that can be recirculated to a surface condenser. But in the air conditioning process, the main fluid is air. Therefore, the hot, humid air is used for conditioning the air to maintain the required temperature and humidity ratio.

0-3: Sensible heating

Sensible heating is a heat transfer process without any mass transfer. When air flows over a heating coil, the air gets heated, which is called sensible heating due to sensible heat transfer. Sensible heating controls the temperature only at the constant specific humidity level. During this process, the relative humidity decreases.

0-4: Heating and dehumidification

Heating and dehumidification can be designed with the adoption of hygroscopic material without the use of water spray. If the hygroscopic material is absorbing the moisture from the air in an isolated condition, the specific humidity of the air decreases. Since the process is isolated, the specific enthalpy is constant. Hence, the dry bulb temperature of the air decreases and results in heating and dehumidification.

0-5: Dehumidification

In the dehumidification process, mass transfers with latent heat transfer similar to the humidification process. The temperature of the fluid is constant. Dehumidification occurs in a cold environment by condensing the moisture from the air.

0-6: Cooling and dehumidification ($t_w < t_{DPT}$)

If chilled water is sprayed over the air stream, the temperature of the air decreases and its moisture condenses. This process occurs if the temperature of the water is less than the dew point temperature of the supply air. Sensible heat and latent heat transfer from the air to water. The cooling process occurs with the sensible heat transfer from air to water. Similarly, the latent heat transfer from air to water influences dehumidification. The temperature of the water increases, and the air temperature drops. Cooling and dehumidification are regular processes in typical air conditioning.

0-7: Sensible cooling

Sensible cooling is a heat transfer process without any mass transfer. When air flows over a cooling coil or chiller, the air gets cooled, which is called sensible cooling due to sensible heat transfer. Sensible cooling controls the temperature only at the constant specific humidity. During this process, the relative humidity increases.

0-8: Cooling and humidification ($t_{DPT} < t_w < t_{WBT}$)

If the water spray temperature is between the wet bulb temperature and the dry bulb temperature of the supply air, the result is cooling and humidification. The sensible heat transfer is from the air to water, and the latent heat transfer is from the water to air. The net heat transfer is from the air to water. Therefore, the resultant process is a cooling process with humidification.

0-9: Adiabatic saturation ($t_w = t_{WBT}$)

An adiabatic saturation process results if the water spray temperature is equal to the wet bulb temperature of the air supply. In this process, the sensible heat transfer from air to water is equal to the latent heat transfer from water to air. Therefore, there is no change in the enthalpy of air as it is an adiabatically process.

0-10: Cooling and humidification ($t_{WBT} < t_w < t_{DBT}$)

If the water spray temperature is set at a difference between the wet bulb temperature and the dry bulb temperature of the supply air, cooling and humidification result. The sensible heat transfer is from the air to water, and the latent heat transfer is from the water to air. The temperature of the air has decreased.

7.4 Basic HDH Desalination

The arrangement and working of the HDH desalination is depicted in Fig. 7.21. The fluid flows in this unit are air, hot water, circulating water, and freshwater. Atmospheric air (1) flows into the unit through the circulating fan (1-2). The air needs to be preheated (2–3) before being supplied to the humidifier to increase the humidification capacity. The untreated water (8) is heated in a solar water heater (SWH) to result in the heating and humidification process in HDH desalination. The required amount of hot water (10) is used in the air preheater (APH) to increase the air temperature. The sensible heating of air in the APH decreases the relative humidity (RH) of air, resulting in more chances of humidification. Therefore, the APH increases the desalination yield. In the humidifier, the hot water (12) is sprayed at the top over the packing. The packing provides the contact surface between the water and air and increases the residence time. The preheated air (3) enters into the humidifier and flows over the wetted packing material. Therefore, the air is humidified (3–4) through the evaporation of the hot water into the air. The balanced brine water

is collected at the bottom of the humidifier (13) and recirculated for continuous operation. The humid air (4) enters into the dehumidifier for the condensation of water to result in fresh water. The dehumidification process (4-5) in this unit is a cooling and dehumidification process. To condense the humid air, normal circulating water, chilled water, or direct use of an evaporator coil of refrigerant can be used. The condensation rate increases with a decrease in the low temperature surface in the dehumidifier. The cooling medium temperature increases (16–17) by absorbing the heat from the humidifier. In the case of an evaporator, the temperature of the refrigerant is constant due to the phase change operation. The dehumidifier's condensate is the resultant freshwater (7). If the cold surface in the dehumidifier is below the ambient temperature, the resultant air (6) has the capacity to be used in an air conditioning unit. Therefore, HDH can be extended to cooling with proper integration of the cold surface. The hot water collected from the APH (11) and humidifier (13) is pumped to SWH for reuse. The supply of saline water (8) to SWH serves as a makeup water to compensate for the removal of freshwater.

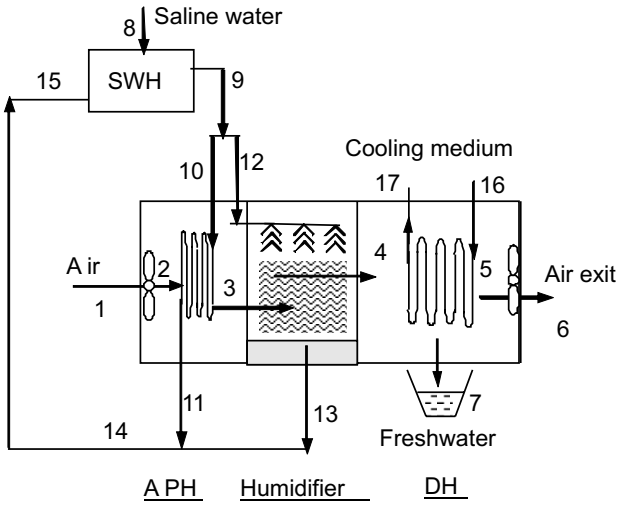

Fig. 7.21: Basic working principle of HDH desalination

7.4.1 Thermodynamic evaluation of HDH desalination

The air flow rate in the HDH plant is fixed at 100 m^3/h. The weightage factor for the high grade energy is 3. The outside temperature is 25 °C and the pressure is 1.01325 bar. The average solar radiation is evaluated at the equinox for the assessment of solar plant efficiency. The considered average global solar radiation is 520 W/m^2 at the location of Jalandhar, India. The RH of atmospheric air is 75% as per the local climatic conditions. The hot water supply temperature is 50 °C. The liquid to air ratio in a humidifier is 1.0. The hot water temperature drop in the APH is 8 °C. In the dehumidifier, the circulating water supply temperature is set at 25 °C.

The air flowing in the desalination duct consists of dry air (da) and moisture (ω). The dry air with moisture is called wet air (wa). The wet air flow is determined by its volume flow rate.

$$m_1 = \frac{V_{wa} MW_{wa}}{22.4} \tag{7.57}$$

From the mass of wet air and its moisture or humidity content, the dry air can be determined or vice versa.

The mass of dry air,

$$m_{da} = \frac{m_a}{1+\omega_1} \tag{7.58}$$

7.4.1.1 Fan

The energy balance applied to fan results the electricity supply to operate it Neglecting the velocity of air at the inlet of fan,

$$W_{fan} = m_{da}(h_2 - h_1)\frac{1}{2000}C_2^2 \tag{7.59}$$

In the above equation C is the velocity of air.

7.4.1.2 Air preheater

Air preheating is a sensible heating as shown in Fig. 7.22. The hot water supply to APH is determined from its temperature drop and heat load of air heater.

$$m_{10} = \frac{m_{da}(h_3 - h_2)}{c_{pw}(T_{10} - T_{11})} \tag{7.60}$$

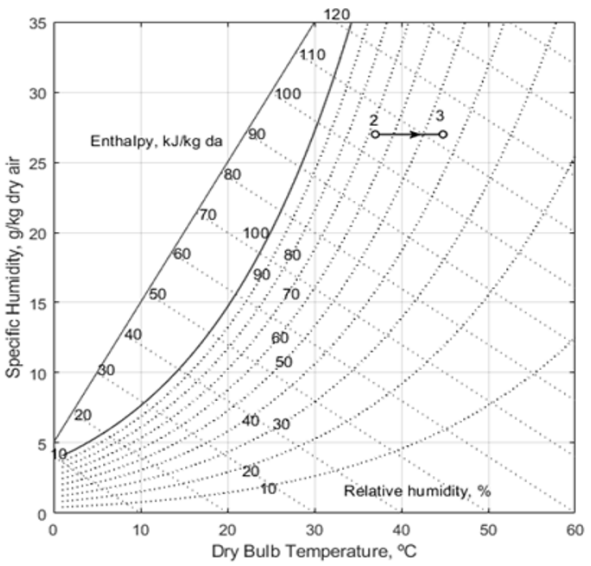

Fig. 7.22: Sensible heating in an air preheater of HDH desalination

7.4.1.3 Humidifier

As per the constraints discussed in the earlier section, in the humidifier, the resultant process may be either heating and humidification or cooling and humidification. Fig. 7.23 shows a typical heating and humidification process in a humidifier.

The brine solution at the bottom of the humidifier is less than the supplied water due to its evaporation.

Therefore, the brine is equal to the hot water supply minus the evaporated water.

$$m_{13} = m_{12} - m_{da}(\omega_4 - \omega_3) \tag{7.61}$$

This evaporated water is added to the preheated air in the humidifier. Therefore,

$$m_4 = m_3 + m_{da}(\omega_4 - \omega_3) \tag{7.62}$$

The energy balance in humidifier, results the brine solution temperature from the humidifier.

$$T_{13} = \frac{m_{12}c_{pw}T_{12} - m_{da}(h_4 - h_3)}{m_{13}c_{pw}} \tag{7.63}$$

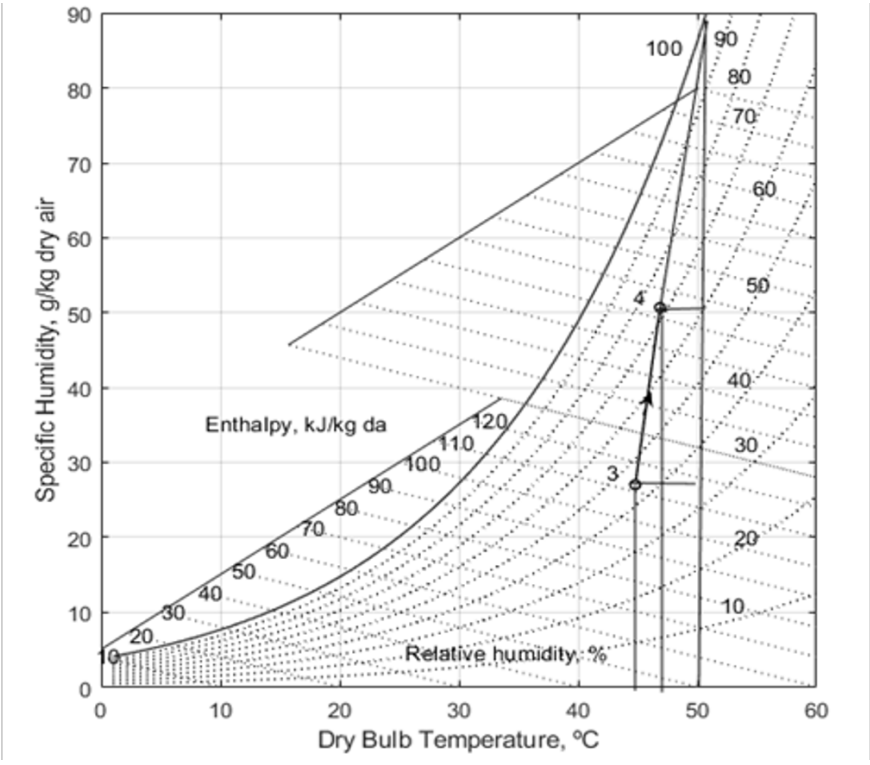

Fig. 7.23: Prediction of exit temperature from the maximum humidifcation limit

7.4.1.4 Dehumidifier

Fig. 7.24 shows the cooling and dehumidification process in a dehumidifier.

In the dehumidifier, the condensate from the humid air forms as a freshwater.

The freshwater from the dehumidifer,

$$m_7 = m_{da}(\omega_4 - \omega_5) \tag{7.64}$$

The circulating water required in the dehumidifier is determined from the energy balance.

$$m_{16} = \frac{m_{da}(h_4 - h_5)}{c_{pw}(T_{17} - T_{16})} \tag{7.65}$$

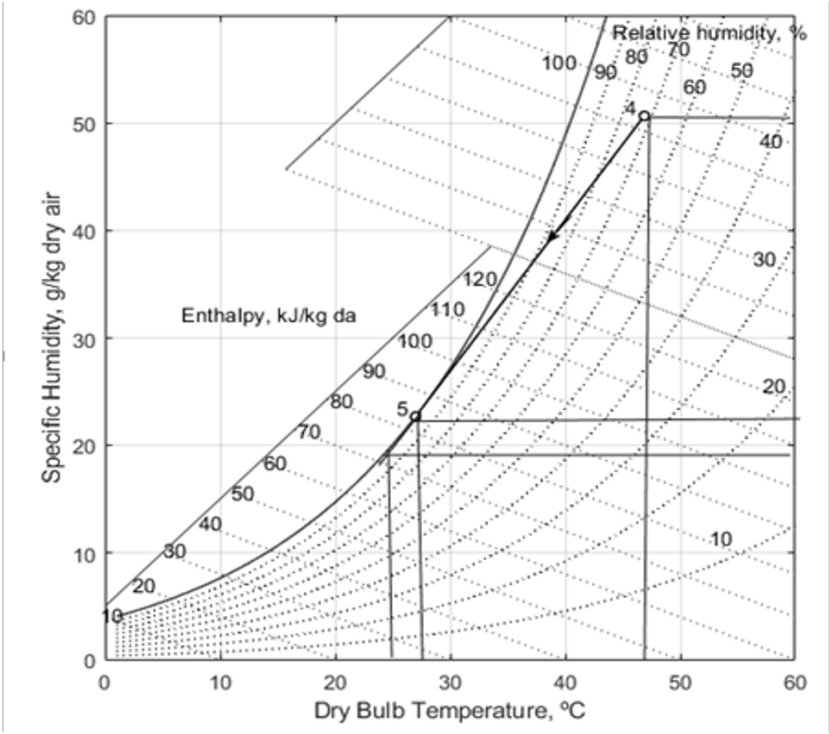

Fig. 7.24: Dehumidification process directed towards the apparatus dew point temperature

7.4.2 Performance of HDH

The specific desalination expressed in g/m^3 of air,

$$m_{fw,\,spe} = \frac{m_{fw} \times 1000}{V_a} \tag{7.66}$$

The EPR is the energy efficiency of HDH system,

EPR of HDH cycle,

$$EPR_C = \frac{m_{fw} h_{fg}}{yW_s + Q_s} \tag{7.67}$$

In EPR, Ws and Qs are the electricity supply and heat supply to operate the HDH desalination. The electricity supply includes two fans and two pumps (for hot water and circulating water). The heat is supplied to the APH and humidifier. The weight factor (y) for the high grade energy is 3, based on the average power plant efficiency of 33.3%.

EPR of HDH plant,

$$\mathrm{EPR}_{\mathrm{pt}} = \frac{m_{fw} h_{fg}}{yW_s + 0.001GA_{SWH}} \tag{7.68}$$

In the above equation, G is global solar radiation and A_{SWH} is the area of solar water heater.

7.4.3 Performance characteristics

The identified independent process conditions in this HDH desalination are hot water supply temperature, atmospheric air temperature, atmospheric air relative humidity, and circulating water supply temperature. The performance conditions analysed in this section are freshwater productivity, the cycle's EPR, and the plant's EPR.

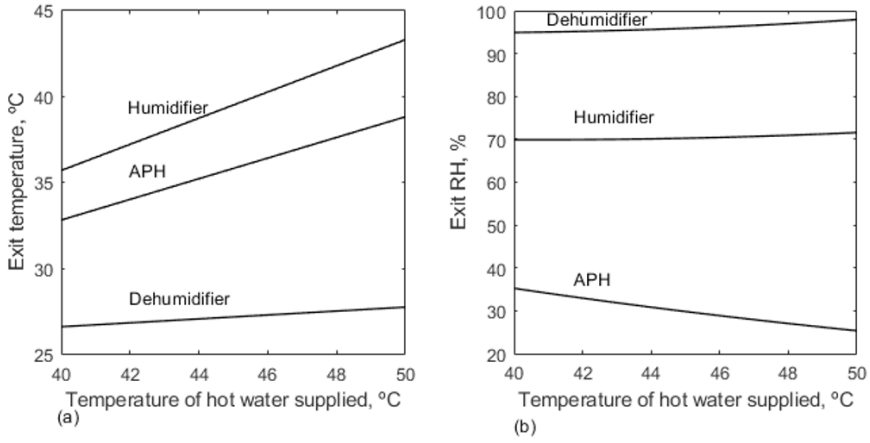

Fig. 7.25: Changes in (a) exit temperature and (b) exit relative humidity of APH, humidifier and dehumidifier of HDH at the stated conditions

Fig. 7.25 simulates the exit conditions (temperature and relative humidity) of the components, viz., APH, humidifier, and dehumidifier. The hot water temperature is increased from 40 °C to 50 °C to study the exit temperatures of components (Fig. 7.25a). The exit temperatures from the APH, humidifier, and dehumidifier increase with an increase in the hot water supply temperature

to the plant. Similarly, the RH at the exit of these three components is studied with the hot water supply temperature (Fig. 7.25b). The RH of APH decreases with the heating of air in APH. It will give more scope for humidification in the humidifier. Therefore, the relative humidity at the exit of the humidifier and dehumidifier also increases with an increase in hot water supply temperature.

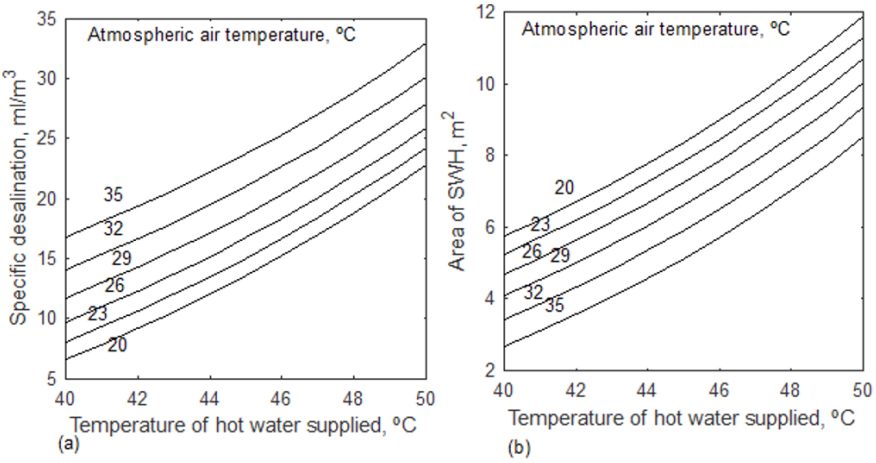

Fig. 7.26: Influence of hot water supply temperature and atmospheric air's temperature on specific desalination from the HDH unit

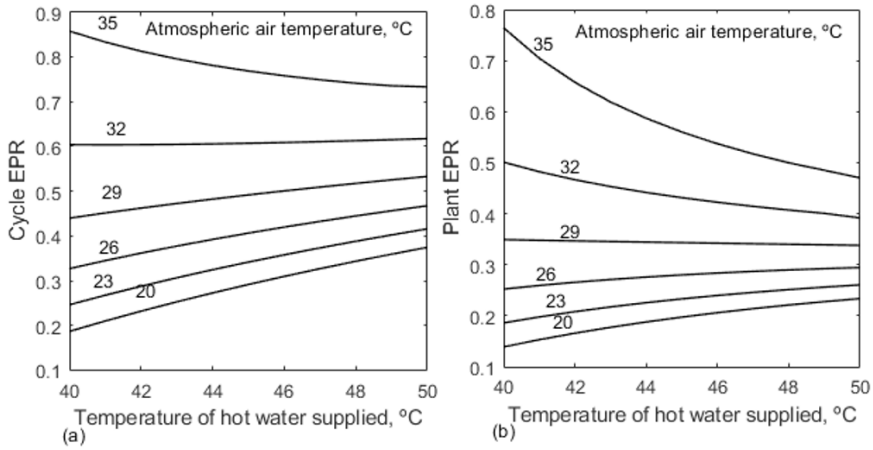

Fig. 7.27 Influence of hot water supply temperature and atmospheric air's temperature on EPR of cycle and plant

Fig. 7.26a shows the effect of hot water temperature, which is the supply to the APR and humidifier, and atmospheric temperature on specific humidity. The specific humidity is expressed in ml/m^3 of air flow. The total desalination can be evaluated by multiplying the specific desalination with

the air flow rate in the unit. The increase in hot water temperature increases the sensible heating and humidification of air. The increase in humidity causes more condensation in the dehumidifier. Therefore, the specific desalination is increased with an increase in the hot water supply temperature. The ambient temperature is increased from 20 °C to 35 °C with a fixed relative humidity. The specific humidity of the supply air to the humidifier increases with an increase in temperature at a fixed relative humidity. This also increases the specific humidity of the air exiting the humidifier. Therefore, humid air condenses more in the dehumidifier.

Fig. 7.26b shows the changes in the solar water heater's area with the change in hot water temperature and atmospheric air temperature. In this analysis, the air flow rate is fixed at 100 m^3/h. The rise in hot water temperature necessitates the use of a large-capacity SWH. Hence, the area of the collector is increasing with an increase in the hot water supply temperature.

Fig. 7.27 analyses the effect of hot water supply temperature and atmospheric air's relative humidity on (a) the EPR of a cycle and (b) the EPR of a plant. The hot water temperature on the EPR is showing favourable and unfavourable conditions. The EPR is increasing with an increase in hot water supply temperature at lower atmospheric temperatures. At higher atmospheric temperatures, the increase in hot water supply temperature decreases the EPR. EPR is a function of input energy and freshwater output. Increased hot water temperature increases freshwater production, but at the expense of increased energy supply. The increase in energy supply causes a decrease in EPR. For maximum EPR, the system requires a low water supply temperature and a high air temperature.

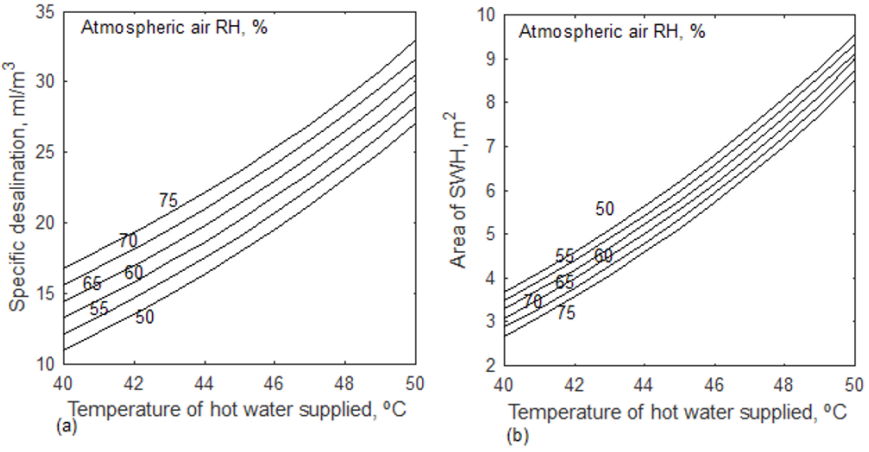

Fig. 7.28: Influence of hot water supply temperature and atmospheric air's relative humidity on specific desalination from the HDH unit

Fig. 7.28 shows the hot water supply temperature and atmospheric air's relative humidity on (a) specific desalination and (b) area of SWH. Specific desalination increases as hot water supply temperature and supply air relative humidity rise. The role of hot water temperature on desalination is discussed in the earlier section. The increase in relative humidity of supply air at a fixed temperature increases the specific humidity of air. It also results in more humid air at the inlet of the dehumidifier. Therefore, more condensate can be observed with the high relative humidity of air. The latent heat load in the humidifier increases as the relative humidity of the air rises. Therefore, the energy supply and area of SWH increase with an increase in RH and also with the hot water supply temperature (Fig. 7.28b).

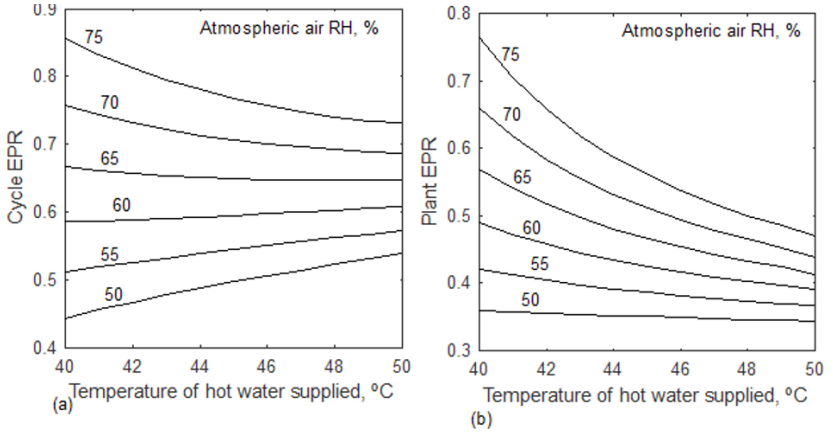

Fig. 7.29: Influence of hot water supply temperature and atmospheric air's relative humidity on EPR of cycle and plant

Fig. 7.29 analyses the influence of hot water supply temperature and atmospheric air's relative humidity on the EPR of (a) cycle and (b) plant. The cycle EPR is increasing with an increase in hot water supply temperature with the low relative humidity. However, it decreases as hot water temperature and relative humidity rise. The plant's EPR is decreasing with an increase in hot water temperature.

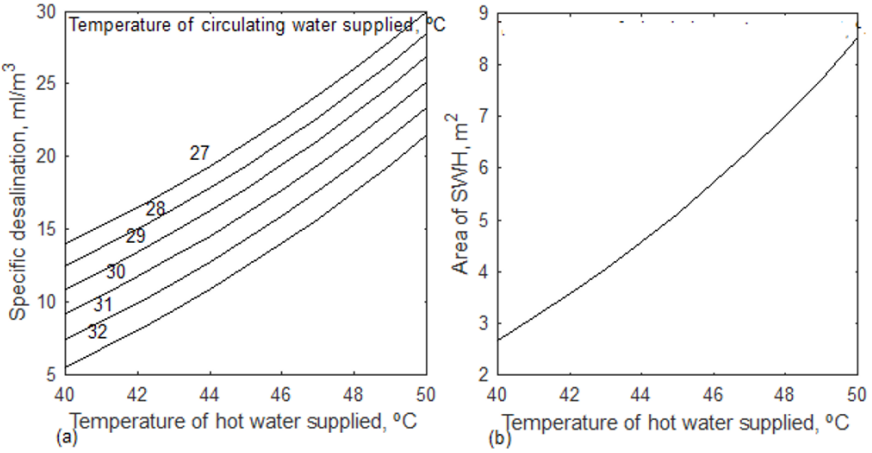

Fig. 7.30: Influence of hot water supply temperature and circulating water supply temperature on specific desalination from the HDH unit

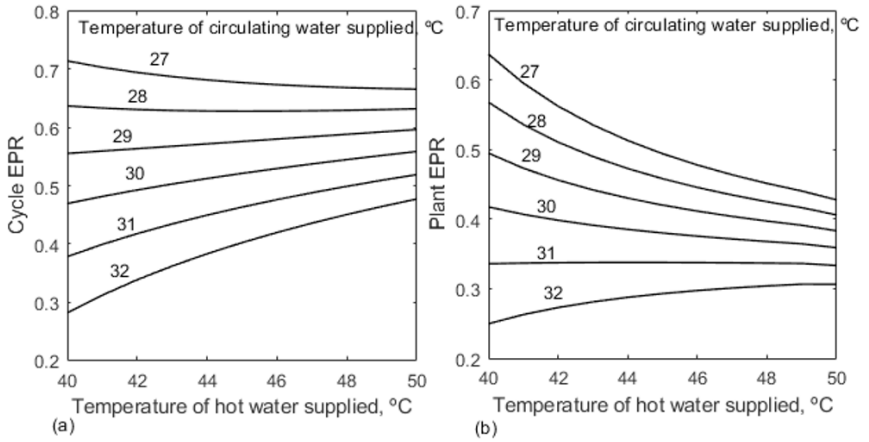

Fig. 7.31: Influence of hot water supply temperature and supply temperature of circulating water on EPR of cycle and plant

Similar to the hot water supply temperature, the low temperature in the dehumidifier also influences the performance of the unit. Fig. 7.30 shows the effect of hot water supply temperature and circulating water supply temperature on (a) specific desalination and (b) area of SWH. The low temperature in the dehumidifier increases the condensate in the dehumidifier. Therefore, the freshwater production is increasing with a decrease in the circulating water supply temperature in the dehumidifier. The temperature of circulating water influences freshwater production but not the energy supply. Therefore, there is no change in the area of SWH with the circulating water temperature.

Fig. 7.31 shows the role of hot water temperature and circulating water supply temperature on the EPR of the (a) cycle and (b) plant. The EPR is increasing with a decrease in circulating water temperature due to an increase in freshwater production.

Table 7.1 Specification of HDH at the hot water supply temperature of 50 °C, circulating water temperature of 25 °C, and air flow rate of 100 m^3/h

S. No.	Particulars	Result
1.	Specific desalination, ml/m^3	35.28
2.	Freshwater production, LPH	3.53
3.	Capacity of APH, kW	0.28
4.	Capacity of humidifier, kW	2.22
5.	Capacity of dehumidifier, kW	3.26
6.	Useful heat in SWH, kW	2.41
7.	Electricity supply, kW	0.15
8.	EPR of cycle	0.78
9.	EPR of plant	0.50

Table 7.1 summarises the performance conditions of the HDH unit at the hot water supply temperature of 50 °C and the air flow rate of 100 m^3/h. The specific desalination is 35.28 ml/m^3. Therefore, the total freshwater at an air flow of 100 m^3/h is 3.53 liters. The heat transfer capacities of the APH, humidifier, and dehumidifier are 0.28 kW, 2.22 kW, and 3.26 kW. Similarly, the useful heat from the SWH is 2.41 kW. The parasitic power includes the electricity supply to fans and pumps, which is equal to 0.15 kW. Based on energy supply to SWH and output of freshwater production, the EUF of the cycle and plant are 0.78 and 0.50, respectively.

7.5 HDH Desalination and Cooling

The once-through arrangement of all the components in the proposed layout allows easy air flow with a minimum pressure drop. It is also easy to remove the brine solution and drinking water by gravity support. The addition of an air reheater (ARH) at the plant's tail allows for the required air supply temperature and relative humidity (Ø) for A/C. In general, dehumidified air is saturated (100%) and unsuitable for air conditioning. Therefore, ARH after the dehumidifier controls the dry bulb temperature (DBT) and Ø of supply air. The refrigeration unit is used as a heat pump (condenser heat is used for air heating) as well as a refrigerator (evaporator coil for dehumidification of humid air). The combined use of the heat pump and refrigerator boosts the coefficient of performance (COP). The total plant is simulated in an off-grid operation mode with solar photovoltaic-thermal (PV/T) supply.

In comparison to the previously reported combined HDH desalination and cooling units, the current work incorporates an air reheater at the end of the dehumidifier to restore the required air conditions, as well as the arrangement of HDH components for easy fluid flow. In the current work, steady state conditions of solar supply have been considered, and dynamic simulation is not the current objective. The work does not extend to the room air conditioning process. The work is carried up to the generation of the A/C supply air. HDH-VCR's air conditioning is not suitable for air recirculation in the room as it is linked to HDH drinking water production. The hybrid plant is suitable for 100% outdoor air circulation.

Fig. 7.32 outlines the schematic flow of the hybrid HDH-VCR plant. The plant is designed to operate in off-grid mode and the energy supply is solar PV and thermal (PV/T). Heat rejection and heat absorption from the heat pump are used in the HDH-VCR unit for water production and A/C. The processes in this combined plant are detailed in a psychrometric chart (Fig. 7.33), and its properties with reference to Fig. 7.32 are listed in Table 7.2. Atmospheric air is forced into the plant by an air circulating fan condenser. An air preheater (APH) is used for sensible heating of air to increase the humidification capacity of the next process. In HDH-VCR, APH is a part of the air-cooled condenser of the VCR unit. The supply of preheated air and hot saline water in the humidifier results in the heating and humidification of the air. The humidifier consists of packing with a wet contact surface to enhance the humidification. The brine solution is collected at the bottom, and humid air flows to the top. After humidification, the air flows over the dehumidifier coil, which is part of the VCR unit (evaporator coil). Air is condensed after touching the cold surface of the dehumidifier. The droplet condensate from the dehumidifier forms the drinking water. After the dehumidifier, APH is used to get the required air supply temperature and humidity ratio for A/C.

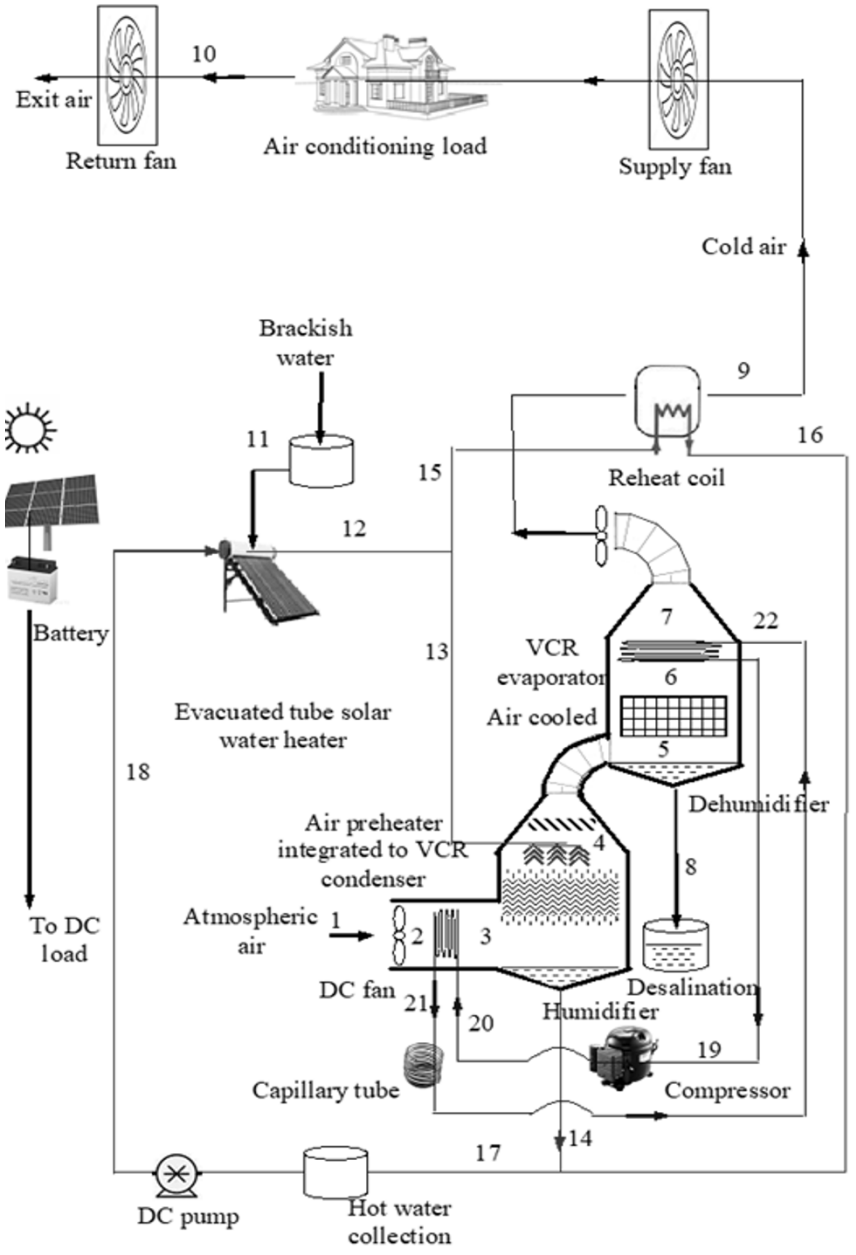

Fig. 7.32: HDH-VCR plant layout with PV/T supply

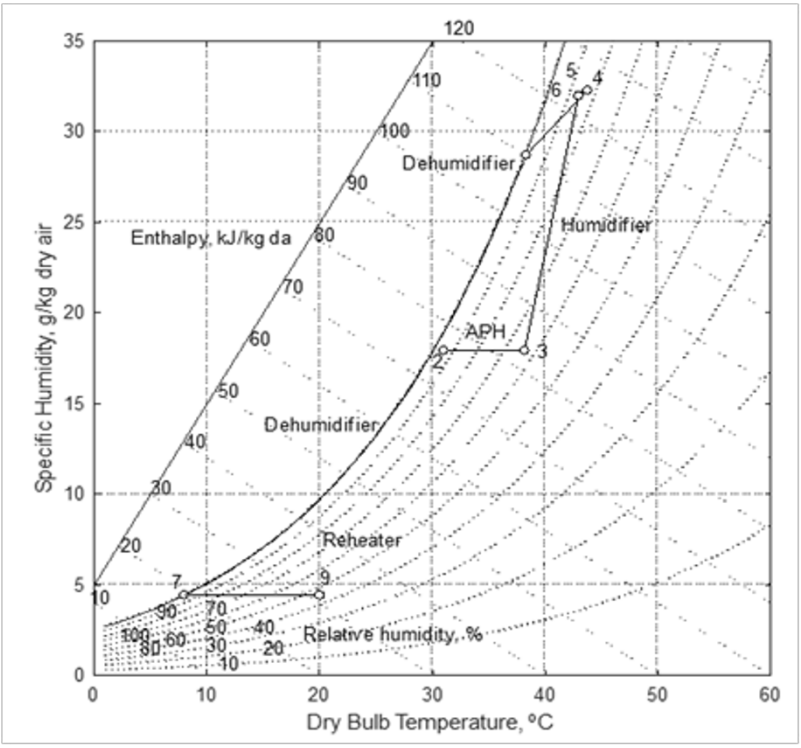

Fig. 7.33: Psychrometric chart for single stage HDH-VCR cycle

Table 7.2 Thermodynamic properties of HDH-VCR cycle

State	P, bar	T, °C	Ø	ω, g/kg	m, kg/h	h, kJ/kg
1	1.01	28.00	75.00	17.95	127.93	73.98
2	1.60	31.00	99.95	17.95	127.93	77.09
3	1.58	38.20	66.37	17.95	127.93	84.56
4	1.57	42.92	89.23	32.01	129.70	125.73
5	1.57	42.92	89.23	32.01	129.70	125.73
6	1.54	41.92	91.21	31.67	129.66	123.77
7	1.52	6.00	100.00	3.84	126.16	15.69
8	1.01	6.00	--	--	3.54	25.08
9	1.51	20.00	39.60	3.84	126.16	29.86
10	1.01	20.00	39.60	--	126.16	34.70
11	1.01	25.00	--	--	1.77	104.50

12	1.01	50.00	--	--	178.93	209.00
13	1.01	50.00	--	--	125.68	209.00
14	1.01	40.73	--	--	123.91	170.23
15	1.01	50.00	--	--	53.26	209.00
16	1.01	42.00	--	--	53.26	175.56
17	1.01	41.11	--	--	177.17	171.83
18	1.01	41.11	--	--	177.17	171.83
19	2.72	-2.00	--	--	96.32	397.43
20	10.17	53.05	--	--	96.32	434.38
21	10.17	40.00	--	--	96.32	256.41
22	2.72	-2.00	--	--	96.32	256.41

The heat load in the humidifier and APH is met by the solar water heater (SWH). Since the SWH handles hard water, indirect heating in the storage tank is preferred. The electricity supply to the vapour compressor, water pumps, and fan/blower is the plant's parasitic power. Since the proposed plant is an off-grid operation, solar PV is connected to meet the plant's parasitic power. In this plant, the dehumidifier consists of two parts: the first part is the natural convective heat exchanger, and the second is the forced convective heat exchanger. The first part of the dehumidifier employs a metallic fin surface to reject heat into the environment. It also shares the cooling load on the subsequent dehumidifier. The refrigeration capacity is saved with this heat sharing. The condensate (soft water) is collected from the dehumidifier by gravity. In addition to this cooling method in the dehumidifier, alternative cooling methods such as chilled water are also used in the dehumidifier (case 2). But chilled water has a constraint on process temperature to avoid the freezing of water. A HDH without A/C (case 1) is included to compare these two dehumidifier methods: chilled water and VCR's evaporator coil with the base method.

A thermodynamic model has been developed to simulate the HDH-VCR cycle using the MATLAB environment. The properties of wet air in the plant are determined from the psychrometric formulation. The HDH-VCR cycle has been depicted on a psychrometric chart (Fig. 7.33). The methodology for evaluating the HDH-VCR cycle has been detailed with the thermodynamic relations. The sections that follow go into great detail about the assumptions and theoretical formulations of plant components used in numerical modelling and simulation. The formulations result from mass balance and energy balance in the components.

The ambient conditions are at 25 °C and 1.01325 bar. The air flow in the plant is assumed to be constant at 1000 m^3/h with no air leakages for easy conversion of specific outputs into total values.

An air circulation fan is used to absorb the atmospheric air and force it into the duct system of the plant via a condenser coil. The inlet condition air has a temperature of 28 °C and a relative humidity of 75%. The velocity of air at the inlet of the fan is not accounted for, and the exit velocity is determined by the cross-sectional area of the duct and its air flow. The enthalpy and kinetic energy functions were used to determine the electrical supply to the fan.

APH is a heat exchanger and part of an air-cooled condenser in case 3. It is used to raise the temperature of the air and decrease the relative humidity. The effectiveness of APH is 0.6.

The saline water supply temperature to the humidifier and ARH is 60 °C. The liquid (water) to air mass ratio in the humidifier is 1. The effectiveness of humidifier heat transfer is 0.75. The humidifier's sensible heat factor is 0.6.

The hot water supply temperature with reference to air influences the humidifier's process. If the hot water supply temperature to the humidifier is less than the dew point temperature (DPT) of inlet air, the resultant process is cooling and dehumidification, which is not acceptable in the humidifier. Therefore, the hot water temperature should be more than the DPT of air. On the other hand, if the hot water temperature is equal to the wet bulb temperature (WBT) of air, the process in the humidifier is an adiabatic saturation. This process is acceptable as the specific humidity of the air increases. If the hot water temperature is in between the DPT and WBT, it results in cooling and humidification. Cooling and humidification is suitable for HDH as it decreases the heat load in the subsequent dehumidification process. If the hot water temperature lies between WBT and air supply temperature, cooling and humidification happens. Therefore, if the hot water temperature is in between DPT and air inlet temperature, cooling and humidification can be expected in the humidifier. If the hot water temperature is higher than the air supply temperature, the humidifier result heating and humdification. It is also an acceptable process as humidity increases but it increases the heat load in the dehumidifier.

If the humidifier is assumed as a heat exchanger, the air exit temperature is simulated by its effectiveness.

$$T_{a,\,e} = T_{a,\,i} + \text{Э}_h\,(T_{hw} - T_{a,\,i}) \tag{7.69}$$

The above enthalpy and temperature of air at the exit of the humidifier result in the relative humidity. The mass of hot water at the exit of the humidifier is less than the inlet due to the evaporation of water particles in the humidifier.

A dehumidifier is a heat exchanger where the humid air is cooled by the cold surface or fluid external to it. Three dehumidification cooling methods are studied in the analysis. These options are water cooling (case 1), chilled

water cooling (case 2), and heat absorption with the VCR's evaporator (case 3). The circulating water temperature (case 1) in the dehumidifier is equal to the DPT of the air inlet. It should not be more than the DPT to ensure cooling and dehumidification. In case 2 and case 3, there is no such constraint due to the maintenance of a low apparatus dew point temperature (ADP) temperature. In the second case, the air exit temperature is 15 °C, with a chilled water supply temperature of 10 °C. In case 3, the air exit temperature is 10 °C, with the cooling coil at 5 °C. In the preliminary stage, dehumidifier heat was rejected by the surroundings via natural convection in order to save heat load in the subsequent stages of three cases. This heat rejection saves the cooling capacity in case 2 and case 3, which is precious. If the cold body in the dehumidifier is above the ADP, the resultant process is humidification instead of dehumidification. Case 2 and case 3 are cooling and dehumidification. The air exit temperature from the dehumidifier is kept above the cold body temperature.

The enthalpy of the exit air in the dehumidifier is determined by the inlet and outlet conditions.

The basic components of the VCR are the vapour compressor, condenser, throttling valve, and evaporator. R134a is the working fluid in the refrigeration plant, with condenser and evaporator temperatures of -2 °C and 40 °C, respectively. The vapour compressor has an isentropic efficiency of 75%. The cooling coil (evaporator) of the VCR is connected to the dehumidifier. Therefore, the dehumidifier's heat load decides the refrigerant flow in the VCR plant.

The refrigerant in VCR,

$$m_r = m_{da} - \left(\frac{h_{a,\,i} - h_{a,\,o})}{h_{e,\,o} - h_{e,\,i})} \right) \tag{7.70}$$

The ARH is located after the dehumidifier and the process is sensible heating. The temperature of air at ARH's exit is 18 °C. ARH is omitted in case 1 as it is not used for air conditioning, which is designed only for drinking water.

The hot water requirement in ARH,

$$m_{hw} = \frac{m_{da}(h_{a,\,o} - h_{a,\,i})}{c_{pw}(h_{hw,\,i} - h_{hw,\,o})} \tag{7.71}$$

The energy supply to the plant is from solar PV and solar thermal collectors. The global radiation from the sun is 720 W/m^2. The solar PV panel electricity efficiency is 15%. The thermal efficiency of SWH is 55%. Solar thermal collectors can be simulated in two ways. The hot water inlet and exit temperatures in SWH are solved with the integration of the HDH-VCR plant. The area of the SWH has been evaluated with the standard method.

The equivalent weight factor for high grade energy (parasitic power to the

plant) supplied to the HDH-VCR cycle is assigned as 3.

The parasitic power supply to the cycle is

$$W_{es} = W_{fan} + W_p + W_r \tag{7.72}$$

The cycle EPR,

$$EPR_c = \frac{m_{dw}h_{fg} + Q_r}{Q_{SWH} + y_e W_{es}} \tag{7.73}$$

The plant EPR,

$$EPR_{pt} = \frac{m_{dw}h_{fg} + Q_r}{0.001 G_g A_{PV+SWH}} \tag{7.74}$$

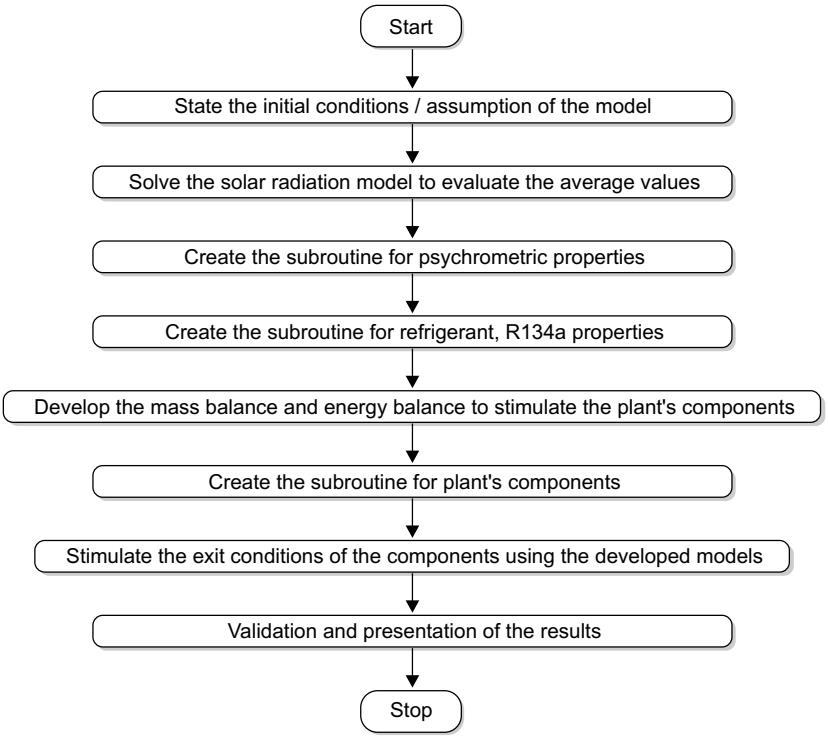

Fig. 7.34: Steps involved in thermodynamic simulation of HDH-VCR plant

The methodology of HDH-VCR plant related is outlined with the flowchart depicted in Fig. 7.34

7.5.1 Simulation results and discussion

The simulation is focused on parametric analysis by varying the hot water supply temperature and evaporator temperature. Three cases are studied in the dehumidifier, viz. C1 (case 1): dehumidification with normal circulating water, C2 (case 2): dehumidification with chilled water, and C3 (case 3): dehumidification with the direct integration of the VCR's evaporator's coil.

The effect of the VCR's evaporator temperature on the hot water temperature has been analysed in case 3. The comparative results are focused on process conditions and performance variations. The identified process conditions are humidifier exit temperature, heat load, relative humidity, and specific humidity at the exit of components. The analysed performance results are specific desalination, specific cooling, cycle EPR and plant EPR.

7.5.1.1 Influence of temperature of hot water supplied

Fig. 7.35a and Fig. 7.35b show the exit temperatures of the plant's components and the heat duties, respectively. The temperature of the supplied hot water is typical for APH, humidifiers, and ARH. The psychrometric process in APH and ARH is sensible heating. Fig. 4a shows the variation in exit temperature of the humidifier, dehumidifier and ARH for three cases. APH in case 3 are different compared to the other two cases. APH influences the humidifier by supplying hot air. The humidifier's exit temperature increases with the increase in the temperature of hot water. The temperature in case 3 differs from case 1 and case 2 due to direct use of air cooled condenser in case 3 in place of APH. The dehumidifier's exit temperature (DH1, DH2 and DH3) is independent of hot water temperature and governed by the cooling method in the dehumidifier. The dehumidifier's outlet temperature is fixed in case 2 and case 3 because of the cold surface used for the dehumidification. In case 1, there is no cold surface and normal circulating water has been used for the dehumidification. There is no need for ARH in Case 1 as it is designed without an air conditioning option. ARH's exit temperature is omitted for case 1. The exit temperature of ARH is fixed to meet the air conditioning conditions. The air exit temperature from ARH in case 2 and case 3 are the same (ARH2 and ARH3). Fig. 4b plots the heat load in the humidifier, dehumidifier and ARH for three plants. The increase in the temperature of hot water increases the heat load in the humidifier. Subsequently, it also increases the heat load in the dehumidifier. The heat load in ARH is not changing as its inlet and exit temperatures are uniform.

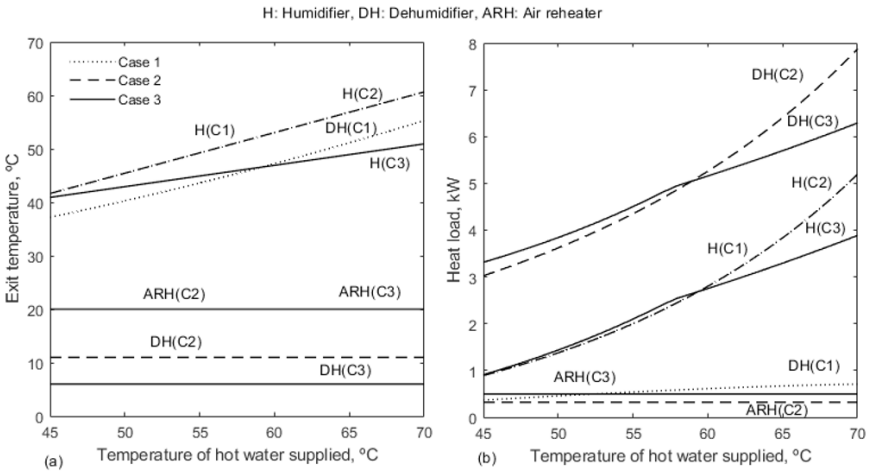

Fig. 7.35: Component's exit temperature and its heat load with temperature of hot water suppled to three plants

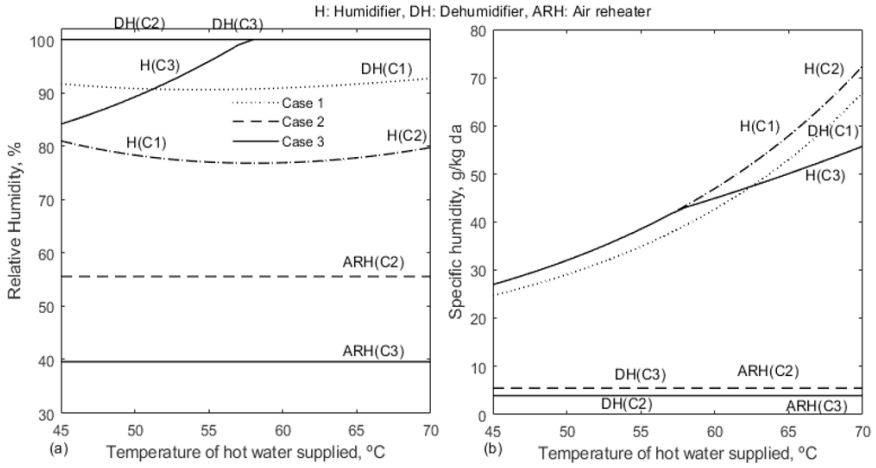

Fig. 7.36: Component's exit relative humidity and specific humidity with temperature of hot water suppled to three plants

Fig. 7.36a and Fig. 7.36b show the changes in relative humidity and specific humidity in the plant's components. The APH conditions in case 1 and case 2 are the same. As a result, the air relative humidity at the exit of the humidifier is the same in these two cases. Heating of the air decreases the relative humidity, and humidification of the air increases the relative humidity. Therefore, the heating and humidification result in the combined effect of these two cases. The condenser has been used as an APH in case 3.

The relative humidity of air at the exit of the humidifier in case 3 increases and reaches the maximum as shown. In case 3, the exit temperature of the humidifier is relatively low. It results in higher relative humidity. As per the initial assumption, the relative humidity in dehumidifiers (DH2 and DH3) and ARH (ARH2 and ARH3) remains the same with a change in the temperature of hot water. In case 1, there is no such fixation due to a lack of a cold body. Fig. 7.36b analyses the specific humidity of air at the exit of HDH components. The specific humidity in the humidifier increases with the humidification of air in a stream of hot air. The dehumidifier exit condition in case 1 is variable, unlike in cases 2 and 3, which have different cooling methods. Accordingly, the specific humidity of the air from the dehumidifier changed. The ARH conditions are also fixed, so there is no change in specific humidity.

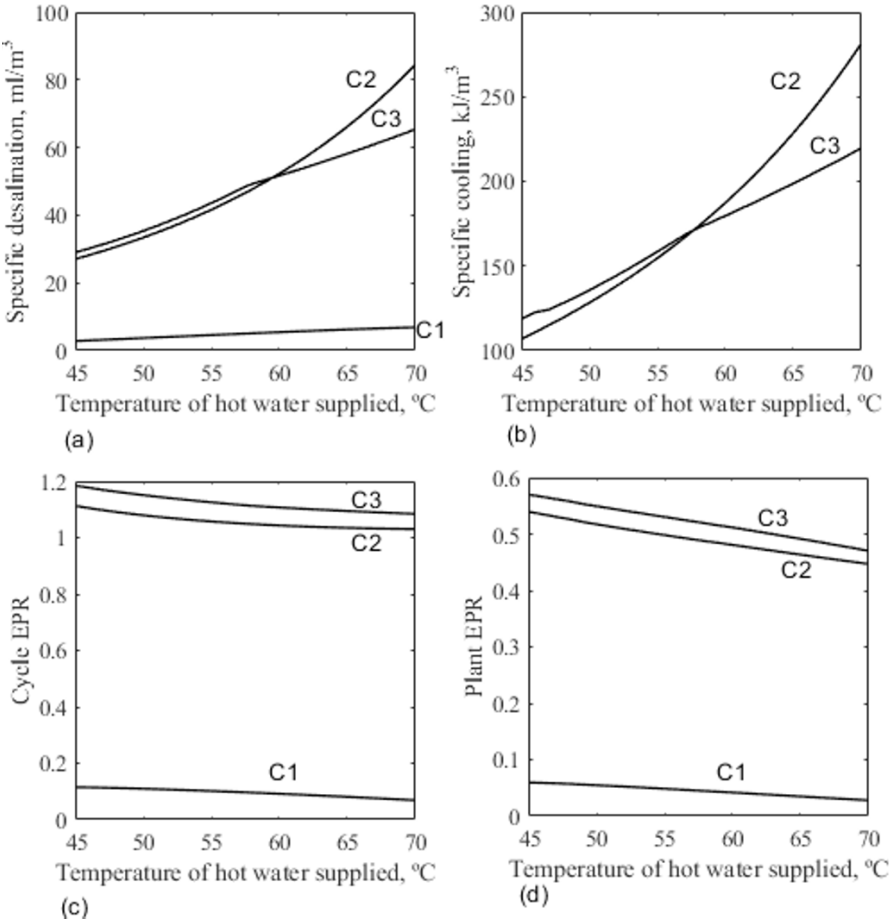

Fig. 7.37: Performance variations of three plants under temperature of hot water suppled

Fig. 7.37 shows the performance results of water productivity and cooling generation, cycle EPR, and plant EPR with a change in the temperature of hot water supplied. The specific outputs from the plant are ml/m^3 of specific water and kJ/m^3 of specific cooling. The capacity of SWH is selected to suit the temperature of hot water. As stated in the earlier section, the heating and humidification in the humidifier increase the specific humidity with the temperature of hot water. Therefore, more moisture is condensed in the dehumidifier, which increases the desalination process. The specific desalination and specific cooling are depicted in Fig. 7.37a and Fig. 7.37b respectively. The dehumidifier load and cooling load increase with the increase in the temperature of hot water. The exit temperature of air after the dehumidifier is fixed to meet the A/C needs. But the dehumidifier inlet conditions differ. The increase in the temperature of hot water increases the cooling load. In case 1, chilled water or VCR is not used and normal water is used in the dehumidifier. Therefore, case 1 is not added in cooling analysis. The increase in water temperature, favours desalination but it raises the cooling capacity. So this option demands additional energy supply for the cycle. The cooling effect is more with direct integration of the VCR compared to the chilled water. EPR is analysed in Fig. 7.37c and Fig. 7.37d with change in temperature of hot water. The EPR of case 3 is higher than the others due to high productivity in water and cooling. The plant heat supply also increases with the water temperature, hence a drop in EPR with the rise in temperature. These results are compared with the reported literature at similar operational conditions for validation purpose. Elattar et al. (2016) and Abdelgaied et al. (2019) reported 25 ml/m^3 of specific desalination from the cooling assisted HDH plant. The current hybrid plant results in 30 ml/m^3 at the temperature of hot water of 30 °C. (Fig. 7.37a). At the saturation temperature of hot water, the specific cooling is 125 kJ/m^3 (Fig. 7.37b). The installed required cooling capacity varies from 65 kJ/m^3 to 75 kJ/m^3. Dalai et al. (2017) experiment resulted in 70 kJ/m^3 of specific cooling and Shafii et al. (2018) experimentation also shows 80 kJ/m^3 of specific cooling. Weight factor has been assigned to high grade energy to determine the EPR. The performance trends are agreed with the literature results. Zhang et al. (2018) proved the rise in the total desalination rate from a combined plant with an increase in the hot water temperature.

7.5.1.2 Influence of evaporator temperature

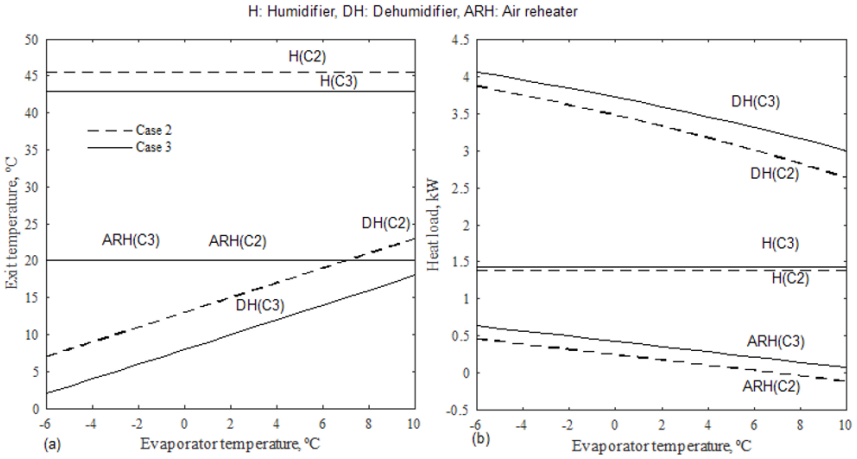

Fig. 7.38: Temperature and heat load changes with evaporator temperature in two plants

Fig. 7.38 shows the influence of evaporator temperature on the exit temperature and heat load of HDH components to interpret the further variations in performance. The evaporator cooling unit is used in cases 2 and 3. Therefore, the results of these two cases are only depicted in this section. The evaporator temperature is linked to the dehumidifier's exit temperature. Therefore, the dehumidifier temperature in cases 2 and 3 is increasing with an increase in evaporator temperature. Other components' temperatures are fixed as they are not related to the evaporator temperature (Fig. 7.38a). The air exit temperature from the dehumidifier is increasing with an increase in evaporator temperature. As a result, the dehumidifier load is decreasing with an increase in evaporator temperature (Fig. 7.38b). The component next to the dehumidifier is called ARH. In connection to the dehumidifier, since the exit temperature of the dehumidifier or inlet temperature of ARH is increasing with an increase in evaporator temperature, the heat load in ARH is decreasing at a fixed exit temperature.

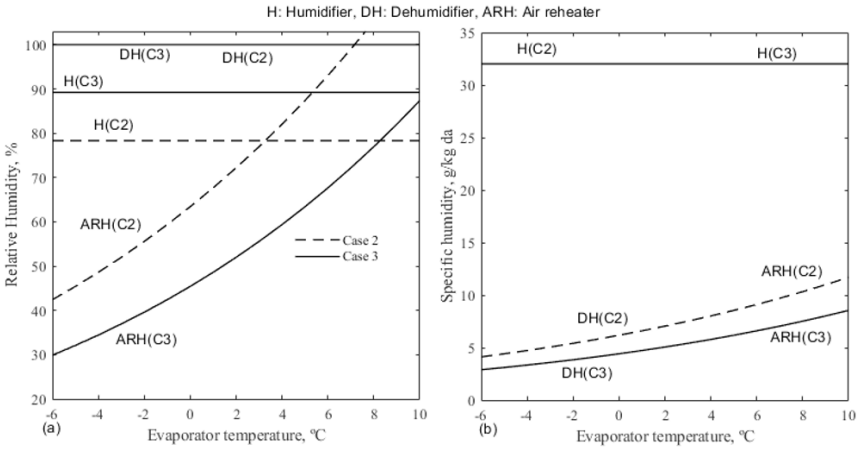

Fig. 7.39: Relative humidity and specific humidity changes with evaporator temperature for the two plants

Fig 7.39 depicts the relative humidity and specific humidity changes with the change in evaporator temperature. The air is saturated at the exit of the dehumidifier with the use of the evaporator's cold body. Hence, its relative humidity is 100%, as shown. The air exit temperature at the exit of the dehumidifier increases with the increase in evaporator temperature. The specific humidity in this state increases with the increase in temperature. Since it is connected to ARH, the relative humidity and specific humidity at the exit of ARH also increase. The humidifier conditions are independent of the evaporator temperature.

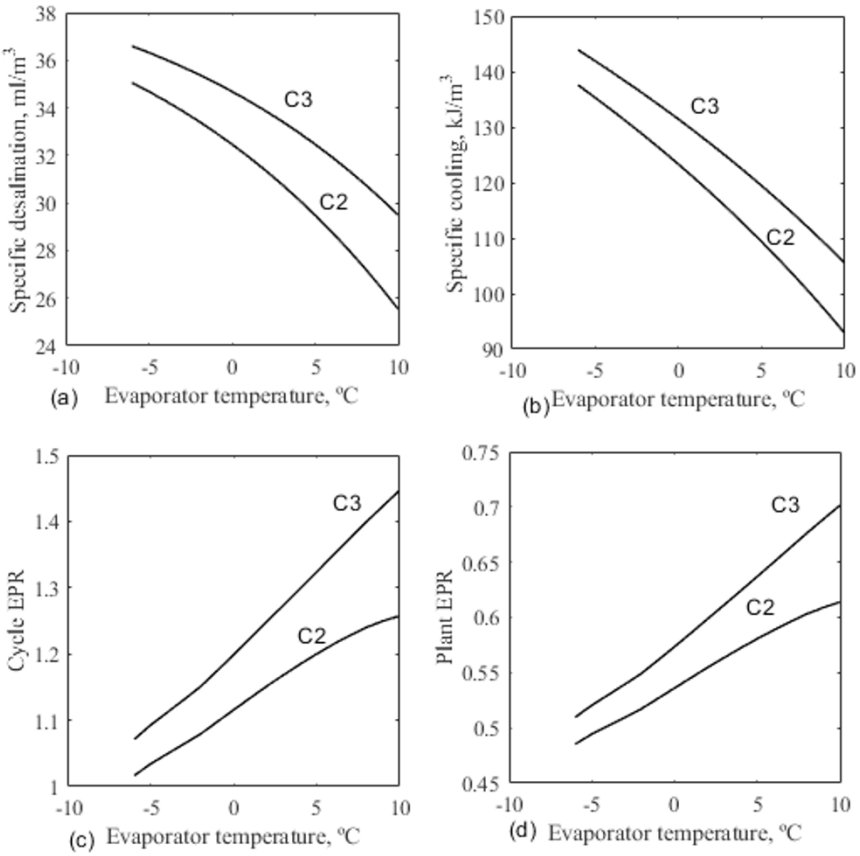

Fig. 7.40: Performance variations of two plants under evaporator temperature

Fig. 7.40 interprets the plant performance of two cases (C2 and C3) with reference to the changes discussed in the earlier section. The water productivity decreased in two models with an increase in evaporator temperature (Fig. 7.40a). The increase in evaporator temperature also increases the air temperature in the dehumidifier. The condensation rate decreases with this effect. The chilled water in the dehumidifier of case 2 has a temperature difference between the refrigerant, chilled water, and dehumidified air. Therefore, the air temperature in case 3 is lower than in case 2 at the dehumidifier. As a result, freshwater production in Case 3 is higher than in Case 2. The low temperature in case 3 also increases the cooling capacity and specific cooling generation (Fig. 7.40b). The cycle and plant EPR increase with an increase in evaporator temperature (Fig. 7.40c and Fig. 7.40d). The decreased heat load in the dehumidifier and ARH (C2 and C3) improves the EPR. The increase in evaporator temperature increases the coefficient of performance (COP) of the VCR unit. The productivity in case 3 is greater than in case 2. Therefore, the EUF of case 3 is greater than that of case 2.

7.5.1.3 Comparison of specifications of three plants

Table 7.3 compares the performance specifications of water and cooling plant models (case 1, case 2, and case 3) at the fixed air supply of 100 m^3/h of air and 50 °C. The freshwater productivity is 3.70 ml/m^3 of air in the base model (case 1). The water productivity in cases 2 and 3 was increased to 33.44 ml/m^3 and 35.40 ml/m^3 respectively with the association of the VCR unit. The air temperature after dehumidification is 11 °C in case 2 and 6 °C in case 3, with an evaporator temperature of -2 °C. For case 1, the cooling capacity and its particulars are omitted. The specific cooling in cases 2 and 3 is 128.38 kJ/m^3 and 135.83 kJ/m^3, respectively. After the dehumidifier, ARH is used in cases 2 and 3 to restore the air temperature to the required state. The ARH load in case 3 are higher than in case 2 with a different dehumidifier temperature. The application of cooling with freshwater increases the driving power of the combined plant from 0.13 kW (case 1) to 1.06 kW in case 2 and 1.11 kW in case 3. With case 2, the cycle EPR increases from 0.11 (case 1) to 1.08. Similarly EPR augments from 0.11 (case 1) to 1.15 with case 3. Similarly, the plant's EPR is also increasing from 0.05 (case 1) to 0.52 (case 2) and 0.55 (case 3). The comparative results conclude that the addition of VCR cooling to HDH gives the favourable outcomes. Finally, case 3 has been recommended compared to cases 1 and 2.

Table 7.3 Comparative study of three plants viz. water cooled dehumidifier (C1), chilled water cooling dehumidifier (C2) and VCR cooled dehumidifier (C3) at hot water temperature of 50 °C, and 100 m^3/h of air

S. No.	Description	Case 1	Case 2	Case 3
1.	Specific desalination, ml/m^3 air	3.70	33.44	35.40
2.	Total desalination, LPH	0.37	3.34	3.54
3.	Specific cooling capacity, kJ/m^3	- -	128.38	135.83
4.	Total cooling capacity, kW	- -	3.56	3.77
5.	Fan/Blower capacity, kW	0.11	0.11	0.11
6.	Pump capacity for hot water, kW	0.01	0.01	0.01
7.	Pump capacity for circulating water	0.01	- -	- -
8.	Pump capacity for chilled water	- -	0.01	- -
9.	Vapor compressor capacity in refrigeration, kW	- -	0.93	0.99
10.	Total parasitic power, kW	0.13	1.06	1.11
11.	Heat supplied to cycle, kW	1.74	2.05	1.88

12.	Area of solar PV plant, m^2	1.63	13.70	14.30
13.	Area of solar water heater, m^2	6.58	7.47	6.79
14.	Total solar collecting area, m^2	8.21	21.17	21.09
15.	Cycle EPR	0.11	1.08	1.15
16.	Plant EPR	0.05	0.52	0.55

7.6 Summary

The process conditions are analysed to increase the freshwater production and the EPR of the cycle and plant. The recommended supply air condition for the desalination plant is a hot and humid state. APH is supporting the desalination plant by increasing the humidity content and producing fresh water. As energy supply increases, so does freshwater production. For enhanced condensation, a higher hot water supply temperature is used. Low temperature is recommended in the dehumidifier. At the stated operational conditions, the resultant cycle EPR and plant EPR are 0.78 and 0.5, respectively.

It has been concluded that VCR integrated into HDH supports the performance for the production of freshwater after comparing the three dehumidifiers, viz., normal water cooling (case 1), chilled water cooling (case 2), and VCR cooling (case 3). The cooling plant capacity is increased from case 2 to case 3 at the same air flow. Since the total production is high in case 3 compared to case 2, the cycle EPR and plant EPR are high in case 3. The cycle EPR is high in case 3 (1.15) compared to case 1 (0.11). The use of chilled water has a constraint on maintaining a low temperature in the dehumidifier compared to direct use of an evaporator for dehumidification. Case 3 yields a specific fresh water density of 35.40 ml/m^3 and a specific cooling density of 135.83 kJ/m^3.

Numerical Solutions

1. Air preheater:

The mass of dry air, m_{da} = 0.035 kg/s (100 m^3/h)

Hot water inlet temperature, $T_{w,\,i}$ = 50 °C

The temperature drop in hot water, ΔT_{water} = 8 °C

The air inlet temperature, $T_{a,\,i}$ = 37 °C

Relative humidity of supply air, $Ø_{a,\,i}$ = 67.20%

Effectiveness of air preheater, $э_{APH}$ = 0.6

Find the exit conditions, unknow flowrates and rating.

Neglect the heat losses and pressure drop.

To find the exit conditios, flow rate and rating, this heat exchanger to be solved with the mass and energy balance equations.

The air temperture at the exit of the air preheater, $T_{a,o}$ from the effectiveness, ε_{APH} and air inlet temperature, $T_{a,i}$,

$$\text{э}_{APH} = \frac{(mc_p)_{\min}(\Delta T)_{\min}}{(mc_p)_{\min}(T_{\max} - T_{\min})}$$

$$= \frac{(\Delta T)_{\min}}{(T_{\max} - T_{\min})}$$

$$\text{э}_{APH} = \frac{T_{a,o} - T_{a,i}}{T_{w,i} - T_{a,i}}$$

$$T_{a,o} = T_{a,i} + \text{э}_{APH}\left(T_{w,i} - T_{a,i}\right)$$

$$= 37 + 0.6\,(50 - 37)$$
$$= 44.8°C$$

From psychrometric chart, at 37 °C DBT and 67.2% of RH (air inlet condition),

specific humidity, $\omega_{a,i} = \omega_2 = 0.027$ kg/kg da (sensible heating)

specific enthalpy, $h_{a,i} = 104.46$ kJ/kg da

Similarly at the exit condition, i.e. 44.8 °C DBT and 0.027 kg/kg da

Relative humidity, $Ø_{a,o} = 44.46\%$

specific enthalpy, $h_{a,o} = 114.81$ kJ/kg da

The energy balane in air preheater,

$m_w\, c_{pw}\,(T_{w,i} - T_{w,o}) = m_{da}\,(h_{a,o} - h_{a,i})$

The hot water supply to air preheater,

$$m_w = \frac{m_{da}(h_{a,o} - h_{a,i})}{c_{pw}(T_{w,i} - T_{w,o})}$$

The rating of air preheater,

$$Q = m_{da}(h_{a,o} - h_{a,i})$$
$$= 0.035\,(114.81 - 104.46)$$
$$= 0.288 \text{ kW}$$

2. Humidifier:

The mass of dry air,

$$m_{da} = 0.035 \text{ kg/s } (100 \text{ m}^3/\text{h})$$

The mass of water spray at the top of humidifier,

$$m_{w,i} = 0.035 \text{ kg/s } (126 \text{ LPH})$$

Hot water inlet temperature, $T_{w,i} = 50$ °C

The air inlet temperature, $T_{a,i} = 44.8$ °C

Relative humidity of supply air, $Ø_{a,i} = 44.46\%$

Based on maximum humidification condition, i.e. if the saturated air

temperature reaches to water supply termperature, simulate the exit temperature of air at the humidifier efficiecy of 40%.

Find the exit conditions, unknow flowrates and rating.

Neglect the heat losses and pressure drop.

To find the exit conditios, flow rate and rating, the humidifier to be solved with the mass and energy balance equations.

At $T_{a,i} = 44.8$ °C and $Ø_{a,i} = 44.46\%$,

Specific enthalpy, $h_{a,i} = 114.81$ kJ/kg da, $\omega_{a,i} = 27$ g/kg da

Comparing the supply water temperatue with the DPT and DBT of supply air,

$T_{w,i} > T_{a,i}$ Results heating and humidification.

The humidifier efficiency, according to the properties on psychometric chart, and similarity triangles,

$$\eta_H = \frac{\omega_{a,o} - \omega_{a,i}}{\omega_{\max} - \omega_{a,i}} = \frac{h_{a,o} - h_{a,i}}{h_{\max} - h_{a,i}} = \frac{T_{a,o} - T_{a,i}}{T_{w,i} - T_{a,i}}$$

At the saturation condition of air, i.e. $T_{a,o} = T_{w,i} = 50$ °C and $Ø = 100\%$,

$$\omega_{max} = 86.2 \text{ g/kg da}$$

From the efficiency of humidifier,

$$\begin{aligned} \omega_{a,o} &= \omega_{a,i} + \eta_H (\omega_{max} - \omega_{a,i}) \\ &= 27 + 0.4 (86.2 - 27) \\ &= 50.7 \text{ g/kg da} \end{aligned}$$

$$\begin{aligned} T_{a,o} &= T_{a,i} + \eta_H (T_{w,i} - T_{a,i}) \\ &= 44.8 + 0.4 (50 - 44.8) \\ &= 46.88 \text{ °C} \end{aligned}$$

At this temperatuer and specific humidity, the relative humidit of exit air,

$$Ø_{a,o} = 72.39\%$$

Specific enthalpy of exit air,

$$h_{a,o} = 178.26 \text{ kJ/kg da}$$

Mass of wet air at the inlet,

$$\begin{aligned} m_{wa,i} &= m_{da}\, \omega_{a,i} \\ &= 0.035 \times 27/1000 \\ &= 0.0359 \text{ kg/s (appriximately)} \end{aligned}$$

Mass of wet air at the exit of humidifier,

$$\begin{aligned} m_{wa,i} &= m_{da}\, \omega_{a,i} + m_{da} (\omega_{a,o} - \omega_{a,i}) \\ &= 0.035 - 0.035 \times (50.7 - 27)/1000 \\ &= 0.0368 \text{ kg/s} \end{aligned}$$

Brine water flow rate,

$$\begin{aligned} m_b &= m_{w,i} - m_{da} (\omega_{a,o} - \omega_{a,i}) \\ &= 0.035 - 0.035 (50.7 - 27)/1000 \\ &= 0.0342 \text{ kg/s} \end{aligned}$$

The heat transfer rate in humidifier,

$$Q_H = m_{da}(h_{a,o} - h_{a,i})$$
$$= 0.035 \times (178.26 - 114.81)$$
$$= 2.22 \text{ kW}$$

3. Dehumidifier:

The mass of dry air, $m_{da} = 0.035$ kg/s (100 m³/h)

The air inlet temperature, $T_{a,i} = 46.88$ °C

Relative humidity of supply air, $Ø_{a,i} = 72.39\%$

The air exit temperature, $T_{a,e} = 27$ °C (It can be determined from the by-pass factor of cooling coil)

Cooling water supply temperature, $T_{w,i} = 25$ °C

The water exit temperature, $T_{w,o} = 36.93$ °C

Find the exit conditions, unknow flowrates and rating.

Neglect the heat losses and pressure drop.

To find the exit conditios, flow rate and rating, the dehumidifier to be solved with the mass and energy balance equations.

At the supply air temperature (46.88 °C) and relative humidity (72.39%) of air,

The specific humidity, $\omega_{a,i} = 50.7$ g/kg da

Specific enthalpy, $h_{a,i} = 178.26$ kJ/kg da

The DPT at the inlet, $T_{dp,i} = 40.65$ °C

The water supply temperature in the dehumidifier is less than the $T_{dp,i}$. Therefore, the resulted process is cooling and dehumidification.

From using similar triangles,

The properties on psychometric chart,

$$\frac{\omega_{a,i} - \omega_{a,o}}{\omega_{a,i} - \omega_{\min}} = \frac{h_{a,i} - h_{a,o}}{h_{a,i} - h_{\min}} = \frac{T_{a,i} - T_{a,o}}{T_{a,i} - T_{w,i}}$$

$$\omega_{a,o} = \omega_{a,i} - \frac{(\omega_{a,i} - \omega_{\min})(T_{a,i} - T_{a,o})}{(T_{a,i} - T_{w,i})}$$

$$= 50.7 - \frac{(50.7 - 20.1)(46.88 - 27)}{(46.88 - 25)}$$

$$= 22.9 \text{g/kg da}$$

At this specific humidity (22.9 g/kg da) and air temperature (27 °C), the relative humidity of exit air,

$$Ø_{a,o} = 100\%$$

Specific enthalpy of exit air,

$$h_{a,o} = 84.97 \text{ kJ/kg da}$$

The circulating water required in the dehumidifier,

$$m_w = \frac{m_{da}(h_{a,i} - h_{a,o})}{c_{pw}(T_{w,o} - T_{w,i})}$$

$$= \frac{0.035(178.26 - 84.97)}{4.18(36.93 - 25)}$$

$$= 0.0655 \text{ kg/s} = 235.63\text{LPH}$$

The heat duty in dehumidifier,

$$Q_{DH} = m_{da}(h_{a,i} - h_{a,o})$$

$$= 0.035 \times (178.26 - 84.97)$$

$$= 3.26 \text{ kW}$$

Review questions

1. What the benefits of HDH desalination compared to other methods?
2. Elaborate the basic working principle of HDH desalination.
3. Formulate the air preheater, humidifier and dehumidifier in a HDH desalination.
4. Identify the key operating conditions in HDH desalination and analyze its effect on the performance with a suitable sketch.
5. In a humidifier, if the hot water supply temperature is greater than the dry bulb temperature of the supply air, what is the resultant process in the humidifier? Analyze the other process conditions in a humidifier based on the hot water supply and air supply properties.
6. How the water spray temperature influence on heating, cooling, humidification and dehumidification? Narrate with the temperature constraints.
7. How the apparatus dew point temperature influence on cooling and dehumidification?
8. What are the design considerations in the bypass factor?
9. Define room sensible heat factor and gross sensible heat factor.

❐

8 Binary Fluid Polygeneration

Abstract

A binary fluid polygeneration plant has been conceptualised to produce power, cooling, freshwater, and hot water from solar thermal energy. Binary fluid cooling cogeneration (BFCC) has been combined with humidification-dehumidification (HDH) desalination. The resulting polygeneration cycle is the BFCC-HDH cycle, developed for multi output generations. The heat sink of the BFCC has been used to generate the hot water which is used to drive the HDH unit, and the additional hot water has been rooted for domestic use. Single stage HDH and double stage HDH have been studied with the integration of BFCC to form a polygeneration. The evaporator of BFCC is linked with HDH by using it as a dehumidifier to condense the moisture in the humid air. Thermodynamic modelling and simulation have been conducted to develop the optimum evaporator temperature for the maximum energy performance ratio (EPR) of polygeneration. The BFCC evaporator temperature is optimised based on the dephlegmator effectiveness, polygeneration plant supply temperature, strong solution concentration, HDH supply temperature, and circulating water supply temperature. The binary fluid polygeneration with single stage HDH results in the cycle EPR and plant EPR being 1.47 and 0.57, respectively. The same polygeneration with double stage HDH results in the cycle EPR and plant EPR being 1.23 and 0.47, respectively.

8.1 Introduction

The system level and stand-alone technologies have been well developed and reported in the open literature. There is a strong need to identify suitable systems with common features and components and integrate them to meet the requirements and refine the existing system. Polygeneration can be developed in a variety of ways, allowing for greater flexibility in process layouts. (Srinivas and Reddy, 2014) reported a novel cooling cogeneration

T. Srinivas, *Thermal Polygeneration*,
https://doi.org/10.1007/978-3-031-37886-7_8

cycle for the generation of power and cooling. The heat rejection from this cooling cogeneration has two parts, viz., the condenser and the absorber. Binary fluid cooling cogeneration (BFCC) allows internal waste heat recovery for thermal desalination. There is no need for external energy to operate the thermal desalination as the hot water from the heat sink of BFCC is hot enough and suitable for the thermal desalination. After using the hot water for the thermal desalination, it will still supply some extra hot water that can be used for any suitable applications such as hospitals, industrial use, commercial use, kitchens, bathing etc. This binary fluid polygeneration will generate electricity, cooling, freshwater, and hot water. The electricity generated by the BFCC is used to drive the polygeneration, and the rest of the power has been shown as a power output from the polygeneration. The goal of this chapter is to combine BFCC with humidification-dehumidification (HDH) desalination and refine the process conditions in order to maximise the energy performance ratio (EPR). In the open literature, the binary fluid polygeneration working on the BFCC-HDH cycle has not been reported or studied for multiple generations.

8.2 Binary Fluid Polygeneration with Single Stage HDH

8.2.1 Plant layout

A binary fluid polygeneration associated with BFCC and HDH desalination is shown in Fig. 8.1. The ammonia-water mixture is used as a working fluid in the BFCC. Binary fluid allows variable heat transfer during the phase change operation in the condenser and boiler. It permits designing a heat exchanger with a minimum entropy generation or irreversibility. A BFCC is a combined cycle to generate electricity and cool the environment Shankar and Srinivas (2018). The condenser pressure in the BFCC is a positive pressure and there is no need for the vacuum pump. It is possible to convert heat at low temperatures into useful forms such as electricity and cooling using the binary fluid.

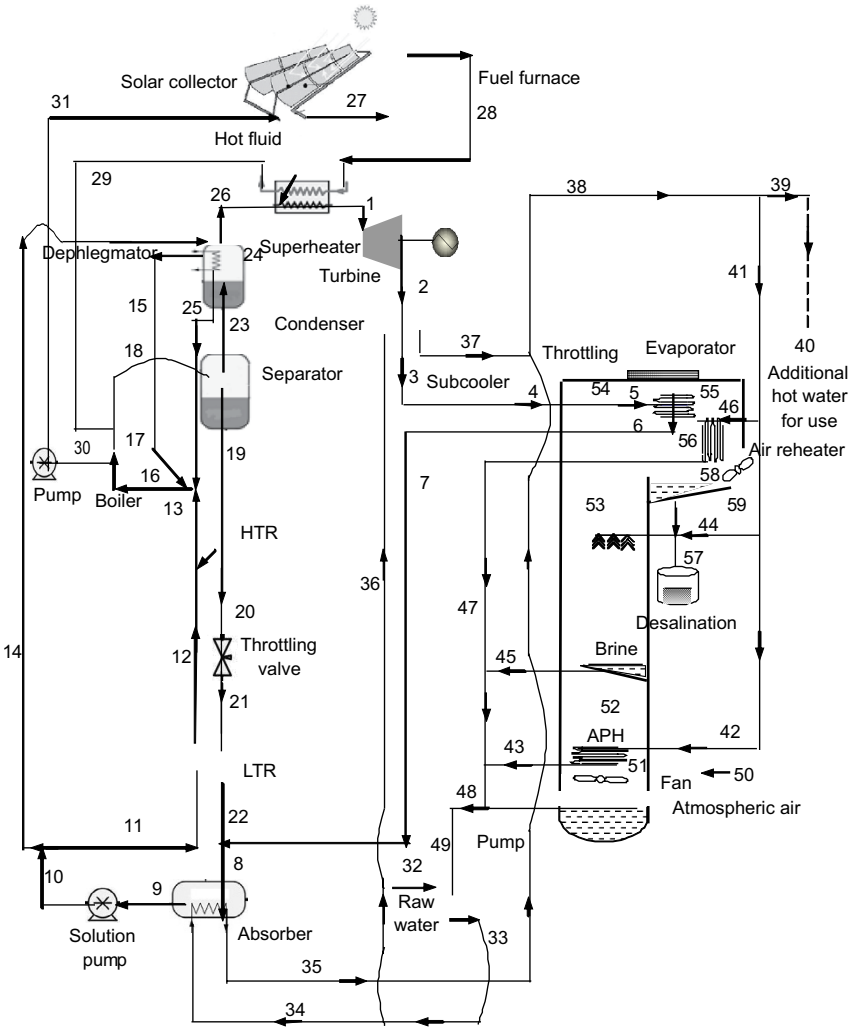

Fig. 8.1: Binary fluid polygeneration plant with single stage HDH desalination

The boiler generates superheated vapour (1), which is supplied to the turbine for electricity generation. The BFCC has three pressures, viz., high pressure (HP), intermediate pressure (IP), and low pressure (LP). The vapour in the turbine is expanded from HP to IP (1-2). The main components of cooling are the condenser, throttling, evaporation, and thermal or mechanical compressor. In a binary fluid system, the thermal compressor consists of a pump and a boiler. At the IP and exit of the turbine, the vapour is condensed (2–3) to a saturated liquid state. The saturated liquid from the condenser is throttled (4-5) to a low pressure and generates low temperature fluid (5) for cooling. This low-temperature fluid (5) enters into the evaporator to condense

the humid air and also generate cold air for space conditioning. The evaporator plays the role of a dehumidifier in the HDH cycle. The air is cooled (55–56) in the dehumidifier or evaporator part of the cooling plant. The heat is absorbed by the refrigerant in the evaporator (5–6). This vapour condensed to a saturated liquid in the absorber (8-9) once more. The vapour passes through the subcooler (6-7) and is mixed with the weak solution before entering the absorber. The subcooler is used to subcool refrigerant at the entry of throttling and heats the vapour before the absorber. The mixing of the weak solution (22) with the vapour (7) permits the easy condensation in the absorber at the sink temperature. The saturated liquid at the exit of the absorber is called a "strong solution" due to its high concentration. It is pumped to boiler pressure (9–10) from the low pressure. In the binary fluid system, a dephlegmator has been used to increase the concentration of the fluid in the cooling plant. The dephlegmator needs a heat rejection process. Therefore, some of the strong solutions have been rooted in dephlegmator to absorb the heat. The strong solution has been supplied to the boiler via a low-temperature regenerator (LTR) and a high-temperature regenerator (HTR). The LTR (11-12) and HTR (12-13) help to preheat the working fluid before supplying it to the boiler through internal heat recovery. The hot fluid for this internal heat recovery is a weak solution. Between HTR and LTR, the weak solution throttles from high pressure to low pressure (20-21). The preheated fluid was mixed with the return fluids from the dephlegmator. The mixed fluid (16) enters the boiler and results in wet vapour (18). This wet vapour is separated into saturated liquid (19) and saturated vapour (23). The vapour is refined in the dephlegmator (23-24-26). The vapour from the dephlegmator (26) is superheated (26-1) and supplied to the turbine, and the cycle repeats for continuous generation of electricity and cooling.

HDH desalination works on the principle of the water cycle, i.e., humidification and dehumidification of the air. Atmospheric air (50) enters the plant with a fan. Later, it is preheated (51–52) in the air preheater (APH). The relative humidity (Ø) of the air in the APH decreases and gives more scope for evaporation in the humidifier. The humidifier consists of packing that provides the wetting surface. The humidifier sprays hot saline water against the preheated air stream at the top of the packing. The air undergoes a heating and humidification process (52-53). The humid air collects at the top, and the brine solution is at the bottom of the humidifier. Later, the air flows over the cooling surface of natural convection and the evaporator's coil for the dehumidifier (54-55). The projected surface into the environment rejects heat from the humid air and contributes to the evaporator load. The final dehumidification (55–56) happens in the evaporator section of the BFCC. The water-cooled condenser and absorber of the BFCC are used to raise the saline water temperature. The evaporator of the BFCC is used for the

dehumidification of air. The condensate from the dehumidification process is collected in a container (57). In dehumidification, the humid air is cooled to condense the moisture in the humid air. After the final dehumidification, the temperature of the air is increased (56–58) in the air reheater (ARH) to reach the required temperature and relative humidity for comfort conditions. The hot saline water is supplied to the APH (42) and humidifier (44) and ARH (46). The total heat load in the condenser and absorber is greater than the HDH heat load (the sum of APR, humidifier, and ARH). If the whole water is recirculated in the circuit, the temperature of water in the plant continuously increases. To keep the sink's operating temperature within the safe limit, saline water at the normal temperature has been supplied (32) to the storage tank. The additional hot water is designed for domestic use (40). The used water from the HDH has been collected and pumped (48-49) to the overhead storage tank, which is kept at an elevated level (elevation not shown in Fig. 8.1). The mixed cool saline water has been supplied to BFCC for heat rejection. Overall, the polygeneration gives electricity, cooling, freshwater and hot water from the solar thermal energy supply.

8.2.2 Thermodynamic model

The thermodynamic model of polygeneration includes the binary fluid system and HDH desalination. In the simulation of the BFCC-HDH polygeneration, the air flow rate in HDH is fixed at 1000 m^3/h. The evaporator in HDH is called a dehumidifier. The capacity of the cooling unit, i.e., the evaporator/dehumidifier, is determined by the air flow rate and the dehumidifier conditions. Based on this cooling capacity, the working fluid in the BFCC has been determined. The pinch point (PP) in the boiler, working fluid flow, and boiler temperatures result in thermic oil circulation in the solar concentrating collectors.

The air around the plant has a relative humidity of about 75%. The average relative humidity in the location (Jalandhar, India) is 75%. The air preheater at the beginning of the HDH unit decreases the relative humidity of the supply air. The air temperature at the APH inlet is 28 °C. The saline water inlet temperature in a humidifier is 50 °C. The mass ratio of water to air in the humidifier is 1 (Dehghani et al., 2018). The chilled coil exit temperature in the VCR is -2 °C. In the refrigeration plant, R134a has been selected as the working fluid. The VCR's condenser phase change temperature is 40 °C. In the refrigeration plant, the vapour compressor's isentropic efficiency is set at 75%. The air reheater's exit temperature is 20 °C.

The wet air consists of dry air and moisture. The mass of wet air can be determined from its volume flow rate and standard air supply conditions.

Mass of wet air,

$$m_{wa} = \frac{P_{wa} V_{wa} M_{wa}}{R_u T_{wa}} \tag{8.1}$$

The dry air in the HDH duct can be determined from wet air flow rate and specific humidity. The specific humidity, ω is the moisture per unit mass of dry air.

$$m_{da} = \frac{m_{wa}}{1+\omega} \tag{8.2}$$

The air exit temperature from the APH is determined from its effectiveness

$$T_{52} = T_{51} + э_{APH}\,(T_{42} - T_{51}) \tag{8.3}$$

The hot water inlet and outlet temperatures for APH have been fixed to find its flow rate. The energy balance equation in the APH results in the hot water flowrate at the known air flow rate, which is fixed as per the assumptions.

Hot water demand in APH,

$$m_{42} = \frac{m_{da}(h_{52} - h_{51})}{c_{p,hw}(T_{43} - T_{42})} \tag{8.4}$$

The amount of brine solution collected at the bottom of the humidifier is less than the hot water supply due to the air humidification. Based on the liquid to air mass ratio in the humidifier, the hot water spray has been determined at a fixed air flow rate.

Let, the m_r liquid to air mass ratio in humidifier

The mass of hot water supplied to the humidifier,

$$m_{hw} = m_r\, m_{wa} \tag{8.5}$$

where $$m_r = \frac{m_{hw}}{m_{wa}}$$

Mass of water at the exit of humidifier,

$$m_{45} = m_{44} - m_{da}(\omega_{53} - \omega_{52}) \tag{8.6}$$

The air exit condition from the humidifier is simulated based on the hot water supply temperature. The heating and humidification process on the psychrometric chart moves towards the hot water temperature at the maximum limit of humidity, i.e., 100% RH.

The temperature of hot water at the humidifier's outlet,

$$T_{45} = \frac{m_{44}c_{pw}T_{44} - m_{da}(h_{53} - h_{52})}{m_{45}c_{pw}} \tag{8.7}$$

The mass of air at the exit of humidifier after picking the moisture,

$$m_{53} = m_{52} + m_{da}\,(\omega_{53} - \omega_{52}) \tag{8.8}$$

Similarly, the cooling and dehumidification processes in a dehumidifier follow the cold body temperature with a maximum limit of 100% RH.

The development of thermodynamic properties for the ammonia-water zeotropic mixture is required for the evaluation of BFCC. After generating the thermodynamic properties of plant fluids, the evaluation of BFCC begins with

the assumptions involved. The heat recovery vapour generator (HRVG) has two sections, viz., an economizer and an evaporator (partial). During the phase change in the HRVG section, the minimum temperature occurs at the end of the economizer or the beginning of the phase change, which is called the bubble point temperature. The temperature difference between the local heat source temperature and the bubble point temperature is called the pinch point. It is a design element to ensure positive heat transfer between the hot fluid and the cold fluid. The working fluid flow in HRVG can be determined by the pinch point constraint. The pinch point in the vapour generator's evaporator is 15 °C. The isentropic efficiency of the pump and the vapour turbine is 75%. Similarly, the mechanical efficiency of machines is 96%. The electrical generator efficiency is 98%. The heat transfer fluid or hot fluid flow temperature at the inlet of the cycle is 175 °C, respectively. The degree of super heat (DSH) in the superheater is 10 °C. The saturated vapour concentration in the separator after evaporation is 0.85. In the ideal dephlegmator (100% effectiveness), the vapour exit condition is pure ammonia. As a result, effectiveness is defined as the ratio of the actual concentration increase to the maximum concentration increase.

Effectiveness of dephlegmator,

$$\text{э}_{deph} = \frac{x_{26} - x_{13}}{1 - x_{23}} \tag{8.9}$$

In the dephlegmator, the vapour is condensed partially to remove the water from the vapour. Hence, the concentration of ammonia increases. The exit concentration (x_{26}) is determined by the effectiveness of the dephlegmator (Eq. 8.9) and the vapour exit concentration (x_{23}). The increased ammonia concentration with the dephlegmator favours the refrigeration performance (output and cooling coefficient of performance). After the liquid-vapour mixture is generated in the boiler, it is separated into a weak solution and a vapour. The concentration of weak solution and vapour along with its flow rate is solved using a lever rule applied to the separation process. The same can be applied to the mixing process. In the separator, the dry fraction of the liquid-vapour fluid is the mass ratio of saturated vapour and total mass.

After simplification of the mass balance equations in the separator, the dry fraction of the fluid can be determined as follows.

$$\delta_{sep} = \frac{x_{18} - x_{19}}{x_{23} - x_{19}} \tag{8.10}$$

Eq. 8.10 shows that the dryness fraction of a mixture is a function of strong solution concentration (x_{18}), weak solution concentration (x_{19}) and vapour concentration (x_{23}). The weak solution concentration is calculated from the high pressure and separator temperature through the saturated liquid state. After partial condensation of vapour in the dephlegmator, another liquid

vapour mixture is formed. The vapour is separated and flows toward the superheater. The liquid drips into the boiler by gravity. Due to distillation, the dryness fraction of the dephlegmator is greater than the dryness fraction of the boiler.

The dryness fraction in dephlegmator,

$$\delta_{deph} = \frac{x_{23} - x_{25}}{x_{26} - x_{25}} \tag{8.11}$$

In the above Eq.8.11, x_{25} is the liquid concentration, determined from high pressure and dephlegmator temperature at saturated liquid state similar to weak solution concentration.

The condensation of vapour in dephlegmator losses heat and also vapour flow. But the heat loss is recovered from the internal fluid flow.

The refrigerant in expansion and refrigeration plant,

$$m_{26} = \frac{\delta_{sep}\delta_{deph}}{1 + \delta_{sep}\delta_{deph} - \delta_{sep}} m_9 \tag{8.12}$$

Eq. 8.12 is derived after simplification of mass balance equations in the boiler's separator and dephlegmator. The strong solution (m_9) may be maintained as a unit mass or determined from the source fluid. In the current work, the strong solution is calculated from the heat source fluid. At the boiler inlet, three fluids mix together and form a liquid or a liquid-vapour mixture. The three fluids are pumped: strong solution, return liquid from the dephlegmator, and heat exchanger fluid from the dephlegmator. The concentration is diluted after mixing. The boiler mass increases with the mixing of streams and is evaluated by the simplification of the mass balance equations.

The actual strong solution after mixing of streams,

$$m_9 = \frac{m_{26}}{\delta_{sep}\delta_{deph}} \tag{8.13}$$

Similarly, the weak solution

$$m_{19} = \frac{\left(1 - \delta_{sep}\right)}{\delta_{sep}\delta_{deph}} m_{26} \tag{8.14}$$

The vapour supply to dephlegmator or at exit of boiler,

$$m_{23} = \frac{m_{26}}{\delta_{deph}} \tag{8.15}$$

The energy balance in the evaporator/dehumidifier results the working fluid flow in BFCC.

$$m_5 = \frac{m_{da}(h_{55} - h_{56})}{(h_6 - h_5)} \tag{8.16}$$

Similarly, the energy balance in the boiler, gives the thermic oil in the solar collector,

$$m_{28} = \frac{m_{17}(h_{18} - h_{17}) + m_1(h_1 - h_{16})}{c_{p,th}(T_{28} - T_{30})} \tag{8.17}$$

The electrical power supply to the cycle/plant is

$$W_e = W_{fans} + W_p + W_r \tag{8.18}$$

The first law of efficiency deals with energy interactions and their performance. The four outputs are different in nature, i.e. one is power and the others are heat, hence the first law performance is expressed in energy performance ratio (EPR). Net power generation is the difference between the turbine's gross output and the pump's input. In EPR, net power generation, freshwater energy, cooling, and hot water are shown as the main outputs from the heat supply in HRVG and superheater. The average solar radiation in Jalandhar, India, has been considered for the study. The equinox position will come in the months of March and September this year. The month of March has been selected to determine the average solar radiation. The average global component of solar radiation is 520 W/m^2. The efficiency of the collector is determined by the plant's process conditions.

The cycle EPR,

$$EPR_c = \frac{W_{net} + m_{fw}h_{fg} + Q_r + m_{hw}Q_{hw}}{Q_g + Q_{sh}} \tag{8.19}$$

The plant EPR,

$$EPR_{pt} = \frac{W_{net} + m_{fw}h_{fg} + Q_r + m_{hw}Q_{hw}}{0.001GA_{CPC}} \tag{8.20}$$

where A_{CPC} is the total solar collecting area for electricity and hot water generation. In Eq. 8.20, the parasitic power has been deducted from the gross power generation; hence, the power supply to drive the plant has not been added to the energy supply.

The results of the mass balance and energy balance equations of the polygeneration plant are furnished in Table 8.1. The binary fluid properties are represented by states 1 through 26. The simulated three pressures in the BFCC are 28.79 bar, 12.44 bar, and 4.41 bar, respectively, HP, IP, and LP. State 27 to 31 are the properties of thermic oil used in the solar concentrating collector and boiler. States 32 through 49 are about water properties. State 50 to 59, (except 57) represents the psychrometric properties of air.

Table 8.1: Material balance and energy balance results of binary fluid polygeneration with single stage HDH at 1000 m^3/h air and the evaporator temperature of 15 °C

State	m, kg/h	P, bar	T, ºC	x or Ø (%)	ω, g/kg	h, kJ/kg	s, kJ/kg K	ε, kJ/kg
1	112.42	28.79	160.00	0.93	--	1661.60	4.91	197.23
2	112.42	12.44	97.97	0.93	--	1547.65	5.00	56.89
3	112.42	12.44	35.00	0.93	--	110.89	0.56	-56.56
4	112.42	12.44	30.00	0.93	--	86.77	0.48	-57.15
5	112.42	4.41	3.04	0.93	--	87.69	0.51	-65.22
6	112.42	4.41	15.00	0.93	--	981.26	3.72	-128.18
7	112.42	4.41	16.68	0.93	--	1005.66	3.81	-128.87
8	351.30	4.41	61.80	0.50	--	233.34	0.49	88.28
9	351.30	4.41	35.00	0.50	--	-82.98	0.37	-192.08
10	351.30	28.79	36.93	0.50	--	-72.30	0.39	-188.78
11	313.52	1.01	36.93	0.50	--	-72.30	0.39	-188.78
12	313.52	1.01	55.07	0.50	--	9.47	0.65	-183.42
13	313.52	1.01	90.22	0.50	--	173.02	1.12	-160.94
14	37.78	1.01	36.93	0.50	--	-72.30	0.39	-188.78
15	37.78	1.01	135.00	0.50	--	731.44	2.54	-26.46
16	369.62	1.01	104.08	0.49	--	239.71	1.30	-148.18
17	369.62	1.01	109.47	0.49	--	266.36	1.37	-142.44
18	369.62	1.01	150.00	0.49	--	968.92	3.10	43.39
19	238.88	1.01	150.00	0.30	--	486.16	1.88	-73.88
20	238.88	1.01	105.06	0.30	--	271.01	1.34	-128.98
21	238.88	1.01	79.87	0.30	--	273.43	1.37	-135.30
22	238.88	1.01	73.61	0.30	--	164.07	1.06	-151.49
23	130.74	1.01	150.00	0.85	--	1704.37	4.99	216.04
24	130.74	1.01	129.12	0.85	--	1472.13	4.44	147.80
25	18.33	28.79	129.12	0.39	--	364.01	1.61	-117.42
26	112.42	28.79	129.12	0.93	--	1571.95	4.70	169.26
27	2613.18	1.01	175.00	--	--	280.95	0.76	53.37
28	2613.18	1.01	175.00	--	--	280.95	0.76	53.37
29	2613.18	1.01	172.94	--	--	276.58	0.75	51.99
30	2613.18	1.01	124.47	--	--	177.72	0.51	24.36
31	2613.18	1.01	117.87	--	--	164.90	0.48	21.35
32	2787.92	1.01	25.00	--	--	79.50	0.00	-25.00
33	4099.08	1.01	30.00	--	--	100.40	0.07	-24.83
34	2167.09	1.01	30.00	--	--	100.40	0.07	-24.83

35	2167.09	1.01	50.00	--	--	184.00	0.34	-20.85
36	1931.99	1.01	30.00	--	--	100.40	0.07	-24.83
37	1931.99	1.01	50.00	--	--	184.00	0.34	-20.85
38	4099.08	1.01	50.00	--	--	184.00	0.34	-20.85
39	2333.70	1.01	50.00	--	--	184.00	0.34	-20.85
40	2333.70	1.01	50.00	--	--	184.00	0.34	-20.85
41	1765.38	1.01	50.00	--	--	184.00	0.34	-20.85
42	449.89	1.01	50.00	--	--	184.00	0.34	-20.85
43	449.89	1.01	42.00	--	--	150.56	0.23	-23.05
44	1270.49	1.01	50.00	--	--	184.00	0.34	-20.85
45	1252.63	1.01	41.13	--	--	146.93	0.22	-23.24
46	45.00	1.01	50.00	--	--	184.00	0.34	-20.85
47	45.00	1.01	42.00	--	--	150.56	0.23	-23.05
48	1747.52	1.01	41.38	--	--	147.96	0.22	-23.19
49	1747.52	1.01	41.48	--	--	148.38	0.22	-23.16
50	1293.30	1.01	28.00	75.00	17.95	73.98	0.26	-0.26
51	1293.30	1.60	31.00	99.95	17.95	77.09	0.27	-0.53
52	1293.30	1.58	42.40	53.08	17.95	88.93	0.31	-0.07
53	1311.17	1.57	45.44	78.32	32.01	128.41	0.44	0.22
54	1311.17	1.57	45.44	78.32	32.01	128.41	0.44	0.22
55	1309.98	1.54	40.61	96.04	31.08	120.86	0.42	-0.05
56	1281.95	1.52	18.84	100.00	9.02	41.80	0.15	0.21
57	29.22	1.01	18.84	- -	- -	53.75	0.00	-50.75
58	1281.95	1.51	20.00	92.11	9.02	42.98	0.16	0.19
59	1281.95	1.01	20.00	50.00	7.28	38.58	0.14	0.53

8.2.3 Performance characteristics of binary fluid polygeneration with single stage HDH

The current polygeneration cycle is an integration of binary fluid systems with HDH desalination for the generation of electricity, cooling, freshwater, and hot water. The influence of operational conditions on polygeneration is different compared to individual systems. The selected key operational conditions are the degree of dephlegmator, evaporator temperature, polygeneration plant supply temperature, strong solution concentration, and HDH plant supply temperature. Energy efficiency is the function of the four outputs of power, cooling, freshwater, and hot water for domestic use. In addition to these four outputs, the input energy consists of heat and electricity, both of which are generated on-site. Therefore, the net electricity from the polygeneration is turbine work minus the driving power for pumps and fans.

Since the output consists of heat and work, energy efficiency is termed as an energy performance ratio. It has been noticed that evaporator temperature can be optimised with polygeneration variables.

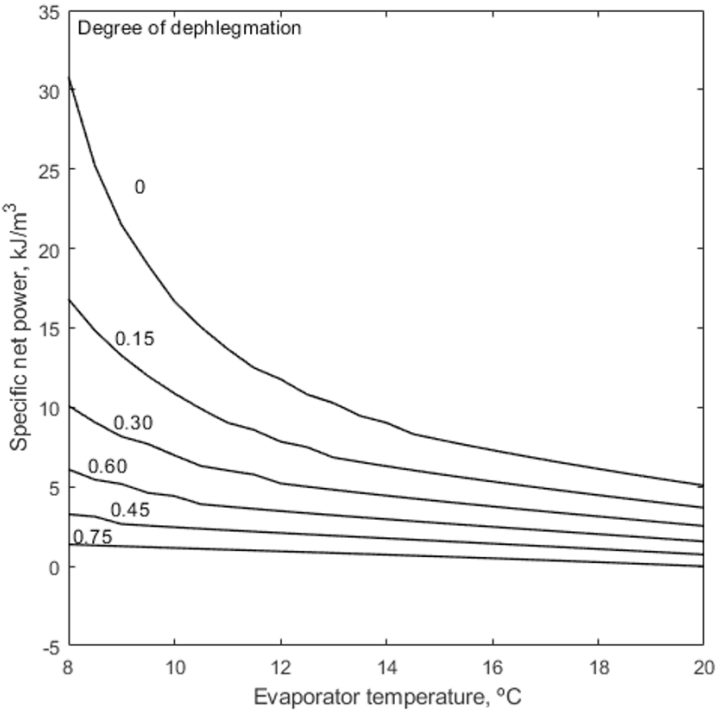

Fig. 8.2: Influence of evaporator temperature and degree of dephlegmation on specific power of polygeneration

Fig. 8.2 depicts the effect of evaporator temperature on cooling with a degree of dephlegmation. The absence of a dephlegmator in the operation of a binary fluid power and cooling unit is indicated by a zero dephlegmator. Theoretically, if the exit concentration of fluid is one, the degree of dephlegmation is also one. The degree of dephlegmator was increased from 0 to 0.75. The BFCC is working on three pressures, viz., HP, IP, and LP. The dephlegmator influences the HP, which is related to power generation. The high pressure level can be decreased with the help of a dephlegmator. However, it reduces the expansion, so the power decreases as the dephlegmation increases. The evaporator in the BFCC plays the role of a dehumidifier in the HDH unit. The plant's power generation is decreasing with an increase in evaporator temperature. The results are generated at the fixed air flow rate in the HDH unit. The decreased evaporator temperature decreases the cooling load on the dehumidifier. According to this drop in cooling, the working fluid in the

binary fluid plant decreases, resulting in power declination. The increase in evaporator exit temperature also increases the air exit temperature of the air in the HDH dehumidifier. It decreases the cooling load in the dehumidifier, and so the cooling load in the evaporator also decreases with an increase in the evaporator temperature. As per the energy balance in the dehumidifier of the HDH or the evaporator of the BFCC, the working fluid in the BFCC decreases. Therefore, proportionately, the power generation decreases with an increase in the evaporator temperature. The increased evaporator temperature decreases the condensation of the humid air in the final dehumidification. Freshwater production decreases with an increase in the evaporator temperature. In BFCC, the refrigerant throttles from intermediate pressure (IP) to low pressure (LP), which is independent of the role of the dephlegmator. According to the simulation constraints, the dephlegmator has no effect on cooling or freshwater production. Therefore, these results are not depicted in this study. The available hot water for external use decreases with an increase in the role of the dephlegmator. Finally, the total energy production decreases with an increase in evaporator temperature and also with an increase in the dephlegmator role.

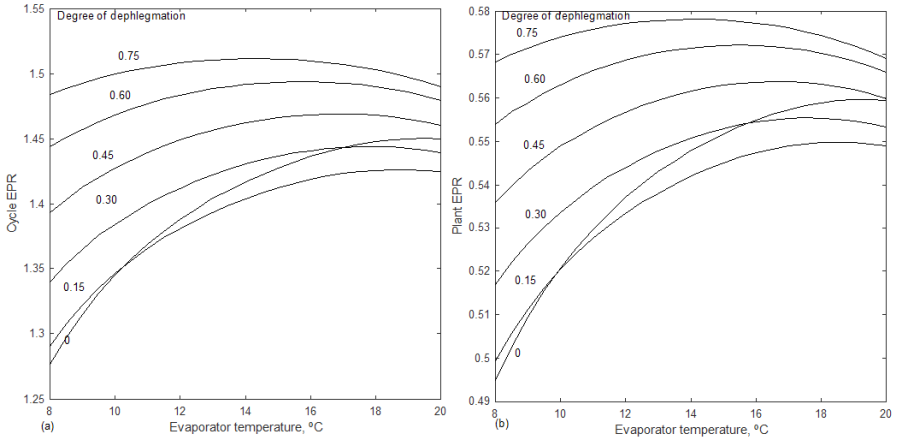

Fig. 8.3: Effect of evaporator temperature and dephlegmation on cycle and plant EPR

Fig. 8.3 shows the influence of the evaporator temperature and degree of dephlegmation on the EPR of the polygeneration cycle and of the plant. The increase in evaporator temperature favours the COP of the refrigeration unit. But the four outputs, viz., power, cooling, freshwater, and hot water, decrease with an increase in the evaporator temperature. The decrease in energy supply and output result an optimum evaporator temperature to maximise the EPR, as shown. The increase in degree of dephlegmation saves pumping power due to the decrease in high pressure. As a result, as the degree of dephlegmation increases, so does the EPR of the cycle and the plant. The optimum evaporator

temperature decreases as the degree of dephlegmation increases. Higher EPR is caused by increased dephlegmation and a low optimum evaporator temperature. The EPR of combined power and cooling is less than unity as per the reported results (Shankar and Srinivas, 2014). The BFCC-HDH polygeneration's cycle EPR is above unity. The waste heat from the absorber and condenser has been utilised for the HDH desalination. Therefore, without much additional energy supply from the HDH, freshwater can be generated.

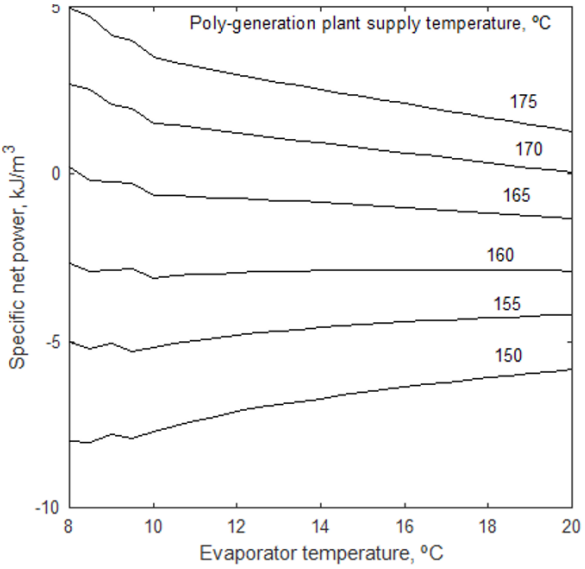

Fig. 8.4: Effect of evaporator temperature and polygeneration plant supply temperature on specific net power generation of the plant

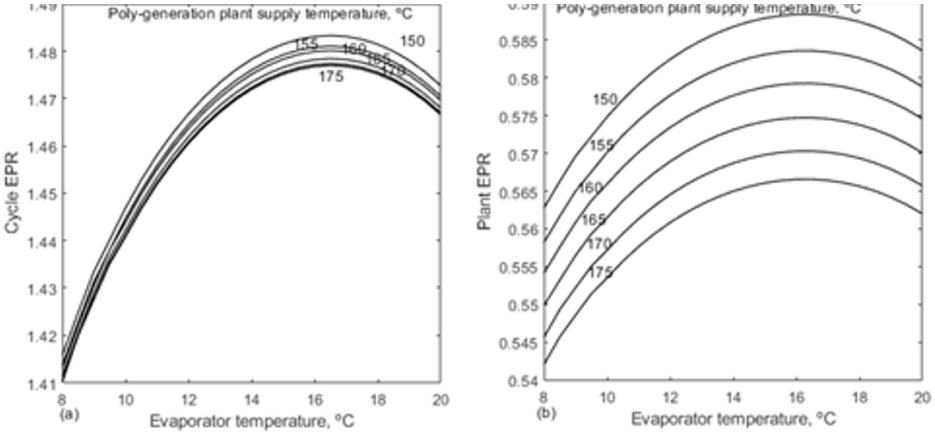

Fig. 8.5: Effect of evaporator temperature and polygeneration plant supply temperature on EPR of cycle and plant

Fig. 8.4 shows the influence of evaporator temperature and polygeneration plant supply temperature on the specific power of the polygeneration plant. Except at the lower supply temperature, the specific power is decreasing with an increase in the evaporator temperature. The generation of power increases as the temperature of the source rises. The enthalpy drops in the turbine increases as the turbine inlet temperature rises.

Fig. 8.5 analyses the role of the evaporator temperature and polygeneration plant supply temperature on the EPR of the cycle and of the plant. The evaporator temperature is optimised for the maximum EPR. Dissimilar to the power augmentation with an increase in the source temperature, the EPR is decreasing with an increase in supply temperature. The increase in source temperature favours the power generation of the BFCC but not the cooling unit of the BFCC. Therefore, the net effect is a drop in EPR with an increase in the source temperature. There is not much change in the optimum evaporator temperature with a change in the polygeneration plant supply temperature.

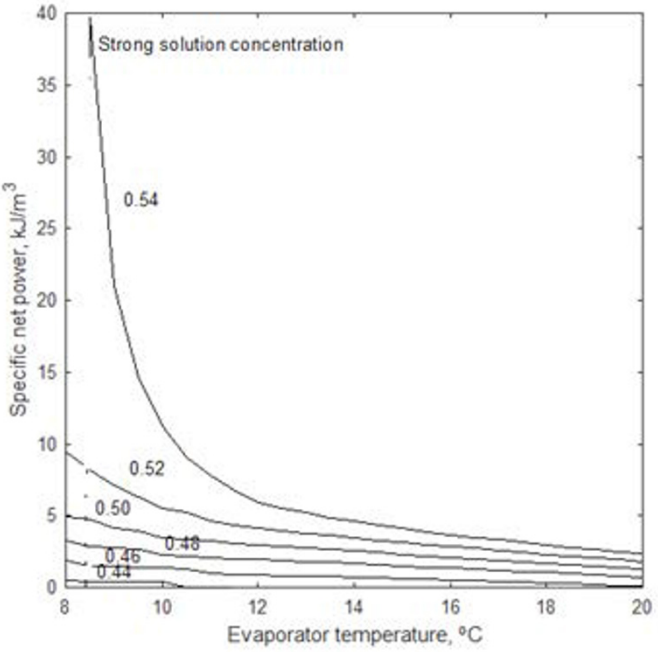

Fig. 8.6: Role of evaporator temperature and strong solution concentration on specific power generation of polygeneration

Fig. 8.6 analyses the effect of evaporator temperature and strong solution concentration on the specific power generation of polygeneration. The net power is decreasing with an increase in evaporator temperature due to a change in the working fluid in the BFCC. The evaporator temperature is

the exit temperature of the unit. Unlike in vapour compression refrigeration, the evaporator temperature is variable in the evaporator of vapour absorption refrigeration. The increase in evaporator temperature, i.e., exit temperature, increases the temperature difference. As a result, the working fluid in the BFCC was reduced. Power generation decreases as the evaporator temperature rises. The low pressure in the BFCC is caused by the high concentration of the solution. It increases the pumping power and so the net power decreases with a drop in strong solution concentration. The high solution concentration has no effect on cooling or freshwater production. The hot water available for external use increases with an increase in the strong solution concentration.

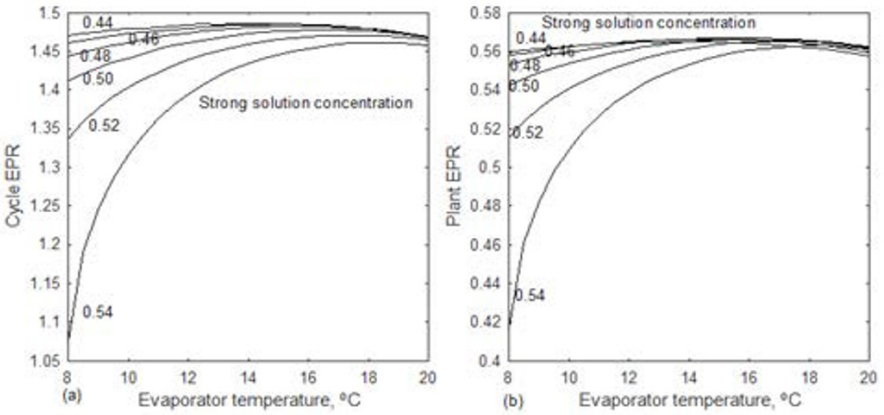

Fig. 8.7: EPR of cycle and plant with change in evaporator temperature and strong solution concentration

Fig. 8.7 analyses the role of evaporator temperature and strong solution concentration on the EPR of the cycle and of the plant. The evaporator temperature is optimised to achieve the highest EPR. The cooling generation increases and later decreases with an increase in the strong solution concentration. The combined changes in the polygeneration outputs result in an optimum strong solution concentration with the evaporator temperature to result in maximum EPR. The optimum evaporator temperature is increased with an increase in the strong solution. For higher EPR, a lower concentration with a lower optimum evaporator temperature is recommended for the maximum cycle EPR. A higher strong solution concentration with a high optimum evaporator temperature is suitable for the maximum EPR of a polygeneration plant.

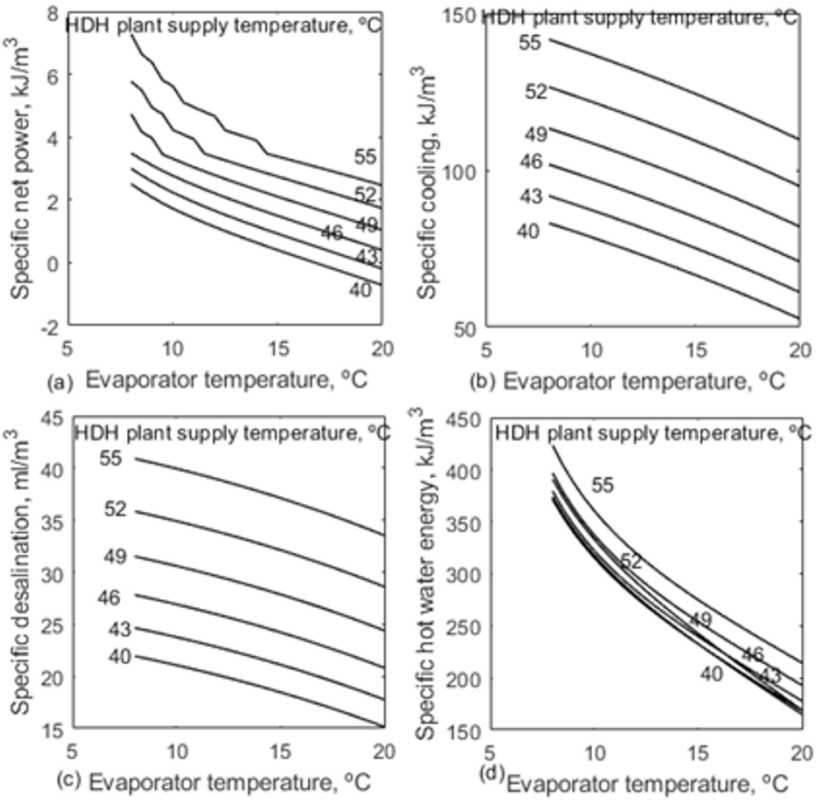

Fig. 8.8: Effect of evaporator temperature and HDH plant supply temperature on four outputs of polygeneration

Fig. 8.8 analyses the effect of evaporator temperature and HDH plant supply temperature on four outputs of polygeneration, viz., specific power, specific cooling, specific freshwater, and specific hot water energy. The air flow rate in the HDH unit is fixed at 1000 m^3/h. The total values can be derived by multiplying the air flow with the specific outputs. The four outputs of polygeneration decrease with an increase in evaporator temperature. The capacities decrease as the working fluid in the BFCC drops at constant air flow in the HDH plant. The role of HDH plant supply temperature is shown in studying the changes in the polygeneration outputs. Power, cooling, freshwater production, and hot water capacity all increase as the HDH supply temperature rises. The increase in HDH supply temperature increases the humidification process and results in more desalination. Since the capacity of HDH is linked with the BFCC, the binary working fluid also increases. Hence, the power, cooling, and heating capacities are also increasing with an increase in the HDH plant's supply temperature.

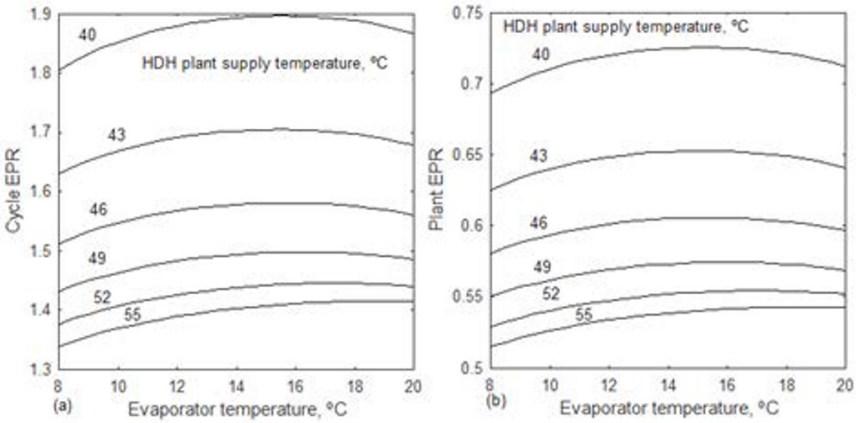

Fig. 8.9: Effect of evaporator temperature and HDH plant supply temperature on EPR of cycle and plant

The role of evaporator temperature and HDH plant supply temperature on the EPR of the cycle and the plant has been analysed in Fig. 8.9. The polygeneration outputs are increasing with an increase in the HDH supply temperature. But it also demands more energy supply from the polygeneration unit. As a result, the EPR decreased with an increase in the HDH unit supply temperature. The optimum evaporator temperature is found to maximise the EPR. The optimum evaporator temperature is increasing with an increase in HDH plant supply temperature.

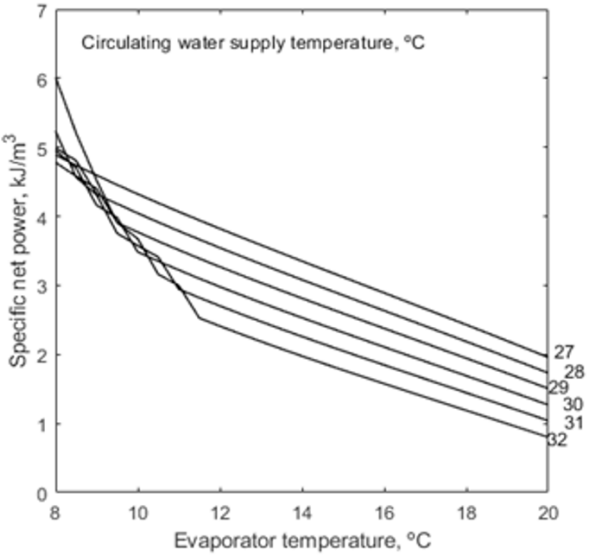

Fig. 8.10: Effect of evaporator temperature and circulating water supply temperature on specific power of polygeneration

Fig. 8.10 shows the role of evaporator temperature and circulating water supply temperature to the absorber and condenser on the specific power generation of a polygeneration plant. The circulating water collected from the storage tank is supplied parallel to the absorber and condenser of the BFCC plant. Therefore, the supply temperature to these two heat exchangers is the same. Compared to a steam power plant, the exit temperature of the circulating water from these two heat exchangers is high due to binary fluid use. The circulating water has been shared and supplied to the absorber and condenser to reach the same exit temperature. Because this exit temperature is excessively high, it is supplied directly to the HDH unit without the use of any additional heaters such as solar water heaters, etc. The increase in circulating water supply temperature or an increase in sink temperature decreases the power generation of the polygeneration. Therefore, a low temperature is required for high power generation. But a lower evaporator temperature demands a higher sink temperature for higher power generation. The energy of the hot water available for the external use is increasing with an increase in circulating water supply temperature. The freshwater production and cooling are remains same with the change in circulating water supply temperature as per the constraints in the simulation.

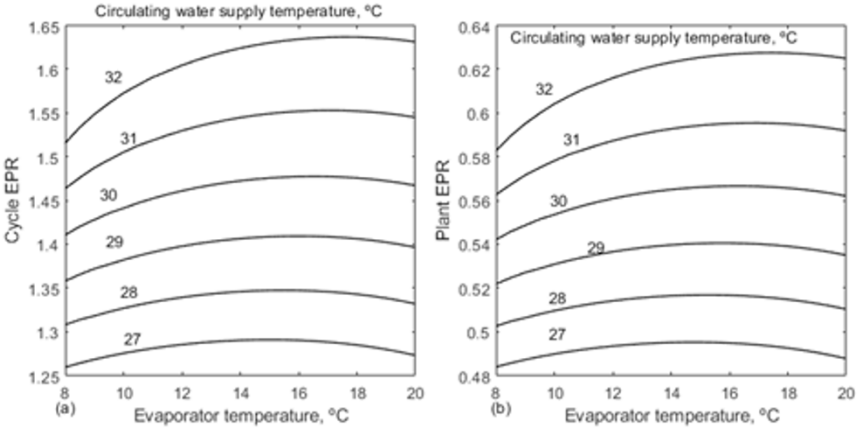

Fig. 8.11: Role of evaporator temperature and circulating water supply temperature on EPR of cycle and plant

Fig. 8.11 analyses the role of evaporator temperature and circulating water supply temperature on the EPR of the polygeneration. The cycle and plant EPR are maximised at the optimum evaporator temperature. The increase in circulating water supply temperature at the fixed outlet temperature decreases the water temperature difference in the absorber and the condenser. It increases the water flowrate in these two heat exchangers. Therefore, more

hot water is available at the same designed temperature for HDH and domestic use. The additional water is supplied for domestic use as the air flowrate and water flowrate in the HDH are fixed. The increased circulating water supply temperature increases the thermal energy for domestic use. Therefore, the EPR is increasing with an increase in the circulating water supply temperature.

Table 8.2: Specifications of binary fluid polygeneration plant at 1000 m^3/h of air in the single stage HDH and 15 °C of refrigerant's exit temperature in the evaporator

Description	Result
Turbine, kW	3.34
Condenser, kW	44.86
Subcooler, kW	0.75
Evaporator, kW	27.90
Absorber, kW	50.32
Solution pump, kW	1.03
LTR, kW	7.12
HTR, kW	14.24
Vapour generator, kW	74.86
Dephlegmator, kW	10.95
Superheater, kW	2.80
Thermic oil pump, kW	0.36
Solar concentrating collector output, kW	84.24
APH, kW	4.18
Humidifier, kW	13.94
1st dehumidifier, kW	2.66
2nd dehumidifier, kW	27.90
HDH fans, kW	1.10
ARH, kW	0.42
Hot water circulating pump, kW	0.20
Specific net power, kJ/m^3	2.31
Specific cooling, kJ/m^3	100.45
Specific freshwater, ml/m^3	32.88
Specific hot water for external use, l/m^3	2.33
Total net power, kW	0.64
Total cooling, kW	27.90
Total freshwater, LPH	32.88

Total hot water, LPH	2333.70
Total energy generation, kW	61.15
Total energy supply to polygeneration cycle, kW	114.60
Total solar energy suppled to collector, kW	202.46
Area of the solar collector, m^2	390.00
Polygeneration cycle EPR	1.47
Polygeneration plant EPR	0.57

Table 8.2 summarises the specifications of BFCC-HDH polygeneration at an air flowrate of 1000 m^3/h and the developed optimised operational conditions. The capacities of binary fluid components and HDH desalination are determined by the developed operational conditions. The electricity supply to the polygeneration is the total electricity supply to the solution pump, circulating pump, and fans. The polygeneration specific results are presented per unit air flowrate, i.e., 1 m^3/s. The production of freshwater and hot water is 32.88 ml/m^3 and 2.33 l/m^3, respectively. The total net power generation, cooling, freshwater, and hot water outcomes are 0.64 kW, 27.90 kW, 32.88 LPH, and 2333.70 LPH, respectively. The EPRs for the cycle and the plant are 1.47 and 0.57, respectively. Compared to the BFCC, addition of HDH to the BFCC results in a higher EPR.

8.3 Binary Fluid Polygeneration with Double Stage HDH

8.3.1 Plant layout

Fig. 8.12 shows the schematic flow details of the binary fluid polygeneration with double stage HDH (BFCC-HDH) for the generation of electricity, cooling, freshwater, and hot water for domestic use.

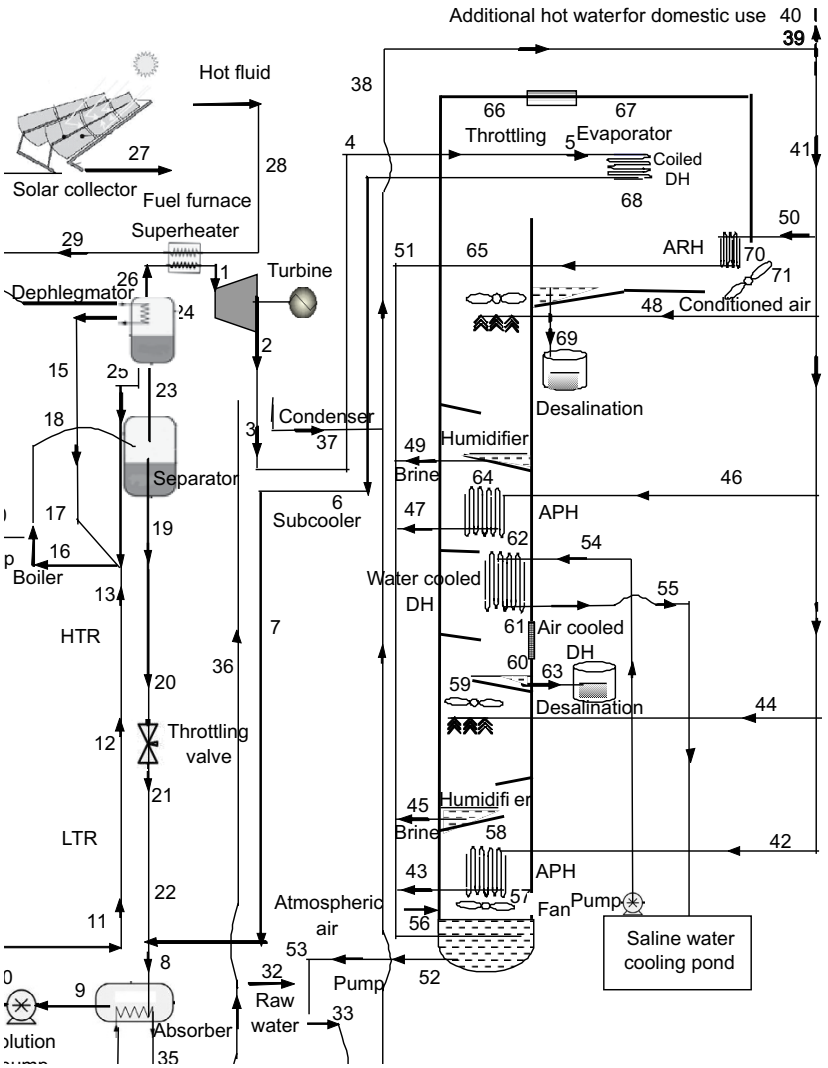

Fig. 8.12: Binary fluid polygeneration with two stage HDH plant; States 1-26: binary fluid, 27-31: thermic oil, 32-55: water, 56-71: HDH desalination

The components used in the BFCC are the vapour turbine, condenser, subcooler, throttling device, evaporator, absorber, solution pump, low temperature regenerator (LTR), high temperature regenerator (HTR), boiler, separator, and dephlegmator. The boiler produces superheated vapour (1), which is used to generate electricity and cool the BFCC.This vapour is expanded in the vapour turbine for power production. BFCC operates at three different pressures: high pressure (HP), intermediate pressure (IP), and low

pressure (LP). The fluid in the turbine expands from HP to IP (1-2). At IP and the exit of the turbine, the vapour is condensed (2-3) to a saturated liquid state. This saturated liquid is expanded (5-6) in the throttling valve. At the exit of the throttling, the fluid's (5) temperature is low and capable of absorbing heat from the surroundings. It is used as a dehumidifier in HDH plants. The humid air passes over the evaporator coil (67–68) and the moisture in the air gets condensed, which is known as desalinated water. The heat is absorbed by the refrigerant, and the refrigerant evapourates (5–6) to a saturated vapour state. The vapour temperature (6) is below the atmospheric temperature and it is to be condensed in the absorber. And the condensate at the IP has the capacity to reject heat from this vapour. Therefore, a subcooler is used to increase the capacity of the evaporator and share the absorber heat load. At the inlet of the absorber, the weak solution has been mixed with the vapour at LP. It dilutes the working fluid in the absorber and allows easy condensation (8–9) with the sink temperature without demanding much high pressure. The saturated liquid at the exit of the absorber is a strong solution. It is pumped to boiler pressure (9–10). The role of the dephlegmator in BFCC is to increase the concentration of working fluid, which favours cooling. The dephlegmator needs heat rejection for the condensation of the water in the dephlegmator. Therefore, some of the strong solutions (14) have been rooted in the dephlegmator to absorb the heat. The strong solution is supplied to the boiler flow via LTR (11-12) and HTR (12-13) for the internal heat recovery from the weak solution. The weak solution rejects the heat in HTR (19–20) and LTR (21-22) before mixing with the absorber. The weak solution is to expand the throttling (20–21) from HP to LP. This preheating of strong solutions shares the boiler load. The preheated strong solution (13) is mixed with the return fluid from the dephlegmator (25) and the cold strong solution (15). With solar thermal collectors, the wet vapour (18) is generated in the boiler. The wet fluid (18) separates into saturated liquid (19), which is also called weak solution and saturated vapour (23). This fluid (23) is refined in the dephlegmator (23-24-26) by rejecting the heat to form a strong solution. The highly concentrated vapour is superheated (26-1), and supplied to the turbine for power generation.

HDH desalination has two-stage operations for more water yield. The components of the HDH plant are the fan, air preheater (APH), humidifier, air cooled dehumidifier, water cooled dehumidifier, refrigerant cooled dehumidifier, and air reheater (ARH). The APH, humidifier, and dehumidifier repeat in the second stage of operation. The atmospheric air (56) enters the plant with a fan. In APH, the temperature of the air is increased (57–58) with sensible heating. The relative humidity (Ø) of the air in the APH decreases and gives more scope for evaporation in the humidifier. The humidifier sprays hot saline water against the preheated air stream at the top of the pack. The air undergoes a heating and humidification process (58–59). Later, the air flows

over the cooling surface of natural convection (60–61), followed by air cooling with the water-cooled dehumidifier (61-62). The projected surface into the environment rejects heat from the humid air and contributes to the evaporator load. The final dehumidification (67–68) happens in the evaporator section of the BFCC. The water-cooled condenser and absorber of the BFCC are used to raise the saline water temperature. The evaporator part of the BFCC is used for the dehumidification of air. The condensate from the dehumidification process is collected in a container from the first stage and second stage (63 and 69). The air reheater (68–70) increases the air temperature and decreases the relative humidity to suit the air conditioning. The hot saline water is supplied to two APHs (42 and 46), two humidifiers (44 and 48), and an ARH (50). The air is humidified in the humidifier (58–59) by spraying hot water (44) over the packing. The packing placed in the humidifier increases the wetting surface and evaporation. The humid air (59) collects at the top, and the brine solution (45) is at the bottom of the humidifier. In dehumidification, the humid air is cooled to condense the moisture in the humid air. A natural convective surface has been provided at the first level to reject heat to the surrounds (60-61). Later, the air is condensed in the water-cooled condenser (61-62). In the second stage of HDH, the APH (62–64), humidifier (64-65) and dehumidifier (66–67–68) are repeated. Since the cold refrigerant in the evaporator provides a lower temperature compared to the water-cooled dehumidifier, more condensation results in the second stage of operation. To restore the required temperature and relative humidity of conditioned air (70), ARH is used.

The total heat load in the condenser and absorber is greater than the HDH heat load (the sum of APR, humidifier, and ARH). If the whole water is recirculated in the circuit, the temperature of water in the plant continuously increases. To keep the sink's operating temperature safe, saline water has been supplied (32) to the storage tank. The additional hot water is designed for domestic use (40). The used water from the HDH has been collected and pumped (52-53) to the overhead storage tank, which is kept at an elevated level (elevation not shown in Fig. 1). The mixed cool saline water from the storage tank has been supplied to BFCC for heat rejection.

8.3.2 Thermodynamic model

Thermodynamic simulation of the polygeneration plant has been conducted at an air flow rate of 1000 m^3/h in HDH plant. Therefore, the HDH formulations are detailed first and followed by BFCC formulation. The heat rejection temperature of the BFCC is suitable to operate the HDH plant. Therefore, the heat sink (absorber and condenser) of BFCC has been used to generate the hot water which drives the HDH plant. The cooling component of evaporator also has been coupled with the HDH plant. The evaporator is used as a dehumidifier in the HDH. The cold surface of the evaporator has been used to condense the moisture in the humid air. Therefore, the evaporator of

BFCC is a dehumidifier in HDH plant. The capacity of the cooling unit, i.e. the evaporator is determined from the air flow rate and the dehumidifier. Based on the resulted BFCC cooling size, the working fluid has been determined. The pinch point (PP) in the boiler, working fluid flow and boiler temperatures result in thermic oil circulation in the solar concentrating collectors.

The assumptions used in the HDH plant are stated in the earlier single stage model. Similarly, the BFCC's assumptions are also furnished in the earlier sections.

The air exit temperature from the APH is determined from its effectiveness

$$T_{58} = T_{57} + э_{APH}(T_{42} - T_{57}) \tag{8.21}$$

The hot water inlet and outlet temperatures to APH have been fixed to find its flow rate. The energy balance equation in the APH results the hot water flowrate at the know air flow rate with is fixed as per the assumptions.

Hot water demand in APH,

$$m_{42} = \frac{m_{da}(h_{58} - h_{57})}{c_{p,hw}(T_{43} - T_{42})} \tag{8.22}$$

The amount of brine solution collected at the bottom of the humidifier is less than the hot water supply due to the air humidification. Based on the liquid to air mass ratio in the humidifier, the hot water spray has been determined at a fixed air flow rate.

Mass of water at the exit of humidifier,

$$m_{45} = m_{44} - m_{da}(\omega_{59} - \omega_{58}) \tag{8.23}$$

The air exit condition from the humidifier is simulated based on the hot water supply temperature. The heating and humidification process on the psychrometric chart moves towards the hot water temperature at the maximum limit of humidification, i.e., 100% RH.

The temperature of hot water at the humidifier's outlet,

$$T_{45} = \frac{m_{44}c_{pw}T_{44} - m_{da}(h_{59} - h_{58})}{m_{45}c_{pw}} \tag{8.24}$$

The mass of air at the exit of humidifier after picking the moisture,

$$m_{59} = m_{58} + m_{da}(\omega_{59} - \omega_{58}) \tag{8.25}$$

The effectiveness of dephlegmator is determined from Eq. 8.9.

In the dephlegmator, the vapour is condensed partially to remove the water from the vapour. Hence, the concentration of ammonia increases. The exit concentration (x_{26}) is determined by the effectiveness of the dephlegmator (Eq. 8.9) and the vapour exit concentration (x_{23}). The increased ammonia concentration with the dephlegmator favours the refrigeration performance (output and cooling coefficient of performance). After the liquid-vapour

mixture is generated in the boiler, it is separated into a weak solution and a vapour. The concentration of weak solution and vapour along with its flow rate is solved using a lever rule applied to the separation process. The same can be applied to the mixing process. In the separator, the dry fraction of the liquid-vapour fluid is the mass ratio of saturated vapour and total mass.

The Eq. 8.10 to 8.20 can be used to solve the BFCC which is integrated with double stage HDH.

The properties of binary fluid polygeneration with double stage HDH have been listed in Table 8.3 with the states 1 to 71. The binary fluid properties are represented by states 1 through 26. The simulated three pressures in the BFCC are 28.79 bar, 12.44 bar, and 4.41 bar, respectively, HP, IP, and LP. State 29 to 31 are the properties of thermic oil used in the solar concentrating collector and boiler. States 32 through 49 are about water properties. State 50 to 59, (except 57) represents the psychrometric properties of air.

Table 8.3: Material balance and energy balance results of polygeneration plant at 1000 m^3/h of air in the double stage HDH and 10 °C of refrigerant's exit temperature in the evaporator

State	m, kg/h	P, bar	T, °C	x or Ø (%)	ω, g/kg	h, kJ/kg	s, kJ/kg K	ε, kJ/kg
1	179.76	28.79	160.00	0.93	- -	1661.60	4.91	197.23
2	179.76	12.44	97.97	0.93	- -	1547.65	5.00	56.89
3	179.76	12.44	35.00	0.93	- -	110.89	0.56	-56.56
4	179.76	12.44	30.00	0.93	- -	86.77	0.48	-57.15
5	179.76	4.41	3.04	0.93	- -	87.69	0.51	-65.22
6	179.76	4.41	10.00	0.93	- -	873.56	3.34	-123.47
7	179.76	4.41	10.85	0.93	- -	897.96	3.43	-124.73
8	561.75	4.41	59.68	0.50	- -	398.27	1.87	-158.70
9	561.75	4.41	35.00	0.50	- -	-82.98	0.37	-192.08
10	561.75	28.79	36.93	0.50	- -	-72.30	0.39	-188.78
11	501.34	28.79	36.93	0.50	- -	-72.30	0.39	-188.78
12	501.34	28.79	55.07	0.50	- -	9.47	0.65	-183.42
13	501.34	28.79	90.22	0.50	- -	173.02	1.12	-160.94
14	60.41	28.79	36.93	0.50	- -	-72.30	0.39	-188.78
15	60.41	28.79	135.00	0.50	- -	731.44	2.54	-26.46
16	591.05	28.79	104.08	0.49	- -	239.71	1.30	-148.18
17	591.05	28.79	109.47	0.49	- -	266.36	1.37	-142.44
18	591.05	28.79	150.00	0.49	- -	968.92	3.10	43.39
19	381.99	28.79	150.00	0.30	- -	486.16	1.88	-73.88
20	381.99	28.79	105.06	0.30	- -	271.01	1.34	-128.98
21	381.99	4.41	79.87	0.30	- -	273.43	1.37	-135.30
22	381.99	4.41	73.61	0.30	- -	164.07	1.06	-151.49

23	209.06	28.79	150.00	0.85	- -	1704.37	4.99	216.04
24	209.06	28.79	129.12	0.85	- -	1472.13	4.44	147.80
25	29.30	28.79	129.12	0.39	- -	364.01	1.61	-117.42
26	179.76	28.79	129.12	0.93	- -	1571.95	4.70	169.26
27	4178.63	1.01	175.00	- -	- -	280.95	0.76	53.37
28	4178.63	1.01	175.00	- -	- -	280.95	0.76	53.37
29	4178.63	1.01	172.94	- -	- -	276.58	0.75	51.99
30	4178.63	1.01	124.47	- -	- -	177.72	0.51	24.36
31	4178.63	1.01	117.87	- -	- -	164.90	0.48	21.35
32	2908.15	1.01	25.00	- -	- -	79.50	0.00	0.00
33	6323.10	1.01	30.00	- -	- -	100.40	0.07	20.90
34	3233.73	1.01	30.00	- -	- -	100.40	0.07	20.90
35	3233.73	1.01	50.00	- -	- -	184.00	0.34	104.50
36	3089.37	1.01	30.00	- -	- -	100.40	0.07	20.90
37	3089.37	1.01	50.00	- -	- -	184.00	0.34	104.50
38	6323.10	1.01	50.00	- -	- -	184.00	0.34	104.50
39	2876.98	1.01	50.00	- -	- -	184.00	0.34	104.50
40	2876.98	1.01	50.00	- -	- -	184.00	0.34	104.50
41	3446.12	1.01	50.00	- -	- -	184.00	0.34	104.50
42	449.89	1.01	50.00	- -	- -	184.00	0.34	104.50
43	449.89	1.01	42.00	- -	- -	150.56	0.23	71.06
44	1270.49	1.01	50.00	- -	- -	184.00	0.34	104.50
45	1252.63	1.01	41.13	- -	- -	146.93	0.22	67.43
46	263.49	1.01	50.00	- -	- -	184.00	0.34	104.50
47	263.49	1.01	42.00	- -	- -	150.56	0.23	71.06
48	1270.49	1.01	50.00	- -	- -	184.00	0.34	104.50
49	1257.19	1.01	43.53	- -	- -	156.97	0.25	77.47
50	191.76	1.01	50.00	- -	- -	184.00	0.34	104.50
51	191.76	1.01	42.00	- -	- -	150.56	0.23	71.06
52	3414.95	1.01	42.25	- -	- -	151.59	0.24	72.09
53	3414.95	1.01	42.42	- -	- -	152.31	0.24	72.81
54	1044.04	1.01	38.85	- -	- -	137.38	0.19	-79.50
55	1044.04	1.01	40.19	- -	- -	143.00	0.21	-79.50
56	1293.30	1.01	28.00	75.00	17.95	73.98	0.26	-0.26
57	1293.30	1.60	31.00	99.95	17.95	77.09	0.27	-0.53
58	1293.30	1.58	42.40	53.08	17.95	88.93	0.31	-0.07
59	1311.17	1.57	45.44	78.32	32.01	128.41	0.44	0.22
60	1311.17	1.57	45.44	78.32	32.01	128.41	0.44	0.22
61	1309.98	1.54	40.61	96.04	31.08	120.86	0.42	-0.05
62	1308.48	1.52	39.11	99.25	29.90	116.24	0.40	-0.15

63	2.68	1.01	39.11	- -	- -	138.48	0.19	-60.63
64	1308.48	1.51	45.64	69.77	29.90	123.18	0.42	0.26
65	1321.79	1.49	47.39	84.00	40.38	152.12	0.52	0.99
66	1321.79	1.49	47.39	84.00	40.38	152.12	0.52	0.99
67	1320.34	1.46	43.64	97.09	39.23	145.11	0.50	0.70
68	1279.94	1.45	15.05	100.00	7.43	33.92	0.12	0.56
69	41.85	1.01	15.05	- -	- -	37.89	-0.14	-41.61
70	1279.94	1.43	20.00	72.41	7.43	38.97	0.14	0.44
71	1279.94	1.43	20.00	50.00	5.11	33.08	0.12	0.84

8.3.3 Performance characteristics of binary fluid polygeneration with double stage HDH

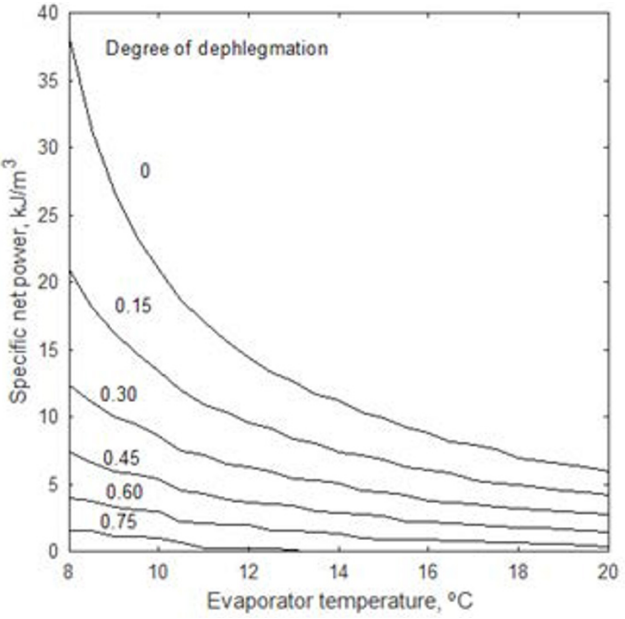

Fig. 8.13: Influence of evaporator temperature and degree of dephlegmation on specific power of polygeneration

Fig. 8.13 depicts the effect of evaporator temperature on the specific net power generation of polygeneration with the degree of dephlegmation. The zero degree of dephlegmation indicates no dephlegmation. Hypothetically, if the exit concentration of fluid is one, the degree of dephlegmation is one. The degree of dephlegmator was increased from 0 to 0.75. The dephlegmator is an important component of the cooling unit. The high pressure can be decreased with the dephlegmator. However, it reduces the expansion, so the

power decreases as the dephlegmation increases. The evaporator in the BFCC plays the role of a dehumidifier in the HDH unit. The plant's power generation is decreasing with an increase in evaporator temperature. The results are generated at the fixed air flow rate in the HDH unit. The decreased evaporator temperature decreases the cooling load on the dehumidifier. According to this drop in cooling, the working fluid in the binary fluid plant decreases, resulting in power declination. The increase in evaporator exit temperature also increases the air exit temperature of the air in the HDH dehumidifier. It decreases the cooling load in the dehumidifier, and so the cooling load in the evaporator also decreases with an increase in the evaporator temperature. As per the energy balance in the dehumidifier of the HDH or the evaporator of the BFCC, the working fluid in the BFCC decreases. Therefore, the power generation decreases with an increase in the evaporator temperature. The freshwater and cooling outputs are independent of the changes in the role of the dephlegmator. But the hot water energy decreases with an increase in the degree of dephlegmator.

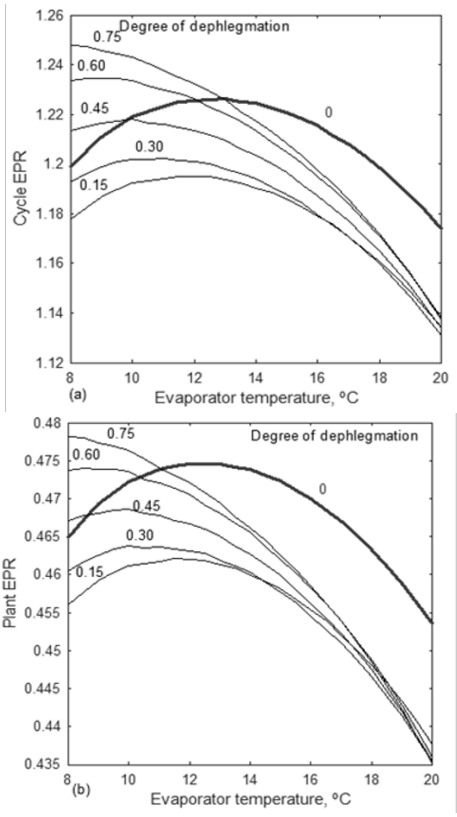

Fig. 8.14: The effect of evaporator temperature and degree of dephlegmation on cycle and plant EPR

Fig. 8.14 shows the influence of the evaporator temperature and degree of dephlegmation on the EPR of the polygeneration cycle and of the plant. The increase in evaporator temperature favours the COP of the refrigeration unit. But the four outputs, viz., power, cooling, fresh water, and hot water, decrease with an increase in the evaporator temperature. The decrease in energy supply and output result an optimum evaporator temperature to maximise the EPR, as shown. The increase in the degree of dephlegmation saves pumping power due to the decrease in high pressure. As a result, as the degree of dephlegmation increases, so does the EPR of the cycle and the plant. The optimum evaporator temperature decreases as the degree of dephlegmation increases. The optimum evaporator temperature without a dephlegmator is higher than the optimum temperature with a dephlemgator. Higher EPR is caused by increased dephlegmation and a low optimum evaporator temperature. The EPR of combined power and cooling is less than unity as per the reported results (Shankar and Srinivas, 2016). The resulted BFCC-HDH polygeneration's cycle EPR is above unity, i.e., more than 100%. Since the waste heat of the BFCC has been used for HDH, without much energy supply to HDH, this polygeneration can be operated in an efficient mode.

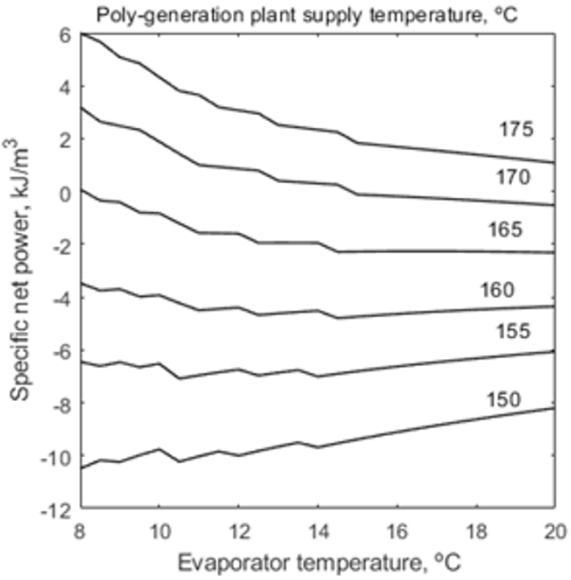

Fig. 8.15: Effect of evaporator temperature and polygeneration plant supply temperature on specific net power generation of the plant

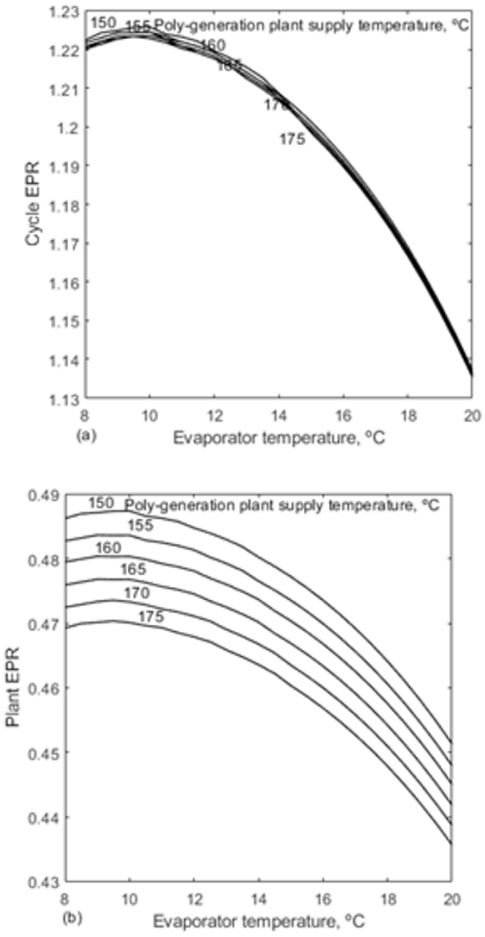

Fig. 8.16: Effect of evaporator temperature and polygeneration plant supply temperature on EPR of cycle and plant

Fig. 8.15 shows the influence of evaporator temperature and polygeneration plant supply temperature on the specific power of the polygeneration plant. At the supply temperature of 160 °C, the specific power decreases with an increase in the evaporator temperature. On the other hand, a high evaporator temperature is required with a lower supply temperature and vice versa for higher power generation. The generation of power increases as the temperature of the source rises. The enthalpy drops in the turbine increases as the turbine inlet temperature rises.

Fig. 8.16 analyses the role of the evaporator temperature and polygeneration plant supply temperature on the EPR of the cycle and of the plant. The evaporator temperature is optimised for the maximum EPR. Dissimilar to the

power augmentation with an increase in the source temperature, the EPR is decreasing with an increase in supply temperature. A high source temperature supports only power production but not the cooling. The cooling quantity of BFCC is more than the electricity generation. Therefore, the net effect is a drop in EPR with an increase in the source temperature. There is not much change in the optimum evaporator temperature with a change in polygeneration plant supply temperature for the maximum EPR.

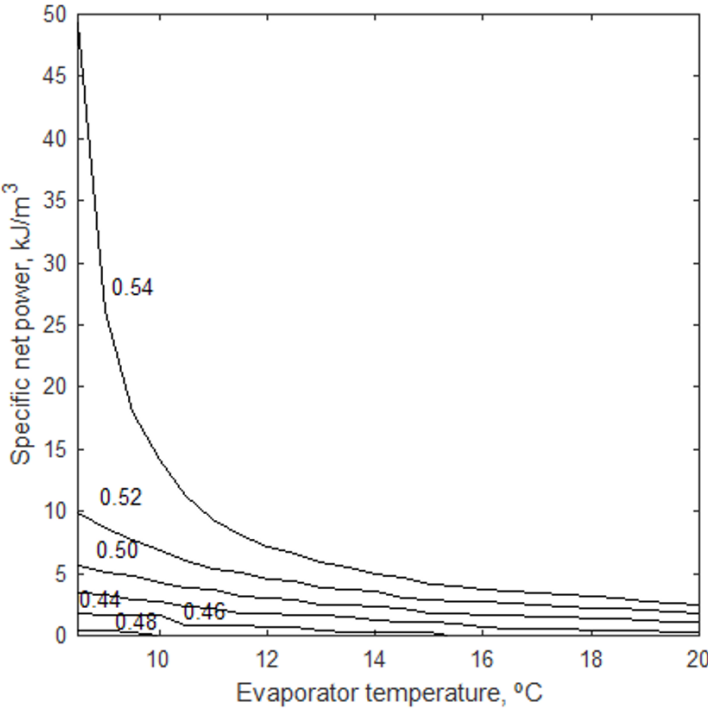

Fig. 8.17: Role of evaporator temperature and strong solution concentration on specific power generation of polygeneration

Fig. 8.17 analyses the effect of evaporator temperature and strong solution concentration on the specific power generation of polygeneration. The strong solution can be controlled during the charging of the fluid in the binary fluid plant. Therefore, it has been taken as an independent variable. The net power is decreasing with an increase in evaporator temperature. The evaporator temperature decides the amount of working fluid required in the BFCC, based on the load in HDH. The fluid demand is decreasing in the BFCC with an increase in evaporator temperature as the cooling load in the dehumidifier is decreasing. The evaporator temperature is the exit temperature of the unit. Unlike in vapour compression refrigeration, the evaporator temperature is variable in the evaporator of vapour absorption refrigeration. The increase in

evaporator temperature, i.e., the exit temperature, increases the temperature difference. As a result, the working fluid in the BFCC was reduced. Power generation decreases as the evaporator temperature rises. The low pressure in the BFCC is caused by the high concentration of the solution. It increases the pumping power and so the net power decreases with a drop in strong solution concentration. Similar to power generation, the available energy of hot water for external use is increasing with an increase in the strong solution concentration. As per the constraints in the simulation, the strong solution concentration is not related to the freshwater production and cooling generation.

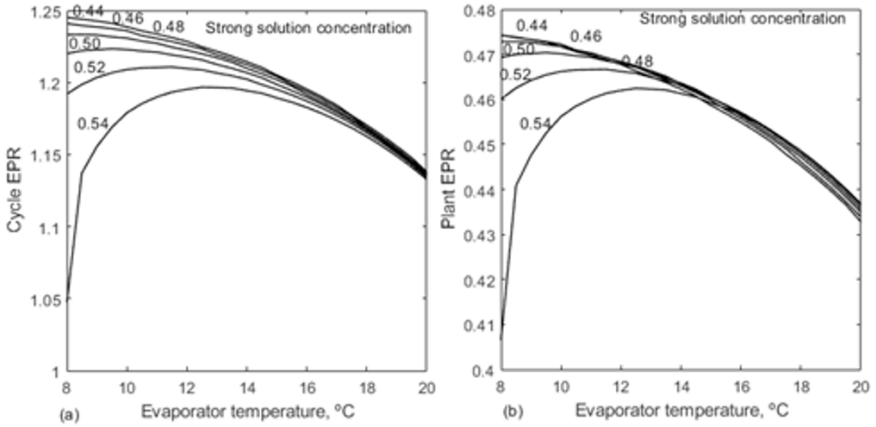

Fig. 8.18: EPR of cycle and plant with change in evaporator temperature and strong solution concentration

Fig. 8.18 analyses the role of evaporator temperature and strong solution concentration on the EPR of the cycle and of the plant. The cooling generation increases and later decreases with an increase in the strong solution concentration. The combined changes in the polygeneration outputs result in an optimum strong solution concentration with the evaporator temperature to achieve maximum EPR. The optimum evaporator temperature is increased with an increase in the strong solution. For higher EPR, a lower concentration with a lower optimum evaporator temperature is recommended for the maximum cycle EPR. A higher strong solution concentration with a high optimum evaporator temperature is suitable for the maximum EPR of a polygeneration plant.

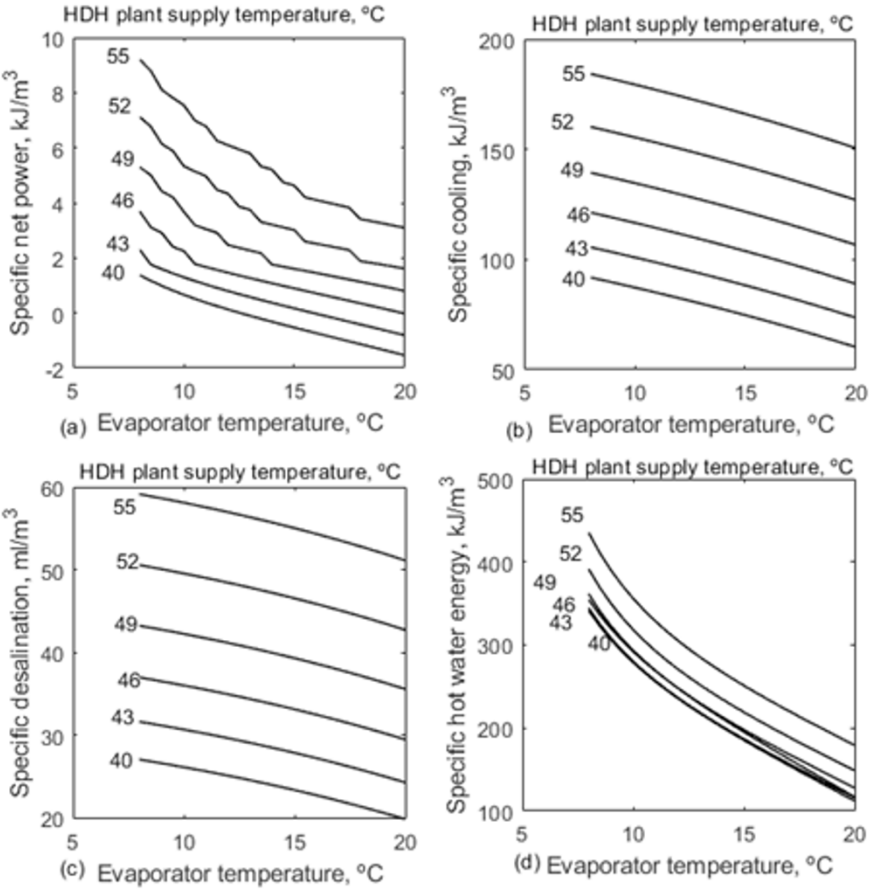

Fig. 8.19: Effect of evaporator temperature and HDH plant supply temperature on four outputs of polygeneration

Fig. 8.19 analyses the effect of evaporator temperature and HDH plant supply temperature on four outputs of polygeneration, viz., specific power, specific cooling, specific freshwater, and specific hot water energy. The air flow rate in the HDH unit is fixed at 1000 m^3/h. The total values can be derived by multiplying the air flow with the specific outputs. The four outputs of polygeneration decrease with an increase in evaporator temperature. The capacities decrease as the working fluid in the BFCC drops below the fixed air flow in the HDH plant. The role of HDH plant supply temperature is shown in studying the changes in the polygeneration outputs. Power, cooling, freshwater production, and hot water capacity all increase as the HDH supply temperature rises. The increase in HDH supply temperature increases the humidification process and results in more desalination. Since the capacity of HDH is linked

with the BFCC, the binary working fluid also increases. Hence, the power, cooling, and heating capacities are also increasing with an increase in the HDH plant's supply temperature.

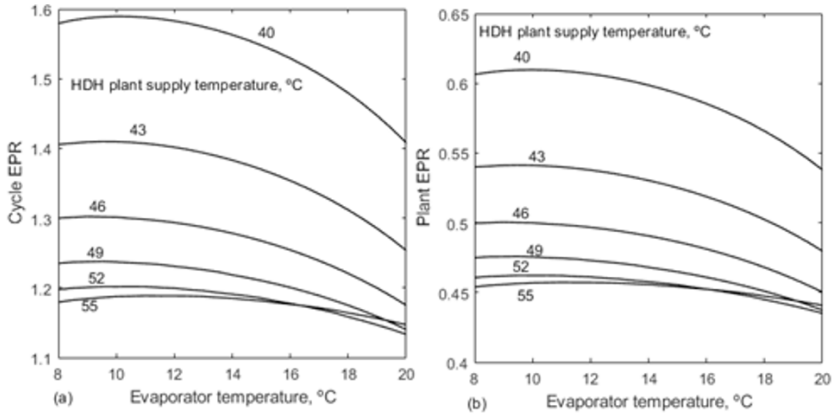

Fig. 8.20: Effect of evaporator temperature and HDH plant supply temperature on EPR of cycle and plant

The role of evaporator temperature and HDH plant supply temperature on the EPR of the cycle and the plant has been analysed in Fig. 8.20. The polygeneration outputs are increasing with an increase in HDH supply temperature. But it also demands more energy supply for the polygeneration unit. As a result, the EPR decreased with an increase in the HDH unit supply temperature. The optimum evaporator temperature is found to maximise the EPR. The optimum evaporator temperature is increasing with an increase in HDH plant supply temperature.

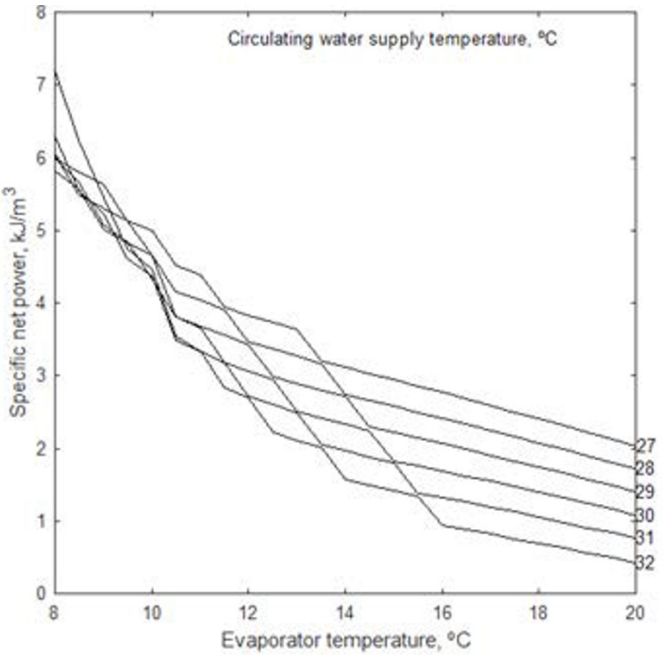

Fig. 8.21: Effect of evaporator temperature and circulating water supply temperature on specific power of polygeneration

Fig. 8.21 shows the role of evaporator temperature and circulating water supply temperature to the absorber and condenser on the specific power generation of a polygeneration plant. The circulating water collected from the storage tank is supplied parallel to the absorber and condenser of the BFCC plant. Therefore, the supply temperature to these two heat exchangers is the same. Compared to a steam power plant, the exit temperature of the circulating water from these two heat exchangers is high due to binary fluid use. The circulating water has been shared and supplied to the absorber and condenser to reach the same exit temperature. Because this exit temperature is excessively high, it is supplied directly to the HDH unit without the use of any additional heaters such as solar water heaters, etc. The increase in circulating water supply temperature or an increase in sink temperature decreases the power generation of the polygeneration. Therefore, a low temperature is required for high power generation. But a lower evaporator temperature demands a higher sink temperature for higher power generation.

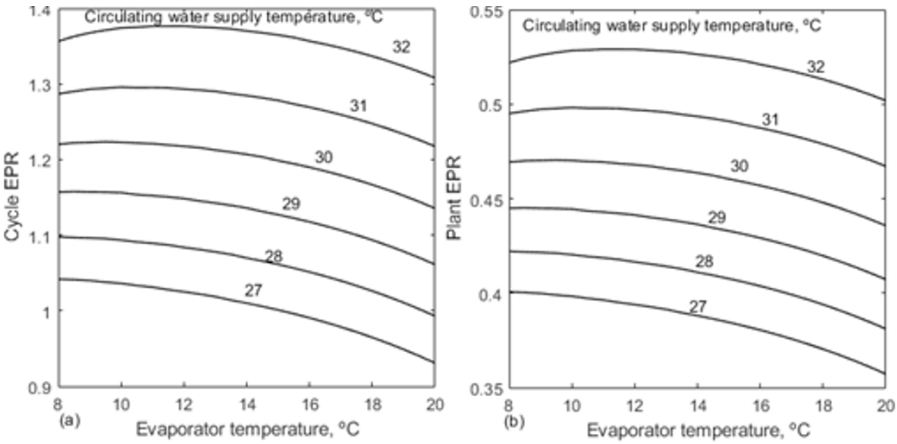

Fig. 8.22: Role of evaporator temperature and circulating water supply temperature on EPR of cycle and plant

Fig. 8.22 analyses the role of evaporator temperature and circulating water supply temperature on the EPR of the polygeneration. The increase in circulating water supply temperature at the fixed outlet temperature decreases the water temperature difference in the absorber and the condenser. It increases the water flowrate in these two heat exchangers. Therefore, more hot water is available at the same designed temperature for HDH and domestic use. The additional water is supplied for domestic use as the air flowrate and water flowrate in the HDH are fixed. The increased circulating water supply temperature increases the thermal energy for domestic use. Therefore, the EPR is increasing with an increase in the circulating water supply temperature.

Table 8.4: Specifications of polygeneration plant at 1000 m^3/h of air in the double stage HDH and 10 °C of refrigerant's exit temperature in the evaporator

Description	Result
Turbine, kW	5.35
Condenser, kW	71.74
Subcooler, kW	1.20
Evaporator, kW	39.24
Absorber, kW	75.09
Solution pump, kW	1.65
LTR, kW	11.38
HTR, kW	22.82
Vapour generator (boiler), kW	119.72
Dephlegmator, kW	17.52
Superheater, kW	4.48

Thermic oil pump, kW	0.71
Solar concentrating collector output, kW	134.71
APH (1), kW	4.17
Humidifier (1), kW	13.93
Dehumidifier (1), kW	0.46
Dehumidifier (2), kW	2.66
APH (2), kW	2.44
Humidifier (2), kW	10.21
Dehumidifier (3), kW	2.47
Dehumidifier (4), kW	39.24
HDH fans, kW	1.10
ARH, kW	1.79
Hot water circulating pump, kW	0.68
Specific net power, kJ/m^3	4.32
Specific cooling, kJ/m^3	141.26
Specific freshwater, ml/m^3	44.53
Specific hot water for external use, l/m^3	2.87
Total net power, kW	1.20
Total cooling, kW	39.24
Total freshwater, LPH	44.53
Total hot water for external use, LPH	2877.00
Total energy generation, kW	151.87
Total energy supply to polygeneration cycle, kW	65.61
Total solar energy suppled to collector, kW	323.00
Area of the solar collector, m^2	622.00
Polygeneration cycle EPR	1.23
Polygeneration plant EPR	0.47

Table 8.4 summarises the specifications of BFCC-HDH polygeneration at an air flowrate of 1000 m^3/h and the developed optimised operational conditions. The ratings of all the heat exchangers and the machines are evaluated at the stated operational conditions within the optimised parameters. The electricity required to operate the polygeneration includes solution pumps, circulating pumps, and fans. Freshwater production is 44.53 ml/m^3 and hot water production is 2.87 l/m^3. The total net power generation, cooling, freshwater, and hot water outcomes are 1.20 kW, 39.24 kW, 44.53 LPH, and 2877.00 LPH, respectively. The EPRs for the cycle and the plant that results are

1.23 and 0.47, respectively. Compared to the BFCC alone, HDH integration to the BFCC augments the EPR.

8.4 Summary

A binary fluid polygeneration has been configured with BFCC and HDH desalination. The designed outputs of polygeneration are power, cooling, fresh water, and hot water for domestic use. A parametric analysis has been conducted to find the efficient operational conditions for the proposed binary fluid polygeneration plant. The selected operational conditions are evaporator temperature, degree of dephlegmation, polygeneration plant supply temperature, strong solution concentration, HDH plant supply temperature, and circulating water supply temperature. The parametric analysis showed that the evaporator temperature can be optimised to result in the maximum EPR for the cycle and the plant. Compared to the reported BFCC, the current polygeneration cycle, which is an extension of an earlier version, results in a higher EPR, which is greater than 100%. The polygeneration cycle efficiency is 3.5 times greater than the BFCC cycle efficiency. The optimum evaporator temperature decreases with increasing dephlegmation, does not change much with increasing polygeneration plant supply temperature, increases with increasing strong solution concentration, increases with increasing HDH plant supply temperature, and increases with increasing circulating water supply temperature. In addition to the optimum evaporator temperature, a higher degree of dephlegmation, low polygeneration plant supply temperature, low strong solution concentration, high HDH plant supply temperature, and high circulating water supply temperature have been recommended to result in a maximum EPR of polygeneration. The resultant optimum evaporator temperature is the same for maximum cycle EPR and maximum plant EPR.

At the evaporator temperature of 15 °C, with 0.5 degree of dephlegmation, polygeneration plant supply temperature of 175 °C, 0.5 strong solution concentration, HDH plant supply temperature of 50 °C, and circulating water supply temperature of 30 °C, the binary fluid polygeneration with double stage HDH results in an EPR of 1.47 and 0.51, respectively, for the cycle and plant. At the same conditions, the binary fluid polygeneration with double stage HDH results in an EPR of 1.23 and 0.43, respectively, for the cycle and plant.

Review questions

1. Analyze the optimum evaporator pressure as a function of operational conditions.
2. How do the single-stage HDH and double-stage HDH influence the performance of a binary fluid polygeneration?
3. Highlight the potential of binary fluid polygeneration compared to the other polygeneration plants.
4. When compared to a single fluid polygeneration plant, the binary fluid plant can generate hot water for thermal desalination. Justify.

❐

9

Heat Pump Polygeneration

Abstract

In a heat pump polygeneration, a humidification-dehumidification and vapor compression refrigeration (HDH-VCR) cycle has been integrated to meet the electricity, freshwater, space conditioning and hot water demands with the minimum floor space. In the refrigeration cycle and heat pump cycle, heat absorption and heat rejection are the desired outputs respectively. In heat pump polygeneration, a water-cooled condenser for humidification and an evaporator for dehumidification are simultaneously used to generate the desired outputs. Thermodynamic simulation and analysis have been focused on studying the effect of evaporator temperature, hot water temperature, circulating water supply temperature to heat pump, atmospheric air temperature, and atmospheric air's relative humidity (RH) on specific outputs, energy performance ratio (EPR), required driving power to operate the polygeneration plant and solar collector's area. Heat absorption and heat rejection have been used in HDH desalination to increase the EPR of the plant. The heat pump polygeneration working on HDH-VCR principle has been simulated to develop its performance characteristics. The study shows that the evaporator temperature can be optimized to maximize the EPR as a function of hot water supply temperature to HDH, circulating water supply temperature to heat pump, atmospheric air temperature, and atmospheric air relative humidity (RH). The resulted EPR for heat pump polygeneration with single stage HDH at 50 °C of hot water temperature is 1.55 and 0.57 respectively for cycle and plant. Similarly, at the same conditions, the heat pump polygeneration with double stage HDH results an EPR of 1.21 and 0.45 respectively for cycle and plant. The double stage HDH in heat pump resulting a freshwater and cooling generations of 45.53 LPH and 40.55 kW, respectively, at an airflow rate of 1000 m^3/h and a hot water supply temperature of 50 °C. The same from the single stage HDH are 32.58 LPH and 34.31 kW. It shows that the double stage HDH polygeneration results higher outputs compared to the single stage HDH polygeneration with the penalty in EPR.

T. Srinivas, *Thermal Polygeneration*,
https://doi.org/10.1007/978-3-031-37886-7_9

9.1 Introduction

According to the literature survey, it has been observed that the results related to heat pump integration with multiple generation and two-stage HDH desalination are limited. This chapter is focused on maximising the energy efficiency of the heat pump polygeneration by optimising the evaporator temperature. The unique features of the plant are: (i) the arrangement of all the two-stage HDH components in a vertical tower; (ii) easy flow of the fluids in the duct; and (iii) minimum floor space for the plant's erection. The process design has the advantage of allowing technology to be commercialised in both the residential and industrial sectors. The effects of evaporator temperature, hot water supply temperature, atmospheric air temperature, and atmospheric air relative humidity on freshwater production, cooling capacity, EPR, and cycle and plant exergy efficiency are studied.

9.2 Heat Pump Polygeneration with Single Stage HDH

9.2.1 Plant layout and description

Fig. 9.1 depicts the plant layout of HDH-VCR to generate the potable water and cooling effect for A/C. It is designed to operate in off-grid mode, i.e. without depending on grid connection. The plant is powered by both high-grade energy (electrical power) and low-grade energy (heat). Pump and SWH supply hot water for the air preheater (APH), humidifier and air reheater. The process components are depicted in Fig. 9.1, the process conditions are depicted on the psychrometric chart (Fig. 9.2), and the same properties at the states are tabulated in Table 9.1.

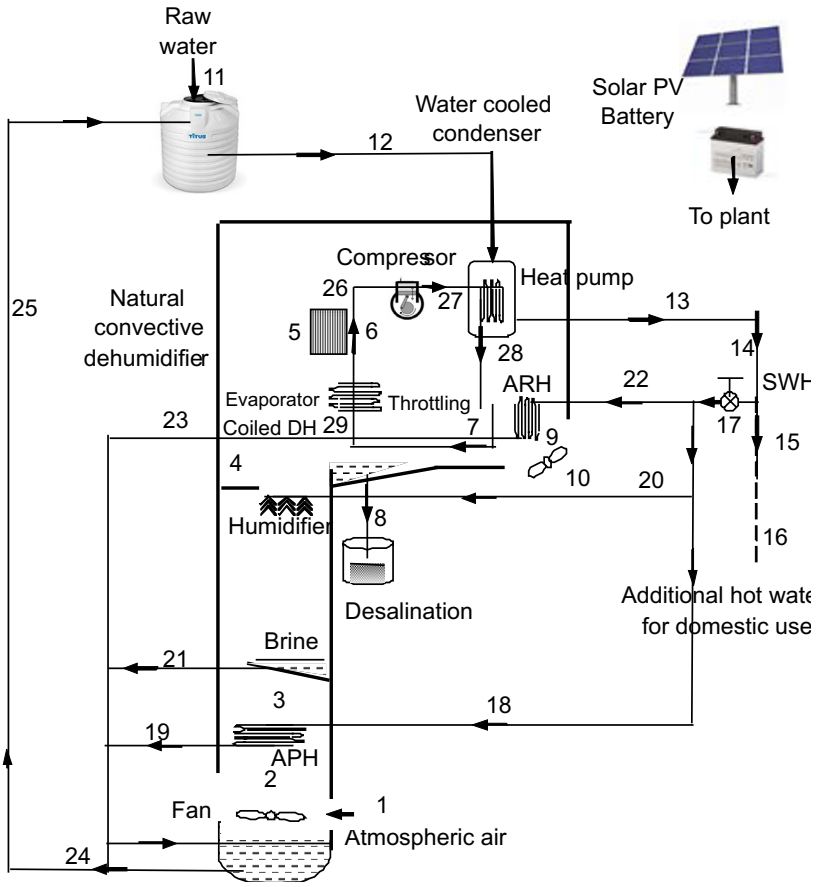

Fig. 9.1: Solar PV/T HDH-VCR cycle with heat pump/refrigerator operation

Atmospheric air (1) enters into the plant with a fan. Next to the fan, the temperature of the air increases in the APH (2–3). On the psychrometric chart, air preheating has been shown as a sensible heating process, i.e., a horizontal line. The relative humidity (Ø) of air in APH decreases and gives more scope for evaporation in the humidifier. The humidifier sprays hot saline water against the preheated air stream at the top of the packing. The air undergoes a heating and humidification process (3–4). Later, the air flows over the cooling surface of the natural convection and evaporator's coil for dehumidification (5-6). The surface exposed to the environment rejects the heat from the humid air and shares the evaporator load. The final dehumidification (6-7) happens at the evaporator section of the VCR heat pump unit. The VCR consists of a vapour compressor (26-27), a water-cooled condenser (27-28), throttling (28-29), and an evaporator (29-26). The water-cooled condenser is used to raise the saline water temperature, and the evaporator is used for the dehumidification

of air. The condensate from the dehumidification processes is collected in a container (8). The air reheater (7-9) increases the air temperature and decreases the relative humidity to suit the space conditioning. The saline water is heated by a heat pump and SWH. This heated saline water is supplied to APH (18), the humidifier (20), and ARH (22).

Table 9.1: Properties of heat pump polygeneration with single stage HDH at 50 °C of hot water and 1000 m³/h of air flowrate (Fig. 9.1 can be referred for the states)

State	m, kg/h	P, bar	T, °C	Ø, %	ω, g/kg	h, kJ/kg	s, kJ/kg K	ε, kJ/kg
1	1293.30	1.01	28.00	75.00	17.95	73.98	0.26	-0.26
2	1293.30	1.60	31.00	99.95	17.95	77.09	0.27	-0.53
3	1293.30	1.58	42.40	53.08	17.95	88.93	0.31	-0.07
4	1311.17	1.57	45.44	78.32	32.01	128.41	0.44	0.22
5	1311.17	1.57	45.44	78.32	32.01	128.41	0.44	0.22
6	1310.92	1.54	44.44	80.35	31.82	126.85	0.44	0.20
7	1278.59	1.52	13.47	100.00	6.37	29.63	0.11	0.77
8	32.58	1.01	13.47	-	-	56.29	-0.16	0.96
9	1278.59	1.51	20.00	65.37	6.37	36.27	0.13	0.58
10	1278.59	1.01	20.00	50.00	7.28	38.58	0.14	0.53
11	4517.21	1.01	25.00	-	-	104.50	0.00	0.00
12	6472.17	1.01	30.00	-	-	125.40	0.07	0.17
13	6472.17	1.01	35.41	-	-	148.00	0.14	0.74
14	6472.17	1.01	50.00	-	-	209.00	0.34	4.15
15	4499.35	1.01	50.00	-	-	209.00	0.34	4.15
16	4499.35	1.01	28.00	-	-	117.04	0.04	0.06
17	1972.82	1.01	50.00	-	-	209.00	0.34	4.15
18	449.89	1.01	50.00	-	-	209.00	0.34	4.15
19	449.89	1.01	42.00	-	-	175.56	0.23	1.95
20	1270.49	1.01	50.00	-	-	209.00	0.34	4.15
21	1252.63	1.01	41.13	-	-	171.93	0.22	1.76
22	252.44	1.01	50.00	-	-	209.00	0.34	4.15
23	252.44	1.01	42.00	-	-	175.56	0.23	1.95
24	1954.95	1.01	41.44	-	-	173.24	0.22	1.83
25	1954.95	1.01	41.55	-	-	173.69	0.23	1.85
26	841.46	3.88	8.00	-	-	403.20	1.72	-110.51
27	841.46	10.17	49.45	-	-	430.25	1.75	-90.06
28	841.46	10.17	40.00	-	-	256.41	1.19	-98.54
29	841.46	3.88	8.00	-	-	256.41	1.20	-101.63

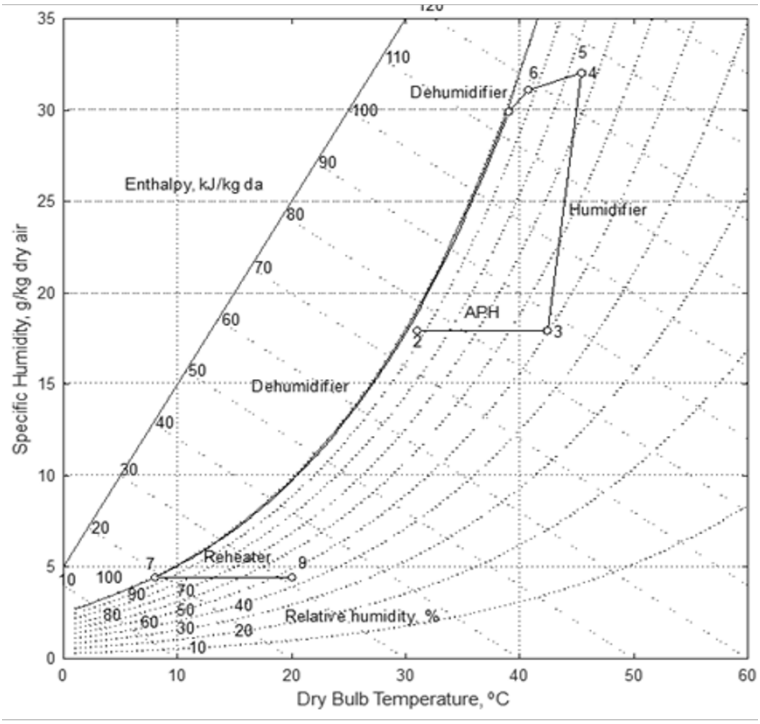

Fig. 9.2: HDH-VCR cycle on psychrometric chart

The packing placed in the humidifier increases the wetting surface and evaporation. The humid air moves upwards and the brine solution at the bottom of the humidifier. The brine from the humidifier recycles in the SWH by periodically changing or maintaining the SWH. In dehumidification, the humid air is cooled to condense the moisture in the humid air. The heat load in the heat pump (water cooled condenser) is greater than the HDH heat load (sum of APR, humidifier and ARH). If the whole water is recirculated in the circuit, the temperature of water in the plant continuously increases. The additional saline water supplied to the storage tank keeps the operating temperature of water in the water cooled condenser at the required limit. The additional hot water is designed for domestic use (15-16). The circulating water has been pumped (24-25) to the storage tank which is kept at an elevated level. The hot water has been collected (17) to the HDH unit with gravity assistance.

9.2.2 Thermodynamic formulation of the HDH-VCR plant

The thermodynamic model has been detailed for the HDH-VCR cycle with the following assumptions: The airflow rate in the duct is assumed to be 1000 m^3/h. The relative humidity of the supply air to the plant is 75%. The average relative humidity at the location (Jalandhar, India) is 75%. The air preheater at

the beginning of the HDH unit decreases the relative humidity of the supply air. Therefore, there are no process difficulties during the dehumidification process. The air temperature at the APH inlet is 28 °C. The saline water inlet temperature in a humidifier is 50 °C. The mass ratio of water to air in the humidifier is 1 (Dehghani et al., 2018). The chilled coil exit temperature in the VCR is -2 °C. In the refrigeration plant, R134a has been selected as the working fluid. The VCR's condenser phase change temperature is 40 °C. In the refrigeration plant, the vapour compressor's isentropic efficiency is set at 75%. The air reheater's exit temperature is 20 °C. Low-grade energy (heat) and high-grade energy (electricity) constitute the function of energy. Therefore, an equivalent weight factor for high-grade energy (ye) has been assigned as 3. That means the electricity is three times more valuable than the thermal cost. In other words, three units of thermal energy are required to generate one unit of electricity. The equivalent thermal efficiency at this weight factor is equal to 1/3 = 0.33% (Tangellapalli, 2021).

The average solar radiation at Jalandhar, India has been considered for the study. The equinox position will come in the months of March and September in a given year. The month of March has been selected to determine the average solar radiation. The average global component of solar radiation is 520 W/m^2. The SWH is a flat plate collector. The size of the collector has been simulated from the average solar radiation, fluid flow rate, inlet temperature, and exit temperature of the fluid. The sizing of the solar PV plant is done at an assumed energy conversion efficiency of 15%. The study and analysis of solar thermal collectors, PV plants, and storage are not the objectives of the current work.

The air exit temperature from the APH is determined from its effectiveness

$$T_{a,\,e} = T_{a,\,i} + \varepsilon_{APH}\,(T_{cond,\,i} - T_{a,\,i}) \tag{9.1}$$

The hot water inlet and outlet temperatures for APH have been fixed to find its flow rate. The energy balance equation in the APH results in the hot water flowrate at the known air flow rate, which is fixed as per the assumptions.

Hot water demand in APH,

$$m_{APH,w} = \frac{m_{da}(h_{a,\,e} - h_{a,\,i})}{c_{p,hw}(T_{hw,\,i} - T_{hw,\,e})} \tag{9.2}$$

The amount of brine solution collected at the bottom of the humidifier is less than the hot water supply due to the air humidification. Based on the liquid to air mass ratio in the humidifier, the hot water spray has been determined at a fixed air flow rate.

Let, the m_r liquid to air mass ratio in humidifier

The mass of hot water supplied to the humidifier,

$$m_{hw} = m_r\, m_a \tag{9.3}$$

where $m_r = \frac{m_{hw}}{m_a}$

Mass of water at the exit of humidifier,

$$m_{hw,e} = m_{hw,\,i} - m_{da}(\omega_e - \omega_i) \tag{9.4}$$

The air exit condition from the humidifier is simulated based on the hot water supply temperature. The heating and humidification process on the psychrometric chart moves towards the hot water temperature with the maximum limit of humidification, i.e. 100% RH.

The temperature of hot water at the exit of humidifier,

$$= \tag{9.5}$$

The mass of air at the exit of humidifier after picking the moisture,

$$m_{a,\,e} = m_{a,\,i} + m_{da}\,(\omega_e - \omega_i) \tag{9.6}$$

Similarly, the cooling and dehumidification processes in a dehumidifier follow the cold body temperature with a maximum limit of 100% RH.

The supply temperature of water to the heat pump should be low enough to reject the heat to the water at a safe limit. To ensure proper heat dissipation, the amount of water to be mixed in the supply tank needs to be determined. The return HDH water is mixed with the normal raw water to control the supply temperature to the heat pump.

The mass balance of the mixing of these fluids,

$$\mathrm{m_{12}} = \mathrm{m_{11}} + \mathrm{m_{25}} \tag{9.7}$$

The energy balance of the mixing of these fluids,

$$\mathrm{m_{12}\,T_{12}} = \mathrm{m_{11}\,T_{11}} + \mathrm{m_{25}\,T_{25}} \tag{9.8}$$

$$(\mathrm{m_{11}} + \mathrm{m_{25}})\,\mathrm{T_{12}} = \mathrm{m_{11}\,T_{11}} + \mathrm{m_{25}\,T_{25}}$$

After the simplification of this equation,

$$m_{11} = \frac{m_{25}(T_{25} - T_{12})}{(T_{12} - T_{11})} \tag{9.9}$$

The electrical power supply to the cycle/plant is

$$W_{es} = W_{fans} + W_p + W_r \tag{9.10}$$

$\mathrm{W_{fans}}$ in Eq. 9.10 include the electricity supply to the suction fan at the inlet and the forced fan for air delivery.

The cycle EPR,

$$EPR_c = \frac{m_{fw}h_{fg} + Q_c + m_{hw}Q_{hw}}{Q_{SWH} + y_e W_{es}} \tag{9.11}$$

The plant EPR,

$$EPR_{pt} = \frac{m_{fw}h_{fg} + Q_c + m_{hw}Q_{hw}}{0.001GA_{SWH+PV}} \quad (9.12)$$

where A_{SWH+PV} is the total solar collecting area for electricity and hot water generation.

Thermodynamic models have been developed for the HDH-VCR plant using MATLAB programming. Subroutines are prepared to generate the psychometric properties and refrigerant (R134a) properties that are used in plant modelling and simulation.

9.2.3 Performance characteristics of heat pump polygeneration with single stage HDH

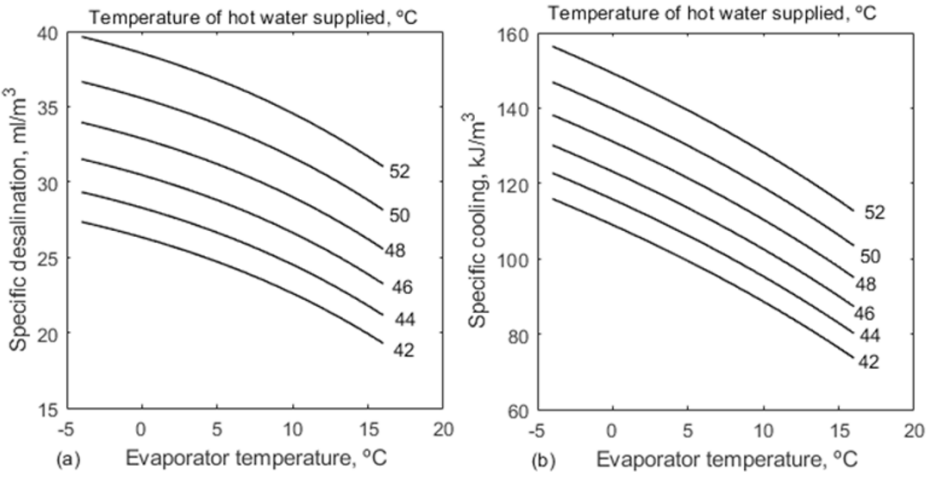

Fig. 9.3: Effect of evaporator temperature and hot water supply temperature to single stage HDH on specific water production and specific cooling of heat pump polygeneration

Fig. 9.3 analyses the effect of evaporator temperature with hot water supply temperature to single stage HDH on specific output of freshwater and specific cooling capacity of heat pump polygeneration operating on HDH-VCR cycle. The evaporator temperature is the refrigerant temperature in the heat exchanger coil. This temperature results the air exit temperature from the final dehumidifier. The increase in evaporator temperature limits the condensation of air in the dehumidifier. Therefore, freshwater production is decreasing with an increase in evaporator temperature. At the designed room temperature, the cooling capacity decreases with an increase in evaporator temperature as it is approaching the design temperature.

The hot water temperature is the hot saline water supply temperature to the HDH plant. The temperature of the saline water is increased first in the

water-cooled condenser of the VCR unit and later in the solar water heater. It is possible to generate the required water temperature with the use of a solar water heater with a water-cooled condenser. The water exit temperature has a limit to ensure heat rejection from the refrigerant. The increase in water temperature results in the heating and humidification of air in the humidifier. This evaporation process is enhanced by an increase in temperature. Therefore, the specific freshwater production at the dehumidifier is increasing with an increase in hot water temperature. But the cooling load in the VCR's evaporator increases with an increase in hot water temperature as the air temperature also increases in the vertical duct. Therefore, the specific cooling capacity increases with an increase in water temperature. The airflow rate is fixed at 1000 m^3/h. The specific results of freshwater and cooling can be expressed independent of airflow so that these results can be converted into total output by multiplying the actual air flowrate. For example, if the specific water production is 35 ml/m3 of air, then the total freshwater production is 35 LPH at 1000 m^3/h of air. The increase in evaporator temperature, which is connected to the final dehumidifier, strongly affects freshwater production and cooling size. The air exit temperature increases with an increase in evaporator temperature from the dehumidifier. Hence, it suppresses the condensation rate, resulting in a drop in specific desalination and total freshwater. Finally, the freshwater and cooling capacity decrease with an increase in evaporator temperature and increase with an increase in water temperature.

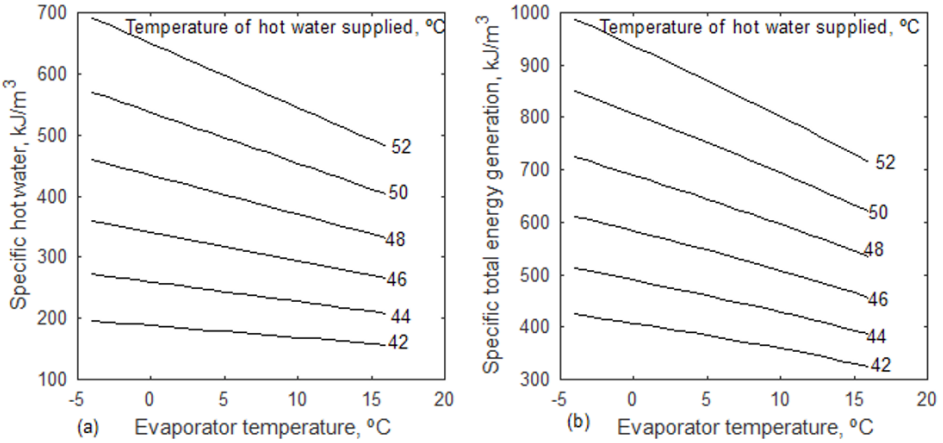

Fig. 9.4: Effect of evaporator temperature and hot water supply temperature to single stage HDH on specific energy of hot water production and total specific energy of heat pump polygeneration

In addition to the freshwater and cooling, the heat pump polygeneration also results in electricity and hot water for use. The electricity is generated as

per the predesigned sizing of the solar PV plant. Fig. 9.4 shows the effect of evaporator temperature on the hot water supply temperature for HDH on hot water energy and total energy developed by the heat pump polygeneration. The increase in the evaporator temperature suppresses the hot water flow in the plant due to the increased temperature difference in the heat pump. The decrease in the hot water flow in the system decreases the amount of hot water energy available for domestic use. The results show that the hot water energy decreases with an increase in evaporator temperature and increases with an increase in hot water supply temperature (Fig. 9.4a). The hot water energy depends on the hot water exit temperature from the HDH plant and its flow rate. The specific hot water energy is increasing with an increase in the hot water supply temperature. Not only the hot water energy, but the other outputs such as freshwater and cooling demand also increase with an increase in the hot water supply temperature as per the earlier section's discussion. Therefore, the total energy output from the heat pump polygeneration also increases with an increase in the hot water supply temperature (Fig. 9.4b). All the outputs are decreasing with an increase in the evaporator temperature. Hence, the total energy generation from the polygeneration decreases with an increase in the evaporator temperature.

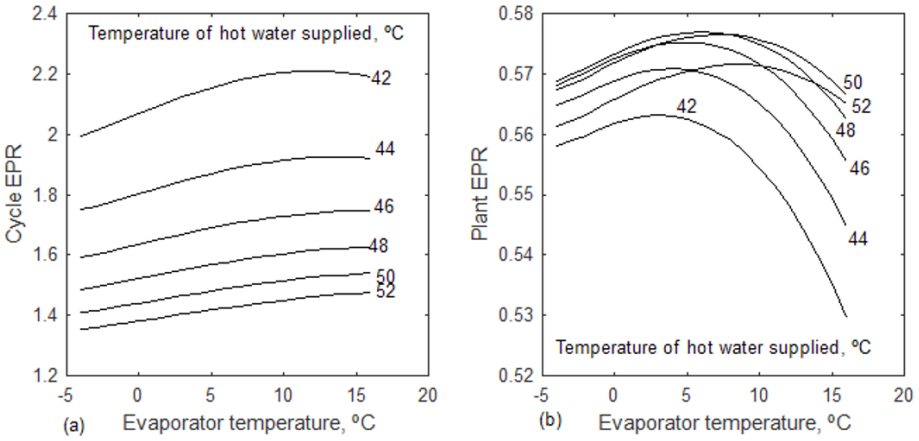

Fig. 9.5: Analysis of EPR of cycle and polygeneration plant with evaporator temperature and hot water supply temperature to single stage HDH

The energy efficiency of the combined unit is defined as EPR as it uses both high-grade and low-grade energy to drive the plant. Fig. 9.5 shows changes in EPR with changes in evaporator temperature and hot water temperature. The outputs, such as freshwater, cooling capacity, and hot water generation, increase with an increase in hot water supply temperature. The rise in hot water

temperatures raises the operating power as the capacity rises. The increased operating power with the increase in water supply temperature demands large-sized solar collectors. The increased input decreases the EPR with an increase in the hot water supply temperature as shown. Evaporator temperature plays a different role in the desalination system and cooling system. The increase in evaporator temperature increases the coefficient of performance (COP) of the heat pump but decreases the desalination rate. The output decreases with an increase in evaporator temperature, and it also decreases the energy supply to the cycle and plant. Therefore, the combined effect of evaporator temperature results in an optimum evaporator temperature to maximise the EPR. The optimum evaporator temperature is increasing with an increase in hot water temperature. Therefore, it has been recommended to select a higher evaporator temperature when the water temperature is high. The comparison of the optimum evaporator temperature for maximum cycle EPR and maximum plant EPR shows that the optimum evaporator temperature for maximum plant EPR is greater than the optimum evaporator temperature for maximum cycle EPR.

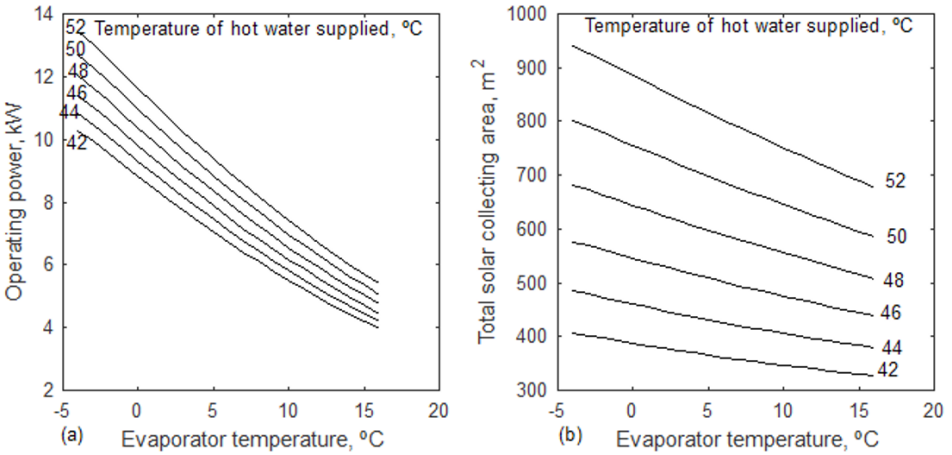

Fig. 9.6: Analysis of evaporator temperature and circulating water supply temperature on operating power and total solar collector's area

Fig. 9.6 shows the effect of evaporator temperature and hot water supply temperature on HDH's operating power and total solar collector area. The collector area includes the flat plate collector for water heating and the solar photovoltaic panel for electricity generation. The increase in hot water supply temperature increases the electricity demand to operate the heat pump polygeneration plant. The vapour compressor supply is the plant's primary source of electricity. The cooling capacity is increasing with an increase in

the water supply temperature. Therefore, the operating power also increases with an increase in the hot water supply temperature. Since the flat plate collector is used for hot water and electricity by the solar PV plant, the total solar collector area is increasing with an increase in water supply temperature. The increase in evaporator temperature decreases the cooling demand. Hence, the operating power to drive the polygeneration is decreasing with an increase in evaporator temperature. The solar collector's area also decreases with an increase in evaporator temperature. Based on this analysis of the operating power required to drive the polygeneration, the capacity of the solar PV plant is fixed at 14 kW.

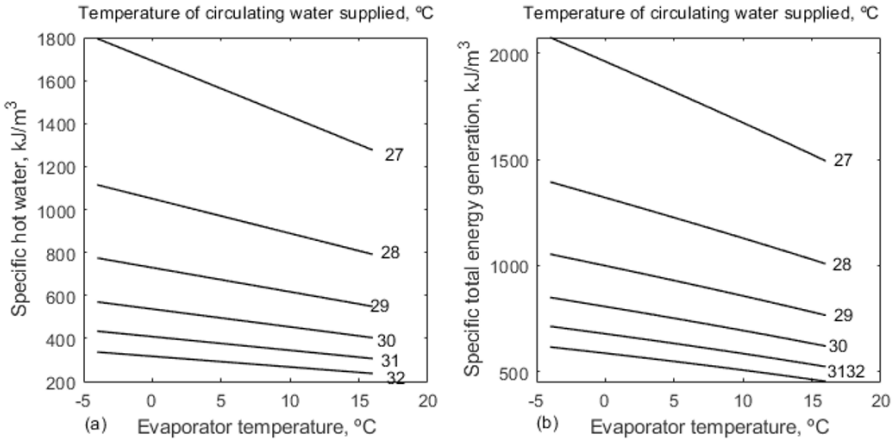

Fig. 9.7: Effect of evaporator temperature and circulating water supply temperature on specific energy of hot water and total specific energy generated by the heat pump polygeneration

The circulating water supply temperature is referred to as the supply temperature of the heat pump. Fig. 9.7 studies the effect of evaporator temperature on the water supply temperature on the heat pump's water-cooled condenser. The water supply temperature to the heat pump is not connected to the operation of the HDH plant as its supply temperature is fixed as per the SWH operation. Therefore, the changes in freshwater production and cooling demand with the water supply temperature to the heat pump are not directed. But the available hot water for domestic use decreases with an increase in the water supply temperature. If more water is supplied as makeup at the storage tank, the resultant water supply temperature decreases at the inlet of the heat pump. But at the higher supply temperature, the heat pump suppresses the makeup water and hence the drop in available hot water for domestic use. It also suppresses the specific total energy output from the polygeneration.

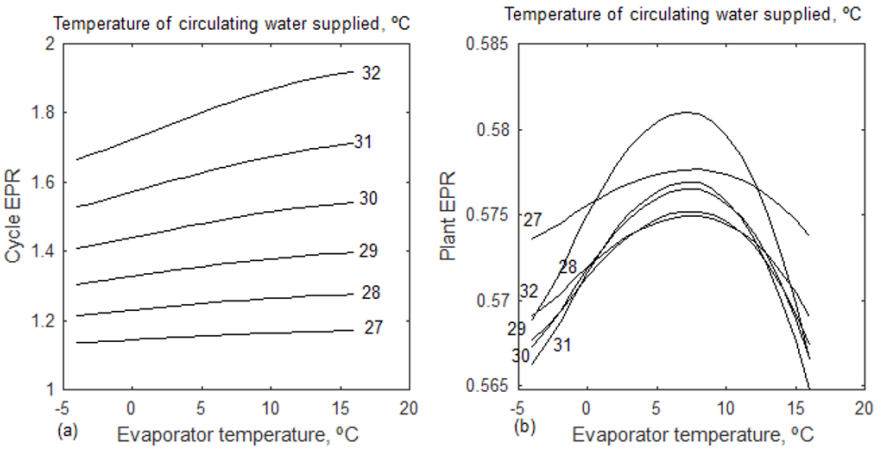

Fig. 9.8: Effect of evaporator temperature and circulating water supply temperature on polygeneration cycle EPR and polygeneration plant EPR

Fig. 9.8 shows the effect of evaporator temperature on the water supply temperature to the heat pump on cycle EPR and plant EPR. The analysis results in an optimum evaporator temperature with water supply temperature to the heat pump to maximise the EPR of the cycle and plant. The optimum evaporator temperature for maximum cycle EPR is greater than the optimum evaporator temperature for maximum plant EPR. The increased polygeneration capacity with an increase in evaporator temperature increases the solar collector's area, which effects the plant's EPR. Therefore, a lower optimum evaporator temperature is recommended to gain a higher plant EPR compared to the cycle EPR.

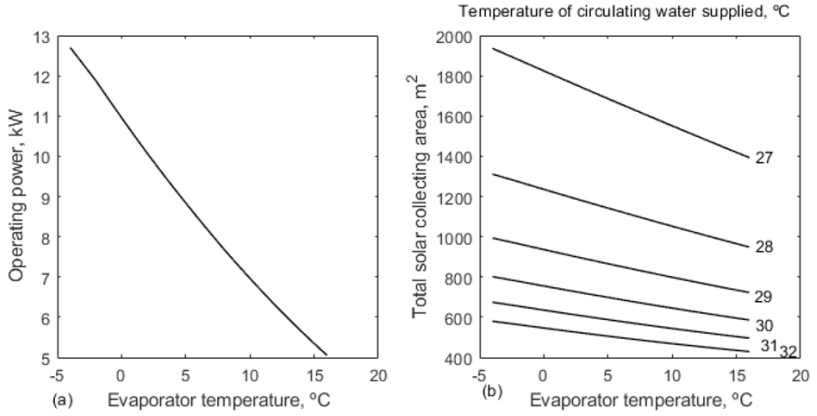

Fig. 9.9: Effect of evaporator temperature and circulating water supply temperature on operating power and area of solar collectors

Fig. 9.9 shows the effect of evaporator temperature and the circulating water supply temperature to the heat pump on the operating power of the polygeneration and solar collector area. The heat pump water supply temperature is not influencing the freshwater production and cooling capacity. Therefore, the operating power of the polygeneration does not change with the change in water supply temperature to the heat pump.

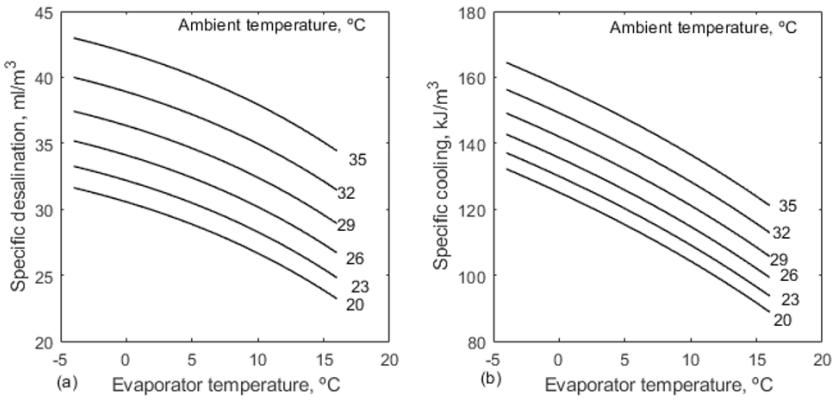

Fig. 9.10: Role of evaporator temperature and ambient temperature on specific freshwater production and specific cooling generation

Fig. 9.10 analyses the evaporator temperature with ambient air temperature on specific freshwater production and specific cooling capacity of the polygeneration plant. The air temperature plays a role in the humidification process. The changes in the humidity due to air temperature variations effect the dehumidification and cooling process. The hot air enhances the humidification process, which results in more condensation during the dehumidification. The results are favouring hot air compared to cold air for satisfactory freshwater production, of course, with the increased cooling capacity. Since the increased cooling capacity has been well justified with the improvement in the EPR (shown in the next section), the hot air has been recommended for the better outcome of the polygeneration.

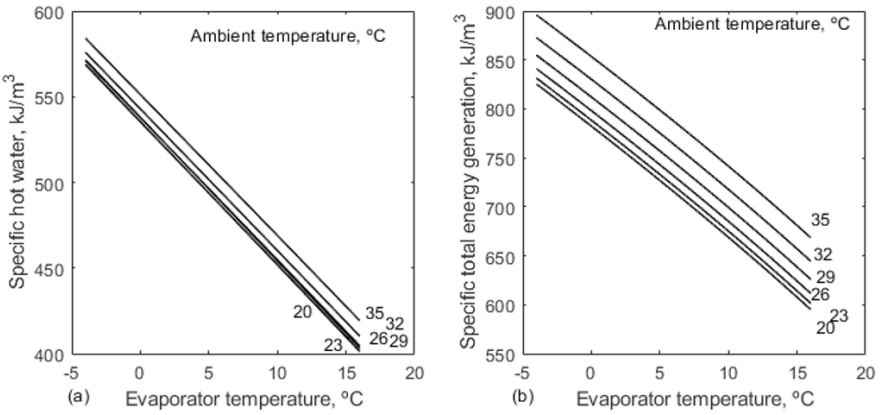

Fig. 9.11: Effect of evaporator temperature and ambient temperature on specific energy of hot water and specific total energy generation from polygeneration

Fig. 9.11 shows the effect of evaporator temperature and the ambient air temperature on the specific energy of hot water generated for domestic use and the total specific energy generated by the polygeneration. The increase in ambient air temperature increases the freshwater production, cooling unit size, and hot water used for the purpose. Therefore, the total specific energy output from the polygeneration also increases with the increase in the ambient air temperature.

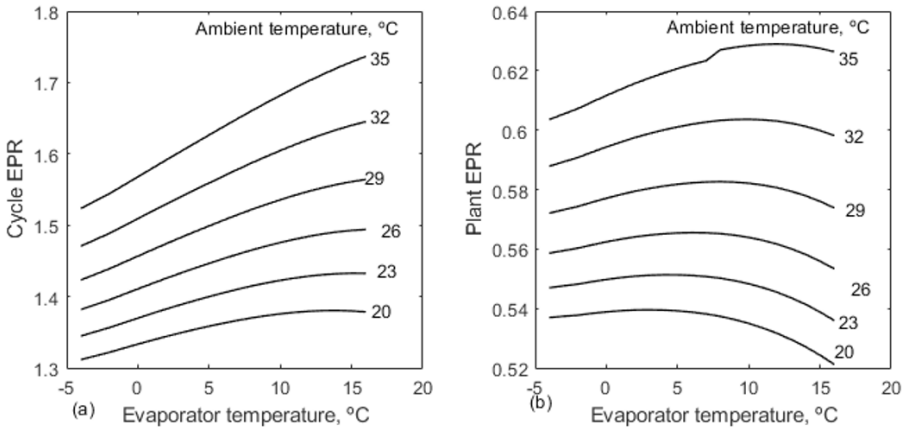

Fig. 9.12: Effect of evaporator temperature and ambient temperature on polygeneration cycle's EPR and polygeneration plant's EPR

Fig. 9.12 shows the role of evaporator temperature in relation to the atmospheric air temperature on cycle EPR and plant EPR. Desalination and cooling are increasing with the increase in atmospheric air temperature at an increasing rate. Therefore, the EPR also increases with an increase in atmospheric air temperature at an increasing rate. The increment in EPR is greater at the higher evaporator temperature. Due to a clash between output and energy supply, the evaporator temperature is optimised for maximum EPR. The optimum evaporator temperature is increasing with an increase in atmospheric air temperature. The evaporator temperature and the atmospheric air temperature are linked to the dehumidification process. A higher atmospheric temperature demands a higher evaporator temperature for effective cooling in the evaporator. The optimum evaporator temperature is increasing with an increase in atmospheric air temperature.

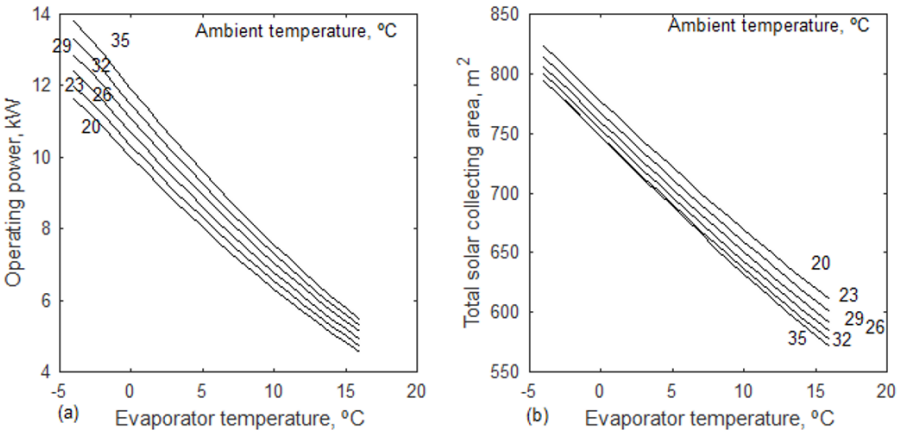

Fig. 9.13: Changes in supply electricity to polygeneration plant and total solar collector's area with evaporator temperature and ambient temperature

Fig. 9.13 studies the effect of evaporator temperature and the ambient air temperature on the electrical power required to operate the polygeneration plant and the required total solar collecting area for the thermal and PV units. Since the capacity of the polygeneration is increasing with an increase in ambient air temperature, the plant needs more power to operate it at the hot air supply.

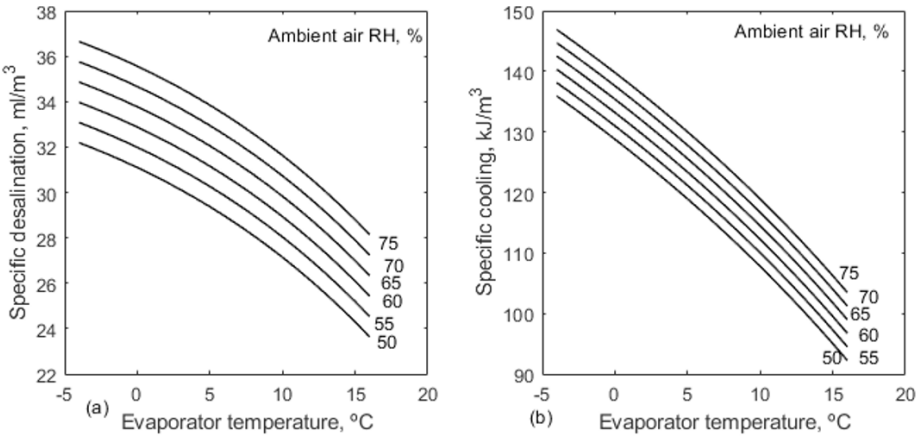

Fig. 9.14: Role of evaporator and ambient air's RH on specific freshwater production and specific cooling generation

Fig. 9.14 depicts the role of evaporator temperature and atmospheric air relative humidity in specific freshwater production and specific cooling capacity of the plant. The humid atmosphere results in more desalination. It condenses more water in the dehumidifier. Therefore, desalination is increasing with an increase in air relative humidity. The latent heat load of air increases with an increase in relative humidity. As shown, the cooling load on the dehumidifier increases with an increase in relative humidity. On the other hand, since the EPR is improving with the hot air, the solar collector's area is decreasing with an increase in the air temperature.

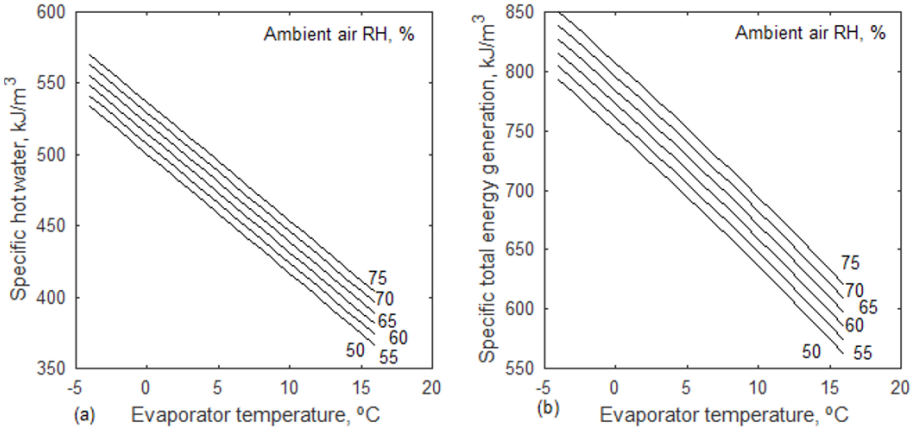

Fig. 9.15: Effect of evaporator temperature and ambient air's RH on specific energy of hot water production and total specific energy generation of polygeneration

After the ambient air temperature, the relative humidity of the ambient air also plays a role in the performance of the polygeneration. Fig. 9.15 highlights the effect of evaporator temperature and the ambient air's RH on specific hot water generation and total specific energy generated from the polygeneration plant. In the simulation, the exit conditions of the polygeneration subsystems are fixed by the constraints. Therefore, the freshwater production and cooling demand with the ambient air's RH have not been addressed due to fixation with the changes in ambient conditions (temperature and RH). However, energy changes in polygeneration utilisation differ from changes in ambient conditions. It also effects polygeneration performance. The humid air favours this by increasing the hot water generation for domestic use and also improving the EPR. Therefore, the total specific energy production by the polygeneration plant increases with an increase in the relative humidity of ambient air.

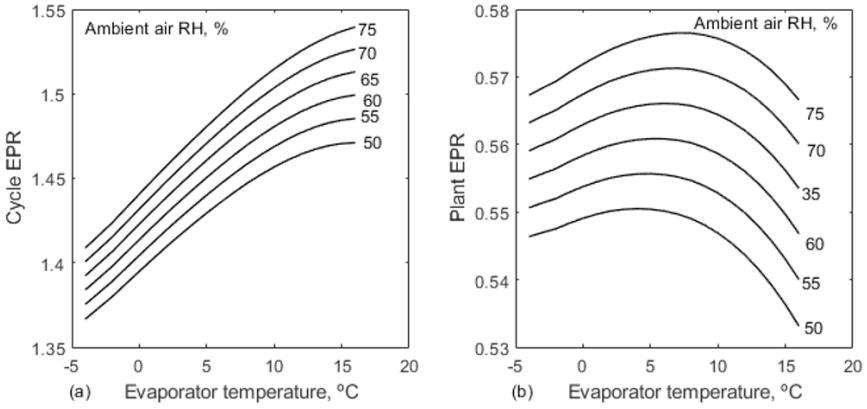

Fig. 9.16: Effect of evaporator temperature and ambient air's RH on polygeneration cycle's EPR and polygeneration plant's EPR

Fig. 9.16 shows the effect of evaporator temperature and the ambient air's RH on cycle EPR and plant EPR. The humid air is generating more energy from the polygeneration plant. Therefore, the EPR of the cycle and plant is increasing with an increase in the RH of ambient air. The optimum evaporator temperature is increasing with an increase in the RH of the ambient air.

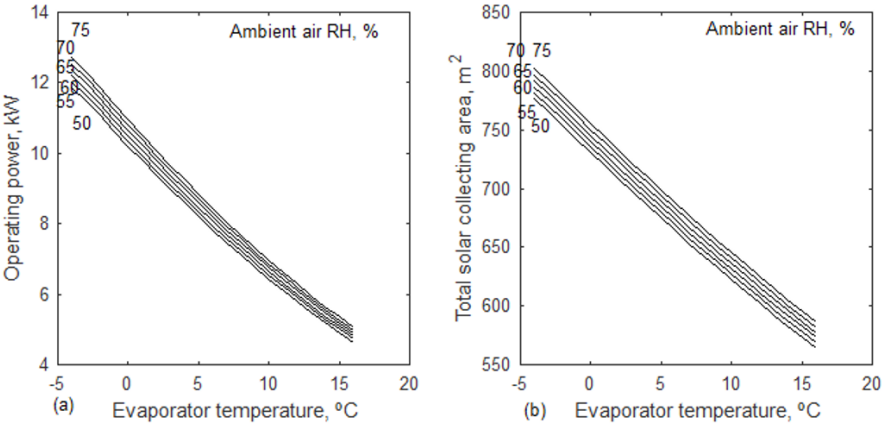

Fig. 9.17: Effect of evaporator temperature and ambient air's RH on plant's electricity supply and solar collector's area

Fig. 9.17 trends the effect of evaporator temperature with the ambient air's RH on the required electrical power to operate the polygeneration plant and the total area of solar thermal collectors and solar PV units. As the relative humidity of the ambient air rises, so does the demand for electricity. The required electricity to operate the polygeneration includes the vapour compressor, hot water pump, circulating water pump, and fans. Since the electrical load of the polygeneration plant is increasing with an increase in the RH, the solar collector's area also increases with the RH.

Table 9.2: Specifications of heat pump polygeneration with single stage HDH at 1000 m^3/h of air and hot water temperature of 50 °C

S. No.	Description	Result
1.	Specific freshwater production, ml/m^3 air	32.58
2.	Total freshwater, LPH	32.58
3.	Specific cooling capacity, kJ/m^3	123.52
4.	Total cooling capacity, kW	34.31
5.	Hot water for domestic use, LPH	1972.80
6.	Energy of hot water for domestic use, kW	130.60
7.	Capacity of fan, kW	1.10
8.	Capacity of hot water pump, kW	0.25
9.	Capacity of vapour compressor, kW	6.32
10.	Total electricity used, kW	7.68
11.	Heat supplied to cycle through SWH, kW	109.66
12.	Area of solar PV plant, m^2	278.41
13.	Area of solar water heater, m^2	387.71

14.	Total solar collecting area, m^2	666.11
15.	Total energy production, kW	199.00
16.	HDH-VCR cycle EPR	1.55
17.	HDH-VCR plant EPR	0.57

Table 9.2 summarises the specifications of the heat pump polygeneration with single stage HDH at an airflow rate of 1000 m^3/h and 50 °C of hot water supply. The specific freshwater productivity and specific cooling capacity are 35 m^3/h and 123.52 kJ/m^3, respectively. At these conditions, the total water production and cooling are 1972.80 LPH and 34.31 kW, respectively. The polygeneration working on the HDH-VCR cycle also generates hot water from the water-cooled condenser and SWH as an additional outcome, in addition to the freshwater and cooling. The hot water used for domestic use (in residential complexes) excluding the HDH processes is 1972 LPH. The energy content of this hot water output is 130.60 kW. At these conditions, the area of the solar PV plant and SWH is 278.41 m^2 and 387.71 m^2, respectively. The operating power includes the electricity supply to the fan, pumps, and vapour compressor, which includes 7.68 kW. The EPR is determined by the four outputs viz. electricity (fixed solar PV capacity), freshwater, cooling, and hot water. The cycle and plant EPR are 1.55 and 0.57, respectively.

9.3 Heat Pump Polygeneration with Double Stage HDH

9.3.1 Plant layout and description

Fig. 9.18 depicts the plant layout of the double stage HDH-VCR for freshwater, cooling and hot water generation. It is designed to operate in an off-grid mode, i.e. without grid power. High-grade energy (parasitic power) and low-grade energy (heat) are used to power the plant.

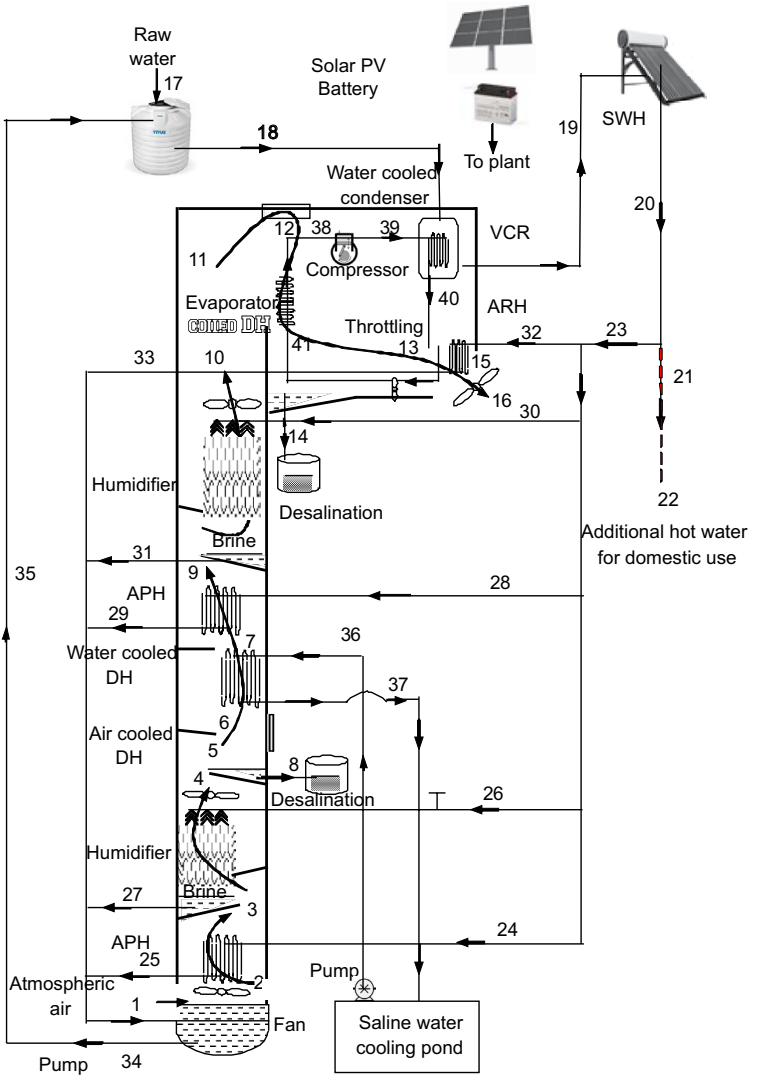

Fig. 9.18: Double stage HDH-VCR plant

The plant components are a fan, air preheater (APH), humidifier, dehumidifier, air reheater (ARH), solar photovoltaic (PV) power plant, solar water heater (SWH), VCR based heat pump and water circulation pumps. The solar PV power plant supplies power to the fan, vapour compressor and pumps. Water cooling condensers (heat pumps) and SWH provide hot water to humidifiers, air preheaters, and air preheating systems. The HDH-VCR cycle process conditions are plotted on the psychrometric chart (Fig. 9.19) and the same properties as the states shown in Fig. 9.18 are tabulated in Table 9.3. The

atmospheric air enters into the plant through a circulating fan. Later, the air temperature is increased in the APH. The hot water from the heat pump and SWH is used in APH to increase the temperature of the air. The preheating of air before humidification increases the humidification capacity in the subsequent process. On the psychrometric chart, air preheating has been shown as a sensible heating process, i.e. a horizontal line. The relative humidity (Ø) of the air in APH decreases and allows more water evaporation in the humidifier.

The saline water is heated by a heat pump and a SWH. This saline water is sprayed on the top of the humidifier. A counter-flow current is developed when the humidifier receives the air from the bottom. The packing material in the humidifier increases the wetting surface and residence time to increase the saline water evaporation. The humid air collects at the top, and the brine water is at the bottom of the humidifier. The brine from the humidifier is recycled into the heat pump and the SWH. To avoid overheating of the heat pump, which is the VCR unit's water-cooled condenser, more saline water was supplied than was required in the HDH plant. The SWH is used to increase the hot water temperature from the heat pump to the required level. After supplying the hot water to the HDH plant, the remaining water is stored for domestic use. The humidified air after the humidifier is cooled by a dehumidifier to condense the water. In the first stage, a water-cooled dehumidifier is used to condense the humid air. The second-stage HDH unit uses the evaporator coil of the VCR unit to condense the air. During dehumidification, the condensate, i.e., freshwater, is collected at the bottom and removed into a container by gravity. Similar to the first stage of operation, the air is preheated in the second APH with hot water. The air temperature was raised to an ARH in the final operation to meet the required temperature and RH of the supply air. In this HDH-VCR unit, the cooling and heating functions of the heat pump are merged with HDH operations. Because the VCR's heating and cooling outputs are used by HDH, the cooling plant functions as both a heat pump and a refrigerator. The vertical arrangement of the humidifier and dehumidifier allows the counterflow of water and air.

Table 9.3: Properties of double stage HDH-VCR cycle with reference to Fig. 9.18

State	m, kg/h	P, bar	T, ºC	Ø, %	ω, g/kg	h, kJ/kg	s, kJ/kg K	ε, kJ/kg
1	1293.30	1.01	28.00	75.00	17.95	73.98	0.26	-0.26
2	1293.30	1.60	31.00	99.95	17.95	77.09	0.27	-0.53
3	1293.30	1.58	42.40	53.08	17.95	88.93	0.31	-0.07
4	1311.17	1.57	45.44	78.32	32.01	128.41	0.44	0.22
5	1311.17	1.57	45.44	78.32	32.01	128.41	0.44	0.22
6	1309.98	1.54	40.61	96.04	31.08	120.86	0.42	-0.05
7	1308.48	1.52	39.11	99.25	29.90	116.24	0.40	-0.15

8	2.68	1.01	39.11	0.00	0.00	163.48	0.19	1.35
9	1308.48	1.51	45.64	69.77	29.90	123.18	0.42	0.26
10	1321.79	1.49	47.39	84.00	40.38	152.12	0.52	0.99
11	1321.79	1.49	47.39	84.00	40.38	152.12	0.52	0.99
12	1320.34	1.46	43.64	97.09	39.23	145.11	0.50	0.70
13	1278.94	1.45	13.35	100.00	6.65	30.21	0.11	0.75
14	42.85	1.01	13.35	-	-	55.79	-0.17	0.98
15	1278.94	1.43	20.00	64.86	6.65	36.98	0.13	0.56
16	1278.94	1.43	20.00	50.00	5.11	33.08	0.12	0.84
17	8643.19	1.01	25.00	-	-	104.50	0.00	0.00
18	12123.57	1.01	30.00	-	-	125.40	0.07	0.17
19	8643.19	1.01	33.41	-	-	139.66	0.12	0.49
20	8643.19	1.01	50.00	-	-	209.00	0.34	4.15
21	5131.63	1.01	50.00	-	-	209.00	0.34	4.15
22	5131.63	1.01	28.00	-	-	117.04	0.04	0.06
23	3511.56	1.01	50.00	-	-	209.00	0.34	4.15
24	449.89	1.01	50.00	-	-	209.00	0.34	4.15
25	449.89	1.01	42.00	-	-	175.56	0.23	1.95
26	1270.49	1.01	50.00	-	-	209.00	0.34	4.15
27	1252.63	1.01	41.13	-	-	171.93	0.22	1.76
28	263.49	1.01	50.00	-	-	209.00	0.34	4.15
29	263.49	1.01	42.00	-	-	175.56	0.23	1.95
30	1270.49	1.01	50.00	-	-	209.00	0.34	4.15
31	1257.19	1.01	43.53	-	-	181.97	0.25	2.31
32	257.20	1.01	50.00	-	-	209.00	0.34	4.15
33	257.20	1.01	42.00	-	-	175.56	0.23	1.95
34	3480.39	1.01	42.24	-	-	176.57	0.23	2.01
35	3480.39	1.01	42.42	-	-	177.30	0.24	2.05
36	1044.04	1.01	38.85	-	-	162.38	0.19	1.30
37	1044.04	1.01	40.19	-	-	168.00	0.21	1.56
38	994.50	3.88	8.00	-	-	403.20	1.72	-110.51
39	994.50	10.17	49.45	-	-	430.25	1.75	-90.06
40	994.50	10.17	40.00	-	-	256.41	1.19	-98.54
41	994.50	3.88	8.00	-	-	256.41	1.20	-101.63

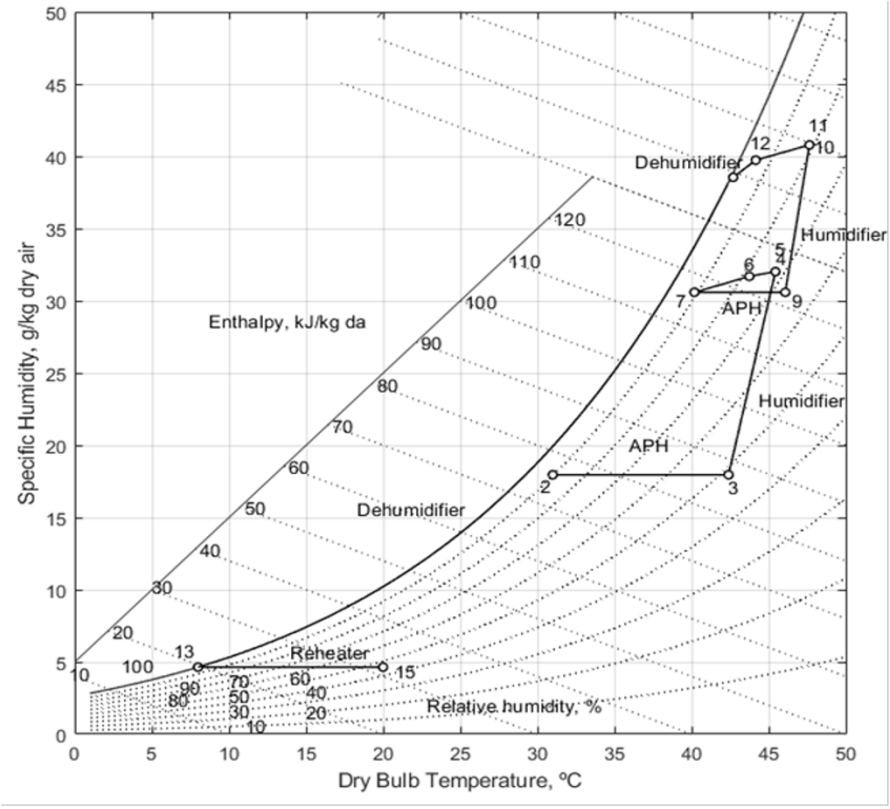

Fig. 9.19: Double stage HDH-VCR plant on psychrometric chart

9.3.2 Thermodynamic model of heat pump polygeneration with double stage HDH

A thermodynamic model has been detailed for the double stage HDH-VCR cycle with the following assumptions: The airflow rate in the duct is assumed to be 1000 m^3/h. The air around the plant has a relative humidity of about 75%, as the majority of the time, the average relative humidity at the considered location (Jalandhar, India) is nearly 75%. The air temperature at the APH inlet is 28 °C. The saline water inlet temperature in a humidifier is 50 °C. The mass ratio of water to air in the humidifier is 1 (Dehghani et al., 2018). The evaporator has a temperature of -2 °C. In the refrigeration plant, R134a has been selected as the working fluid. The VCR's condenser's phase change temperature is 40 °C. The refrigeration plant's vapour compressor has an isentropic efficiency of 75%. The air reheater (ARH) is used to maintain the conditioned air temperature of 20 °C. EPR is the function of low-grade energy (heat) and high-grade energy (electricity). Therefore, an equivalent weight factor for high-grade energy (y_e) is assigned to 3. As per the average power plant efficiency of 33.33%, electricity is three times more valuable

than the thermal cost of 33%. In other words, three units of thermal energy are required to generate one unit of electricity. The average solar radiation at Jalandhar, India has been considered for the study. The equinox position will come in the months of March and September in a given year. The month of March has been selected to determine the average solar radiation. The average global component of solar radiation is 520 W/m^2. The SWH is a flat plate collector. The size of the collector has been simulated based on the average solar radiation, fluid flow rate, inlet temperature, and exit temperature of the fluid. The sizing of the solar PV plant is done at an assumed energy conversion efficiency of 15%. The study and analysis of solar thermal collectors, PV plants, and storage are not the objectives of the current work.

The following are the formulations developed from the mass balance and energy balance of the components.

APH is a heat exchanger and it handles air and hot water. The air exit temperature from the APH is determined from its effectiveness

$$T_{a,\,e} = T_{a,\,i} + \varepsilon_{APH}\,(T_{cond,\,i} - T_{a,\,i}) \tag{9.15}$$

The brine water collected at the bottom of humidifier is less than the water supply at the top. This difference is equal to the water evaporation. Mass of water at the exit of humidifier,

$$m_{hw,e} = m_{hw,\,i} - m_{da}(\omega_e - \omega_i) \tag{9. 16}$$

As per the psychrometric conditions, the resulted process in the humidifier is heating and humidification. The temperature of hot water at the exit of humidifier,

$$T_{hw,\,e} = \frac{m_{hw,\,i}c_{p,hw}T_{hw,\,i} - m_{da}(h_{a,\,e} - h_{a,\,i})}{m_{hw,e}c_{p,hw}} \tag{9.17}$$

The mass of air at the exit of humidifier after picking the moisture,

$$m_{a,\,e} = m_{a,\,i} + m_{da}\,(\omega_e - \omega_i) \tag{9.18}$$

Circulating water has been used in the first stage of dehumidifier. The energy balance in the dehumidifier results the water requirement in the dehumidifier.

Circulating water in 1st dehumidifier,

$$m_{cw} = \frac{m_{da}(h_{a,\,i} - h_{a,\,e})}{c_{p,hw}(T_{cw,\,e} - T_{cw,\,i})} \tag{9.19}$$

The temperature difference of hot water in the APH is fixed. From the energy balance and the temperature difference of hot water, the hot water requirement in the APH can be determined.

Hot water demand in APH,

$$m_{APH,w} = \frac{m_{da}(h_{a,\,e} - h_{a,\,i})}{c_{p,hw}(T_{hw,\,i} - T_{hw,\,e})} \tag{9.20}$$

The electricity to drive the combined plant includes the supply of fan, pump and VCR's compressor.

The electrical supply to the cycle/plant is

$$W_{es} = W_{fans} + W_{p} + W_{r} \tag{9.21}$$

The outputs from the unit are three, viz., freshwater, cooling and hot water.

The cycle EPR,

$$EPR_{c} = \frac{m_{fw}h_{fg} + Q_{cg} + m_{hw}h_{hw}}{Q_{SWH} + y_{e}W_{es}} \tag{9.22}$$

The plant EPR,

$$EPR_{pt} = \frac{m_{fw}h_{fg} + Q_{cg} + m_{hw}h_{hw}}{0.001GA_{SWH+PV}} \tag{9.23}$$

where A_{SWH+PV} is the total solar collecting area for electricity and hot water generation.

9.3.3 Performance characteristics heat pump polygeneration with double stage HDH

Fig. 9.20 analyses the role of evaporator temperature and hot water supply temperature on the specific outcome of freshwater and cooling. Freshwater and cooling are strongly related to the evaporator's temperature. The increase in evaporator temperature suppresses the function of the final dehumidifier. It decreases the condensation rate of the water. Hence, the cooling capacity was decreased. The increase in hot water temperatures favours the humidification process. The increased humidification results in more desalination. But the increase in hot water temperature in the humidifier increases the cooling load as the temperature drop of air in the dehumidifier increases. Therefore, as per the analysis, the water productivity and cooling productivity decrease with an increase in evaporator temperature and increase with an increase in hot water supply temperature.

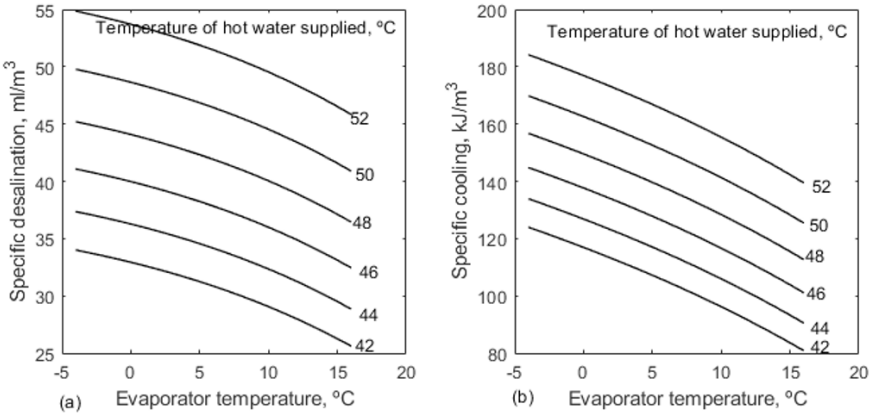

Fig. 9.20: Effect of evaporator temperature with hot water supply temperature on specific desalination and specific cooling

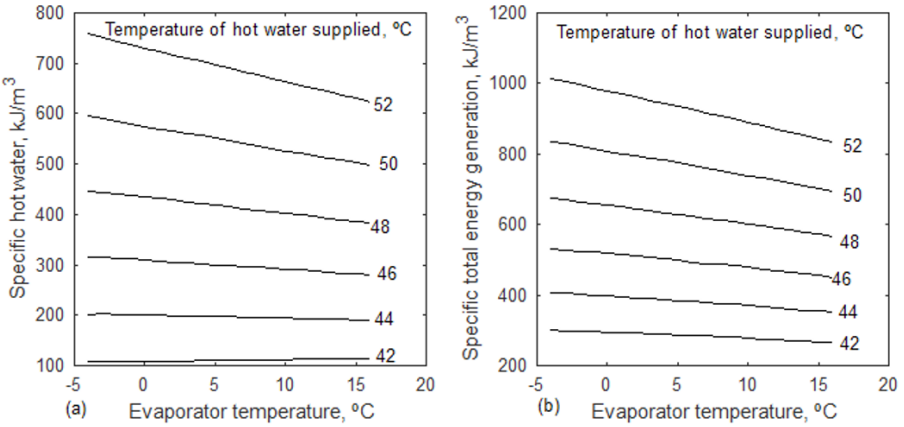

Fig. 9.21: Effect of evaporator temperature with hot water supply temperature on specific energy of hot water used for the domestic use and total specific energy output by the heat pump polygeneration plant

Fig. 9.21 analyses the effect of evaporator temperature on water supply temperature on the heat pump's water-cooled condenser. The increase in evaporator temperature also suppresses the hot water generation for domestic use, which is similar to the freshwater production and cooling capacity. The decrease in heat pump capacity with an increase in evaporator temperature also decreases the water flow rate in the water-cooled condenser. Therefore, the available hot water from the polygeneration decreases with an increase in the evaporator temperature. Since all the four outputs, i.e. electricity generation, cooling output, freshwater production, and hot water for use, are decreasing

with an increase in evaporator temperature, the total energy output from the polygeneration is decreasing with the evaporator temperature. The increase in hot water supply temperature to HDH increases the evaporation rate in the humidifier and also increases the cooling capacity. Therefore, with this, the electricity generation, freshwater production, cooling capacity, and hot water for use all increase with an increase in the hot water supply temperature to the HDH.

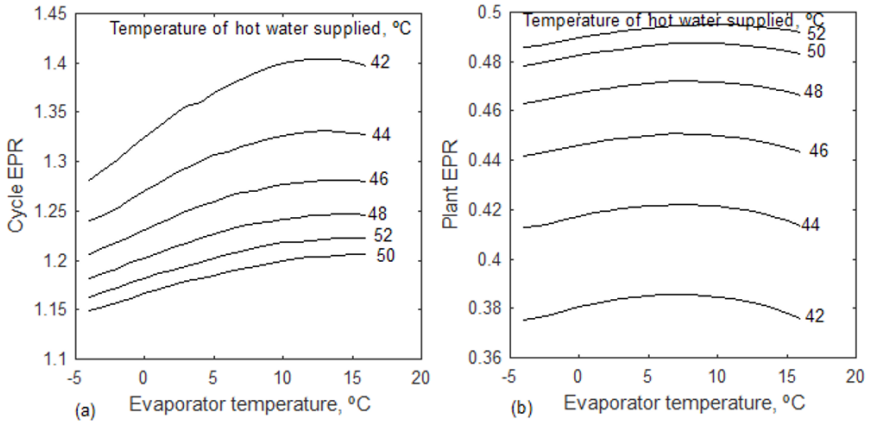

Fig. 9.22: Effect of evaporator temperature with hot water supply temperature on EPR of cycle and plant

Fig. 9.22 shows the effect of evaporator temperature and hot water evaporator temperature on the energy conversion efficiency of the HDH-VCR cycle and plant. The energy conversion efficiency is termed as the energy performance ratio (EPR) as it generates water, cooling, and hot water with the supply of high-grade energy and low-grade energy. As per the earlier discussion, the evaporator temperature and hot water temperature greatly influence the output of the HDH-VCR unit. They are also linked to the EPR of plants and cycles. The increase in evaporator temperature supports increasing the refrigeration/heat pump's coefficient of performance (COP). But the same thing suppresses freshwater production and cooling capacity. The combined effect of these two effects results in an optimum evaporator temperature for maximum EPR. The optimum evaporator temperature increases with an increase in the hot water temperature.

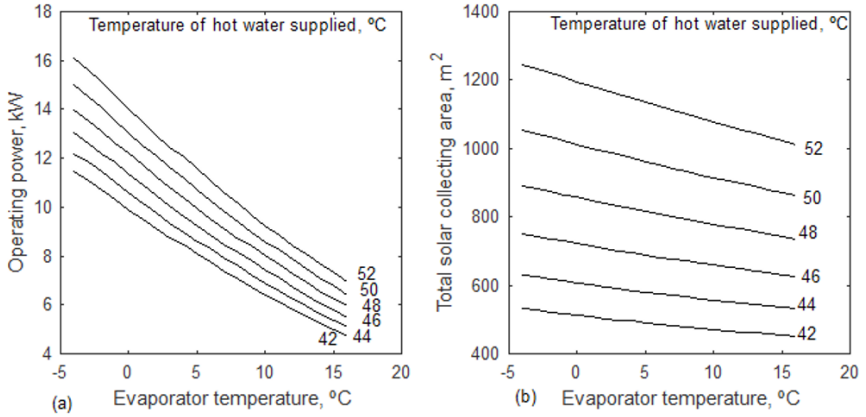

Fig. 9.23: Effect of evaporator temperature with hot water supply temperature on electricity supply to the polygeneration plant and area of PV and thermal solar collectors

Fig. 9.23 shows the effect of evaporator temperature with hot water supply temperature on required electrical energy to drive the polygeneration and total required solar collecting area. Since the heat pump capacity and the polygeneration capacity is decreasing with an increase in evaporator temperature, the operating power for the polygeneration and the required solar collectors (thermal and PV) are decreasing with an increase in evaporator temperature. But the hot water increases the capacity of the polygeneration; hence, the operating power and solar area are increasing with an increase in hot water supply temperature to the HDH plant. Based on this analysis, the solar PV plant size has been fixed at the 18 kW during the analysis.

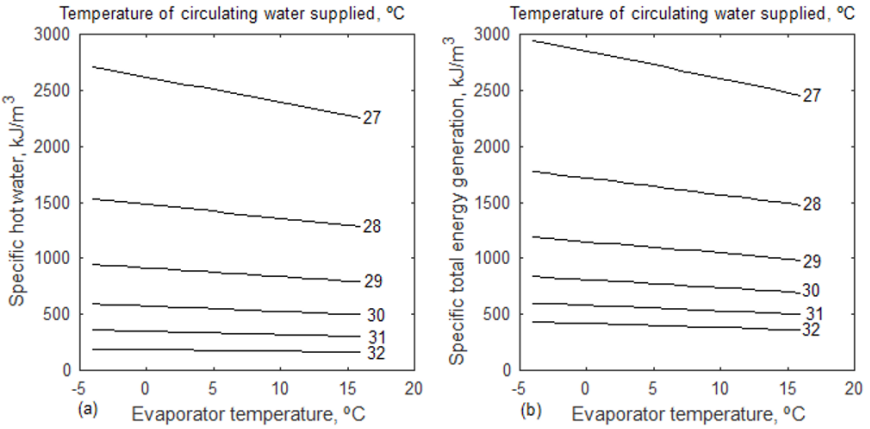

Fig. 9.24: Effect of evaporator temperature with temperature of the circulating water supply to the heat pump on specific energy of hot water generated for domestic use and specific energy of total output of the polygeneration plant

The fixed freshwater production and cooling capacity are fixed as per the constraints in the HDH unit. Therefore, these results are not depicted with a change in water supply temperature to the heat pump heat rejection. Fig. 9.24 analyses the effect of evaporator temperature and the water supply temperature to the heat pump's condenser on the specific energy of hot water generated for use and the total specific energy of the polygeneration plant. The increase in water temperature for the heat pump drops the water flow rate in the heat pump while the water flow in the HDH unit remains the same. Hence, the available hot water for use decreases with an increase in the water supply temperature to the heat pump. Therefore, the total specific energy output from the polygeneration also decreases with an increase in the water supply temperature.

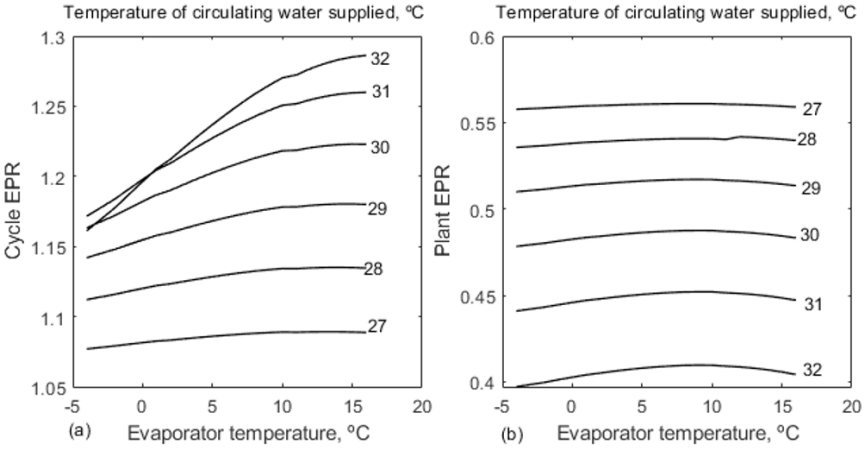

Fig. 9.25: Effect of evaporator temperature with temperature of circulating water supplied to the heat pump on EPR of HDH-VCR cycle and plant

Fig. 9.25 studies the effect of evaporator temperature and water supply temperature on the heat pump's EPR. The maximum cycle EPR demands a higher water supply temperature for the heat pump. However, due to the heat rejection of the heat pump, the maximum plant EPR necessitates a lower water temperature. The increased water supply temperature to the heat pump drops the flow rate in the SWH while the water supply to HDH is fixed. It drops the amount of hot water from the SWH. The amount of hot water available for domestic use is decreasing with a decrease in energy supply to SWH. The cycle EPR is increasing with an increase in water supply temperature to the heat pump with the influence of a drop in energy supply to SWH. The decrease in hot water output for domestic use has a greater impact on the plant than the decrease in flat plate collector area. Therefore, the plant's EPR is decreasing with an increase in temperature.

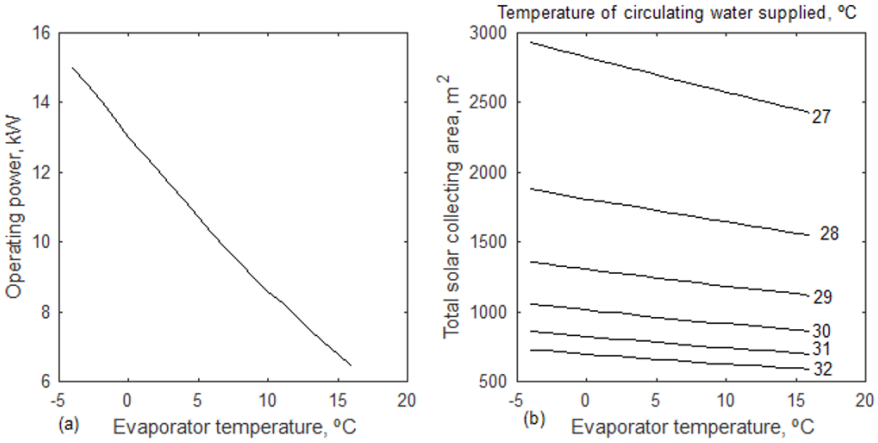

Fig. 9.26: Effect of evaporator temperature with temperature of water supplied to the heat pump on electricity supplied to operate the plant total areas of solar thermal and solar PV panels

Fig. 9.26 shows the effect of evaporator temperature on the water supply temperature to the heat pump on the electrical power required to operate the polygeneration plant and the required area to install the solar thermal collectors and solar PV panels. The electrical power demand for the polygeneration is independent of the water supply temperature for the heat pump as the HDH and heat pump components are operating at a fixed rate. The decrease in SWH size effects the total solar collecting area of the polygeneration plant. Though the solar PV size is fixed, the drop in the flat plate collector's size decreases the total size of the solar plant (thermal + PV) with an increase in the water supply temperature to the heat pump.

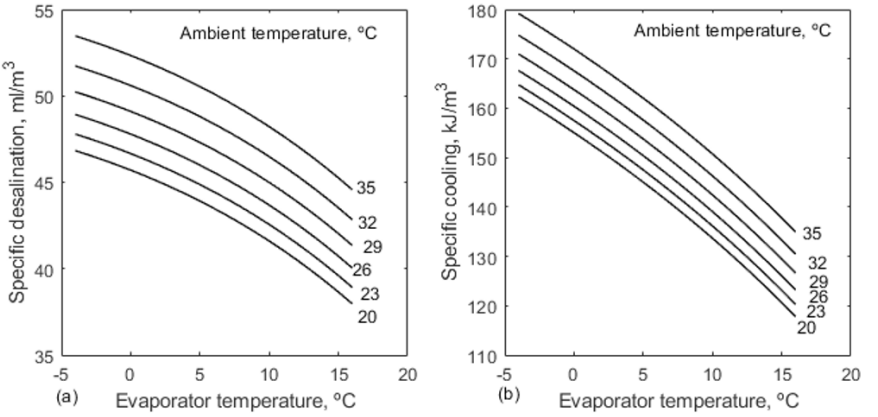

Fig. 9.27: Effect of evaporator temperature with ambient temperature on specific desalination output and specific cooling load demand

Fig. 9.27 analyses the effect of evaporator temperature and ambient air temperature on freshwater production and cooling generation of heat pump polygeneration with a single-stage HDH unit. The hot air augments the humidification process; hence, it favours freshwater production. It also increases the cooling unit size.

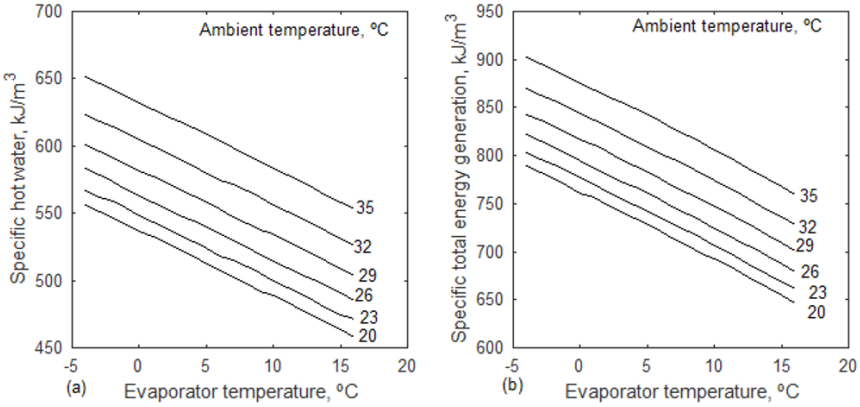

Fig. 9.28: Effect of evaporator temperature and ambient temperature on specific energy of hot water generated for domestic use and specific energy to total outputs from the polygeneration plant

Fig. 9.28 shows the effect of evaporator temperature and ambient air temperature on hot water output and total energy generation from the polygeneration. The increase in ambient temperature drops the hot water supply to the HDH unit. Since the same conditions are maintained at the heat pump, the amount of balanced available hot water for external use increases with an increase in ambient air temperature.

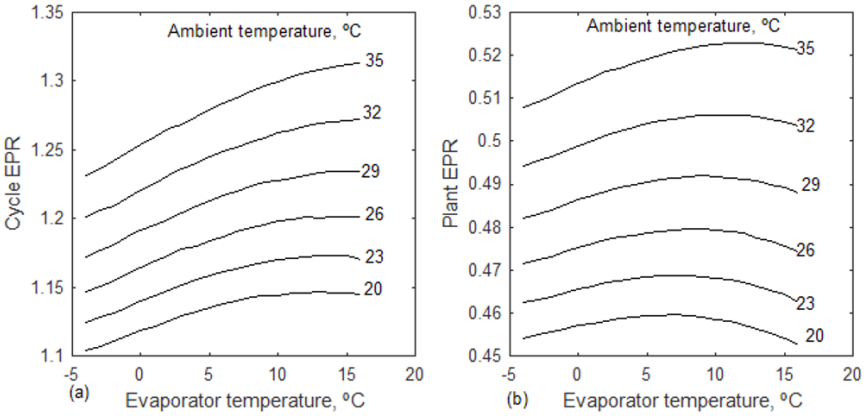

Fig. 9.29: Influence of evaporator temperature with ambient temperature on cycle and plant EPR

Fig. 9.29 shows the effect of evaporator temperature and atmospheric air temperature on the EPR of the polygeneration cycle and polygneration plant. The hot air in the humidifier increases the evaporation rate and also increases the cooling needs. With a small increase in energy supply to the cycle and plant, since the total outputs from the polygneration are increasing, the EPR of the cycle and plant increases with an increase in the atmospheric air temperature.

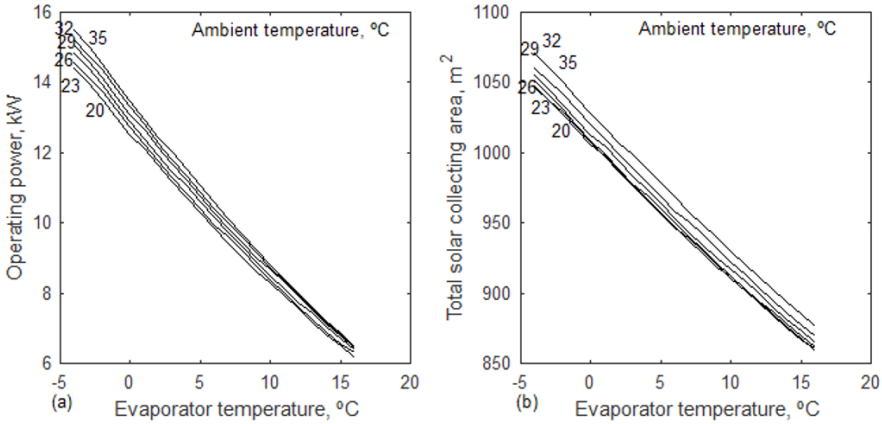

Fig. 9.30: Effect of evaporator temperature with ambient temperature on electrical energy supply to the polygeneration plant and total collecting area of solar thermal and solar PV unit

Fig. 9.30 reveals the effect of evaporator temperature and the ambient air temperature on the operating power of the polygeneration plant and the total required area of solar collection. The increased hot water flow in the flat plate collector increases the size of the solar water heater. Similarly, the increased

cooling capacity demands more power for the vapour compressor. Therefore, the operating power of the polygeneation is increasing with an increase in ambient air temperature. As per the discussion, the increased total area of the solar collectors is also depicted in Fig. 9.30b.

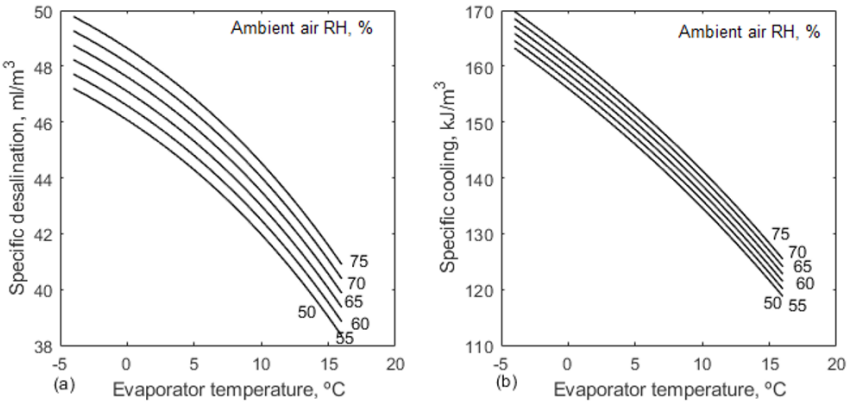

Fig. 9.31: Effect of evaporator temperature with ambient air's RH on specific freshwater production and specific cooling demand

Fig. 9.31 reveals the influence of the evaporator temperature and the ambient air's RH on freshwater generation and the specific cooling capacity of the polygeneration. Similar to the air inlet temperature, its relative humidity also helps in boosting the freshwater and cooling capacity. The humid air causes more evaporation in the humidifier and enhances the freshwater production. It also increases the latent heat load in the final dehumidifier and increases the cooling size for the dehumidification.

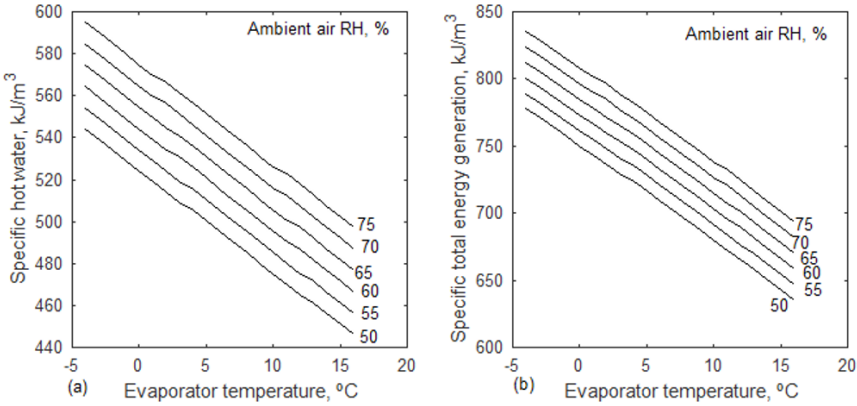

Fig. 9.32: Effect of evaporator temperature with ambient air's RH on specific energy of hot water generated for the domestic use and total specific energy output of the polygeneration

Similar to the freshwater and cooling, Fig. 9.32 shows the effect of evaporator temperature and ambient air's RH on the specific energy of hot water generated for use and the total specific energy generated from the polygeneration plant. The hot water supply to the HDH unit decreases with an increase in the RH of the supply air. It enhances the available hot water for domestic use. Therefore, the specific energy of hot water increases with an increase in the relative humidity of air. Because freshwater, cooling, and hot water supplies are increasing, so does the total energy production from polygeneration.

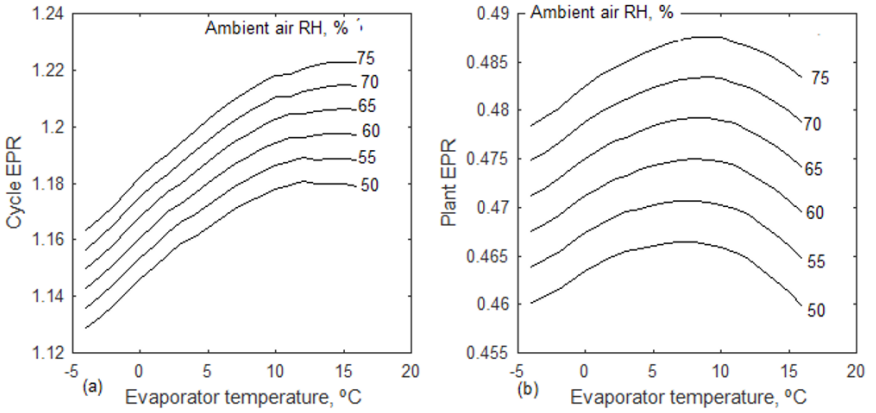

Fig. 9.33: Effect of evaporator temperature and ambient air's RH on cycle and plant EPR

Fig. 9.33 analyses the role of evaporator temperature and atmospheric air RH on cycle EPR and plant EPR. The increase in relative humidity increases the total energy production of the polygeneration. Therefore, the EPR of cycle and plant is increasing as energy supply increases for cycle and plant.

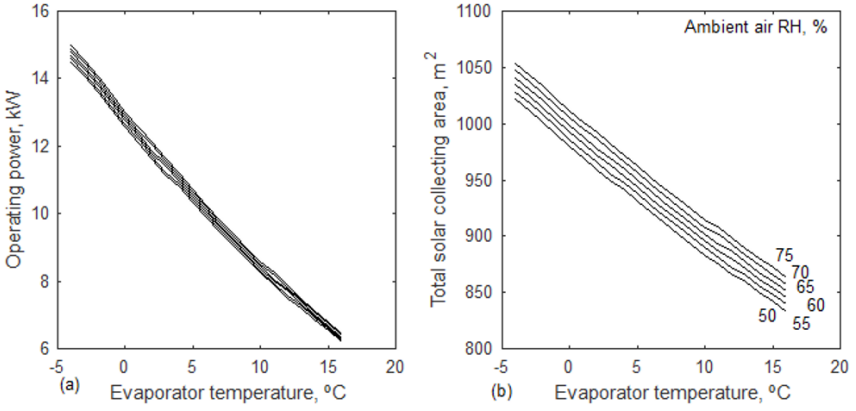

Fig. 9.34: Effect of evaporator temperature with ambient air's RH on electrical energy supply to polygeneration plant and total area of solar thermal and solar PV unit

Fig. 9.34 studies the required electricity to operate the polygeneration plant and area of the solar collectors with changes in evaporator temperature and ambient air's RH. Since the capacity of the polygeneration (freshwater, cooling and hot water at fixed electricity generation) is increasing with an increase in RH, the operating power and area of the solar collectors increases with an increase in the RH.

Table 9.4: Specifications of heat pump polygeneration with double stage HDH at the air flow rate of 1000 m^3/h and hot water temperature of 50 °C

S. No.	Description	Result
1.	Fan, kW	1.10
2.	1st Air preheater, kW	4.18
3.	1st Humidifier, kW	13.93
4.	Total first stage dehumidifier, kW	2.66
5.	2nd Air preheater, kW	4.29
6.	2nd Humidifier, Kw	10.21
7.	Air cooled dehumidifier	2.47
8.	VCR's dehumidifier/evaporator, kW	40.55
9.	VCR's compressor, kW	7.47
10.	Heat rejection from heat pump, kW	48.02
11.	Air reheater, kW	2.40
12.	Specific water production, ml/m^3 air	45.53
13.	Water production, LPH	45.53
14.	Specific cooling, kJ/m^3	145.98
15.	Cooling capacity, kW	40.55
16.	Hot water pump, kW	0.71
17.	Normal water pump, kW	0.10
18.	Hot water used for domestic use, kW	149.00
19.	Heat supplied to heat pump polygeneration cycle, kW	101.93
20.	Heat used for heat pump polygeneration cycle, kW	33.16
21.	Heat generated at solar water heater, kW	166.47
22.	Total electrical energy supplied to plant, kW	9.38
23.	Size of solar PV plant, m^2	351.65
24.	Size of solar water heater, m^2	581.14
25.	Total size of solar collection, m^2	932.79
26.	Total energy production, kW	236.00
27.	EPR of heat pump polygeneration cycle	1.21
28.	EPR of heat pump polygeneration plant	0.48

Table 9.4 lists the specifications of the HDH-VCR plant developed at an airflow rate of 1000 m^3/h and 50 °C. The parasitic power to drive the plant includes the electricity supply to the fan, circulating pump and compressor. The sizes of the first APH and second APH are nearly same. When compared to the first stage dehumidifier, the temperature drop in the final dehumidifier is greater. Therefore, the size of the second stage dehumidifier is much higher than the first stage dehumidifier. At the pre-stated conditions, the specific and total desalination are 45.53 m^3/h and 45.53 LPH respectively with 1000 m^3/h of air. Similarly, the specific cooling and total cooling are 145.98 kJ/m^3 and 40.55 kW respectively. The EPR of the HDH-VCR cycle and plant is 1.21 and 0.48 respectively.

9.4 Summary

The heat pump polygeneration with single stage HDH and double stage HDH has been studied to generate four outputs, i.e., electricity, freshwater, cooling, and hot water. Through the parametric analysis, the evaporator temperature has been optimised to maximise the EPR of the cycle and plant. The optimum evaporator temperature for maximum plant EPR is less than the optimum evaporator temperature for maximum cycle EPR. The optimum evaporator temperature is increasing with an increase in water temperature due to the heat pump, atmospheric air temperature, and atmospheric air relative humidity. The analysis of the HDH-VCR unit concludes that water productivity and cooling productivity are inversely related to the evaporator temperature and directly related to the hot water supply temperature. The optimum evaporator temperature increases with an increase in hot water temperature, atmospheric air temperature, and relative humidity of atmospheric air to result in maximum EPR. Hot and humid air favours the performance of the HDH-VCR unit. The heat pump polygeneration plant results in an EPR of 0.57 and 0.45, respectively, with single-stage HDH and double-stage HDH. The total energy production is increased from 199 kW to 236 kW from a heat pump polygeneration plant with a single stage HDH to a double stage HDH.

Review questions

1. Analyse the evaporator temperature to maximise the energy efficiency of heat pump polygeneration as a function of operational conditions.
2. The selection of single-stage HDH or double-stage HDH depends on the objective of the heat pump polygeneration plant. Justify.
3. What is the role of the hot water supply temperature to the HDH on the performance of the heat pump polygeneration?
4. How do the single stage HDH and double stage HDH influence the performance of heat pump polygeneration?
5. Formulate the performance of heat pump polygeneration with single-stage HDH and double-stage HDH.

❐

10

Polygeneration – A Comparative Study

Abstract

Polygeneration has the merits of high energy conversion, minimal energy losses, generation of multiple needs, etc. In the current work, various polygeneration systems are compared to draw the merits and demerits and select the most suitable. The current work is focused on the development of two polygeneration plants to generate electricity, cooling, freshwater, and hot water. In one polygeneration option, humidification-dehumidification (HDH) desalination has been combined with vapour compression refrigeration (VCR), which is known as heat pump polygeneration. The second polygeneration integrates the binary fluid cooling cogeneration (BFCC) and HDH desalination, which is known as binary fluid polygeneration. These two polygeneration plants are studied with the single-stage HDH and double-stage HDH. The comparative results show that polygeneration with single-stage HDH results in a higher energy performance ratio (EPR) compared with double-stage HDH. Heat pump polygeneration (VCR-HDH) results in a higher EPR compared to binary fluid polygeneration (BFCC-HDH). The double-stage HDH poly-generation generates more output but with a penalty in EPR compared to the single stage due to higher operating energy. The EPR with single-stage HDH is greater than with double-stage HDH. The EPR of heat pump polygeneration and binary fluid polygeneration are closely associated. However, the maximum EPR of heat pump polygeneration is slightly higher than the maximum EPR of binary fluid polygeneration at the simulated conditions.

T. Srinivas, *Thermal Polygeneration*,
https://doi.org/10.1007/978-3-031-37886-7_10

10.1 Introduction

The study on polygeneration demonstrates the potential of integration and possible future inventions to meet societal needs. It has been observed that the heat pump polygeneration (VCR-HDH) and binary fluid polygeneration (BFCC-HDH) are not reported in the open literature. The polygeneration system gives electricity, cooling, freshwater, and hot water. Heat pump polygeneration and binary fluid polygeneration are compared under the evaporator temperature to analyse the four outputs and energy performance ratio (EPR). The studies identified evaporator temperature as the optimum operational condition to maximise the EPR. The evaporator temperature is optimised to result in a maximum EPR for the heat pump polygeneration with single-stage HDH and double-stage HDH. Similarly, the binary fluid polygeneration was also analysed to develop the optimum evaporator temperature with single-stage HDH and double-stage HDH for the maximum EPR.

10.2 Comparative Studies

The results of four polygeneration plants are compared. The four polygeneration plants considered are single-stage VCR-HDH, double-stage VCR-HDH, single-stage BFCC-HDH, and double-stage BFCC-HDH plants. The first two heat pump polygeneration plants combine HDH with VCR for the generation of electricity, cooling, freshwater, and hot water. The third and fourth are the integration of BFCC with the HDH unit for the generation of the same outputs. The evaporator of the cooling system, either in VCR or BFCC, plays a different role in the outputs linked. For example, in a heat pump polygeneration, a lower evaporator temperature results in more freshwater but demands more electricity to drive the vapour compressor. A lower evaporator temperature in BFCC favours the four outputs with more energy demand. Therefore, there will be an optimum evaporator temperature to result in maximum energy conversion efficiency, i.e., the EPR of the polygeneration plant. The results focused on finding the influence of evaporator temperature on the performance of the polygeneration. The performance of the four polygenerations is compared with a change in evaporator temperature. This comparative study allows us to differentiate between the various poly-generation plants and select the best one. The expected outcome is the optimum evaporator temperature to maximise the EPR of the polygeneration.

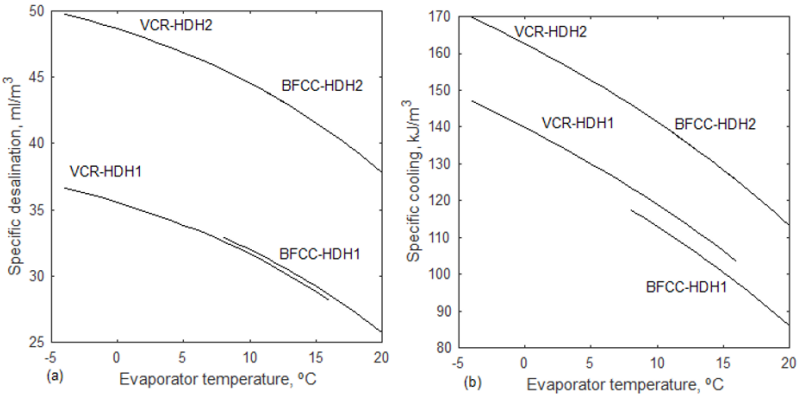

Fig. 10.1: Effect of evaporator temperature on specific desalination and specific cooling of four polygeneration plants

The role of evaporator temperature on specific outcomes of freshwater (Fig. 10.1a) and cooling (Fig. 10.1b) has been analysed with four polygenerations. Freshwater and cooling are strongly related to the evaporator's temperature. The increase in evaporator temperature suppresses the function of the final dehumidifier in the HDH unit. It decreases the condensation rate of the water. Hence, freshwater production is decreasing with an increase in evaporator temperature. The cooling output is determined by the evaporator temperature. At a fixed air flow in HDH, cooling output decreases with an increase in evaporator temperature as the temperature difference decreases. Therefore, as per the analysis, water productivity and cooling productivity decrease with an increase in evaporator temperature. The selected evaporator temperature range is different from the category of the poly-generation. The cooling in the BFCC-HDH polygeneration works on the principle of vapour absorption refrigeration (VAR). The cooling in VCR-HDH works on the principle of vapour compression refrigeration (VCR). Therefore, the selected temperature for VCR is relatively lower compared to VAR. Since VCR is suitable to operate at a lower evaporator temperature, the low temperature benefits, i.e., high freshwater yield and cooling output, can be obtained. The two-stage HDH polygeneration (both VCR-HDH and BFCC-HDH) results in higher freshwater production compared to the single stage operation. The multiple stages in HDH result in multiple condensations of the humid air in the dehumidifier. The added freshwater at each stage results in additional production compared to the single stage at the same air flow rate. The double stage also results in more cooling as it demands more cooling capacity as the heating of air takes place in two stages in both the APR and humidifier. The supply of air at the final dehumidifier is relatively higher with two-stage operation compared to single-stage. Therefore, specific cooling with two-stage HDH poly-generation is higher than with single-stage HDH polygeneration.

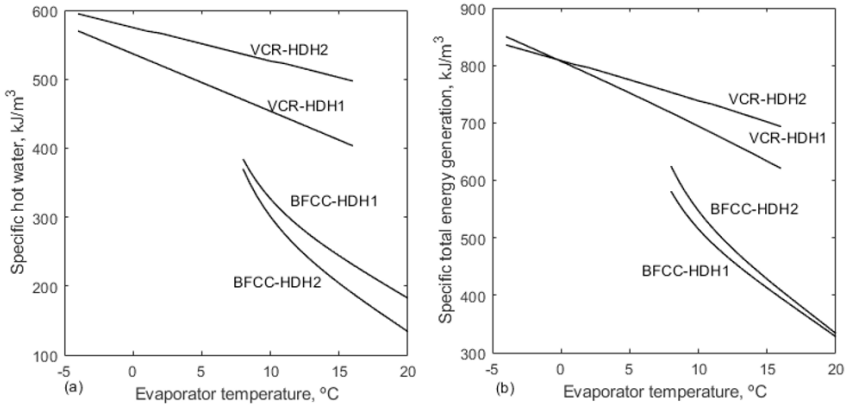

Fig. 10.2: Effect of evaporator temperature on specific energy of hot water and specific total energy generation for four polygeneration plants

Fig. 10.2 shows the influence of evaporator temperature on specific hot water energy production and specific total energy production of the polygeneration plant. The energy of the hot water generated in polygeneration depends on its temperature and flowrate. The dehumidifier capacity and BFCC working fluid decrease with an increase in evaporator temperature. It suppresses the sink load of BFCC and its circulating water flow. The decreased water flow rate in the absorber and condenser of the BFCC drops the energy content of the hot water supply for domestic use. The same is repeated even with the VCR unit of the VCR-HDH polygeneration. The hot water use in the two-stage HDH is greater compared to the single stage. Therefore, the amount of hot water that is meant for domestic use decreases with the two-stage polygeneration compared to the single-stage HDH polygeneration.

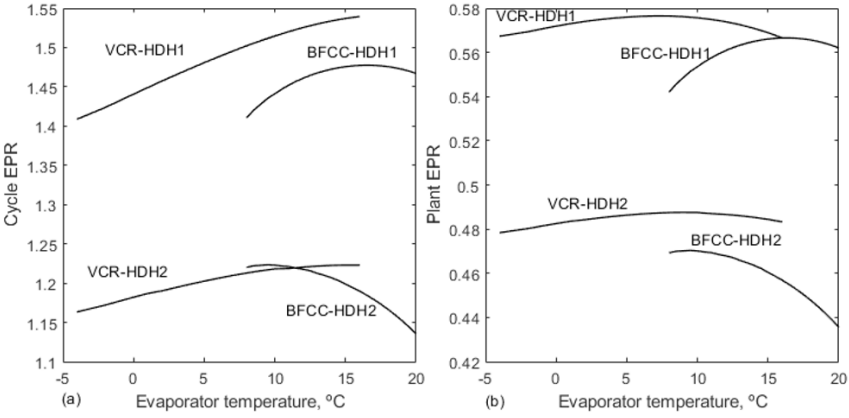

Fig. 10.3: Effect of evaporator temperature EPR of polygeneration cycle and polygeneration plant for four polygeneration plants

Fig. 10.3 shows the effect of evaporator temperature on the EPR of the cycle and plant for four polygeneration plants. The low evaporator temperature favours some elements, such as fresh water productivity, but demands more energy to operate. Therefore, to balance these effects, there will be an optimum evaporator temperature to be selected to operate at a high efficiency condition. The EPR is maximum at an optimum evaporator temperature as shown. The increase in evaporator temperature supports increasing the refrigeration/heat pump's coefficient of performance (COP). But the same thing suppresses freshwater production and cooling capacity. The combined effect of these two effects results in an optimum evaporator temperature for maximum EPR. The two-stage polygeneration results in more output, but it also demands more energy to drive the poly-generation plant. Therefore, the EPR of two-stage HDH polygeneration is less than the single-stage HDH poly-generation. The optimum evaporator temperature is varied from 10 °C to 15 °C for the maximum EPR of the cycle and plant at the specified operational conditions.

Table 10.1: Comparison of specifications of four polygeneration plants 1000 m^3/h of air and 50 °C of HDH supply temperature

S. No.	Description	Heat pump polygeneration		Binary fluid polygeneration	
		VCR-HDH1	VCR-HDH2	BFCC-HDH1	BFCC-HDH2
1.	Hot water supply to HDH, LPH	1972.80	3511.60	1765.40	3446.10
2.	Hot water to domestic use, LPH	4499.40	5131.60	2333.70	2877.00
3.	Water from SWH, LPH	6472,20	8643.20	--	--
4.	Net power generation, kW	14.00	18.00	0.64	1.20
5.	Useful heat from SWH, kW	109.66	166.47	--	--
6.	Cooling production, kW	34.31	40.55	27.90	39.24
7.	Freshwater production, LPH	32.58	45.53	29.21	44.53
8.	Specific freshwater output, ml/m^3	32.58	45.53	29.21	44.53
9.	Specific cooling, kJ/m^3	123.52	145.98	100.45	141.26
10.	Heat used for HDH plant, kW	20.45	33.16	18.53	16.72
11.	Electricity supplied, kW	7.67	9.38	2.70	4.15
12.	Total solar radiation supplied, kW	345.79	484.21	202.46	323.06

13.	Total energy supplied to cycle, kW	117.34	175.85	77.67	124.19
14.	Total energy generated, kW	199.34	236.05	114.60	151.87
15.	Area of SWH, m^2	387.71	581.14	--	--
16.	Area of concentrating collectors, m^2	--	--	390.02	622.33
17.	Area of PV plant, m^2	278.41	351.64	--	--
18.	Total area of PV/T collectors, m^2	666.11	932.78	390.02	622.33
19.	EPR of polygeneration cycle	1.50	1.21	1.47	1.22
20.	EPR of polygeneration plant	0.57	0.48	0.57	0.47

The specifications of four stated polygeneration plants are compared in Table 10.1 at the HDH air flow of 1000 m^3/h and their hot water supply temperature of 50°C. The optimum evaporator temperature depends on operational conditions, the number of HDH stages, and the nature of polygeneration integration. The optimum evaporator temperature in VCR-HDH1 and VCR-HDH2 heat pump poly-generations is considered to be 8 °C. The optimum evaporator temperatures in the binary fluid polygenerations BFCC-HDH1 and BFCC-HDH2 are 15 °C and 10 °C, respectively, according to the results. The hot water supply to HDH is nearly the same with VCR integration and BFCC integration. The hot water usage on the double stage is more than on the single stage. Hot water is generated in a heat pump and a SWH to power the HDH unit in a heat pump polygeneration system. Whereas, in the binary fluid polygeneration, the hot water is generated from the heat recovery of the BFCC's sink (condenser and absorber). The BFCC generates hot water at the required temperature. But the heat pump has a constraint on the hot water generated temperature. Therefore, SWH is not used in BFCC. The supply temperature to the heat sink of the BFCC and heat pump should be sufficiently low to reject the heat. Therefore, extra water has been supplied to control the inlet temperature of water at the inlet of heat exchangers. This additional water has been substituted by hot water used for domestic use. After using the hot water for HDH, the balanced hot water is used for domestic use. Similar to the hot water supply to HDH, the available hot water for domestic use has been increased from a single stage to a double stage. The heat rejection of BFCC is less than the heat rejection of the heat pump. Therefore, the available hot water for domestic use with the binary fluid polygeneration is lower than with the heat pump polygeneration. In binary fluid polygeneration, there is no need for SWH. Therefore, the particulars of SWH are not furnished with this plant. The electricity demand to operate the heat pump polygeneration is higher than the

binary fluid polygeneration due to the mechanical compressor in the heat pump. In the heat pump polygeneration, the electricity supply, excluding the parasitic power to drive, is fixed at 14 kW and 18 kW, respectively, with single-stage HDH and double-stage HDH as per its usage. But the net power generation from the binary fluid polygeneration depends on the generated working fluid in the polygeneration. The heat load and working fluid in the binary fluid polygeneration with double stage HDH are greater than in the binary fluid polygeneration with single stage HDH. Therefore, electricity generation from double-staged HDH polygeneration with BFCC is nearly double that of single-stage polygeneration. The HDH's heat load in VCR-HDH2 is 150% of the VCR-HDH1 poly-generation, i.e., 50% additional load. Therefore, the useful heat of SWH in VCR-HDH2 polygeneration is greater than in VCR-HDH1 polygeneration. The cooling production does not change much by switching from the BFCC to the VCR mode of operation. The double-stage HDH results in more cooling as its heat exchanger capacity increases compared to the single-stage HDH polygeneration. Similarly, the production of freshwater also does not vary much between the BFCC and VCR modes of poly-generation. The cooling and freshwater generation in the double stage is more than in the single stage polygeneration. The electricity to drive the double-stage HDH polygeneration is more than the single-stage HDH polygeneration. The VCR needs electricity for its operation, and the BFCC requires only heat and a little electricity to drive the pump. Therefore, the binary fluid polygeneration needs lower driving power to operate the plant compared to the heat pump polygeneration. The heat pump polygeneration is equipped with solar thermal (SWH) and solar PV units, respectively, for hot water and electricity. The binary fluid polygeneration has only one solar thermal source with a concentrating collector. The turbine generates the electricity required to operate the plant and the additional external load. Therefore, the total collector area and solar radiation supplied to the binary fluid polygeneration is less than the heat pump polygeneration. But due to increased heat load in double stage HDH, the EPR of the double stage is decreasing compared to the single stage in both heat pump polygeneration and binary fluid polygeneration. The cycle ERP of the heat pump polygeneration is closely matched with the cycle ERP of the binary fluid polygeneration. The same is applied to the plant.

10.3 Merits and Demerits of Two Polygeneration Plants

The following are the advantages and disadvantages of the binary fluid polygeneration plant.

The benefits of binary fluid polygeneration

1. The exit temperature of the evaporator in the refrigeration cycle is high due to the variable temperature during the phase change compared to heat pump polygeneration.

2. The energy supply to binary fluid polygeneration is heat, which is low grade energy.
3. The heat rejection of the power plant and cooling plant (cooling cogeneration) is used for the process heat of the HDH desalination.
4. The binary fluid power plant requires less floor space than a solar PV plant.

Disadvantages of binary fluid polygeneration

1. The binary working fluid, which is an ammonia-water mixture, has certain constraints such as corrosion with some materials, toxic properties, and being leak proof etc.
2. The COP of VAR in binary fluid polygeneration is low compared to the COP of VCR used in heat pump polygeneration.
3. Bulky due to the large number of heat exchangers in power and cooling of binary fluid polygeneration.
4. Due to the toxic nature of binary fluid, it is suitable for industrial applications but not for domestic or commercial use.

The following are the advantages and disadvantages of the heat pump polygeneration plant.

1. The benefits of heat pump polygeneration
2. The COP of a heat pump is higher than the COP of a binary fluid system.
3. Compact in size compared to the binary fluid polygeneration,
4. Material constraints in the use of refrigerant in heat pump polygeneration.
5. It can be used at all levels, such as domestic, commercial, and industrial, without any limitations.

Disadvantages of heat pump polygeneration

1. It uses high grade energy to drive the heat pump.
2. The evaporator exit temperature is low compared to the binary fluid polygeneration.
3. More floor space is required to install the solar PV plant to drive the heat pump polygeneration.

10.4 Summary

The polygeneration survey shows the need and projects its future development. Two polygeneration plants are investigated and compared to highlight their relative merits and demerits. Two polygeneration plants are extended with single-stage HDH desalination and double-stage HDH desalination. Double stage HDH polygeneration results in higher outputs

compared to single stage HDH polygeneration. But since single stage HDH demands low energy, its polygeneration efficiency is higher than the single stage HDH polygeneration. Evaporator temperature can be optimised to achieve maximum EPR due to its adverse and favourable effects on polygeneration. The optimal evaporator temperature increased from 10 to 15 degrees Celsius. Due to high temperature losses from the concentrating collector, the binary fluid polygeneration results in low EPR compared to the VCR-HDH polygeneration. In binary fluid polygeneration, the refrigerant temperature is variable in the evaporator. Therefore, it has high binary fluid polygeneration compared to heat pump polygeneration.

Review Questions

1. The selection of process conditions in binary fluid polygeneration and heat pump polygeneration depends on the objective function. Justify.
2. Why the single stage HDH results higher energy efficiency compared to the double stage HDH in a polygeneration?
3. Analyze the optimum evaporator temperature in a cooler for the maximum performance as a function of process conditions?
4. Compare the relative merits and demerits of binary fluid polygeneration and heat pump polygeneration.

❒

Appendix A

Binary Fluid Properties – Ammonia-Water Mixture

Compared to single fluid system, the binary fluid system needs an additional property i.e. concentration to find the thermodynamic properties such as saturation pressure, saturation temperature, internal energy, enthalpy, entropy, exergy etc. Therefore, the binary fluid properties involve more tedious calculations. The mixture can be grouped into two viz., azeotropic mixture and zeotropic mixture. The azeotropic mixture behaves as a single fluid system as they can not be separated by heating or absorbed by rejecting the heat. On otherhand, zeotropic mixture can be separated and absorbed respectively with heat addition and heat rejection. Ammonia-water is an example of the zeoptropic mixture widely used in vapour absorption systemsRefrigerant and steam properties are available in the literature. Currently to refer the ammonia-water mixture properties, property charts such as enthalpy-concentration are available for the graphical solutions. But for the analytical solutions, the mixture properties are not available in the tabular form. The mixture properties have been developed as a function of pressure, temperature and concentration. This appendix is focused on presentation of ammonia-water mixture properties in the form of tables and graphs. The tables are categories into saturated liquid properties, saturated vapour properties and liquid-vapour mixture properties. The liquid-vapour mixture properties changes from the bubble point temperature (BPT) to dew point temperature (DPT). Therefore, these properties are listed between these two temperatures.

T. Srinivas, *Thermal Polygeneration*,
https://doi.org/10.1007/978-3-031-37886-7

Table A.1 tabulates the saturated liquid properties from zero concentration to one-unit concentration. The pressure is changed from 0.15 bar to 54 bar. These tables can be used to solve vapour absorption refrigeration (VAR) cycles, Kalina cycles, aqua ammonia-based cooling cogeneration cycles, and similar thermal systems. The selected pressures are close to each other to avoid iteration in the direction of multiple variables. Similar to saturated liquid properties, the saturated vapour properties are also listed in Table A.2.

The collection of saturated properties in the liquid state and vapour state is a straight method without using the lever rule in graphical solution. To solve the liquid-vapour properties, the lever rule has to be applied. More iterations of mass balance and energy balance equations are required to find the liquid-vapour mixture properties. To avoid the multiple iterations and simplify the length of the procedure of liquid-vapour properties solutions, these properties are developed and presented in Table A.3. The properties can be directly picked from the unsaturated mixture properties with reference to the temperature, which lies between the bubble point temperature and the dew point temperature. Sometimes a minimum number of iterations is required to find the properties with the mixture temperature.

The bubble point temperature and dew point temperature can be determined from the saturated liquid and saturated vapour properties at zero concentration and unit concentration, respectively. These are not repeated in the unsaturated fluid properties. For the saturated fluid, the presented properties are temperature, specific volume, specific enthalpy, and specific entropy. The unsaturated fluid properties include temperature, specific volume, specific enthalpy, specific entropy, liquid concentration, vapour concentration, liquid specific enthalpy, and vapour specific enthalpy. The temperature of the fluid changes between the bubble point temperature and the dew point temperature. The temperature is increased in steps of 10% increments up to the dew point temperature.

The temperature between BPT and DPT is refered as a temperature ratio, $\theta = f(T)$ for the easy interpretation of the properties,

The temperature ratio between BPT and DPT is

$$\theta = \frac{T - T_{bp}}{T_{dp} - T_{bp}} \tag{1}$$

The value $\theta = 0$ indicates BPT and $\theta = 1$ is equal to the DPT.

Therefore, θ, BPT and DPT results the temperature between the BPT and DPT as follows,

$$T = T_{bp} + \theta = f(T)\,(T_{dp} - T_{bp}) \tag{2}$$

The dryness fraction of liquid-vapour mixture

Dryness fraction, $\partial = \frac{m_v}{m_l + m_v}$

$$m = m_l + m_v \tag{3}$$

The total ammonia portion before separation and after separation is same.

$$m\,x = m_l\,x_l + m_v\,x_v \tag{4}$$

Eliminating m_{liquid},

$$\begin{aligned} m\,x &= (m - m_v)\,x_l + m_v\,x_v \\ m\,x &= m\,x_l - m_v\,x_l + m_v\,x_v \\ m\,(x - x_l) &= m_v\,(x_v - x_l) \end{aligned}$$

Therefore, the dryness fraction of the mixture is defined from the simplification

$$\partial = \frac{m_v}{m} = \frac{x - x_l}{x_v - x_l} = \frac{x - x_l}{x_v - x_l} \tag{5}$$

Similarly,

$$\partial = \frac{h - h_l}{h_v - h_l} = \frac{s - s_l}{s_v - s_l} \tag{6}$$

Table A.1 Saturated liquid properties

P, bar	Property	Ammonia concentration (mass fraction), x										
		0	**0.1**	**0.2**	**0.3**	**0.4**	**0.5**	**0.6**	**0.7**	**0.8**	**0.9**	**1**
0.15	T, °C	54.309	23.376	4.447	-12.125	-27.608	-40.961	-51.130	-57.822	-61.605	-63.6292	-65.094
	v, m^3/kg	0.001	0.001	0.001	0.001	0.001	0.001	0.001	0.001	0.001	0.0014	0.001
	h, kJ/kg	227.583	30.730	-116.342	-245.710	-356.252	-438.031	-481.383	-481.794	-442.710	-374.7695	-291.3586
	s, kJ/kg K	0.763	0.389	0.060	-0.284	-0.637	-0.959	-1.202	-1.332	-1.346	-1.2782	-1.2037
0.20	T, °C	60.359	29.445	10.106	-6.866	-22.660	-36.243	-46.584	-53.410	-57.298	-59.4043	-60.9311
	v, m^3/kg	0.001	0.001	0.001	0.001	0.001	0.001	0.001	0.001	0.001	0.0014	0.0014
	h, kJ/kg	252.911	56.223	-91.940	-222.014	-332.625	-414.070	-457.143	-457.788	-419.710	-353.5903	-272.8622
	s, kJ/kg K	0.839	0.474	0.147	-0.194	-0.542	-0.857	-1.094	-1.221	-1.238	-1.1782	-1.1157
0.30	T, °C	69.293	38.414	18.504	0.968	-15.267	-29.183	-39.780	-46.808	-50.864	-53.1093	-54.7502
	v, m^3/kg	0.001	0.001	0.001	0.001	0.001	0.001	0.001	0.001	0.001	0.0014	0.0014
	h, kJ/kg	290.3312	93.8223	-55.9639	-187.1263	-297.9398	-379.0263	-421.7986	-422.8269	-386.1627	-322.5445	-245.4466
	s, kJ/kg K	0.95	0.60	0.27	-0.0649	-0.4053	-0.7113	-0.9404	-1.0644	-1.0848	-1.0351	-0.9884
0.40	T, °C	75.96	45.11	24.80	6.8577	-9.694	-23.8521	-34.6395	-41.8246	-46.013	-48.3739	-50.1146
	v, m^3/kg	0.00	0.00	0.00	0.001	0.0011	0.0012	0.0013	0.0014	0.0014	0.0014	0.0014
	h, kJ/kg	318.27	121.85	-29.15	-161.1584	-272.2022	-353.122	-395.7541	-397.0938	-361.4298	-299.5358	-224.9056
	s, kJ/kg K	1.03	0.69	0.36	0.0288	-0.3066	-0.6063	-0.8301	-0.952	-0.9748	-0.9317	-0.8954
0.50	T, °C	81.34	50.51	29.8858	11.635	-5.1656	-19.5163	-30.4573	-37.7708	-42.0707	-44.5307	-46.3596
	v, m^3/kg	0.001	0.001	0.001	0.001	0.0011	0.0012	0.0013	0.0014	0.0014	0.0015	0.0014
	h, kJ/kg	340.8433	144.4738	-7.5117	-140.228	-251.5056	-332.3517	-374.9202	-376.5256	-341.6347	-281.0475	-208.2683
	s, kJ/kg K	1.0949	0.7563	0.4354	0.1029	-0.2288	-0.5238	-0.7436	-0.864	-0.8885	-0.8502	-0.8215

0.60	T, °C	85.8781	55.0754	34.1914	15.6837	-1.3227	-15.8337	-26.9043	-34.3275	-38.7241	-41.2714	-43.1795
	v, m^3/kg	0.001	0.001	0.001	0.001	0.0011	0.0012	0.0013	0.0014	0.0014	0.0015	0.0014
	h, kJ/kg	359.9187	163.5778	10.7626	-122.5643	-234.0719	-314.8965	-357.4443	-359.2831	-325.0219	-265.4815	-194.1731
	s, kJ/kg K	1.1484	0.8148	0.4952	0.1644	-0.1642	-0.4555	-0.6721	-0.7913	-0.8171	-0.7827	-0.7599
0.70	T, °C	89.8276	59.0426	37.9411	19.2149	2.0328	-12.6164	-23.7994	-31.3189	-35.8012	-38.4267	-40.4068
	v, m^3/kg	0.001	0.001	0.001	0.001	0.0011	0.0012	0.0013	0.0014	0.0014	0.0015	0.0014
	h, kJ/kg	376.524	180.1998	26.664	-107.2042	-218.935	-299.7704	-342.3237	-344.3719	-310.6414	-251.9709	-181.8761
	s, kJ/kg K	1.1943	0.8651	0.5466	0.2173	-0.1089	-0.3971	-0.6112	-0.7293	-0.7562	-0.7248	-0.7068

Table A.1 Saturated liquid properties (contd.,)

P, bar	Property	Ammonia concentration (mass fraction), x										
		0	**0.1**	**0.2**	**0.3**	**0.4**	**0.5**	**0.6**	**0.7**	**0.8**	**0.9**	**1**
0.80	T, °C	93.3345	62.5647	41.2741	22.3576	5.0218	-9.7488	-21.0315	-28.6369	-33.1966	-35.8932	-37.9393
	v, m^3/kg	0.001	0.001	0.001	0.001	0.0011	0.0012	0.0013	0.0014	0.0014	0.0015	0.0014
	h, kJ/kg	391.2828	194.9682	40.794	-93.5626	-205.5093	-286.3764	-328.9524	-331.1911	-297.9191	-239.9903	-170.9243
	s, kJ/kg K	1.2348	0.9093	0.5918	0.2636	-0.0604	-0.346	-0.5579	-0.6752	-0.703	-0.6741	-0.66
0.90	T, °C	96.497	65.7403	44.2824	25.1971	7.7245	-7.1547	-18.5271	-26.2105	-30.8407	-33.6027	-35.7098
	v, m^3/kg	0.001	0.001	0.001	0.001	0.0011	0.0012	0.0013	0.0014	0.0014	0.0015	0.0015
	h, kJ/kg	404.6042	208.2949	53.5465	-81.2563	-193.4116	-274.3246	-316.9349	-319.349	-286.4803	-229.1966	-161.0202
	s, kJ/kg K	1.2709	0.9488	0.6321	0.305	-0.0172	-0.3006	-0.5105	-0.627	-0.6556	-0.6289	-0.6182
1.00	T, °C	99.3831	68.6377	47.0296	27.7926	10.1966	-4.781	-16.2352	-23.99	-28.6851	-31.5076	-33.6716
	v, m^3/kg	0.001	0.001	0.001	0.001	0.0011	0.0012	0.0013	0.0014	0.0014	0.0015	0.0015
	h, kJ/kg	416.7721	220.4656	65.1947	-70.0199	-182.3767	-263.3457	-305.9982	-308.5753	-276.0665	-219.3523	-151.9574
	s, kJ/kg K	1.3037	0.9846	0.6686	0.3425	0.0219	-0.2595	-0.4678	-0.5836	-0.6129	-0.588	-0.5802

2.00	T, °C	119.8535	89.1709	66.5568	46.2987	27.8634	12.2059	0.1773	-8.0884	-13.2565	-16.5269	-19.1188
	v, m^3/kg	0.0011	0.001	0.001	0.001	0.0011	0.0012	0.0013	0.0014	0.0015	0.0015	0.0015
	h, kJ/kg	503.4342	307.1399	148.229	9.9871	-104.077	-185.7942	-229.0256	-232.8278	-202.6659	-149.5098	-86.9027
	s, kJ/kg K	1.5299	1.2305	0.92	0.6002	0.2896	0.0203	-0.1778	-0.2894	-0.3223	-0.3082	-0.3171
3.00	T, °C	133.1788	102.5174	79.2957	58.4175	39.4655	23.3812	10.9844	2.3846	-3.0981	-6.6712	-9.5568
	v, m^3/kg	0.0011	0.001	0.001	0.001	0.0011	0.0012	0.0013	0.0014	0.0015	0.0015	0.0015
	h, kJ/kg	560.2596	364.0297	202.8415	62.5559	-52.8469	-135.3434	-179.1833	-183.8412	-155.0362	-103.7988	-43.6892
	s, kJ/kg K	1.6718	1.3845	1.0776	0.7614	0.4562	0.1933	0.0005	-0.1087	-0.1431	-0.134	-0.1507
4.00	T, °C	143.3246	112.6681	89.0041	67.6738	48.3415	31.9398	19.2661	10.4127	4.689	0.8825	-2.231
	v, m^3/kg	0.0011	0.001	0.001	0.001	0.0011	0.0012	0.0013	0.0014	0.0015	0.0016	0.0016
	h, kJ/kg	603.7908	407.6785	244.8238	102.9609	-13.5599	-96.7809	-141.189	-146.5253	-118.6778	-68.7243	-10.2419
	s, kJ/kg K	1.7774	1.4988	1.1948	0.8813	0.5798	0.3211	0.1319	0.0243	-0.0109	-0.0048	-0.0261
5.00	T, °C	151.6244	120.965	96.9506	75.2616	55.6259	38.9691	26.0711	17.011	11.0901	7.0917	3.7901
	v, m^3/kg	0.0011	0.001	0.001	0.0011	0.0011	0.0012	0.0014	0.0015	0.0015	0.0016	0.0016
	h, kJ/kg	639.5937	443.6386	279.4721	136.3131	18.8238	-65.0641	-109.9972	-115.9044	-88.798	-39.795	17.511
	s, kJ/kg K	1.8622	1.5908	1.2892	0.9777	0.679	0.4235	0.2369	0.1305	0.0949	0.0991	0.0746

Table A.1 Saturated liquid properties (contd.,)

P, bar	Property	Ammonia concentration (mass fraction), x										
		0	**0.1**	**0.2**	**0.3**	**0.4**	**0.5**	**0.6**	**0.7**	**0.8**	**0.9**	**1**
6.00	T, °C	158.7027	128.0359	103.7299	81.7423	61.853	44.9816	31.894	22.6584	16.5694	12.4072	8.9447
	v, m^3/kg	0.0011	0.001	0.001	0.0011	0.0011	0.0013	0.0014	0.0015	0.0015	0.0016	0.0016
	h, kJ/kg	670.2763	474.5073	309.2634	164.9994	46.6511	-37.8533	-83.273	-89.6778	-63.1766	-14.9207	41.4806
	s, kJ/kg K	1.9336	1.6682	1.3687	1.059	0.7625	0.5094	0.3249	0.2196	0.1837	0.1864	0.1598

7.00	T, °C	164.906	134.2293	109.6728	87.4286	67.3205	50.2632	37.0108	27.622	21.3861	17.0804	13.4766
	v, m^3/kg	0.0011	0.001	0.001	0.0011	0.0012	0.0013	0.0014	0.0015	0.0016	0.0016	0.0016
	h, kJ/kg	697.2866	501.7259	335.5717	190.3422	71.2191	-13.8583	-59.7316	-66.5803	-40.5911	7.0539	62.7302
	s, kJ/kg K	1.9955	1.7353	1.4377	1.1296	0.8349	0.5838	0.401	0.2965	0.2604	0.2622	0.234
8.00	T, °C	170.4483	139.76	114.9834	92.5137	72.2128	54.9911	41.5923	32.0674	25.7006	21.2667	17.5368
	v, m^3/kg	0.0011	0.001	0.001	0.0011	0.0012	0.0013	0.0014	0.0015	0.0016	0.0016	0.0016
	h, kJ/kg	721.5189	526.1835	359.2448	213.1567	93.3262	7.7131	-38.5855	-45.8366	-20.2917	26.8393	81.9174
	s, kJ/kg K	2.0502	1.7946	1.4988	1.1921	0.8991	0.6497	0.4682	0.3645	0.3283	0.3293	0.2999
9.00	T, °C	175.4715	144.7705	119.7973	97.1261	76.6525	59.2831	45.7525	36.1046	29.6195	25.0697	21.2256
	v, m^3/kg	0.0011	0.001	0.001	0.0011	0.0012	0.0013	0.0014	0.0015	0.0016	0.0016	0.0016
	h, kJ/kg	743.5672	548.4704	380.8453	233.9838	113.5011	27.3845	-19.3148	-26.9352	-1.7831	44.9062	99.4793
	s, kJ/kg K	2.0993	1.848	1.5538	1.2484	0.9568	0.7088	0.5286	0.4255	0.3893	0.3898	0.3593
10.00	T, °C	180.075	149.3606	124.2094	101.356	80.7257	63.222	49.5713	39.8112	33.2179	28.5621	24.6135
	v, m^3/kg	0.0011	0.001	0.001	0.0011	0.0012	0.0013	0.0014	0.0015	0.0016	0.0016	0.0017
	h, kJ/kg	763.8475	568.9999	400.7674	253.2019	132.1136	45.5215	-1.5571	-9.5194	15.2804	61.5835	115.7229
	s, kJ/kg K	2.1441	1.8966	1.604	1.2997	1.0093	0.7627	0.5835	0.481	0.4448	0.4448	0.4136
11.00	T, °C	184.3313	153.6031	128.2892	105.2691	84.4953	66.8683	53.1071	43.2436	36.5506	31.7971	27.752
	v, m^3/kg	0.0011	0.001	0.001	0.0011	0.0012	0.0013	0.0014	0.0015	0.0016	0.0017	0.0017
	h, kJ/kg	782.6637	588.0738	419.2989	271.0873	149.4329	62.3901	14.9513	6.6696	31.1498	77.1109	130.8725
	s, kJ/kg K	2.1851	1.9413	1.6501	1.3469	1.0577	0.8122	0.634	0.532	0.4958	0.4954	0.4637
12.00	T, °C	188.2951	157.5528	132.0889	108.9151	88.0088	70.2677	56.4041	46.4447	39.6591	34.8148	30.68
	v, m^3/kg	0.0011	0.001	0.001	0.0011	0.0012	0.0013	0.0014	0.0015	0.0016	0.0017	0.0017
	h, kJ/kg	800.2448	605.9197	436.6567	287.8481	165.6619	78.1904	30.4081	21.8267	46.0141	91.6688	145.0975
	s, kJ/kg K	2.2232	1.9827	1.6929	1.3907	1.1025	0.858	0.6807	0.5792	0.5431	0.5424	0.5102

Table A.1 Saturated liquid properties (contd.,)

P, bar	Property	Ammonia concentration (mass fraction), x										
		0	**0.1**	**0.2**	**0.3**	**0.4**	**0.5**	**0.6**	**0.7**	**0.8**	**0.9**	**1**
13.00	T, °C	192.0087	161.2522	135.6489	112.3325	91.303	73.4556	59.4965	49.4475	42.5754	37.6462	33.4277
	v, m^3/kg	0.0011	0.0011	0.001	0.0011	0.0012	0.0013	0.0014	0.0015	0.0016	0.0017	0.0017
	h, kJ/kg	816.7683	622.7136	453.0088	303.6455	180.9574	93.077	44.9663	36.1019	60.0191	105.3968	158.5291
	s, kJ/kg K	2.2586	2.0213	1.7328	1.4316	1.1443	0.9008	0.7242	0.6231	0.5871	0.5862	0.5536
14.00	T, °C	195.5055	164.7346	139.0013	115.5517	94.407	76.4601	62.4114	52.2783	45.325	40.316	36.0188
	v, m^3/kg	0.0012	0.0011	0.0011	0.0011	0.0012	0.0013	0.0014	0.0015	0.0016	0.0017	0.0017
	h, kJ/kg	832.3744	638.5949	468.4882	318.6068	195.4435	107.1718	58.7463	49.6137	73.2798	118.4051	171.2714
	s, kJ/kg K	2.2918	2.0575	1.7703	1.47	1.1836	0.9409	0.765	0.6644	0.6284	0.6274	0.5945
15.00	T, °C	198.8124	168.0273	142.1718	118.5972	97.3443	79.3037	65.1707	54.9583	47.9284	42.8442	38.4727
	v, m^3/kg	0.0012	0.0011	0.0011	0.0011	0.0012	0.0013	0.0014	0.0016	0.0016	0.0017	0.0017
	h, kJ/kg	847.1764	653.676	483.2018	332.8349	209.2199	120.573	71.8451	62.4572	85.8888	130.7825	183.4084
	s, kJ/kg K	2.323	2.0915	1.8056	1.5061	1.2206	0.9787	0.8035	0.7032	0.6674	0.6662	0.633
16.00	T, °C	201.9515	171.1521	145.1816	121.4891	100.1342	82.0051	67.7922	57.5048	50.4023	45.247	40.805
	v, m^3/kg	0.0012	0.0011	0.0011	0.0011	0.0012	0.0013	0.0014	0.0016	0.0017	0.0017	0.0017
	h, kJ/kg	861.2669	668.0487	497.2376	346.4137	222.3684	133.3609	84.3419	74.7104	97.9217	142.6018	195.0087
	s, kJ/kg K	2.3525	2.1237	1.839	1.5404	1.2556	1.0145	0.8398	0.7399	0.7042	0.7029	0.6696
17.00	T, °C	204.9411	174.1276	148.0481	124.2442	102.7925	84.5795	70.2909	59.9323	52.7609	47.5378	43.0291
	v, m^3/kg	0.0012	0.0011	0.0011	0.0011	0.0012	0.0013	0.0015	0.0016	0.0017	0.0017	0.0017
	h, kJ/kg	874.7228	681.7895	510.6683	359.4131	234.9567	145.6021	96.3023	86.4375	109.4411	153.923	206.1297
	s, kJ/kg K	2.3805	2.1543	1.8708	1.5729	1.2889	1.0485	0.8744	0.7748	0.7391	0.7378	0.7043
18.00	T, °C	207.7966	176.9689	150.786	126.8764	105.3328	87.04	72.6793	62.2528	55.0158	49.7282	45.1557
	v, m^3/kg	0.0012	0.0011	0.0011	0.0011	0.0012	0.0013	0.0015	0.0016	0.0017	0.0017	0.0018
	h, kJ/kg	887.6086	694.9625	523.5552	371.8917	247.0417	157.3522	107.7811	97.6925	120.4997	164.7968	216.8193
	s, kJ/kg K	2.4071	2.1835	1.901	1.6039	1.3206	1.0808	0.9073	0.808	0.7724	0.771	0.7374

19.00	T, °C	210.5309	179.6892	153.4079	129.3975	107.7664	89.3975	74.968	64.4767	57.1769	51.8277	47.1944
	v, m^3/kg	0.0012	0.0011	0.0011	0.0011	0.0012	0.0013	0.0015	0.0016	0.0017	0.0017	0.0018
	h, kJ/kg	899.9792	707.622	535.9502	383.8993	258.6716	168.6587	118.8251	108.5212	131.1418	175.266	227.1184
	s, kJ/kg K	2.4325	2.2113	1.9299	1.6336	1.3509	1.1117	0.9387	0.8397	0.8043	0.8028	0.7691

Table A.1 Saturated liquid properties (contd.,)

P, bar	Property	Ammonia concentration (mass fraction), x										
		0	**0.1**	**0.2**	**0.3**	**0.4**	**0.5**	**0.6**	**0.7**	**0.8**	**0.9**	**1**
20.00	T, °C	213.1526	182.2971	155.9219	131.8155	110.1008	91.6592	77.1638	66.6106	59.2508	53.8427	49.1511
	v, m^3/kg	0.0012	0.0011	0.0011	0.0011	0.0012	0.0014	0.0015	0.0016	0.0017	0.0018	0.0018
	h, kJ/kg	911.8698	719.8028	547.886	395.467	269.8767	179.5513	129.4635	118.9524	141.3956	185.3576	237.0522
	s, kJ/kg K	2.4568	2.2378	1.9575	1.662	1.3799	1.1413	0.9687	0.87	0.8347	0.8332	0.7995
21.00	T, °C	215.6791	184.8099	158.3446	134.1461	112.3513	93.8399	79.2813	68.6684	61.251	55.7862	51.0386
	v, m^3/kg	0.0012	0.0011	0.0011	0.0011	0.0012	0.0014	0.0015	0.0016	0.0017	0.0018	0.0018
	h, kJ/kg	923.356	731.5809	559.4364	406.6659	280.7257	190.097	139.7622	129.0506	151.324	195.1328	246.6803
	s, kJ/kg K	2.4801	2.2634	1.9841	1.6892	1.4078	1.1698	0.9976	0.8992	0.864	0.8625	0.8287
22.00	T, °C	218.111	187.2282	160.6767	136.39	114.5183	95.94	81.3207	70.6506	63.1777	57.6585	52.8571
	v, m^3/kg	0.0012	0.0011	0.0011	0.0012	0.0012	0.0014	0.0015	0.0016	0.0017	0.0018	0.0018
	h, kJ/kg	934.438	742.9556	570.5995	417.4938	291.2167	200.294	149.7196	138.8143	160.9254	204.5896	255.9998
	s, kJ/kg K	2.5025	2.2879	2.0097	1.7155	1.4346	1.1971	1.0254	0.9272	0.8921	0.8906	0.8569
23.00	T, °C	220.4582	189.562	162.9276	138.5562	116.6107	97.9679	83.2901	72.565	65.0387	59.467	54.6138
	v, m^3/kg	0.0012	0.0011	0.0011	0.0012	0.0013	0.0014	0.0015	0.0016	0.0017	0.0018	0.0018
	h, kJ/kg	945.1584	753.9694	581.4164	427.9902	301.3878	210.1798	159.3722	148.2795	170.2349	213.762	265.0435
	s, kJ/kg K	2.524	2.3115	2.0343	1.7408	1.4605	1.2234	1.0521	0.9542	0.9192	0.9177	0.884

24.00	T, °C	222.7272	191.8176	165.1035	140.6506	118.6339	99.929	85.1949	74.4166	66.8389	61.2166	56.3135
	v, m^3/kg	0.0012	0.0011	0.0011	0.0012	0.0013	0.0014	0.0015	0.0016	0.0017	0.0018	0.0018
	h, kJ/kg	955.5445	764.6494	591.913	438.1797	311.2628	219.7775	168.7432	157.4686	179.2744	222.6713	273.8318
	s, kJ/kg K	2.5448	2.3343	2.0581	1.7652	1.4854	1.2489	1.0779	0.9802	0.9453	0.9439	0.9102
25.00	T, °C	224.9236	194.0009	167.2099	142.6784	120.5931	101.8283	87.0398	76.2101	68.5827	62.9115	57.9601
	v, m^3/kg	0.0012	0.0011	0.0011	0.0012	0.0013	0.0014	0.0015	0.0016	0.0017	0.0018	0.0018
	h, kJ/kg	965.6203	775.0197	602.1122	448.0845	320.8632	229.1081	177.8528	166.4016	188.0634	231.3362	282.3828
	s, kJ/kg K	2.5648	2.3563	2.081	1.7888	1.5096	1.2734	1.1028	1.0054	0.9706	0.9692	0.9355
26.00	T, °C	227.0527	196.1169	169.2516	144.6443	122.4928	103.67	88.8289	77.9495	70.274	64.5556	59.5574
	v, m^3/kg	0.0012	0.0011	0.0011	0.0012	0.0013	0.0014	0.0015	0.0016	0.0017	0.0018	0.0018
	h, kJ/kg	975.4074	785.1015	612.0343	457.7238	330.2076	238.1899	186.7191	175.0964	196.6193	239.7737	290.7126
	s, kJ/kg K	2.5841	2.3776	2.1033	1.8116	1.5329	1.2972	1.127	1.0298	0.9951	0.9937	0.96

Table A.1 Saturated liquid properties (contd.,)

P, bar	Property	Ammonia concentration (mass fraction), x										
		0	**0.1**	**0.2**	**0.3**	**0.4**	**0.5**	**0.6**	**0.7**	**0.8**	**0.9**	**1**
27.00	T, °C	229.1188	198.1702	171.2331	146.5525	124.3368	105.458	90.5659	79.6385	71.9163	66.1521	61.1087
	v, m^3/kg	0.0012	0.0011	0.0011	0.0012	0.0013	0.0014	0.0015	0.0016	0.0017	0.0018	0.0018
	h, kJ/kg	984.925	794.914	621.6977	467.1154	339.3131	247.0395	195.3585	183.5688	204.9576	247.9988	298.8356
	s, kJ/kg K	2.6029	2.3983	2.1248	1.8338	1.5556	1.3203	1.1504	1.0534	1.0188	1.0175	0.9839
28.00	T, °C	231.1261	200.1648	173.1582	148.4066	126.1289	107.1957	92.2542	81.2802	73.5128	67.7042	62.617
	v, m^3/kg	0.0012	0.0011	0.0011	0.0012	0.0013	0.0014	0.0015	0.0016	0.0018	0.0018	0.0019
	h, kJ/kg	994.1904	804.4744	631.1189	476.2748	348.1949	255.6717	203.7853	191.8331	213.0922	256.0248	306.7649
	s, kJ/kg K	2.6211	2.4183	2.1457	1.8553	1.5775	1.3427	1.1731	1.0763	1.0418	1.0406	1.007

29.00	T, °C	233.0784	202.1044	175.0305	150.2101	127.8722	108.8863	93.8969	82.8776	75.0663	69.2146	64.0848
	v, m^3/kg	0.0012	0.0011	0.0011	0.0012	0.0013	0.0014	0.0015	0.0017	0.0018	0.0018	0.0019
	h, kJ/kg	1003.2192	813.7981	640.3125	485.2163	356.8666	264.0998	212.0128	199.9021	221.0356	263.8641	314.5122
	s, kJ/kg K	2.6387	2.4377	2.166	1.8761	1.5989	1.3644	1.1951	1.0985	1.0642	1.063	1.0294
30.00	T, °C	234.9788	203.9924	176.8531	151.966	129.5697	110.5326	95.4966	84.4333	76.5795	70.6859	65.5147
	v, m^3/kg	0.0012	0.0011	0.0011	0.0012	0.0013	0.0014	0.0015	0.0017	0.0018	0.0018	0.0019
	h, kJ/kg	1012.0256	822.8993	649.2922	493.9528	365.3407	272.3361	220.0528	207.7875	228.7992	271.5277	322.088
	s, kJ/kg K	2.6558	2.4566	2.1858	1.8965	1.6197	1.3856	1.2165	1.1202	1.0859	1.0848	1.0513
31.00	T, °C	236.8305	205.8318	178.629	153.6771	131.2241	112.1373	97.056	85.9499	78.0545	72.1202	66.9088
	v, m^3/kg	0.0012	0.0011	0.0011	0.0012	0.0013	0.0014	0.0015	0.0017	0.0018	0.0019	0.0019
	h, kJ/kg	1020.6223	831.7907	658.07	502.4959	373.6285	280.3914	227.9162	215.4999	236.3934	279.0255	329.5022
	s, kJ/kg K	2.6725	2.4749	2.205	1.9162	1.6399	1.4062	1.2374	1.1412	1.1071	1.106	1.0726
32.00	T, °C	238.6363	207.6254	180.3608	155.346	132.8377	113.7025	98.5771	87.4294	79.4937	73.5197	68.2691
	v, m^3/kg	0.0012	0.0011	0.0011	0.0012	0.0013	0.0014	0.0015	0.0017	0.0018	0.0019	0.0019
	h, kJ/kg	1029.0211	840.484	666.6572	510.8563	381.7402	288.2759	235.6127	223.0489	243.8276	286.3667	336.7634
	s, kJ/kg K	2.6887	2.4928	2.2237	1.9355	1.6596	1.4262	1.2577	1.1618	1.1277	1.1267	1.0934
33.00	T, °C	240.3985	209.3756	182.051	156.9749	134.4129	115.2306	100.0622	88.8739	80.8989	74.8863	69.5975
	v, m^3/kg	0.0012	0.0011	0.0011	0.0012	0.0013	0.0014	0.0015	0.0017	0.0018	0.0019	0.0019
	h, kJ/kg	1037.2327	848.9897	675.0639	519.0437	389.6853	295.9986	243.1513	230.4434	251.1103	293.5598	343.8798
	s, kJ/kg K	2.7044	2.5102	2.2419	1.9543	1.6788	1.4458	1.2776	1.1818	1.1478	1.1468	1.1136

Table A.1 Saturated liquid properties (contd.,)

P, bar	Property	Ammonia concentration (mass fraction), x										
		0	**0.1**	**0.2**	**0.3**	**0.4**	**0.5**	**0.6**	**0.7**	**0.8**	**0.9**	**1**
34.00	T, °C	242.1197	211.0848	183.7017	158.5659	135.9516	116.7234	101.5132	90.2853	82.2719	76.2216	70.8957
	v, m^3/kg	0.0012	0.0011	0.0011	0.0012	0.0013	0.0014	0.0016	0.0017	0.0018	0.0019	0.0019
	h, kJ/kg	1045.267	857.3178	683.2995	527.0671	397.4724	303.5681	250.5403	237.6913	258.2495	300.6123	350.8589
	s, kJ/kg K	2.7198	2.5272	2.2598	1.9726	1.6975	1.4649	1.2969	1.2013	1.1674	1.1665	1.1334
35.00	T, °C	243.8018	212.7552	185.3151	160.1211	137.4558	118.1827	102.9317	91.6652	83.6144	77.5274	72.1651
	v, m^3/kg	0.0012	0.0011	0.0011	0.0012	0.0013	0.0014	0.0016	0.0017	0.0018	0.0019	0.0019
	h, kJ/kg	1053.1329	865.4771	691.3726	534.9348	405.1095	310.992	257.7873	244.8002	265.2524	307.5313	357.7073
	s, kJ/kg K	2.7348	2.5438	2.2771	1.9906	1.7159	1.4835	1.3158	1.2203	1.1866	1.1858	1.1527
36.00	T, °C	245.4469	214.3886	186.8929	161.6422	138.9271	119.6103	104.3194	93.0153	84.9279	78.805	73.4073
	v, m^3/kg	0.0012	0.0011	0.0011	0.0012	0.0013	0.0014	0.0016	0.0017	0.0018	0.0019	0.0019
	h, kJ/kg	1060.8387	873.476	699.2912	542.6542	412.6039	318.2775	264.8992	251.7768	272.1257	314.3233	364.4315
	s, kJ/kg K	2.7495	2.56	2.2941	2.0081	1.7338	1.5017	1.3343	1.239	1.2053	1.2046	1.1716
37.00	T, °C	247.0568	215.9869	188.4369	163.1309	140.3672	121.0077	105.6779	94.3369	86.2138	80.0558	74.6235
	v, m^3/kg	0.0012	0.0012	0.0012	0.0012	0.0013	0.0014	0.0016	0.0017	0.0018	0.0019	0.0019
	h, kJ/kg	1068.3923	881.3221	707.0625	550.2326	419.9623	325.4312	271.8825	258.6275	278.8756	320.9944	371.0372
	s, kJ/kg K	2.7638	2.5758	2.3108	2.0252	1.7513	1.5195	1.3523	1.2572	1.2236	1.2229	1.19
38.00	T, °C	248.633	217.5517	189.9487	164.5887	141.7776	122.3763	107.0084	95.6314	87.4734	81.2811	75.815
	v, m^3/kg	0.0012	0.0012	0.0012	0.0012	0.0013	0.0014	0.0016	0.0017	0.0018	0.0019	0.0019
	h, kJ/kg	1075.8006	889.0226	714.6933	557.6762	427.1911	332.4592	278.7432	265.3581	285.5078	327.55	377.5298
	s, kJ/kg K	2.7777	2.5913	2.327	2.0419	1.7684	1.537	1.37	1.275	1.2415	1.2409	1.2081
39.00	T, °C	250.1773	219.0847	191.4299	166.017	143.1595	123.7174	108.3123	96.9	88.708	82.4821	76.9829
	v, m^3/kg	0.0013	0.0012	0.0012	0.0012	0.0013	0.0014	0.0016	0.0017	0.0018	0.0019	0.0019
	h, kJ/kg	1083.0704	896.5839	722.1901	564.9912	434.2959	339.3671	285.4867	271.9741	292.0275	333.9954	383.9144
	s, kJ/kg K	2.7914	2.6065	2.3429	2.0583	1.7852	1.554	1.3873	1.2924	1.2591	1.2586	1.2258

40.00	T, °C	251.691	220.5872	192.8817	167.4173	144.5143	125.0323	109.5907	98.144	89.9185	83.6598	78.1282
	v, m^3/kg	0.0013	0.0012	0.0012	0.0012	0.0013	0.0014	0.0016	0.0017	0.0018	0.0019	0.002
	h, kJ/kg	1090.2077	904.0123	729.5585	572.1832	441.2824	346.1601	292.1183	278.4804	298.4398	340.3354	390.1956
	s, kJ/kg K	2.8048	2.6213	2.3585	2.0744	1.8016	1.5708	1.4042	1.3095	1.2763	1.2758	1.2432

Table A.1 Saturated liquid properties (contd.,)

P, bar	Property	Ammonia concentration (mass fraction), x										
		0	**0.1**	**0.2**	**0.3**	**0.4**	**0.5**	**0.6**	**0.7**	**0.8**	**0.9**	**1**
41.00	T, °C	253.1755	222.0606	194.3055	168.7906	145.8432	126.3221	110.8448	99.3644	91.1061	84.8153	79.2519
	v, m^3/kg	0.0013	0.0012	0.0012	0.0012	0.0013	0.0015	0.0016	0.0017	0.0018	0.0019	0.002
	h, kJ/kg	1097.2184	911.3134	736.8042	579.2575	448.1554	352.8433	298.6427	284.8819	304.7492	346.5744	396.3777
	s, kJ/kg K	2.8179	2.6358	2.3738	2.0902	1.8177	1.5872	1.4208	1.3263	1.2931	1.2927	1.2602
42.00	T, °C	254.632	223.5061	195.7025	170.1381	147.1473	127.5879	112.0756	100.5621	92.2718	85.9495	80.355
	v, m^3/kg	0.0013	0.0012	0.0012	0.0012	0.0013	0.0015	0.0016	0.0017	0.0018	0.0019	0.002
	h, kJ/kg	1104.1076	918.4925	743.9322	586.2188	454.9198	359.4211	305.0645	291.1828	310.96	352.7167	402.4649
	s, kJ/kg K	2.8307	2.6501	2.3888	2.1056	1.8335	1.6032	1.4371	1.3427	1.3096	1.3093	1.2769
43.00	T, °C	256.0618	224.925	197.0739	171.461	148.4276	128.8307	113.2841	101.7382	93.4164	87.0633	81.4383
	v, m^3/kg	0.0013	0.0012	0.0012	0.0012	0.0013	0.0015	0.0016	0.0017	0.0018	0.0019	0.002
	h, kJ/kg	1110.8805	925.5547	750.9473	593.0718	461.5798	365.8979	311.3877	297.3873	317.0762	358.766	408.4609
	s, kJ/kg K	2.8433	2.664	2.4035	2.1208	1.849	1.619	1.4531	1.3588	1.3258	1.3256	1.2933
44.00	T, °C	257.4658	226.3183	198.4206	172.7603	149.6851	130.0514	114.4712	102.8934	94.5409	88.1574	82.5027
	v, m^3/kg	0.0013	0.0012	0.0012	0.0012	0.0013	0.0015	0.0016	0.0017	0.0019	0.0019	0.002
	h, kJ/kg	1117.5417	932.5046	757.8539	599.8208	468.1397	372.2777	317.6163	303.4993	323.1016	364.7262	414.3692
	s, kJ/kg K	2.8556	2.6777	2.4179	2.1357	1.8643	1.6345	1.4688	1.3746	1.3417	1.3416	1.3094
45.00	T, °C	258.8452	227.687	199.7436	174.0368	150.9207	131.2509	115.6377	104.0288	95.6459	89.2328	83.5487
	v, m^3/kg	0.0013	0.0012	0.0012	0.0012	0.0013	0.0015	0.0016	0.0017	0.0019	0.0019	0.002
	h, kJ/kg	1124.0956	939.3466	764.6563	606.4697	474.6033	378.5641	323.754	309.5222	329.0396	370.6006	420.1933
	s, kJ/kg K	2.8677	2.6912	2.432	2.1503	1.8792	1.6497	1.4842	1.3902	1.3574	1.3573	1.3251

46.00	T, °C	260.2009	229.0321	201.0439	175.2915	152.1352	132.43	116.7845	105.1449	96.7324	90.2901	84.5773
	v, m^3/kg	0.0013	0.0012	0.0012	0.0012	0.0013	0.0015	0.0016	0.0017	0.0019	0.002	0.002
	h, kJ/kg	1130.5463	946.0848	771.3584	613.0223	480.9742	384.7608	329.8042	315.4595	334.8937	376.3924	425.9362
	s, kJ/kg K	2.8796	2.7044	2.4459	2.1646	1.8939	1.6646	1.4993	1.4054	1.3727	1.3727	1.3407
47.00	T, °C	261.5338	230.3545	202.3224	176.5252	153.3295	133.5895	117.9123	106.2426	97.8009	91.33	85.5889
	v, m^3/kg	0.0013	0.0012	0.0012	0.0012	0.0014	0.0015	0.0016	0.0018	0.0019	0.002	0.002
	h, kJ/kg	1136.8977	952.723	777.9639	619.4822	487.2558	390.8711	335.7702	321.3143	340.6668	382.1047	431.6008
	s, kJ/kg K	2.8913	2.7174	2.4596	2.1787	1.9083	1.6793	1.5142	1.4204	1.3878	1.3879	1.3559

Table A.1 Saturated liquid properties (contd.,)

P, bar	Property	Ammonia concentration (mass fraction), x										
		0	**0.1**	**0.2**	**0.3**	**0.4**	**0.5**	**0.6**	**0.7**	**0.8**	**0.9**	**1**
48.00	T, °C	262.8448	231.6551	203.5798	177.7387	154.5043	134.7302	119.0217	107.3225	98.8522	92.3532	86.5843
	v, m^3/kg	0.0013	0.0012	0.0012	0.0013	0.0014	0.0015	0.0016	0.0018	0.0019	0.002	0.002
	h, kJ/kg	1143.1535	959.2649	784.4763	625.8528	493.4515	396.898	341.6551	327.0897	346.3619	387.7404	437.1901
	s, kJ/kg K	2.9027	2.7301	2.473	2.1926	1.9225	1.6938	1.5288	1.4352	1.4026	1.4028	1.3709
49.00	T, °C	264.1346	232.9347	204.817	178.9327	155.6603	135.8526	120.1135	108.3852	99.8868	93.3602	87.5641
	v, m^3/kg	0.0013	0.0012	0.0012	0.0013	0.0014	0.0015	0.0016	0.0018	0.0019	0.002	0.002
	h, kJ/kg	1149.317	965.714	790.8988	632.1371	499.5641	402.8446	347.4616	332.7885	351.9818	393.3021	442.7066
	s, kJ/kg K	2.914	2.7426	2.4862	2.2062	1.9365	1.7079	1.5431	1.4497	1.4172	1.4174	1.3857
50.00	T, °C	265.404	234.1939	206.0346	180.108	156.7982	136.9576	121.1883	109.4315	100.9054	94.3516	88.5287
	v, m^3/kg	0.0013	0.0012	0.0012	0.0013	0.0014	0.0015	0.0016	0.0018	0.0019	0.002	0.002
	h, kJ/kg	1155.3916	972.0734	797.2347	638.3382	505.5966	408.7135	353.1925	338.4133	357.5291	398.7923	448.1528
	s, kJ/kg K	2.925	2.7549	2.4992	2.2197	1.9502	1.7219	1.5573	1.4639	1.4315	1.4319	1.4002

51.00	T, °C	266.6538	235.4336	207.2334	181.2651	157.9187	138.0456	122.2467	110.4618	101.9085	95.328	89.4788
	v, m^3/kg	0.0013	0.0012	0.0012	0.0013	0.0014	0.0015	0.0016	0.0018	0.0019	0.002	0.002
	h, kJ/kg	1161.3803	978.3463	803.4868	644.4588	511.5516	414.5076	358.8504	343.9666	363.0062	404.2136	453.5311
	s, kJ/kg K	2.9359	2.7671	2.512	2.2329	1.9637	1.7357	1.5712	1.478	1.4457	1.4461	1.4145
52.00	T, °C	267.8847	236.6545	208.414	182.4048	159.0223	139.1173	123.2892	111.4768	102.8967	96.2899	90.4148
	v, m^3/kg	0.001	0.001	0.001	0.001	0.001	0.002	0.002	0.002	0.002	0.002	0.002
	h, kJ/kg	1167.286	984.536	809.658	650.502	517.432	420.229	364.438	349.451	368.416	409.5681	458.8436
	s, kJ/kg K	2.9466	2.779	2.525	2.246	1.977	1.749	1.585	1.492	1.460	1.46	1.4286
53.00	T, °C	269.0972	237.8571	209.577	183.528	160.110	140.173	124.317	112.477	103.870	97.2378	91.3372
	v, m^3/kg	0.0013	0.0012	0.001	0.001	0.001	0.002	0.002	0.002	0.002	0.002	0.002
	h, kJ/kg	1173.1115	990.6438	815.751	656.469	523.240	425.881	369.957	354.868	373.759	414.8581	464.0925
	s, kJ/kg K	2.9571	2.7907	2.537	2.259	1.990	1.763	1.598	1.505	1.473	1.4738	1.4424
54.00	T, °C	270.292	239.042	210.723	184.634	161.181	141.214	125.329	113.463	104.830	98.1722	92.2465
	v, m^3/kg	0.001	0.001	0.0012	0.0013	0.0014	0.0015	0.0016	0.0018	0.0019	0.002	0.002
	h, kJ/kg	1178.859	996.674	821.77	662.3642	528.9773	431.4642	375.4098	360.2209	379.0393	420.0855	469.2797
	s, kJ/kg K	2.967	2.802	2.549	2.271	2.003	1.776	1.612	1.519	1.4867	1.4873	1.4561

Table A.2 Saturated vapour properties

P, bar	Property	Ammonia concentration (mass fraction), x										
		0	**0.1**	**0.2**	**0.3**	**0.4**	**0.5**	**0.6**	**0.7**	**0.8**	**0.9**	**1**
0.15	T, °C	53.968	51.201	48.798	46.525	44.114	41.244	37.510	32.362	24.9391	13.4007	-57.9271
	v, m^3/kg	10.019	9.997	9.984	9.974	9.959	9.928	9.867	9.759	9.5744	9.2536	6.9565
	h, kJ/kg	2598.768	2468.652	2340.548	2214.000	2088.457	1963.238	1837.467	1709.952	1578.8422	1440.2617	1179.6958
	s, kJ/kg K	8.010	8.023	7.961	7.868	7.751	7.612	7.448	7.257	7.0283	6.741	5.8815

0.20	T, °C	60.193	57.357	54.808	52.340	49.721	46.664	42.808	37.647	30.3592	19.0478	-54.447
	v, m^3/kg	7.650	7.633	7.621	7.610	7.595	7.568	7.521	7.441	7.307	7.073	5.2933
	h, kJ/kg	2609.716	2479.674	2351.486	2224.747	2098.969	1973.544	1847.683	1720.284	1589.5729	1451.5394	1185.7827
	s, kJ/kg K	7.911	7.923	7.861	7.767	7.648	7.508	7.344	7.153	6.9254	6.6407	5.7702
0.30	T, °C	69.3371	66.4016	63.6438	60.8988	57.9735	54.6307	50.56	45.3114	38.1033	26.9493	-49.2238
	v, m^3/kg	0.00	5.22	5.2091	5.199	5.1853	5.1641	5.1304	5.0767	4.9901	4.8378	3.6028
	h, kJ/kg	290.52	2495.66	2367.3823	2240.395	2114.2921	1988.5576	1862.5084	1735.155	1604.802	1467.2263	1194.7061
	s, kJ/kg K	0.95	7.78	7.7203	7.6246	7.5046	7.3625	7.1974	7.0059	6.7799	6.4975	5.6145
0.40	T, °C	76.13	73.12	70.2154	67.2707	64.1212	60.5592	56.3065	50.9456	43.715	32.5575	-45.249
	v, m^3/kg	3.99	3.99	3.9773	3.9682	3.956	3.9383	3.9116	3.8707	3.8062	3.6926	2.743
	h, kJ/kg	2637.16	2507.3644	2379.0397	2251.8949	2125.5691	1999.604	1873.3814	1745.9783	1615.7373	1478.2633	1201.3159
	s, kJ/kg K	7.6737	7.6855	7.6212	7.5245	7.4033	7.26	7.094	6.9021	6.6764	6.3948	5.5051
0.50	T, °C	81.6007	78.5316	75.5084	72.4071	69.0795	65.3384	60.9274	55.4506	48.1577	36.9315	-41.9895
	v, m^3/kg	3.2406	3.2336	3.2266	3.2183	3.2074	3.1921	3.1697	3.1364	3.0847	2.9936	2.2205
	h, kJ/kg	2646.3487	2516.654	2388.3122	2261.0586	2134.567	2008.419	1882.0409	1754.5539	1624.3195	1486.7963	1206.6144
	s, kJ/kg K	7.5978	7.6094	7.5447	7.4472	7.3251	7.1809	7.0142	6.8218	6.5961	6.3148	5.4209
0.60	T, °C	86.2087	83.0901	79.9712	76.741	73.2652	69.3716	64.8202	59.2302	51.8571	40.532	-39.2006
	v, m^3/kg	2.7319	2.726	2.7198	2.7123	2.7025	2.6888	2.6695	2.6412	2.5979	2.5215	1.8685
	h, kJ/kg	2653.9827	2524.3853	2396.0416	2268.7092	2142.088	2015.7892	1889.2717	1761.6875	1631.4068	1493.7602	1211.0574
	s, kJ/kg K	7.5359	7.5475	7.4824	7.3843	7.2616	7.1166	6.9492	6.7564	6.5306	6.2492	5.3526
0.70	T, °C	90.2091	87.0478	83.8477	80.5077	76.9046	72.878	68.2001	62.5013	55.04	43.6014	-36.7481
	v, m^3/kg	2.3646	2.3596	2.3541	2.3472	2.3382	2.3259	2.3088	2.2841	2.2466	2.1806	1.615
	h, kJ/kg	2660.5263	2531.0205	2402.6847	2275.2939	2148.568	2022.1414	1895.498	1767.8122	1637.4565	1499.6469	1214.8937
	s, kJ/kg K	7.4838	7.4953	7.4299	7.3314	7.2081	7.0625	6.8946	6.7013	6.4752	6.1935	5.2951

Table A.2 Saturated vapour properties (contd.,)

P, bar	Property	Ammonia concentration (mass fraction), x										
		0	**0.1**	**0.2**	**0.3**	**0.4**	**0.5**	**0.6**	**0.7**	**0.8**	**0.9**	**1**
0.80	T, °C	93.7556	90.5568	87.286	83.8505	80.1358	75.9908	71.1975	65.3948	57.8419	46.2828	-34.5497
	v, m^3/kg	2.0866	2.0823	2.0773	2.071	2.0627	2.0515	2.036	2.014	1.9809	1.9226	1.4234
	h, kJ/kg	2666.2584	2536.8399	2408.5187	2281.0837	2154.2714	2027.7347	1900.9767	1773.1888	1642.7416	1504.7473	1218.2747
	s, kJ/kg K	7.4387	7.4502	7.3845	7.2857	7.1619	7.0158	6.8473	6.6537	6.4273	6.1452	5.2456
0.90	T, °C	96.9492	93.7168	90.3835	86.8633	83.0489	78.7972	73.8977	67.9959	60.3505	48.668	-32.5509
	v, m^3/kg	1.8687	1.8649	1.8603	1.8545	1.8468	1.8365	1.8223	1.8025	1.7728	1.7204	1.2734
	h, kJ/kg	2671.3617	2542.0267	2413.7247	2286.2565	2159.3717	2032.7384	1905.8755	1777.9869	1647.4389	1509.248	1221.3001
	s, kJ/kg K	7.399	7.4105	7.3447	7.2455	7.1213	6.9747	6.8058	6.6118	6.385	6.1026	5.2021
1.00	T, °C	99.8596	96.5968	93.2074	89.6111	85.7068	81.3576	76.3596	70.3633	62.6258	50.8193	-30.7137
	v, m^3/kg	1.6931	1.6898	1.6855	1.6801	1.6729	1.6633	1.6503	1.6322	1.6051	1.5576	1.1526
	h, kJ/kg	2675.9624	2546.7077	2418.4284	2290.9351	2163.9888	2037.27	1910.3103	1782.3234	1651.6693	1513.2757	1224.0392
	s, kJ/kg K	7.3635	7.375	7.309	7.2096	7.0851	6.9381	6.7688	6.5744	6.3473	6.0644	5.1634
2.00	T, °C	120.3808	116.91	113.1475	109.043	104.5262	99.4913	93.7622	87.0047	78.4434	65.5011	-17.3582
	v, m^3/kg	0.8844	0.883	0.8807	0.8775	0.8731	0.8673	0.8598	0.8495	0.8346	0.8086	0.5984
	h, kJ/kg	2706.8909	2578.3246	2450.3506	2322.829	2195.5769	2068.3342	1940.6873	1811.8728	1680.1512	1539.783	1242.675
	s, kJ/kg K	7.131	7.1429	7.0763	6.9755	6.849	6.6996	6.5275	6.3301	6.0999	5.8122	4.912
3.00	T, °C	133.6085	130.0093	126.0254	121.6175	116.7259	111.2537	105.0302	97.7154	88.4963	74.6323	-8.4068
	v, m^3/kg	0.6046	0.6037	0.6022	0.5999	0.5968	0.5926	0.5871	0.5796	0.569	0.5504	0.4075
	h, kJ/kg	2725.2257	2597.2271	2469.5901	2342.1922	2214.8688	2087.3756	1959.306	1829.8763	1697.2382	1555.1841	1253.7852
	s, kJ/kg K	6.9953	7.0076	6.9411	6.8399	6.7124	6.5617	6.388	6.1887	5.9559	5.6641	4.7675
4.00	T, °C	143.602	139.9086	135.7662	131.1403	125.9753	120.1769	113.5726	105.8122	96.0478	81.4144	-1.4854
	v, m^3/kg	0.4613	0.4608	0.4597	0.4579	0.4554	0.4521	0.4477	0.4418	0.4333	0.4186	0.3099
	h, kJ/kg	2738.1208	2610.6216	2483.3159	2356.0879	2228.7792	2101.1483	1972.7817	1842.8647	1709.4471	1565.9459	1261.5174
	s, kJ/kg K	6.8988	6.9117	6.8453	6.7439	6.616	6.4645	6.2897	6.0888	5.8539	5.5586	4.6661

5.00	T, °C	151.7241	147.956	143.6898	138.8932	133.512	127.4512	120.5346	112.3999	102.1674	86.8714	4.2321
	v, m^3/kg	0.3738	0.3735	0.3727	0.3712	0.3692	0.3664	0.3627	0.3578	0.3507	0.3383	0.2504
	h, kJ/kg	2747.9378	2620.892	2493.9055	2366.8653	2239.6133	2111.905	1983.3149	1852.9939	1718.8974	1574.1216	1267.2806
	s, kJ/kg K	6.8236	6.837	6.7709	6.6695	6.5413	6.3893	6.2136	6.0116	5.7748	5.4764	4.5881

Table A.2 Saturated vapour properties (contd.,)

P, bar	Property	Ammonia concentration (mass fraction), x										
		0	**0.1**	**0.2**	**0.3**	**0.4**	**0.5**	**0.6**	**0.7**	**0.8**	**0.9**	**1**
6.00	T, °C	158.6118	154.7816	150.4137	145.4767	139.916	133.6349	126.4519	117.9929	107.3488	91.4687	9.1412
	v, m^3/kg	0.3147	0.3145	0.3139	0.3127	0.3109	0.3085	0.3054	0.3011	0.2949	0.2842	0.2102
	h, kJ/kg	2755.7647	2629.1382	2502.4587	2375.613	2248.4412	2120.6927	1991.927	1861.2606	1726.5601	1580.638	1271.737
	s, kJ/kg K	6.762	6.7758	6.71	6.6086	6.4803	6.3279	6.1516	5.9485	5.7102	5.4091	4.5247
7.00	T, °C	164.6182	160.7347	156.2804	151.2239	145.5096	139.0381	131.6221	122.8757	111.8631	95.4593	13.4647
	v, m^3/kg	0.272	0.2719	0.2714	0.2703	0.2688	0.2667	0.2639	0.2601	0.2547	0.2451	0.0016
	h, kJ/kg	2762.1967	2635.9628	2509.5787	2382.9296	2255.8521	2128.0878	1999.1803	1868.2116	1732.965	1585.9954	62.6743
	s, kJ/kg K	6.7095	6.7238	6.6583	6.5571	6.4287	6.276	6.0991	5.8951	5.6555	5.3519	0.2338
8.00	T, °C	169.9605	166.0302	161.5009	156.3404	150.4916	143.8519	136.2284	127.2234	115.8765	98.9967	17.342
	v, m^3/kg	0.2396	0.2396	0.2392	0.2383	0.237	0.2351	0.2326	0.2292	0.2242	0.2156	0.1592
	h, kJ/kg	2767.5957	2641.7329	2515.6335	2389.1807	2262.2063	2134.4434	2005.4191	1874.1811	1738.4343	1590.4955	1278.0603
	s, kJ/kg K	6.6639	6.6786	6.6134	6.5123	6.3839	6.231	6.0537	5.8489	5.608	5.3023	4.4257
9.00	T, °C	174.7828	170.8108	166.2151	160.9624	154.9939	148.2035	140.3924	131.152	119.4985	102.1817	20.8664
	v, m^3/kg	0.2143	0.2143	0.2139	0.2131	0.2119	0.2103	0.208	0.2049	0.2004	0.1924	0.142
	h, kJ/kg	2772.1992	2646.6892	2520.8651	2394.6069	2267.7413	2139.9922	2010.87	1879.3892	1743.1794	1594.3348	1280.3048
	s, kJ/kg K	6.6234	6.6386	6.5737	6.4727	6.3443	6.1912	6.0135	5.8081	5.566	5.2583	4.3856

10.00	T, °C	179.1857	175.176	170.5207	165.1853	159.1088	152.1817	144.1994	134.7424	122.8053	105.0841	24.1038
	v, m^3/kg	0.1938	0.1939	0.1936	0.1929	0.1918	0.1903	0.1882	0.1853	0.1811	0.1738	0.1281
	h, kJ/kg	2776.1711	2650.9985	2525.4409	2399.3751	2272.622	2144.8961	2015.6909	1883.9885	1747.3465	1597.6487	1282.0934
	s, kJ/kg K	6.5869	6.6026	6.538	6.4372	6.3088	6.1556	5.9776	5.7715	5.5284	5.2188	4.3499
11.00	T, °C	183.2425	179.1985	174.4891	169.0786	162.9037	155.8514	147.7113	138.0535	125.8524	107.7543	27.1027
	v, m^3/kg	0.177	0.177	0.1768	0.1762	0.1752	0.1738	0.1719	0.1692	0.1653	0.1585	0.1166
	h, kJ/kg	2779.6296	2654.7811	2529.4822	2403.606	2276.9678	2149.2722	2019.996	1888.0896	1751.0412	1600.5343	1283.5027
	s, kJ/kg K	6.5538	6.5699	6.5055	6.405	6.2766	6.1233	5.945	5.7384	5.4943	5.1829	4.3178
12.00	T, °C	187.0084	182.9328	178.174	172.6947	166.4293	159.2615	150.9749	141.1299	128.6815	110.23	29.8998
	v, m^3/kg	0.1628	0.1629	0.1627	0.1622	0.1613	0.16	0.1582	0.1557	0.152	0.1457	0.107
	h, kJ/kg	2782.663	2658.1267	2533.0793	2407.39	2280.868	2153.2082	2023.8708	1891.7751	1754.3423	1603.0638	1284.5905
	s, kJ/kg K	6.5234	6.5398	6.4758	6.3755	6.2472	6.0938	5.9152	5.7081	5.4631	5.1501	4.2888

Table A.2 Saturated vapour properties (contd.,)

P, bar	Property	Ammonia concentration (mass fraction), x										
		0	**0.1**	**0.2**	**0.3**	**0.4**	**0.5**	**0.6**	**0.7**	**0.8**	**0.9**	**1**
13.00	T, °C	190.526	186.4211	181.6167	176.0739	169.7249	162.4497	154.0263	144.0057	131.3245	112.5404	32.5236
	v, m^3/kg	0.1508	0.1509	0.1508	0.1503	0.1494	0.1482	0.1465	0.1442	0.1408	0.1347	0.0988
	h, kJ/kg	2785.3386	2661.104	2536.3015	2410.7963	2284.3912	2156.7716	2027.3811	1895.1085	1757.3104	1605.2925	1285.4014
	s, kJ/kg K	6.4953	6.5121	6.4484	6.3482	6.22	6.0666	5.8878	5.6802	5.4344	5.1197	4.2623
14.00	T, °C	193.8288	189.6967	184.8501	179.2483	172.8214	165.4458	156.8942	146.7081	133.8069	114.7081	34.9968
	v, m^3/kg	0.1405	0.1406	0.1405	0.14	0.1392	0.1381	0.1365	0.1343	0.1311	0.1254	0.0918
	h, kJ/kg	2787.7092	2663.767	2539.2033	2413.8791	2287.5913	2160.0154	2030.5785	1898.1399	1759.9927	1607.2633	1285.9706
	s, kJ/kg K	6.4691	6.4863	6.4229	6.3229	6.1948	6.0413	5.8623	5.6543	5.4077	5.0916	4.2379

15.00	T, °C	196.9441	192.7865	187.9004	182.2437	175.7438	168.274	159.6015	149.2589	136.1489	116.7515	37.3378
	v, m^3/kg	0.1315	0.1316	0.1315	0.1311	0.1304	0.1293	0.1278	0.1257	0.1226	0.1172	0.0856
	h, kJ/kg	2789.8168	2666.1584	2541.8279	2416.682	2290.5115	2162.9819	2033.5044	1900.909	1762.4273	1609.0108	1286.3266
	s, kJ/kg K	6.4446	6.4622	6.399	6.2993	6.1713	6.0177	5.8385	5.6301	5.3827	5.0653	4.2155
16.00	T, °C	199.8939	195.7122	190.7891	185.0809	178.5125	170.9539	162.1669	151.6757	138.3671	118.6853	39.5616
	v, m^3/kg	0.1235	0.1237	0.1236	0.1232	0.1225	0.1215	0.1201	0.1181	0.1152	0.11	0.0802
	h, kJ/kg	2791.6954	2668.3131	2544.2105	2419.2403	2293.1866	2165.7056	2036.1925	1903.4484	1764.6448	1610.5627	1286.4925
	s, kJ/kg K	6.4216	6.4395	6.3766	6.2771	6.1492	5.9956	5.8162	5.6074	5.3594	5.0406	4.1946
17.00	T, °C	202.6964	198.4921	193.5342	187.7774	181.1445	173.5017	164.6062	153.9735	140.4752	120.522	41.6808
	v, m^3/kg	0.1165	0.1167	0.1166	0.1163	0.1156	0.1147	0.1133	0.1114	0.1086	0.1036	0.0754
	h, kJ/kg	2793.373	2670.2598	2546.3802	2421.5829	2295.6457	2168.215	2038.6704	1905.7848	1766.6706	1611.9418	1286.4875
	s, kJ/kg K	6.3998	6.4181	6.3555	6.2561	6.1283	5.9748	5.7953	5.5861	5.3374	5.0173	4.1753
18.00	T, °C	205.3671	201.1413	196.1506	190.348	183.6538	175.9312	166.9323	156.1645	142.4848	122.2718	43.7059
	v, m^3/kg	0.1103	0.1104	0.1104	0.11	0.1095	0.1085	0.1073	0.1054	0.1027	0.098	0.0711
	h, kJ/kg	2794.873	2672.0222	2548.3611	2423.734	2297.9127	2170.5338	2040.9613	1907.9405	1768.5258	1613.1671	1286.3278
	s, kJ/kg K	6.3792	6.3978	6.3355	6.2363	6.1087	5.9551	5.7754	5.566	5.3166	4.9953	4.1572
19.00	T, °C	207.9189	203.6727	198.6509	192.8048	186.0526	178.254	169.1563	158.2593	144.4056	123.9433	45.6459
	v, m^3/kg	0.1046	0.1048	0.1048	0.1045	0.1039	0.103	0.1018	0.1001	0.0975	0.0929	0.0673
	h, kJ/kg	2796.2147	2673.6203	2550.1734	2425.7142	2300.008	2172.682	2043.0849	1909.9344	1770.2282	1614.2546	1286.0271
	s, kJ/kg K	6.3596	6.3786	6.3165	6.2176	6.09	5.9365	5.7567	5.5469	5.2969	4.9745	4.1402

Table A.2 Saturated vapour properties (contd.,)

P, bar	Property	Ammonia concentration (mass fraction), x										
		0	**0.1**	**0.2**	**0.3**	**0.4**	**0.5**	**0.6**	**0.7**	**0.8**	**0.9**	**1**
20.00	T, °C	210.3627	206.0971	201.0458	195.1584	188.3508	180.4798	171.2876	160.2666	146.2457	125.5438	47.5084
	v, m^3/kg	0.0996	0.0998	0.0997	0.0994	0.0989	0.0981	0.0969	0.0952	0.0927	0.0883	0.0638
	h, kJ/kg	2797.4192	2675.0754	2551.8385	2427.5444	2301.9523	2174.68	2045.0608	1911.7855	1771.7958	1615.2209	1285.6035
	s, kJ/kg K	6.341	6.3603	6.2985	6.1997	6.0722	5.9187	5.7388	5.5287	5.2782	4.9547	4.1244
21.00	T, °C	212.7089	208.4247	203.3452	197.4185	190.5581	182.6176	173.3349	162.1947	148.0128	127.0801	49.3005
	v, m^3/kg	0.0949	0.0951	0.0951	0.0949	0.0944	0.0936	0.0924	0.0908	0.0884	0.0841	0.0606
	h, kJ/kg	2798.4873	2676.3892	2553.359	2429.2281	2303.7497	2176.5322	2046.8936	1913.4984	1773.2328	1616.0684	1285.048
	s, kJ/kg K	6.3231	6.3427	6.2812	6.1826	6.0553	5.9018	5.7217	5.5114	5.2603	4.9357	4.1094
22.00	T, °C	214.9649	210.663	205.5567	199.5923	192.6814	184.6745	175.3047	164.0497	149.7126	128.5574	51.0275
	v, m^3/kg	0.0907	0.0909	0.0909	0.0907	0.0902	0.0895	0.0884	0.0868	0.0845	0.0803	0.0577
	h, kJ/kg	2799.4445	2677.5871	2554.7597	2430.7897	2305.4239	2178.2614	2048.6055	1915.0942	1774.5591	1616.8162	1284.3885
	s, kJ/kg K	6.306	6.3259	6.2647	6.1663	6.0391	5.8856	5.7055	5.4948	5.2432	4.9176	4.0953
23.00	T, °C	217.1384	212.8194	207.6874	201.6871	194.7278	186.657	177.2034	165.8377	151.3507	129.9805	52.6946
	v, m^3/kg	0.0869	0.0871	0.0871	0.0869	0.0864	0.0857	0.0846	0.0831	0.0809	0.0768	0.0551
	h, kJ/kg	2800.2971	2678.6757	2556.0477	2432.2363	2306.9822	2179.8752	2050.2039	1916.5802	1775.7817	1617.47	1283.6264
	s, kJ/kg K	6.2896	6.3098	6.2488	6.1506	6.0235	5.8701	5.6899	5.479	5.2268	4.9003	4.0821
24.00	T, °C	219.2357	214.9004	209.7437	203.7089	196.7031	188.5709	179.0365	167.564	152.9319	131.3537	54.3065
	v, m^3/kg	0.0834	0.0836	0.0836	0.0834	0.0829	0.0822	0.0812	0.0798	0.0776	0.0736	0.0527
	h, kJ/kg	2801.0543	2679.6645	2557.2327	2433.5779	2308.4345	2181.3834	2051.6983	1917.9654	1776.909	1618.0373	1282.7684
	s, kJ/kg K	6.2738	6.2943	6.2336	6.1356	6.0086	5.8552	5.6749	5.4638	5.2111	4.8837	4.0695
25.00	T, °C	221.2625	216.9114	211.7311	205.6632	198.6127	190.4212	180.8089	169.2329	154.4605	132.6808	55.867
	v, m^3/kg	0.0801	0.0803	0.0803	0.0801	0.0797	0.079	0.0781	0.0766	0.0745	0.0707	0.0504
	h, kJ/kg	2801.7241	2680.5619	2558.3233	2434.8229	2309.7894	2182.7942	2053.0968	1919.2578	1777.9485	1618.5248	1281.8206
	s, kJ/kg K	6.2586	6.2794	6.2189	6.1211	5.9943	5.8409	5.6605	5.4491	5.196	4.8677	4.0576

26.00	T, °C	223.2238	218.8575	213.6545	207.5547	200.4611	192.2125	182.5248	170.8487	155.9401	133.965	57.3797
	v, m^3/kg	0.0771	0.0773	0.0773	0.0771	0.0767	0.0761	0.0751	0.0738	0.0717	0.068	0.0483
	h, kJ/kg	2802.3137	2681.3753	2559.3268	2435.979	2311.0543	2184.1153	2054.407	1920.4646	1778.9069	1618.9385	1280.7884
	s, kJ/kg K	6.2439	6.265	6.2048	6.1072	5.9804	5.8271	5.6467	5.4351	5.1815	4.8523	4.0464

Table A.2 Saturated vapour properties (contd.,)

P, bar	Property	Ammonia concentration (mass fraction), x										
		0	**0.1**	**0.2**	**0.3**	**0.4**	**0.5**	**0.6**	**0.7**	**0.8**	**0.9**	**1**
27.00	T, °C	225.1241	220.7432	215.5183	209.3878	202.2526	193.9488	184.1881	172.4149	157.3741	135.2094	58.8479
	v, m^3/kg	0.0743	0.0745	0.0745	0.0743	0.074	0.0733	0.0724	0.0711	0.0691	0.0654	0.0464
	h, kJ/kg	2802.8296	2682.1111	2560.2501	2437.053	2312.2362	2185.3534	2055.6352	1921.5919	1779.7902	1619.2835	1279.6767
	s, kJ/kg K	6.2298	6.2511	6.1911	6.0937	5.9671	5.8138	5.6333	5.4215	5.1675	4.8375	4.0357
28.00	T, °C	226.9676	222.5725	217.3265	211.1663	203.991	195.6337	185.8023	173.9349	158.7657	136.4166	60.2743
	v, m^3/kg	0.0717	0.0719	0.0719	0.0718	0.0714	0.0708	0.0699	0.0686	0.0666	0.0631	0.0446
	h, kJ/kg	2803.2773	2682.7754	2561.0991	2438.0508	2313.341	2186.5144	2056.7874	1922.6455	1780.6036	1619.5645	1278.4897
	s, kJ/kg K	6.216	6.2377	6.1779	6.0807	5.9542	5.801	5.6204	5.4084	5.154	4.8231	4.0256
29.00	T, °C	228.7576	224.3489	219.0825	212.8937	205.6795	197.2704	187.3704	175.4115	160.1174	137.589	61.6615
	v, m^3/kg	0.0692	0.0695	0.0695	0.0693	0.069	0.0684	0.0675	0.0663	0.0643	0.0609	0.0429
	h, kJ/kg	2803.662	2683.3732	2561.8791	2438.9779	2314.3742	2187.6037	2057.8689	1923.6304	1781.3518	1619.7857	1277.2313
	s, kJ/kg K	6.2028	6.2247	6.1651	6.0681	5.9417	5.7885	5.6079	5.3957	5.1409	4.8093	4.0159
30.00	T, °C	230.4977	226.0757	220.7896	214.5731	207.3213	198.862	188.8954	176.8474	161.4317	138.7287	63.012
	v, m^3/kg	0.067	0.0672	0.0672	0.0671	0.0667	0.0662	0.0653	0.0641	0.0622	0.0588	0.0413
	h, kJ/kg	2803.9881	2683.9094	2562.595	2439.8392	2315.3406	2188.6261	2058.8842	1924.5511	1782.0391	1619.9508	1275.9052
	s, kJ/kg K	6.1899	6.2121	6.1528	6.0559	5.9296	5.7765	5.5958	5.3834	5.1282	4.7959	4.0068
31.00	T, °C	232.1908	227.7559	222.4507	216.2074	208.9192	200.4112	190.3797	178.2451	162.7109	139.8378	64.3278
	v, m^3/kg	0.0648	0.0651	0.0651	0.065	0.0646	0.0641	0.0633	0.0621	0.0602	0.0569	0.0398
	h, kJ/kg	2804.2599	2684.3881	2563.2511	2440.639	2316.2446	2189.586	2059.8378	1925.4118	1782.6694	1620.0633	1274.5146
	s, kJ/kg K	6.1773	6.1998	6.1407	6.044	5.9179	5.7648	5.5841	5.3715	5.1159	4.7829	3.9981

32.00	T, °C	233.8395	229.3922	224.0684	217.7992	210.4756	201.9202	191.8257	179.6067	163.957	140.9179	65.6108
	v, m^3/kg	0.0628	0.0631	0.0631	0.063	0.0627	0.0621	0.0613	0.0602	0.0583	0.0551	0.0385
	h, kJ/kg	2804.4809	2684.8132	2563.8514	2441.3814	2317.0902	2190.4873	2060.7334	1926.2161	1783.2461	1620.1262	1273.0624
	s, kJ/kg K	6.1652	6.1879	6.129	6.0325	5.9065	5.7535	5.5728	5.36	5.104	4.7703	3.9898
33.00	T, °C	235.4465	230.9869	225.6452	219.3508	211.9928	203.3914	193.2355	180.9342	165.1718	141.9708	66.863
	v, m^3/kg	0.061	0.0612	0.0612	0.0611	0.0608	0.0603	0.0595	0.0584	0.0566	0.0534	0.0371
	h, kJ/kg	2804.6546	2685.1882	2564.3993	2442.0699	2317.8811	2191.3336	2061.5747	1926.9676	1783.7725	1620.1423	1271.5513
	s, kJ/kg K	6.1533	6.1763	6.1177	6.0213	5.8955	5.7425	5.5617	5.3488	5.0925	4.758	3.9819

Table A.2 Saturated vapour properties (contd.,)

P, bar	Property	Ammonia concentration (mass fraction), x										
		0	**0.1**	**0.2**	**0.3**	**0.4**	**0.5**	**0.6**	**0.7**	**0.8**	**0.9**	**1**
34.00	T, °C	237.0138	232.5425	227.1834	220.8644	213.4731	204.8269	194.6112	182.2295	166.357	142.9979	68.0858
	v, m^3/kg	0.0592	0.0594	0.0595	0.0593	0.059	0.0585	0.0578	0.0567	0.0549	0.0518	0.0359
	h, kJ/kg	2804.784	2685.5162	2564.8982	2442.7079	2318.6205	2192.1283	2062.3647	1927.6692	1784.2515	1620.1142	1269.9839
	s, kJ/kg K	6.1418	6.165	6.1066	6.0105	5.8847	5.7318	5.551	5.3379	5.0812	4.7462	3.9744
35.00	T, °C	238.5437	234.0609	228.6849	222.3421	214.9183	206.2284	195.9543	183.4943	167.5142	144.0006	69.2808
	v, m^3/kg	0.0575	0.0577	0.0578	0.0577	0.0574	0.0569	0.0562	0.055	0.0533	0.0503	0.0347
	h, kJ/kg	2804.8719	2685.8002	2565.3511	2443.2983	2319.3115	2192.8743	2063.1066	1928.3239	1784.6857	1620.0441	1268.3624
	s, kJ/kg K	6.1305	6.154	6.0958	5.9999	5.8742	5.7214	5.5405	5.3273	5.0703	4.7346	3.9672
36.00	T, °C	240.038	235.5441	230.1515	223.7857	216.3302	207.5977	197.2667	184.7301	168.6448	144.9801	70.4494
	v, m^3/kg	0.0559	0.0561	0.0562	0.0561	0.0558	0.0553	0.0546	0.0535	0.0519	0.0488	0.0336
	h, kJ/kg	2804.9209	2686.0428	2565.7605	2443.8439	2319.9568	2193.5743	2063.8029	1928.9342	1785.0775	1619.9343	1266.6889
	s, kJ/kg K	6.1196	6.1433	6.0853	5.9895	5.864	5.7112	5.5304	5.317	5.0597	4.7234	3.9604

37.00	T, °C	241.4986	236.9937	231.5852	225.1968	217.7105	208.9365	198.5499	185.9383	169.7502	145.9376	71.5928
	v, m^3/kg	0.0544	0.0546	0.0547	0.0546	0.0543	0.0539	0.0532	0.0521	0.0505	0.0475	0.0326
	h, kJ/kg	2804.9333	2686.2464	2566.1292	2444.3474	2320.5591	2194.231	2064.4562	1929.5025	1785.4292	1619.7866	1264.9655
	s, kJ/kg K	6.1089	6.1329	6.0751	5.9795	5.8541	5.7014	5.5204	5.3069	5.0493	4.7124	3.9539
38.00	T, °C	242.927	238.4115	232.9874	226.577	219.0606	210.2461	199.8052	187.1204	170.8316	146.8742	72.7123
	v, m^3/kg	0.053	0.0532	0.0533	0.0532	0.0529	0.0525	0.0518	0.0507	0.0491	0.0462	0.0316
	h, kJ/kg	2804.9112	2686.4133	2566.4592	2444.8109	2321.1206	2194.8467	2065.0687	1930.031	1785.7429	1619.6029	1263.1939
	s, kJ/kg K	6.0984	6.1226	6.0651	5.9696	5.8444	5.6917	5.5108	5.2971	5.0392	4.7017	3.9477
39.00	T, °C	244.3248	239.7989	234.3596	227.9278	220.3821	211.528	201.0339	188.2774	171.89	147.7909	73.8089
	v, m^3/kg	0.0516	0.0519	0.0519	0.0518	0.0516	0.0511	0.0505	0.0494	0.0478	0.045	0.0306
	h, kJ/kg	2804.8567	2686.5455	2566.7529	2445.2366	2321.6435	2195.4234	2065.6426	1930.5218	1786.0204	1619.3848	1261.3758
	s, kJ/kg K	6.0882	6.1127	6.0553	5.96	5.8349	5.6823	5.5013	5.2875	5.0293	4.6913	3.9418
40.00	T, °C	245.6934	241.1574	235.7032	229.2505	221.6762	212.7835	202.2374	189.4106	172.9266	148.6886	74.8837
	v, m^3/kg	0.0503	0.0506	0.0506	0.0506	0.0503	0.0499	0.0492	0.0482	0.0466	0.0438	0.0297
	h, kJ/kg	2804.7715	2686.645	2567.012	2445.6266	2322.1299	2195.9632	2066.1798	1930.9767	1786.2635	1619.1339	1259.5129
	s, kJ/kg K	6.0782	6.1029	6.0458	5.9506	5.8256	5.6731	5.4921	5.2782	5.0197	4.6812	3.9362

Table A.2 Saturated vapour properties (contd.,)

P, bar	Property	Ammonia concentration (mass fraction), x										
		0	**0.1**	**0.2**	**0.3**	**0.4**	**0.5**	**0.6**	**0.7**	**0.8**	**0.9**	**1**
41.00	T, °C	247.0341	242.4882	237.0195	230.5465	222.9442	214.0136	203.4166	190.5211	173.9423	149.5681	75.9377
	v, m^3/kg	0.0491	0.0493	0.0494	0.0493	0.0491	0.0487	0.048	0.047	0.0455	0.0427	0.0288
	h, kJ/kg	2804.6573	2686.7134	2567.2385	2445.9827	2322.5815	2196.468	2066.6821	1931.3975	1786.4738	1618.8515	1257.6066
	s, kJ/kg K	6.0684	6.0933	6.0364	5.9414	5.8166	5.6641	5.4831	5.2691	5.0103	4.6713	3.9308

42.00	T, °C	248.3481	243.7926	238.3097	231.8168	224.1872	215.2195	204.5727	191.6098	174.938	150.4302	76.9716
	v, m^3/kg	0.0479	0.0482	0.0482	0.0482	0.0479	0.0475	0.0469	0.0459	0.0444	0.0416	0.028
	h, kJ/kg	2804.5158	2686.7524	2567.434	2446.3066	2323.0001	2196.9394	2067.1512	1931.7858	1786.6529	1618.5391	1255.6583
	s, kJ/kg K	6.0588	6.084	6.0273	5.9325	5.8077	5.6553	5.4743	5.2601	5.0011	4.6616	3.9257
43.00	T, °C	249.6366	245.0716	239.5749	233.0625	225.4062	216.4023	205.7067	192.6776	175.9147	151.2758	77.9864
	v, m^3/kg	0.0468	0.047	0.0471	0.0471	0.0468	0.0464	0.0458	0.0448	0.0433	0.0406	0.0272
	h, kJ/kg	2804.3483	2686.7636	2567.6001	2446.5999	2323.3873	2197.3791	2067.5887	1932.1432	1786.8022	1618.1977	1253.6693
	s, kJ/kg K	6.0494	6.0748	6.0183	5.9237	5.799	5.6467	5.4657	5.2514	4.9921	4.6521	3.9209
44.00	T, °C	250.9006	246.3263	240.8162	234.2848	226.6023	217.5629	206.8194	193.7255	176.873	152.1054	78.9828
	v, m^3/kg	0.0458	0.046	0.0461	0.046	0.0458	0.0454	0.0448	0.0438	0.0423	0.0397	0.0265
	h, kJ/kg	2804.1562	2686.7483	2567.7381	2446.864	2323.7447	2197.7885	2067.996	1932.471	1786.923	1617.8286	1251.6408
	s, kJ/kg K	6.0402	6.0658	6.0095	5.915	5.7905	5.6382	5.4572	5.2429	4.9833	4.6429	3.9162
45.00	T, °C	252.1412	247.5578	242.0345	235.4845	227.7763	218.7022	207.9117	194.7541	177.8138	152.9197	79.9616
	v, m^3/kg	0.0447	0.045	0.045	0.045	0.0448	0.0444	0.0438	0.0428	0.0414	0.0387	0.0257
	h, kJ/kg	2803.9407	2686.7079	2567.8496	2447.1004	2324.0735	2198.1691	2068.3745	1932.7705	1787.0164	1617.4329	1249.574
	s, kJ/kg K	6.0311	6.057	6.0009	5.9066	5.7822	5.63	5.449	5.2345	4.9747	4.6339	3.9118
46.00	T, °C	253.3593	248.767	243.2307	236.6625	228.9293	219.821	208.9845	195.7644	178.7377	153.7195	80.9234
	v, m^3/kg	0.0438	0.044	0.0441	0.044	0.0438	0.0434	0.0428	0.0419	0.0405	0.0378	0.0251
	h, kJ/kg	2803.7031	2686.6435	2567.9357	2447.3103	2324.3751	2198.5221	2068.7255	1933.0429	1787.0838	1617.0114	1247.4699
	s, kJ/kg K	6.0223	6.0484	5.9924	5.8983	5.774	5.6219	5.4409	5.2263	4.9662	4.625	3.9077
47.00	T, °C	254.5557	249.9547	244.4057	237.8197	230.0619	220.9202	210.0385	196.757	179.6454	154.5051	81.8689
	v, m^3/kg	0.0428	0.043	0.0431	0.0431	0.0429	0.0425	0.0419	0.041	0.0396	0.037	0.0244
	h, kJ/kg	2803.4444	2686.5563	2567.9976	2447.495	2324.6508	2198.8487	2069.0502	1933.2895	1787.126	1616.5653	1245.3296
	s, kJ/kg K	6.0136	6.0399	5.9842	5.8902	5.766	5.614	5.4329	5.2183	4.958	4.6163	3.9037

Table A.2 Saturated vapour properties (contd.,)

P, bar	Property	Ammonia concentration (mass fraction), x										
		0	**0.1**	**0.2**	**0.3**	**0.4**	**0.5**	**0.6**	**0.7**	**0.8**	**0.9**	**1**
48.00	T, °C	255.7312	251.1217	245.5604	238.9569	231.175	222.0005	211.0744	197.7325	180.5376	155.2772	82.7987
	v, m^3/kg	0.0419	0.0421	0.0422	0.0422	0.042	0.0416	0.041	0.0401	0.0387	0.0362	0.0237
	h, kJ/kg	2803.1657	2686.4475	2568.0365	2447.6556	2324.9016	2199.1501	2069.3497	1933.5113	1787.1442	1616.0952	1243.154
	s, kJ/kg K	6.005	6.0316	5.976	5.8822	5.7582	5.6062	5.4251	5.2104	4.9499	4.6079	3.8999
49.00	T, °C	256.8868	252.2689	246.6954	240.0748	232.2692	223.0626	212.0928	198.6917	181.4147	156.0363	83.7134
	v, m^3/kg	0.0411	0.0413	0.0414	0.0413	0.0411	0.0408	0.0402	0.0393	0.0379	0.0354	0.0231
	h, kJ/kg	2802.8678	2686.3179	2568.0533	2447.7931	2325.1286	2199.4274	2069.625	1933.7094	1787.1393	1615.6021	1240.9441
	s, kJ/kg K	5.9966	6.0234	5.968	5.8744	5.7505	5.5985	5.4175	5.2026	4.9419	4.5995	3.8963
50.00	T, °C	258.023	253.3969	247.8116	241.1741	233.3454	224.1071	213.0945	199.6351	182.2773	156.7828	84.6135
	v, m^3/kg	0.0402	0.0404	0.0405	0.0405	0.0403	0.0399	0.0394	0.0385	0.0372	0.0346	0.0225
	h, kJ/kg	2802.5517	2686.1685	2568.0491	2447.9085	2325.3328	2199.6815	2069.8772	1933.8845	1787.1122	1615.0867	1238.7007
	s, kJ/kg K	5.9884	6.0153	5.9602	5.8667	5.7429	5.591	5.41	5.1951	4.9341	4.5914	3.8929
51.00	T, °C	259.1407	254.5065	248.9095	242.2556	234.4041	225.1348	214.0801	200.5632	183.1261	157.5172	85.4995
	v, m^3/kg	0.0394	0.0396	0.0397	0.0397	0.0395	0.0392	0.0386	0.0377	0.0364	0.0339	0.022
	h, kJ/kg	2802.2183	2686.0003	2568.0247	2448.0028	2325.5153	2199.9134	2070.1071	1934.0378	1787.0637	1614.5497	1236.4247
	s, kJ/kg K	5.980	6.007	5.953	5.859	5.736	5.584	5.403	5.188	4.9265	4.5834	3.8897
52.00	T, °C	260.240	255.598	249.990	243.320	235.446	226.146	215.050	201.477	183.9613	158.24	86.3719
	v, m^3/kg	0.0387	0.039	0.039	0.039	0.039	0.038	0.038	0.037	0.0357	0.0332	0.0214
	h, kJ/kg	2801.8682	2685.814	2567.981	2448.077	2325.677	2200.124	2070.316	1934.170	1786.9946	1613.9918	1234.1168
	s, kJ/kg K	5.9723	6.000	5.945	5.852	5.728	5.576	5.395	5.180	4.919	4.5756	3.8867
53.00	T, °C	261.3228	256.673	251.053	244.367	236.472	227.142	216.005	202.376	184.7836	158.9515	87.2312
	v, m^3/kg	0.0379	0.038	0.038	0.038	0.038	0.038	0.037	0.036	0.035	0.0326	0.0209
	h, kJ/kg	2801.502	2685.610	2567.919	2448.132	2325.818	2200.314	2070.504	1934.282	1786.9056	1613.4137	1231.7777
	s, kJ/kg K	5.964	5.992	5.9374	5.8444	5.721	5.5693	5.3883	5.1731	4.9116	4.5679	3.8838

54.00	T, °C	262.389	257.73	252.1001	245.3987	237.4813	228.1221	216.9451	203.2616	185.5934	159.6521	88.0778
	v, m^3/kg	0.037	0.037	0.038	0.038	0.037	0.037	0.036	0.0356	0.0343	0.0319	0.0204
	h, kJ/kg	2801.121	2685.390	2567.839	2448.168	2325.940	2200.485	2070.672	1934.3741	1786.7974	1612.8159	1229.4082
	s, kJ/kg K	5.957	5.985	5.930	5.837	5.714	5.562	5.381	5.166	4.9043	4.5604	3.8811

Table A.3 Ammonia-water liquid-vapour mixture properties at 3 bar

θ = f(T)	Property	Ammonia concentration (mass fraction), x								
		0.1	**0.2**	**0.3**	**0.4**	**0.5**	**0.6**	**0.7**	**0.8**	**0.9**
0.1	T, °C	105.2656	83.9677	64.7366	47.1906	32.1675	20.3881	11.9168	6.0604	1.4583
	v, m^3/kg	0.0147	0.0209	0.0281	0.0382	0.0543	0.0808	0.1241	0.1903	0.2812
	h, kJ/kg	420.3585	286.1835	174.9657	97.0425	68.4748	107.4858	232.8798	457.4003	780.3663
	s, kJ/kg K	1.5337	1.3128	1.0974	0.9292	0.869	0.9915	1.3801	2.099	3.1611
	x_l, kg/kg	0.0913	0.181	0.2713	0.3551	0.4398	0.5178	0.5866	0.6462	0.7063
	x_v, kg/kg	0.6039	0.8428	0.9402	0.9789	0.9925	0.9972	0.9989	0.9995	0.9998
	h_l, kJ/kg	389.4792	240.6947	109.4663	-6.778	-92.2316	-148.3373	-177.9274	-188.3158	-185.2415
	h_v, kJ/kg	1955.378	1639.4924	1503.8265	1415.926	1362.5254	1327.8491	1305.0916	1290.0027	1277.9184
0.2	T, °C	108.0149	88.6408	71.0567	54.9168	40.9549	29.7928	21.45	15.22	9.5887
	v, m^3/kg	0.03	0.042	0.055	0.0722	0.0974	0.1341	0.1858	0.2529	0.3323
	h, kJ/kg	482.6073	372.964	285.5029	233.9243	234.9604	303.1313	446.4573	661.0569	932.9141
	s, kJ/kg K	1.6973	1.5543	1.4217	1.3511	1.4053	1.6456	2.1152	2.8157	3.7084
	x_l, kg/kg	0.0809	0.1601	0.2409	0.3151	0.3889	0.4544	0.5101	0.558	0.6087
	x_v, kJ/kg	0.5618	0.8033	0.9152	0.9661	0.9859	0.9937	0.9969	0.9984	0.9992
	h_l, kJ/kg	408.4343	273.4044	151.7269	41.1813	-43.6743	-104.5094	-143.8503	-167.914	-183.4051
	h_v, kg/kg	2009.5251	1693.9258	1546.9713	1450.061	1392.0881	1355.156	1330.8067	1313.8085	1299.0443

0.3	T, °C	110.7642	93.3139	77.3768	62.6429	49.7423	39.1974	30.9831	24.3795	17.7191
	v, m^3/kg	0.0477	0.0648	0.0826	0.105	0.1355	0.1768	0.23	0.2936	0.3636
	h, kJ/kg	553.3912	466.0452	397.8594	364.6639	382.06	459.85	599.1654	791.0137	1020.7026
	s, kJ/kg K	1.8818	1.8097	1.7451	1.7446	1.8661	2.1533	2.6233	3.2573	4.0129
	x_l, kg/kg	0.0708	0.1399	0.2112	0.2815	0.3417	0.3987	0.447	0.4897	0.5379
	x_v, kg/kg	0.5168	0.7567	0.8815	0.9469	0.9753	0.9875	0.9931	0.996	0.9979
	h_l, kJ/kg	427.3151	306.1807	194.9283	95.7123	8.8072	-53.7352	-98.4061	-130.8007	-158.9568
	h_v, kJ/kg	2066.9895	1756.403	1599.0583	1491.1613	1426.5629	1385.8429	1358.8219	1339.1168	1320.5299
0.4	T, °C	113.5135	97.9869	83.6969	70.369	58.5296	48.6021	40.5163	33.5391	25.8496
	v, m^3/kg	0.0688	0.0906	0.1122	0.1381	0.1717	0.2149	0.2673	0.327	0.3892
	h, kJ/kg	636.7512	569.6678	516.8019	495.7685	521.0998	599.1281	727.3982	895.6972	1090.1574
	s, kJ/kg K	2.0974	2.09	2.081	2.1301	2.29	2.591	3.0364	3.6017	4.2465
	x_l, kg/kg	0.061	0.1203	0.1822	0.2442	0.3	0.3476	0.3913	0.4315	0.4798
	x_v, kg/kg	0.4691	0.7028	0.8449	0.9183	0.9581	0.977	0.9864	0.9917	0.9954
	h_l, kJ/kg	446.161	338.8966	238.8041	147.0782	64.6075	1.8109	-46.1999	-84.961	-123.9187
	h_v, kJ/kg	2127.9107	1827.3351	1636.5724	1541.8809	1468.2687	1421.7396	1390.5122	1366.8881	1343.3784

Table A.3 Ammonia-water liquid-vapour mixture properties at 3 bar (contd.,)

θ = f(T)	Property	Ammonia concentration (mass fraction), x								
		0.1	**0.2**	**0.3**	**0.4**	**0.5**	**0.6**	**0.7**	**0.8**	**0.9**
0.5	T, °C	116.2628	102.66	90.017	78.0952	67.317	58.0068	50.0495	42.6986	33.98
	v, m^3/kg	0.0953	0.1212	0.1456	0.1737	0.2087	0.2519	0.3025	0.3578	0.4129
	h, kJ/kg	739.3149	690.4525	649.2139	634.9556	661.832	734.1346	847.6659	992.146	1154.143
	s, kJ/kg K	2.3605	2.4121	2.4478	2.5299	2.7075	3.0029	3.412	3.9092	4.4555
	x_l, kg/kg	0.0517	0.1014	0.1541	0.2078	0.2588	0.3	0.3401	0.3792	0.4289
	x_v, kg/kg	0.4185	0.6415	0.7903	0.877	0.9309	0.9593	0.9748	0.9842	0.9914
	h_l, kJ/kg	465.0501	371.435	283.0565	199.8859	126.5918	60.7717	10.7017	-33.5385	-82.597
	h_v, kJ/kg	2192.4727	1907.0277	1711.4685	1605.6432	1520.4936	1465.5311	1427.8832	1398.4764	1368.3085

0.6	T, °C	119.0121	107.3331	96.3371	85.8213	76.1043	67.4115	59.5827	51.8582	42.1105
	v, m^3/kg	0.1303	0.1595	0.1858	0.2145	0.2494	0.2911	0.3386	0.3889	0.4366
	h, kJ/kg	872.8186	839.5653	806.0402	793.2501	815.6875	876.8424	971.8195	1090.4908	1219.1368
	s, kJ/kg K	2.7005	2.8043	2.8739	2.9739	3.1519	3.4258	3.7882	4.2136	4.662
	x_l, kg/kg	0.0426	0.0834	0.1271	0.1727	0.2171	0.2583	0.2967	0.3307	0.3825
	x_v, kJ/kg	0.3647	0.5725	0.7227	0.828	0.8891	0.9305	0.9554	0.9718	0.9848
	h_l, kJ/kg	484.1186	403.7401	327.3611	253.6527	186.167	127.2239	75.86	21.9258	-36.9738
	h_v, kg/kg	2260.9189	1995.7913	1801.3067	1660.1539	1587.7462	1521.1279	1473.8956	1435.8384	1396.2995
0.7	T, °C	121.7614	112.0062	102.6572	93.5474	84.8917	76.8162	69.1159	61.0177	50.2409
	v, m^3/kg	0.1804	0.2114	0.2379	0.2656	0.2982	0.3365	0.3791	0.4229	0.4617
	h, kJ/kg	1060.1844	1037.6979	1006.5211	988.8023	999.6217	1042.5612	1112.7388	1200.1944	1290.3097
	s, kJ/kg K	3.1743	3.3186	3.4085	3.5097	3.6691	3.9029	4.2027	4.5434	4.8823
	x_l, kg/kg	0.0339	0.0663	0.1014	0.1389	0.1768	0.2138	0.2501	0.2896	0.3391
	x_v, kg/kg	0.3076	0.4956	0.6415	0.7542	0.8355	0.8849	0.9237	0.9516	0.9745
	h_l, kJ/kg	503.6664	435.8317	371.4165	307.8183	247.1501	191.0647	138.6396	85.1299	11.8837
	h_v, kJ/kg	2333.5668	2094.0715	1906.9767	1759.7446	1649.6419	1594.0197	1532.8672	1481.8169	1428.7102
0.8	T, °C	124.5107	116.6792	108.9773	101.2736	93.679	86.2209	78.649	70.1772	58.3714
	v, m^3/kg	0.2598	0.289	0.3126	0.336	0.3632	0.3946	0.4288	0.4628	0.4896
	h, kJ/kg	1353.3746	1328.542	1288.9566	1255.6	1243.3368	1255.9512	1289.1642	1333.5248	1373.4426
	s, kJ/kg K	3.9108	4.0642	4.1481	4.2241	4.3364	4.4999	4.7069	4.9333	5.1331
	x_l, kg/kg	0.0255	0.0503	0.0773	0.1069	0.1383	0.1709	0.2053	0.2451	0.3
	x_v, kg/kg	0.247	0.4105	0.5464	0.6604	0.7528	0.8246	0.8735	0.9191	0.9585
	h_l, kJ/kg	524.3762	467.9168	415.0521	361.806	308.74	256.4496	203.7158	145.7839	62.3553
	h_v, kJ/kg	2410.8312	2202.5833	2029.2564	1882.4531	1761.637	1664.7657	1610.8211	1540.4797	1467.4363
0.9	T, °C	127.26	121.3523	115.2974	108.9997	102.4664	95.6255	88.1822	79.3368	66.5018
	v, m^3/kg	0.4101	0.4235	0.435	0.4466	0.4608	0.4779	0.4965	0.5137	0.5225
	h, kJ/kg	1900.8145	1824.2991	1744.3163	1668.5278	1607.4373	1563.5834	1533.5988	1509.7359	1476.4247
	s, kJ/kg K	5.2774	5.3204	5.3206	5.3059	5.308	5.3369	5.3859	5.4347	5.4364
	x_l, kg/kg	0.0175	0.0352	0.0549	0.0772	0.1022	0.1301	0.1622	0.2021	0.2627
	x_v, kg/kg	0.1823	0.3164	0.4366	0.546	0.6441	0.731	0.8075	0.8689	0.934
	h_l, kJ/kg	548.1982	500.7047	458.4064	415.2056	370.0908	322.3799	270.1891	208.4766	121.1614
	h_v, kJ/kg	2493.2542	2322.4759	2169.3725	2029.7212	1903.5476	1790.4144	1688.2365	1617.3758	1515.0959

Table A.3 Ammonia-water liquid-vapour mixture properties at 4 bar

θ = f(T)	Property	Ammonia concentration (mass fraction), x									
		0.1	**0.2**	**0.3**	**0.4**	**0.5**	**0.6**	**0.7**	**0.8**	**0.9**	
0.1	T, °C	115.3913	93.6794	74.0196	56.104	40.7626	28.6959	19.9517	13.824		8.9348
	v, m^3/kg	0.0118	0.0164	0.0218	0.0295	0.0416	0.0614	0.0938	0.1432		0.2116
	h, kJ/kg	464.974	328.4413	214.8562	134.6271	103.3385	138.3937	257.5791	473.2955		786.5927
	s, kJ/kg K	1.6466	1.4243	1.2066	1.0346	0.9662	1.0717	1.4285	2.0973		3.0968
	x_l, kg/kg	0.0915	0.1814	0.2718	0.3557	0.4407	0.5192	0.5891	0.6507		0.7142
	x_v, kg/kg	0.5812	0.8241	0.9299	0.9742	0.9904	0.9963	0.9984	0.9993		0.9997
	h_l, kJ/kg	433.1507	282.4339	149.5693	32.1971	-54.0442	-110.6945	-140.5889	-150.8557		-146.7061
	h_v, kJ/kg	1998.221	1677.4687	1534.5422	1438.7599	1380.314	1342.5375	1317.7873	1301.2689		1288.4124
0.2	T, °C	118.1154	98.3558	80.3663	63.8675	49.5864	38.1266	29.4918	22.96		16.9881
	v, m^3/kg	0.0239	0.0328	0.0426	0.0556	0.0745	0.1022	0.1411	0.1918		0.252
	h, kJ/kg	528.5483	416.0198	325.6363	271.0379	268.4816	332.0071	469.4336	677.4001		943.0973
	s, kJ/kg K	1.8092	1.6614	1.5227	1.4435	1.4837	1.7015	2.1381	2.7966		3.6437
	x_l, kg/kg	0.0813	0.1609	0.2418	0.3163	0.3904	0.4566	0.5136	0.5633		0.6171
	x_v, kJ/kg	0.5405	0.7836	0.9027	0.9597	0.9827	0.9921	0.996	0.9978		0.9989
	h_l, kJ/kg	451.9022	314.8868	191.5818	79.8451	-5.9095	-67.4764	-107.4007	-131.823		-147.0848
	h_v, kg/kg	2050.483	1732.8898	1580.108	1475.4624	1412.0617	1371.5942	1344.8807	1326.1186		1309.7314
0.3	T, °C	120.8396	103.0321	86.7131	71.631	58.4102	47.5574	39.0318	32.0959		25.0414
	v, m^3/kg	0.0379	0.0507	0.064	0.0809	0.1039	0.1351	0.1753	0.2235		0.2765
	h, kJ/kg	601.0573	510.4553	438.9752	402.3463	415.7579	488.7943	622.6948	808.932		1033.3331
	s, kJ/kg K	1.9933	1.9136	1.8401	1.828	1.9326	2.1958	2.6345	3.2319		3.9486
	x_l, kg/kg	0.0713	0.141	0.2126	0.2832	0.3438	0.4016	0.4511	0.4955		0.5466
	x_v, kg/kg	0.4974	0.7368	0.8669	0.9383	0.9705	0.9848	0.9915	0.995		0.9973
	h_l, kJ/kg	470.609	347.4358	234.5202	134.0461	46.1149	-17.3628	-62.9201	-96.1171		-124.7416
	h_v, kJ/kg	2105.6858	1795.575	1634.3376	1519.2741	1449.0406	1404.3645	1374.5545	1352.6749		1331.9885

0.4	T, °C	123.5637	107.7084	93.0598	79.3945	67.234	56.9881	48.5719	41.2319	33.0947
	v, m^3/kg	0.0548	0.071	0.0872	0.1067	0.1321	0.1647	0.2043	0.2494	0.2965
	h, kJ/kg	686.6097	616.0217	559.6314	534.9604	556.1547	629.4773	752.6583	915.7746	1105.0005
	s, kJ/kg K	2.2088	2.1916	2.1718	2.2075	2.3491	2.6262	3.0421	3.5743	4.1836
	x_l, kg/kg	0.0617	0.1217	0.1841	0.2464	0.3	0.3511	0.396	0.4379	0.4888
	x_v, kg/kg	0.4517	0.6834	0.829	0.9074	0.9514	0.9729	0.9838	0.9901	0.9946
	h_l, kJ/kg	489.3128	379.9692	278.1465	185.0835	101.0383	37.5076	-11.6625	-51.6022	-91.6007
	h_v, kJ/kg	2163.978	1865.8062	1670.6501	1572.6156	1493.4596	1442.6445	1408.1802	1381.8989	1355.7197

Table A.3 Ammonia-water liquid-vapour mixture properties at 4 bar (contd.,)

θ = f(T)	Property	Ammonia concentration (mass fraction), x								
		0.1	**0.2**	**0.3**	**0.4**	**0.5**	**0.6**	**0.7**	**0.8**	**0.9**
0.5	T, °C	126.2879	112.3847	99.4065	87.1579	76.0579	66.4189	58.1119	50.3679	41.148
	v, m^3/kg	0.0758	0.0951	0.1134	0.1345	0.161	0.1936	0.2318	0.2736	0.315
	h, kJ/kg	791.9039	739.3857	694.4684	676.5072	699.2361	766.9086	875.4997	1014.8527	1171.2336
	s, kJ/kg K	2.4721	2.5121	2.5355	2.6033	2.7624	3.0344	3.4158	3.8821	4.3945
	x_l, kg/kg	0.0524	0.103	0.1564	0.2106	0.2621	0.3037	0.3453	0.3861	0.4384
	x_v, kg/kg	0.4034	0.6233	0.7736	0.8641	0.922	0.9535	0.971	0.9819	0.9901
	h_l, kJ/kg	508.0925	412.393	322.1966	237.5592	162.9473	95.9666	44.3029	-1.4437	-52.0401
	h_v, kJ/kg	2225.5599	1943.8201	1746.3318	1638.5133	1548.3419	1488.9707	1447.6833	1415.0981	1381.6146
0.6	T, °C	129.012	117.061	105.7533	94.9214	84.8817	75.8496	67.652	59.5039	49.2013
	v, m^3/kg	0.1037	0.1254	0.145	0.1666	0.1928	0.2243	0.2601	0.2979	0.3334
	h, kJ/kg	928.7126	891.7327	854.3642	837.8473	856.1829	912.762	1002.7879	1116.122	1238.4903
	s, kJ/kg K	2.8117	2.9026	2.9587	3.0441	3.2039	3.4554	3.7916	4.1876	4.603
	x_l, kg/kg	0.0435	0.0852	0.1297	0.1759	0.221	0.2631	0.3	0.3382	0.3925
	x_v, kJ/kg	0.3523	0.5565	0.7065	0.8139	0.8782	0.9229	0.9502	0.9686	0.9831
	h_l, kJ/kg	527.0858	444.6502	366.378	291.0365	222.0483	161.5755	102.8655	52.7873	-8.0999
	h_v, kg/kg	2290.6928	2029.9119	1835.5111	1691.499	1617.6888	1546.8979	1495.7956	1454.0892	1410.5801

0.7	T, °C	131.7362	121.7373	112.1	102.6849	93.7055	85.2804	77.1921	68.6399	57.2545
	v, m^3/kg	0.1432	0.1664	0.186	0.2066	0.2311	0.2598	0.2917	0.3244	0.3529
	h, kJ/kg	1119.7716	1093.671	1058.351	1036.7348	1043.424	1081.7683	1146.8604	1228.6293	1311.7193
	s, kJ/kg K	3.2829	3.4136	3.4889	3.5752	3.717	3.9296	4.2048	4.5176	4.8241
	x_l, kg/kg	0.0348	0.0681	0.1042	0.1425	0.1813	0.2192	0.2567	0.2977	0.3498
	x_v, kg/kg	0.298	0.4826	0.6272	0.7405	0.8239	0.8759	0.9173	0.9475	0.9724
	h_l, kJ/kg	546.5972	476.7727	410.4228	345.0174	282.6143	224.7582	170.4405	114.8495	39.1141
	h_v, kJ/kg	2359.7222	2124.5447	1938.8448	1790.6651	1677.7574	1621.2409	1556.35	1501.4116	1443.8287
0.8	T, °C	134.4603	126.4136	118.4468	110.4484	102.5293	94.7111	86.7321	77.7758	65.3078
	v, m^3/kg	0.2052	0.2271	0.2443	0.2616	0.2816	0.3049	0.3303	0.3553	0.3744
	h, kJ/kg	1415.7706	1388.2173	1343.9579	1306.1449	1289.404	1297.2496	1325.2399	1363.7221	1396.2167
	s, kJ/kg K	4.0083	4.1501	4.2183	4.2787	4.3738	4.5176	4.7021	4.9032	5.0731
	x_l, kg/kg	0.0264	0.052	0.08	0.1107	0.1431	0.1768	0.2125	0.254	0.3092
	x_v, kg/kg	0.2403	0.4011	0.5354	0.649	0.7421	0.8157	0.8668	0.9148	0.9563
	h_l, kJ/kg	567.2965	508.9585	454.1797	398.9865	343.9348	289.5787	234.6511	174.3093	88.9202
	h_v, kJ/kg	2433.1038	2228.4847	2057.0381	1910.5568	1788.4777	1689.0896	1634.5155	1560.5675	1482.9896
0.9	T, °C	137.1845	131.0899	124.7935	118.2118	111.3531	104.1419	96.2722	86.9118	73.3611
	v, m^3/kg	0.3202	0.3311	0.3389	0.3467	0.3565	0.3686	0.382	0.3941	0.3995
	h, kJ/kg	1957.124	1883.7217	1798.8833	1717.6539	1651.3122	1602.4532	1567.6037	1538.6676	1498.9194
	s, kJ/kg K	5.3269	5.3752	5.3614	5.3308	5.3165	5.3282	5.3595	5.3894	5.3688
	x_l, kg/kg	0.0184	0.0368	0.0575	0.0809	0.1071	0.1364	0.17	0.2117	0.2749
	x_v, kg/kg	0.1788	0.3112	0.4303	0.539	0.6372	0.7247	0.8024	0.8657	0.9323
	h_l, kJ/kg	591.0581	541.8927	497.7745	452.5653	405.2529	355.1627	300.4078	235.878	145.2729
	h_v, kJ/kg	2511.4453	2342.9706	2191.358	2052.3861	1925.9283	1811.5513	1707.3196	1636.1967	1530.2392

Table A.3 Ammonia-water liquid-vapour mixture properties at 5 bar

θ = f(T)	Property	Ammonia concentration (mass fraction), x									
		0.1	**0.2**	**0.3**	**0.4**	**0.5**	**0.6**	**0.7**	**0.8**	**0.9**	
0.1	T, °C	123.6632	101.6236	81.6238	63.4137	47.8164	35.5166	26.549	20.1969		15.0688
	v, m^3/kg	0.0099	0.0137	0.018	0.0241	0.0338	0.0497	0.0754	0.1148		0.1694
	h, kJ/kg	501.5903	363.2855	247.8389	165.7271	132.1818	163.9726	278.062	486.4704		791.4042
	s, kJ/kg K	1.7371	1.5142	1.2948	1.1199	1.0452	1.1375	1.4694	2.099		3.0481
	x_l, kg/kg	0.0916	0.1817	0.2721	0.3562	0.4414	0.5204	0.5912	0.6544		0.7206
	x_v, kg/kg	0.5637	0.8086	0.9208	0.9699	0.9884	0.9953	0.998	0.9991		0.9996
	h_l, kJ/kg	469.098	316.8767	182.6899	64.347	-22.597	-79.7496	-109.9315	-120.11		-115.0384
	h_v, kJ/kg	2031.3531	1708.1907	1559.7003	1457.6282	1394.9305	1354.4406	1327.9079	1310.0993		1296.1285
0.2	T, °C	126.3624	106.2976	87.9871	71.2024	56.6647	44.963	36.0879	29.3047		23.0468
	v, m^3/kg	0.02	0.0272	0.035	0.0454	0.0606	0.0828	0.114	0.1547		0.2031
	h, kJ/kg	566.0521	451.4381	358.8229	301.8171	296.327	356.0198	488.5314	690.8589		951.1149
	s, kJ/kg K	1.8985	1.7477	1.6046	1.5189	1.5483	1.7485	2.1591	2.7843		3.5946
	x_l, kg/kg	0.0816	0.1616	0.2426	0.3173	0.3917	0.4585	0.5164	0.5677		0.6241
	x_v, kJ/kg	0.5242	0.7677	0.8919	0.9538	0.9797	0.9905	0.9951	0.9973		0.9986
	h_l, kJ/kg	487.6475	349.0951	224.4937	111.7587	25.2263	-36.9851	-77.421	-102.1465		-117.165
	h_v, kg/kg	2082.0103	1763.9888	1606.9988	1496.3466	1428.4881	1384.9958	1356.2022	1335.861		1318.0091
0.3	T, °C	129.0616	110.9716	94.3504	78.9911	65.513	54.4095	45.6269	38.4126		31.0249
	v, m^3/kg	0.0317	0.042	0.0526	0.0662	0.0847	0.1097	0.142	0.1807		0.2234
	h, kJ/kg	639.6925	546.8352	472.9088	433.605	443.8004	512.9252	642.2858	823.6981		1043.395
	s, kJ/kg K	2.0815	1.997	1.9173	1.8965	1.988	2.2325	2.6465	3.2147		3.9
	x_l, kg/kg	0.0718	0.1419	0.2138	0.2846	0.3456	0.4039	0.4544	0.5004		0.5539
	x_v, kg/kg	0.4826	0.721	0.8547	0.9306	0.9661	0.9823	0.99	0.9941		0.9969
	h_l, kJ/kg	506.1735	381.4348	267.2149	165.7079	76.9059	12.6274	-33.6889	-67.5638		-96.5431
	h_v, kJ/kg	2135.3632	1826.4311	1662.6676	1542.206	1467.4687	1419.49	1387.274	1363.4735		1340.909

0.4	T, °C	131.7608	115.6456	100.7136	86.7798	74.3613	63.8559	55.1659	47.5204	39.003
	v, m^3/kg	0.0458	0.0588	0.0718	0.0875	0.1079	0.134	0.1659	0.2022	0.2399
	h, kJ/kg	726.6443	653.7506	594.8275	567.3903	585.2936	654.7614	773.6611	932.2922	1116.8628
	s, kJ/kg K	2.296	2.2726	2.2452	2.2711	2.3988	2.6571	3.0498	3.5554	4.1358
	x_l, kg/kg	0.0624	0.1229	0.1857	0.2482	0.3019	0.354	0.3998	0.4431	0.4964
	x_v, kg/kg	0.4386	0.6683	0.8159	0.898	0.9454	0.9691	0.9815	0.9886	0.9938
	h_l, kJ/kg	524.7178	413.7887	310.6257	216.4852	131.5807	66.9781	16.8247	-24.1157	-64.9684
	h_v, kJ/kg	2191.57	1895.7479	1698.0762	1597.4318	1513.9717	1459.6679	1422.4711	1393.8822	1365.3484

Table A.3 Ammonia-water liquid-vapour mixture properties at 5 bar (contd.,)

θ = f(T)	Property	Ammonia concentration (mass fraction), x								
		0.1	**0.2**	**0.3**	**0.4**	**0.5**	**0.6**	**0.7**	**0.8**	**0.9**
0.5	T, °C	134.46	120.3197	107.0769	94.5685	83.2096	73.3023	64.7049	56.6282	46.9811
	v, m^3/kg	0.0634	0.0788	0.0935	0.1105	0.1317	0.1579	0.1886	0.2221	0.2552
	h, kJ/kg	833.5687	778.8406	731.3973	710.6989	730.1836	794.0885	898.5234	1033.4334	1184.8502
	s, kJ/kg K	2.558	2.5908	2.6059	2.6633	2.8084	3.0622	3.4217	3.8632	4.348
	x_l, kg/kg	0.0532	0.1044	0.1583	0.2128	0.2647	0.307	0.3496	0.3918	0.4463
	x_v, kg/kg	0.3921	0.6095	0.7604	0.8533	0.9143	0.9483	0.9676	0.9797	0.989
	h_l, kJ/kg	543.3632	446.0739	354.4824	268.6931	193.0119	124.9008	72.0514	25.0204	-26.8679
	h_v, kJ/kg	2250.8376	1972.1653	1773.9311	1664.7444	1570.7924	1507.9247	1463.6331	1428.3398	1391.9828
0.6	T, °C	137.1592	124.9937	113.4402	102.3572	92.058	82.7488	74.2439	65.7361	54.9591
	v, m^3/kg	0.0865	0.104	0.1197	0.137	0.1581	0.1833	0.212	0.2422	0.2704
	h, kJ/kg	972.1114	933.2462	893.3913	874.2246	889.4209	942.3042	1028.1739	1136.8964	1253.7813
	s, kJ/kg K	2.8951	2.9786	3.0258	3.1008	3.247	3.4811	3.7966	4.1691	4.5575
	x_l, kg/kg	0.0442	0.0867	0.1318	0.1785	0.2241	0.2669	0.3025	0.3444	0.4009
	x_v, kJ/kg	0.3429	0.5445	0.6939	0.8026	0.8692	0.9162	0.9457	0.9657	0.9817
	h_l, kJ/kg	562.246	478.2449	398.5247	321.9215	251.7331	190.0046	130.8384	78.2503	15.6743
	h_v, kg/kg	2313.437	2055.9942	1862.1699	1716.5196	1641.5421	1567.5239	1513.2941	1468.5384	1421.6526

0.7	T, °C	139.8584	129.6677	119.8034	110.1459	100.9063	92.1952	83.7829	74.8439	62.9372
	v, m^3/kg	0.1191	0.1379	0.1536	0.1701	0.1897	0.2127	0.2381	0.264	0.2864
	h, kJ/kg	1164.497	1137.3171	1099.5693	1075.3454	1078.9703	1113.647	1174.4923	1251.3746	1328.4222
	s, kJ/kg K	3.3602	3.4847	3.5509	3.627	3.7558	3.9521	4.2079	4.4983	4.7786
	x_l, kg/kg	0.0356	0.0697	0.1064	0.1454	0.1848	0.2235	0.262	0.3	0.3587
	x_v, kg/kg	0.2908	0.4729	0.6163	0.7297	0.8144	0.8683	0.9119	0.944	0.9707
	h_l, kJ/kg	581.6621	510.3353	442.513	375.7168	311.9487	252.6567	196.7588	134.4748	61.5212
	h_v, kJ/kg	2379.7244	2147.7297	1963.3676	1814.9056	1700.1973	1642.7718	1574.9109	1516.7751	1455.4502
0.8	T, °C	142.5576	134.3417	126.1667	117.9346	109.7546	101.6417	93.3219	83.9517	70.9153
	v, m^3/kg	0.1699	0.188	0.2017	0.2153	0.2312	0.2497	0.2697	0.2893	0.3039
	h, kJ/kg	1459.4337	1433.1102	1386.6299	1346.0996	1326.2146	1330.3554	1354.0323	1387.4949	1413.6845
	s, kJ/kg K	4.0689	4.2098	4.2697	4.32	4.403	4.5319	4.6987	4.8794	5.0253
	x_l, kg/kg	0.0273	0.0535	0.0823	0.1137	0.147	0.1816	0.2184	0.2613	0.3187
	x_v, kg/kg	0.2353	0.3942	0.5272	0.6403	0.7337	0.8085	0.8613	0.9111	0.9545
	h_l, kJ/kg	602.2684	542.5414	486.3025	429.6108	373.0085	317.0004	260.2574	197.8646	109.9734
	h_v, kJ/kg	2450.1715	2248.173	2078.2483	1932.2672	1809.5189	1708.3941	1653.033	1576.135	1494.8049
0.9	T, °C	145.2568	139.0157	132.5299	125.7233	118.6029	111.0881	102.8609	93.0596	78.8934
	v, m^3/kg	0.2619	0.2725	0.2788	0.2846	0.2921	0.3013	0.3116	0.3207	0.3241
	h, kJ/kg	1987.9972	1924.6608	1839.0645	1755.1574	1685.5467	1633.0625	1594.3012	1561.0191	1515.7967
	s, kJ/kg K	5.3316	5.4017	5.3845	5.3459	5.3211	5.3207	5.3383	5.3528	5.3139
	x_l, kg/kg	0.0192	0.0383	0.0597	0.084	0.1111	0.1415	0.1763	0.2196	0.285
	x_v, kg/kg	0.1761	0.3074	0.4256	0.5338	0.6318	0.7198	0.7984	0.863	0.931
	h_l, kJ/kg	625.8428	575.5141	530.0162	483.2575	434.2267	382.2415	325.3884	258.486	165.0827
	h_v, kJ/kg	2525.4123	2358.6089	2208.1361	2069.7773	1943.2556	1828.0743	1722.3302	1650.6167	1541.578

Table A.3 Ammonia-water liquid-vapour mixture properties at 6 bar

θ = f(T)	Property	Ammonia concentration (mass fraction), x								
		0.1	**0.2**	**0.3**	**0.4**	**0.5**	**0.6**	**0.7**	**0.8**	**0.9**
0.1	T, °C	130.7096	108.3974	88.1149	69.6584	53.846	41.3489	32.1909	25.6465	20.3125
	v, m^3/kg	0.0087	0.0118	0.0154	0.0205	0.0286	0.0418	0.0631	0.0957	0.1411
	h, kJ/kg	532.906	393.2053	276.2238	192.5105	157.025	186.0206	295.7591	497.8685	795.3575
	s, kJ/ kg K	1.8129	1.5899	1.3694	1.1921	1.1123	1.1937	1.5052	2.1025	3.0095
	x_l, kg/kg	0.0918	0.182	0.2725	0.3567	0.442	0.5214	0.5929	0.6574	0.726
	x_v, kg/kg	0.5495	0.7955	0.9126	0.9658	0.9865	0.9944	0.9975	0.9988	0.9995
	h_l, kJ/kg	499.9299	346.4788	211.1789	91.9854	4.4057	-53.2114	-83.6628	-93.7731	-87.8935
	h_v, kJ/kg	2058.3318	1733.9397	1581.0512	1473.7718	1407.3956	1364.4819	1336.3244	1317.3274	1302.3269
0.2	T, °C	133.3843	113.0659	94.4884	77.4648	62.7114	50.8048	41.7245	34.7245	28.2187
	v, m^3/kg	0.0174	0.0233	0.0298	0.0386	0.0513	0.0698	0.0958	0.1297	0.1701
	h, kJ/kg	597.9697	481.7749	387.3651	328.3527	320.3676	376.7757	505.0401	702.4147	957.7313
	s, kJ/ kg K	1.973	1.8203	1.674	1.5831	1.6036	1.7894	2.1786	2.7761	3.5553
	x_l, kg/kg	0.0819	0.1621	0.2433	0.3181	0.3927	0.46	0.5188	0.5715	0.6302
	x_v, kJ/kg	0.5111	0.7545	0.8824	0.9484	0.9768	0.9889	0.9942	0.9968	0.9984
	h_l, kJ/kg	518.276	378.4874	252.8053	139.2041	51.9828	-10.8061	-51.6993	-76.6862	-91.4543
	h_v, kg/kg	2107.6082	1789.7921	1629.6472	1514.1298	1442.492	1396.348	1365.6863	1343.9039	1324.7046

0.3	T, °C	136.0589	117.7344	100.8619	85.2712	71.5769	60.2607	51.258	43.8026	36.125
	v, m^3/kg	0.0274	0.036	0.0449	0.0562	0.0717	0.0926	0.1196	0.1519	0.1876
	h, kJ/kg	672.3636	577.8634	502.026	460.5279	468.0187	533.7986	659.2121	836.3478	1051.7579
	s, kJ/ kg K	2.1547	2.0669	1.9825	1.9549	2.0359	2.2649	2.6585	3.2023	3.861
	x_l, kg/kg	0.0723	0.1428	0.2148	0.2857	0.347	0.4059	0.4573	0.5045	0.5602
	x_v, kg/kg	0.4707	0.7081	0.85	0.9238	0.9621	0.9799	0.9886	0.9932	0.9964
	h_l, kJ/kg	536.6214	410.623	295.3295	192.9503	103.3845	38.402	-8.5807	-43.0423	-72.294
	h_v, kJ/kg	2159.4053	1851.7971	1656.9099	1561.6012	1483.1268	1432.3085	1397.9666	1372.4338	1348.1572
0.4	T, °C	138.7336	122.4028	107.2355	93.0776	80.4423	69.7166	60.7916	52.8806	44.0312
	v, m^3/kg	0.0395	0.0504	0.0612	0.0744	0.0915	0.1133	0.14	0.1703	0.2017
	h, kJ/kg	760.19	685.7399	624.9031	595.2415	610.4071	676.5883	791.7623	946.3996	1126.7302
	s, kJ/ kg K	2.3676	2.3401	2.3071	2.3253	2.4418	2.6847	3.0582	3.5416	4.0975
	x_l, kg/kg	0.0629	0.1239	0.187	0.2497	0.3038	0.3564	0.403	0.4476	0.503
	x_v, kg/kg	0.428	0.6561	0.8049	0.8898	0.9399	0.9657	0.9793	0.9873	0.9931
	h_l, kJ/kg	554.9991	442.7995	338.5462	243.5074	157.7552	92.329	41.3182	-0.4924	-42.0612
	h_v, kJ/kg	2213.8863	1920.1645	1720.9666	1618.2463	1531.2943	1474.0506	1434.4804	1403.84	1373.1853

Table A.3 Ammonia-water liquid-vapour mixture properties at 6 bar (contd.,)

θ = f(T)	Property	Ammonia concentration (mass fraction), x								
		0.1	**0.2**	**0.3**	**0.4**	**0.5**	**0.6**	**0.7**	**0.8**	**0.9**
0.5	T, °C	141.4083	127.0713	113.609	100.884	89.3077	79.1725	70.3251	61.9586	51.9375
	v, m^3/kg	0.0546	0.0676	0.0799	0.0941	0.1118	0.1338	0.1594	0.1873	0.2148
	h, kJ/kg	868.052	812.0257	762.7551	739.9171	756.7356	817.4435	918.2584	1049.2087	1196.1348
	s, kJ/kg K	2.6274	2.6558	2.6648	2.7143	2.8481	3.087	3.4283	3.8491	4.3104
	x_l, kg/kg	0.0538	0.1056	0.1599	0.2147	0.2669	0.3099	0.3533	0.3967	0.4532
	x_v, kg/kg	0.383	0.5985	0.7494	0.85	0.9075	0.9437	0.9645	0.9778	0.988
	h_l, kJ/kg	573.495	474.9385	382.2217	295.4792	218.8921	149.8098	95.9308	47.7792	-5.2163
	h_v, kJ/kg	2271.2621	1995.1283	1796.6855	1656.9634	1589.5988	1523.8412	1476.9846	1439.3209	1400.4109

0.6	T, °C	144.0829	131.7398	119.9825	108.6904	98.1732	88.6284	79.8587	71.0367	59.8437
	v, m^3/kg	0.0744	0.0892	0.1023	0.1168	0.1344	0.1555	0.1794	0.2045	0.2278
	h, kJ/kg	1007.3508	967.7381	926.2321	905.0712	917.7308	967.501	1049.7604	1154.3853	1266.36
	s, kJ/kg K	2.9607	3.0402	3.0813	3.1484	3.2838	3.5038	3.8021	4.1548	4.5203
	x_l, kg/kg	0.045	0.088	0.1336	0.1807	0.2267	0.2701	0.3066	0.3497	0.4082
	x_v, kJ/kg	0.3354	0.535	0.6837	0.7931	0.8614	0.9104	0.9417	0.9631	0.9804
	h_l, kJ/kg	592.2449	507	426.1189	348.4821	277.293	214.4946	154.0972	100.1603	36.1216
	h_v, kg/kg	2331.8077	2077.0214	1883.9131	1737.2687	1661.3353	1584.7017	1527.8436	1480.4581	1430.6151
0.7	T, °C	146.7576	136.4083	126.3561	116.4968	107.0386	98.0843	89.3922	80.1147	67.75
	v, m^3/kg	0.1022	0.1182	0.1313	0.1451	0.1614	0.1806	0.2017	0.2231	0.2413
	h, kJ/kg	1199.64	1172.913	1133.7935	1107.7351	1108.9542	1140.5789	1197.7531	1270.319	1342.0153
	s, kJ/kg K	3.4179	3.5406	3.601	3.6696	3.7884	3.9715	4.2111	4.4827	4.7409
	x_l, kg/kg	0.0364	0.0711	0.1084	0.1478	0.1878	0.2271	0.2666	0.3054	0.3664
	x_v, kg/kg	0.285	0.4652	0.6077	0.7209	0.8065	0.8619	0.9071	0.9409	0.9692
	h_l, kJ/kg	611.5373	539.0191	470.019	402.0981	337.2036	276.6985	219.4398	155.7005	80.7901
	h_v, kJ/kg	2395.8817	2166.3647	1983.2038	1834.7494	1718.8047	1660.5366	1590.2132	1529.352	1464.7915
0.8	T, °C	149.4323	141.0768	132.7296	124.3032	115.9041	107.5402	98.9258	89.1927	75.6562
	v, m^3/kg	0.1449	0.1608	0.1722	0.1836	0.1968	0.212	0.2286	0.2446	0.2562
	h, kJ/kg	1491.3624	1468.52	1421.2772	1379.0839	1356.8712	1357.9941	1377.9845	1407.0374	1427.7026
	s, kJ/kg K	4.1076	4.2534	4.309	4.3528	4.4267	4.5437	4.6959	4.8594	4.985
	x_l, kg/kg	0.0281	0.0549	0.0843	0.1164	0.1503	0.1856	0.2234	0.2675	0.3269
	x_v, kg/kg	0.2313	0.3887	0.5207	0.6333	0.7269	0.8025	0.8567	0.908	0.953
	h_l, kJ/kg	632.0071	571.1937	513.7892	455.8883	398.0154	340.6258	282.3281	218.1469	128.0741
	h_v, kJ/kg	2463.9608	2263.9847	2095.3196	1949.8681	1826.7408	1724.3333	1668.1656	1588.7642	1504.213
0.9	T, °C	152.1069	145.7452	139.1032	132.1096	124.7695	116.9961	108.4593	98.2708	83.5625
	v, m^3/kg	0.2208	0.2318	0.2373	0.2421	0.2481	0.2555	0.2637	0.2709	0.2731
	h, kJ/kg	2004.0818	1954.1948	1870.1305	1785.1756	1713.459	1658.24	1616.2165	1579.119	1529.1018
	s, kJ/kg K	5.3128	5.4122	5.3974	5.3549	5.3233	5.3137	5.3201	5.3217	5.2674
	x_l, kg/kg	0.02	0.0396	0.0616	0.0866	0.1145	0.1458	0.1817	0.2263	0.2937
	x_v, kg/kg	0.1739	0.3044	0.422	0.5297	0.6276	0.7158	0.795	0.8608	0.9299
	h_l, kJ/kg	655.3026	604.1398	557.5461	509.5372	459.0994	405.5353	346.9025	277.9453	182.1088
	h_v, kJ/kg	2536.6861	2371.187	2221.6362	2083.8188	1957.3248	1841.5727	1734.6412	1662.2137	1550.5039

Table A.3 Ammonia-water liquid-vapour mixture properties at 7 bar

θ = f(T)	Property	Ammonia concentration (mass fraction), x								
		0.1	**0.2**	**0.3**	**0.4**	**0.5**	**0.6**	**0.7**	**0.8**	**0.9**
0.1	T, °C	136.879	114.3327	93.8072	75.1385	59.1398	46.471	37.1465	30.4329	24.9174
	v, m^3/kg	0.0078	0.0104	0.0135	0.0179	0.0249	0.0361	0.0543	0.082	0.1207
	h, kJ/kg	560.4224	419.589	301.3023	216.1917	178.9946	205.5336	311.4582	508.0066	798.7354
	s, kJ/kg K	1.8785	1.6556	1.4343	1.2551	1.1708	1.243	1.5374	2.1073	2.9778
	x_l, kg/kg	0.0919	0.1822	0.2727	0.3571	0.4425	0.5222	0.5944	0.6601	0.7308
	x_v, kg/kg	0.5375	0.7842	0.9051	0.9619	0.9846	0.9935	0.997	0.9986	0.9993
	h_l, kJ/kg	527.0949	372.6133	236.3497	116.3934	28.2318	-29.8171	-60.5221	-70.5771	-63.9752
	h_v, kJ/kg	2081.0686	1756.0624	1599.6098	1487.9068	1418.2873	1373.1769	1343.519	1323.4127	1307.4467
0.2	T, °C	139.5296	118.9935	100.1869	82.9575	68.0174	55.9322	46.6719	39.4807	32.7554
	v, m^3/kg	0.0154	0.0205	0.0261	0.0336	0.0445	0.0604	0.0826	0.1117	0.1464
	h, kJ/kg	625.8826	508.4522	412.5499	351.8145	341.6555	395.1753	519.6783	712.6015	963.3582
	s, kJ/kg K	2.0371	1.8831	1.7343	1.6392	1.6523	1.8258	2.1968	2.7706	3.5227
	x_l, kg/kg	0.0822	0.1626	0.2439	0.3188	0.3936	0.4614	0.5208	0.5747	0.6355
	x_v, kJ/kg	0.5001	0.7432	0.8739	0.9433	0.974	0.9874	0.9934	0.9963	0.9981
	h_l, kJ/kg	545.2439	404.4211	277.8116	163.4465	75.6052	12.2913	-29.016	-54.2325	-68.7462
	h_v, kg/kg	2129.1387	1811.7917	1649.2088	1529.6308	1454.7177	1406.208	1373.8438	1350.7288	1330.2733
0.3	T, °C	142.1802	123.6544	106.5665	90.7766	76.8949	65.3935	56.1974	48.5285	40.5933
	v, m^3/kg	0.0242	0.0316	0.0392	0.049	0.0623	0.0803	0.1034	0.1311	0.1617
	h, kJ/kg	700.7671	605.0496	527.6553	484.3023	489.4529	552.2913	674.1968	847.463	1058.8991
	s, kJ/kg K	2.2172	2.1272	2.0392	2.006	2.0781	2.2941	2.6702	3.1931	3.8286
	x_l, kg/kg	0.0727	0.1435	0.2157	0.2867	0.3483	0.4077	0.4598	0.5082	0.5658
	x_v, kg/kg	0.4607	0.6971	0.8416	0.9175	0.9582	0.9776	0.9872	0.9924	0.9959
	h_l, kJ/kg	563.4056	436.363	320.1602	217.0176	126.7725	61.1598	13.5817	-21.3973	-50.8596
	h_v, kJ/kg	2179.5947	1873.2748	1675.3533	1578.4082	1496.7509	1443.4401	1407.1876	1380.0706	1354.2115

0.4	T, °C	144.8309	128.3153	112.9461	98.5956	85.7725	74.8547	65.7229	57.5763	48.4313
	v, m^3/kg	0.0348	0.0442	0.0536	0.0649	0.0796	0.0984	0.1212	0.1472	0.1741
	h, kJ/kg	789.1201	713.6174	651.2709	619.762	632.5794	695.8813	807.7322	958.7455	1135.1544
	s, kJ/kg K	2.4283	2.398	2.3607	2.3727	2.4798	2.7097	3.0667	3.5309	4.0655
	x_l, kg/kg	0.0635	0.1248	0.1881	0.251	0.3054	0.3585	0.4059	0.4516	0.5088
	x_v, kg/kg	0.4192	0.6458	0.7954	0.8824	0.9349	0.9624	0.9772	0.986	0.9924
	h_l, kJ/kg	581.6136	468.3608	363.1913	267.3803	180.8838	114.7273	62.9544	20.3734	-21.8056
	h_v, kJ/kg	2232.6033	1940.719	1740.5619	1636.1577	1546.2866	1486.5039	1444.8307	1412.3361	1379.7416

Table A.3 Ammonia-water liquid-vapour mixture properties at 7 bar (contd.,)

θ = f(T)	Property	Ammonia concentration (mass fraction), x								
		0.1	**0.2**	**0.3**	**0.4**	**0.5**	**0.6**	**0.7**	**0.8**	**0.9**
0.5	T, °C	147.4815	132.9761	119.3258	106.4146	94.6501	84.3159	75.2484	66.6241	56.2693
	v, m^3/kg	0.0481	0.0593	0.0699	0.0821	0.0974	0.1162	0.1382	0.1622	0.1856
	h, kJ/kg	897.4383	840.7241	790.0887	765.5155	780.07	837.9886	935.5812	1062.9365	1205.7316
	s, kJ/kg K	2.6854	2.711	2.7154	2.7585	2.8831	3.1094	3.4352	3.8379	4.2789
	x_l, kg/kg	0.0544	0.1067	0.1612	0.2163	0.2689	0.3123	0.3565	0.401	0.4593
	x_v, kg/kg	0.3754	0.5892	0.7401	0.8426	0.9014	0.9394	0.9617	0.976	0.9871
	h_l, kJ/kg	599.9528	500.3487	406.6949	319.1427	241.7701	171.8307	117.039	67.8924	13.9325
	h_v, kJ/kg	2288.377	2014.3699	1815.9816	1673.9185	1605.7622	1537.5497	1488.4515	1448.6715	1407.4538
0.6	T, °C	150.1321	137.637	125.7054	114.2336	103.5277	93.7772	84.7738	75.6719	64.1073
	v, m^3/kg	0.0654	0.0783	0.0896	0.1021	0.1172	0.1353	0.1558	0.1772	0.1969
	h, kJ/kg	1036.8436	997.2495	954.6292	931.9182	942.4527	989.5241	1068.5731	1169.4888	1276.9853
	s, kJ/kg K	3.0142	3.0918	3.1285	3.1894	3.316	3.524	3.8076	4.1431	4.4888
	x_l, kg/kg	0.0456	0.0891	0.1352	0.1826	0.229	0.2729	0.3102	0.3544	0.4146
	x_v, kJ/kg	0.3291	0.527	0.6752	0.785	0.8545	0.9052	0.938	0.9608	0.9792
	h_l, kJ/kg	618.5556	532.2857	450.4429	371.9391	299.8906	236.1572	174.6697	119.5332	54.2074
	h_v, kg/kg	2347.1909	2094.58	1902.2067	1754.9381	1678.2133	1599.3924	1540.2678	1490.5626	1438.0773

0.7	T, °C	152.7828	142.2978	132.085	122.0526	112.4053	103.2384	94.2993	84.7197	71.9453
	v, m^3/kg	0.0895	0.1036	0.115	0.1269	0.1409	0.1573	0.1753	0.1935	0.2087
	h, kJ/kg	1228.1481	1202.8551	1163.0324	1135.6586	1134.9199	1163.917	1217.8429	1286.5242	1353.3908
	s, kJ/kg K	3.4627	3.5861	3.6428	3.7058	3.8164	3.9884	4.2142	4.4694	4.7085
	x_l, kg/kg	0.0371	0.0723	0.1101	0.15	0.1904	0.2303	0.2705	0.3104	0.3732
	x_v, kg/kg	0.2801	0.4589	0.6005	0.7135	0.7997	0.8563	0.9029	0.9382	0.9678
	h_l, kJ/kg	637.7038	564.2129	494.2361	425.375	359.5217	297.9698	239.5126	174.3342	97.8351
	h_v, kJ/kg	2409.4037	2181.8913	1999.7948	1851.4837	1734.6476	1675.6119	1603.1874	1539.9454	1472.523
0.8	T, °C	155.4334	146.9587	138.4647	129.8716	121.2829	112.6996	103.8248	93.7675	79.7833
	v, m^3/kg	0.1262	0.1406	0.1506	0.1604	0.1717	0.1847	0.1987	0.2121	0.2216
	h, kJ/kg	1515.39	1497.3621	1450.2745	1407.1064	1383.1133	1381.7073	1398.4614	1423.576	1439.2952
	s, kJ/kg K	4.1322	4.2863	4.3403	4.3796	4.4463	4.5534	4.6932	4.8419	4.95
	x_l, kg/kg	0.0289	0.0562	0.0861	0.1187	0.1532	0.1891	0.2277	0.2729	0.3341
	x_v, kg/kg	0.2279	0.3842	0.5154	0.6275	0.7212	0.7974	0.8527	0.9053	0.9516
	h_l, kJ/kg	658.0006	596.3198	537.9538	479.0467	420.0973	361.5184	301.8639	236.0955	144.0872
	h_v, kJ/kg	2475.4893	2277.1455	2109.5471	1964.608	1841.2596	1737.8572	1680.9027	1599.3229	1511.9377
0.9	T, °C	158.084	151.6195	144.8443	137.6906	130.1605	122.1609	113.3502	102.8153	87.6213
	v, m^3/kg	0.1902	0.2017	0.2068	0.211	0.216	0.2223	0.229	0.2349	0.2361
	h, kJ/kg	2011.0353	1976.1283	1894.9536	1809.9629	1736.9174	1679.5494	1634.7331	1594.243	1539.9307
	s, kJ/kg K	5.2813	5.4129	5.4036	5.36	5.3237	5.3069	5.304	5.2945	5.2268
	x_l, kg/kg	0.0208	0.0408	0.0634	0.0889	0.1175	0.1495	0.1864	0.2322	0.3
	x_v, kg/kg	0.1721	0.3019	0.419	0.5263	0.6241	0.7124	0.7922	0.8589	0.9289
	h_l, kJ/kg	680.9804	629.2101	581.706	532.6529	481.0289	426.1178	365.9346	295.1641	193.7416
	h_v, kJ/kg	2546.0878	2381.6563	2232.8791	2095.5436	1969.1186	1852.9344	1745.0291	1671.8391	1557.7612

Table A.3 Ammonia-water liquid-vapour mixture properties at 8 bar

θ = f(T)	Property	Ammonia concentration (mass fraction), x								
		0.1	**0.2**	**0.3**	**0.4**	**0.5**	**0.6**	**0.7**	**0.8**	**0.9**
0.1	T, °C	142.3861	119.6342	98.8955	80.0398	63.8762	51.055	41.5821	34.7172	29.0388
	v, m^3/kg	0.007	0.0094	0.0121	0.016	0.022	0.0319	0.0477	0.0718	0.1054
	h, kJ/kg	585.0631	443.2917	323.8706	237.5158	198.7882	223.1281	325.6433	517.1952	801.705
	s, kJ/kg K	1.9364	1.7138	1.4918	1.311	1.2229	1.2871	1.5668	2.1128	2.9512
	x_l, kg/kg	0.0921	0.1824	0.273	0.3574	0.443	0.523	0.5957	0.6625	0.7349
	x_v, kg/kg	0.5272	0.7742	0.8982	0.9582	0.9827	0.9925	0.9965	0.9983	0.9992
	h_l, kJ/kg	551.4851	396.1217	259.0096	138.3603	49.6612	-8.7915	-39.7351	-49.745	-42.4908
	h_v, kJ/kg	2100.7075	1775.424	1616.0238	1500.4884	1427.9688	1380.8457	1349.7889	1328.6372	1311.7564
0.2	T, °C	145.0132	124.2861	105.2783	87.8678	72.7624	60.5187	51.0978	43.7349	36.8119
	v, m^3/kg	0.0138	0.0183	0.0232	0.0298	0.0394	0.0533	0.0727	0.0981	0.1284
	h, kJ/kg	650.7793	532.3608	435.1857	372.9382	360.8408	411.7736	532.8865	721.7514	968.2446
	s, kJ/kg K	2.0935	1.9387	1.7879	1.6891	1.6958	1.8588	2.2139	2.7668	3.495
	x_l, kg/kg	0.0825	0.1631	0.2444	0.3195	0.3945	0.4626	0.5227	0.5777	0.6403
	x_v, kJ/kg	0.4906	0.7333	0.8662	0.9386	0.9714	0.9859	0.9925	0.9958	0.9978
	h_l, kJ/kg	569.4415	427.7356	300.32	185.2672	96.8601	33.0641	-8.6225	-34.0434	-48.3008
	h_v, kg/kg	2147.7063	1830.9286	1666.4125	1543.3729	1465.5722	1414.9244	1380.9919	1356.6322	1334.994
0.3	T, °C	147.6403	128.9379	111.661	95.6957	81.6486	69.9824	60.6135	52.7526	44.585
	v, m^3/kg	0.0217	0.0282	0.035	0.0435	0.0552	0.0709	0.0911	0.1154	0.1422
	h, kJ/kg	725.9546	629.3234	550.634	505.6737	508.7508	568.9602	687.6881	857.403	1065.1144
	s, kJ/kg K	2.2719	2.1804	2.0894	2.0515	2.1161	2.3208	2.6816	3.186	3.8009
	x_l, kg/kg	0.0731	0.1441	0.2164	0.2876	0.3495	0.4092	0.462	0.5115	0.5708
	x_v, kg/kg	0.4521	0.6876	0.8335	0.9117	0.9546	0.9754	0.9858	0.9915	0.9955
	h_l, kJ/kg	587.4215	459.4943	342.5016	238.6845	147.824	81.6392	33.5216	-1.9202	-31.5449
	h_v, kJ/kg	2196.9839	1891.8603	1692.2912	1593.2311	1508.8095	1453.2765	1415.2848	1386.7027	1359.3659

0.4	T, °C	150.2675	133.5898	118.0438	103.5237	90.5348	79.4462	70.1292	61.7703	52.3581
	v, m^3/kg	0.0312	0.0395	0.0477	0.0576	0.0705	0.087	0.107	0.1298	0.1533
	h, kJ/kg	814.578	738.3841	674.8235	641.7385	652.4899	713.2219	822.0625	969.7384	1142.4798
	s, kJ/kg K	2.4809	2.4488	2.4081	2.4148	2.5139	2.7325	3.0752	3.5224	4.0381
	x_l, kg/kg	0.0639	0.1256	0.1891	0.2522	0.3069	0.3604	0.4084	0.4552	0.5141
	x_v, kg/kg	0.4116	0.637	0.7871	0.8757	0.9303	0.9594	0.9752	0.9848	0.9918
	h_l, kJ/kg	605.4587	491.318	385.3596	288.8691	201.7073	134.8932	82.4329	39.1604	-3.5456
	h_v, kJ/kg	2248.7064	1958.4272	1757.6552	1651.8604	1559.4936	1497.4769	1453.9123	1419.7213	1385.3323

Table A.3 Ammonia-water liquid-vapour mixture properties at 8 bar (contd.,)

θ = f(T)	Property	Ammonia concentration (mass fraction), x								
		0.1	**0.2**	**0.3**	**0.4**	**0.5**	**0.6**	**0.7**	**0.8**	**0.9**
0.5	T, °C	152.8946	138.2416	124.4266	111.3517	99.421	88.9099	79.6449	70.788	60.1312
	v, m^3/kg	0.043	0.053	0.0623	0.073	0.0865	0.103	0.1222	0.1431	0.1635
	h, kJ/kg	923.0145	866.0434	814.375	788.3551	800.9396	856.3742	951.0455	1075.0924	1214.0438
	s, kJ/kg K	2.735	2.7591	2.76	2.7977	2.9143	3.1298	3.4419	3.8287	4.2516
	x_l, kg/kg	0.055	0.1076	0.1625	0.2178	0.2706	0.3145	0.3594	0.4049	0.4649
	x_v, kg/kg	0.3688	0.5813	0.732	0.8355	0.8959	0.9355	0.959	0.9743	0.9862
	h_l, kJ/kg	623.635	523.146	428.6927	340.4408	262.3734	191.6651	136.0524	86.0105	31.1993
	h_v, kJ/kg	2303.088	2030.8885	1832.6881	1689.3576	1619.9154	1549.5722	1498.4816	1456.7859	1413.4542
0.6	T, °C	155.5217	142.8935	130.8093	119.1797	108.3072	98.3736	89.1606	79.8057	67.9043
	v, m^3/kg	0.0583	0.0699	0.0799	0.0908	0.1041	0.12	0.1378	0.1565	0.1735
	h, kJ/kg	1062.0764	1023.0259	979.6658	955.7167	964.4346	1009.1121	1085.2581	1182.769	1286.1312
	s, kJ/kg K	3.0588	3.1361	3.1695	3.2254	3.3444	3.5421	3.8128	4.1332	4.4613
	x_l, kg/kg	0.0463	0.0902	0.1366	0.1843	0.231	0.2754	0.3134	0.3586	0.4205
	x_v, kJ/kg	0.3237	0.5203	0.6678	0.7779	0.85	0.9005	0.9347	0.9587	0.9781
	h_l, kJ/kg	642.0832	554.9526	472.2932	393.0428	320.2404	255.6757	193.2096	136.9917	70.519
	h_v, kg/kg	2360.4017	2109.6137	1917.9491	1770.2837	1692.8945	1612.2006	1551.0826	1499.2974	1444.4148

0.7	T, °C	158.1488	147.5453	137.1921	127.0077	117.1934	107.8373	98.6763	88.8234	75.6774
	v, m^3/kg	0.0796	0.0924	0.1025	0.1129	0.1252	0.1395	0.1552	0.171	0.184
	h, kJ/kg	1251.7822	1228.5948	1188.5271	1160.2021	1157.8255	1184.5218	1235.5239	1300.6587	1363.1007
	s, kJ/kg K	3.4981	3.6241	3.6784	3.737	3.8408	4.0033	4.217	4.4579	4.68
	x_l, kg/kg	0.0378	0.0734	0.1116	0.1519	0.1927	0.2331	0.274	0.3149	0.3794
	x_v, kg/kg	0.2758	0.4535	0.5943	0.7071	0.7937	0.8514	0.8992	0.9357	0.9666
	h_l, kJ/kg	661.0701	586.7706	515.97	446.3036	379.6172	317.1375	257.608	191.1333	113.2114
	h_v, kJ/kg	2421.0034	2195.1602	2014.0081	1865.9051	1748.4012	1688.6692	1614.4131	1549.0533	1479.0552
0.8	T, °C	160.776	152.1972	143.5749	134.8356	126.0795	117.301	108.192	97.8411	83.4505
	v, m^3/kg	0.1116	0.1251	0.1341	0.1427	0.1525	0.1638	0.1759	0.1875	0.1953
	h, kJ/kg	1533.8354	1521.4118	1475.1043	1431.4143	1406.0225	1402.45	1416.3219	1437.861	1449.0842
	s, kJ/kg K	4.1475	4.3117	4.3656	4.4019	4.4629	4.5617	4.6907	4.8263	4.9189
	x_l, kg/kg	0.0296	0.0574	0.0877	0.1207	0.1557	0.1923	0.2315	0.2778	0.3407
	x_v, kg/kg	0.2249	0.3804	0.5109	0.6226	0.7162	0.7929	0.85	0.9029	0.9504
	h_l, kJ/kg	681.1782	618.7903	559.6118	499.8445	439.9667	380.3438	319.4792	252.282	158.5359
	h_v, kJ/kg	2485.362	2288.3784	2121.7013	1977.2428	1853.7662	1749.563	1691.855	1608.3436	1518.4183
0.9	T, °C	163.4031	156.849	149.9576	142.6636	134.9657	126.7647	117.7077	106.8588	91.2236
	v, m^3/kg	0.1665	0.1785	0.1835	0.1872	0.1916	0.1969	0.2026	0.2074	0.2081
	h, kJ/kg	2012.1896	1992.73	1915.2678	1830.9028	1757.053	1697.9557	1650.7156	1607.1548	1548.9456
	s, kJ/kg K	5.243	5.4073	5.4054	5.3623	5.3229	5.3003	5.2895	5.2701	5.1905
	x_l, kg/kg	0.0216	0.042	0.065	0.0911	0.1202	0.1529	0.1905	0.2374	0.3037
	x_v, kg/kg	0.1705	0.2998	0.4164	0.5234	0.6211	0.7095	0.7897	0.8572	0.9281
	h_l, kJ/kg	703.8294	651.5854	603.3258	553.3823	500.7352	444.6438	383.0901	310.6912	205.9873
	h_v, kJ/kg	2554.1109	2390.5831	2242.473	2105.5686	1979.232	1862.7062	1753.9778	1680.0108	1563.7954

Table A.3 Ammonia-water liquid-vapour mixture properties at 9 bar

θ = f(T)	Property	Ammonia concentration (mass fraction), x								
		0.1	**0.2**	**0.3**	**0.4**	**0.5**	**0.6**	**0.7**	**0.8**	**0.9**
0.1	T, °C	147.3736	124.4381	103.5089	84.4857	68.1742	55.2156	45.6084	38.6065	32.78
	v, m^3/kg	0.0065	0.0085	0.011	0.0144	0.0198	0.0285	0.0425	0.0637	0.0934
	h, kJ/kg	607.4513	464.8818	344.4587	256.9859	216.8632	239.2072	338.6376	525.6339	804.3669
	s, kJ/kg K	1.9883	1.7661	1.5437	1.3614	1.27	1.3273	1.5938	2.1188	2.9285
	x_l, kg/kg	0.0922	0.1826	0.2732	0.3577	0.4434	0.5237	0.5969	0.6646	0.7387
	x_v, kg/kg	0.5181	0.7652	0.8919	0.9546	0.9809	0.9916	0.996	0.998	0.9991
	h_l, kJ/kg	573.6952	417.564	279.693	158.4093	69.21	10.3778	-20.7917	-30.7634	-22.9125
	h_v, kJ/kg	2117.9845	1792.6144	1630.7319	1511.8278	1436.6856	1387.7018	1355.331	1333.187	1315.4329
0.2	T, °C	149.9777	129.08	109.8926	92.32	77.0663	64.6797	55.1133	47.5945	40.4913
	v, m^3/kg	0.0126	0.0166	0.021	0.0269	0.0354	0.0477	0.0649	0.0874	0.1144
	h, kJ/kg	673.3063	554.0849	455.8052	392.2095	378.3656	426.9486	544.9648	730.0797	972.5535
	s, kJ/kg K	2.1438	1.9886	1.8361	1.7343	1.7354	1.8889	2.2301	2.7644	3.471
	x_l, kg/kg	0.0827	0.1635	0.2449	0.32	0.3952	0.4636	0.5244	0.5803	0.6446
	x_v, kJ/kg	0.4822	0.7245	0.8593	0.9341	0.9688	0.9844	0.9916	0.9953	0.9976
	h_l, kJ/kg	591.4654	448.9939	320.8606	205.1836	116.2559	52.0131	9.976	-15.6287	-29.6303
	h_v, kg/kg	2164.0204	1847.8367	1681.7547	1555.7129	1475.3329	1422.7319	1387.342	1361.811	1339.051
0.3	T, °C	152.5819	133.7219	116.2763	100.1542	85.9585	74.1438	64.6181	56.5825	48.2026
	v, m^3/kg	0.0198	0.0255	0.0316	0.0392	0.0496	0.0636	0.0815	0.1031	0.1269
	h, kJ/kg	748.6245	651.3041	571.515	525.1392	526.3555	584.1761	699.9928	866.4095	1070.5998
	s, kJ/kg K	2.3205	2.228	2.1346	2.0927	2.1506	2.3453	2.6926	3.1805	3.7768
	x_l, kg/kg	0.0735	0.1447	0.2171	0.2884	0.3505	0.4106	0.464	0.5144	0.5754
	x_v, kg/kg	0.4445	0.6792	0.8261	0.9064	0.9512	0.9733	0.9845	0.9907	0.9951
	h_l, kJ/kg	609.2646	480.5732	362.8841	258.4626	167.0388	100.3293	51.7176	15.8575	-13.8916
	h_v, kJ/kg	2212.2447	1908.2113	1707.387	1606.4804	1519.6213	1462.082	1422.4914	1392.5428	1363.8152

0.4	T, °C	155.186	138.3638	122.66	107.9884	94.8506	83.6079	74.123	65.5705	55.9139
	v, m^3/kg	0.0283	0.0358	0.0431	0.052	0.0634	0.0781	0.0959	0.1161	0.1369
	h, kJ/kg	837.3267	760.7097	696.1524	661.6965	670.6051	729.004	835.0815	979.6532	1148.9351
	s, kJ/kg K	2.5273	2.494	2.4506	2.4528	2.5449	2.7536	3.0834	3.5155	4.014
	x_l, kg/kg	0.0644	0.1264	0.19	0.2532	0.3082	0.3621	0.4107	0.4584	0.5189
	x_v, kg/kg	0.4048	0.6293	0.7796	0.8697	0.926	0.9565	0.9734	0.9836	0.9912
	h_l, kJ/kg	627.1299	512.2249	405.5794	308.4827	220.7175	153.3043	100.2172	56.317	13.1511
	h_v, kJ/kg	2262.825	1973.9523	1772.7841	1665.8202	1571.2837	1507.2751	1461.9895	1426.2305	1390.1666

Table A.3 Ammonia-water liquid-vapour mixture properties at 9 bar (contd.,)

θ = f(T)	Property	Ammonia concentration (mass fraction), x								
		0.1	**0.2**	**0.3**	**0.4**	**0.5**	**0.6**	**0.7**	**0.8**	**0.9**
0.5	T, °C	157.7901	143.0057	129.0438	115.8227	103.7428	93.072	83.6278	74.5585	63.6252
	v, m^3/kg	0.0389	0.0479	0.0563	0.0659	0.0778	0.0925	0.1096	0.1281	0.1461
	h, kJ/kg	945.6333	888.7158	836.2566	809.0066	819.8467	873.036	965.0266	1085.9991	1221.3418
	s, kJ/kg K	2.7782	2.8015	2.7996	2.8329	2.9426	3.1484	3.4485	3.821	4.2275
	x_l, kg/kg	0.0556	0.1085	0.1636	0.2191	0.2722	0.3165	0.362	0.4084	0.4699
	x_v, kg/kg	0.363	0.5744	0.7248	0.8291	0.8908	0.9318	0.9565	0.9727	0.9854
	h_l, kJ/kg	645.1416	543.8958	448.7474	359.873	281.1845	209.7795	153.4197	102.5633	46.9929
	h_v, kJ/kg	2315.9734	2045.33	1847.3856	1703.0741	1632.4852	1560.263	1507.3776	1463.9272	1418.6393
0.6	T, °C	160.3943	147.6475	135.4275	123.6569	112.6349	102.5361	93.1326	83.5465	71.3365
	v, m^3/kg	0.0527	0.0632	0.0721	0.082	0.0938	0.1079	0.1237	0.1403	0.1552
	h, kJ/kg	1084.0316	1045.8979	1002.0766	977.1179	984.2442	1026.7647	1100.2523	1194.6099	1294.1149
	s, kJ/kg K	3.0968	3.1747	3.2058	3.2575	3.3699	3.5586	3.8178	4.1246	4.4369
	x_l, kg/kg	0.0469	0.0912	0.1379	0.1859	0.2329	0.2776	0.3162	0.3624	0.4258
	x_v, kJ/kg	0.3189	0.5144	0.6614	0.7716	0.8491	0.8963	0.9316	0.9567	0.9771
	h_l, kJ/kg	663.4262	575.5648	492.1964	412.2945	338.8201	273.5051	210.1508	152.9482	85.443
	h_v, kg/kg	2371.9606	2122.7283	1931.7311	1783.813	1673.965	1623.5292	1560.6327	1506.959	1449.8762

0.7	T, °C	162.9984	152.2894	141.8112	131.4911	121.5271	112.0002	102.6375	92.5345	79.0478
	v, m^3/kg	0.0716	0.0834	0.0925	0.1019	0.1128	0.1255	0.1394	0.1533	0.1646
	h, kJ/kg	1271.739	1251.0957	1211.119	1182.0909	1178.3269	1202.964	1251.303	1313.1655	1371.5116
	s, kJ/kg K	3.5266	3.6564	3.7093	3.7645	3.8624	4.0165	4.2195	4.4475	4.6544
	x_l, kg/kg	0.0385	0.0745	0.1131	0.1537	0.1948	0.2356	0.2771	0.319	0.385
	x_v, kg/kg	0.2721	0.4488	0.589	0.7016	0.7885	0.85	0.8958	0.9335	0.9655
	h_l, kJ/kg	682.2477	607.2637	535.7497	465.3833	397.9612	334.6502	274.1494	206.4928	127.2836
	h_v, kJ/kg	2431.1382	2206.715	2026.4061	1878.5412	1760.5219	1671.443	1624.2733	1557.0043	1484.6583
0.8	T, °C	165.6025	156.9313	148.195	139.3254	130.4192	121.4643	112.1423	101.5225	86.7591
	v, m^3/kg	0.0999	0.1127	0.1209	0.1286	0.1374	0.1474	0.158	0.1681	0.1747
	h, kJ/kg	1548.1965	1541.8289	1496.7199	1452.8286	1426.3347	1420.8599	1432.1312	1450.3889	1457.4792
	s, kJ/kg K	4.1562	4.3316	4.3866	4.4207	4.4771	4.5686	4.6881	4.8121	4.8908
	x_l, kg/kg	0.0303	0.0585	0.0892	0.1226	0.158	0.1951	0.235	0.2822	0.3466
	x_v, kg/kg	0.2223	0.3771	0.507	0.6183	0.7119	0.789	0.85	0.9007	0.9493
	h_l, kJ/kg	702.1552	639.1798	579.2956	518.7866	458.0927	397.5387	335.5827	267.0851	171.763
	h_v, kJ/kg	2493.9688	2298.1459	2132.2768	1988.2651	1864.7173	1759.8507	1671.7995	1616.1738	1523.9418
0.9	T, °C	168.2067	161.5732	154.5787	147.1596	139.3114	130.9283	121.6471	110.5105	94.4704
	v, m^3/kg	0.1476	0.1601	0.1649	0.1684	0.1723	0.1769	0.1818	0.1859	0.1861
	h, kJ/kg	2009.4486	2005.4495	1932.1968	1848.9018	1774.6191	1714.1155	1664.7204	1618.3645	1556.5714
	s, kJ/kg K	5.2011	5.3976	5.4042	5.3627	5.3212	5.2939	5.276	5.2478	5.1576
	x_l, kg/kg	0.0224	0.0431	0.0665	0.093	0.1227	0.1559	0.1943	0.2421	0.31
	x_v, kg/kg	0.169	0.298	0.4143	0.521	0.6185	0.707	0.7876	0.8557	0.9273
	h_l, kJ/kg	724.4703	671.8607	622.953	572.2357	518.6916	461.5547	398.7674	324.8944	218.3712
	h_v, kJ/kg	2561.0753	2398.3308	2250.8084	2114.2945	1988.0547	1871.2485	1761.8079	1687.064	1568.8962

Table A.3 Ammonia-water liquid-vapour mixture properties at 10 bar

θ = f(T)	Property	Ammonia concentration (mass fraction), x								
		0.1	0.2	0.3	0.4	0.5	0.6	0.7	0.8	0.9
0.1	T, °C	151.9412	128.8397	107.738	88.5631	72.117	59.0332	49.3034	42.1757	36.2134
	v, m^3/kg	0.006	0.0079	0.0101	0.0132	0.018	0.0258	0.0383	0.0573	0.0839
	h, kJ/kg	628.0146	484.7646	363.4445	274.9503	233.5486	254.0611	350.661	533.4664	806.7894
	s, kJ/kg K	2.0354	1.8138	1.591	1.4075	1.3131	1.3641	1.619	2.1251	2.9089
	x_l, kg/kg	0.0923	0.1828	0.2734	0.358	0.4438	0.5243	0.598	0.6665	0.7421
	x_v, kg/kg	0.5099	0.7571	0.886	0.9512	0.9791	0.9906	0.9955	0.9977	0.9989
	h_l, kJ/kg	594.1393	437.3317	298.7733	176.9062	87.2387	28.0483	-3.3357	-13.2747	-4.8734
	h_v, kJ/kg	2133.4016	1808.0532	1644.0499	1522.1481	1444.6115	1393.8961	1360.2834	1337.192	1318.5992
0.2	T, °C	154.5229	133.4709	114.121	96.4015	81.0131	68.4961	58.7966	51.1346	43.8657
	v, m^3/kg	0.0116	0.0152	0.0192	0.0245	0.0322	0.0432	0.0587	0.0789	0.1031
	h, kJ/kg	693.9195	574.0449	474.7917	409.9779	394.5365	440.9617	556.12	737.7422	976.3978
	s, kJ/kg K	2.1894	2.0339	1.8801	1.7755	1.7716	1.9168	2.2454	2.763	3.4499
	x_l, kg/kg	0.083	0.1638	0.2453	0.3206	0.3959	0.4646	0.5259	0.5828	0.6486
	x_v, kJ/kg	0.4747	0.7166	0.8528	0.9299	0.9664	0.983	0.9908	0.9948	0.9973
	h_l, kJ/kg	611.7268	468.5862	339.8085	223.5588	134.1479	69.4884	27.125	1.3534	-12.3932
	h_v, kg/kg	2178.5623	1862.9604	1695.5847	1566.9047	1484.1965	1429.797	1393.0433	1366.403	1342.5725
0.3	T, °C	157.1045	138.1021	120.5041	104.2399	89.9092	77.959	68.2898	60.0934	51.518
	v, m^3/kg	0.0181	0.0234	0.0288	0.0357	0.0451	0.0576	0.0738	0.0932	0.1145
	h, kJ/kg	769.266	671.435	590.6968	543.0503	542.5762	598.202	711.3249	874.6532	1075.4927
	s, kJ/kg K	2.3643	2.2711	2.1758	2.1303	2.1822	2.368	2.7032	3.1762	3.7555
	x_l, kg/kg	0.0738	0.1452	0.2178	0.2891	0.3515	0.4119	0.4659	0.5172	0.5797
	x_v, kg/kg	0.4377	0.6718	0.8195	0.9014	0.948	0.9713	0.9832	0.99	0.9946
	h_l, kJ/kg	629.3501	499.9873	381.6814	276.7083	184.767	117.5722	68.5043	32.2624	2.4198
	h_v, kJ/kg	2225.8344	1922.7865	1720.9839	1618.4468	1529.4127	1470.0454	1428.9727	1397.7408	1367.6955

0.4	T, °C	159.6862	142.7333	126.8871	112.0783	98.8053	87.4219	77.783	69.0522	59.1703
	v, m^3/kg	0.0259	0.0327	0.0393	0.0473	0.0577	0.0709	0.0869	0.105	0.1237
	h, kJ/kg	857.9001	781.0606	715.6746	680.0083	687.2517	743.5129	847.0286	988.6882	1154.6834
	s, kJ/kg K	2.5687	2.5348	2.4891	2.4874	2.5733	2.7731	3.0914	3.5098	3.9927
	x_l, kg/kg	0.0649	0.127	0.1909	0.2542	0.3094	0.3636	0.4128	0.4614	0.5234
	x_v, kg/kg	0.3988	0.6224	0.7729	0.8642	0.922	0.9538	0.9716	0.9824	0.9906
	h_l, kJ/kg	647.0429	531.4747	424.218	326.5767	238.2592	170.2951	116.631	72.1561	28.586
	h_v, kJ/kg	2275.3848	1987.7513	1786.3306	1678.3704	1581.9209	1516.1145	1469.2488	1432.0294	1394.3908

Table A.3 Ammonia-water liquid-vapour mixture properties at 10 bar (contd.,)

θ = f(T)	Property	Ammonia concentration (mass fraction), x								
		0.1	**0.2**	**0.3**	**0.4**	**0.5**	**0.6**	**0.7**	**0.8**	**0.9**
0.5	T, °C	162.2678	147.3646	133.2702	119.9167	107.7013	96.8849	87.2763	78.0111	66.8226
	v, m^3/kg	0.0356	0.0438	0.0514	0.06	0.0708	0.084	0.0994	0.116	0.1321
	h, kJ/kg	965.8903	909.267	856.1983	827.8841	837.1567	888.2913	977.797	1095.8847	1227.8167
	s, kJ/kg K	2.8163	2.8396	2.8355	2.8649	2.9684	3.1657	3.4548	3.8144	4.206
	x_l, kg/kg	0.0561	0.1093	0.1646	0.2203	0.2736	0.3183	0.3643	0.4116	0.4746
	x_v, kg/kg	0.3578	0.5683	0.7185	0.8234	0.8862	0.9284	0.9542	0.9712	0.9846
	h_l, kJ/kg	664.8897	562.988	467.2283	377.7983	298.5413	226.5008	169.4546	117.8508	61.5977
	h_v, kJ/kg	2327.4238	2058.136	1860.48	1715.393	1643.7723	1569.8716	1515.3523	1470.2813	1423.1683
0.6	T, °C	164.8495	151.9958	139.6532	127.7551	116.5974	106.3478	96.7695	86.9699	74.4749
	v, m^3/kg	0.048	0.0577	0.0659	0.0747	0.0854	0.0981	0.1123	0.1271	0.1404
	h, kJ/kg	1103.3927	1066.4453	1022.367	996.5731	1002.2839	1042.8437	1113.8717	1205.2798	1301.1598
	s, kJ/kg K	3.1297	3.2088	3.2382	3.2864	3.3931	3.5736	3.8226	4.117	4.4148
	x_l, kg/kg	0.0475	0.0921	0.1391	0.1873	0.2345	0.2796	0.3189	0.3658	0.4307
	x_v, kJ/kg	0.3145	0.5092	0.6557	0.766	0.8442	0.8923	0.9288	0.9548	0.9762
	h_l, kJ/kg	683.0111	594.5103	510.5267	430.0437	355.9642	289.9648	225.7979	167.6902	99.2478
	h_v, kg/kg	2382.2197	2134.3349	1943.9599	1795.8849	1685.0793	1633.665	1569.161	1513.756	1454.635

0.7	T, °C	167.4311	156.627	146.0362	135.5935	125.4935	115.8107	106.2627	95.9288	82.1272
	v, m^3/kg	0.0651	0.0761	0.0844	0.0929	0.1028	0.1142	0.1266	0.139	0.1489
	h, kJ/kg	1288.8326	1271.0274	1231.3806	1201.8478	1196.8787	1219.657	1265.5381	1324.3579	1378.8799
	s, kJ/kg K	3.55	3.6842	3.7365	3.7889	3.8817	4.0284	4.2217	4.4381	4.6311
	x_l, kg/kg	0.0392	0.0755	0.1144	0.1552	0.1967	0.2379	0.28	0.3228	0.3902
	x_v, kg/kg	0.2687	0.4447	0.5843	0.6966	0.7838	0.8488	0.8927	0.9314	0.9644
	h_l, kJ/kg	701.6582	626.0868	553.9477	482.9662	414.8838	350.8178	289.4279	220.688	140.3044
	h_v, kJ/kg	2440.1185	2216.9244	2037.3733	1889.7578	1771.331	1678.2065	1633.0387	1564.0282	1489.5201
0.8	T, °C	170.0127	161.2583	152.4193	143.432	134.3896	125.2736	115.7559	104.8876	89.7795
	v, m^3/kg	0.0903	0.1025	0.1101	0.1172	0.1251	0.134	0.1435	0.1524	0.1581
	h, kJ/kg	1559.489	1559.4117	1515.7894	1471.9416	1444.5538	1437.3963	1446.2859	1461.5123	1464.7641
	s, kJ/kg K	4.1603	4.3473	4.4042	4.437	4.4894	4.5746	4.6855	4.7989	4.865
	x_l, kg/kg	0.031	0.0595	0.0906	0.1243	0.1601	0.1976	0.2382	0.2862	0.3521
	x_v, kg/kg	0.2199	0.3741	0.5035	0.6145	0.7081	0.7854	0.8492	0.8987	0.9483
	h_l, kJ/kg	721.3607	657.8873	597.3939	536.2275	474.8066	413.4129	350.4609	280.77	184.0065
	h_v, kJ/kg	2501.5746	2306.7616	2141.6107	1998.0137	1874.4303	1769.002	1677.7329	1623.0571	1528.7059
0.9	T, °C	172.5944	165.8895	158.8023	151.2704	143.2856	134.7365	125.2491	113.8465	97.4318
	v, m^3/kg	0.1322	0.145	0.1498	0.1531	0.1566	0.1607	0.165	0.1685	0.1683
	h, kJ/kg	2004.1579	2015.261	1946.5074	1864.5856	1790.1318	1728.472	1677.1511	1628.217	1563.1004
	s, kJ/kg K	5.1578	5.3851	5.4008	5.3617	5.3188	5.2875	5.2635	5.2274	5.1274
	x_l, kg/kg	0.0231	0.0441	0.0679	0.0948	0.1249	0.1587	0.1977	0.2465	0.3158
	x_v, kg/kg	0.1677	0.2964	0.4123	0.5188	0.6162	0.7048	0.7856	0.8544	0.9266
	h_l, kJ/kg	743.3337	690.4422	640.973	589.5746	535.2327	477.1569	413.2495	338.0251	229.8385
	h_v, kJ/kg	2567.2006	2405.1484	2258.1515	2121.9944	1995.8542	1878.8121	1768.744	1693.2291	1573.2603

Table A.3 Ammonia-water liquid-vapour mixture properties at 11 bar

θ = f(T)	Property	Ammonia concentration (mass fraction), x								
		0.1	**0.2**	**0.3**	**0.4**	**0.5**	**0.6**	**0.7**	**0.8**	**0.9**
0.1	T, °C	156.1617	132.9083	111.6491	92.3353	75.7657	62.5667	52.7237	45.4799	39.3919
	v, m^3/kg	0.0056	0.0073	0.0093	0.0122	0.0166	0.0236	0.0349	0.052	0.076
	h, kJ/kg	647.0678	503.2303	381.0992	291.663	249.0789	267.8942	361.8797	540.7955	809.0218
	s, kJ/kg K	2.0787	1.8576	1.6346	1.45	1.3529	1.3982	1.6426	2.1316	2.8917
	x_l, kg/kg	0.0924	0.183	0.2736	0.3583	0.4442	0.5249	0.599	0.6683	0.7452
	x_v, kg/kg	0.5025	0.7498	0.8805	0.948	0.9773	0.9897	0.995	0.9974	0.9988
	h_l, kJ/kg	613.1257	455.7136	316.531	194.1185	104.0102	44.4801	12.8921	2.9812	11.8928
	h_v, kJ/kg	2147.3159	1822.0497	1656.2091	1531.6144	1451.8761	1399.5386	1364.7467	1340.7465	1321.3444
0.2	T, °C	158.7214	137.5284	118.0302	100.1762	84.6641	72.0272	62.2048	54.4102	46.9877
	v, m^3/kg	0.0108	0.0141	0.0177	0.0225	0.0295	0.0395	0.0536	0.0718	0.0938
	h, kJ/kg	712.9517	592.5409	492.4202	426.4948	409.5785	454.0048	566.5038	744.8493	979.8591
	s, kJ/kg K	2.2311	2.0755	1.9206	1.8136	1.8052	1.9428	2.2599	2.7623	3.4312
	x_l, kg/kg	0.0832	0.1642	0.2457	0.3211	0.3966	0.4656	0.5273	0.585	0.6523
	x_v, kJ/kg	0.4679	0.7095	0.85	0.926	0.964	0.9816	0.99	0.9943	0.997
	h_l, kJ/kg	630.533	486.7981	357.4361	240.6574	150.7953	85.7447	43.0759	17.1519	3.6584
	h_v, kg/kg	2191.6735	1876.624	1678.6953	1577.1387	1492.3101	1436.2423	1398.2049	1370.5089	1345.6518
0.3	T, °C	161.281	142.1485	124.4112	108.0171	93.5625	81.4877	71.6859	63.3404	54.5836
	v, m^3/kg	0.0168	0.0216	0.0265	0.0328	0.0413	0.0528	0.0674	0.085	0.1043
	h, kJ/kg	788.2355	690.0327	608.4658	559.6715	557.6406	611.2368	721.8435	882.2587	1079.894
	s, kJ/kg K	2.4041	2.3106	2.2136	2.1649	2.2116	2.3893	2.7134	3.1727	3.7365
	x_l, kg/kg	0.0742	0.1457	0.2184	0.2898	0.3523	0.4131	0.4676	0.5197	0.5836
	x_v, kg/kg	0.4315	0.665	0.8134	0.8968	0.9449	0.9693	0.982	0.9892	0.9942
	h_l, kJ/kg	647.9806	518.0295	399.1643	293.6845	201.2641	133.6173	84.1252	47.5323	17.622
	h_v, kJ/kg	2238.0752	1935.9168	1733.3366	1629.348	1538.3531	1477.3054	1434.85	1402.406	1371.1056

0.4	T, °C	163.8407	146.7686	130.7923	115.8581	102.4609	90.9482	81.167	72.2707	62.1794
	v, m^3/kg	0.0239	0.0302	0.0362	0.0435	0.0529	0.0649	0.0795	0.0959	0.1128
	h, kJ/kg	876.6869	799.788	733.7035	696.9545	702.6709	756.9557	858.0773	996.9873	1159.8443
	s, kJ/kg K	2.6061	2.572	2.5245	2.5193	2.5996	2.7914	3.0992	3.5049	3.9735
	x_l, kg/kg	0.0653	0.1277	0.1917	0.2551	0.3105	0.365	0.4148	0.4641	0.5275
	x_v, kg/kg	0.3933	0.6162	0.7669	0.8591	0.9183	0.9512	0.9698	0.9814	0.99
	h_l, kJ/kg	665.505	549.3504	441.546	343.4103	254.5841	186.1097	131.9106	86.9055	42.9779
	h_v, kJ/kg	2286.6867	2000.1525	1798.5757	1689.7529	1591.5986	1524.1563	1475.8278	1437.2392	1398.1115

Table A.3 Ammonia-water liquid-vapour mixture properties at 11 bar (contd.,)

θ = f(T)	Property	Ammonia concentration (mass fraction), x								
		0.1	**0.2**	**0.3**	**0.4**	**0.5**	**0.6**	**0.7**	**0.8**	**0.9**
0.5	T, °C	166.4003	151.3887	137.1734	123.699	111.3594	100.4087	90.6481	81.201	69.7752
	v, m^3/kg	0.0328	0.0404	0.0473	0.0552	0.065	0.0771	0.091	0.1061	0.1206
	h, kJ/kg	984.2182	928.0687	874.5321	845.2853	853.1335	902.3703	989.5545	1104.9216	1233.6092
	s, kJ/kg K	2.8503	2.874	2.8681	2.8941	2.9922	3.1817	3.4609	3.8086	4.1865
	x_l, kg/kg	0.0566	0.1101	0.1656	0.2214	0.2749	0.32	0.3665	0.4146	0.4789
	x_v, kg/kg	0.3531	0.5628	0.7127	0.8181	0.8819	0.9252	0.9519	0.9698	0.9839
	h_l, kJ/kg	683.1836	580.7077	484.4039	394.4707	314.6955	242.0676	184.3863	132.0915	75.2202
	h_v, kJ/kg	2337.7168	2069.6213	1872.2656	1726.5553	1653.9976	1578.5839	1522.5641	1475.9841	1427.1569
0.6	T, °C	168.9599	156.0088	143.5544	131.5399	120.2578	109.8692	100.1292	90.1313	77.371
	v, m^3/kg	0.0441	0.0531	0.0606	0.0688	0.0785	0.09	0.1029	0.1163	0.1282
	h, kJ/kg	1120.6541	1085.0898	1040.9098	1014.4132	1018.8581	1057.6108	1126.3453	1214.9778	1307.4295
	s, kJ/kg K	3.1584	3.2394	3.2674	3.3126	3.4142	3.5875	3.827	4.1102	4.3946
	x_l, kg/kg	0.0481	0.093	0.1402	0.1886	0.2361	0.2815	0.3213	0.3691	0.4353
	x_v, kJ/kg	0.3106	0.5045	0.6506	0.7609	0.8397	0.8887	0.9261	0.9531	0.9753
	h_l, kJ/kg	701.1386	612.0859	527.5541	446.5467	371.9164	305.292	240.3721	181.4272	112.1281
	h_v, kg/kg	2391.4291	2144.7265	1954.9292	1806.7626	1695.1482	1642.8163	1576.8471	1519.8402	1458.8173

0.7	T, °C	171.5196	160.6289	149.9355	139.3809	129.1562	119.3297	109.6103	99.0616	84.9668
	v, m^3/kg	0.0596	0.07	0.0777	0.0854	0.0944	0.1048	0.116	0.1272	0.136
	h, kJ/kg	1303.6472	1288.8739	1249.7331	1219.8436	1213.8141	1234.8983	1278.4992	1334.4637	1385.3911
	s, kJ/kg K	3.5694	3.7085	3.7607	3.8107	3.8991	4.0391	4.2237	4.4293	4.6096
	x_l, kg/kg	0.0398	0.0765	0.1156	0.1567	0.1985	0.2401	0.2827	0.3263	0.395
	x_v, kg/kg	0.2656	0.441	0.5801	0.6922	0.7795	0.8452	0.8899	0.9295	0.9635
	h_l, kJ/kg	719.6193	643.5292	570.8417	499.3073	430.6292	365.871	303.6636	233.9195	152.4574
	h_v, kJ/kg	2448.1648	2226.0501	2047.1846	1899.82	1781.0637	1687.055	1640.9048	1570.2917	1493.7762
0.8	T, °C	174.0792	165.249	156.3165	147.2218	138.0546	128.7903	119.0913	107.9919	92.5626
	v, m^3/kg	0.0823	0.0941	0.1012	0.1077	0.1149	0.123	0.1316	0.1395	0.1444
	h, kJ/kg	1568.4273	1574.7312	1532.7951	1489.1663	1461.0465	1452.3855	1459.0836	1471.4819	1471.144
	s, kJ/kg K	4.161	4.3598	4.4191	4.4511	4.5001	4.5797	4.6828	4.7867	4.8412
	x_l, kg/kg	0.0317	0.0605	0.0919	0.1259	0.162	0.2	0.2411	0.2899	0.3572
	x_v, kg/kg	0.2178	0.3715	0.5005	0.6111	0.7047	0.7823	0.8466	0.8969	0.9474
	h_l, kJ/kg	739.1014	675.2071	614.1764	552.4257	490.3494	428.1911	364.32	293.5265	195.4383
	h_v, kJ/kg	2508.3699	2314.4483	2149.9426	2006.7299	1883.1353	1777.2222	1685.0008	1629.1674	1532.8524
0.9	T, °C	176.6389	169.8691	162.6976	155.0627	146.953	138.2508	128.5724	116.9222	100.1585
	v, m^3/kg	0.1195	0.1325	0.1373	0.1404	0.1437	0.1473	0.1511	0.1541	0.1537
	h, kJ/kg	1997.1729	2022.845	1958.7448	1878.4038	1803.9876	1741.3521	1688.2889	1636.9604	1568.7419
	s, kJ/kg K	5.1142	5.3709	5.3959	5.3595	5.3159	5.2812	5.2517	5.2084	5.0995
	x_l, kg/kg	0.0238	0.0451	0.0692	0.0965	0.127	0.1613	0.2009	0.2505	0.3212
	x_v, kg/kg	0.1666	0.295	0.4106	0.5169	0.6141	0.7028	0.7839	0.8532	0.926
	h_l, kJ/kg	760.743	707.6262	657.6635	605.6607	550.602	491.6739	426.7404	350.2681	240.5497
	h_v, kJ/kg	2572.6445	2411.2132	2264.6924	2128.8635	2002.8232	1885.5783	1774.9484	1698.6746	1577.0287

Table A.3 Ammonia-water liquid-vapour mixture properties at 12 bar

θ = f(T)	Property	Ammonia concentration (mass fraction), x								
		0.1	**0.2**	**0.3**	**0.4**	**0.5**	**0.6**	**0.7**	**0.8**	**0.9**
0.1	T, °C	160.0899	136.6965	115.2922	95.85	79.1662	65.8603	55.9123	48.5604	42.3554
	v, m^3/kg	0.0053	0.0068	0.0087	0.0113	0.0153	0.0218	0.0321	0.0477	0.0694
	h, kJ/kg	664.8485	520.4999	397.6272	307.3219	263.6311	280.8684	372.4196	547.7008	811.0951
	s, kJ/kg K	2.1186	1.8981	1.675	1.4894	1.3898	1.43	1.6649	2.1384	2.8766
	x_l, kg/kg	0.0926	0.1831	0.2738	0.3585	0.4445	0.5254	0.5999	0.6699	0.7481
	x_v, kg/kg	0.4957	0.743	0.8753	0.9449	0.9756	0.9888	0.9945	0.9971	0.9986
	h_l, kJ/kg	630.8784	472.9274	333.1692	210.2472	119.7221	59.8689	28.0862	18.1998	27.588
	h_v, kJ/kg	2159.9905	1834.8384	1667.3892	1540.3532	1458.5771	1404.7134	1368.7966	1343.9216	1323.7353
0.2	T, °C	162.628	141.3051	121.6702	103.6921	88.0656	75.3175	65.3809	57.4628	49.897
	v, m^3/kg	0.0101	0.0131	0.0164	0.0209	0.0273	0.0364	0.0493	0.066	0.086
	h, kJ/kg	730.6537	609.8018	508.8986	441.9504	423.6678	466.2287	576.2357	751.4853	982.9987
	s, kJ/kg K	2.2694	2.114	1.9581	1.8489	1.8364	1.9672	2.2738	2.7622	3.4143
	x_l, kg/kg	0.0834	0.1645	0.2461	0.3215	0.3971	0.4664	0.5287	0.5871	0.6558
	x_v, kJ/kg	0.4616	0.703	0.8471	0.9222	0.9617	0.9803	0.9891	0.9938	0.9967
	h_l, kJ/kg	648.1102	503.8449	373.9462	256.6787	166.3932	100.9738	58.0177	31.9533	18.711
	h_v, kg/kg	2203.6056	1889.0726	1687.1489	1586.5592	1499.7852	1442.161	1402.9097	1374.2045	1348.3588
0.3	T, °C	165.1661	145.9137	128.0483	111.5343	96.9651	84.7747	74.8495	66.3651	57.4386
	v, m^3/kg	0.0156	0.0201	0.0246	0.0304	0.0382	0.0487	0.0621	0.0782	0.0958
	h, kJ/kg	805.8016	707.3384	625.0382	575.1982	571.7274	623.4275	731.6683	889.3241	1083.8796
	s, kJ/kg K	2.4406	2.347	2.2486	2.1971	2.2389	2.4093	2.7232	3.1699	3.7193
	x_l, kg/kg	0.0745	0.1462	0.2189	0.2905	0.3532	0.4142	0.4691	0.522	0.5873
	x_v, kg/kg	0.4259	0.6589	0.8077	0.8925	0.942	0.9675	0.9808	0.9884	0.9938
	h_l, kJ/kg	665.3813	534.9099	415.5387	309.5915	216.7227	148.6525	98.7637	61.8462	31.8896
	h_v, kJ/kg	2249.2049	1947.8491	1744.6406	1639.3478	1546.5709	1483.969	1440.2158	1406.6213	1374.12

0.4	T, °C	167.7042	150.5223	134.4263	119.3764	105.8646	94.2318	84.3182	75.2674	64.9803
	v, m^3/kg	0.0222	0.028	0.0336	0.0403	0.049	0.06	0.0733	0.0883	0.1037
	h, kJ/kg	893.9794	817.1471	750.4694	712.7424	717.0521	769.49	868.3615	1004.661	1164.5083
	s, kJ/kg K	2.6402	2.6062	2.557	2.5488	2.624	2.8085	3.1066	3.5008	3.956
	x_l, kg/kg	0.0657	0.1283	0.1924	0.256	0.3116	0.3664	0.4166	0.4667	0.5314
	x_v, kg/kg	0.3883	0.6105	0.7613	0.8543	0.9147	0.9488	0.9682	0.9803	0.9894
	h_l, kJ/kg	682.7405	566.0685	457.7715	359.1807	269.8822	200.9318	146.2338	100.7367	56.4912
	h_v, kJ/kg	2296.9527	2011.3981	1809.7323	1700.1546	1600.4661	1531.5223	1481.8311	1441.9524	1401.4087

Table A.3 Ammonia-water liquid-vapour mixture properties at 12 bar (contd.,)

θ = f(T)	Property	Ammonia concentration (mass fraction), x								
		0.1	**0.2**	**0.3**	**0.4**	**0.5**	**0.6**	**0.7**	**0.8**	**0.9**
0.5	T, °C	170.2423	155.1309	140.8044	127.2186	114.7641	103.689	93.7868	84.1698	72.5219
	v, m^3/kg	0.0304	0.0375	0.0439	0.0512	0.0602	0.0712	0.084	0.0977	0.1109
	h, kJ/kg	1000.9417	945.4041	891.5115	861.4386	867.9781	915.4505	1000.4516	1113.2379	1238.8267
	s, kJ/kg K	2.881	2.9054	2.8981	2.9211	3.0142	3.1966	3.4667	3.8035	4.1686
	x_l, kg/kg	0.0571	0.1108	0.1665	0.2224	0.2761	0.3216	0.3686	0.4174	0.483
	x_v, kg/kg	0.3488	0.5578	0.7075	0.8132	0.8779	0.9222	0.9498	0.9684	0.9832
	h_l, kJ/kg	700.2542	597.2709	500.4775	410.0878	329.8343	256.66	198.387	145.4499	88.0155
	h_v, kJ/kg	2347.0552	2080.0179	1882.9638	1736.744	1663.3312	1586.5396	1529.1319	1481.1391	1430.6922
0.6	T, °C	172.7804	159.7396	147.1824	135.0607	123.6636	113.1462	103.2554	93.0721	80.0635
	v, m^3/kg	0.0408	0.0493	0.0562	0.0637	0.0726	0.0832	0.095	0.1072	0.1179
	h, kJ/kg	1136.1851	1102.1413	1057.9818	1030.8989	1034.191	1071.2648	1137.847	1223.8551	1313.0478
	s, kJ/kg K	3.1838	3.267	3.2941	3.3367	3.4337	3.6002	3.8311	4.1039	4.3761
	x_l, kg/kg	0.0487	0.0938	0.1412	0.1898	0.2375	0.2833	0.3236	0.3721	0.4395
	x_v, kJ/kg	0.307	0.5003	0.646	0.7563	0.8355	0.8854	0.9236	0.9515	0.9745
	h_l, kJ/kg	718.0434	628.5022	543.4813	462.0015	386.8662	319.6613	254.0413	194.3168	124.2301
	h_v, kg/kg	2399.7729	2154.1179	1964.8564	1816.6432	1704.3361	1651.1404	1583.8251	1525.3274	1462.5175

0.7	T, °C	175.3185	164.3482	153.5605	142.9029	132.563	122.6034	112.724	101.9745	87.6052
	v, m^3/kg	0.055	0.0648	0.072	0.0792	0.0874	0.0969	0.1072	0.1173	0.1251
	h, kJ/kg	1316.6149	1304.9967	1266.4931	1236.3619	1229.3954	1248.9125	1290.3843	1343.6599	1391.1883
	s, kJ/kg K	3.5856	3.73	3.7824	3.8305	3.9149	4.0489	4.2254	4.4212	4.5897
	x_l, kg/kg	0.0404	0.0773	0.1167	0.1581	0.2001	0.2421	0.2852	0.3295	0.3995
	x_v, kg/kg	0.2628	0.4376	0.5763	0.6881	0.7756	0.8418	0.8873	0.9277	0.9626
	h_l, kJ/kg	736.345	659.8116	586.6339	514.602	445.3769	379.9851	317.0175	246.3385	163.8799
	h_v, kJ/kg	2455.44	2234.2837	2056.0428	1908.9244	1789.8976	1695.1085	1648.0182	1575.9213	1497.5282
0.8	T, °C	177.8566	168.9568	159.9386	150.745	141.4625	132.0605	122.1926	110.8768	95.1468
	v, m^3/kg	0.0755	0.0869	0.0937	0.0997	0.1063	0.1137	0.1215	0.1286	0.1329
	h, kJ/kg	1575.5287	1588.2098	1548.0968	1504.8183	1476.1039	1466.0726	1470.7412	1480.4876	1476.7721
	s, kJ/kg K	4.1593	4.3698	4.4319	4.4634	4.5096	4.5841	4.6801	4.7751	4.819
	x_l, kg/kg	0.0324	0.0614	0.0931	0.1275	0.1639	0.2022	0.2438	0.2934	0.3619
	x_v, kg/kg	0.2158	0.3691	0.4977	0.6081	0.7015	0.7794	0.8442	0.8953	0.9466
	h_l, kJ/kg	755.6137	691.3591	629.8528	567.5748	504.904	442.0409	377.3245	305.5041	206.1869
	h_v, kJ/kg	2514.4943	2321.3694	2157.449	2014.5944	1891.004	1784.6658	1691.5868	1634.6353	1536.488
0.9	T, °C	180.3947	173.5654	166.3166	158.5872	150.362	141.5177	131.6613	119.7791	102.6884
	v, m^3/kg	0.1087	0.1219	0.1267	0.1297	0.1327	0.1361	0.1395	0.142	0.1414
	h, kJ/kg	1989.0737	2028.6924	1969.3089	1890.69	1816.4618	1752.9955	1698.3483	1644.7883	1573.6508
	s, kJ/kg K	5.0711	5.3555	5.3898	5.3566	5.3126	5.2749	5.2405	5.1905	5.0735
	x_l, kg/kg	0.0246	0.0461	0.0705	0.098	0.1289	0.1636	0.2038	0.2542	0.3262
	x_v, kg/kg	0.1655	0.2936	0.4091	0.5151	0.6123	0.701	0.7823	0.8521	0.9255
	h_l, kJ/kg	776.9394	723.635	673.2367	620.6922	564.9831	505.2753	439.3953	361.7651	250.6255
	h_v, kJ/kg	2577.5236	2416.6562	2270.571	2135.0466	2009.1042	1891.6823	1780.5438	1703.5231	1580.3056

Table A.3 Ammonia-water liquid-vapour mixture properties at 13 bar

θ = f(T)	Property	Ammonia concentration (mass fraction), x								
		0.1	**0.2**	**0.3**	**0.4**	**0.5**	**0.6**	**0.7**	**0.8**	**0.9**
0.1	T, °C	163.7682	140.2448	118.7057	99.1443	82.3541	68.9486	58.9024	51.4494	45.1347
	v, m^3/kg	0.005	0.0064	0.0081	0.0106	0.0143	0.0202	0.0297	0.0439	0.0639
	h, kJ/kg	681.5404	536.7423	413.193	322.0751	277.3481	293.1037	382.3719	554.2374	813.0368
	s, kJ/kg K	2.1558	1.9359	1.7127	1.5262	1.4244	1.4599	1.686	2.1452	2.8633
	x_l, kg/kg	0.0927	0.1833	0.274	0.3588	0.4448	0.5259	0.6008	0.6714	0.7507
	x_v, kg/kg	0.4894	0.7368	0.8705	0.9418	0.974	0.9879	0.994	0.9968	0.9984
	h_l, kJ/kg	647.5778	489.1378	348.8477	225.4475	134.5272	74.3658	42.3966	32.5319	42.3666
	h_v, kJ/kg	2171.6248	1846.6016	1677.7274	1548.4649	1464.7923	1409.4854	1372.4922	1346.7718	1325.8234
0.2	T, °C	166.2852	144.8417	125.08	106.9866	91.2536	78.4017	68.3583	60.3244	52.6242
	v, m^3/kg	0.0094	0.0123	0.0154	0.0195	0.0254	0.0338	0.0456	0.061	0.0794
	h, kJ/kg	747.2192	626.0022	524.3945	456.4982	436.936	477.7459	585.4046	757.7144	985.8637
	s, kJ/kg K	2.305	2.1499	1.9931	1.882	1.8657	1.9901	2.2871	2.7625	3.3991
	x_l, kg/kg	0.0836	0.1648	0.2464	0.322	0.3977	0.4672	0.5299	0.5891	0.659
	x_v, kJ/kg	0.4559	0.697	0.842	0.9186	0.9595	0.9789	0.9883	0.9933	0.9965
	h_l, kJ/kg	664.6356	519.8942	389.5041	271.7776	181.0926	115.3241	72.0965	45.9023	32.909
	h_v, kg/kg	2214.549	1900.4933	1697.4746	1595.2791	1506.7101	1447.6263	1407.2219	1377.5486	1350.7475
0.3	T, °C	168.8021	149.4386	131.4542	114.8289	100.1531	87.8548	77.8143	69.1994	60.1138
	v, m^3/kg	0.0146	0.0187	0.023	0.0283	0.0355	0.0452	0.0576	0.0724	0.0886
	h, kJ/kg	822.1665	723.536	640.5892	589.7821	584.9707	634.8906	740.8974	895.9229	1087.5087
	s, kJ/kg K	2.4743	2.3808	2.2812	2.2271	2.2646	2.4281	2.7327	3.1677	3.7036
	x_l, kg/kg	0.0748	0.1467	0.2195	0.2911	0.3539	0.4152	0.4706	0.5242	0.5908
	x_v, kg/kg	0.4207	0.6532	0.8025	0.8884	0.9392	0.9656	0.9796	0.9877	0.9934
	h_l, kJ/kg	681.7382	550.7961	430.9611	324.5817	231.2918	162.8231	112.5614	75.342	45.3572
	h_v, kJ/kg	2259.4028	1958.7724	1755.0484	1648.5743	1554.1665	1490.1188	1445.1417	1410.451	1376.7961

0.4	T, °C	171.3191	154.0354	137.8285	122.6712	109.0526	97.3079	87.2702	78.0744	67.6033
	v, m^3/kg	0.0207	0.0262	0.0314	0.0376	0.0456	0.0557	0.068	0.0818	0.0959
	h, kJ/kg	910.0032	833.3384	766.1508	727.533	730.5378	781.2443	877.9858	1011.7957	1168.7461
	s, kJ/kg K	2.6716	2.6378	2.5873	2.5763	2.6469	2.8246	3.1138	3.4972	3.9399
	x_l, kg/kg	0.0661	0.1289	0.1931	0.2568	0.3125	0.3676	0.4183	0.4691	0.535
	x_v, kg/kg	0.3837	0.6054	0.7562	0.85	0.9114	0.9464	0.9666	0.9793	0.9889
	h_l, kJ/kg	698.9308	581.7954	473.0506	374.0368	284.3005	214.9038	159.738	113.782	69.2527
	h_v, kJ/kg	2306.3501	2021.6739	1819.9649	1709.7185	1608.6386	1538.3076	1487.3409	1446.2401	1404.3445

Table A.3 Ammonia-water liquid-vapour mixture properties at 13 bar (contd.,)

θ = f(T)	Property	Ammonia concentration (mass fraction), x								
		0.1	**0.2**	**0.3**	**0.4**	**0.5**	**0.6**	**0.7**	**0.8**	**0.9**
0.5	T, °C	173.8361	158.6323	144.2027	130.5135	117.9521	106.7609	96.7261	86.9495	75.0928
	v, m^3/kg	0.0283	0.035	0.0409	0.0477	0.056	0.0662	0.0779	0.0906	0.1026
	h, kJ/kg	1016.3105	961.4922	907.3302	876.5192	881.8537	927.6687	1010.6059	1120.9345	1243.5502
	s, kJ/kg K	2.9089	2.9343	2.9258	2.9462	3.0348	3.2106	3.4722	3.7989	4.1521
	x_l, kg/kg	0.0576	0.1115	0.1673	0.2234	0.2773	0.323	0.3705	0.42	0.4868
	x_v, kg/kg	0.3448	0.5532	0.7027	0.8088	0.8741	0.9194	0.9478	0.9671	0.9825
	h_l, kJ/kg	716.2798	612.8433	515.6087	424.7995	344.1024	270.4172	211.5904	158.0529	100.1033
	h_v, kJ/kg	2355.5936	2089.5017	1892.7443	1746.1026	1671.9028	1593.8475	1535.1488	1485.826	1433.8416
0.6	T, °C	176.3531	163.2292	150.5769	138.3557	126.8516	116.214	106.182	95.8245	82.5823
	v, m^3/kg	0.038	0.0459	0.0524	0.0594	0.0676	0.0774	0.0882	0.0994	0.1092
	h, kJ/kg	1150.2685	1117.8566	1073.8096	1046.2231	1048.457	1083.9676	1148.5179	1232.0293	1318.1106
	s, kJ/kg K	3.2065	3.2921	3.3186	3.3589	3.4517	3.6121	3.835	4.0981	4.3588
	x_l, kg/kg	0.0492	0.0946	0.1422	0.191	0.2389	0.2849	0.3257	0.3749	0.4436
	x_v, kJ/kg	0.3037	0.4964	0.6417	0.752	0.8317	0.8822	0.9213	0.9499	0.9737
	h_l, kJ/kg	733.9022	643.9301	558.4663	476.5559	400.9542	333.2081	266.9345	206.4808	135.6666
	h_v, kg/kg	2407.3898	2162.6716	1973.9087	1825.6802	1712.7722	1658.7614	1590.1992	1530.306	1465.8085

0.7	T, °C	178.8701	167.8261	156.9512	146.198	135.7511	125.6671	115.638	104.6995	90.0718
	v, m^3/kg	0.051	0.0604	0.0671	0.0738	0.0814	0.0901	0.0996	0.1088	0.1159
	h, kJ/kg	1328.0635	1319.6724	1281.9046	1251.6176	1243.817	1261.8828	1301.3499	1352.0791	1396.3783
	s, kJ/kg K	3.5993	3.7491	3.802	3.8486	3.9294	4.0578	4.2269	4.4135	4.5711
	x_l, kg/kg	0.041	0.0782	0.1178	0.1594	0.2016	0.2439	0.2875	0.3325	0.4037
	x_v, kg/kg	0.2602	0.4345	0.5728	0.6845	0.772	0.8387	0.8848	0.926	0.9617
	h_l, kJ/kg	752.0257	675.1	601.4834	528.9974	459.2736	393.2921	329.6145	258.0615	174.6778
	h_v, kJ/kg	2462.0673	2241.7705	2064.1019	1917.223	1797.9702	1702.4857	1654.4946	1581.013	1500.8539
0.8	T, °C	181.3871	172.423	163.3254	154.0403	144.6506	135.1202	125.0939	113.5745	97.5614
	v, m^3/kg	0.0697	0.0808	0.0872	0.0928	0.099	0.1058	0.1129	0.1193	0.1231
	h, kJ/kg	1581.1772	1600.1672	1561.9696	1519.1403	1489.9371	1478.6589	1481.4255	1488.6736	1481.7656
	s, kJ/kg K	4.1558	4.3779	4.4429	4.4743	4.518	4.5879	4.6774	4.7642	4.7982
	x_l, kg/kg	0.0331	0.0623	0.0943	0.1289	0.1656	0.2042	0.2464	0.2967	0.3664
	x_v, kg/kg	0.214	0.3669	0.4952	0.6053	0.6987	0.7767	0.842	0.8937	0.9458
	h_l, kJ/kg	771.0833	706.5144	644.5811	581.8281	518.6122	455.1	389.5934	316.8138	216.3518
	h_v, kJ/kg	2520.0549	2327.6494	2164.2643	2021.7431	1898.1675	1791.4518	1697.5926	1639.5607	1539.693
0.9	T, °C	183.9041	177.0198	169.6997	161.8826	153.5502	144.5733	134.5498	122.4495	105.0509
	v, m^3/kg	0.0995	0.1128	0.1177	0.1206	0.1234	0.1265	0.1295	0.1317	0.1309
	h, kJ/kg	1980.2621	2033.1656	1978.5008	1901.6874	1827.7721	1763.6032	1707.4902	1651.8406	1577.9432
	s, kJ/kg K	5.029	5.3394	5.383	5.353	5.309	5.2687	5.2299	5.1737	5.049
	x_l, kg/kg	0.0252	0.047	0.0717	0.0995	0.1307	0.1659	0.2066	0.2577	0.3309
	x_v, kg/kg	0.1645	0.2924	0.4077	0.5135	0.6106	0.6994	0.7809	0.8511	0.9249
	h_l, kJ/kg	792.084	738.6422	687.8561	634.8174	578.5194	518.0936	451.332	372.6197	260.1584
	h_v, kJ/kg	2581.9273	2421.5768	2275.8943	2140.6533	2014.8068	1897.2276	1785.6246	1707.8691	1583.1704

Table A.3 Ammonia-water liquid-vapour mixture properties at 14 bar

θ = f(T)	Property	Ammonia concentration (mass fraction), x								
		0.1	**0.2**	**0.3**	**0.4**	**0.5**	**0.6**	**0.7**	**0.8**	**0.9**
0.1	T, °C	167.2299	143.5853	121.9204	102.2476	85.3577	71.8588	61.7204	54.1723	47.7544
	v, m^3/kg	0.0047	0.0061	0.0077	0.0099	0.0134	0.0189	0.0276	0.0407	0.0591
	h, kJ/kg	697.2848	552.0979	427.9214	336.0414	290.3377	304.6945	391.8173	560.4572	814.8668
	s, kJ/kg K	2.1906	1.9714	1.7481	1.5608	1.4569	1.4881	1.7061	2.152	2.8513
	x_l, kg/kg	0.0928	0.1834	0.2741	0.359	0.4451	0.5264	0.6016	0.6728	0.7532
	x_v, kg/kg	0.4836	0.731	0.8659	0.9389	0.9723	0.9869	0.9934	0.9965	0.9983
	h_l, kJ/kg	663.3619	504.4777	363.6946	239.8429	148.5462	88.09	55.9419	46.0967	56.3521
	h_v, kJ/kg	2182.3739	1857.4828	1687.3364	1556.0285	1470.5828	1413.9067	1375.8798	1349.3406	1327.6492
0.2	T, °C	169.7263	148.1703	128.2902	110.0891	94.2564	81.3072	71.1635	63.0206	55.1937
	v, m^3/kg	0.0089	0.0116	0.0144	0.0183	0.0237	0.0316	0.0425	0.0567	0.0737
	h, kJ/kg	762.7973	641.2886	539.0351	470.2548	449.4896	488.6472	594.0805	763.5916	988.4913
	s, kJ/kg K	2.3383	2.1834	2.0259	1.913	1.8933	2.0118	2.2999	2.7633	3.3853
	x_l, kg/kg	0.0838	0.1651	0.2467	0.3224	0.3982	0.468	0.531	0.5909	0.6621
	x_v, kJ/kg	0.4505	0.6914	0.8373	0.9152	0.9573	0.9776	0.9875	0.9928	0.9962
	h_l, kJ/kg	680.2501	535.0739	404.2332	286.0759	195.0126	128.9126	85.4275	59.1128	46.3659
	h_v, kg/kg	2224.6509	1911.0337	1707.0692	1603.3903	1513.1549	1452.696	1411.1926	1380.5874	1352.8605
0.3	T, °C	172.2226	152.7552	134.66	117.9306	103.1551	90.7556	80.6066	71.8689	62.633
	v, m^3/kg	0.0137	0.0176	0.0216	0.0265	0.0332	0.0422	0.0537	0.0674	0.0823
	h, kJ/kg	837.505	738.7802	655.2512	603.5502	597.4773	645.7169	749.6048	902.1145	1090.8291
	s, kJ/kg K	2.5057	2.4124	2.3117	2.2554	2.2887	2.4459	2.7419	3.166	3.6892
	x_l, kg/kg	0.0751	0.1471	0.22	0.2916	0.3547	0.4162	0.472	0.5263	0.5941
	x_v, kg/kg	0.4158	0.648	0.7976	0.8845	0.9365	0.9638	0.9784	0.9869	0.993
	h_l, kJ/kg	697.1848	565.8212	445.5601	338.7758	245.0892	176.244	125.6303	88.1289	58.1318
	h_v, kJ/kg	2268.8084	1968.8343	1764.6826	1657.1315	1561.2215	1495.821	1449.6855	1413.9461	1379.1794

0.4	T, °C	174.7189	157.3402	141.0297	125.7722	112.0538	100.2039	90.0496	80.7171	70.0723
	v, m^3/kg	0.0195	0.0246	0.0294	0.0352	0.0426	0.052	0.0634	0.0762	0.0893
	h, kJ/kg	924.9362	848.5166	780.8972	741.4613	743.2436	792.3166	887.0326	1018.4606	1172.6136
	s, kJ/kg K	2.7005	2.6672	2.6156	2.6021	2.6684	2.8398	3.1208	3.494	3.9251
	x_l, kg/kg	0.0665	0.1294	0.1938	0.2575	0.3135	0.3688	0.4199	0.4714	0.5385
	x_v, kg/kg	0.3794	0.6006	0.7514	0.85	0.9082	0.9442	0.9651	0.9783	0.9883
	h_l, kJ/kg	714.2137	596.6605	487.5085	388.1036	297.9552	228.1385	172.5322	126.146	81.3628
	h_v, kJ/kg	2315.0083	2031.1236	1829.4041	1687.3711	1616.2076	1544.5892	1492.4219	1450.1591	1406.9678

Table A.3 Ammonia-water liquid-vapour mixture properties at 14 bar (contd.,)

θ = f(T)	Property	Ammonia concentration (mass fraction), x								
		0.1	**0.2**	**0.3**	**0.4**	**0.5**	**0.6**	**0.7**	**0.8**	**0.9**
0.5	T, °C	177.2152	161.9252	147.3995	133.6137	120.9524	109.6523	99.4927	89.5654	77.5116
	v, m^3/kg	0.0265	0.0328	0.0384	0.0447	0.0524	0.0619	0.0728	0.0845	0.0955
	h, kJ/kg	1030.521	976.501	922.1512	890.674	894.8844	939.1397	1020.1162	1128.0922	1247.8466
	s, kJ/kg K	2.9345	2.961	2.9516	2.9696	3.054	3.2238	3.4775	3.7947	4.1368
	x_l, kg/kg	0.058	0.1122	0.1681	0.2243	0.2784	0.3244	0.3723	0.4225	0.4904
	x_v, kg/kg	0.3411	0.549	0.6983	0.8046	0.8706	0.9167	0.9459	0.9659	0.9818
	h_l, kJ/kg	731.4004	627.5587	529.9189	438.7249	357.6129	283.4499	224.102	170.001	111.5778
	h_v, kJ/kg	2363.4509	2098.2101	1901.7402	1754.7452	1679.8155	1600.5956	1540.6881	1490.108	1436.6578
0.6	T, °C	179.7115	166.5102	153.7693	141.4552	129.8511	119.1007	108.9358	98.4137	84.9509
	v, m^3/kg	0.0355	0.0431	0.0491	0.0556	0.0633	0.0724	0.0824	0.0927	0.1017
	h, kJ/kg	1163.1254	1132.4209	1088.5607	1060.5421	1061.8025	1095.8419	1158.4654	1239.5927	1322.6937
	s, kJ/kg K	3.2268	3.3151	3.3412	3.3795	3.4684	3.6232	3.8386	4.0927	4.3426
	x_l, kg/kg	0.0497	0.0954	0.1431	0.192	0.2401	0.2865	0.3277	0.3775	0.4474
	x_v, kJ/kg	0.3006	0.4928	0.6378	0.7481	0.8281	0.8793	0.9191	0.9484	0.9729
	h_l, kJ/kg	748.8557	658.4986	572.6356	490.329	414.2934	346.0428	279.1545	218.0155	146.5263
	h_v, kg/kg	2414.3882	2170.5138	1982.2145	1833.9934	1720.5589	1665.7755	1596.0534	1534.8464	1468.7476

0.7	T, °C	182.2078	171.0951	160.139	149.2968	138.7498	128.5491	118.3789	107.262	92.3902
	v, m^3/kg	0.0475	0.0565	0.0628	0.0691	0.0762	0.0843	0.093	0.1015	0.1079
	h, kJ/kg	1338.2468	1333.1178	1296.1532	1265.7937	1257.2359	1273.9468	1311.5172	1359.8276	1401.0478
	s, kJ/kg K	3.6109	3.7662	3.8198	3.8651	3.9427	4.0659	4.2281	4.4063	4.5537
	x_l, kg/kg	0.0416	0.079	0.1189	0.1606	0.2031	0.2456	0.2897	0.3354	0.4077
	x_v, kg/kg	0.2578	0.4317	0.5696	0.6811	0.7688	0.8358	0.8825	0.9245	0.9609
	h_l, kJ/kg	766.8025	689.5307	615.5165	542.6177	472.4313	405.8985	341.556	269.1808	184.9347
	h_v, kJ/kg	2468.1425	2248.6229	2071.4813	1924.8331	1805.3892	1709.2786	1660.4227	1585.6429	1503.8142
0.8	T, °C	184.7041	175.6801	166.5088	157.1383	147.6485	137.9974	127.822	116.1103	99.8295
	v, m^3/kg	0.0646	0.0754	0.0816	0.0869	0.0926	0.0989	0.1054	0.1113	0.1146
	h, kJ/kg	1585.6633	1610.8515	1574.6283	1532.3166	1502.7172	1490.2929	1491.2773	1496.1596	1486.2165
	s, kJ/kg K	4.1509	4.3843	4.4525	4.4839	4.5255	4.5911	4.6746	4.7538	4.7785
	x_l, kg/kg	0.0337	0.0632	0.0954	0.1302	0.1671	0.2062	0.2487	0.2997	0.3706
	x_v, kg/kg	0.2123	0.3649	0.4928	0.6028	0.6961	0.7743	0.8399	0.8923	0.9451
	h_l, kJ/kg	785.6457	720.8073	658.4892	595.3	531.5834	467.4699	401.2246	327.5427	226.011
	h_v, kJ/kg	2525.1343	2333.3839	2170.4916	2028.2824	1904.7292	1797.6746	1703.1	1644.0214	1542.5304
0.9	T, °C	187.2004	180.2651	172.8786	164.9799	156.5471	147.4458	137.265	124.9586	107.2688
	v, m^3/kg	0.0916	0.1049	0.1098	0.1127	0.1153	0.1181	0.1209	0.1228	0.1219
	h, kJ/kg	1971.0195	2036.5386	1986.5524	1911.6157	1838.0891	1773.3177	1715.8531	1658.2297	1581.7147
	s, kJ/kg K	4.9881	5.3228	5.3755	5.349	5.3051	5.2627	5.2196	5.1578	5.0259
	x_l, kg/kg	0.0259	0.0479	0.0728	0.1009	0.1325	0.168	0.2092	0.261	0.3354
	x_v, kg/kg	0.1636	0.2913	0.4064	0.5121	0.6091	0.6979	0.7796	0.8502	0.9245
	h_l, kJ/kg	806.3312	752.7813	701.6486	648.1651	591.3237	530.2279	462.6483	382.9204	269.2209
	h_v, kJ/kg	2585.9254	2426.0527	2280.7443	2145.7692	2020.0158	1902.2952	1790.2636	1711.7852	1585.6846

Table A.3 Ammonia-water liquid-vapour mixture properties at 15 bar

θ = f(T)	Property	Ammonia concentration (mass fraction), x								
		0.1	**0.2**	**0.3**	**0.4**	**0.5**	**0.6**	**0.7**	**0.8**	**0.9**
0.1	T, °C	170.5023	146.7438	124.9609	105.1834	88.1998	74.6129	64.3875	56.7495	50.234
	v, m^3/kg	0.0045	0.0058	0.0073	0.0094	0.0126	0.0177	0.0258	0.038	0.0549
	h, kJ/kg	712.2068	566.6736	441.9147	349.3148	302.6886	315.7233	400.8147	566.3936	816.6006
	s, kJ/kg K	2.2233	2.0048	1.7814	1.5934	1.4877	1.5148	1.7252	2.1589	2.8406
	x_l, kg/kg	0.0929	0.1835	0.2743	0.3592	0.4454	0.5268	0.6023	0.6742	0.7555
	x_v, kg/kg	0.4781	0.7255	0.8615	0.9361	0.9707	0.986	0.9929	0.9962	0.9981
	h_l, kJ/kg	678.3443	519.055	377.8087	253.5325	161.8765	101.1375	68.8174	58.9893	69.6426
	h_v, kJ/kg	2192.3596	1867.5977	1696.3053	1563.11	1475.9986	1418.019	1378.9971	1351.6625	1329.2453
0.2	T, °C	172.9783	151.3167	131.3257	113.0234	97.097	84.056	73.8176	65.5717	57.6249
	v, m^3/kg	0.0084	0.0109	0.0136	0.0172	0.0223	0.0296	0.0397	0.0529	0.0687
	h, kJ/kg	777.5205	655.7713	552.9249	483.3161	461.4128	499.0044	602.3254	769.1576	990.9114
	s, kJ/kg K	2.3694	2.215	2.0569	1.9423	1.9194	2.0325	2.3122	2.7643	3.3726
	x_l, kg/kg	0.084	0.1654	0.2471	0.3228	0.3987	0.4687	0.5321	0.5926	0.6649
	x_v, kJ/kg	0.4455	0.6862	0.8328	0.9119	0.9552	0.9763	0.9867	0.9923	0.9959
	h_l, kJ/kg	695.0658	549.4979	418.2345	299.672	208.2496	141.8336	98.1035	71.6763	59.173
	h_v, kg/kg	2234.028	1920.8125	1716.0222	1610.9661	1519.1762	1457.4178	1414.8632	1383.3587	1354.732
0.3	T, °C	175.4543	155.8897	137.6904	120.8635	105.9941	93.4992	83.2478	74.3938	65.0157
	v, m^3/kg	0.013	0.0166	0.0203	0.025	0.0312	0.0396	0.0503	0.063	0.0769
	h, kJ/kg	851.9434	753.1871	669.1333	616.5992	609.3392	655.9855	757.8521	907.9472	1093.8769
	s, kJ/kg K	2.535	2.4421	2.3404	2.282	2.3115	2.4629	2.7507	3.1646	3.6759
	x_l, kg/kg	0.0754	0.1475	0.2204	0.2922	0.3553	0.4171	0.4733	0.5283	0.5972
	x_v, kg/kg	0.4113	0.6431	0.7931	0.8808	0.9339	0.9621	0.9773	0.9862	0.9926
	h_l, kJ/kg	711.8364	580.0899	459.4315	352.2713	258.21	189.0075	138.0605	100.2947	70.2986
	h_v, kJ/kg	2277.5316	1978.1527	1773.6407	1665.1018	1567.801	1501.13	1453.8932	1417.1475	1381.3063

0.4	T, °C	177.9304	160.4626	144.0552	128.7035	114.8912	102.9424	92.6779	83.216	72.4065
	v, m^3/kg	0.0183	0.0232	0.0277	0.0331	0.0401	0.0488	0.0594	0.0713	0.0834
	h, kJ/kg	938.9211	862.8176	794.8219	754.6301	755.2612	802.7879	895.5732	1024.7117	1176.1563
	s, kJ/kg K	2.7274	2.6947	2.6421	2.6264	2.6887	2.8543	3.1275	3.4913	3.9114
	x_l, kg/kg	0.0668	0.13	0.1944	0.2582	0.3143	0.3699	0.4214	0.4735	0.5418
	x_v, kg/kg	0.3753	0.5961	0.747	0.8473	0.9052	0.942	0.9636	0.9773	0.9878
	h_l, kJ/kg	728.7033	610.7741	501.246	401.4772	310.9404	240.7266	184.7037	137.913	92.9019
	h_v, kJ/kg	2323.0303	2039.8614	1838.1543	1694.1675	1623.2491	1550.4285	1497.1267	1453.7551	1409.318

Table A.3 Ammonia-water liquid-vapour mixture properties at 15 bar (contd.,)

θ = f(T)	Property	Ammonia concentration (mass fraction), x								
		0.1	**0.2**	**0.3**	**0.4**	**0.5**	**0.6**	**0.7**	**0.8**	**0.9**
0.5	T, °C	180.4064	165.0356	150.4199	136.5436	123.7884	112.3856	102.1081	92.0381	79.7973
	v, m^3/kg	0.0249	0.0309	0.0362	0.0421	0.0493	0.0581	0.0682	0.0791	0.0893
	h, kJ/kg	1043.7303	990.5795	936.0966	904.0145	907.1728	949.9515	1029.0582	1134.7763	1251.7691
	s, kJ/kg K	2.958	2.9859	2.9757	2.9915	3.0721	3.2362	3.4826	3.7909	4.1225
	x_l, kg/kg	0.0585	0.1128	0.1689	0.2252	0.2794	0.3257	0.374	0.4248	0.4939
	x_v, kg/kg	0.3376	0.5451	0.6942	0.8007	0.8673	0.9141	0.944	0.9647	0.9812
	h_l, kJ/kg	745.7263	641.5217	543.5144	451.9578	370.4615	295.8468	236.007	181.3749	122.5151
	h_v, kJ/kg	2370.7212	2106.2508	1910.058	1762.7641	1687.1546	1606.8536	1545.8104	1494.0363	1439.1836
0.6	T, °C	182.8824	169.6085	156.7847	144.3836	132.6855	121.8287	111.5382	100.8603	87.1882
	v, m^3/kg	0.0333	0.0405	0.0463	0.0524	0.0595	0.068	0.0773	0.0869	0.0951
	h, kJ/kg	1174.9321	1145.9875	1102.3733	1073.9784	1074.3388	1106.9891	1167.7782	1246.624	1326.8585
	s, kJ/kg K	3.2452	3.3363	3.3622	3.3986	3.4841	3.6335	3.8421	4.0876	4.3275
	x_l, kg/kg	0.0503	0.0961	0.144	0.1931	0.2413	0.2879	0.3296	0.38	0.451
	x_v, kJ/kg	0.2977	0.4895	0.6342	0.7445	0.8248	0.8765	0.917	0.947	0.9722
	h_l, kJ/kg	763.0164	672.3167	586.0893	503.4176	426.9779	358.251	290.7838	228.9986	156.8808
	h_v, kg/kg	2420.8529	2177.7441	1989.8775	1841.68	1727.7785	1672.2601	1601.4536	1539.0049	1471.3806

0.7	T, °C	185.3584	174.1815	163.1494	152.2237	141.5826	131.2719	120.9684	109.6824	94.579
	v, m^3/kg	0.0444	0.0531	0.0591	0.065	0.0717	0.0792	0.0873	0.0951	0.101
	h, kJ/kg	1347.3648	1345.5054	1309.4055	1279.0251	1269.7753	1285.218	1320.9914	1366.9911	1405.2629
	s, kJ/kg K	3.6208	3.7816	3.8362	3.8804	3.955	4.0735	4.2292	4.3994	4.5371
	x_l, kg/kg	0.0422	0.0798	0.1198	0.1618	0.2044	0.2473	0.2917	0.3381	0.4115
	x_v, kg/kg	0.2555	0.429	0.5666	0.6779	0.7657	0.8331	0.8804	0.923	0.9602
	h_l, kJ/kg	780.786	703.2087	628.8338	555.5551	484.9393	417.8904	352.9206	279.7706	194.7175
	h_v, kJ/kg	2473.7414	2254.9298	2078.2763	1931.8497	1812.2415	1715.5632	1665.8745	1589.8719	1506.4579
0.8	T, °C	187.8344	178.7545	169.5142	160.0637	150.4797	140.7151	130.3986	118.5046	101.9698
	v, m^3/kg	0.0602	0.0707	0.0767	0.0817	0.087	0.0929	0.0989	0.1043	0.1072
	h, kJ/kg	1589.2107	1620.4581	1586.2348	1544.5138	1514.5816	1501.0973	1500.4015	1503.0358	1490.1983
	s, kJ/kg K	4.1451	4.3894	4.4608	4.4925	4.5322	4.5939	4.6718	4.7438	4.7599
	x_l, kg/kg	0.0343	0.064	0.0964	0.1315	0.1687	0.208	0.251	0.3	0.3746
	x_v, kg/kg	0.2107	0.363	0.4907	0.6004	0.6937	0.772	0.838	0.891	0.9444
	h_l, kJ/kg	799.4212	734.3475	671.6802	608.0943	543.9131	479.2358	412.2943	332.4024	235.2274
	h_v, kJ/kg	2529.7985	2338.6489	2176.2135	2034.2968	1910.7706	1803.4086	1708.1733	1648.0814	1545.0503
0.9	T, °C	190.3105	183.3274	175.8789	167.9038	159.3769	150.1583	139.8287	127.3267	109.3606
	v, m^3/kg	0.0847	0.098	0.1029	0.1058	0.1083	0.1109	0.1134	0.1151	0.114
	h, kJ/kg	1961.5459	2039.0215	1993.6302	1920.6206	1847.5493	1782.2581	1723.5366	1664.0454	1585.0363
	s, kJ/kg K	4.9486	5.306	5.3675	5.3446	5.301	5.2566	5.2098	5.1427	5.0041
	x_l, kg/kg	0.0266	0.0488	0.0739	0.1023	0.1341	0.1699	0.2116	0.2641	0.3396
	x_v, kg/kg	0.1627	0.2903	0.4052	0.5108	0.6077	0.6965	0.7783	0.85	0.924
	h_l, kJ/kg	819.8032	766.1661	714.7207	660.8286	603.4818	541.769	473.4186	392.7354	277.8718
	h_v, kJ/kg	2589.5728	2430.145	2285.1866	2150.4618	2024.7989	1906.9501	1794.5209	1715.3323	1587.8969

Table A.3 Ammonia-water liquid-vapour mixture properties at 16 bar

θ = f(T)	Property	Ammonia concentration (mass fraction), x								
		0.1	**0.2**	**0.3**	**0.4**	**0.5**	**0.6**	**0.7**	**0.8**	**0.9**
0.1	T, °C	173.6072	149.7414	127.8474	107.9711	90.8991	77.2288	66.921	59.1979	52.5899
	v, m^3/kg	0.0043	0.0055	0.0069	0.0089	0.0119	0.0167	0.0242	0.0355	0.0513
	h, kJ/kg	726.3983	580.5591	455.2569	361.9784	314.4715	326.2519	409.4122	572.0823	818.2527
	s, kJ/kg K	2.2542	2.0364	1.813	1.6244	1.5168	1.5401	1.7436	2.1658	2.8311
	x_l, kg/kg	0.093	0.1837	0.2744	0.3594	0.4457	0.5272	0.6031	0.6754	0.7577
	x_v, kg/kg	0.4729	0.7204	0.8574	0.9334	0.9691	0.9851	0.9924	0.9959	0.9979
	h_l, kJ/kg	692.617	532.9566	391.2794	266.5973	174.5975	113.5867	81.101	71.2884	82.3186
	h_v, kJ/kg	2201.6814	1877.0414	1704.7073	1569.7627	1481.0815	1421.8572	1381.8746	1353.766	1330.6381
0.2	T, °C	176.0633	154.3023	134.2067	115.809	99.794	86.6664	76.3382	67.9945	59.9338
	v, m^3/kg	0.008	0.0104	0.0129	0.0163	0.021	0.0279	0.0373	0.0497	0.0644
	h, kJ/kg	791.4853	669.5432	566.1497	495.7588	472.7803	508.882	610.1854	774.447	993.1485
	s, kJ/kg K	2.3988	2.2448	2.0861	1.9701	1.9442	2.0521	2.3241	2.7656	3.3609
	x_l, kg/kg	0.0842	0.1656	0.2474	0.3231	0.3992	0.4693	0.5332	0.5943	0.6677
	x_v, kJ/kg	0.4407	0.6813	0.8285	0.9088	0.9532	0.975	0.9859	0.9918	0.9956
	h_l, kJ/kg	709.1746	563.2492	431.5932	312.6468	220.8822	154.1642	110.2002	83.668	71.4058
	h_v, kg/kg	2242.774	1929.9254	1724.4071	1618.0667	1524.8221	1461.8304	1418.2676	1385.8929	1356.3897
0.3	T, °C	178.5195	158.8632	140.566	123.647	108.689	96.1039	85.7554	76.7911	67.2778
	v, m^3/kg	0.0123	0.0157	0.0192	0.0236	0.0295	0.0373	0.0473	0.0592	0.0721
	h, kJ/kg	865.5893	766.8543	682.3225	629.0106	620.627	665.7565	765.6882	913.4608	1096.6841
	s, kJ/kg K	2.5625	2.47	2.3676	2.3071	2.3332	2.4791	2.7593	3.1636	3.6636
	x_l, kg/kg	0.0756	0.1479	0.2209	0.2927	0.356	0.418	0.4746	0.5301	0.6001
	x_v, kg/kg	0.407	0.6386	0.7888	0.8774	0.9314	0.9604	0.9762	0.9855	0.9922
	h_l, kJ/kg	725.7833	593.6895	472.6658	365.1485	270.7318	201.1895	149.9257	111.9111	81.928
	h_v, kJ/kg	2285.6606	1986.8229	1782.0046	1672.5527	1573.959	1506.0899	1457.8032	1420.0892	1383.2066

0.4	T, °C	180.9756	163.424	146.9252	131.4849	117.584	105.5415	95.1726	85.5876	74.6217
	v, m^3/kg	0.0173	0.0219	0.0262	0.0313	0.0378	0.046	0.0559	0.0671	0.0783
	h, kJ/kg	952.0743	876.3417	808.02	767.126	766.6718	812.7232	903.6622	1030.5952	1179.4125
	s, kJ/kg K	2.7525	2.7206	2.6671	2.6493	2.708	2.868	3.134	3.4889	3.8986
	x_l, kg/kg	0.0672	0.1305	0.195	0.2589	0.3151	0.371	0.4229	0.4756	0.5449
	x_v, kg/kg	0.3715	0.592	0.7429	0.8437	0.9023	0.9399	0.9621	0.9764	0.9873
	h_l, kJ/kg	742.4913	624.2219	514.3461	414.2367	323.3326	252.7422	196.3242	149.1517	103.9361
	h_v, kJ/kg	2330.4979	2047.9793	1846.3012	1701.6783	1629.8239	1555.8762	1501.4982	1457.0657	1411.4271

Table A.3 Ammonia-water liquid-vapour mixture properties at 16 bar (contd.,)

θ = f(T)	Property	Ammonia concentration (mass fraction), x								
		0.1	**0.2**	**0.3**	**0.4**	**0.5**	**0.6**	**0.7**	**0.8**	**0.9**
0.5	T, °C	183.4317	167.9849	153.2845	139.3228	126.479	114.9791	104.5898	94.3842	81.9657
	v, m^3/kg	0.0235	0.0292	0.0342	0.0397	0.0465	0.0548	0.0643	0.0744	0.0839
	h, kJ/kg	1056.0663	1003.8358	949.2697	916.6347	918.8009	960.1785	1037.4959	1141.0408	1255.3613
	s, kJ/kg K	2.9798	3.0092	2.9983	3.0121	3.0891	3.248	3.4875	3.7873	4.109
	x_l, kg/kg	0.0589	0.1134	0.1696	0.226	0.2804	0.3269	0.3756	0.427	0.4972
	x_v, kg/kg	0.3343	0.5414	0.6904	0.797	0.8642	0.9117	0.9423	0.9635	0.9805
	h_l, kJ/kg	759.3537	654.8211	556.4743	464.5839	382.719	307.6808	247.3748	192.2407	132.977
	h_v, kJ/kg	2377.4809	2113.7111	1917.7836	1770.2339	1693.9879	1612.6792	1550.5643	1497.6526	1441.4537
0.6	T, °C	185.8878	172.5457	159.6438	147.1608	135.3739	124.4166	114.007	103.1808	89.3096
	v, m^3/kg	0.0313	0.0383	0.0437	0.0495	0.0562	0.0641	0.0728	0.0817	0.0893
	h, kJ/kg	1185.8307	1158.6816	1115.3606	1086.6427	1086.1594	1117.4902	1176.5293	1253.184	1330.6561
	s, kJ/kg K	3.262	3.356	3.3818	3.4166	3.4988	3.6433	3.8453	4.0828	4.3131
	x_l, kg/kg	0.0508	0.0968	0.1449	0.194	0.2425	0.2893	0.3313	0.3824	0.4544
	x_v, kJ/kg	0.295	0.4864	0.6309	0.741	0.8217	0.8739	0.915	0.9457	0.9715
	h_l, kJ/kg	776.4791	685.4712	598.9103	515.8995	439.0806	369.9051	301.8901	239.4931	166.7883
	h_v, kg/kg	2426.8534	2184.443	1996.9805	1848.8177	1734.5001	1678.2805	1606.4545	1542.8276	1473.745

0.7	T, °C	188.3439	177.1066	166.003	154.9987	144.2689	133.8542	123.4242	111.9774	96.6535
	v, m^3/kg	0.0416	0.0501	0.0558	0.0614	0.0676	0.0747	0.0822	0.0895	0.0949
	h, kJ/kg	1355.5774	1356.9749	1321.7802	1291.426	1281.5465	1295.7869	1329.852	1373.6399	1409.0806
	s, kJ/kg K	3.6294	3.7957	3.8512	3.8945	3.9664	4.0804	4.2301	4.3928	4.5215
	x_l, kg/kg	0.0428	0.0806	0.1208	0.1629	0.2057	0.2489	0.2937	0.3407	0.4152
	x_v, kg/kg	0.2534	0.4266	0.5639	0.675	0.7628	0.8305	0.8784	0.9216	0.9594
	h_l, kJ/kg	794.0743	716.2189	641.5188	567.8894	496.8721	429.3376	363.7749	289.8917	204.0811
	h_v, kJ/kg	2478.9257	2260.7624	2084.5625	1938.3481	1818.5981	1721.4009	1670.908	1593.7489	1508.8246
0.8	T, °C	190.8	181.6674	172.3623	162.8366	153.1639	143.2918	132.8414	120.7739	103.9975
	v, m^3/kg	0.0562	0.0666	0.0723	0.0771	0.0821	0.0876	0.0932	0.0982	0.1007
	h, kJ/kg	1591.9938	1629.1435	1596.9465	1555.8492	1525.6375	1511.1726	1508.8863	1509.3774	1493.7706
	s, kJ/kg K	4.1386	4.3934	4.4681	4.5003	4.5381	4.5963	4.669	4.7343	4.7422
	x_l, kg/kg	0.0349	0.0648	0.0974	0.1327	0.1701	0.2097	0.2531	0.3009	0.3784
	x_v, kg/kg	0.2092	0.3612	0.4887	0.5982	0.6914	0.7699	0.8363	0.8897	0.9437
	h_l, kJ/kg	812.4998	747.2212	684.2373	620.2862	555.673	490.4667	422.868	342.75	244.0519
	h_v, kJ/kg	2534.1006	2343.5061	2181.4955	2039.8544	1916.3584	1808.7157	1712.8667	1651.7907	1547.2935
0.9	T, °C	193.2561	186.2283	178.7216	170.6746	162.0589	152.7293	142.2586	129.5705	111.3414
	v, m^3/kg	0.0787	0.092	0.0969	0.0996	0.102	0.1045	0.1068	0.1082	0.1071
	h, kJ/kg	1951.9838	2040.7784	1999.9099	1928.828	1856.2632	1790.5213	1730.6253	1669.3571	1587.9669
	s, kJ/kg K	4.9106	5.2892	5.3593	5.3399	5.2968	5.2507	5.2003	5.1282	4.9833
	x_l, kg/kg	0.0273	0.0496	0.0749	0.1035	0.1356	0.1718	0.2139	0.267	0.3436
	x_v, kg/kg	0.1619	0.2893	0.4041	0.5095	0.6063	0.6952	0.7772	0.85	0.9236
	h_l, kJ/kg	832.5848	778.8855	727.155	672.8871	615.0744	552.783	483.7063	402.1186	286.1586
	h_v, kJ/kg	2592.9146	2433.9032	2289.2747	2154.7864	2029.2107	1911.2443	1798.4435	1718.5568	1589.8469

Table A.3 Ammonia-water liquid-vapour mixture properties at 17 bar

θ = f(T)	Property	Ammonia concentration (mass fraction), x								
		0.1	**0.2**	**0.3**	**0.4**	**0.5**	**0.6**	**0.7**	**0.8**	**0.9**
0.1	T, °C	176.5631	152.5958	130.5966	110.6268	93.4709	79.7215	69.3355	61.5314	54.8354
	v, m^3/kg	0.0042	0.0053	0.0066	0.0085	0.0113	0.0158	0.0228	0.0334	0.0481
	h, kJ/kg	739.9388	593.8287	468.0158	374.0954	325.751	336.3314	417.6561	577.5448	819.8291
	s, kJ/kg K	2.2834	2.0664	1.843	1.6538	1.5445	1.5643	1.7613	2.1728	2.8224
	x_l, kg/kg	0.093	0.1838	0.2746	0.3596	0.4459	0.5276	0.6037	0.6766	0.7598
	x_v, kg/kg	0.4681	0.7156	0.8535	0.9308	0.9676	0.9842	0.9919	0.9956	0.9977
	h_l, kJ/kg	706.2554	546.2536	404.1728	279.1046	186.775	125.5025	92.8569	83.0582	94.4467
	h_v, kJ/kg	2210.4189	1885.8917	1712.606	1576.0315	1485.8659	1425.4496	1384.538	1355.6747	1331.8496
0.2	T, °C	178.9997	157.1445	136.95	118.4621	102.3632	89.1532	78.7397	70.303	62.1339
	v, m^3/kg	0.0076	0.0099	0.0123	0.0154	0.0199	0.0263	0.0352	0.0468	0.0605
	h, kJ/kg	804.7752	682.6814	578.7785	507.6528	483.649	518.3285	617.7005	779.4886	995.2225
	s, kJ/kg K	2.4265	2.273	2.1139	1.9965	1.9678	2.0709	2.3356	2.7671	3.3502
	x_l, kg/kg	0.0844	0.1659	0.2477	0.3235	0.3996	0.47	0.5342	0.5958	0.6702
	x_v, kJ/kg	0.4363	0.6767	0.8245	0.9058	0.9512	0.9738	0.9851	0.9913	0.9953
	h_l, kJ/kg	722.6531	576.4021	444.3768	325.067	232.9755	165.9683	121.7807	95.1499	83.1258
	h_v, kg/kg	2250.9661	1938.4516	1732.2865	1624.7443	1530.1316	1465.9662	1421.434	1388.2157	1357.857
0.3	T, °C	181.4362	161.6932	143.3035	126.2974	111.2555	98.5848	88.144	79.0745	69.4324
	v, m^3/kg	0.0117	0.015	0.0183	0.0224	0.0279	0.0352	0.0446	0.0558	0.0679
	h, kJ/kg	878.5321	779.863	694.8983	640.8523	631.4009	675.082	773.159	918.6886	1099.2765
	s, kJ/kg K	2.5884	2.4964	2.3933	2.331	2.3538	2.4945	2.7675	3.1628	3.6522
	x_l, kg/kg	0.0759	0.1482	0.2213	0.2932	0.3566	0.4188	0.4758	0.5319	0.6029
	x_v, kg/kg	0.4029	0.6343	0.7848	0.8741	0.929	0.9588	0.9751	0.9848	0.9918
	h_l, kJ/kg	739.1036	606.6922	485.3281	377.4738	282.7192	212.8527	161.2871	123.0375	93.0779
	h_v, kJ/kg	2293.2675	1994.9226	1789.8407	1679.5427	1579.7401	1510.7378	1461.4468	1422.7993	1384.9051

0.4	T, °C	183.8728	166.242	149.6569	134.1327	120.1478	108.0164	97.5482	87.846	76.7309
	v, m^3/kg	0.0164	0.0208	0.0249	0.0297	0.0358	0.0435	0.0528	0.0633	0.0738
	h, kJ/kg	964.4921	889.1754	820.5707	779.021	777.5378	822.1823	911.3468	1036.1486	1182.4113
	s, kJ/kg K	2.7761	2.7449	2.6907	2.671	2.7262	2.8812	3.1402	3.4867	3.8865
	x_l, kg/kg	0.0675	0.1309	0.1955	0.2595	0.3159	0.372	0.4242	0.4775	0.5479
	x_v, kg/kg	0.3679	0.5881	0.739	0.8402	0.8995	0.9379	0.9607	0.9755	0.9868
	h_l, kJ/kg	755.6527	637.0758	526.8771	426.4474	335.1957	264.2471	207.4532	159.9193	114.5196
	h_v, kJ/kg	2337.4787	2055.5533	1853.9147	1708.7245	1635.9831	1560.9743	1505.5733	1460.122	1413.3217

Table A.3 Ammonia-water liquid-vapour mixture properties at 17 bar (contd.,)

θ = f(T)	Property	Ammonia concentration (mass fraction), x								
		0.1	**0.2**	**0.3**	**0.4**	**0.5**	**0.6**	**0.7**	**0.8**	**0.9**
0.5	T, °C	186.3093	170.7907	156.0103	141.968	129.0401	117.448	106.9524	96.6176	84.0294
	v, m^3/kg	0.0222	0.0277	0.0324	0.0377	0.0441	0.0518	0.0607	0.0702	0.0791
	h, kJ/kg	1067.6342	1016.3638	961.7559	928.6101	929.8439	969.8826	1045.4827	1146.9306	1258.6596
	s, kJ/kg K	3.0001	3.031	3.0197	3.0316	3.1053	3.2592	3.4922	3.784	4.0963
	x_l, kg/kg	0.0593	0.114	0.1703	0.2268	0.2813	0.3281	0.3771	0.4291	0.5003
	x_v, kg/kg	0.3312	0.538	0.6868	0.7936	0.8612	0.9093	0.9406	0.9624	0.98
	h_l, kJ/kg	772.3519	667.5279	568.8688	476.6648	394.4555	319.0126	258.2635	202.6532	143.0151
	h_v, kJ/kg	2383.7918	2120.6623	1924.9885	1777.2177	1700.3715	1618.1197	1554.9905	1500.9918	1443.4967
0.6	T, °C	188.7459	175.3394	162.3637	149.8033	137.9324	126.8797	116.3566	105.3891	91.3279
	v, m^3/kg	0.0296	0.0363	0.0415	0.0469	0.0532	0.0607	0.0689	0.0772	0.0842
	h, kJ/kg	1195.9381	1170.6062	1127.6118	1098.6172	1097.3424	1127.4199	1184.7794	1259.3243	1334.1258
	s, kJ/kg K	3.2774	3.3743	3.4001	3.4334	3.5126	3.6524	3.8483	4.0783	4.2995
	x_l, kg/kg	0.0512	0.0974	0.1457	0.1949	0.2435	0.2907	0.333	0.3847	0.4577
	x_v, kJ/kg	0.2924	0.4835	0.6277	0.7378	0.8187	0.8714	0.9131	0.9444	0.9708
	h_l, kJ/kg	789.321	698.0345	611.166	527.8395	450.6641	381.0636	312.5296	249.552	176.2972
	h_v, kg/kg	2432.4457	2190.6757	2003.5919	1855.4717	1740.779	1683.889	1611.1014	1546.3529	1475.8715

0.7	T, °C	191.1824	179.8881	168.7172	157.6386	146.8248	136.3113	125.7609	114.1606	98.6265
	v, m^3/kg	0.0392	0.0474	0.0529	0.0582	0.0641	0.0707	0.0778	0.0845	0.0895
	h, kJ/kg	1363.0144	1367.6409	1333.3808	1303.0909	1292.6319	1305.737	1338.1672	1379.8319	1412.5469
	s, kJ/kg K	3.6367	3.8085	3.8651	3.9076	3.977	4.0869	4.2309	4.3864	4.5066
	x_l, kg/kg	0.0433	0.0813	0.1217	0.1639	0.207	0.2503	0.2955	0.3431	0.4186
	x_v, kg/kg	0.2513	0.4243	0.5613	0.6723	0.7602	0.8281	0.8765	0.9203	0.9587
	h_l, kJ/kg	806.7398	728.6412	653.6392	579.6857	508.2918	440.2987	374.1738	299.5946	213.0708
	h_v, kJ/kg	2483.7449	2266.1796	2090.403	1944.3917	1824.5172	1726.8423	1675.5733	1597.3162	1510.9468
0.8	T, °C	193.619	184.4368	175.0706	165.4739	155.7171	145.7429	135.1651	122.9322	105.925
	v, m^3/kg	0.0527	0.0629	0.0684	0.073	0.0778	0.0829	0.0881	0.0927	0.095
	h, kJ/kg	1594.1508	1637.035	1606.8671	1566.4252	1535.988	1520.5978	1516.8047	1515.2466	1496.9823
	s, kJ/kg K	4.1316	4.3965	4.4745	4.5072	4.5435	4.5984	4.6661	4.7251	4.7253
	x_l, kg/kg	0.0355	0.0656	0.0984	0.1338	0.1715	0.2114	0.2552	0.3036	0.3821
	x_v, kg/kg	0.2077	0.3596	0.4869	0.5962	0.6893	0.7679	0.8346	0.8885	0.9431
	h_l, kJ/kg	824.9628	759.5039	696.2298	631.9398	566.9231	501.2184	432.9996	352.0924	252.5272
	h_v, kJ/kg	2538.084	2348.0052	2186.3924	2045.011	1921.547	1813.6457	1717.2238	1655.191	1549.2932
0.9	T, °C	196.0555	188.9855	181.424	173.3092	164.6094	155.1745	144.5693	131.7037	113.2235
	v, m^3/kg	0.0733	0.0866	0.0915	0.0942	0.0965	0.0988	0.1009	0.1022	0.101
	h, kJ/kg	1942.4354	2041.9389	2005.4927	1936.3411	1864.314	1798.1873	1737.189	1674.231	1590.5548
	s, kJ/kg K	4.874	5.2724	5.3508	5.335	5.2924	5.2448	5.1912	5.1143	4.9634
	x_l, kg/kg	0.0279	0.0504	0.076	0.1048	0.1371	0.1736	0.2161	0.2698	0.3474
	x_v, kg/kg	0.1611	0.2884	0.4031	0.5084	0.6051	0.694	0.7761	0.85	0.9232
	h_l, kJ/kg	844.7585	791.0094	739.0221	684.4079	626.161	563.3244	493.5636	411.1176	294.1207
	h_v, kJ/kg	2595.9872	2437.3683	2293.0511	2158.7876	2033.2962	1915.2214	1802.0716	1721.4976	1591.5667

Table A.3 Ammonia-water liquid-vapour mixture properties at 18 bar

θ = f(T)	Property	Ammonia concentration (mass fraction), x								
		0.1	**0.2**	**0.3**	**0.4**	**0.5**	**0.6**	**0.7**	**0.8**	**0.9**
0.1	T, °C	179.3852	155.3216	133.2226	113.164	95.9282	82.1037	71.6431	63.7618	56.9817
	v, m^3/kg	0.004	0.0051	0.0063	0.0081	0.0108	0.015	0.0216	0.0315	0.0453
	h, kJ/kg	752.895	606.5423	480.2542	385.7208	336.5757	346.0109	425.5792	582.8074	821.3401
	s, kJ/kg K	2.3112	2.0949	1.8716	1.6818	1.571	1.5875	1.7783	2.1796	2.8146
	x_l, kg/kg	0.0931	0.1839	0.2747	0.3598	0.4462	0.528	0.6044	0.6777	0.7617
	x_v, kg/kg	0.4635	0.7111	0.85	0.9283	0.9661	0.9833	0.9913	0.9953	0.9975
	h_l, kJ/kg	719.3261	559.0111	416.5467	291.111	198.4644	136.9395	104.1395	94.3537	106.0835
	h_v, kJ/kg	2218.6394	1894.2137	1720.0526	1581.9542	1490.3807	1428.821	1387.0087	1357.4082	1332.8982
0.2	T, °C	181.8026	159.8582	139.5699	120.9962	104.8175	91.5291	81.0344	72.5088	64.2361
	v, m^3/kg	0.0073	0.0094	0.0117	0.0147	0.0189	0.025	0.0333	0.0442	0.0571
	h, kJ/kg	817.4606	695.2508	590.876	519.0512	494.0685	527.3865	624.9045	784.3052	997.1506
	s, kJ/kg K	2.4528	2.2999	2.1404	2.0216	1.9903	2.089	2.3467	2.7688	3.3402
	x_l, kg/kg	0.0846	0.1661	0.2479	0.3238	0.4001	0.4706	0.5351	0.5973	0.6727
	x_v, kJ/kg	0.432	0.6724	0.8206	0.9029	0.9493	0.9726	0.9843	0.9908	0.9951
	h_l, kJ/kg	735.5665	589.0146	456.6443	336.9889	244.5844	177.2995	132.8976	106.1739	94.3852
	h_v, kg/kg	2258.6671	1946.4567	1739.712	1631.0411	1535.1382	1469.8525	1424.3862	1390.3482	1359.153
0.3	T, °C	184.2199	164.3947	145.9171	128.8284	113.7067	100.9545	90.4256	81.2558	71.4906
	v, m^3/kg	0.0111	0.0143	0.0174	0.0213	0.0265	0.0334	0.0422	0.0527	0.0641
	h, kJ/kg	890.8463	792.2779	706.9208	652.1794	641.7121	684.0057	780.2986	923.6586	1101.676
	s, kJ/kg K	2.6129	2.5215	2.4177	2.3538	2.3735	2.5094	2.7756	3.1622	3.6415
	x_l, kg/kg	0.0762	0.1486	0.2217	0.2937	0.3572	0.4196	0.4769	0.5336	0.6056
	x_v, kg/kg	0.3991	0.6303	0.7809	0.8709	0.9267	0.9572	0.974	0.9841	0.9914
	h_l, kJ/kg	751.861	619.1591	497.4756	389.3036	294.2264	224.0497	172.1958	133.7239	103.797
	h_v, kJ/kg	2300.4124	2002.5171	1797.2064	1686.1191	1585.1835	1515.1047	1464.8515	1425.3012	1386.4224

0.4	T, °C	186.6373	168.9313	152.2644	136.6606	122.5959	110.3799	99.8169	90.0028	78.745
	v, m^3/kg	0.0156	0.0198	0.0237	0.0282	0.034	0.0413	0.0501	0.0599	0.0697
	h, kJ/kg	976.2482	901.3914	832.5376	790.3736	787.9136	831.2104	918.6668	1041.4071	1185.1798
	s, kJ/kg K	2.7982	2.768	2.7132	2.6916	2.7436	2.8937	3.1463	3.4848	3.8752
	x_l, kg/kg	0.0679	0.1314	0.1961	0.2601	0.3167	0.3729	0.4255	0.4794	0.5507
	x_v, kg/kg	0.3645	0.5844	0.7353	0.837	0.8969	0.9359	0.9594	0.9746	0.9863
	h_l, kJ/kg	768.2547	649.3959	538.8968	438.1645	346.5834	275.293	218.1406	170.2636	124.6984
	h_v, kJ/kg	2344.0288	2062.6456	1861.0547	1715.3532	1641.7693	1565.7595	1509.3818	1462.9502	1415.0242

Table A.3 Ammonia-water liquid-vapour mixture properties at 18 bar (contd.,)

θ = f(T)	Property	Ammonia concentration (mass fraction), x								
		0.1	**0.2**	**0.3**	**0.4**	**0.5**	**0.6**	**0.7**	**0.8**	**0.9**
0.5	T, °C	189.0546	173.4678	158.6117	144.4928	131.4851	119.8053	109.2082	98.7498	85.9995
	v, m^3/kg	0.0211	0.0264	0.0308	0.0358	0.0419	0.0492	0.0576	0.0665	0.0748
	h, kJ/kg	1078.5217	1028.242	973.6235	940.0121	940.3588	979.1142	1053.0636	1152.4822	1261.6944
	s, kJ/kg K	3.019	3.0516	3.0398	3.0501	3.1206	3.2699	3.4967	3.781	4.0843
	x_l, kg/kg	0.0597	0.1145	0.171	0.2276	0.2822	0.3292	0.3786	0.4311	0.5033
	x_v, kg/kg	0.3282	0.5347	0.6834	0.7904	0.8584	0.9071	0.939	0.9613	0.9794
	h_l, kJ/kg	784.7974	679.7021	580.7549	488.2567	405.7202	329.8928	268.7215	212.6585	152.6723
	h_v, kJ/kg	2389.7048	2127.1628	1931.731	1783.7682	1706.3549	1623.2167	1559.1233	1504.0828	1445.3368
0.6	T, °C	191.4719	178.0044	164.9589	152.325	140.3744	129.2307	118.5995	107.4968	93.2539
	v, m^3/kg	0.028	0.0345	0.0394	0.0446	0.0506	0.0576	0.0653	0.0731	0.0797
	h, kJ/kg	1205.3507	1181.8473	1139.2145	1109.974	1107.9506	1136.8341	1192.5778	1265.0885	1337.3036
	s, kJ/kg K	3.2915	3.3914	3.4173	3.4493	3.5256	3.6611	3.8511	4.0739	4.2866
	x_l, kg/kg	0.0517	0.0981	0.1464	0.1958	0.2446	0.2919	0.3347	0.3869	0.4609
	x_v, kJ/kg	0.2899	0.4808	0.6248	0.7348	0.8159	0.8691	0.9113	0.9432	0.9701
	h_l, kJ/kg	801.6034	710.0669	622.9125	539.2947	461.7795	391.7759	322.7495	259.2192	185.448
	h_v, kg/kg	2437.676	2196.496	2009.768	1861.6964	1746.664	1689.1299	1615.432	1549.6122	1477.786

0.7	T, °C	193.8893	182.541	171.3062	160.1572	149.2636	138.6561	127.9907	116.2438	100.5084
	v, m^3/kg	0.037	0.045	0.0503	0.0553	0.0609	0.0671	0.0738	0.0801	0.0846
	h, kJ/kg	1369.7819	1377.5897	1344.2935	1314.099	1303.1039	1315.1302	1345.9943	1385.616	1415.7005
	s, kJ/kg K	3.6431	3.8202	3.878	3.9198	3.9869	4.0929	4.2315	4.3803	4.4923
	x_l, kg/kg	0.0438	0.082	0.1225	0.1649	0.2081	0.2518	0.2973	0.3454	0.4219
	x_v, kg/kg	0.2494	0.4221	0.5589	0.6697	0.7576	0.8259	0.8747	0.919	0.9581
	h_l, kJ/kg	818.8515	740.5333	665.2544	590.9978	519.2506	450.8225	384.1629	308.9216	221.7247
	h_v, kJ/kg	2488.2409	2271.2293	2095.8492	1950.0319	1830.0475	1731.9304	1679.9099	1600.6072	1512.8515
0.8	T, °C	196.3066	187.0775	177.6534	167.9894	158.1528	148.0815	137.382	124.9908	107.7629
	v, m^3/kg	0.0496	0.0596	0.0649	0.0693	0.0738	0.0787	0.0836	0.0878	0.0898
	h, kJ/kg	1595.8146	1644.2368	1616.0906	1576.3274	1545.7055	1529.4509	1524.2179	1520.6952	1499.8741
	s, kJ/kg K	4.1243	4.3988	4.4801	4.5134	4.5484	4.6002	4.6633	4.7162	4.7091
	x_l, kg/kg	0.0361	0.0664	0.0993	0.1349	0.1728	0.2129	0.2571	0.3061	0.3856
	x_v, kg/kg	0.2064	0.3581	0.4851	0.5943	0.6874	0.7661	0.833	0.8874	0.9425
	h_l, kJ/kg	836.8711	771.2548	707.7141	643.1115	577.7164	511.5413	442.7317	361.0748	260.6888
	h_v, kJ/kg	2541.7853	2352.1877	2190.9481	2049.8124	1926.3818	1818.2409	1721.2809	1658.3172	1551.0769
0.9	T, °C	198.724	191.6141	184.0007	175.8216	167.042	157.5069	146.7733	133.7378	115.0173
	v, m^3/kg	0.0686	0.0817	0.0866	0.0893	0.0915	0.0937	0.0956	0.0968	0.0955
	h, kJ/kg	1932.9736	2042.6066	2010.474	1943.245	1871.7926	1805.3173	1743.286	1678.7136	1592.8398
	s, kJ/kg K	4.8389	5.2557	5.3423	5.3299	5.288	5.2389	5.1823	5.101	4.9445
	x_l, kg/kg	0.0285	0.0512	0.0769	0.1059	0.1385	0.1753	0.2182	0.2725	0.3511
	x_v, kg/kg	0.1603	0.2876	0.4021	0.5073	0.604	0.6929	0.7751	0.85	0.9228
	h_l, kJ/kg	856.3839	802.6037	750.3801	695.446	636.7927	573.4431	503.0319	419.7706	301.7912
	h_v, kJ/kg	2598.8218	2440.5739	2296.5521	2162.5022	2037.0922	1918.9167	1805.4376	1694.2926	1593.083

Table A.3 Ammonia-water liquid-vapour mixture properties at 19 bar

θ = f(T)	Property	Ammonia concentration (mass fraction), x								
		0.1	**0.2**	**0.3**	**0.4**	**0.5**	**0.6**	**0.7**	**0.8**	**0.9**
0.1	T, °C	182.0867	157.9313	135.7373	115.5941	98.2823	84.3859	73.854	65.8989	59.0384
	v, m^3/kg	0.0039	0.0049	0.0061	0.0078	0.0103	0.0143	0.0205	0.0298	0.0427
	h, kJ/kg	765.3235	618.7583	492.0198	396.9014	346.9889	355.326	433.2095	587.8841	822.7947
	s, kJ/kg K	2.3377	2.1222	1.8989	1.7086	1.5963	1.6097	1.7947	2.1865	2.8075
	x_l, kg/kg	0.0932	0.184	0.2749	0.3599	0.4464	0.5284	0.605	0.6788	0.7636
	x_v, kg/kg	0.459	0.7068	0.85	0.9258	0.9646	0.9825	0.9908	0.9949	0.9974
	h_l, kJ/kg	731.8838	571.2774	428.452	302.6645	209.7127	147.944	114.9944	105.2201	117.2764
	h_v, kJ/kg	2226.3985	1902.0626	1696.2732	1587.5642	1494.6515	1431.9917	1389.305	1358.9834	1333.7993
0.2	T, °C	184.4851	162.4557	142.0782	123.4228	107.168	93.8048	83.2324	74.6218	66.25
	v, m^3/kg	0.007	0.009	0.0112	0.014	0.018	0.0237	0.0316	0.0418	0.054
	h, kJ/kg	829.6008	707.3034	602.4907	530.0009	504.0812	536.0902	631.8244	788.9206	998.9459
	s, kJ/kg K	2.4779	2.3255	2.1656	2.0457	2.0119	2.1063	2.3575	2.7706	3.3309
	x_l, kg/kg	0.0848	0.1663	0.2482	0.3242	0.4005	0.4712	0.536	0.5988	0.6751
	x_v, kJ/kg	0.428	0.6683	0.817	0.9001	0.9474	0.9714	0.9836	0.9903	0.9948
	h_l, kJ/kg	747.9653	601.1405	468.4415	348.46	255.7553	188.2034	143.5956	116.7842	105.2287
	h_v, kg/kg	2265.9304	1953.9964	1746.7289	1636.9939	1539.87	1473.5131	1427.1446	1392.3087	1360.2942
0.3	T, °C	186.8836	166.9801	148.419	131.2515	116.0538	103.2238	92.6108	83.3448	73.4617
	v, m^3/kg	0.0106	0.0136	0.0166	0.0203	0.0252	0.0318	0.0401	0.05	0.0607
	h, kJ/kg	902.5952	804.1637	718.4432	663.0449	651.6041	692.5631	787.1376	928.3934	1103.9012
	s, kJ/kg K	2.6361	2.5454	2.4411	2.3755	2.3923	2.5236	2.7834	3.1619	3.6314
	x_l, kg/kg	0.0764	0.1489	0.2221	0.2941	0.3578	0.4204	0.478	0.5352	0.6082
	x_v, kg/kg	0.3954	0.6264	0.7773	0.8679	0.9245	0.9557	0.973	0.9835	0.991
	h_l, kJ/kg	764.1101	631.1379	509.1599	400.6824	305.2994	234.8255	182.6954	144.0126	114.1264
	h_v, kJ/kg	2307.145	2009.6609	1804.1495	1692.3226	1590.3211	1519.218	1468.0398	1427.6149	1387.7758

0.4	T, °C	189.282	171.5045	154.7598	139.0803	124.9395	112.6427	101.9891	92.0678	80.6733
	v, m^3/kg	0.0149	0.0189	0.0226	0.0269	0.0324	0.0393	0.0476	0.0568	0.0661
	h, kJ/kg	987.4242	913.0513	843.9833	801.2403	797.8454	839.848	925.656	1046.3972	1187.7403
	s, kJ/kg K	2.8191	2.7899	2.7345	2.7113	2.7603	2.9057	3.1522	3.483	3.8645
	x_l, kg/kg	0.0682	0.1318	0.1966	0.2607	0.3174	0.3739	0.4268	0.4812	0.5535
	x_v, kg/kg	0.3613	0.581	0.7318	0.8338	0.8944	0.9341	0.958	0.9737	0.9858
	h_l, kJ/kg	780.3484	661.2347	550.4519	449.4366	357.541	285.924	228.4287	180.2252	134.5114
	h_v, kJ/kg	2350.194	2069.3086	1867.7703	1721.6065	1647.2204	1570.2617	1512.9497	1465.5723	1416.5533

Table A.3 Ammonia-water liquid-vapour mixture properties at 19 bar (contd.,)

θ = f(T)	Property	Ammonia concentration (mass fraction), x								
		0.1	**0.2**	**0.3**	**0.4**	**0.5**	**0.6**	**0.7**	**0.8**	**0.9**
0.5	T, °C	191.6805	176.0289	161.1007	146.909	133.8253	122.0616	111.3675	100.7908	87.885
	v, m^3/kg	0.0201	0.0252	0.0294	0.0342	0.0399	0.0468	0.0547	0.0631	0.0709
	h, kJ/kg	1088.8028	1039.5367	984.9407	950.8938	950.396	987.9219	1060.2754	1157.7308	1264.4917
	s, kJ/kg K	3.0367	3.071	3.0589	3.0676	3.1352	3.28	3.501	3.7781	4.0729
	x_l, kg/kg	0.0601	0.1151	0.1716	0.2283	0.283	0.3303	0.38	0.433	0.5062
	x_v, kg/kg	0.3254	0.5317	0.6802	0.7873	0.8557	0.905	0.9374	0.9602	0.9788
	h_l, kJ/kg	796.7378	691.3977	592.1802	499.4052	416.5581	340.3646	278.7899	222.2955	161.9852
	h_v, kJ/kg	2395.2631	2133.2624	1938.061	1789.9298	1711.9779	1628.0039	1562.9916	1506.9504	1446.9942
0.6	T, °C	194.0789	180.5533	167.4415	154.7377	142.711	131.4806	120.7459	109.5137	95.0967
	v, m^3/kg	0.0266	0.0328	0.0376	0.0425	0.0482	0.0548	0.0621	0.0694	0.0756
	h, kJ/kg	1214.1495	1192.4775	1150.2305	1120.7743	1118.0455	1145.7828	1199.9722	1270.5136	1340.2189
	s, kJ/kg K	3.3045	3.4074	3.4336	3.4643	3.538	3.6693	3.8538	4.0698	4.2742
	x_l, kg/kg	0.0522	0.0987	0.1472	0.1967	0.2456	0.2931	0.3362	0.3889	0.4639
	x_v, kJ/kg	0.2876	0.4782	0.622	0.732	0.8133	0.8668	0.9096	0.942	0.9695
	h_l, kJ/kg	813.3861	721.6199	634.2034	550.3071	472.4754	402.0883	332.5898	268.5323	194.2751
	h_v, kg/kg	2442.5835	2201.9494	2015.5563	1867.5368	1752.1941	1694.0408	1619.4779	1552.6334	1479.51

0.7	T, °C	196.4774	185.0777	173.7823	162.5664	151.5968	140.8995	130.1242	118.2367	102.3083
	v, m^3/kg	0.035	0.0428	0.0479	0.0527	0.058	0.0639	0.0702	0.0761	0.0803
	h, kJ/kg	1375.968	1386.919	1354.591	1324.5129	1313.0239	1324.0219	1353.3818	1391.0316	1418.5738
	s, kJ/kg K	3.6486	3.831	3.8901	3.9313	3.9962	4.0985	4.232	4.3744	4.4786
	x_l, kg/kg	0.0444	0.0827	0.1234	0.1659	0.2093	0.2531	0.299	0.3477	0.4251
	x_v, kg/kg	0.2476	0.4201	0.5567	0.6673	0.7553	0.8238	0.8729	0.9178	0.9574
	h_l, kJ/kg	830.4622	751.9471	676.4121	601.8732	529.7913	460.9512	393.7808	317.9085	230.075
	h_v, kJ/kg	2492.4483	2275.9518	2100.9441	1955.3125	1835.2301	1736.7014	1683.9522	1603.6507	1514.5617
0.8	T, °C	198.8758	189.6021	180.1232	170.3951	160.4825	150.3185	139.5026	126.9597	109.52
	v, m^3/kg	0.0468	0.0566	0.0618	0.066	0.0703	0.0749	0.0795	0.0834	0.0852
	h, kJ/kg	1597.0283	1650.8356	1624.6958	1585.6278	1554.8554	1537.7864	1531.1747	1525.7671	1502.4805
	s, kJ/kg K	4.1167	4.4006	4.4851	4.5191	4.5528	4.6016	4.6604	4.7076	4.6936
	x_l, kg/kg	0.0367	0.0671	0.1002	0.136	0.174	0.2144	0.259	0.3085	0.3889
	x_v, kg/kg	0.2051	0.3566	0.4835	0.5925	0.6855	0.7643	0.8315	0.8864	0.942
	h_l, kJ/kg	848.2805	782.5263	718.7423	653.848	588.0973	521.4758	452.1033	369.7312	268.5667
	h_v, kJ/kg	2545.2346	2356.0879	2195.2005	2054.298	1930.9012	1822.5366	1725.0697	1661.1984	1552.6679
0.9	T, °C	201.2743	194.1265	186.464	178.2238	169.3683	159.7374	148.8809	135.6826	116.7316
	v, m^3/kg	0.0643	0.0774	0.0823	0.085	0.0871	0.0891	0.0909	0.0919	0.0905
	h, kJ/kg	1923.6506	2042.8653	2014.9328	1949.6109	1878.7548	1811.9787	1748.9614	1682.8468	1594.4176
	s, kJ/kg K	4.8052	5.2393	5.3336	5.3246	5.2835	5.2332	5.1736	5.0882	4.9251
	x_l, kg/kg	0.0291	0.052	0.0779	0.1071	0.1399	0.1769	0.2202	0.2751	0.3546
	x_v, kg/kg	0.1596	0.2868	0.4012	0.5063	0.6029	0.6918	0.7742	0.85	0.9225
	h_l, kJ/kg	867.5245	813.7194	761.2794	706.0483	647.0144	583.1796	512.1499	428.111	309.198
	h_v, kJ/kg	2601.4435	2443.5479	2299.8073	2165.9616	2040.6304	1922.3604	1808.5695	1696.1231	1594.4179

Table A.3 Ammonia-water liquid-vapour mixture properties at 20 bar

θ = f(T)	Property	Ammonia concentration (mass fraction), x								
		0.1	**0.2**	**0.3**	**0.4**	**0.5**	**0.6**	**0.7**	**0.8**	**0.9**
0.1	T, °C	184.6762	160.4334	138.1489	117.9249	100.5404	86.5753	75.9753	67.9494	61.0119
	v, m^3/kg	0.0037	0.0047	0.0059	0.0074	0.0099	0.0136	0.0195	0.0283	0.0404
	h, kJ/kg	777.2666	630.5119	503.3477	407.668	357.0212	364.3047	440.5742	592.7955	824.1983
	s, kJ/kg K	2.3631	2.1482	1.9251	1.7343	1.6206	1.631	1.8105	2.1934	2.8011
	x_l, kg/kg	0.0933	0.1841	0.275	0.3601	0.4466	0.5287	0.6056	0.6798	0.7653
	x_v, kg/kg	0.4549	0.7027	0.8478	0.9235	0.9631	0.9816	0.9903	0.9946	0.9972
	h_l, kJ/kg	743.9628	583.0891	439.9203	313.7963	220.5503	158.5456	125.4509	115.6869	128.0547
	h_v, kJ/kg	2233.7133	1909.4661	1701.6292	1592.8851	1498.6965	1434.9773	1391.4412	1360.4137	1334.5662
0.2	T, °C	187.0563	164.9459	144.4833	125.75	109.4225	95.9878	85.341	76.649	68.1821
	v, m^3/kg	0.0067	0.0087	0.0107	0.0134	0.0172	0.0226	0.0301	0.0398	0.0512
	h, kJ/kg	841.2478	718.8895	613.6629	540.5386	513.7185	544.4732	638.4883	793.3526	1000.6264
	s, kJ/kg K	2.5017	2.3499	2.1898	2.0687	2.0326	2.1229	2.368	2.7726	3.3223
	x_l, kg/kg	0.0849	0.1666	0.2485	0.3245	0.4009	0.4717	0.5368	0.6001	0.6774
	x_v, kJ/kg	0.4241	0.6644	0.8135	0.8974	0.9456	0.9702	0.9828	0.9898	0.9945
	h_l, kJ/kg	759.8937	612.8147	479.8089	359.5129	266.5195	198.7102	153.9039	127.0096	115.6829
	h_v, kg/kg	2272.7729	1961.0986	1753.3626	1642.6306	1544.35	1476.9663	1429.7255	1394.1124	1361.2948
0.3	T, °C	189.4364	169.4584	150.8176	133.5751	118.3047	105.4003	94.7067	85.3486	75.3523
	v, m^3/kg	0.0102	0.0131	0.0159	0.0194	0.0241	0.0303	0.0382	0.0476	0.0577
	h, kJ/kg	913.8428	815.5694	729.512	673.4886	661.1125	700.791	793.7041	932.919	1105.9712
	s, kJ/kg K	2.6583	2.5682	2.4633	2.3964	2.4103	2.5373	2.791	3.1617	3.622
	x_l, kg/kg	0.0767	0.1493	0.2225	0.2945	0.3583	0.4211	0.4791	0.5368	0.6107
	x_v, kg/kg	0.3919	0.6228	0.7739	0.865	0.9223	0.9542	0.972	0.9828	0.9907
	h_l, kJ/kg	775.8882	642.6727	520.4137	411.6474	315.9704	245.2108	192.8156	153.9319	124.0931
	h_v, kJ/kg	2313.4828	2016.3824	1810.699	1698.1862	1595.1797	1523.0994	1471.0307	1429.7576	1388.9811

0.4	T, °C	191.8165	173.9709	157.152	141.4002	127.1868	114.8128	104.0724	94.0482	82.5225
	v, m^3/kg	0.0142	0.0181	0.0216	0.0257	0.0309	0.0375	0.0453	0.0541	0.0628
	h, kJ/kg	998.0936	924.2184	854.9596	811.6676	807.3747	848.1332	932.3459	1051.1467	1190.1157
	s, kJ/kg K	2.839	2.8108	2.7549	2.7301	2.7762	2.9173	3.1579	3.4815	3.8545
	x_l, kg/kg	0.0685	0.1323	0.1971	0.2613	0.3181	0.3747	0.428	0.4829	0.5561
	x_v, kg/kg	0.3582	0.5777	0.7286	0.8309	0.892	0.9323	0.9568	0.9729	0.9854
	h_l, kJ/kg	791.9777	672.628	561.5839	460.2973	368.1019	296.1715	238.3476	189.8324	143.9841
	h_v, kJ/kg	2355.9924	2075.5714	1874.0931	1727.5118	1652.3676	1574.5073	1516.2995	1468.0085	1417.9264

Table A.3 Ammonia-water liquid-vapour mixture properties at 20 bar (contd.,)

θ = f(T)	Property	Ammonia concentration (mass fraction), x								
		0.1	**0.2**	**0.3**	**0.4**	**0.5**	**0.6**	**0.7**	**0.8**	**0.9**
0.5	T, °C	194.1966	178.4834	163.4864	149.2253	136.069	124.2252	113.4381	102.7477	89.6927
	v, m^3/kg	0.0191	0.024	0.0281	0.0326	0.0381	0.0447	0.0522	0.0601	0.0674
	h, kJ/kg	1098.5803	1050.3263	995.7701	961.3133	960.0072	996.349	1067.1608	1162.7082	1267.0788
	s, kJ/kg K	3.0535	3.0894	3.0771	3.0843	3.1491	3.2898	3.5051	3.7754	4.0621
	x_l, kg/kg	0.0605	0.1156	0.1722	0.229	0.2838	0.3313	0.3813	0.4349	0.509
	x_v, kg/kg	0.3227	0.5288	0.6772	0.7844	0.8532	0.9029	0.9359	0.9592	0.9783
	h_l, kJ/kg	808.215	702.6484	603.1843	510.1469	427.0047	350.4606	288.4996	231.5926	170.9792
	h_v, kJ/kg	2400.4844	2138.9892	1944.0106	1795.7336	1717.2775	1632.5123	1566.6216	1509.6168	1448.4879
0.6	T, °C	196.5767	182.9958	169.8208	157.0504	144.9511	133.6377	122.8038	111.4473	96.8629
	v, m^3/kg	0.0253	0.0314	0.0359	0.0406	0.046	0.0523	0.0592	0.0661	0.0718
	h, kJ/kg	1222.4698	1202.596	1160.7418	1131.089	1127.6864	1154.3204	1207.0075	1275.6393	1342.9034
	s, kJ/kg K	3.3168	3.4226	3.449	3.4786	3.5497	3.6771	3.8563	4.0658	4.2625
	x_l, kg/kg	0.0526	0.0993	0.1479	0.1975	0.2465	0.2943	0.3377	0.3909	0.4668
	x_v, kJ/kg	0.2853	0.4758	0.6193	0.7293	0.8108	0.8647	0.9079	0.9409	0.9689
	h_l, kJ/kg	824.7083	732.7349	645.0758	560.9196	482.7857	412.0315	342.0817	277.5198	202.8034
	h_v, kg/kg	2447.1865	2207.0632	2020.9887	1873.0256	1757.4004	1698.6569	1623.271	1555.4419	1481.0646

0.7	T, °C	198.9568	187.5083	176.1552	164.8755	153.8333	143.0502	132.1695	120.1469	104.0332
	v, m^3/kg	0.0333	0.0408	0.0458	0.0504	0.0554	0.061	0.0669	0.0725	0.0763
	h, kJ/kg	1381.7557	1395.7511	1364.3785	1334.4306	1322.4647	1332.4781	1360.3837	1396.1293	1421.2031
	s, kJ/kg K	3.6537	3.8411	3.9014	3.9421	4.005	4.1038	4.2324	4.3687	4.4656
	x_l, kg/kg	0.0449	0.0834	0.1242	0.1668	0.2103	0.2544	0.3	0.3498	0.4282
	x_v, kg/kg	0.2458	0.4181	0.5545	0.6651	0.753	0.8217	0.8713	0.9167	0.9568
	h_l, kJ/kg	841.6154	762.9258	687.1544	612.3504	539.9522	470.7161	401.4833	326.5842	238.1463
	h_v, kJ/kg	2496.3854	2280.373	2105.7185	1960.2659	1840.0962	1741.1844	1687.7347	1606.4758	1516.1001
0.8	T, °C	201.3369	192.0208	182.4896	172.7006	162.7155	152.4627	141.5352	128.8465	111.2034
	v, m^3/kg	0.0442	0.0539	0.059	0.063	0.0671	0.0715	0.0758	0.0795	0.0811
	h, kJ/kg	1598.071	1657.0145	1632.8241	1594.4412	1563.5338	1545.6852	1537.7483	1530.5143	1504.842
	s, kJ/kg K	4.1093	4.402	4.4897	4.5244	4.5569	4.603	4.6575	4.6994	4.6787
	x_l, kg/kg	0.0372	0.0678	0.1011	0.137	0.1752	0.2159	0.2607	0.3108	0.3921
	x_v, kg/kg	0.2038	0.3552	0.4819	0.5908	0.6838	0.7627	0.8301	0.8854	0.9415
	h_l, kJ/kg	859.2421	793.3652	729.3556	664.1883	598.1028	531.0565	461.1478	378.0909	276.1853
	h_v, kJ/kg	2548.4511	2359.7308	2199.1776	2058.4975	1935.1353	1826.5618	1728.6164	1663.866	1554.0907
0.9	T, °C	203.717	196.5333	188.824	180.5257	171.5976	161.8751	150.9009	137.5461	118.3736
	v, m^3/kg	0.0605	0.0735	0.0783	0.081	0.0831	0.085	0.0866	0.0875	0.086
	h, kJ/kg	1914.8289	2042.9864	2019.0714	1955.5947	1885.3237	1818.2643	1754.3015	1686.6912	1595.5968
	s, kJ/kg K	4.7736	5.2235	5.3252	5.3195	5.2792	5.2276	5.1653	5.0759	4.906
	x_l, kg/kg	0.0297	0.0528	0.0788	0.1082	0.1412	0.1785	0.2222	0.2775	0.358
	x_v, kg/kg	0.159	0.286	0.4004	0.5053	0.6019	0.6908	0.7733	0.85	0.9221
	h_l, kJ/kg	878.2237	824.4035	771.766	716.2569	656.8644	592.5691	520.9506	436.168	316.3652
	h_v, kJ/kg	2603.8726	2446.3137	2302.842	2169.1922	2043.9373	1925.5794	1811.4918	1697.8165	1595.5971

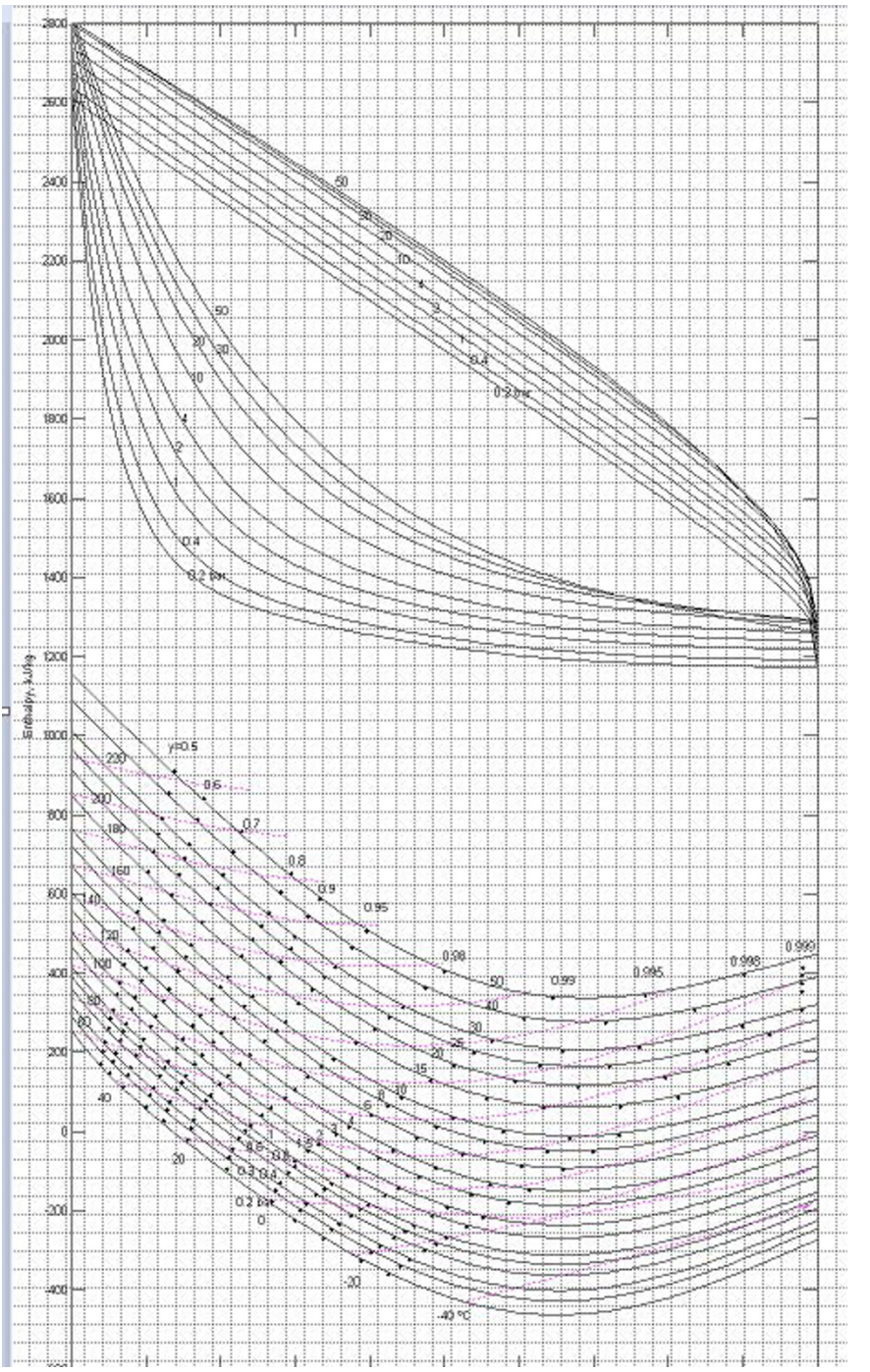

Fig. A.1: Specific enthalpy-concentration chart for ammonia-water mixture

Appendix B

Refrigerants and Psychrometric Properties

The refrigeration data book consists of the properties of refrigerants and wet air. The properties of refrigerants are used in the solutions used for refrigeration. Psychrometry deals with the properties of the wet air, i.e., a mixture of dry air and moisture. In the unsaturated air, the moisture is in the superheated steam condition. Psychrometric properties can be used in the evaluation and design of air conditioning systems. In terms of polygeneration, these psychrometric properties can be used in humidification-dehumidification (HDH) desalination solutions in addition to air conditioning.

So far, in the literature, a psychrometric chart has been developed for the graphical solution. The formulae and corrulation equations have been used in the analytical solutions of psychrometry. But there are no psychrometric tables similar to the steam tables or refrigerant tables to evaluate the problems with the use of tables in an easy method. For the first time in this section, the psychrometric tables are presented to solve the pscyometric properties, processes, and systems.

This section is focused on the critical pressure and the critical pressure of some refrigerants, formulation, and correlations of the psychrometric properties, psychrometric properties tables, and psychrometric charts. The properties of the refrigerant can be found in tables and charts published by the American Society of Heating, Refrigerating, and Air-Conditioning Engineers (ASHRAE).

T. Srinivas, *Thermal Polygeneration*,
https://doi.org/10.1007/978-3-031-37886-7

Table B.1: Critical temperature and critical pressure of some refrigerants

ASHRAE Number	Normal Boiling or Bubble/Dew /Azeotropic Point(s), °C	Critical Temperature, °C	Critical pressure (absolute), bar
R10	76.72	283.35	45.60
R11	23.77	197.96	44.08
R12	−29.80	111.97	41.36
R12B1	−3.70	153.80	41.02
R12B2	22.80	198.11	41.30
R13	−81.50	28.73	38.77
R13B1	−57.75	67.00	39.64
R14	−127.80	−45.64	37.50
R20	61.20	262.35	54.80
R21	8.92	178.45	51.80
R22	−40.70	96.14	49.90
R22B1	−14.60	138.83	51.32
R23	−82.10	25.92	48.36
R30	39.60	235.15	60.80
R31	−9.10	151.76	51.31
R32	−52.00	78.11	57.82
R40	−24.20	143.05	66.60
R41	−78.20	44.13	58.97
R50	−162.00	−82.30	46.40
R123	27.60	183.68	36.62
R124	−12.00	122.28	36.24
R125	−48.50	66.18	36.29
R150	84.00	292.83	53.70
R150a	57.20	249.83	50.70
R401A	-34.40/-28.80	105.27	46.13
R401B	-35.70/-30.80	103.54	46.82
R402A	-49.20/-47.00	76.03	42.34
R402B	-47.20/-44.90	83.03	45.25
R403A	-44.00/-42.30	91.22	46.88
R403B	-43.80/-42.30	88.72	43.99
R404A	-46.60/-45.80	72.14	37.35
R405A	-32.90/-24.50	106	42.89
R500	−33/00	102.15	41.73
R501	−41.00/-41.00	96.19	47.64
R502	−45.00/19.00	80.73	40.19
R503	−88.00/88.00	18.43	42.65

ASHRAE Number	Normal Boiling or Bubble/Dew /Azeotropic Point(s), °C	Critical Temperature, °C	Critical pressure (absolute), bar
R504	−57.00/17.00	62.13	44.39
R505	−30.00/115.00	117.78	47.30
R506	−12.00/18.00	142.22	51.57
R600	0.00	152.01	37.96
R600a	−11.70	134.70	36.40
R601	36.10	196.56	33.58
R601a	27.70	187.78	33.78
R610	34.60	193.65	36.40
R611	32.00	213.55	60.00
R630	−6.00	156.89	74.60
R631	16.60	183.00	56.20
R702	−252.87	−239.95	13.00
R704	−268.93	−267.96	2.27
R717	−33.34	132.40	112.80
R718	100.00	373.94	220.60
R720	−246.08	−228.75	27.60
R728	−195.79	−146.90	33.90
R729	−192.97	−140.53	37.85
R732	−182.95	−118.60	50.50
R740	−185.85	−122.40	48.70
R744	−78.00	31.04	73.80
R744A	−88.48	36.40	72.40
R764	−10.00	157.65	78.80
R784	−153.22	−63.80	55.00

B.1 Calculation of psychrometric properties from P, DBT and WBT

Modified Aphohn equation,

$$P_v = P'_v - \frac{1.8P(DBT - WBT')}{2700} \tag{1}$$

Modified Ferrel equation,

$$P_v = P'_v - 0.00066(DBT - WBT)\left(1 + \frac{1.8DBT}{1571}\right) \tag{2}$$

Carrier equation,

$$P_v = P_v' - \frac{1.8(P - P_v')(DBT - WBT)}{2800 - 1.3(1.8DBT + 32)} \quad (3)$$

P_v' is the saturation vapor pressure at wet-bulb temperature

Psychrometric Properties

Table B.2: Psychrometric Tables

DBT, °C	RH, %	DPT °C	WBT °C	Specific Volume, m^3/kg da	Degree of saturation	Specific humidity, g/kg da	Saturated specific humidity, g/kg da	Specific Enthalpy, kJ/ kg da	Specific entropy, kJ/kg da K	Specific exergy, kJ/ kg da
8	10	-21.84	0.16	0.80	0.10	0.66	6.65	9.70	0.04	2.92
	20	-13.62	1.11	0.80	0.20	1.32	6.65	11.36	0.04	2.64
	30	-8.53	2.05	0.80	0.30	1.98	6.65	13.02	0.05	2.41
	40	-4.78	2.96	0.80	0.40	2.64	6.65	14.69	0.06	2.22
	50	-1.79	3.86	0.80	0.50	3.31	6.65	16.36	0.06	2.04
	60	0.71	4.73	0.80	0.60	3.97	6.65	18.04	0.07	1.89
	70	2.86	5.57	0.80	0.70	4.64	6.65	19.72	0.07	1.74
	80	4.76	6.40	0.80	0.80	5.31	6.65	21.40	0.08	1.62
	90	6.46	7.21	0.80	0.90	5.98	6.65	23.09	0.09	1.50
	100	8.00	8.00	0.81	1.00	6.65	6.65	24.78	0.09	1.39
9	10	-21.07	0.81	0.80	0.10	0.71	7.12	10.82	0.04	2.84
	20	-12.79	1.81	0.80	0.20	1.41	7.12	12.60	0.05	2.55
	30	-7.66	2.80	0.80	0.30	2.12	7.12	14.38	0.05	2.31
	40	-3.88	3.75	0.80	0.40	2.83	7.12	16.17	0.06	2.11
	50	-0.87	4.69	0.80	0.50	3.54	7.12	17.96	0.07	1.93
	60	1.65	5.60	0.80	0.60	4.25	7.12	19.76	0.07	1.77
	70	3.82	6.48	0.81	0.70	4.97	7.12	21.56	0.08	1.62
	80	5.74	7.34	0.81	0.80	5.69	7.12	23.36	0.09	1.49
	90	7.45	8.18	0.81	0.90	6.40	7.12	25.17	0.09	1.37
	100	9.00	9.00	0.81	1.00	7.12	7.12	26.98	0.10	1.26
10	10	-20.29	1.45	0.80	0.10	0.75	7.62	11.95	0.04	2.76
	20	-11.95	2.51	0.80	0.20	1.51	7.62	13.86	0.05	2.46
	30	-6.79	3.54	0.81	0.30	2.27	7.62	15.77	0.06	2.21
	40	-2.98	4.54	0.81	0.40	3.03	7.62	17.68	0.07	2.00
	50	0.06	5.52	0.81	0.50	3.79	7.62	19.60	0.07	1.81
	60	2.59	6.46	0.81	0.60	4.55	7.62	21.52	0.08	1.65
	70	4.78	7.38	0.81	0.70	5.32	7.62	23.45	0.09	1.50
	80	6.71	8.28	0.81	0.80	6.08	7.62	25.38	0.09	1.37
	90	8.43	9.15	0.81	0.90	6.85	7.62	27.32	0.10	1.25
	100	10.00	10.00	0.81	1.00	7.62	7.62	29.26	0.11	1.14

Table B.2 Psychrometric Tables (contd.,)

DBT, °C	RH, %	DPT °C	WBT °C	Specific Volume, m^3/kg da	Degree of saturation	Specific humidity, g/kg da	Saturated specific humidity, g/kg da	Specific Enthalpy, kJ/ kg da	Specific entropy, kJ/kg da K	Specific exergy, kJ/ kg da
11	10	-19.51	2.09	0.81	0.10	0.81	8.16	13.09	0.05	2.68
	20	-11.12	3.20	0.81	0.20	1.61	8.16	15.13	0.06	2.37
	30	-5.91	4.28	0.81	0.30	2.42	8.16	17.17	0.06	2.11
	40	-2.08	5.33	0.81	0.40	3.24	8.16	19.22	0.07	1.89
	50	0.98	6.34	0.81	0.50	4.05	8.16	21.27	0.08	1.70
	60	3.54	7.33	0.81	0.60	4.87	8.16	23.33	0.09	1.53
	70	5.74	8.29	0.81	0.70	5.69	8.16	25.40	0.09	1.38
	80	7.68	9.21	0.81	0.80	6.51	8.16	27.47	0.10	1.25
	90	9.42	10.12	0.81	0.90	7.33	8.16	29.54	0.11	1.12
	100	11.00	11.00	0.82	1.00	8.16	8.16	31.63	0.12	1.02
12	10	-18.73	2.72	0.81	0.10	0.86	8.72	14.23	0.05	2.61
	20	-10.28	3.88	0.81	0.20	1.73	8.72	16.41	0.06	2.28
	30	-5.04	5.01	0.81	0.30	2.59	8.72	18.60	0.07	2.02
	40	-1.18	6.11	0.81	0.40	3.46	8.72	20.79	0.08	1.79
	50	1.90	7.17	0.81	0.50	4.33	8.72	22.99	0.08	1.59
	60	4.48	8.19	0.81	0.60	5.20	8.72	25.20	0.09	1.42
	70	6.70	9.19	0.82	0.70	6.08	8.72	27.41	0.10	1.27
	80	8.66	10.15	0.82	0.80	6.96	8.72	29.62	0.11	1.13
	90	10.41	11.09	0.82	0.90	7.84	8.72	31.85	0.12	1.01
	100	12.00	12.00	0.82	1.00	8.72	8.72	34.07	0.12	0.90
13	10	-17.96	3.34	0.81	0.10	0.92	9.32	15.39	0.06	2.54
	20	-9.45	4.56	0.81	0.20	1.84	9.32	17.72	0.07	2.20
	30	-4.17	5.74	0.81	0.30	2.77	9.32	20.06	0.07	1.92
	40	-0.28	6.89	0.82	0.40	3.70	9.32	22.40	0.08	1.69
	50	2.82	7.99	0.82	0.50	4.63	9.32	24.75	0.09	1.49
	60	5.42	9.06	0.82	0.60	5.56	9.32	27.11	0.10	1.31
	70	7.66	10.09	0.82	0.70	6.50	9.32	29.48	0.11	1.15
	80	9.63	11.09	0.82	0.80	7.44	9.32	31.85	0.12	1.02
	90	11.40	12.06	0.82	0.90	8.38	9.32	34.23	0.12	0.89
	100	13.00	13.00	0.82	1.00	9.32	9.32	36.61	0.13	0.79
14	10	-17.18	3.96	0.81	0.10	0.98	9.96	16.55	0.06	2.48
	20	-8.62	5.24	0.82	0.20	1.97	9.96	19.04	0.07	2.12
	30	-3.30	6.47	0.82	0.30	2.96	9.96	21.54	0.08	1.83
	40	-0.62	7.66	0.82	0.40	3.95	9.96	24.05	0.09	1.59
	50	3.75	8.81	0.82	0.50	4.94	9.96	26.56	0.10	1.38
	60	6.36	9.92	0.82	0.60	5.94	9.96	29.08	0.11	1.20
	70	8.62	10.99	0.82	0.70	6.94	9.96	31.61	0.12	1.05
	80	10.61	12.03	0.82	0.80	7.94	9.96	34.15	0.12	0.91
	90	12.38	13.03	0.83	0.90	8.95	9.96	36.69	0.13	0.79
	100	14.00	14.00	0.83	1.00	9.96	9.96	39.25	0.14	0.68
15	10	-16.41	4.56	0.82	0.10	1.05	10.64	17.73	0.06	2.41
	20	-7.78	5.91	0.82	0.20	2.10	10.64	20.38	0.07	2.04
	30	-2.43	7.20	0.82	0.30	3.15	10.64	23.05	0.08	1.75
	40	1.51	8.44	0.82	0.40	4.21	10.64	25.73	0.09	1.50
	50	4.67	9.63	0.82	0.50	5.27	10.64	28.42	0.10	1.28
	60	7.30	10.79	0.82	0.60	6.34	10.64	31.11	0.11	1.10
	70	9.58	11.90	0.83	0.70	7.41	10.64	33.81	0.12	0.94
	80	11.58	12.97	0.83	0.80	8.48	10.64	36.53	0.13	0.80
	90	13.37	14.00	0.83	0.90	9.56	10.64	39.25	0.14	0.68
	100	15.00	15.00	0.83	1.00	10.64	10.64	41.98	0.15	0.58

Table B.2 Psychrometric Tables (contd.,)

DBT, °C	RH, %	DPT °C	WBT °C	Specific Volume, m^3/kg da	Degree of saturation	Specific humidity, g/kg da	Saturated specific humidity, g/kg da	Specific Enthalpy, kJ/ kg da	Specific entropy, kJ/kg da K	Specific exergy, kJ/ kg da
16	10	-15.64	5.17	0.82	0.10	1.12	11.36	18.91	0.07	2.35
	20	-6.95	6.57	0.82	0.20	2.24	11.36	21.75	0.08	1.97
	30	-1.56	7.92	0.82	0.30	3.36	11.36	24.59	0.09	1.66
	40	2.41	9.21	0.83	0.40	4.49	11.36	27.45	0.10	1.40
	50	5.59	10.45	0.83	0.50	5.63	11.36	30.32	0.11	1.19
	60	8.24	11.65	0.83	0.60	6.76	11.36	33.20	0.12	1.00
	70	10.53	12.80	0.83	0.70	7.91	11.36	36.09	0.13	0.84
	80	12.55	13.91	0.83	0.80	9.05	11.36	38.99	0.14	0.70
	90	14.36	14.97	0.83	0.90	10.20	11.36	41.90	0.15	0.59
	100	16.00	16.00	0.83	1.00	11.36	11.36	44.82	0.16	0.48
17	10	-14.87	5.77	0.82	0.10	1.19	12.12	20.10	0.07	2.29
	20	-6.12	7.23	0.83	0.20	2.39	12.12	23.13	0.08	1.89
	30	-0.69	8.64	0.83	0.30	3.59	12.12	26.17	0.10	1.58
	40	3.31	9.98	0.83	0.40	4.79	12.12	29.22	0.11	1.31
	50	6.51	11.27	0.83	0.50	6.00	12.12	32.28	0.12	1.09
	60	9.18	12.51	0.83	0.60	7.21	12.12	35.36	0.13	0.91
	70	11.49	13.70	0.83	0.70	8.43	12.12	38.44	0.14	0.75
	80	13.53	14.84	0.83	0.80	9.66	12.12	41.54	0.15	0.61
	90	15.35	15.94	0.84	0.90	10.88	12.12	44.65	0.16	0.49
	100	17.00	17.00	0.84	1.00	12.12	12.12	47.77	0.17	0.40
18	10	-14.10	6.36	0.83	0.10	1.27	12.92	21.31	0.08	2.24
	20	-5.29	7.89	0.83	0.20	2.54	12.92	24.54	0.09	1.82
	30	0.17	9.35	0.83	0.30	3.82	12.92	27.78	0.10	1.49
	40	4.21	10.75	0.83	0.40	5.11	12.92	31.03	0.11	1.23
	50	7.43	12.09	0.83	0.49	6.40	12.92	34.30	0.12	1.00
	60	10.12	13.37	0.84	0.60	7.69	12.92	37.58	0.14	0.81
	70	12.45	14.60	0.84	0.70	8.99	12.92	40.88	0.15	0.65
	80	14.50	15.78	0.84	0.80	10.30	12.92	44.19	0.16	0.52
	90	16.33	16.91	0.84	0.90	11.61	12.92	47.51	0.17	0.41
	100	18.00	18.00	0.84	1.00	12.92	12.92	50.84	0.18	0.31
19	10	-13.33	6.94	0.83	0.1	1.35	13.78	22.52	0.08	2.18
	20	-4.47	8.54	0.83	0.2	2.71	13.78	25.96	0.09	1.75
	30	1.04	10.07	0.83	0.3	4.07	13.78	29.42	0.11	1.42
	40	5.1	11.52	0.83	0.39	5.44	13.78	32.89	0.12	1.14
	50	8.35	12.91	0.84	0.49	6.81	13.78	36.38	0.13	0.92
	60	11.06	14.24	0.84	0.59	8.19	13.78	39.88	0.14	0.73
	70	13.41	15.5	0.84	0.7	9.58	13.78	43.4	0.16	0.57
	80	15.47	16.72	0.84	0.8	10.97	13.78	46.93	0.17	0.44
	90	17.32	17.88	0.84	0.9	12.37	13.78	50.48	0.18	0.33
	100	19	19	0.85	1	13.78	13.78	54.04	0.19	0.24
20	10	-12.56	7.52	0.83	0.10	1.44	14.68	23.75	0.09	2.13
	20	-3.64	9.19	0.83	0.20	2.88	14.68	27.42	0.10	1.69
	30	1.91	10.78	0.84	0.30	4.33	14.68	31.10	0.11	1.34
	40	6.00	12.29	0.84	0.39	5.79	14.68	34.80	0.13	1.06
	50	9.27	13.73	0.84	0.49	7.26	14.68	38.52	0.14	0.83
	60	12.00	15.10	0.84	0.59	8.73	14.68	42.25	0.15	0.64
	70	14.36	16.41	0.84	0.70	10.21	14.68	46.00	0.17	0.49
	80	16.44	17.66	0.85	0.80	11.69	14.68	49.77	0.18	0.36
	90	18.31	18.85	0.85	0.90	13.18	14.68	53.56	0.19	0.26
	100	20.00	20.00	0.85	1.00	14.68	14.68	57.37	0.20	0.18

Table B.2 Psychrometric Tables (contd.,)

DBT, °C	RH, %	DPT °C	WBT °C	Specific Volume, m^3/kg da	Degree of saturation	Specific humidity, g/kg da	Saturated specific humidity, g/kg da	Specific Enthalpy, kJ/ kg da	Specific entropy, kJ/kg da K	Specific exergy, kJ/ kg da
21	10	-11.79	8.10	0.84	0.10	1.53	15.64	24.99	0.09	2.08
	20	-2.81	9.84	0.84	0.20	3.07	15.64	28.90	0.10	1.62
	30	2.77	11.49	0.84	0.29	4.61	15.64	32.82	0.12	1.27
	40	6.89	13.06	0.84	0.39	6.16	15.64	36.76	0.13	0.98
	50	10.19	14.55	0.84	0.49	7.72	15.64	40.72	0.15	0.75
	60	12.94	15.96	0.85	0.59	9.29	15.64	44.71	0.16	0.56
	70	15.32	17.31	0.85	0.69	10.87	15.64	48.71	0.18	0.41
	80	17.42	18.60	0.85	0.80	12.45	15.64	52.73	0.19	0.29
	90	19.30	19.82	0.85	0.90	14.04	15.64	56.77	0.20	0.19
	100	21.00	21.00	0.85	1.00	15.64	15.64	60.83	0.22	0.12
22	10	-11.03	8.67	0.84	0.10	1.63	16.65	26.24	0.09	2.04
	20	-1.98	10.49	0.84	0.20	3.26	16.65	30.40	0.11	1.56
	30	3.64	12.20	0.84	0.29	4.90	16.65	34.58	0.13	1.20
	40	7.79	13.83	0.85	0.39	6.56	16.65	38.78	0.14	0.91
	50	11.11	15.36	0.85	0.49	8.22	16.65	43.00	0.16	0.68
	60	13.88	16.82	0.85	0.59	9.89	16.65	47.24	0.17	0.49
	70	16.28	18.21	0.85	0.69	11.56	16.65	51.51	0.18	0.34
	80	18.39	19.53	0.85	0.80	13.25	16.65	55.80	0.20	0.22
	90	20.28	20.79	0.86	0.90	14.95	16.65	60.11	0.21	0.14
	100	22.00	22.00	0.86	1.00	16.65	16.65	64.44	0.23	0.07
23	10	-10.26	9.24	0.84	0.10	1.73	17.73	27.51	0.10	2.00
	20	-1.16	11.13	0.84	0.20	3.47	17.73	31.93	0.12	1.50
	30	4.50	12.91	0.85	0.29	5.21	17.73	36.38	0.13	1.13
	40	8.68	14.59	0.85	0.39	6.97	17.73	40.85	0.15	0.84
	50	12.02	16.18	0.85	0.49	8.74	17.73	45.35	0.16	0.61
	60	14.82	17.69	0.85	0.59	10.52	17.73	49.87	0.18	0.42
	70	17.23	19.12	0.86	0.69	12.30	17.73	54.41	0.19	0.28
	80	19.36	20.47	0.86	0.80	14.10	17.73	58.98	0.21	0.17
	90	21.27	21.76	0.86	0.90	15.91	17.73	63.58	0.23	0.09
	100	23.00	23.00	0.86	1.00	17.73	17.73	68.20	0.24	0.04
24	10	-9.50	9.80	0.84	0.10	1.84	18.86	28.79	0.10	1.95
	20	-0.33	11.77	0.85	0.20	3.68	18.86	33.50	0.12	1.44
	30	5.37	13.62	0.85	0.29	5.54	18.86	38.23	0.14	1.06
	40	9.58	15.36	0.85	0.39	7.41	18.86	42.98	0.15	0.77
	50	12.94	17.00	0.85	0.49	9.29	18.86	47.77	0.17	0.54
	60	15.76	18.55	0.86	0.59	11.18	18.86	52.59	0.19	0.36
	70	18.19	20.02	0.86	0.69	13.08	18.86	57.43	0.21	0.22
	80	20.34	21.41	0.86	0.80	15.00	18.86	62.30	0.22	0.12
	90	22.26	22.74	0.86	0.90	16.92	18.86	67.20	0.24	0.05
	100	24.00	24.00	0.87	1.00	18.86	18.86	72.13	0.26	0.01
25	10	-8.73	10.36	0.85	0.10	1.95	20.06	30.09	0.11	1.92
	20	0.49	12.41	0.85	0.19	3.91	20.06	35.09	0.13	1.39
	30	6.23	14.33	0.85	0.29	5.89	20.06	40.12	0.14	1.00
	40	10.47	16.13	0.86	0.39	7.87	20.06	45.18	0.16	0.71
	50	13.86	17.82	0.86	0.49	9.87	20.06	50.28	0.18	0.48
	60	16.70	19.42	0.86	0.59	11.88	20.06	55.40	0.20	0.30
	70	19.15	20.92	0.86	0.69	13.91	20.06	60.56	0.22	0.17
	80	21.31	22.35	0.87	0.79	15.95	20.06	65.75	0.23	0.08
	90	23.24	23.71	0.87	0.90	18.00	20.06	70.97	0.25	0.02
	100	**25.00**	**25.00**	**0.87**	**1.00**	**20.06**	**20.06**	**76.23**	**0.27**	**0.00**

Table B.2 Psychrometric Tables (contd.,)

DBT, °C	RH, %	DPT °C	WBT °C	Specific Volume, m^3/kg da	Degree of saturation	Specific humidity, g/kg da	Saturated specific humidity, g/kg da	Specific Enthalpy, kJ/ kg da	Specific entropy, kJ/kg da K	Specific exergy, kJ/ kg da
26	10	-7.97	10.91	0.85	0.10	2.07	21.33	31.41	0.11	1.88
	20	1.32	13.04	0.85	0.19	4.15	21.33	36.72	0.13	1.34
	30	7.09	15.03	0.86	0.29	6.25	21.33	42.06	0.15	0.94
	40	11.36	16.89	0.86	0.39	8.36	21.33	47.45	0.17	0.65
	50	14.78	18.64	0.86	0.49	10.49	21.33	52.86	0.19	0.42
	60	17.64	20.28	0.86	0.59	12.63	21.33	58.32	0.21	0.25
	70	20.10	21.83	0.87	0.69	14.78	21.33	63.81	0.23	0.13
	80	22.28	23.29	0.87	0.79	16.95	21.33	69.34	0.25	0.05
	90	24.23	24.68	0.87	0.90	19.13	21.33	74.90	0.26	0.01
	100	26.00	26.00	0.88	1.00	21.33	21.33	80.51	0.28	0.00
27	10	-7.21	11.46	0.85	0.10	2.20	22.67	32.74	0.12	1.85
	20	2.14	13.68	0.86	0.19	4.41	22.67	38.38	0.14	1.29
	30	7.96	15.74	0.86	0.29	6.63	22.67	44.06	0.16	0.89
	40	12.26	17.66	0.86	0.39	8.88	22.67	49.78	0.18	0.59
	50	15.69	19.46	0.87	0.49	11.13	22.67	55.54	0.20	0.37
	60	18.57	21.15	0.87	0.59	13.41	22.67	61.34	0.22	0.21
	70	21.06	22.73	0.87	0.69	15.70	22.67	67.19	0.24	0.10
	80	23.25	24.23	0.88	0.79	18.01	22.67	73.07	0.26	0.03
	90	25.22	25.65	0.88	0.90	20.33	22.67	79.00	0.28	0.01
	100	27.00	27.00	0.88	1.00	22.67	22.67	84.97	0.30	0.02
28	10	-6.45	12.01	0.86	0.10	2.33	24.09	34.08	0.12	1.81
	20	2.96	14.31	0.86	0.19	4.67	24.09	40.07	0.14	1.24
	30	8.82	16.44	0.86	0.29	7.04	24.09	46.11	0.17	0.84
	40	13.15	18.43	0.87	0.39	9.42	24.09	52.19	0.19	0.54
	50	16.61	20.28	0.87	0.49	11.82	24.09	58.31	0.21	0.32
	60	19.51	22.01	0.87	0.59	14.23	24.09	64.48	0.23	0.17
	70	22.01	23.64	0.88	0.69	16.67	24.09	70.70	0.25	0.07
	80	24.22	25.18	0.88	0.79	19.13	24.09	76.97	0.27	0.02
	90	26.20	26.62	0.88	0.90	21.60	24.09	83.28	0.29	0.02
	100	28.00	28.00	0.89	1.00	24.09	24.09	89.64	0.31	0.05
29	10	-5.69	12.55	0.86	0.10	2.47	25.59	35.45	0.13	1.78
	20	3.78	14.94	0.86	0.19	4.96	25.59	41.81	0.15	1.20
	30	9.68	17.15	0.87	0.29	7.46	25.59	48.21	0.17	0.79
	40	14.04	19.19	0.87	0.39	9.99	25.59	54.67	0.19	0.49
	50	17.53	21.10	0.87	0.49	12.54	25.59	61.18	0.22	0.28
	60	20.45	22.88	0.88	0.59	15.11	25.59	67.74	0.24	0.14
	70	22.97	24.55	0.88	0.69	17.70	25.59	74.35	0.26	0.06
	80	25.20	26.12	0.88	0.79	20.31	25.59	81.02	0.28	0.03
	90	27.19	27.60	0.89	0.90	22.94	25.59	87.74	0.31	0.04
	100	29.00	29.00	0.89	1.00	25.59	25.59	94.52	0.33	0.09
30	10	-4.93	13.09	0.86	0.10	2.61	27.17	36.84	0.13	1.76
	20	4.60	15.57	0.87	0.19	5.25	27.17	43.58	0.16	1.16
	30	10.54	17.85	0.87	0.29	7.91	27.17	50.38	0.18	0.74
	40	14.93	19.96	0.87	0.39	10.59	27.17	57.23	0.20	0.45
	50	18.44	21.92	0.88	0.49	13.30	27.17	64.15	0.23	0.25
	60	21.39	23.75	0.88	0.59	16.02	27.17	71.12	0.25	0.12
	70	23.93	25.46	0.88	0.69	18.78	27.17	78.15	0.28	0.05
	80	26.17	27.06	0.89	0.79	21.55	27.17	85.25	0.30	0.04
	90	28.18	28.57	0.89	0.90	24.35	27.17	92.40	0.32	0.08
	100	30.00	30.00	0.90	1.00	27.17	27.17	99.62	0.35	0.16

Table B.2 Psychrometric Tables (contd.,)

DBT, °C	RH, %	DPT °C	WBT °C	Specific Volume, m^3/kg da	Degree of satu-ration	Specific humidity, g/kg da	Satu-rated specific humidity, g/kg da	Specific Enthalpy, kJ/ kg da	Specific entropy, kJ/kg da K	Specific exergy, kJ/ kg da
31	10	-4.17	13.62	0.87	0.10	2.77	28.85	38.24	0.14	1.73
	20	5.43	16.20	0.87	0.19	5.56	28.85	45.39	0.16	1.12
	30	11.40	18.56	0.87	0.29	8.38	28.85	52.61	0.19	0.70
	40	15.82	20.73	0.88	0.39	11.23	28.85	59.88	0.21	0.41
	50	19.36	22.74	0.88	0.49	14.10	28.85	67.23	0.24	0.22
	60	22.32	24.62	0.89	0.59	16.99	28.85	74.64	0.26	0.11
	70	24.88	26.37	0.89	0.69	19.92	28.85	82.11	0.29	0.06
	80	27.14	28.00	0.89	0.79	22.87	28.85	89.66	0.31	0.07
	90	29.16	29.54	0.90	0.90	25.84	28.85	97.27	0.34	0.14
	100	31.00	31.00	0.90	1.00	28.85	28.85	104.95	0.36	0.24
32	10	-3.41	14.16	0.87	0.10	2.93	30.62	39.67	0.14	1.71
	20	6.24	16.83	0.87	0.19	5.89	30.62	47.25	0.17	1.08
	30	12.26	19.26	0.88	0.29	8.88	30.62	54.90	0.20	0.66
	40	16.71	21.50	0.88	0.39	11.89	30.62	62.62	0.22	0.38
	50	20.27	23.57	0.89	0.49	14.94	30.62	70.42	0.25	0.20
	60	23.26	25.49	0.89	0.59	18.01	30.62	78.29	0.28	0.11
	70	25.84	27.27	0.89	0.69	21.12	30.62	86.23	0.30	0.08
	80	28.11	28.95	0.90	0.79	24.25	30.62	94.25	0.33	0.12
	90	30.15	30.52	0.90	0.90	27.42	30.62	102.36	0.36	0.21
	100	32.00	32.00	0.91	1.00	30.62	30.62	110.53	0.38	0.35
33	10	-2.65	14.69	0.87	0.10	3.10	32.48	41.12	0.15	1.69
	20	7.06	17.45	0.88	0.19	6.24	32.48	49.15	0.17	1.05
	30	13.12	19.97	0.88	0.29	9.40	32.48	57.26	0.20	0.63
	40	17.60	22.27	0.88	0.39	12.60	32.48	65.45	0.23	0.36
	50	21.19	24.39	0.89	0.49	15.83	32.48	73.72	0.26	0.19
	60	24.19	26.36	0.89	0.59	19.09	32.48	82.08	0.29	0.12
	70	26.79	28.19	0.90	0.69	22.39	32.48	90.52	0.32	0.12
	80	29.08	29.89	0.90	0.79	25.72	32.48	99.05	0.34	0.18
	90	31.13	31.49	0.91	0.90	29.08	32.48	107.67	0.37	0.30
	100	33.00	33.00	0.91	1.00	32.48	32.48	116.38	0.40	0.48
34	10	-1.90	15.22	0.87	0.10	3.28	34.45	42.59	0.15	1.67
	20	7.88	18.08	0.88	0.19	6.60	34.45	51.09	0.18	1.02
	30	13.98	20.68	0.88	0.29	9.95	34.45	59.69	0.21	0.60
	40	18.49	23.04	0.89	0.39	13.34	34.45	68.37	0.24	0.34
	50	22.10	25.22	0.89	0.49	16.76	34.45	77.15	0.27	0.19
	60	25.13	27.23	0.90	0.59	20.22	34.45	86.03	0.30	0.14
	70	27.74	29.10	0.90	0.69	23.72	34.45	95.00	0.33	0.16
	80	30.05	30.84	0.91	0.79	27.26	34.45	104.06	0.36	0.26
	90	32.12	32.47	0.91	0.90	30.84	34.45	113.23	0.39	0.42
	100	34.00	34.00	0.92	1.00	34.45	34.45	122.50	0.42	0.63
35	10	-1.14	15.74	0.88	0.09	3.47	36.54	44.08	0.16	1.66
	20	8.70	18.71	0.88	0.19	6.98	36.54	53.09	0.19	1.00
	30	14.84	21.38	0.89	0.29	10.53	36.54	62.19	0.22	0.58
	40	19.38	23.82	0.89	0.39	14.12	36.54	71.40	0.25	0.33
	50	23.02	26.05	0.90	0.49	17.75	36.54	80.71	0.28	0.20
	60	26.07	28.10	0.90	0.59	21.42	36.54	90.13	0.31	0.17
	70	28.70	30.01	0.91	0.69	25.13	36.54	99.66	0.35	0.23
	80	31.02	31.78	0.91	0.79	28.89	36.54	109.30	0.38	0.36
	90	33.11	33.44	0.92	0.89	32.69	36.54	119.04	0.41	0.55
	100	35.00	35.00	0.92	1.00	36.54	36.54	128.90	0.44	0.81

Table B.2 Psychrometric Tables (contd.,)

DBT, °C	RH, %	DPT °C	WBT °C	Specific Volume, m^3/kg da	Degree of saturation	Specific humidity, g/kg da	Saturated specific humidity, g/kg da	Specific Enthalpy, kJ/ kg da	Specific entropy, kJ/kg da K	Specific exergy, kJ/ kg da
36	10	-0.39	16.27	0.88	0.09	3.67	38.73	45.60	0.16	1.65
	20	9.52	19.33	0.89	0.19	7.38	38.73	55.13	0.19	0.97
	30	15.70	22.09	0.89	0.29	11.13	38.73	64.78	0.23	0.56
	40	20.27	24.59	0.90	0.39	14.94	38.73	74.54	0.26	0.33
	50	23.93	26.88	0.90	0.48	18.78	38.73	84.41	0.30	0.22
	60	27.00	28.98	0.91	0.59	22.68	38.73	94.41	0.33	0.22
	70	29.65	30.92	0.91	0.69	26.62	38.73	104.52	0.36	0.31
	80	31.99	32.73	0.92	0.79	30.61	38.73	114.76	0.40	0.47
	90	34.09	34.42	0.92	0.89	34.65	38.73	125.13	0.43	0.71
	100	36.00	36.00	0.93	1.00	38.73	38.73	135.62	0.46	1.02
37	10	0.37	16.79	0.88	0.09	3.88	41.06	47.15	0.17	1.64
	20	10.33	19.96	0.89	0.19	7.80	41.06	57.23	0.20	0.95
	30	16.55	22.80	0.90	0.29	11.77	41.06	67.44	0.24	0.55
	40	21.16	25.37	0.90	0.38	15.80	41.06	77.78	0.27	0.33
	50	24.84	27.71	0.91	0.48	19.87	41.06	88.25	0.31	0.25
	60	27.94	29.85	0.91	0.58	24.00	41.06	98.85	0.34	0.28
	70	30.61	31.84	0.92	0.69	28.18	41.06	109.59	0.38	0.40
	80	32.96	33.67	0.92	0.79	32.42	41.06	120.47	0.42	0.61
	90	35.08	35.39	0.93	0.89	36.71	41.06	131.49	0.45	0.90
	100	37.00	37.00	0.94	1.00	41.06	41.06	142.66	0.49	1.26
38	10	10	1.12	17.31	0.89	0.09	4.09	43.51	48.72	0.17
	20	20	11.15	20.59	0.89	0.19	8.24	43.51	59.38	0.21
	30	30	17.41	23.51	0.90	0.29	12.44	43.51	70.19	0.25
	40	40	22.04	26.15	0.91	0.38	16.70	43.51	81.14	0.28
	50	50	25.76	28.54	0.91	0.48	21.02	43.51	92.24	0.32
	60	60	28.87	30.73	0.92	0.58	25.39	43.51	103.49	0.36
	70	70	31.56	32.75	0.92	0.69	29.83	43.51	114.89	0.40
	80	80	33.94	34.62	0.93	0.79	34.32	43.51	126.44	0.43
	90	90	36.07	36.37	0.94	0.89	38.88	43.51	138.16	0.47
	100	100	38.00	38.00	0.94	1.00	43.51	43.51	150.04	0.51
39	10	10	1.87	17.83	0.89	0.09	4.32	46.09	50.32	0.18
	20	20	11.96	21.22	0.90	0.19	8.70	46.09	61.60	0.22
	30	30	18.27	24.22	0.90	0.29	13.15	46.09	73.03	0.26
	40	40	22.93	26.92	0.91	0.38	17.65	46.09	84.63	0.30
	50	50	26.67	29.37	0.92	0.48	22.22	46.09	96.39	0.34
	60	60	29.81	31.61	0.92	0.58	26.86	46.09	108.31	0.37
	70	70	32.51	33.67	0.93	0.68	31.56	46.09	120.41	0.41
	80	80	34.91	35.57	0.94	0.79	36.34	46.09	132.69	0.45
	90	90	37.05	37.34	0.94	0.89	41.18	46.09	145.14	0.50
	100	100	39.00	39.00	0.95	1.00	46.09	46.09	157.78	0.54
40	10	10	2.62	18.35	0.89	0.09	4.56	48.83	51.95	0.18
	20	20	12.78	21.84	0.90	0.19	9.19	48.83	63.87	0.22
	30	30	19.12	24.94	0.91	0.28	13.88	48.83	75.96	0.27
	40	40	23.82	27.70	0.91	0.38	18.65	48.83	88.24	0.31
	50	50	27.58	30.21	0.92	0.48	23.49	48.83	100.70	0.35
	60	60	30.74	32.49	0.93	0.58	28.40	48.83	113.34	0.39
	70	70	33.47	34.58	0.93	0.68	33.39	48.83	126.18	0.43
	80	80	35.88	36.52	0.94	0.79	38.46	48.83	139.22	0.48
	90	90	38.04	38.32	0.95	0.89	43.60	48.83	152.45	0.52
	100	100	40.00	40.00	0.96	1.00	48.83	48.83	165.90	0.56

Table B.2 Psychrometric Tables (contd.,)

DBT, °C	RH, %	DPT °C	WBT °C	Specific Volume, m^3/kg da	Degree of saturation	Specific humidity, g/kg da	Saturated specific humidity, g/kg da	Specific Enthalpy, kJ/ kg da	Specific entropy, kJ/kg da K	Specific exergy, kJ/ kg da
41	10	10	3.37	18.87	0.90	0.09	4.81	51.71	53.61	0.19
	20	20	13.59	22.47	0.90	0.19	9.70	51.71	66.20	0.23
	30	30	19.98	25.65	0.91	0.28	14.66	51.71	78.99	0.28
	40	40	24.70	28.49	0.92	0.38	19.70	51.71	91.98	0.32
	50	50	28.49	31.04	0.93	0.48	24.82	51.71	105.18	0.36
	60	60	31.67	33.37	0.93	0.58	30.03	51.71	118.58	0.41
	70	70	34.42	35.50	0.94	0.68	35.32	51.71	132.21	0.45
	80	80	36.85	37.47	0.95	0.79	40.69	51.71	146.05	0.50
	90	90	39.02	39.29	0.96	0.89	46.16	51.71	160.12	0.54
	100	100	41.00	41.00	0.96	1.00	51.71	51.71	174.42	0.59
42	10	10	4.12	19.38	0.90	0.09	5.07	54.76	55.30	0.19
	20	20	14.40	23.10	0.91	0.19	10.23	54.76	68.60	0.24
	30	30	20.83	26.37	0.92	0.28	15.47	54.76	82.12	0.29
	40	40	25.59	29.27	0.92	0.38	20.80	54.76	95.87	0.33
	50	50	29.41	31.88	0.93	0.48	26.22	54.76	109.84	0.38
	60	60	32.61	34.25	0.94	0.58	31.74	54.76	124.05	0.43
	70	70	35.37	36.42	0.95	0.68	37.34	54.76	138.50	0.47
	80	80	37.82	38.42	0.95	0.79	43.05	54.76	153.20	0.52
	90	90	40.01	40.27	0.96	0.89	48.85	54.76	168.16	0.57
	100	100	42.00	42.00	0.97	1.00	54.76	54.76	183.37	0.62
43	10	10	4.87	19.90	0.90	0.09	5.35	57.98	57.02	0.20
	20	20	15.21	23.73	0.91	0.19	10.79	57.98	71.07	0.25
	30	30	21.68	27.08	0.92	0.28	16.33	57.98	85.36	0.30
	40	40	26.48	30.05	0.93	0.38	21.96	57.98	99.90	0.35
	50	50	30.32	32.72	0.94	0.48	27.70	57.98	114.69	0.40
	60	60	33.54	35.13	0.94	0.58	33.54	57.98	129.75	0.45
	70	70	36.33	37.33	0.95	0.68	39.48	57.98	145.08	0.49
	80	80	38.79	39.37	0.96	0.79	45.53	57.98	160.69	0.55
	90	90	40.99	41.25	0.97	0.89	51.70	57.98	176.59	0.60
	100	100	43.00	43.00	0.98	1.00	57.98	57.98	192.78	0.65
44	10	10	5.61	20.41	0.91	0.09	5.64	61.37	58.78	0.20
	20	20	16.03	24.37	0.92	0.19	11.38	61.37	73.61	0.26
	30	30	22.54	27.80	0.92	0.28	17.22	61.37	88.71	0.31
	40	40	27.36	30.84	0.93	0.38	23.18	61.37	104.08	0.36
	50	50	31.23	33.56	0.94	0.48	29.24	61.37	119.74	0.41
	60	60	34.47	36.01	0.95	0.58	35.43	61.37	135.70	0.46
	70	70	37.28	38.25	0.96	0.68	41.73	61.37	151.96	0.52
	80	80	39.76	40.32	0.97	0.78	48.15	61.37	168.54	0.57
	90	90	41.98	42.22	0.98	0.89	54.70	61.37	185.43	0.62
	100	100	44.00	44.00	0.99	1.00	61.37	61.37	202.66	0.68
45	10	10	6.36	20.93	0.91	0.09	5.94	64.96	60.58	0.21
	20	20	16.84	25.00	0.92	0.18	11.99	64.96	76.22	0.27
	30	30	23.39	28.52	0.93	0.28	18.16	64.96	92.17	0.32
	40	40	28.25	31.63	0.94	0.38	24.45	64.96	108.43	0.37
	50	50	32.14	34.40	0.95	0.48	30.87	64.96	125.00	0.43
	60	60	35.41	36.90	0.96	0.58	37.42	64.96	141.91	0.48
	70	70	38.23	39.17	0.97	0.68	44.09	64.96	159.16	0.54
	80	80	40.73	41.27	0.98	0.78	50.91	64.96	176.76	0.60
	90	90	42.97	43.20	0.99	0.89	57.86	64.96	194.72	0.65
	100	100	45.00	45.00	1.00	1.00	64.96	64.96	213.05	0.71

Table B.2 Psychrometric Tables (contd.,)

DBT, °C	RH, %	DPT °C	WBT °C	Specific Volume, m^3/kg da	Degree of saturation	Specific humidity, g/kg da	Saturated specific humidity, g/kg da	Specific Enthalpy, kJ/ kg da	Specific entropy, kJ/kg da K	Specific exergy, kJ/ kg da
46	10	10	7.10	21.44	0.91	0.09	6.25	68.76	62.41	0.22
	20	20	17.65	25.63	0.92	0.18	12.63	68.76	78.91	0.27
	30	30	24.24	29.25	0.93	0.28	19.15	68.76	95.75	0.33
	40	40	29.13	32.42	0.94	0.38	25.79	68.76	112.94	0.39
	50	50	33.05	35.24	0.95	0.47	32.58	68.76	130.48	0.45
	60	60	36.34	37.78	0.96	0.57	39.51	68.76	148.40	0.51
	70	70	39.18	40.10	0.97	0.68	46.59	68.76	166.69	0.56
	80	80	41.70	42.22	0.98	0.78	53.82	68.76	185.37	0.62
	90	90	43.95	44.18	0.99	0.89	61.20	68.76	204.46	0.69
	100	100	46.00	46.00	1.00	1.00	68.76	68.76	223.97	0.75
47	10	10	7.85	21.96	0.92	0.09	6.58	72.77	64.28	0.22
	20	20	18.46	26.27	0.93	0.18	13.31	72.77	81.68	0.28
	30	30	25.09	29.97	0.94	0.28	20.18	72.77	99.46	0.34
	40	40	30.01	33.21	0.95	0.37	27.20	72.77	117.63	0.40
	50	50	33.96	36.08	0.96	0.47	34.37	72.77	136.19	0.47
	60	60	37.27	38.67	0.97	0.57	41.71	72.77	155.17	0.53
	70	70	40.14	41.02	0.98	0.68	49.21	72.77	174.57	0.59
	80	80	42.67	43.17	0.99	0.78	56.88	72.77	194.41	0.65
	90	90	44.94	45.15	1.00	0.89	64.73	72.77	214.70	0.72
	100	100	47.00	47.00	1.01	1.00	72.77	72.77	235.47	0.78
48	10	10	8.59	22.47	0.92	0.09	6.93	77.00	66.19	0.23
	20	20	19.26	26.91	0.93	0.18	14.01	77.00	84.54	0.29
	30	30	25.94	30.70	0.94	0.28	21.26	77.00	103.31	0.36
	40	40	30.90	34.00	0.95	0.37	28.67	77.00	122.50	0.42
	50	50	34.87	36.93	0.96	0.47	36.26	77.00	142.14	0.48
	60	60	38.20	39.56	0.97	0.57	44.02	77.00	162.24	0.55
	70	70	41.09	41.94	0.99	0.67	51.97	77.00	182.81	0.62
	80	80	43.63	44.12	1.00	0.78	60.11	77.00	203.88	0.68
	90	90	45.92	46.13	1.01	0.89	68.45	77.00	225.46	0.75
	100	100	48.00	48.00	1.02	1.00	77.00	77.00	247.57	0.82
49	10	10	9.34	22.98	0.92	0.09	7.29	81.48	68.14	0.24
	20	20	20.07	27.54	0.93	0.18	14.75	81.48	87.48	0.30
	30	30	26.79	31.42	0.95	0.27	22.39	81.48	107.29	0.37
	40	40	31.78	34.80	0.96	0.37	30.22	81.48	127.57	0.44
	50	50	35.78	37.77	0.97	0.47	38.24	81.48	148.34	0.50
	60	60	39.13	40.44	0.98	0.57	46.45	81.48	169.63	0.57
	70	70	42.04	42.86	0.99	0.67	54.88	81.48	191.45	0.64
	80	80	44.60	45.07	1.01	0.78	63.52	81.48	213.82	0.71
	90	90	46.91	47.11	1.02	0.89	72.38	81.48	236.77	0.79
	100	100	49.00	49.00	1.03	1.00	81.48	81.48	260.31	0.86
50	10	10	10.08	23.50	0.93	0.09	7.67	86.22	70.14	0.24
	20	20	20.88	28.18	0.94	0.18	15.52	86.22	90.52	0.31
	30	30	27.64	32.15	0.95	0.27	23.58	86.22	111.41	0.38
	40	40	32.66	35.59	0.96	0.37	31.84	86.22	132.83	0.45
	50	50	36.69	38.62	0.97	0.47	40.31	86.22	154.81	0.53
	60	60	40.07	41.33	0.99	0.57	49.01	86.22	177.35	0.60
	70	70	42.99	43.79	1.00	0.67	57.94	86.22	200.49	0.67
	80	80	45.57	46.03	1.01	0.78	67.11	86.22	224.26	0.75
	90	90	47.89	48.09	1.03	0.89	76.54	86.22	248.66	0.82
	100	100	50.00	50.00	1.04	1.00	86.22	86.22	273.74	0.90

Table B.2 Psychrometric Tables (contd.,)

DBT, °C	RH, %	DPT °C	WBT °C	Specific Volume, m^3/kg da	Degree of saturation	Specific humidity, g/kg da	Saturated specific humidity, g/kg da	Specific Enthalpy, kJ/ kg da	Specific entropy, kJ/kg da K	Specific exergy, kJ/ kg da
51	10	10	10.82	24.01	0.93	0.09	8.06	91.23	72.18	0.25
	20	20	21.69	28.83	0.94	0.18	16.33	91.23	93.65	0.32
	30	30	28.49	32.88	0.96	0.27	24.82	91.23	115.69	0.40
	40	40	33.54	36.39	0.97	0.37	33.54	91.23	138.31	0.47
	50	50	37.59	39.47	0.98	0.47	42.50	91.23	161.55	0.55
	60	60	41.00	42.22	0.99	0.57	51.70	91.23	185.43	0.62
	70	70	43.94	44.71	1.01	0.67	61.17	91.23	209.97	0.70
	80	80	46.54	46.98	1.02	0.78	70.90	91.23	235.21	0.78
	90	90	48.88	49.07	1.04	0.89	80.92	91.23	261.18	0.86
	100	100	51.00	51.00	1.05	1.00	91.23	91.23	287.90	0.95
52	10	10	11.56	24.53	0.93	0.09	8.47	96.53	74.27	0.26
	20	20	22.49	29.47	0.95	0.18	17.17	96.53	96.88	0.33
	30	30	29.34	33.62	0.96	0.27	26.12	96.53	120.12	0.41
	40	40	34.42	37.19	0.97	0.37	35.32	96.53	144.01	0.49
	50	50	38.50	40.32	0.99	0.46	44.79	96.53	168.59	0.57
	60	60	41.93	43.11	1.00	0.56	54.53	96.53	193.88	0.65
	70	70	44.89	45.63	1.02	0.67	64.57	96.53	219.91	0.73
	80	80	47.51	47.93	1.03	0.78	74.90	96.53	246.73	0.82
	90	90	49.86	50.04	1.05	0.89	85.55	96.53	274.35	0.90
	100	100	52.00	52.00	1.06	1.00	96.53	96.53	302.83	0.99

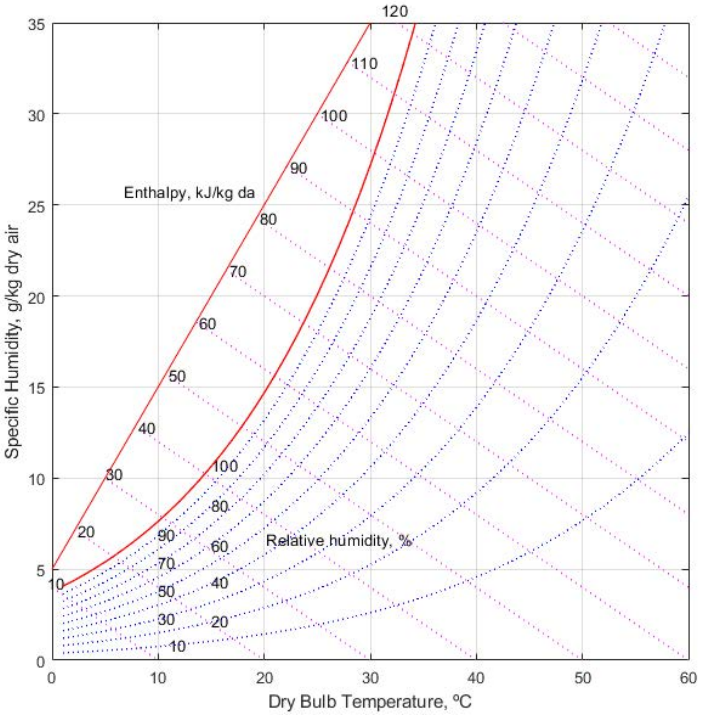

Fig. B.1: Psychrometric chart drawn with MATLAB plot

References

1. Abdelgaied, M., Kabeel, A.E. and Zakaria, Y 2019. Performance improvement of desiccant air conditioner coupled with humidification-dehumidification desalination unit using solar reheating of regeneration air. Energy Conversion and Management, 198: 111808.
2. Ahmadi, Pouria, Marc A. Rosen, and Ibrahim Dincer. 2012. Multi-Objective Exergy-Based Optimization of a Polygeneration Energy System Using an Evolutionary Algorithm. Energy 46(1):21–31.
3. Aichmayer, Lukas, James Spelling, and Björn Laumert. 2014. Small Scale Hybrid Solar Power Plants for Polygeneration in Rural Areas. Energy Procedia 57:1536–45.
4. Bracco, Stefano, Federico Delfino, Fabio Pampararo, Michela Robba, and Mansueto Rossi. 2012. Economic and Environmental Performances Quantification of the University of Genoa Smart Polygeneration Microgrid. 2012 IEEE International Energy Conference and Exhibition, ENERGYCON 2012 593–98.
5. Buonomano, Annamaria, Francesco Calise, Gabriele Ferruzzi, and Laura Vanoli. 2014. A Novel Renewable Polygeneration System for Hospital Buildings: Design, Simulation and Thermo-Economic Optimization. Applied Thermal Engineering 67(1–2):43–60.
6. Calise, Francesco, Adolfo Palombo, and Laura Vanoli. 2012. Design and Dynamic Simulation of a Novel Polygeneration System Fed by Vegetable Oil and by Solar Energy. Energy Conversion and Management 60(x):204–13.
7. Calise, Francesco, Adriano Macaluso, Antonio Piacentino, and Laura Vanoli. 2017. A Novel Hybrid Polygeneration System Supplying Energy and Desalinated Water by Renewable Sources in Pantelleria Island. Energy 137:1086–1106.
8. Calise, F., di Vastogirardi, G.D.N., d'Accadia, M.D. and Vicidomini, M., 2018. Simulation of polygeneration systems. Energy, 163, pp.290-337.
9. Chen, Dengyu, Xiaojuan Chen, Jun Sun, Zhongcheng Zheng, and Kexin Fu. 2016a. Pyrolysis Polygeneration of Pine Nut Shell: Quality of Pyrolysis Products and Study on the Preparation of Activated Carbon from Biochar. Bioresource Technology 216:629–36.
10. Chen, Hanping, Guiying Lin, Yingquan Chen, Wei Chen, and Haiping Yang. 2016b. Biomass Pyrolytic Polygeneration of Tobacco Waste: Product Characteristics and Nitrogen Transformation. Energy and Fuels 30(3):1579–88.
11. Chen, Yang, Thomas A. Adams, and Paul I. Barton. 2011. Optimal Design and Operation of Flexible Energy Polygeneration Systems. Industrial and Engineering Chemistry Research 50(8):4553–66.
12. Chen, Y., Yang, H., Wang, X., Zhang, S. and Chen, H., 2012. Biomass-based pyrolytic polygeneration system on cotton stalk pyrolysis: influence of temperature. Bioresource technology, 107, pp.411-418.

T. Srinivas, *Thermal Polygeneration*,
https://doi.org/10.1007/978-3-031-37886-7

13. Dalai P, Nanda P, Mund C, Mishra D and Gupta A 2017 An Experimental Study on Water Harvesting from a Modified Window Air-Conditioner. Energy Procedia, 109: 253-260.
14. Dehghani, S., Date, A. and Akbarzadeh, A., 2018. Performance analysis of a heat pump driven humidification-dehumidification desalination system. Desalination, 445, pp.95-104.
15. Duffie, J.A. and Beckman, W.A., 2013. Solar engineering of thermal processes. John Wiley & Sons.
16. Elattar H F, Fouda, A. and Nada, S A 2016. Performance investigation of a novel solar hybrid air conditioning and humidification–dehumidification water desalination system. Desalination 382: 28-42.
17. Farhat, Karim and Stefan Reichelstein. 2016. Economic Value of Flexible Hydrogen-Based Polygeneration Energy Systems. Applied Energy 164:857–70.
18. Ganesh, N.S. and Srinivas, T., 2012. Design and modeling of low temperature solar thermal power station. Applied energy, 91(1), pp.180-186.
19. Gao, Lin, Hongqiang Li, Bin Chen, Hongguang Jin, Rumou Lin, and Hui Hong. 2008. Proposal of a Natural Gas-Based Polygeneration System for Power and Methanol Production. Energy 33(2):206–12.
20. Gassner, Martin and Franois Maréchal. 2012. Thermo-Economic Optimisation of the Polygeneration of Synthetic Natural Gas (SNG), Power and Heat from Lignocellulosic Biomass by Gasification and Methanation. Energy and Environmental Science 5(2):5768–89.
21. Guo, Zhihang, Qinhui Wang, Mengxiang Fang, Zhongyang Luo, and Kefa Cen. 2014. Thermodynamic and Economic Analysis of Polygeneration System Integrating Atmospheric Pressure Coal Pyrolysis Technology with Circulating Fluidized Bed Power Plant. Applied Energy 113:1301–14.
22. Guo, Zhihang, Qinhui Wang, Mengxiang Fang, Zhongyang Luo, and Kefa Cen. 2015. Simulation of a Lignite-Based Polygeneration System Coproducing Electricity and Tar with Carbon Capture. Chemical Engineering and Technology 38(3):463–72.
23. Gutkowski, Gary P. 1983. 1983 (20th) Space: The Next Twenty Years Kennedy Space Center Polygeneration Facility. 1983:0–7.
24. Hao, Yan Hong and Jie Feng. 2012. Exergoeconomic Analysis of Parallel Polygeneration System with Co-Riched Gas Once Through. Applied Mechanics and Materials 229–231:2671–79.
25. Hao, Yanhong, Yi Huang, Minhui Gong, Wenying Li, Jie Feng, and Qun Yi. 2015. A Polygeneration from a Dual-Gas Partial Catalytic Oxidation Coupling with an Oxygen-Permeable Membrane Reactor. Energy Conversion and Management 106:466–78.
26. Hu, Lin, Jin Hongguang, Gao Lin, and Han Wei. 2011. Techno-Economic Evaluation of Coal-Based Polygeneration Systems of Synthetic Fuel and Power with CO2 Recovery. Energy Conversion and Management 52(1):274–83.
27. James, Olusola O., Biswajit Chowdhury, Aline Auroux, and Sudip Maity. 2013. Low CO2 Selective Iron Based Fischer-Tropsch Catalysts for Coal

Based Polygeneration. Applied Energy 107:377–83.

28. Jana, Kuntal and Sudipta De. 2015. Polygeneration Performance Assessments: Multi-Dimensional Viewpoint. Clean Technologies and Environmental Policy 17(6):1547–61.
29. Kaniyal, Ashok A., Philip J. Van Eyk, Graham J. Nathan, Peter J. Ashman, and Jonathan J. Pincus. 2013. Polygeneration of Liquid Fuels and Electricity by the Atmospheric Pressure Hybrid Solar Gasification of Coal. Energy and Fuels 27(6):3538–55.
30. Kasaeian, A., Bellos, E., Shamaeizadeh, A. and Tzivanidis, C., 2020. Solar-driven polygeneration systems: Recent progress and outlook. Applied Energy, 264, p.114764.
31. Khan, Ershad Ullah and Andrew R. Martin. 2015. Optimization of Hybrid Renewable Energy Polygeneration System with Membrane Distillation for Rural Households in Bangladesh. Energy 93:1116–27.
32. Khojasteh Salkuyeh Yaser and Thomas A. Adams. 2015a. A Novel Polygeneration Process to Co-Produce Ethylene and Electricity from Shale Gas with Zero CO_2 Emissions via Methane Oxidative Coupling. Energy Conversion and Management 92:406–20.
33. Khojasteh Salkuyeh Yaser and Thomas A. Adams. 2015b. Integrated Petroleum Coke and Natural Gas Polygeneration Process with Zero Carbon Emissions. Energy 91:479–90.
34. Kribus, Abraham and Gur Mittelman. 2008. Potential of Polygeneration with Solar Thermal and Photovoltaic Systems. Journal of Solar Energy Engineering, Transactions of the ASME 130(1):0110011–15.
35. Kyriakarakos, George, Anastasios I. Dounis, Stelios Rozakis, Konstantinos G. Arvanitis, and George Papadakis. 2011. Polygeneration Microgrids: A Viable Solution in Remote Areas for Supplying Power, Potable Water and Hydrogen as Transportation Fuel. Applied Energy 88(12):4517–26.
36. Kyriakarakos, George, Dimitrios D. Piromalis, Konstantinos G. Arvanitis, Anastasios I. Dounis, and George Papadakis. 2015. On Battery-Less Autonomous Polygeneration Microgrids: Investigation of the Combined Hybrid Capacitors/Hydrogen Alternative. Energy Conversion and Management 91:405–15.
37. Li, Xiang and Paul I. Barton. 2015. Optimal Design and Operation of Energy Systems under Uncertainty. Journal of Process Control 30:1–9.
38. Li, Yuanyuan, Guoqiang Zhang, Yongping Yang, Dailong Zhai, Kai Zhang, and Gang Xu. 2014. Thermodynamic Analysis of a Coal-Based Polygeneration System with Partial Gasification. Energy 72:201–14.
39. Lin, Hu, Hongguang Jin, Lin Gao, and Na Zhang. 2014. A Polygeneration System for Methanol and Power Production Based on Coke Oven Gas and Coal Gas with CO_2 Recovery. Energy 74(C):174–80.
40. Liu, P., Gerogiorgis, D.I. and Pistikopoulos, E.N., 2007. Modeling and optimization of polygeneration energy systems. Catalysis Today, 127(1-4), pp.347-359.
41. Lythcke-Jørgensen, Christoffer and Fredrik Haglind. 2015. Design Optimization of a Polygeneration Plant Producing Power, Heat, and

Lignocellulosic Ethanol. Energy Conversion and Management 91:353–66.

42. Maraver, Daniel, Javier Uche, and Javier Royo. 2012. Assessment of High Temperature Organic Rankine Cycle Engine for Polygeneration with MED Desalination: A Preliminary Approach. Energy Conversion and Management 53(1):108–17.
43. Mata-Torres, Carlos, Rodrigo A. Escobar, José M. Cardemil, Yeliz Simsek, and José A. Matute. 2017. Solar Polygeneration for Electricity Production and Desalination: Case Studies in Venezuela and Northern Chile. Renewable Energy 101:387–98.
44. Meerman, J. C., A. Ramírez, W. C. Turkenburg, and A. P. C. Faaij. 2011. Performance of Simulated Flexible Integrated Gasification Polygeneration Facilities. Part A: A Technical-Energetic Assessment. Renewable and Sustainable Energy Reviews 15(6):2563–87.
45. Meerman, J. C., A. Ramírez, W. C. Turkenburg, and A. P. C. Faaij. 2012. Performance of Simulated Flexible Integrated Gasification Polygeneration Facilities, Part B: Economic Evaluation. Renewable and Sustainable Energy Reviews 16(8):6083–6102.
46. Murugan, S. and Bohumil Horák. 2016. Tri and Polygeneration Systems-A Review. Renewable and Sustainable Energy Reviews 60:1032–51.
47. Ng, Kok Siew and Elias Martinez Hernandez. 2016. A Systematic Framework for Energetic, Environmental and Economic (3E) Assessment and Design of Polygeneration Systems. Chemical Engineering Research and Design 106(0):1–25.
48. Ng Kok Siew, Nan Zhang, and Jhuma Sadhukhan. 2013. CO_2 Abatement Strategies for Polygeneration Systems: Process Integration and Analysis. Chemical Engineering Journal 219:96–108.
49. Ortiga, J., J. C. Bruno, and A. Coronas. 2012. Operational Experience of the Polygeneration Plant in Parc de l'Alba (Spain): Start-up and First Results. Proceedings of the 2011 International Conference and Utility Exhibition on Power and Energy Systems: Issues and Prospects for Asia, ICUE 2011 1–5.
50. Ortiga, Jordi, Joan Carles Bruno, Alberto Coronas, and Ignacio E. Grossman. 2007. Review of Optimization Models for the Design of Polygeneration Systems in District Heating and Cooling Networks. Computer Aided Chemical Engineering 24:1121–26.
51. Paleta, Rita, Andre Pina, and Carlos A. Santos Silva. 2014. Polygeneration Energy Container: Designing and Testing Energy Services for Remote Developing Communities. IEEE Transactions on Sustainable Energy 5(4):1348–55.
52. Pradeep Varma, G.V. and Srinivas, T., 2017. Power-augmented steam power plant in a cogeneration cement factory. Journal of Energy Engineering, 143(1), p.04016020.
53. Ray, Avishek, Kuntal Jana, and Sudipta De. 2017. Polygeneration for an Off-Grid Indian Village: Optimization by Economic and Reliability Analysis. Applied Thermal Engineering 116(2017):182–96.
54. Rossi, Iacopo, Larry Banta, Alessandra Cuneo, Mario Luigi Ferrari, Alberto Nicola Traverso, and Alberto Traverso. 2016. Real-Time Management Solutions for a Smart Polygeneration Microgrid. Energy Conversion and

Management 112:11–20.

55. Rubio-Maya, Carlos, Javier Uche-Marcuello, Amaya Martínez-Gracia, and Angel A. Bayod-Rújula. 2011. Design Optimization of a Polygeneration Plant Fuelled by Natural Gas and Renewable Energy Sources. Applied Energy 88(2):449–57.
56. Sahoo, U., R. Kumar, P. C. Pant, and R. Chaudhury. 2015. Scope and Sustainability of Hybrid Solar-Biomass Power Plant with Cooling, Desalination in Polygeneration Process in India. Renewable and Sustainable Energy Reviews 51(May):304–16.
57. Salomón, Marianne, Maria Fernanda Gomez, and Andrew Martin. 2013. Technical Polygeneration Potential in Palm Oil Mills in Colombia: A Case Study. Sustainable Energy Technologies and Assessments 3:40–52.
58. Serra, L.M., Lozano, M.A., Ramos, J., Ensinas, A.V. and Nebra, S.A., 2009. Polygeneration and efficient use of natural resources. Energy, 34(5), pp.575-586.
59. Shafii M B Jafargholi, H and Faegh, M 2018 Experimental investigation of heat recovery in a humidification-dehumidification desalination system via a heat pump. Desalination, 437: 81-88.
60. Shankar, R. and Srinivas, T., 2018. Performance investigation of Kalina cooling cogeneration cycles. International Journal of Refrigeration, 86, pp.163-185.
61. Shankar, R. and Srinivas, T., 2014. Investigation on operating processes for a new solar cooling cogeneration plant. Journal of solar energy engineering, 136(3).
62. Soutullo, S., L. A. Bujedo, J. Samaniego, D. Borge, J. A. Ferrer, R. Carazo, and M. R. Heras. 2016. Energy Performance Assessment of a Polygeneration Plant in Different Weather Conditions through Simulation Tools. Energy and Buildings 124:7–18.
63. Srinivas, T. and Reddy, B.V., 2014. Thermal optimization of a solar thermal cooling cogeneration plant at low temperature heat recovery. Journal of Energy Resources Technology, 136(2).
64. Tangellapalli, S., 2021. Humidification-dehumidification and heat pump integration for water purifier and air conditioning. Energy Conversion and Management, 244, p.114472.
65. Varma, G.P. and Srinivas, T., 2017. Power generation from low temperature heat recovery. Renewable and Sustainable Energy Reviews, 75, pp.402-414.
66. Vidal, Marta and Mariano Martín. 2015. Optimal Coupling of a Biomass Based Polygeneration System with a Concentrated Solar Power Facility for the Constant Production of Electricity over a Year. Computers and Chemical Engineering 72:273–83.
67. Wang, Zhifang, Danxing Zheng, and Hongguang Jin. 2009. Energy Integration of Acetylene and Power Polygeneration by Flowrate-Exergy Diagram. Applied Energy 86(3):372–79.
68. Wright, Vincent P. 1986. World Energy Outlook. 23–28.
69. Xin, Shanzhi, Haiping Yang, Yingquan Chen, Xianhua Wang, and Hanping Chen. 2013. Assessment of Pyrolysis Polygeneration of Biomass Based on

Major Components: Product Characterization and Elucidation of Degradation Pathways. Fuel 113:266–73.

70. Yi, Qun, Jie Feng, Yanli Wu, and Wenying Li. 2014. 3E (Energy, Environmental, and Economy) Evaluation and Assessment to an Innovative Dual-Gas Polygeneration System. Energy 66:285–94.
71. Yi. Qun, Yang Fan, Wenying Li, and Jie Feng. 2013. CO_2 Capture and Use in a Novel Coal-Based Polygeneration System. Industrial and Engineering Chemistry Research 52(39):14231–40.
72. Yu, Bor Yih and I. Lung Chien. 2015. Design and Economic Evaluation of a Coal-Based Polygeneration Process to Coproduce Synthetic Natural Gas and Ammonia. Industrial and Engineering Chemistry Research 54(41):10073–87.
73. Yu, Ge wen, Yuan yuan Xu, Xu Hao, Yong wang Li, and Guang qi Liu. 2010. Process Analysis for Polygeneration of Fischer-Tropsch Liquids and Power with CO_2 Capture Based on Coal Gasification. Fuel 89(5):1070–76.
74. Zhang, Y Zhu, C, Zhang, H, Zheng, W, You, S and Zhen, Y, 2018 Experimental study of a humidification-dehumidification desalination system with heat pump unit. Desalination, 442: 108-117.
75. Zeghici, Răzvan Mihai, Andrei Damian, Rodica Frunzulicə, and Florin Iordache. 2014. Energy Performance Assessment of a Complex District Heating System Which Uses Gas-Driven Combined Heat and Power, Heat Pumps and High Temperature Aquifer Thermal Energy Storage. Energy and Buildings 84:142–51.
76. Zhu, Lin, Zheng Zhang, Junming Fan, and Peng Jiang. 2016. Polygeneration of Hydrogen and Power Based on Coal Gasification Integrated with a Dual Chemical Looping Process: Thermodynamic Investigation. Computers and Chemical Engineering 84:302–12.

❐❐❐